UNIVERSITY OF CANTERBURY
Te Whare Wānanga o Waitaha
CHRISTCHURCH NEW ZEALAND

DEVELOPMENT OF MAGNESIUM SILICATE HYDRATE BINDER SYSTEMS

A thesis submitted in partial fulfilment of the requirements for the degree of

DOCTOR OF PHILOSOPHY IN CIVIL ENGINEERING

ENCI790

By

HUNG TRAN

Supervisors:

Assoc. Prof. Allan Scott

Prof. Rajesh Dhakal

Department of Civil and Natural Resources Engineering

University of Canterbury

Apr, 2019

Abstract

Studies on magnesium-based cement have been of interest to mitigate the increasing impact of climate change due to the high CO_2 emissions associated with cement production industry. Although magnesium silicate hydrate (M-S-H) phases in concrete were discovered in the 1950s, the strengths of M-S-H binders as construction materials have been known only since 2006. Research on M-S-H binders is very limited, compared to Portland cement (PC), and mainly focused on properties of cement paste and mortar. The publications focused on mechanical properties and initially studied the reaction mechanisms of the formation of hydration products and the influence of different material sources. There was a controversy on the strength capacity of M-S-H binders while very little research characterized long-term properties, chemical compositions of pore solutions, and properties of concrete with the effect of aggregates. The poor workability was also reported as a significant limitation of the development of M-S-H cement for environmental benefits.

In this research, a comprehensive experimental programme was conducted to improve properties of M-S-H binders, derived from the characterization of the microstructures and chemical reactions of the binders, then followed by the optimization of the binders for strength, workability, and durability.

Firstly, microstructures and hydration processes have been analyzed by various methods such as XRD, SEM/EDS, and pore solution analysis (ICP-MS). Binders included MgO and silica within the optimal contents from 40-60% and were cured for a long-term duration up to 365 days age. The XRD and SEM/EDS results confirmed the formation of the hydration products including brucite and M-S-H phases. The brucite formed in the first stage and mainly completed after 7 days whereas M-S-H phases were formed slowly and still developed significantly from 28 to 90 days, which is very different from the hydration of PC. SEM/EDS images provided the microstructures of raw materials and hydration products, showing highly porous structures of M-S-H binder compared to PC. Pore solution analysis by ICP-MS showed important characteristics such as pHs and ion concentrations, which reveal the trend of forming hydration products and directly relate to the durability of M-S-H cementitious materials.

Secondly, M-S-H binders were found to have adequate strength for construction materials. Optimized M-S-H mortar using ternary binder systems (MgO - silica fume- quartz filler) obtained high strength of approximately 90 MPa. The optimal binder composition for strength and working was the balance between maximizing hydration products and improving the microstructure homogeneity and packing density. In addition, among high range water reducers, the use of polymer-based super plasticizer Sika Viscocrete-5-555 was a key factor to reduce w/c ratio to below 0.40 to improve strength and workability. Quartz filler also played an important role in improving microstructure and packing density, resulting in superior strength and improved workability of M-S-H binders.

Thirdly, M-S-H binder concrete was produced and tested based on the optimization of M-S-H cement pastes and mortars in previous phases. The binder using 60% MgO-40% silica fume with 10% quartz filler yielded strength of over 40 MPa which could be sufficient for structural concrete materials. However, some unexpected results were also observed such as low tensile strength and elastic modulus. In addition, further studies are required regarding the long-term strength and the permeability of the M-S-H binder concrete.

Another finding showed the strong influence of silica sources on the microstructure and mechanical properties of resulting M-S-H cementitious materials. The high-performance M-S-H binders require high reactivity binder constituents. The M-S-H phases readily formed with highly reactive silica such as silica fume, natural pozzolan, and rice husk ash. However, poor performance was observed with FA type F.

The extensive experimental programmes in this research have yielded valuable results for a variety of related topics which are of fundamental importance for the application of M-S-H binders. The research findings have closed a number of current research gaps, and also give directions for future studies of the M-S-H binders as new cementitious materials focused on sustainable development.

UNIVERSITY OF CANTERBURY
Te Whare Wānanga o Waitaha
CHRISTCHURCH NEW ZEALAND

Deputy Vice-Chancellor's Office
Postgraduate Office

Co-Authorship Form

This form is to accompany the submission of any thesis that contains research reported in co-authored work that has been published, accepted for publication, or submitted for publication. A copy of this form should be included for each co-authored work that is included in the thesis. Completed forms should be included at the front (after the thesis abstract) of each copy of the thesis submitted for examination and library deposit.

Please indicate the chapter/section/pages of this thesis that are extracted from co-authored work and provide details of the publication or submission from the extract comes:

1. Chapter 6:

Tran, H. M., & Scott, A. (2017). Strength and workability of magnesium silicate hydrate binder systems. *Construction and Building Materials*, *131*, 526-535.

2. Chapter 7:

Tran H.M., Scott A., Dhakal R.P. (2017). Strength development of mortars using a magnesium silicate hydrate binder system under different curing conditions. *Proceedings of the 2nd International RILEM Conference on Bio-based Building Materials, 21-23 June 2017, Clermont-Ferrand, France,* 87-91.

3. Chapter 8:

Tran, H.M., Scott, A., Dhakal, R.P. (2017). Mechanical and durability properties of a concrete using magnesium silicate hydrate binder system. *Proceedings of the Concrete 2017, the 28th Biennial National Conference of the Concrete Institute of Australia, held in conjunction with the 3rd International Congress on Durability of Concrete (ICDC), Adelaide, Australia, 22 October to 25 October 2017.*

Tran H., Scott A. and Dhakal R. (2019). Mechanical and durability properties of magnesium silicate hydrate binder concrete. *Magazine of Concrete Research*, https://doi.org/10.1680/jmacr.18.00217

Please detail the nature and extent (%) of contribution by the candidate:
The candidate was responsible for the developing the test plan, conducting the experiments, analysing the data and writing the papers.

Certification by Co-authors:

If there is more than one co-author then a single co-author can sign on behalf of all

The undersigned certifys that:

- The above statement correctly reflects the nature and extent of the PhD candidate's contribution to this co-authored work
- In cases where the candidate was the lead author of the co-authored work he or she wrote the text

Name: Allan Scott Signature: 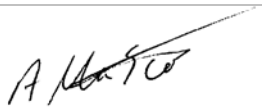 Date: 18/04/2019

Dedicated to my father

My dream of doing a PhD continues my father's dream

He pursued his PhD 30 years ago and it was disrupted

ACKNOWLEDGEMENTS

First of all, I would like to thank the Ministry of Education and Hanoi University of Mining and Geology (Vietnam) for their financial support. Without this invaluable scholarship, I would haven't had the life-changing opportunity to start my PhD study at University of Canterbury, New Zealand.

My greatest gratitude is devoted to Associate Professor Allan Scott, my main supervisor, for his trust, expertise, and passion to guide me throughout my study.

I would like to thank Professor Rajesh Dhakal for his co-supervision and great support. His professionalism and career success have highly motivated me to complete my study and pursue an academic career.

I truly appreciate the enormous support of Mr. Tim Perigo and other university staff for their guidance and assistance in experimental work.

Finally, I express my special thanks and love to my parents, my wife and children (Nina and Cherry), other family members, and my friends for their emotional support. I know they are looking forward to my graduation day. In the last four years, whenever I was struggling, I was thinking of them and kept going.

Thanks for all your encouragement!

TABLE OF CONTENTS

LIST OF FIGURES

LIST OF TABLES

APPENDICES

ABBREVIATIONS

PC	Portland cement
M-S-H	Magnesium silicate hydrate
C-S-H	Calcium silicate hydrate
UHPC	Ultra-high performance concrete
M	Magnesium oxide
SF	Silica fume
MS	Microsilica 600 (natural pozzolan)
RHA	Rice husk ash
FA	Fly ash
QF	Crushed quartz filler
SEM	Scanning electron microscope
EDS	Energy dispersive X-ray spectroscopy
XRD	X-ray diffraction
ICP-MS	inductively coupled plasma mass spectrometry
OPI	Oxygen Permeability Index
MOE	Static modulus of elasticity
w/c	water to cement ratio
w/b	water to binder ratio
w/s	water to solids ratio

CHAPTER 1 INTRODUCTION

1.1. RESEARCH BACKGROUND AND MOTIVATION

Production of Portland cement and its impact to the environment

Throughout the nearly 200 years since its inception in 1824 (Hall, 1976), Portland cement has brought great changes to human history in contributing to the supply of dwellings and infrastructure. Cement is now the most consumed construction material and the second most consumed substance worldwide, after water (Mariel, 2015). Reasons for the popularity in use of Portland cement (PC) might lie in the availability of lime and other minerals of cement production as well as its excellent engineering properties that are required in construction.

The cement production mainly includes the sintering of limestone ($CaCO_3$) with clay (SiO_2, FeO, Al_2O_3) in a kiln at temperatures of about 1400-1500°C. The first stage includes decarbonation of the mixture to produce calcium oxide (CaO) from limestone in which large amount CO_2 is released. As continued heating, various calcium silicates are produced in which the majority is C_3S ($3CaO.SiO_2$), C_2S ($2CaO.SiO_2$), C_3A ($3CaO.Al_2O_3$), C_4AF ($4CaO.Al_2O_3.Fe_2O_3$).

The first two mineral C_3S, C_2S account for the largest proportion of PC, and when hydrate in water form solid phases, with the most important hydration product being C-S-H gel. The microstructure of C-S-H gel phases is stable with layers that are intrinsically strong and well connected with other solid phases.

Despite the intensive use of PC in the last centuries and many benefits, there are some negative issues with the widespread use of cement which cannot be ignored. Global cement production was 1.39 billion tons/year in 1995, 3.31 billion tons/year in 2010, 4.1 billion tons/year in 2017 and is predicted to continue to increase in the future (U.S Geological Survey, 2018) This high demand is associated with environmental issue in particular the high CO_2 emission during PC production. The ratio of anthropogenic CO_2 for each ton of cement product is estimated at 0.65-0.95 (Mariel, 2015) and therefore billions of tons of total CO_2 emissions generated from cement industry each year now account for 5-8% of total CO_2 emissions in the atmosphere. This scenario calls for an urgent need to find more sustainable binder materials that the production will not cause such negative impact to the environment while retaining the well-performed engineering properties in construction.

Overview of current PC replacement

The first step in cement industry to reduce anthropogenic CO_2 emission is the introduction of blended cements to replace a certain amount of clinker used in Portland cement by other minerals utilized from industrial by-products or waste materials.

In the last few decades pozzolanic materials including silica fume, rice husk ash, fly ash, pulverized fuel ash, ground granulated blast-furnace slag (GGBFS) and the presence of superplasticizers have made it possible to increase the effective use of PC considerably. The application of binary and ternary blended cements has allowed for a significant level of PC replacement while maintaining expected cementitious properties. It is reported that the use of silica fume at 10-20% as additive to PC can improve strength of concrete dramatically. Even a concrete in which 25 vol.% of cement is replaced by silts and clay with a water/cement ratio of 0.5 adequate durability can still be obtained (Chan, 2000). It is reported (ACI Committee, 1996) that concrete with 20-30% cement replacement with Class C Fly Ash gained higher 28 days compressive strengths than PC control samples. In specific conditions, Fly Ash content of up to 50% may be suitable for most structural elements provided adequate moist-curing and the early-age strength requirements can be met (Thomas, 2007; Tarun et al., 1995). At higher replacement rate of 60%, although compressive strength of fly ash concrete was slightly lower than the reference sample, it appears that fly ash concrete can meet adequate strengths for structural applications (Malhotra V.M. and Painter, 1989). In addition, in an experiment and economic calculation, Dale et al. (2013) demonstrated that ternary mixture of high volume fly ash (45%) and fine limestone powder (15%) is capable not only to increase concrete strength but also reduce the cost considerably. Ecocem (2015) demonstrated that concrete made with 50% PC replacement by GGBFS obtained the same 28–day strength as concrete made with ordinary Portland cement (CEM I or CEM II/A), and the long-term strength even developed higher with GGBFS concrete.

The improved/comparable effect of PC replacement by pozzolanic materials has been well studied in the literature. As calcium hydroxide is a weak chemical binding phase which accounts for 15-19% of hydration products (Neville, 1981; The science of concrete, 2015), most of previous studies focused on the consumption and conversion of this undesirable product. Once pozzolanic reaction of pozzolans and calcium hydroxide is activated, calcium silicate hydrate gel is formed and the transformation from weak binding phase of calcium hydroxide to strong binding phase of calcium silicate hydrate gel is the main cause for strength improvement in concrete.

Alternatively, Aydin and Baradan (2013) demonstrated the production of concrete without Portland cement. This type of binder, also called geopolymer, utilized GGBFS in combination with

silica fume as the binder to obtain excellent mechanical properties and even enable to produce ultra-high strength concrete (Aydin and Baradan, 2013). Geopolymer consumes industrial by-products to form a solid binder with similar mechanical functions to OPC and thus has positive effect to environment. However, it also presents problems of rapid setting and durability and further research is ongoing for future applications.

Although having contributed to the effort of reducing CO_2 emissions, most of the past research on PC replacement focused on blending PC with silica for pozzolanic reactions to produce additional C-S-H gels. The nature of the hydration and reaction mechanism of PC has not changed and the C-S-H is still the main binding phases in blended cements. In such conditions and the high demand of cement in construction, the PC production with its energy-intensive nature of high temperature calcination still releases a high amount of CO_2 and causes a large impact to the environment.

Introduction of Magnesium-based cement

A new stage of cement development has been initiated when the issue of reducing CO_2 emissions and waste recycling became more important and the idea of finding alternative binders based on reactive magnesia gradually became of interest in materials engineering. The novel idea of using magnesium-based cement for green built environment lies in its potential of incorporating waste materials and light burn reactive magnesium oxide obtained from a low temperature (700-800^{o}C) calcination process, compared to PC production.

The CO_2 emission from magnesia production is dependent on magnesite sources and production technology. The calcination of magnesite to produce magnesia releases CO_2 emission, regardless of any technical arrangements. It is reported that 50% of the raw material diffuses as CO_2 during the firing process (Trojer, 2009). The amount of CO_2 emission from fuel combustion depends on the origin of the deposit, the different chemical compositions of the magnesite and the calcined temperature (Trojer, 2009) whereas different magnesia sources require different fuel consumption. Accordingly, the use of light burnt magnesia is beneficial from a less energy-intensive calcination process, which leads to less CO_2 emission compared to other magnesium-based cement using hard-burnt or dead-burnt magnesia. Another breakthrough technology if successful can largely reduce CO_2 emission as magnesia is not obtained from magnesite. The process involves CO_2 sequestration by magnesium-rich minerals such as olivine and serpentine to form magnesium carbonates which are then decarbonated to obtain magnesium hydroxide for magnesia production (Pacheco-Torgal, 2014).

Reactive MgO was first used as an additive to compensate for the shrinkage of concrete in several dam construction projects in China in 1966-1976 at low content of 4.5% binder (Du, 2005). Hydration of MgO results in magnesium hydroxide ($Mg(OH)_2$) and the expansion effect occurs due to the larger volume of $Mg(OH)_2$ compared to its precursors. Another application of magnesium-based cement was developed for masonry blocks (Tececo, 2015). In such system, hydrated MgO absorbs a significant amount of CO_2 to form magnesium carbonate. This binder system requires high porosity for the CO_2 penetration and carbonation, thus only suitable for low strength concrete.

The other research focuses on magnesia silicate hydrate (M-S-H) systems synthesized from reactions of reactive magnesia and amorphous silica. The strength of hardened M-S-H binders is mainly dependent on M-S-H gel phases, which are considered to have stronger bonding effect than brucite and potentially can be used for concrete material to achieve adequate strength for structural applications.

The formation of M-S-H as hydration products was first discovered in 1953 during the investigation of deteriorated mechanism of concrete in sea water (Cole, 1953). The M-S-H formation since then had been considered a detrimental constituent without cementing properties in concrete and attracted little research interest for a long period. From 1977 to 2005, a number of studies had been performed and confirmed the formation of M-S-H gel phases. Remarkable publications included those of Mitsuda and Taguchi (1977) and Brew and Glasser (2005) studying the microstructure of M-S-H phases synthesized in the laboratory have laid the foundation for the development of M-S-H binders.

Following these works, cementing properties of M-S-H binders have been studied in the last decade. Wei et al. (2006) studied compressive and flexural strength of M-S-H mortars prepared and cured at room temperature. Magnesium content in the binders varied from 60-90%, combined with 10-40% silica fume. The samples were then tested at 3 and 28 days, resulted in the highest compressive strength of 57.4 MPa with the binder composition containing 70% magnesia and 30% silica fume. The authors confirmed that M-S-H binder system had comparable strength compared to traditional Portland cement. In another study, Zhang (2012) proposed a M-S-H binder composition containing 20% MgO, 5% $MgCO_3$, 25% silica fume and 50% quart sand filler (by weight) for immobilization of nuclear waste. The compressive strengths of MgO/SF mortar samples reached over 30 MPa at 7 days, 50 MPa at 14 days, 70 MPa at 28 days and increased to 80 MPa at 90 days. However, apart from those encouraging experimental results, most of other studies reported the poor compressive strengths of materials using magnesium silicate hydrate binder systems.

The microstructure and chemical formula of M-S-H gel have been also investigated without clear confirmation of the chemical formulas of hydration products. The Mg/Si molar ratio varied widely in a range of 0.67-4.0 as reported in the literature. In a well-known study of M-S-H gel formation by Brew and Glasser (2005), mixtures of magnesia and silica fume at Mg/Si molar ratios in a range of 0.5-2.0 were prepared. However, results showed that at room temperature, M-S-H gel with low Mg/Si stoichiometric molar ratios of only 0.6-1.0 were the most likely hydration products. Other authors, Wei et al. (2006) suggested that M-H-S gel with chemical formulas of higher Mg/Si ratios (up to 1.4) were achieved after 28 days, while Roosz et al. (2015) reported Mg/Si ratios at 1.07±0.13 were formed after one year curing at room temperature.

It can be seen that M-S-H binders have potential applications for immobilization of nuclear wastes. In addition, the developing binders can be used for PC replacement in structural concrete and other cementitious materials such as concrete block and building partitions if adequate workability, mechanical and durability properties can be achieved. However, the lack of thorough understanding and the inconsistency of research results on the mechanical properties and microstructure are among the main issues of the developing M-S-H binder systems. This research, therefore, is motivated to understand those problems in order to characterize the various influencing factors and propose novel M-S-H binder systems that are sustainable and viable for structural applications.

1.2. RESEARCH AIM AND OBJECTIVES

1.2.1. Aim

The purpose of this research is to develop magnesium silicate hydrate binder systems using less energy-intensive and recyclable materials for PC replacement to reduce negative environmental impact while maintaining structural performances.

1.2.2. Objective

The research project focuses on challenges or matters limiting the use of M-S-H binder systems, including the following objectives:

1. Microstructure properties

(i) Examine the microstructure of the pastes of M-S-H binder systems by SEM analysis.

(ii) Study the XRD results of the pastes samples (phases and composition) of M-S-H binder systems.

(iii) Measure and evaluate the pH development in the cement pastes of M-S-H binders.

(iv) Express the pore solutions and analyze the ion concentrations of the pore solutions of M-S-H cement pastes.

2. Workability and mechanical properties

(v) Investigate fresh properties of M-S-H pastes and mortars, effect of binder's constituents and superplasticizers on the workability of the pastes and mortars.

(vi) Optimize mix design and proportioning method focusing on the influence of MgO/silica ratio and particle packing density in order to improve strength of M-S-H binder systems.

(vii) Investigate the ternary binder systems of magnesia, silica fume quartz filler

(viii) Evaluate pozzolanic reactivity of different silica sources (silica fume, microsilica, rice husk ash, fly ash) and its effect on fresh and hardened cementitious materials.

(ix) Investigate effect of different curing regimes (hydrothermal conditions and duration) on strength development of produced M-S-H mortars.

(x) Compare mechanical properties of concrete produced with M-S-H binders and PC.

(xi) Study stress-strain behaviors of M-S-H cement pastes made of different silica sources.

3. Durability properties

(xii) Examine porosity, permeability and resistivity of M-S-H concrete in comparison to PC concrete.

1.3. SCOPE OF WORK AND THESIS ORGANIZATION

The research project is divided into 3 phases to achieve the abovementioned aim and objectives.

Phase 1 studies the reaction mechanism and microstructure of the formation of M-S-H binder systems. The strength capacity and workability of the binders are also included.

Phase 2 performs further experiments on the effects of different curing conditions and different material sources for the improvement of the mechanical properties of the M-S-H cement paste and mortar.

Phase 3 focuses on the production of M-S-H structural concrete to characterize mechanical and durability properties of M-S-H concrete.

The thesis presents the experimental work completed and highlights the major findings of the project. Thesis structure is organized in the following chapters:

Chapter 1 introduces the research problem and the motivation of the project, leading to the aim, objectives and outline of the thesis.

Chapter 2 provides a comprehensive review of the literature on the advances and challenges of the cement industry related to developing M-S-H-based binders as alternatives to PC. The research gaps are pointed out and the rationale behind the research aim and objectives of the project is presented.

Chapter 3 describes the primary properties (chemical composition and morphology) of a wide range of materials used in this investigation. This chapter also explains the key methods and techniques used for the experimental program.

Chapter 4 examines the hydration process and microstructure of the M-S-H pastes using different techniques including XRD, SEM-EDS analysis. The reactions mechanism of the formation of the M-S-H binding phases, hydration products, hydration rate, and texture properties are discussed. In addition, the critical influence of the material sources and the binder compositions on the hydration products can be evaluated.

Chapter 5 investigates the pH and ion concentrations of the pore solutions of the M-S-H cement pastes. The extraction apparatus was produced based on similar devices used for PC in the literature. The ICP-MS method was used to measure the concentrations of alkalis, magnesium and silicon to study the hydration process and the formation of the hydration products. The pH of the pore solutions were measured to provide an understanding of the pH development and its effect to the durability of the M-S-H binders.

Chapter 6 addresses the questions on strength capacity and workability of the M-S-H cementitious materials. Different binder compositions were designed and compared for the pastes and mortars to achieve a workable M-S-H mix with a range of strengths. Ground quartz sand is used as filler in ternary systems to improve strength and workability of M-S-H binders.

Chapter 7 presents effects of curing and material sources on short term and long term (365 days) strengths of the mortar samples using M-S-H binder systems. Different hydrothermal conditions were tested with various moistures (dry, sealed, water-cured) and temperatures (20^{o}C, 50^{o}C and

100°C). Effects of reactivity and morphology of the materials on the strengths of the resulting mortar samples are evaluated from the experimental results.

Chapter 8 discusses the potential of M-S-H binders to produce concrete for structural applications. The concrete produced with selected M-S-H binders and local aggregates are tested for compressive strength, split tensile strength and modulus of elasticity. Other experiments on durability properties were performed to understand the permeability, porosity and resistivity of the resulting concrete. Effect of quartz filler on properties of M-S-H binder concrete is also discussed in comparison to control samples using PC.

Chapter 9 details the experimental study on modulus of elasticity and Poisson's ratio of magnesium silicate hydrate (M-S-H) cement pastes in comparison with Portland cement. Mixtures of MgO with various silica sources (silica fume, microsilica, rice husk ash) were prepared with silica content varies between 40-60%, w/c=0.45. The axial and lateral stress-strain behaviors of cement pastes samples at 28 days age are presented.

Chapter 10 summarizes the main conclusions and findings of the research on the development of M-S-H binder systems, including the microstructure and the ion concentrations to characterize the reaction mechanism of the formation of M-S-H binding phases. The strength capacity and the workability of the new binders with different binder compositions and effect of the filler are also concluded. The optimal curing condition for M-S-H binders and the effect of material sources have been suggested to achieve sufficient strengths for the mortars. In addition, mechanical and durability properties of the M-S-H concrete are included for potential use in large scale in structural applications. Finally, this chapter proposes recommendations and directions for future research towards further improvement of the M-S-H binder system as sustainable cement.

1.4. REFERENCES

ACI Committee 232 (1996). Report 232.2R-96 Use of Fly Ash in Concrete. ACI

Aydin S., Baradan B. (2013). Engineering properties of reactive powder concrete without Portland cement. ACI Materials Journal Technical Paper. Nov-Dec 2013, 619-627.

Brew D.R.M., Glasser F.P. (2005) Synthesis and characterisation of magnesium silicate hydrate gels. Cement and Concrete Research 35 (2005) 85– 98

Roosz C., Grangeon S., Blanc P., Montouillout V., Lothenbach B., Henocq P., Giffaut E. (2015) *Crystal structure of magnesium silicate hydrates (M-S-H): The relation with 2:1 Mg–Si phyllosilicates*. Cement and Concrete Research, Volume 73, July 2015, Pages 228–237

Chan W.W.J. , Wu C.M.L. (2000). *Durability of concrete with high cement replacement*. Cement and Concrete Research 30 (2000) 865 - 879

Cole WF. A (1953). *Crystalline hydrated magnesium silicate formed in the breakdown of a concrete sea-wall.* Nat 1953;171:354–5.

Dale Bentz, Jussara Tanesi, Ahmad Adani (2013) Enhancing the Performance of High Volume Fly Ash Concretes Using Fine Limestone Powder. American Concrete Institute, ACI Spring Convention Green Green Cement Sessions (Apri 16, 2013). Available at: https://www.youtube.com/watch?v=vXBpoXLZbhI&index=55&list=PLA28CDF778D6BE0F8.

Du C. J. (2005) A Review of Magnesium Oxide in Concrete - A serendipitous discovery leads to new concrete for dam construction. Concrete international, p45-50

Ecocem. (2015). Strength Development. Ecocem. Available at: http://www.ecocem.ie/technical,strength.htm (Accessed: 10 Aug 2015)

Hall C. (1976). On the history of Portland cement after 150 years, J. Chem. Educ.,53 (4).

Harrison, A. J. W. (2013). Low Carbon Cements and Concretes in Modern Construction. In Proceedings of the UKIERI Concrete Congress–Innovations in Concrete Construction. 5–8 March 2013. Jalandhar (pp. 723-746). Available at: http://www.tececo.com/files/conference%20presentations/JHarrisonLowCarbonCement&Concrete.pdf

Malhotra V.M. and Painter K.E. (1989). Early-Age Strength Properties, and Freezing and Thawing Resistance of Concrete Incorporating High-Volumes of ASTM Class F Fly Ash, the International Journal of Cement Composites and Lightweight Concrete, Vol. 11, No. 2, February 1989.

Mariel V., Carlos A. (2015). Cement, waste and carbon markets-problems related to waste incineration in cement kilns under the EU ETS. European commission. Available at http://www.ec.europa.eu/clima/consultations/docs/0017/.../global_3_en.pdf (Accessed: 5 May 2015).

Mitsuda T. and Taguchi H. (1977) Formation of Magnesium Silicate Hydrate and Its Crystallization to Talc. Cement and concrete research. 7(3), p223-230

Neville A.M. (1981). *Properties of Concrete.* 3rd edn. Longman, Essex, England (1981)

Naik T. R., Singh S. S., Hossain M. M. (1995). Properties of high performance concrete systems incorporating large amounts of high-lime fly ash. Construction and Building Materials, Volume 9, Issue 4, August 1995, Pages 195–204

Tececo Pty. Ltd. (2015). Eco-cement. Tececo Pty. Ltd. Available at: http://www.tececo.com/simple.eco-cement.php (Access: 31 Dec 2015)

Infrastructure Technology Institute (2015). The Science of Concrete. Infrastructure Technology Institute, Northwestern University. Available at: http://iti.northwestern.edu/cement (Accessed: 07 May 2015).

Thomas, M.D.A. (2007). Optimizing the Use of Fly Ash in Concrete. PCA Report IS548, Portland Cement Association.

Trojer, M. (2009). MSc. Thesis - Principles of benchmarking criteria for the European Magnesia Industry. Mining Engineering University of Leoben (Austria).

U.S. Geological Survey (2018). Cement Statistics and Information - Mineral Commodity Summaries. U.S. Geological Survey. Available at: http://minerals.usgs.gov/minerals/pubs/commodity/cement (Access: 28 Dec 2018).

Wei J. X., Chen Y. M., Li Y. X. (2006). *The Reaction Mechanism between MgO and Microsilica at Room Temperature.* Journal of Wuhan University of Technology - Mater. Sci. Ed. 21(2), p88-91

Zhang, T., Cheeseman, C., & Vandeperre, L. J. (2012). Characterisation of corrosion of nuclear metal wastes encapsulated in magnesium silicate hydrate (M-S-H) cement. Ceramic Materials for Energy Applications II, 159-167.

CHAPTER 2
LITERATURE REVIEW

A review of the most state-of-the-art aspects of the development of magnesium silicate hydrate binders, as a potential alternative for the replacement of conventional Portland cement, is presented in this chapter. At the beginning of the chapter the development of high-content magnesium oxide cement that maximizes carbonation in permeable concrete is outlined. Thereafter, an overview is presented for different aspects of the new magnesium silicate hydrate binder system including: reaction mechanism, workability, mechanical properties and microstructure. The mix proportioning methods, theories of packing density, pore solution analysis and curing methods, which have been widely applied to PC concrete, are also mentioned as important factors in the development of magnesium silicate hydrate binder systems.

2.1. MgO-H_2O SYSTEM

2.1.1. Reaction mechanism and hydration products

The development of MgO-H_2O binder benefits from the use of reactivity magnesia which requires low calcining temperature. As opposed to crystalline magnesia, reactive magnesia dissolves rapidly. The hydrated reactive magnesia will form magnesium hydroxide (brucite) at an early age and then the brucite enters further reaction with permeated CO_2 forming nesquehonite for the full strength. The reactions can be described as follows:

$$MgO + 2H_2O \rightarrow Mg(OH)_2.H_2O$$

$$Mg(OH)_2.H_2O + CO_2 + H_2O \rightarrow MgCO_3.3H_2O$$

The formation of brucite from reactive magnesia has been observed with SEM images (Figure 2.1) as reported by Unluer and Al-Tabbaa (2011) in a study of reactive magnesia porous blocks. The mixtures comprised 85% aggregate and 15% binder containing magnesia (4-10%) and pulverized fuel ash (5-11%). The SEM micrographs showed the presence of magnesium carbonation product even at 1 day age. Various magnesium carbonates, along with non-carbonated brucite were found at the end of 28 days curing period.

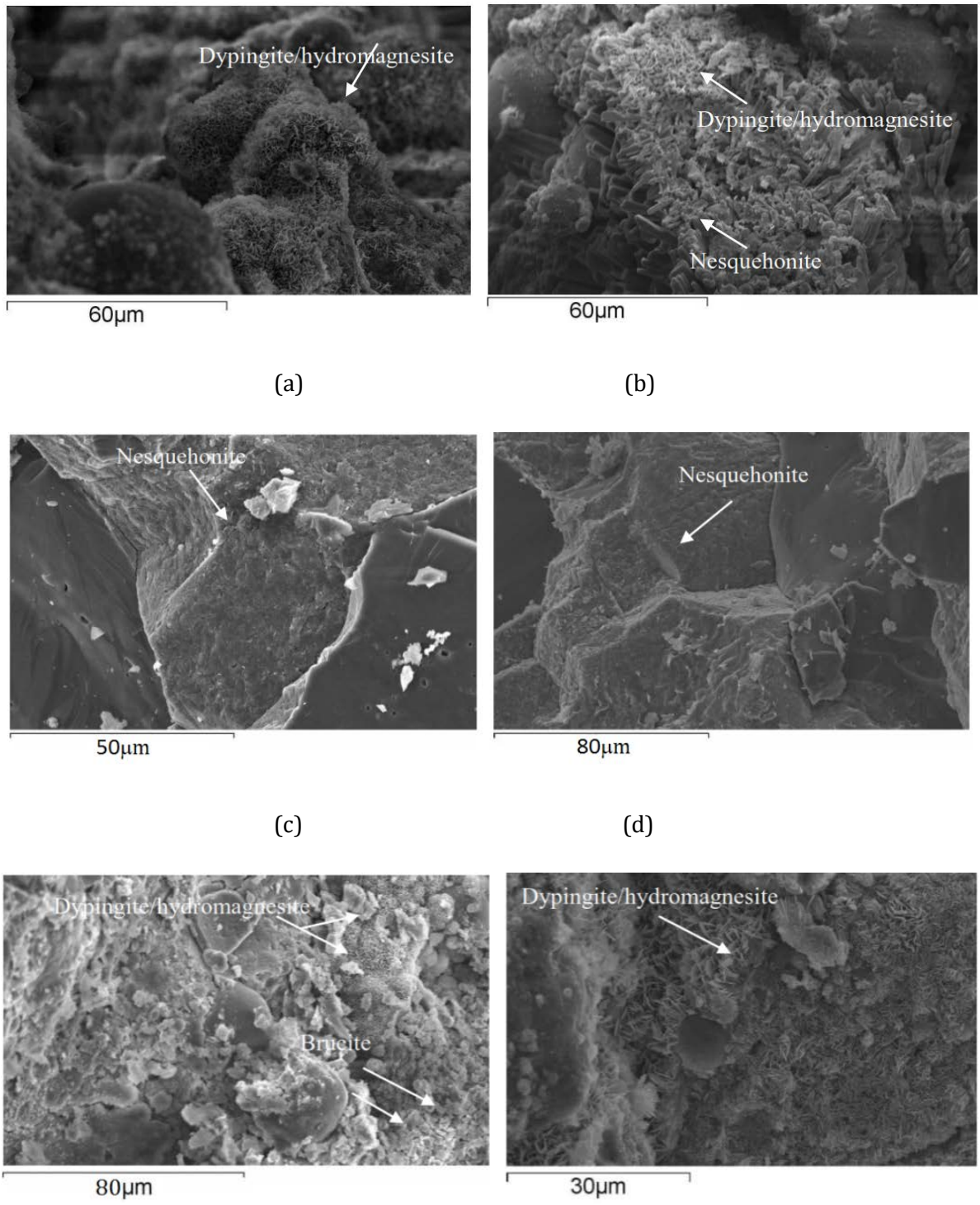

Figure 2.1. SEM micrographs of magnesium hydration and carbonation products

Mix with 10% MgO content w/c=0.8 at 28-day Carbonation (a) and at 1-day carbonation (b);
Mix with 7% MgO content w/c=0.76 28-day carbonation (c) and at 1-day curing (d);
Mix with 4% MgO content w/c=0.68 28day carbonation (e) and at 1-day curing (f)
(Unluer and Al-Tabbaa, 2011)

2.1.2. **Strength and Mix proportion**

The strength of cementitious materials is very much dependent on its binding phases. For MgO-H_2O system, binding phases include only brucite and magnesium carbonates.

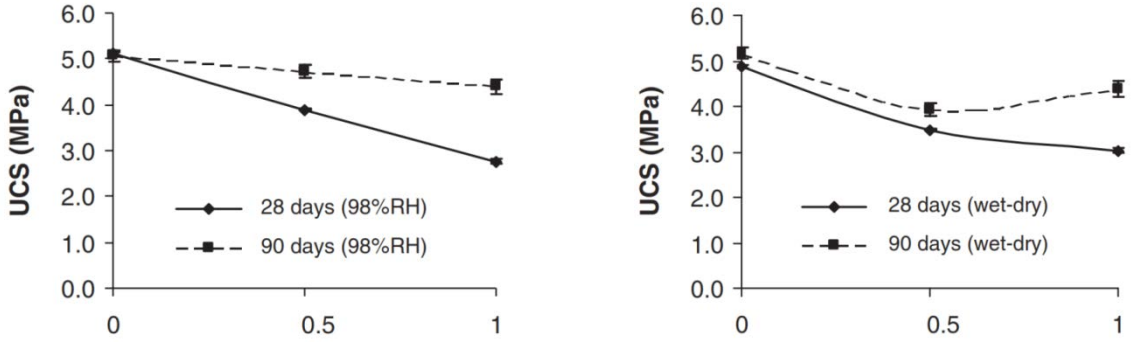

Figure 2.2. Unconfined compressive strength (UCS) of PC/MgO binder porous block, aggregate/binder ratio 9:1 (Vlasopoulos and Cheeseman, 2007)

Vlasopoulos and Cheeseman (2007) replaced PC by MgO-H_2O binders in porous blocks using lightweight aggregate. Three replacement ratios were selected (MgO/PC=0, 0.5, and 1.0). It was clear that increasing PC replacement ratio by MgO reduced compressive strength at 28 days at which MgO-containing samples gained only 60-75% strength compared to PC-containing samples. However, increasing curing times was critical for the strength development of MgO-containing samples, thus, after 90 days the MgO samples achieved similar compressive strengths to those prepared using PC.

In a study by Unluer and Al-Tabbaa (2011), the mixtures of porous blocks including reactive magnesia (4-10%), pulverized fuel ash (PFA) (5-11% and sand (85%) have been tested to examine carbonation rate and the influence of water content on strength. Mixtures containing magnesia (at 4%, 7%, 10%) and PFA (at 11%, 8%, 5%) were mixed with different w/b ratios to achieve standard consistency ±12%.

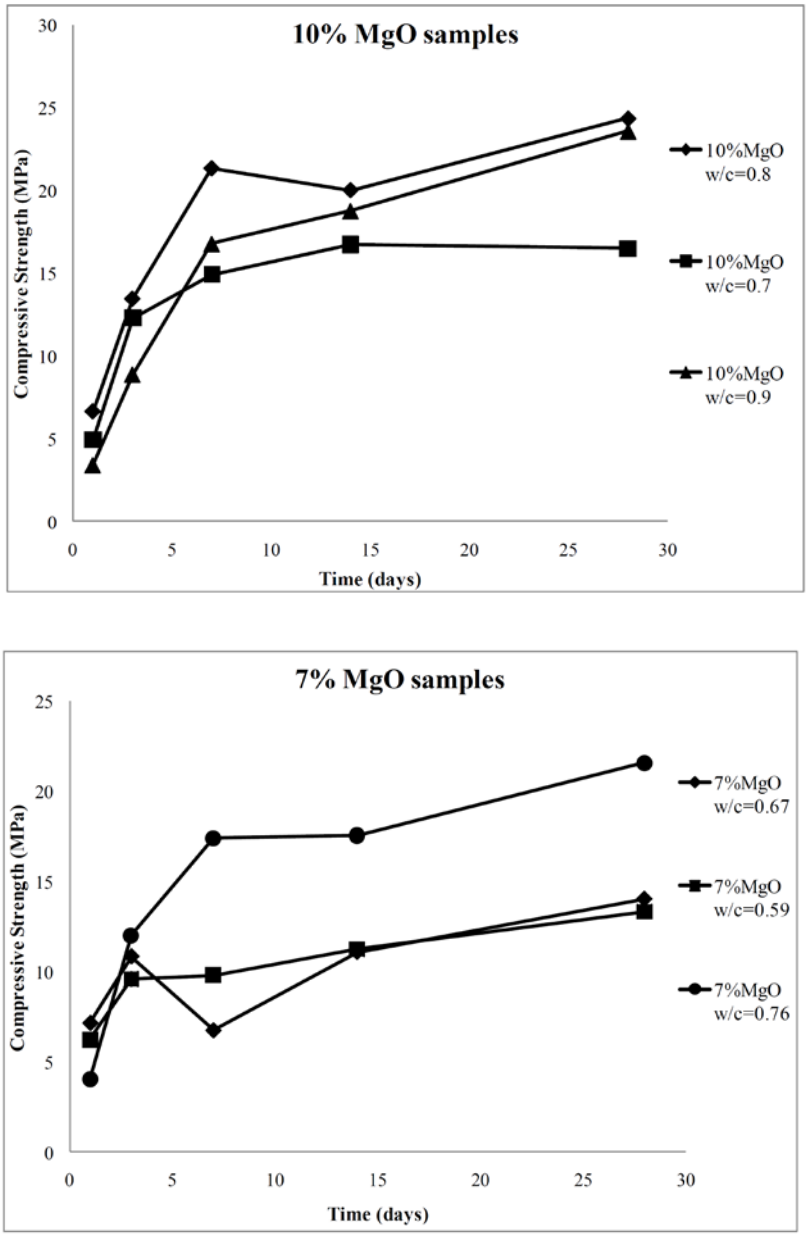

Figure 2.3. Compressive strength of porous block with Magnesia-PFA binder (a): 10% MgO, (b): 7% MgO (Unluer and Al-Tabbaa, 2011)

The testing results for compressive strength at 3, 7, 14 and 28 days showed a direct relationship between density and strength after carbonation. It was explained that higher MgO content resulted in higher $Mg(OH)_2$ and also higher $MgCO_3$ was formed. The influence of water content on strength development was not clear as the lowest w/b did not always result in highest strength. Among samples containing 10% MgO, those with a w/s of 0.8 produced the best compressive strength at 24.4 MPa. It can be seen that the carbonation process requires a high porosity for CO_2 sequestration. Therefore, magnesium oxide binder systems are generally suitable for low strength applications such as porous blocks. Figure 2.4 expresses a high porosity concrete to allow CO_2 penetration for carbonation.

Figure 2.4. Permecocrete - An Example of a monosize and gap graded Eco-Cement Concrete (TecEco, 2015)

2.2. MAGNESIUM SILICATE HYDRATE BINDER SYSTEM (MgO-SiO_2-H_2O)

The discovery of magnesium silicate hydrate phases in cement and concrete has been reported since 1950s by Cole (1953), however, there has been an increase in interest in the formation mechanism of magnesium silicate hydrate (M-S-H) as a binder for construction industry in the last decades. The idea of combining reactive magnesia and silica for cementitious materials was proposed recently by Wei et al. (2006) as an alternative for Portland cement with its potential benefits from an environmental perspective.

2.2.1. Formation of magnesium silicate hydrate - reaction mechanism

Hydration of magnesia (MgO)

It has been demonstrated that reactive MgO - which is essentially amorphous and different in nature from crystalline magnesia - dissolves in water to form brucite ($Mg(OH)_2$). The hydration occurs at an early age and nearly complete in 3 days (Wei, 2006; TecEco, 2015; Fang, 2004).

As studied by Silva (2011), hydration of MgO in water occurs in stages. The first process is controlled by proton attack onto the surface of magnesia:

$$MgO_{surface} + H^+ \rightarrow MgO \cdot H^+_{surface} \rightarrow Mg^{2+} + OH^-_{solution}$$

As the concentration of Mg^{2+} in solution increases, the dissolution of hydroxyl and cation begins and control the reaction:

$$MgOH^{+}_{surface} + OH^{-}_{solution} \rightarrow MgOH^{+} \cdot OH^{-}_{solution} \rightarrow Mg^{2+} + 2OH^{-}_{solution}$$

The reaction proceeds and achieves super-saturation, followed by precipitation of $Mg(OH)_2$ on the MgO surface and slow the reaction rate. The reaction path for the hydration of magnesium in water is describes as:

$$MgO + H_2O \rightarrow Mg^{2+} + 2OH^{-}_{solution} \longleftrightarrow Mg(OH)_2$$

Hydration of silica (SiO_2)

In the presence of reactive siliceous powder in high pH solution, reactions between MgO and silica to form M-S-H gel have been reported. The first stage is the dissolution of reactive silica in water to form silicic acid (Rimstidt and Barnes, 1980). The reaction rate is dependent on the reactivity of the reactants as well as the hydrothermal conditions, following the equation:

$$SiO_{2(s)} + 2H_2O_{(l)} \longleftrightarrow H_4SiO_{4(aq)}$$

The equation consists of two opposing reactions at equal rates when the system is at equilibrium, as described below:

$$SiO_2 + 2H_2O \rightarrow SiO_2 \cdot 2H_2O \rightarrow H_4SiO_4$$

$$H_4SiO_4 \rightarrow SiO_2 \cdot 2H_2O \rightarrow SiO_2 + 2H_2O$$

Formation of magnesium silicate hydrate gels

With the availability of both magnesia and silica in the solution, the formation of magnesium silicate hydrate was observed (Mitsuda and Taguchi, 1977; Brew, 2005; Zhang, 2014; Li et al., 2014). At room temperature, Li et al. (2014) proposed some potential reaction equations based on a thermodynamic analysis in which M-S-H gel has the crystalline structure of talc ($Mg_3(Si_4O_{10})(OH)_2$) or serpentine ($Mg_3(Si_2O_5)(OH)_4$), described by the following equations:

$$3Mg^{2+} + 6OH^{-} + 4SiO_2 \rightarrow Mg_3Si_4O_{10}(OH)_2 + 2H_2O$$

$$3Mg^{2+} + 6OH^{-} + 2SiO_2 \rightarrow Mg_3Si_2O_5(OH)_4 + H_2O$$

Such reaction mechanisms of M-S-H formation can be explained by the presence of anions and cations of brucite and silicic acid in the solution, as follows:

Chemical reactions for the formation of serpentine:

$$3Mg(OH)_2 \rightarrow 3Mg^{2+} + 6OH^-$$

$$2SiO_2 + 4H_2O \rightarrow 2SiO_4^{4-} + 8H^+$$

$$3Mg^{2+} + 6OH^- + 2SiO_4^{4-} + 8H^+ \rightarrow Mg_3Si_2O_5(OH)_4 + 5H_2O$$

$$3Mg(OH)_2 + 2SiO_2 \leftrightarrow Mg_3Si_2O_5(OH)_4 + H_2O$$

Chemical reactions for the formation of talc:

$$3Mg(OH)_2 \rightarrow 3Mg^{2+} + 6OH^-$$

$$4SiO_2 + 8H_2O \rightarrow 4SiO_4^{4-} + 16H^+$$

$$3Mg^{2+} + 6OH^- + 4SiO_4^{4-} + 16H^+ \rightarrow Mg_3Si_4O_{10}(OH)_2 + 10H_2O$$

$$3Mg(OH)_2 + 4SiO_2 \leftrightarrow Mg_3Si_2O_5(OH)_4 + 2H_2O$$

In a recent study, Zhang et al. (2014) confirmed the formation of M-S-H gel and $Mg(OH)_2$ as hydration products of $MgO\text{-}SiO_2\text{-}H_2O$ system. Also, the result has shown that if mixture containing 60 wt.% SF and 40 wt.% MgO (molar ratio of Mg/Si=1.0), all the brucite reacts with silica fume and converts into M-S-H gel on condition that sufficient water is supplied (w/s=0.8). The M-S-H gel chemical formula was calculated as $M_8Si_8O_{20}(OH)_8.12H_2O$ based on the weight loss assumptions and TGA data at 285 days, as shown in the equation:

$$8MgO + 8SiO2 + 16H_2O \rightarrow M_8Si_8O_{20}(OH)_8.12H_2O$$

The reaction of brucite and silica to form magnesium silicate hydrate, thus, can be written in general form below in which M-S-H gel was reported as a secondary hydration product, formed by the reaction of brucite (the hydration product of magnesium in water) with silica.

$$xMg^{2+}\ 2x(OH)^- + ySiO_2 \rightarrow xMgO.ySiO_2.zH_2O$$

2.2.2. **Microstructures of magnesia silicate hydrate**

The formation of M-S-H gel in natural and synthesized phases exhibits a wide range of Mg/Si molar ratios. M-S-H was firstly reported to occur in cement mortars decomposed by sulfate attack of sea water with the chemical composition of $4MgO.SiO_2.8.5H_2O$ (Cole,1953). Bonen and Cohen (1992) simulated the sulfate attack of blended PC, contain MgO, in magnesium sulfate and suggested another formula of lower Mg/Si ratio ($2MgO.SiO_2.H_2O$). In an experiment on sulfate attack to form

M-S-H gel, Gollop and Taylor (1996) calculated Mg/Si molar ratio to be 1.37 and close to serpentine $C_3S_2H_2$. Mitsuda and Taguchi (1977) found that synthesized M-S-H gel has crystallized structure with Mg/Si =0.75 ratio and similar to talc microstructure ($Mg_3(Si_4O_{10})(OH)_2$). After long-term curing of magnesia and siliceous gels at room temperature for up to 7 years, Mitsuda and Taguchi (1977) concluded that magnesium silicate hydrates are disordered intermediate phases and most likely to formation of talc (Mg/Si=0.75), chrysotile (Mg/Si=1.5), or deweylite-like materials at Mg/Si ratios between the two minerals (Figure 2.5). Similar results of the M-S-H gel formation with Mg/Si ratios of 0.7-1.5 were reported by Lothenbach et al. (2015). For mixtures of magnesia and silica having a low Mg/Si ratio = 0.5, the M-S-H gel formed also have Mg/Si=0.5 with microstructures similar to clay minerals such as crystalline sepiolite and smectite (The Mineral Society, 1991).

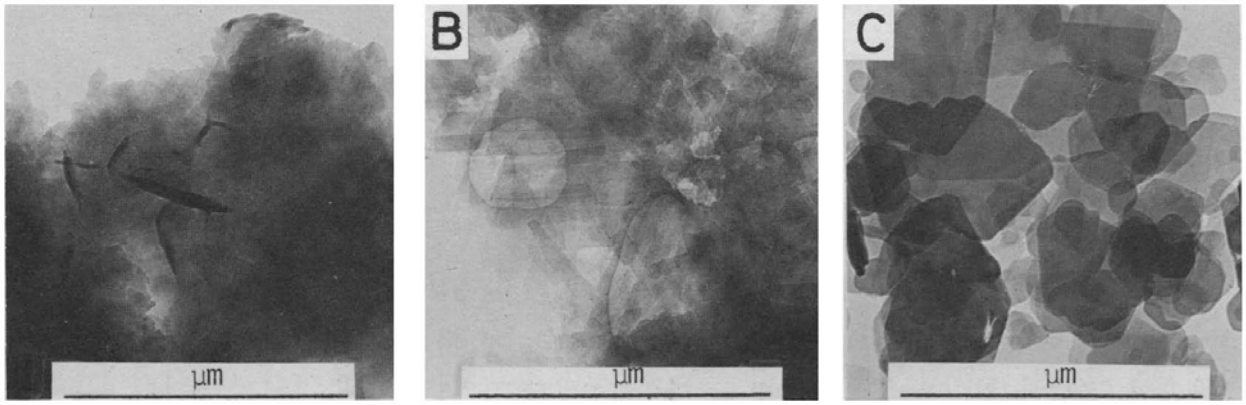

Figure 2.5. Electron images of M-S-H: (A) Poorly Crystalline Magnesium Silicate Hydrate,(B) Poorly Crystalline Talc, and (C) Highly Crystalline Talc. (Mitsuda and Taguchi, 1977)

In a study by Brew and Glasser (2005), two forms of M-S-H gel were synthesized and characterized for comparison. One form of M-S-H gel precipitated in reactions between sodium metasilicate ($Na_2SiO3.5H_2O$) and magnesium nitrate (Mg(NO3)2.6H2O. Other forms of M-S-H gel are products from exposure of Portland cement containing low initial magnesia in $MgSO_4$ solution. All M-S-H gel were cured in short and long period (24 hours and 6 months) to characterize Mg/Si molar ratios and crystallinity. The author discussed that the chemical and mineralogical nature of the magnesium phase is a function of silica reactivity. In mixtures with low reactive silica, brucite ($Mg(OH)_2$) is the favoured final product while in mixtures of highly reactive silica, brucite may be completely reacted to result in M-S-H gel. Brew and Glasser (2005) also suggested a narrow band of M-S-H gel composition. At low target ratios of Mg/Si = 0.5-0.75, the actual obtained Mg/Si ratio was in a range of 0.66-0.82. While in an increased target ratio of Mg/Si from 1.0-2.0, the actual Mg/Si ratio obtained increased to 0.86-0.96. The M-S-H phases have poor crystallinity close to known M-S-H minerals: sepiolite: $Mg_4(Si_2O_5)_3(OH)_2.4H_2O$ (Mg/Si = 0.67); talc: $Mg_3(Si_2O_5)_2(OH)_2$ (Mg/ Si = 0.75) and serpentine: $Mg_2(Si_2O_5)(OH)_4$ (Mg/Si = 1.0).

Wei (2006) has performed an analysis on the composition of M-S-H gel in high MgO/SiO_2 ratios at room temperature. A wide range of hydrated magnesium silicates were obtained with Mg/Si molar ratios varying from 0.82 to 1.83 with a mean value of 1.40.

Recently, Li et al. (2014) tested the formation of M-S-H gel at room temperature in which MgO/SF pastes with different Mg/Si ratios from 0.67-4.0 were prepared with a water content of 5.0. The mixtures were cured for 1 year to ensure all the reactions were completed. Figure 2.6 shows the XRD patterns of the mixtures where there was no residual brucite in mixtures of Mg/Si molar ratios of 0.67 and 1.0. As Mg/Si was of 1.5 or higher, the hydration products included both M-S-H gel and residual brucite. The chemical compositions (Mg/Si ratios) of hydration products are dependent on the Mg/Si ratios of the reactants. Lothenbach et al. (2015) by XRD analysis suggested that for 0.8<Mg/Si<1.0 the M-S-H structure is related to talc ($3MgO.4SiO_2.H_2O$) while at higher Mg/Si ratio M-S-H was reported to correspond to serpentine ($3MgO.2SiO_2.2H_2O$).

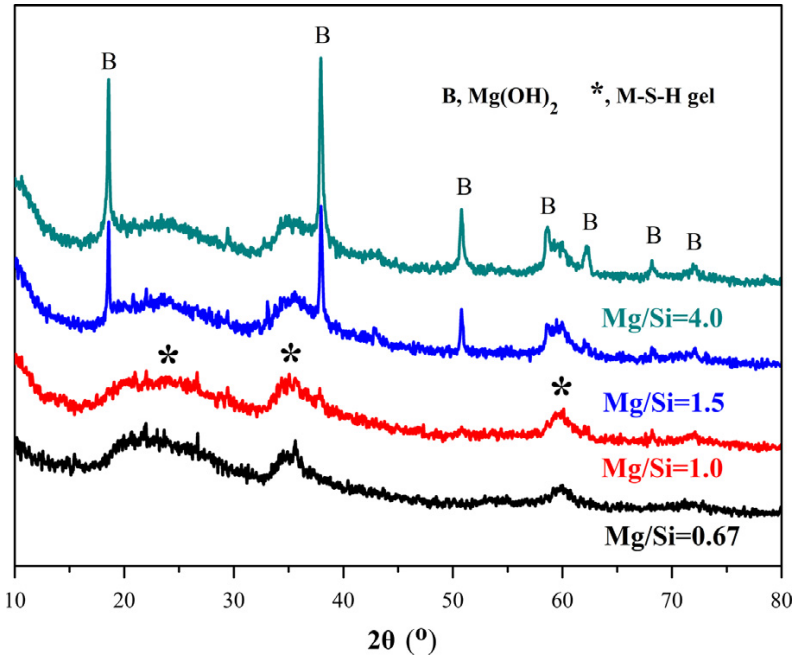

Figure 2.6. XRD patterns of the fully hydrated MgO/SF pastes with different Mg/Si ratios. (Li et al., 2014)

In terms of hydrothermal treatment effect on the microstructure of M-S-H hydration product, previous studies have shown that the increased temperature and curing period shows improvement in crystallinity and local ordering of M-S-H gel structures. Mitsuda and Taguchi (1977) investigated hydration of $Mg(OH)_2$ and colloidal silica at 180 °C to 600°C in the period from 4 h to 8 weeks. The results confirmed that the M-S-H gel had a poor crystalline structure and the crystallization was proportional with temperature and curing time. The weak interlayer binding force was attributed as the cause of disordered layer silicates. Brew and Glasser (2005) also

observed the improvement of crystallinity and local order of M-S-H gel synthesized and cured for 6 months at 85°C, compared to control sample cured at 25°C in 24 hours.

It is seen that considerable divergence of M-S-H compositions exists in the literature. One influencing factor is the reactivity and purity of light burn MgO that varies considerably dependent on the material sources. The other factors of Mg/Si mixing ratio and hydrothermal treatment play important role in the composition of M-S-H gel phase and crystallinity. At room temperature, it is noted that the most likely synthesized M-S-H gel has Mg/Si molar ratio of 0.67-1.5, close to talc and serpentine or in between.

2.2.3. Mix proportion and mechanical properties

The formation of magnesium silicate hydrate gel in paste was mainly observed during sulfate attack of concrete (Cole, 1953; Bonen, 1992; Gollop, 1992) with limited or detrimental cementing properties (Zhang, 2014). For this reason, it is not surprised that there was no research on magnesia silicate hydrate as potential construction materials (Jin and Al-Tabbaa, 2014).

The first M-S-H-based material with compressive strength of over 50 MPa was reported in a study by Wei et al. (2006). The mortar mixes contained 60%-90% reactive MgO and 40%-10% silica fume were prepared with w/b=0.5 and cured at room temperature. The compressive and flexural strengths of samples are listed in table 2.1.

Table 2.1. Mix proportions and strengths of MgO-SiO_2-H_2O mixtures (Wei et al., 2006)

MgO	MS	Additive	Water/cm (MgO+MS)	Flexural strength		Compressive strength	
				3 days	28 days	3 days	28 days
90	10	2%	0.5	3.12	5.56	17.6	45.2
80	20	2%	0.5	4.38	8.35	24.3	56.4
70	30	2%	0.5	4.64	9.95	20.6	57.4
60	40	2%	0.5	4.02	7.05	16.4	53.2

Testing results indicated that the M-S-H system had cementing properties and the strengths were dependent on the mix proportions. The lowest 28-day compressive strength was 45.2 MPa obtained with the mixture containing the least SiO_2 content (10%). A decrease in MgO content to 70% accompanied by an increase of SiO_2 to 30% led to an increase of 28-day compressive strength to the highest value of 57.4 MPa. It is explained that SiO_2 reacts with $Mg(OH)_2$ to form M-S-H gel - the hydration product that gains strength better than $Mg(OH)_2$.

In comparison to Portland cement system for nuclear waste immobilization, Zhang et al. (2012) proposed a magnesia silicate cement system consists of 50% MgO/SF blend and 50% quartz sand added as inert fillers. The binder composition included 20 wt.% MgO, 5 wt.% $MgCO_3$ (to achieve low pH), 25 wt.% SF, 25 wt.% coarse quartz sand (176μm mean particle sizes) and 25% wt.% milled quartz sand (51μm mean particle sizes). The w/b=0.55 and 1% inorganic superplasticizer sodium hexametaphosphate (NaHMP) was used for workability.

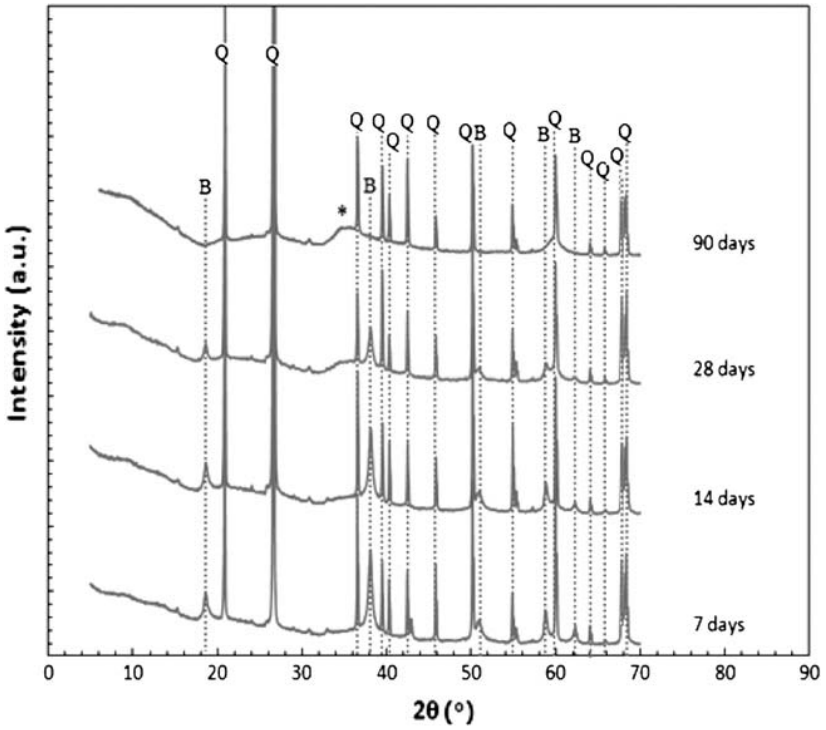

*Figure 2.7. XRD patterns of MgO/SF samples over 90 days. (B: brucite ($Mg(OH)_2$);Q: quartz (SiO_2); *: magnesium-silicate-hydrate (M-S-H) gel)(Zhang et al., 2012).*

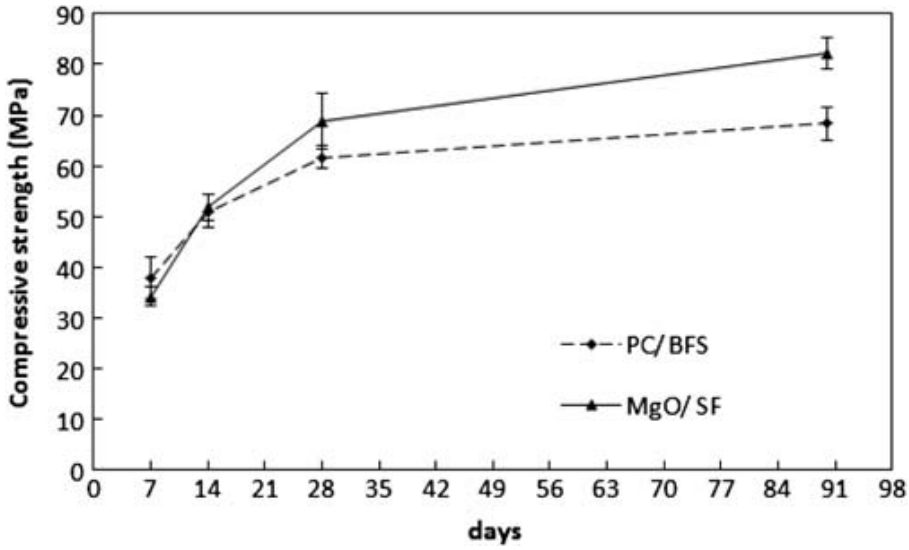

Figure 2.8. Compressive strengths of PC/BFS and MgO/SF samples over 90 days (Zhang et al., 2012).

The compressive strengths of MgO-SF mortar samples reached over 30 MPa at 7 days, 68 MPa at 28 days and 80 MPa at 90 days. Except for a lower compressive strength at the early age of 7 days, the compressive strength of MgO/SF cement system afterwards increased higher than control sample containing 25 wt.% PC and 75 wt.% blast furnace slag (BFS) mixtures (w/s=0.35). The XRD analysis also indicated that most of MgO reacted with SF to form M-S-H gel at 90 days age as no peaks of brucite was observed with XRD pattern at this age.

Compressive strengths of M-S-H pastes were also reported by Zhang et al. (2014), using mixtures of MgO and SiO_2 at molar ratio of 1.0 (40% MgO - 60% SF by mass).

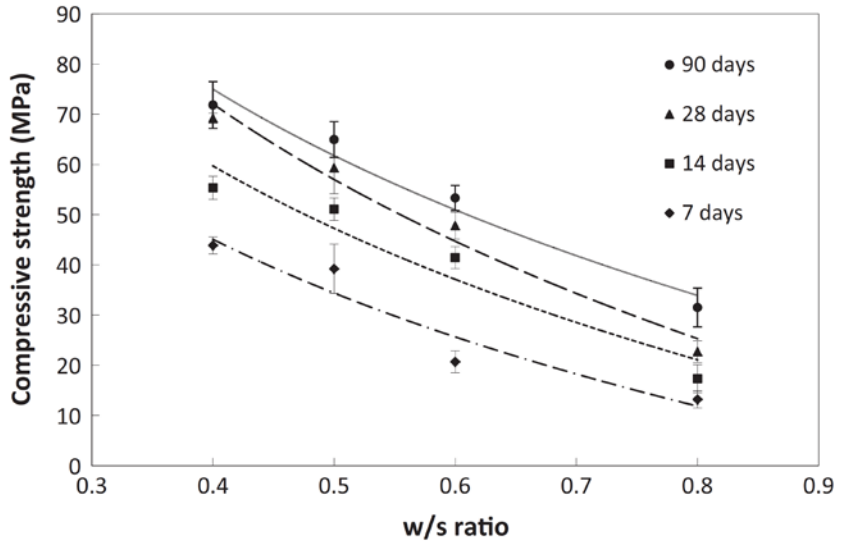

Figure 2.9. Compressive strength of 40% MgO+60% SF samples with 1% NaHMP at different w/s ratios over 90 days (Zhang et al (2014).

The compressive strength was highly dependent on water content and curing period. The highest compressive strength achieved with lowest w/s=0.4 at 7, 28 and 90 days were about 45 MPa, 68 MPa and 72 MPa. The XRD, TGA test result indicated the main hydration product of the 40% MgO + 60% SF system was M-S-H gel for all selected w/s ratios.

Jin and Al-Tabbaa (2014) performed experiments with different commercial magnesium and siliceous materials to evaluate reactivity by measuring hydration rates. Magnesia-silicate-water mixtures with silica contents of 15%, 30% and 50% were prepared and cured at ambient temperature. Due to the fineness of MgO and SF, the binder required high w/b from 0.59 to 0.87 to achieve standard consistency and consequently obtained very low strength. The maximum compressive strength of M1 series (less reactive magnesia) over 90 days was only 15 MPa while the Figure of M2 series (high reactive magnesia) was higher at 17 MPa (Figure 2.10).

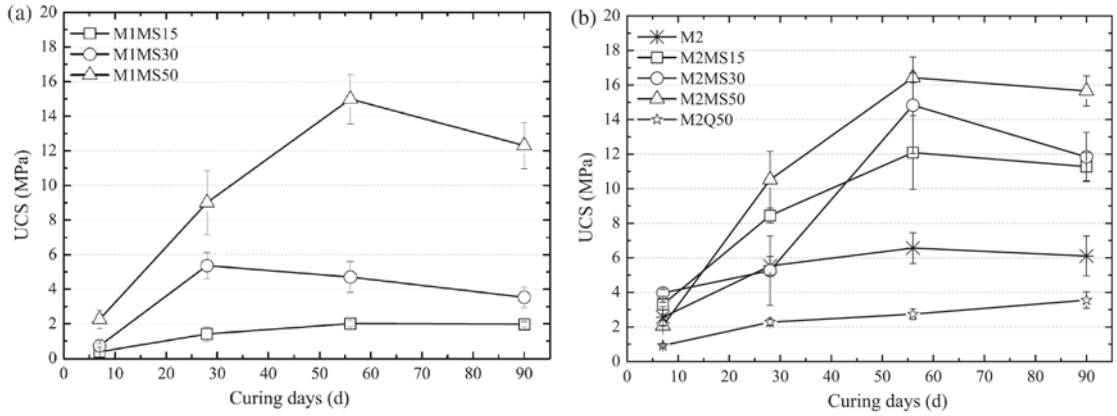

Figure 2.10. Compressive strength of MgO-MS mixtures (Jin and Al-Tabbaa, 2014)

The compressive strength is also proportional to the increase in silica fume content from 0-50%. This is inconsistent with the previous study by Wei (2006) reported that the maximum compressive strength obtained with a mix containing 30% of silica fume. Surprisingly, the compressive strength only increased with water curing up to 56 days and reduced with longer curing in water up to 90 days. Jin and Al-Tabbaa (2014) proposed that the reaction between MgO and silica was completed within 2 months and further curing in water resulted in the dissolution of the hydration products and consequently reduced the paste's strength.

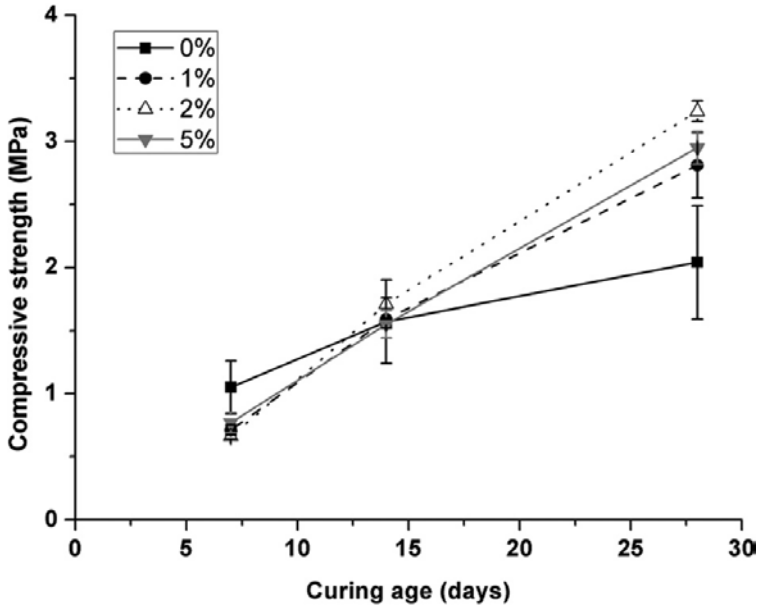

Figure 2.11. Compressive strengths of 1:1 $Mg(OH)_2$: SiO_2 pastes, w/b = 1.0, with 0–5 wt% $(NaPO_3)_6$. (Walling et al., 2015)

Walling et al. (2015) blended slurry $Mg(OH)_2$ with silica fume at mix proportion of 1:1 to produce a cementitious system for immobilization of Magnox sludge. Despite the addition of $(NaPO_3)_6$ as an inorganic dispersant, the high water demand required for workability was reported the biggest

challenge of the $Mg(OH)_2$-SiO_2-H_2O system to achieve high strength. As a result, the compressive strength of all samples mixed with high w/b ratio of 1.0 was only 1 MPa at 7 days and increased to over 3 MPa at 28 days.

The compressive strengths of M-S-H pastes and mortars from previous studies are summarized in Table 2.2. It is shown that there have been limited publications on strengths of magnesium silicate hydrate binder systems with somewhat contradictory results. The binder compositions (MgO/SiO_2 ratio) and different material sources were among the key factors of the wide variation of compressive strengths. The strength of magnesium oxide binder system without silica, based on carbonation of brucite as the only hydration product was generally lower than equivalent Portland cement binders. On the other hand, the presence of both reactive silica and magnesia led to the formation of M-S-H gel with higher cementitious properties in which 28-day compressive strength could reach 70 MPa. Among reported publications, only a few studies (Wei et al., 2006; Zhang, 2012, 2014) showed equivalent strength results to Portland cement. The optimal M-S-H binder composition for strength was not clear and there was no prescribed method of mixture design in presence of aggregates.

Table 2.2. Compressive strengths of M-S-H paste and mortar in previous studies

Reference	Binder		Quartz Sand (% of binder by weight)	w/b	Super-plasticizer (% of binder by weight)	Curing	Compressive strength (MPa)					
	Magnesium content (% of binder)	Silica fume (% of binder)					3 days	7 days	14 days	28 days	56 days	90 days
Wei et al. (2006)	90	10	-	0.50	2%	Water cured at 20°C	18.0	-	-	**45**	-	-
	80	20	-	0.50	2%		24.0	-	-	**56**	-	-
	70	30	-	0.50	2%		21.0	-	-	**57**	-	-
	60	40	-	0.50	2%		16.0	-	-	**53**	-	-
Zhang et al. (2012)	40% MgO +10% $MgCO_3$	50	100	0.55*	1 % (NaHMP)	Moist cured (RH95%) at 22°C	-	33	51	**68**	-	80
Zhang et al. (2014)	40	60	0	0.40	1 % (NaHMP)	Wet cured	-	43	55	**68**	-	**72**
	40	60	0	0.50	1 % (NaHMP)		-	40	50	**60**	-	65
	40	60	0	0.60	1 % (NaHMP)		-	20	43	**48**	-	55
	40	60	0	0.80	1 % (NaHMP)		-	13	18	**22**	-	32
Jin and Al-Tabbaa (2014)	100	0	-	0.87	-	Water cured	-	3	-	**5**	7	6
	85	15	-	0.87	-		-	3.5	-	**8.5**	12	11
	70	30	-	0.87	-		-	4	-	**5**	15	12
	50	50	-	0.87	-		-	2	-	**11**	17	15.5
Walling et al. (2015)	50% $Mg(OH)_2$	50	-	1.0	0%	Moist cured (RH95%) at 40°C	-	<1	-	**2**	-	-
	50% $Mg(OH)_2$	50	-	1.0	1%		-	<1	-	**2.8**	-	-
	50% $Mg(OH)_2$	50	-	1.0	2%		-	<1	-	**3.3**	-	-
	50% $Mg(OH)_2$	50	-	1.0	5%		-	<1	-	**2.9**	-	-

**: w/s =0.275 (solid content: MgO, SF, quartz sand as inert filler)*

2.3. WORKABILITY

Workability is defined in ACI 116R "Cement and Concrete Terminology" as "that property of freshly mixed concrete which determines the ease and homogeneity with which it can be mixed, placed, compacted, and finished."

As green building materials generally require a reduction in cement content and increase use of industrial by-products and/or recycling resources as supplementary cementitious materials, there is a question whether an M-S-H binder for sustainable concrete can be achieved with the same workability as PC mixture. Dale et al (2013) have mentioned several disadvantages in workability and constructability with cement incorporating industrial by-products and/or recycling resources such as improper hydration, delayed setting times, reduced early-age strength and increased sensitivity to curing conditions.

2.3.1. Water demand of silica fume and M-S-H-based cementitious materials

It is well known that water to binder ratio has a considerable influence on strength of concrete due to excess water resulting in high porosity which weakens the material. Effect of water content to the strength of M-S-H binder system are even more important than PC as M-S-H binder system contains a very high content of siliceous materials.

Water demand of silica fume concrete with Portland cement has been studied extensively in the literature. ACI 363R-92 (1992) suggests that the high silica fume content used in high strength PC concrete results in significant change in water demand. Due to this limitation, the maximum PC replacement ratio by silica fume is normally limited at 25% (ACI 211.1,1991) and in practice typically around 10%.

Rao (2003) examined the influence of high silica fume volume on the consistency of cement pastes and mortars. Silica fume replaced cement up to 30% at a constant increment of 2.5%-5% by weight of cement. The test result showed that the consistency (percentage of water to achieve standard consistency) of the paste increased proportionally with the increase of silica fume content. The standard consistency of pure cement paste was only 31.5% whereas that value increased to 40% at 20% SF content. An additional water requirement of as much as 44.25% was observed for the paste containing 30% SF. The reason for the increase in water demand was due to the fineness and low specific gravity of SF resulted in increased specific surface and binder volume of the high SF content mixture.

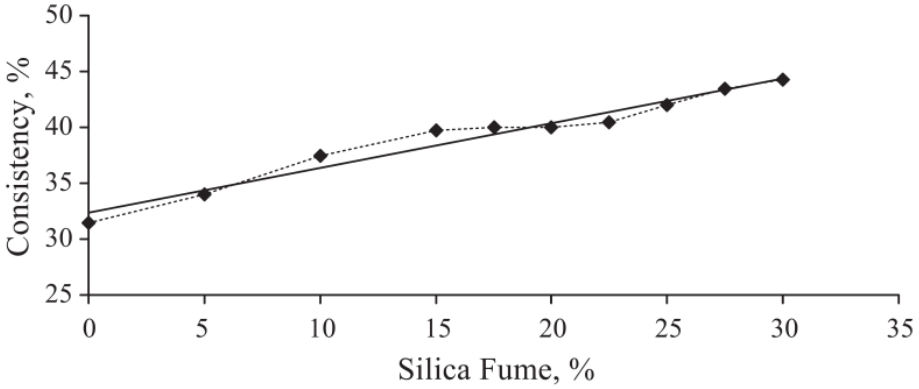

Figure 2.12. Variation of consistency of cement paste containing different percentages of silica fume (Rao, 2003)

The workability measured by % flow of high silica content PC mortar is reported in Figure 2.13. The replacement of PC with silica fume up to 15% did not affect the flow. As silica fume content exceeded 15%, the flow reduced due to the increase of water demand effect. However, the effect of silica fume content to workability was not clear, possibly due to the selection of high w/b ratios of 0.45 and 0.50.

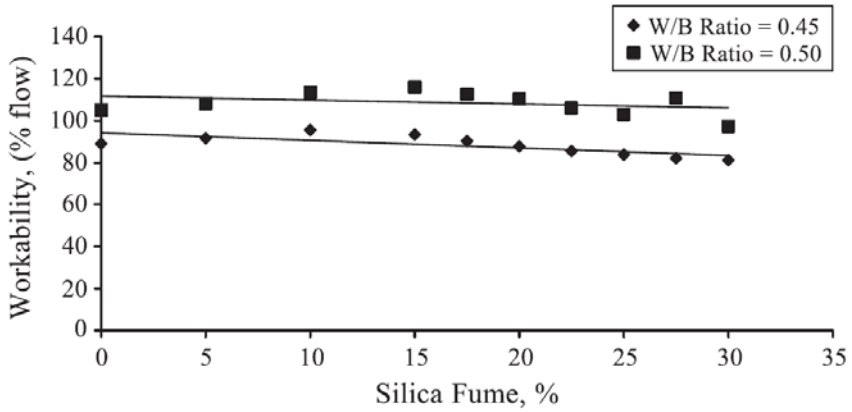

Figure 2.13. Variation of workability (% Flow) of cement mortars with different silica fume contents (Rao, 2003)

There have been few publications on water demand of magnesium silicate hydrate binder system in which the common argument is that the extremely high water demand is due to the very high content of silica fume. Fine, light burned magnesia also tends to have a high water demand. Coarser MgO powders calcining at higher temperatures requires lower water demand but cause damage due to expansion during the late hydration (Vandeperre, 2007) and are not usually used for magnesium silicate hydrate binder system.

Zhang et al. (2010) conducted flow tests of M-S-H binder to compare with Portland cement. To achieve flow diameter of 185 mm, the control sample of 100% PC required w/c as low as 0.33 while the mixture of 50% MgO + 50% SF required a w/b=1.3 for a flow of 183 mm. An extremely

high w/b=1.6 was observed with a mixture of 20% MgO + 80% SF to obtain similar flow to PC (Table 2.3).

Table 2.3. Consistency by flow table of PC and MgO+SF binder (Zhang et al., 2010)

Sample description	Value (mm)	Water/ Solid ratio
100PC	185	0.33
75BFS/25PC	184	0.35
50MgO/50SF	183	1.3
20MgO/80SF	185	1.6

Jin and Al-Tabbaa (2014) tested the standard consistency of M-S-H binder and each individual constituent of the binder system. Reactive magnesia (MgO) had water demand for standard consistency of 0.48 and 0.52 while microsilica required much higher at 1.2. A binder of 50% MgO + 50% microsilica required w/b=0.87 to achieve standard consistency.

2.3.2. Setting time

Due to the high water demand, M-S-H binder is known to have longer setting times compared to Portland cement. In the study by Zhang et al. (2010), the final setting time of M-S-H mixes in Table 2.3 last very long. The 50 wt.% MgO + 50 wt.% SF mix final setting time was 48h and the final setting time of 20 wt.% MgO + 80 wt.% SF mix was up to 72 hours whereas the PC and blended PC mixes had final setting times of only 4.5 and 5 hours (Figure 2.14).

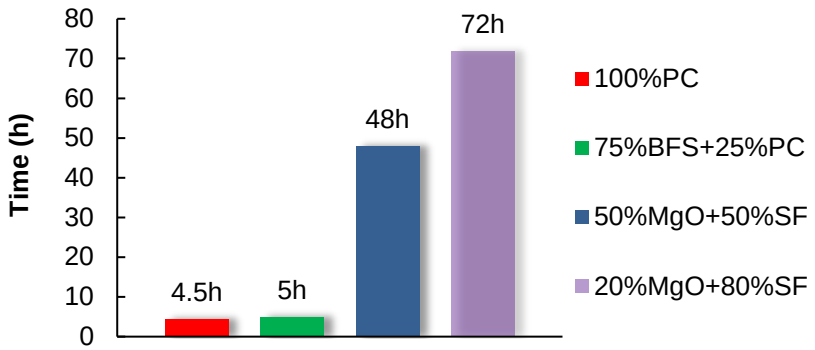

Figure 2.14. Comparison of setting time of PC and MgO+SF binder (Zhang et al., 2010)

The disadvantage of high silica fume content to workability of PC was also reported (Rao, 2003). Low percentages of SF did not affect the setting times considerably. However, at higher SF contents, the initial setting time significantly decreased. Testing results in Figure 2.15 described that initial setting time was only 30 min as SF presented at 30%. Thus, the negative effect of high SF content to the workability of both PC and M-S-H binder system poses a real challenge for the development of M-S-H binder system to achieve low water content mixtures with reasonable workability and high strength cementitious materials.

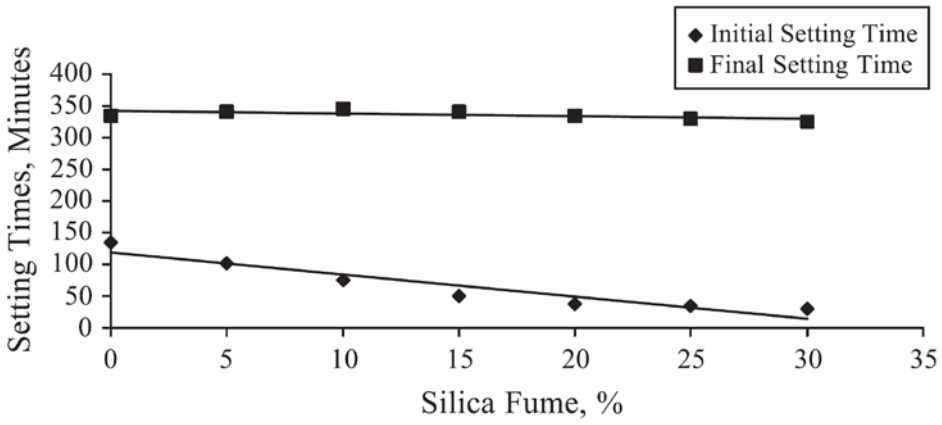

Figure 2.15. Variation of setting times of cement pastes with different percentages of SF addition (Rao, 2003).

2.3.3. **Use of dispersant additives and superplasticizers**

It was shown in previous studies that the M-S-H binder system has an extremely high water demand. The high w/b ratio consequently results in low compressive strength, and without measures to reduce water demand, it is a very big challenge to produce normal or high strength M-S-H cementitious materials.

The water reducing effect of additives has been well studied in the published literature. For Portland cement silica fume concrete, ACI 211.1 (1991) recommends that silica fume should always be used with a water-reducing admixture, preferably high-range water reducers (HRWR) to maximize the full strength-producing potential in concrete. The reason for use of HRWR is to assist in achieving uniform dispersion. The dosage of the HRWR will depend on the percentages of silica fume and the type of HRWR used. There is also a need to mix adequately with higher mixing time compared to mixtures without silica fume additive.

Table 2.4. Castable composition wt.% (Myhre et al., 1997)

Castable components:	Spinel	Forsterite	Magnesite
Magnesite: -100 micron	35	35	35
Microsilica 983U	8	8	8
Calcined alumina: BACO MA95D2	5	5	5
Spinel AR78: 01-3mm	28		
Spinel AR78: 0.5-1mm	12		
Spinel AR78: 0-0.5mm	12		
Olivine 1-5mm		20	
Olivine AFS20		20	
Olivine AFS30		12	
Magnesite: 1-4mm			28
Magnesite: 0.5-1mm			19
Magnesite: <0.5mm			5
Vanisperse CB (deflocculant)	0.25	0.25	0.25
Water (13 vol%)	4.57	4.65	4.5

The use of dispersant for M-S-H bonding system has been reported since 1989 in studies of MgO-SiO_2 system for pumpable MgO based castables. One example of a good flow mixture was achieved (Fisher, 1989) in which the bond phase comprised 15wt.% of MgO (10μm), 5wt.% of MgO (45μm), 6wt.% microsilica, 5wt.% water and 0.3 wt.% sodium hexametaphosphate (NaHMP), which was used as deflocculant. Myhre (1997) used another deflocculant (Vanisperse CB) to produce self-flowing castables of MgO-SiO_2-H_2O bond system mixed with different aggregates include periclase, spinel and olivine (forsterite); the flowability was well attained at low water addition (Table 2.4).

Further studies on M-S-H bond system in refractories were presented with the focus on the effect of additives and raw materials on flow and set. Ødegård et al. (2001) tested the flow and setting time of castable mixtures with different additives and reported that either Vanisperse CB or Castament FS10 was identified as interesting additives to obtain good workability. The increase in additive dosage led to the increase in flow and also retard the set time of the mixture (Table 2.5). Effect of Castament FS10 additive to the improvement of rheology of MgO-SF mixture was also demonstrated in study by Myhre (2002) in which mixes of different dead burnt magnesia and Microsilica (6-8%) were deflocculated by Castament FS10 (0.5 wt.%) to obtain good flow at water content as low as 4%.

Table 2.5. Effect of additives on flow and set of MgO-SF castables (Ødegård et al., 2001)

Additives (wt.%)	**Calgon S**	**Vanisperse CB**		**Calgon**	**Castament FS10**
	0.2	0.2	0.3	0.2	0.25
Nedmag MgO (wt.%)	94	94	94	94	94
Microsilica 971U (wt.%)	6	6	6	6	6
Water (wt.%)	4.50/13.1	4.50/13.1	4.50/13.1	4.50/13.1	4.50/13.1
Free-flow (%)	41	6	16	16	76
Vibra-flow (%)	120	100	116	120	128
Set time (hours:min)	1:00	0:30	2:15	0:50	1:15

In previous studies, there are a number of additives which have been used effectively for mixing of workable refractories and castables containing MgO and microsilica whereby MgO content was predominant. In recent studies on strength of reactive magnesia silicate hydrate as a cementitious material, Wei et al. (2011) suggested that inorganic phosphate salts such as sodium hexametaphosphate (NaHMP: chemical formula is $Na(PO_3)_6$) and potassium hexametaphosphate (KHMP) are able to improve the fluidity of MgO-microsilica systems.

Zhang et al (2012) designed a low pH M-S-H cement formulation contained 20 wt.% MgO, 5 wt.% $MgCO_3$, 25 wt.% SF, 50 wt.% quartz sand micro-fillers to encapsulate the problematic nuclear waste. It was reported that by addition of NaHMP of 1% by weight of the solids, the rheology of the mix was well improved with water to solid ratio of only 0.275 (w/b=0.55).

In a study by Zhang (2014) on the formation of magnesium silicate hydrate (M-S-H) cement pastes using sodium hexametaphosphate (NaHMP), the solid phase included 40%MgO+60%SF by weight were mixed with different NaHMP dosages to find the optimal amount of additive. The results showed that 1% NaHMP additive resulted in optimal water reduction for workability. The minimum water to binder ratio to form a thick paste was reduced to 0.40 (Figure 2.16).

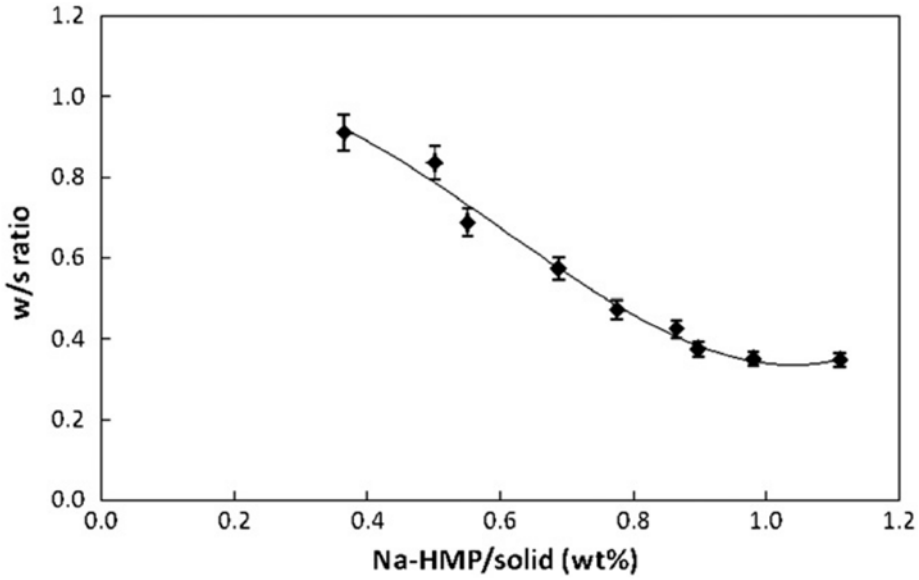

Figure 2.16. Minimum w/s ratio at which a paste formed for different NaHMP dosages (Zhang, 2014)

Walling et al (2015) investigated the influence of NaHMP additive on the workability of M-S-H binder composition of $Mg(OH)_2$ and Silica fume (1:1 ratio) in which the range of superplasticizers used varied extensively from 0 to 5% as shown in Figure 2.17.

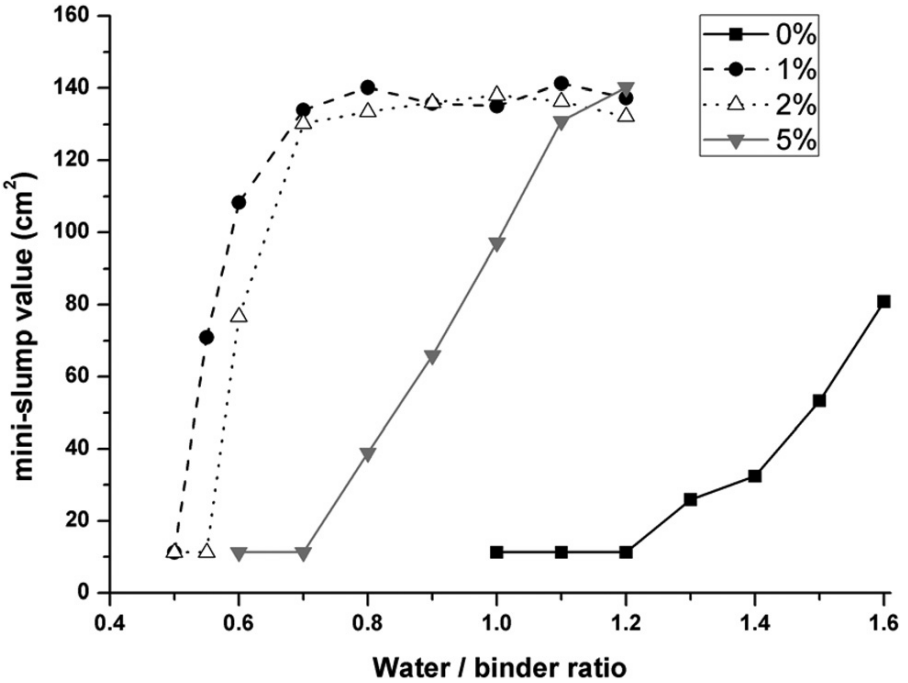

Figure 2.17. Mini-slump values for 1:1 $Mg(OH)_2$:SiO_2 with 0–5 wt%$(NaPO_3)_6$at different water/binder ratios (Walling et al., 2015)

The addition of $(NaPO_3)_6$ as an inorganic dispersant resulted in major differences in the workability of the prepared samples. The paste without $(NaPO_3)_6$ addition lacked fluidity and required w/b as high as 1.6 to achieve a mini-slump of approximate 80 cm^2. Mixes with added

NaHMP at 1-2 wt% obtained a similar mini-slump but at a lower w/b at 0.55-0.60. The most effective dosage of additive was found at 1% to obtain highest fluidity (mini-slump of 130 cm^2) with a w/b down to 0.7. The addition of 5 wt% $(NaPO_3)_6$ increased fluidity, compared to non-plasticizer sample, however required much higher water content as observed in the formulations with 1 and 2 wt% $(NaPO_3)_6$. The loss of fluidity as NaHMP added exceeding 2% indicated a threshold limit beyond that the dispersion is no longer effective.

2.3.4. **Micro-fillers and rheology**

The use of micro-fillers was well studied to improve workability and strength of Portland cement concrete. In a study by Nehdi (1998), the influence of ultrafine fillers to the rheology of high-strength concrete has been assessed, including factors such as superplasticizer efficiency, slump, and flow resistance. The testing fillers include silica fume, ground silica, limestone with different binary blends of 5, 10, 15, 20% weight content for cement replacement. The water to cement ratio is controlled at 0.33 and slump was required as 220mm ± 20mm by adjustment of superplasticizers content.

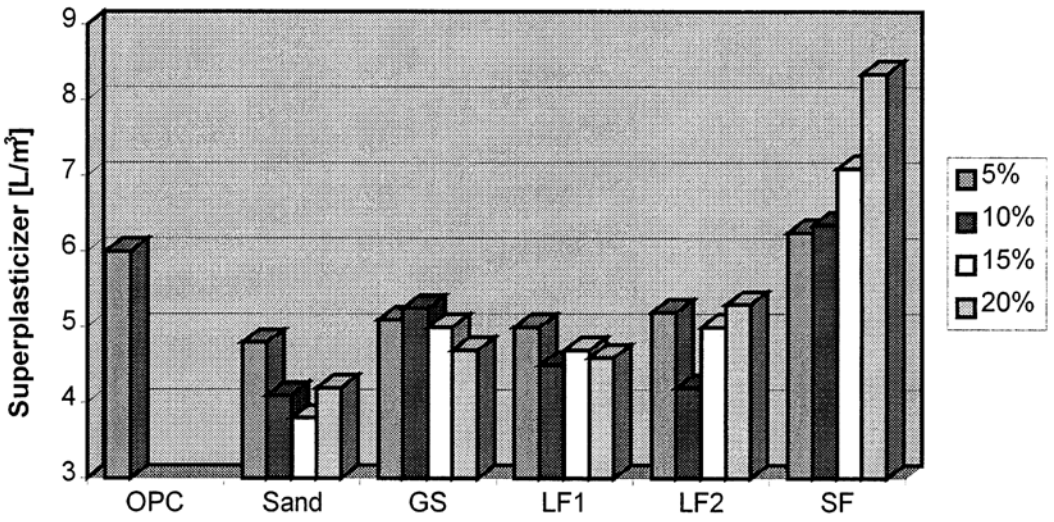

Figure 2.18. Superplasticizer dosage for constant workability

The integration of the ultrafine fillers of ground silica and limestone significantly improved rheology of concrete mixtures by reduction of superplasticizers from 25% up to 70% compared to controlled PC sample without ultrafine fillers. In contrast, silica fume significantly increased superplasticizer dosages, especially at high cement replacement ratio (20%). Other authors (Siddique and Khan, 2011) also concluded that silica fume in the amount exceeding 5% from the mass of cement considerably increases the water demand of the binder due to the increase in the fine fraction volume.

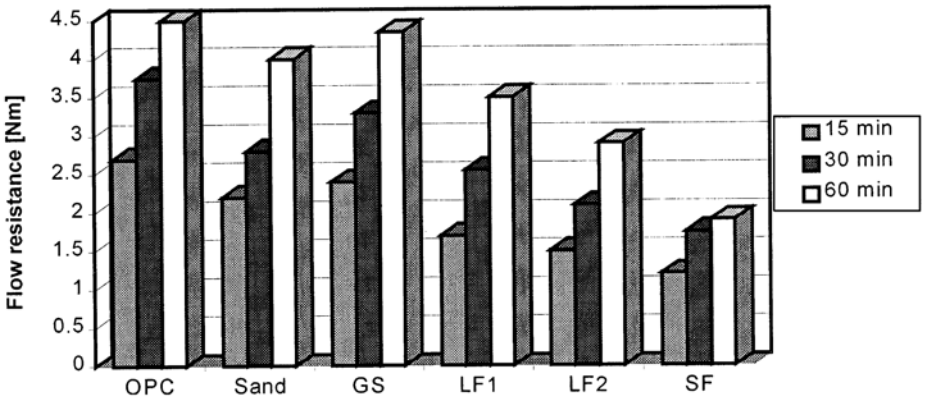

Figure 2.19. Flow resistance at various ages for concretes made with 15% of various fillers (Neidi, 1998)

The decrease of flow resistance with the inclusion of 15% ultrafine fillers improved the workability of the mixtures (Figure 2.19). Surprisingly, the replacement of 15% cement by silica fume gave the lowest flow resistance, due to the combined effect of spherical particle shape with high superplasticizer content. However, it should be noted that in another study, Hedda and Harald (2009) pointed out that the flow resistance decreased whereby silica fume content was as low as 9% and over that weight percentage, the flow resistance actually increased.

The idea of combining superplasticizer and suitable ultrafine particles to make the concrete easier to place and improve rheology was also explained by Nehdi (1998). The principle was that the superplasticizer can combat the electrostatic forces to disperse ultrafine particles, while the spherical microfillers can reduce the viscous and friction forces between aggregates. In the presence of superplasticizer, the finer and the more spherical filler resulted in the better rheology. It is also suggested that for the good rheology with minimum viscosity of suspensions, the deviation from ideal grading should be minimal to target the high particle packing with broad particle-size ranges of fillers for the finer particles to fit into the gaps between coarser particles. Barnes (1989) proposed that gradation for optimized particle packing of the binder might enhance the flow of concrete.

Daukšys (2010) examined the influence of finely ground quartz sand and plasticizing admixtures on rheological properties of Portland cement paste. The testing Portland cement had a specific surface area of 353 m^2/kg and water demand for normal consistency of 27.5 %. The quartz sand was ground to specific surface area of 255 m^2/kg.

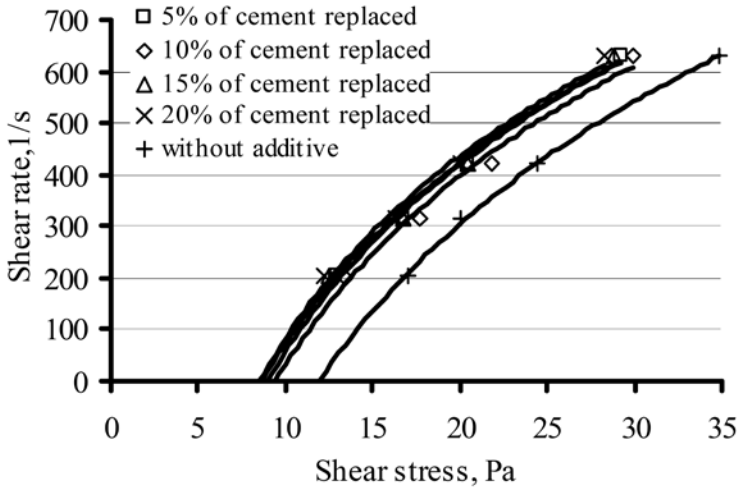

Figure 2.20. Flow curve of cement pastes in addition of finely ground quartz replaces Portland cement (0-20%), w/c = 0.55 (Daukšys, 2010)

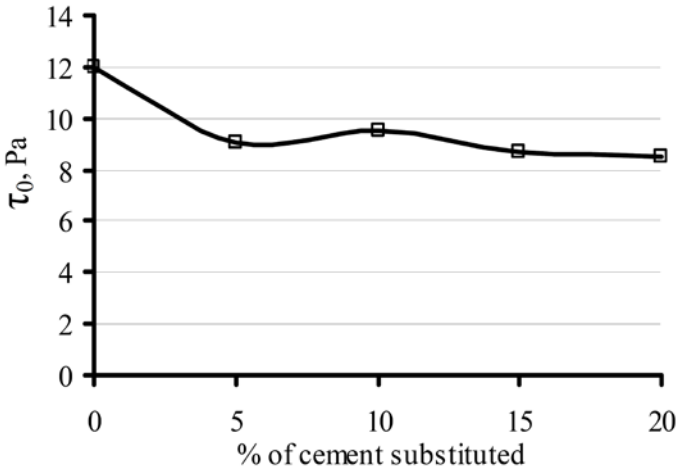

Figure 2.21. Yield stress of cement pastes in addition of finely ground quartz replaces Portland cement (0-20%), w/c = 0.55 (Daukšys, 2010)

It was shown in Figure 2.20 and Figure 2.21 that flowability of the paste was improved as finely ground quartz replacing from 5 % cement reduced the shear and yield stress of the cement paste while higher amounts of the filler up to 20% only have negligible improvement on the rheology properties of the paste.

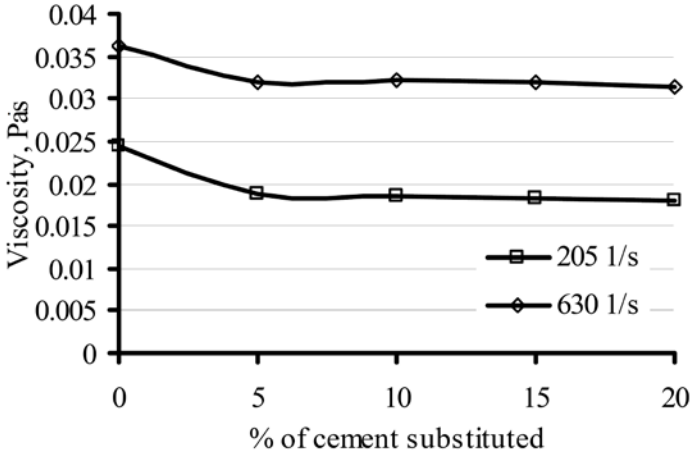

Figure 2.22. Dependence of viscosity on the ground quartz filler content (0-20%), w/c = 0.55 without superplasticizer (Daukšys, 2010)

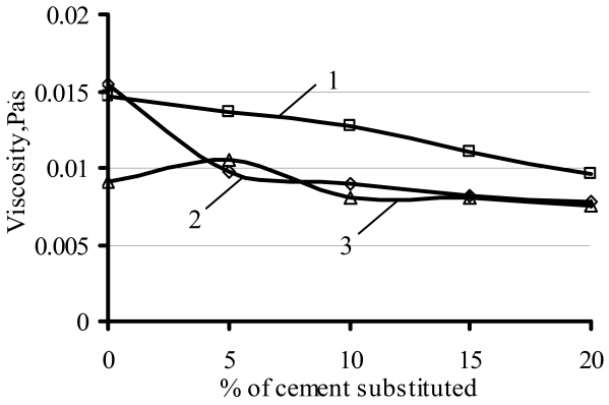

Figure 2.23. Dependence of viscosity on the ground quartz filler content (0-20%), w/c = 0.55with different superplasticizers (1,2,3) at velocity gradient 205 s^{-1}(Daukšys, 2010)

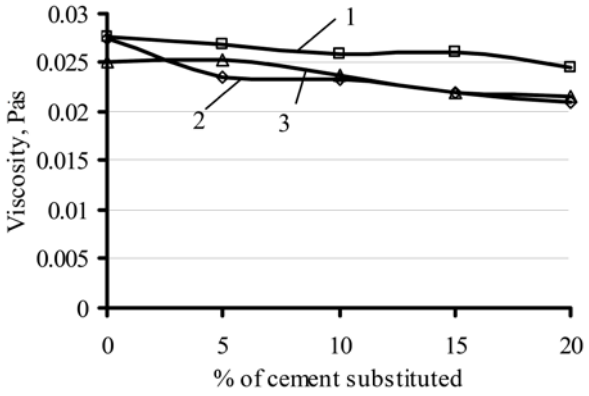

Figure 2.24. Dependence of viscosity on the ground quartz filler content (0-20%), w/c = 0.55with different superplasticizers (1,2,3) at velocity gradient 630 s^{-1} (Daukšys, 2010)

The combined effect of quartz fillers and three different plasticizers on viscosity was also reported. The use of plasticizing admixtures decreased the viscosity of the cement paste at

different rate subjected to the chemical composition of the admixture. The test results indicated a possibility to reduce the viscosity of cement pastes with the addition of finely ground quartz sand and plasticizing admixtures (Figure 2.22 – 2.26).

The only M-S-H binder mixtures incorporating crushed quartz fillers was reported by Zhang (2012) in which the role of quartz filler is to reduce shrinkage resulted from high silica fume content. The effect of micro fillers on the workability of M-S-H binder has not been studied extensively in the literature.

Silica fume is very much finer with a significant increase in its specific surface area compared to Portland cement, consequently results in extremely high water demand of M-S-H binder system. The workability of M-S-H binder system can be improved by using a number of dispersive additives to reduce water demand effectively such as Sodium hexametaphosphate, Vanisperse or Castament FS10. The optimal superplasticizer dosage (solid content) for M-S-H binder system was found in a range of 1-2%. However, no experiments of polycarboxylate-based superplasticizer with M-S-H binder system were found in the literature. The lowest water to cementitious materials at which M-S-H paste can be formed was still very high (w/b=0.40), compared to Portland cement. The introduction of some types of fillers to the binder system in presence of superplasticizer led to the improvement of the workability by reducing shear stress, viscosity and increasing particle packing density.

2.4. CONCRETE MIX PROPORTIONING METHODS

The mix proportions play an important role in the mechanical properties and durability of cementitious materials. For PC concrete, mix design methods were well studied and reported in the literature. For example, ACI 211.1 provides a design method for normal, heavyweight and mass concrete to achieve desirable workability and compressive strengths. There are also guidance for high strength concrete mix design using supplementary cementitious materials such as fly ash (ACI 211.4R) and silica fume (ACI 234R). For other materials such as high-performance concrete or ultra-high performance concrete (UHPC), numerous studies have been published as a basis for the mix proportions selection. The optimization of mix proportions of UHPC considering the use of silica fume and crushed quartz filler fillers resulted in over 200 MPa concrete with high durability. However, studies on mix design methods for proportioning M-S-H concrete have not been found extensively in the literature. In addition, the reported strengths of M-S-H cementitious materials are somewhat lower than those achieved with PC. Therefore, the advanced mix proportioning methods of PC concrete and theory of packing density is reviewed and presented in Appendix A as guidance for the development of high strength M-S-H cementitious materials.

2.5. CURING OF M-S-H CEMENTITIOUS MATERIALS AND STRENGTH DEVELOPMENT

The M-S-H binder systems have been studied recently as a cementitious material and there has been very limited publication on the effect of different curing regime to its mechanical properties and durability. Most of previous studies adopted standard curing in water at ambient temperature. As opposed to conventional PC paste, M-S-H paste and mortar were observed to develop strength slowly. A detailed discussion of PC is provided in Appendix A.

The slow strength development of M-S-H binder was demonstrated in a number of studies as described in Figure 2.25. At the age of 7 days, M-S-H samples achieved only 30-67% of the compressive strength compared to 28-day samples (Wei et al., 2006; Zhang et al., 2012, 2014). Further curing to 56 and 90 days improved compressive strength considerably to 106-146% of 28-day compressive strength while some samples exhibited an abnormal strength increase upto 240% (Jin and Al-Tabbaa, 2014). The linear-like strength development from 7 days to 90 days (Figure 2.25) indicates a longer curing period beyond 28 days for M-S-H cementitious materials to achieve its optimum strength.

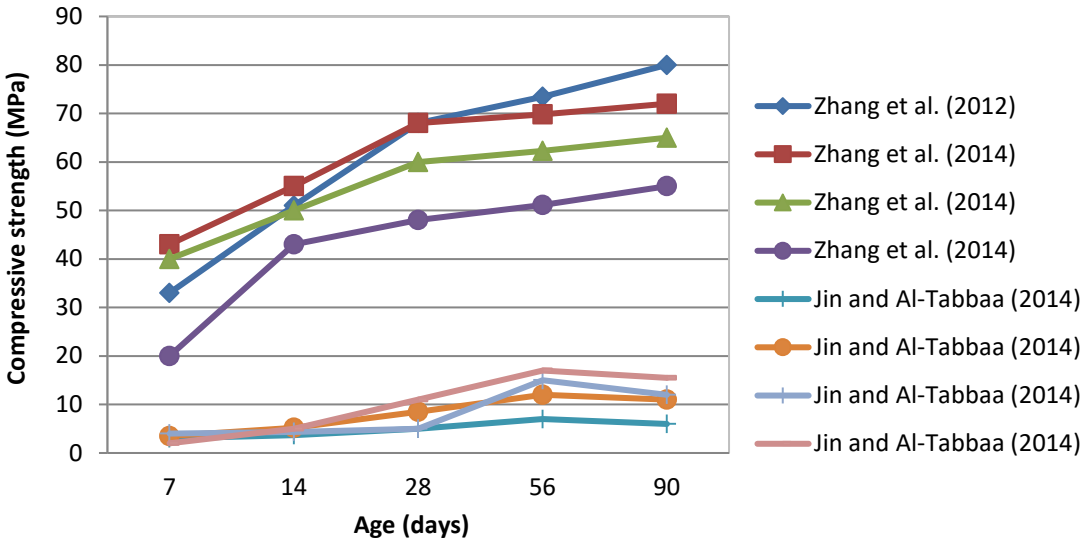

Figure 2.25. Strength development of M-S-H pastes and mortars

Jin and Al-Tabbaa (2014) suggested an optimal water curing period at 56 days for M-S-H paste samples. It was surprising that further curing of M-S-H samples in water for more than 56 days reduced the compressive strength. The adverse effect of water curing for longer than 56 days was explained that while full hydration was completed within 56 days, further soaking in water led to the dissolution of the hydration products and strength reduction. This controversial effect of water curing needs to be investigated further along with studies on temperature curing of M-S-H binder systems.

2.6. PORE SOLUTION ANALYSIS

The chemical compositions of the pore solution reflect the ongoing processes of cement hydration. The ion concentrations over the time can determine which solid phases are stable and may precipitate, and which phases are unstable and may dissolve (Vollpracht et al., 2016). The study of cement pore solutions, therefore, is necessary to the understanding of the reaction mechanisms of the formation of cement hydration products.

The solution in the pores of the cement pastes can be collected in different methods. A vacuum filtration or centrifuge is able to separate the liquid phase during the first hours of hydration (Goldschmidt, 1982; Michaux et al., 1989). After hardening, a high pressure device is generally required to extract the pore solutions from the pastes prepared with high w/c ratios (Locher et al., 1976, 1983; Vernet et al., 1980a, 1980b; Way and Shayan, 1989). Such a high pressure device was first introduced by Longuet et al. (1973) to extract pore solutions from hardened cement pastes. Numerous studies (Barneyback and Diamond, 1981; Page et al., 1986; Kawamura et al., 1988; Andersson et al., 1989; Hussain and Al-Gahtani, 1991; Duchesne and Bérubé, 1994; Tritthart and Häußler, 2003; Buckley et al., 2007) have successfully applied similar techniques to obtain pore solutions of cement pastes with w/c = 0.60 and below. Chemical compositions of the pore solutions can be analyzed by ICP MS or ICP-OES methods which determine elements available in the solution and their concentrations.

Pore solution analysis has been widely applied to study durability of concrete in the literature (Hooton et al., 2010). For example, the hydroxyl concentration is directly related to the pH which is among the key factors affecting the corrosion of embedded steel reinforcement. Anstice et al. (2005) undertook a study to clarify whether accelerated carbonation regimes, required to produce carbonated cement paste for laboratory investigations over reasonable time scales, may affect pH and the corrosion-related properties of concrete.

Pore solution expression also allows analysis of the chemical composition at a particular age and condition of samples and provides a “snapshot” of existing concentrations at the time (Buckley et al., 2007). Accordingly, it is very useful for analysis of particularly important elemental ions such as chloride as their high concentrations lead to loss of corrosion protection in embedded steel reinforcement (Page and Vennesland, 1983).

Research on pore solutions of PC incorporating supplementary cementitious materials such as silica fume, fly ash, and GGBS have been well studied and published extensively (Diamond, 1981; Page and Vennesland, 1983; Larbi et al., 1990; Lorenzo et al., 1996; Rothstein et al., 2002). Hooton (2009) showed that the inclusion of SCMs generally lowers the concentration of alkalis and hydroxyl in the pore fluid due to the pozzolanic reactions forming secondary C-S-H phases. The

pH change also depends on the PC replacement level and the type of SCMs. For example, Fly ashes unusually high in alkali can increase alkali concentrations in the pore fluid.

Comparison of ion concentrations of ordinary PC and blended cement has shown the effect of SCMs on the alkali-silica reactions (ASR) in concrete (Kawamura and Takemoto, 1986; Nixon et al., 1986; Canham et al., 1987). There is a close relationship between ASR expansion and pore solution alkalinity. The ability of SCMs to reduce alkalinity in pore solutions to below ASR threshold and maintain its depressed levels over time is effective to control the ASR expansion of PC concrete (Hooton, 2009).

While the pore solution of Portland cement systems has been studied quite extensively few studies on pore solutions extracted from M-S-H binder systems have been found in the literature. The M-S-H binders contain very high contents of alkalis and SCMs, which is similar to blended cement to a certain degree. The main reactions of hydrated MgO and reactive silica are comparable to pozzolanic reactions in PC and the formation of M-S-H phases may be indicated by the change of the alkalinity of the pore solutions. The material source is also reported to be one of the major causes for the strength variations of M-S-H binders (Jin et al., 2013). From the effectiveness of the pore solution analysis of PC, it can be seen that this method is capable to analyze M-S-H cement pastes pore solutions for the understanding of the reaction mechanisms and the effect of material sources on the hydration products and durability.

2.7. RESEARCH GAPS AND DIRECTIONS

As previously summarized, there is an urgent need to develop new sustainable materials in construction and magnesium-based cements have been evaluated by researchers as a potential binder to replace PC. Previous studies show that there are two main cement systems using reactive magnesium oxide as the main binder constituent: (i) $MgO\text{-}H_2O$ and $MgO\text{-}SiO_2\text{-}H_2O$ (M-S-H). Research on $MgO\text{-}H_2O$ systems show that this cement has a relatively low early-age strength compared to PC but the strength is approximately the same as a PC at 28 days age. This type of binder shows the suitability to develop porous blocks for buildings with low required strengths due to the very high porosity requirement of the pastes and mortars to accelerate CO_2 penetration. The binder is based on carbonation of brucite to form magnesium carbonates to develop strength. This type of cement also shows great environmental benefit as it can absorb a large amount of carbon dioxide in the carbonation process. However, it appears that this cement may not be suitable to develop high strength cementitious materials to compare to PC for a wide range of applications in materials and structures.

The research direction focusing on the formation of M-S-H systems has been initiated in the last decades, with the intention of developing construction materials using M-S-H cement. Most of previous studies have confirmed M-S-H phases as the main hydration product of reactive MgO and amorphous silica in M-S-H binders. So far, there have been a few studies showing the advantages of M-S-H binders compared to PC in mechanical properties. Most previous research results have been quite inconsistent. Performance of M-S-H binder systems is highly dependent on material sources, especially the MgO sources with different levels of reactivity. Some studies also show that M-S-H binders require very high water demand for workability.

Thus, it can be seen that despite its potential benefits, there are still a number of limitations and challenges for M-S-H binders to achieve desirable engineering properties. Previous studies have not fully studied the properties of M-S-H binders, so a better understanding is in demand for the new M-S-H binders to be technically feasible for PC replacement. The key issues in developing M-S-H binder systems are summarized below but not limited to:

(1) There have been very limited studies on the workability of M-S-H binder systems, particularly the use of polymer-based super-plasticizers. This type of super-plasticizer has been used widely as a high range water reducer for ultra-high performance concrete using PC and could be effectively reduce water demand for M-S-H binders. The selection and experiments of the effect of different superplasticiers are among the key factors to improve strength and durability of M-S-H binder systems due to the inclusion of large amounts of very fine particles of reactive MgO and silica.

(2) There is still a lack of studies on the performance of M-S-H binders with various amorphous silica sources. Most of previous studies used highly reactive silica fume in MgO-SiO_2 mixtures. The effect of MgO sources has been mentioned, however it should be noted that reactivity of silica fume is also crucial to the formation of the hydration products. In addition, silica fume is a high cost material while other silica sources such as natural silica, fly ash or agricultural waste material (rice husk ash) should be studied for the ability to combine with reactive MgO. It is necessary to evaluate the strength and microstructure of M-S-H binders with different silica sources to improve the properties and reduce material costs.

(3) Previous studies have mentioned M-S-H as a low-pH binder and have benefits on the immobilization of problematic nuclear wastes. However, the effect of different silica sources on pH has not been studied. So far, there has not been any experimental work extracting pore solutions from hardened M-S-H cement pastes or mortars, so the previous studies on pH development did not reflect the actual pHs of M-S-H pore solutions in the real samples. In addition, no studies on ion concentrations of the pore solutions of M-S-H samples have found. The chemical

composition of the pore solutions is useful for the understanding of reaction mechanisms and hydration products, the solubility of binder constituents, and the hydration process. Pore solutions analysis also indicates the durability of the material over the time.

(4) Most of previous studies focused on mechanical properties and microstructure of M-S-H samples at early age to 90 days, however, the understanding of the long-term properties are more important to the durability of the new binders. Currently, the lack of studies on long-term properties of M-S-H binders is still a limitation for the use of the new binders in practice. Experimental work on strength development, microstructures or hydration process in the long-term (at least up to 6 months or 1 year) should be performed to characterize the durability of M-S-H binder systems.

(5) Curing regime has a decisive role on the strength development and durability of concrete. For PC, numerous studies on different curing regimes have been performed, however, such studies on M-S-H binders are scarce in the literature. Water-curing at room temperature is the most common curing regime which was applied to M-S-H binders and no optimal curing condition has been suggested. It is known that factors such as heated treatment and moisture conditions have crucial impact on the strength development and microstructure of cementitious materials. In addition, M-S-H binders are found to be highly dependent on material sources and therefore research on curing effect is necessary to the understanding of whether this new binder is sensitive to the variation of the curing conditions.

(6) Binary systems of MgO-SiO_2 have shown some limitations such as high water demand for workability and low strengths compared to PC. Nonetheless there is very limited research on ternary systems incorporating fillers to improve properties of fresh and hardened cement pastes, mortars and concrete. In the meanwhile, quartz fillers are widely used in high performance and ultra-high performance concrete to improve microstructure and increase strengths. Studies of multi-component systems are required to explore potential benefits of fillers in M-S-H binder systems.

(7) The past research on M-S-H binders only focuses on testing cement pastes and mortars. So far, little research has been carried out on M-S-H concrete samples for the practical purpose of PC replacement in construction applications. The effect of coarse aggregates on the properties of concrete has not been studied. For structural materials, properties other than compressive strength such as tensile strength, elastic modulus and durability properties are also important and the lack of studies on these properties has limited the use of M-S-H binders in current practice.

This thesis focuses on developing M-S-H binder systems using reactive MgO and amorphous silica. The research topics include the key characteristics of cement such as workability, mechanical properties, microstructure, long-term durability, and effects of other factors such as curing conditions, sources of materials and fillers. Potential use of M-S-H binders in large scale is evaluated by producing and testing M-S-H concrete samples. The study will attempt to analyze the current research gaps and limitations as mentioned above to develop M-S-H binder systems for a wide range of applications in the future. The next chapters will present the experimental results and findings of the thesis.

2.8. REFERENCES

ACI Committee 211 (1991). Standard Practice for Selecting Proportions for Normal, Heavyweight and Mass Concrete, ACI 211.1-91. American Concrete Institute, Farmington Hills, Michigan.

ACI (1992). ACI 363R-92 State-of-the-Art Report on High-Strength Concrete. American Concrete Institute, Farmington Hills, Michigan.

ACI (2005). Building code requirements for structural concrete and commentary (ACI 318M-05)

ACI Committee 211 (1993). Guide for Selecting Proportions for High-Strength Concrete with Portland Cement and Fly Ash, ACI 211.4R-93. American Concrete Institute, Farmington Hills, Michigan.

ACI Committee 232 (1996). Report 232.2R-96 Use of Fly Ash in Concrete. American Concrete Institute, Farmington Hills, Michigan.

ACI Committee 234 (2006). Guide for the use of silica fume, ACI 234R-06, American Concrete Institute, Farmington Hills, Michigan.

Acquaye L. (2006). Effect of high curing temperatures on the strength, durability and potential of delayed ettringite formation in mass concrete structures. Phd Thesis. University of Florida.

Aggarwal, M. I. (2002). Mixture Experiments. In Design Workshop lecture notes. University of Delhi, Delhi. India (pp. 77-89).

Alexander, M. G., Mackechnie, J. R., & Ballim, Y. (1999). Guide to the use of durability indexes for achieving durability in concrete structures. Research monograph, 2.

Andersson, K., Allard, B., Bengtsson, M. and Magnusson, B. (1989). Chemical composition of cement pore solutions. Cement and Concrete Research, 19(3), pp.327-332.

Anstice, D. J., Page, C. L., & Page, M. M. (2005). The pore solution phase of carbonated cement pastes. *Cement and Concrete Research*, *35*(2), 377-383.

Atis C.D., Ozcan F., Kılıc A. et al. (2005). Influence of dryand wet curing conditions on compressive strength of silica fume concrete. Building and Environment 40 (2005) 1678–1683.

Aydin S., Baradan B. (2013). Engineering properties of reactive powder concrete without Portland cement. ACI MATERIALS JOURNAL TECHNICAL PAPER. Nov-Dec 2013, 619-627.

Aydin S., Yazici H., Yardimci M.Y., and Yiğiter H. (2010). Effect of Aggregate Type on Mechanical Properties of Reactive Powder Concrete. ACI MATERIALS JOURNAL TECHNICAL PAPER. Title no. 107-M50, 441-449.

Barnes H.A., Hutton J.F., Walters K. (1989). An Introduction to Rheology, Elsevier (1989), p. 115

Barneyback, R.S. and Diamond, S. (1981). Expression and analysis of pore fluids from hardened cement pastes and mortars. Cement and Concrete Research, 11(2), pp.279-285.

Benezet J.C., Benhassaine A. (1999). Grinding and pozzolanic reactivity of quartz powders. Powder Technology. 105(1999), 167-171.

Bentz D., Tanesi J., Adani A. (2013). Enhancing the Performance of High Volume Fly Ash Concretes Using Fine Limestone Powder. American Concrete Institute, ACI Spring Convention Green Green Cement Sessions (Apri 16,2013). Available at: https://www.youtube.com/watch?v=vXBpoXLZbhI&index=55&list=PLA28CDF778D6BE0F8.

Blais P. and Couture M. (1999). Precast, prestressed pedestrian bridge – world's first reactive powder concrete structure. PCI J. IX–X, 60–71.

Blais Y.P., Couture M. (1999). Precast, Prestressed Pedestrian Bridge — World's First Reactive Powder Concrete Structure. PCI Journal, p. 60-71.

Bonneau, O., Lachemi, M., Dallaire, E., Dugat, J., and Aitcin, P. (1997). Mechanical properties and durability of two industrial reactive powder concretes, ACI Materials Journal, 94(4), 286-290.

Bonen, D., and Cohen, M.P. (1992). Magnesium sulfate attack on Portland cement pastes. Cement and Concrete Research 22, 169–180, 707–718

Brew D.R.M., Glasser F.P. (2005). Synthesis and characterisation of magnesium silicate hydrate gels. Cement and Concrete Research 35 (2005) 85– 98

Brew DRM, Glasser FP. (2005). The magnesia-silica gels phase in slag cements: alkali (K, Cs) sorption potential of synthetic gels. Cem Concr Res 35(1):77–83.

British Standard (1995). BS EN196-1:1995 Methods of testing cements. Part 1: Determination of strength. BSI, 1995.

Buckley, L. J., Carter, M. A., Wilson, M. A., & Scantlebury, J. D. (2007). Methods of obtaining pore solution from cement pastes and mortars for chloride analysis. Cement and Concrete Research, 37(11), 1544-1550.

Canbaz M. (2014). The effect of high temperature on reactive powder concrete. Construction and Building Materials 70 (2014) 508–513.

Canham I, Page CL, Nixon PJ. (1987). Aspects of the pore solution chemistry of blended cements related to the control of alkali silica reaction. Cem Concr Res 17(5): 839–844

Roosz, C., Grangeon, S., Blanc, P., Montouillout, V., Lothenbach, B., Henocq, P., ... & Gaboreau, S. (2015). Crystal structure of magnesium silicate hydrates (MSH): The relation with 2: 1 Mg–Si phyllosilicates. Cement and Concrete Research, 73, 228-237.

Chan W.W.J., Wu C.M.L. (2000). *Durability of concrete with high cement replacement*. Cement and Concrete Research 30 (2000) 865 - 879

Charron J., Denari´e E., Bruhwiler E. (2007). Permeability of ultra high performance fiber reinforced concretes (UHPFRC) under high stresses. Materials and Structures, 40 p.269-277

Cheyrezy M. (1999). Structural applications of RPC. Concrete. 33(1), pp. 20-23.

Cheyrezy M., Maret V., Frouin L. (1995). MICROSTRUCTURAL ANALYSIS OF RPC (REACTIVE POWDER CONCRETE). Cement and Concrete Research. Vol 25 (7), 1491-1500.

Cole WF. A (1953). *Crystalline hydrated magnesium silicate formed in the breakdown of a concrete sea-wall.* Nat 1953;171:354–5.

Collepardi S., Coppola L., Troli R., and Collepardi M. (1997). Mechanical properties of modified reactive powder concrete. American Concrete Institute 173, 1–22.

Cornell, J. A. (2011). *Experiments with mixtures: designs, models, and the analysis of mixture data* (Vol. 895). John Wiley & Sons.

Daukšys M., Skripkiūnas G., Grinys A. (2010). finely ground quartz sand and plasticizing admixtures influence on rheological properties of portland cement paste. materials science (Medžiagotyra). vol. 16, no. 4. 2010

Diamond S (1981). Effects of two Danish fly ashes on alkali contents of pore solutions of cement–fly ash pastes. Cem Concr Res 11(3):383–394

Du Chongjiang (2005). A Review of Magnesium Oxide in Concrete - A serendipitous discovery leads to new concrete for dam construction. Concrete international, p45-50

Duchesne, J., & Bérubé, M. A. (1994). Evaluation of the validity of the pore solution expression method from hardened cement pastes and mortars. Cement and Concrete Research, 24(3), 456-462.

Dugat J., Roux N., Bernier G. (1996). Mechanical properties of reactive powder concretes. Materials and structures. Springer

Ecocem. (2015). Strength Development. Ecocem. Available at: http://www.ecocem.ie/technical,strength.htm (Accessed: 10 Aug 2015)

Fang, K.H. (2004). Hydration of MgO and its Influence on Autogenous Volume Expansion. Journal of Hydroelectric Engineering, 4, p45-49, (in Chinese).

FIB. (1988). Condensed silica fume in concrete. Thomas Telford Ltd., London.

Fisher R. E. (1989). Advances in refractories technology. Vol. 4. Amer Ceramic Society.

Furnas C.C. (1929). Flow of gases through beds of broken solids. Bureau of Mines Bulletin 307.

Goldschmidt A. (1982). About the hydration theory and the composition of the liquid phase of Portland cement. Cem Concr Res 12(6):743–746

Gollop R, Taylor H. (1996). Microstructural and microanalytical studies of sulfate attack. IV. Reactions of a slag cement paste with sodium and magnesium sulfate solutions. Cem Concr Res 26(7): 1013–28.

Graybeal B.A., Hartmann J.L. (2003). Strength and durability of ultra-high performance concrete. 2003 concrete Bridge Conference. http://www.ductal.com/20-FHWA._Strength_and_Durability._UHPC.pdf (accessed 17.07.2015)

Graybeal, B. (2006). Material Property Characterization of Ultra-High Performance Concrete. Report No. FHWA-HRT-06-103. McLean, VA.

Habel K, Viviani M, Denarié E, Brühwiler E. (2006). Development of the mechanical properties of an Ultra-High Performance Fiber Reinforced Concrete (UHPFRC). Cem Concrete Research 36(7):1362–70

Hall C. (1976). On the history of Portland cement after 150 years, J. Chem. Educ.,53 (4).

Harrison, A. J. W. (2013). Low Carbon Cements and Concretes in Modern Construction. In Proceedings of the UKIERI Concrete Congress–Innovations in Concrete Construction. 5–8 March 2013. Jalandhar (pp. 723-746). Available at: http://www.tececo.com/files/conference%20presentations/JHarrisonLowCarbonCement&Concrete.pdf

HDR. 2002.Tensile properties of VHSC, HDR, Inc (adapted from Lubbers 2003)

Hedda V., Harald J. (2009). PARAMETERS DETERMINING THE FLOW OF CONCRETE MATRIX. Design, Performance and Use of Self-Consolidating Concrete SCC'2009. (RILEM Proceedings : Vol. 65)

Hooton, R. D., & Thomas, M. D. (2009). Pore Solution Analysis as a Tool for Studying Early–Age Hydration & Predicting Future Durability. *Cement Hydration Summit, Quebec*.

Hooton RD, Thomas MDA, Ramlochan T (2010) Use of pore solution analysis in design for concrete durability. Adv Cem Res 22(4):203–210. doi:10.1680/adcr.2010.22.4.20

Hussain, S.E. and Al-Gahtani, A.S. (1991). Pore solution composition and reinforcement corrosion characteristics of microsilica blended cement concrete. Cement and Concrete Research, 21(6), pp.1035-1048.

Jin. F, Al-Tabbaa A. (2014). Strength and hydration products of reactive MgO–silica pastes. Cement & Concrete Composites 52 (2014) 27–33

Jin F, Gu K, Abdollahzadeh A and Al-Tabbaa A (2013). Effects of different reactive MgOs on the hydration of MgO-activated GGBS paste. Journal of Materials in Civil Engineering 27(7): B4014001

Kamal M.M., Safan M.A., Etman Z.A., Salama R.A. (2013). Behavior and strength of beams cast with ultra high strength concrete containing different types of fibers. Housing and Building

National Research Center. HBRC Journal (2013).

Kawamura M, Takemoto K (1986). Effects of pozzolans and a blast furnace slag on alkali hydroxides concentrations in pore solutions and alkali-silica expansion. In: Review of the 40th general meeting, technical session, 1986. Cement Association of Japan, Tokyo, pp 262–265

Kawamura, M., Kayyali, O. A., & Haque, M. N. (1988). Effects of a fly ash on pore solution composition in calcium and sodium chloride-bearing mortars. Cement and Concrete Research, 18(5), 763-773.

Kjellsen K.O., Detwiler R.J., and Gjorv O.E. (1990a). Pore Structure of Plain cement pastes hydrated at different Temperatures. Cement and Concrete Research. Vol. 20, pp. 927-933, 1990a.

Kjellsen K.O., Detwiler R.J., and Gjorv O.E. (1990b). Development of Microstructure in plain hydrated at different Temperatures. Cement and Concrete Research. Vol. 21, pp. 179-189, 1990b.

Larbi JA, Fraay ALA, Bijen JM. (1990). The chemistry of the pore fluid of silica fume-blended cement systems. Cem Concr Res 20(4):506–516

Larrard F. and Sedran T. (1994). Optimization of ultra-high-performance concrete by the use of a packing model. Cement and Concrete Research, Vol. 24, No. 6, pp. 997-1009.

Larrard F. and Sedran T. (1994). Optimization of ultra-high-performance concrete by the use of a packing model. Cement and Concrete Research, Vol. 24, No. 6, pp. 997-1009.

Lee N.P. and Chisholm D.H. (2005). Reactive Powder Concrete. Study Report SR 146, BRANZ Ltd, Judgeford, New Zealand.

Li, Z., Zhang, T., Hu, J., Tang, Y., Niu, Y., Wei, J., & Yu, Q. (2014). Characterization of reaction products and reaction process of MgO–SiO2–H2O system at room temperature. Construction and Building Materials, 61, 252-259.

Longuet P, Burglen L, Zelwer A. (1973). La phase liquide du ciment hydrate. Rev mate´r constr 676:35–41

Lorenzo P, Gon˜i S, Hernandez S, Guerrero A. (1996). Effect of fly ashes with high alkali content on the alkalinity of the pore solution of hydrated Portland cement paste. J Am Ceram Soc 79(2):470–474. doi:10.1111/j.1151-2916.1996.tb08146.x

Lothenbach, B., Nied, D., L'Hopital, E., Achiedo, G., Dauzeres, A. (2015). Magnesium and calcium silicate hydrates. Cement and concrete research, 77, 60-68

Máca P., Sovjak R., Vavrinik T. (2013). Experimental Investigation of Mechanical Properties of UHPFRC. Procedia Engineering. 65, 14-19.

Máca P., Zatloukal J., and Maca P.K. (2012). Development of Ultra High Performance Fiber Reinforced Concrete Mixture. 2012 IEEE Symposium on Business, Engineering and Industrial Applications.

Makovic' I. (2006). High-Performance Hybrid-Fibre Concrete- Development and Utilisation. PhD Thesis. Delft University Press.

Malhotra V.M. and Painter K.E. (1989). Early-Age Strength Properties, and Freezing and Thawing Resistance of Concrete Incorporating High-Volumes of ASTM Class F Fly Ash, the International Journal of Cement Composites and Lightweight Concrete, Vol. 11, No. 2, February 1989.

Mariel V., Carlos A. (2015). Cement, waste and carbon markets-problems related to waste incineration in cement kilns under the EU ETS. European commission. Available at http://www.ec.europa.eu/clima/consultations/docs/0017/.../global_3_en.pdf (Accessed: 5 May 2015).

Mathews, P. G. (2005). Design of Experiments with MINITAB. ASQ Quality Press.

Menzel, C.A. (1934). Strength and volume change of steam-cured portland cement mortar and concrete, Journal of ACI Proceedings, Vol. 31, pp. 125-148

Michaux M, Fletcher P, Vidick B (1989). Evolution at early hydration times of the chemical composition of liquid phase of oil-well cement pastes with and without additives. Part I. Additive free cement pastes. Cem Concr Res 19(3):443–456

Mitsuda and Taguchi H. (1977). Formation of Magnesium Silicate Hydrate and Its Crystallization to Talc. Cement and concrete research. 7(3), p223-230

Monosi S., Pignoloni G., Collepardi S., Troli R., and Collepardi M. (2000). Modified Reactive Powder Concrete with Artificial Aggregates. ACI SP 195-28, 447-460.

Myhre B. , Sandberg B., Hundere A. M. (1997). Castables with MgO-SiO2-Al2O3 as bond phase. Proc. of the XXVI ALAFAR Congress in San Juan, Puerto Rico, Oct. 30 – Nov. 1, 1997.

Myhre, B., Ødegård, C., & Feldborg, H. (2002). Periclase castables based on the bond MgO–SiO2–H2O: Properties and current status. In INREFCON (5th India International Refractories Congress) in Bhubaneswar, India. Available at: https://www.elkem.com/documents/esm/refractories/research-papers/50-periclase-castables-based-on-the-bond-mgo-sio2-h2o-properties-and-current-status.pdf

Nehdi M., Mindess S., and Aitcin P. (1998). Rheology of high-performance concrete: effect of ultrafine particles. Cement and Concrete Research, Vol. 28, No. 5, pp. 687–697, 1998

Neville A.M. (1981). *Properties of Concrete.* 3rd edn. Longman, Essex, England (1981)

Nixon PJ, Page CL, Bollinghaus R, Canham I. (1986). The effect of a PFA with a high total alkali content on pore solution composition and alkali silica reaction. Mag Concr Res 38(134):30–35

Ødegård C., Chen Z., Myhre B. et al. (2003). MgO – SiO2 – H2O bonded MgO castables - Part 1: Effect on flow, set and hot properties when substituting microsilica with alumina in pumpable MgO

based castables. Elkem ASA Materials, Presented at the Fourth International Symposium on Refractories in Dalian, China, March 24-28, 2003. Available at: https://www.elkem.com/documents/esm/refractories/research-papers/51-mgo-sio2-h2o-bonded-mgo-castables-part-1-effect-on-flow-set-and-hot-properties-when-substituting-microsilica-with-alumina-in-pumpable-mgo-based-castables.pdf (Accessed 21 may 2015).

Ødegård C., Feldborg H. and Myhre B. (2001). Magnesia-Silicate-Hydrate bonded MgO Castables. In Proc. UNITECR'01, Nov. 4-8. 2001, Cancun, Mexico.

Ojovan M. I., Lee W. E. (2005). An Introduction to Nuclear Waste Immobilisation. London: Elsevier.

Ozyildirim H.C. (1998). Effects of temperature on the development of low permeability in concretes. Virginia Transportation Research Council. Available at: http://www.virginiadot.org/vtrc/main/online_reports/pdf/98-r14.pdf (Accessed: 10 Aug 2015)

Page, C.L., Short, N.R., Holden, W.R. and Materials Research Group (1986). The influence of different cements on chloride-induced corrosion of reinforcing steel. Cement and Concrete Research, 16(1), pp.79-86.

Page, C. L., & Vennesland, Ø. (1983). Pore solution composition and chloride binding capacity of silica-fume cement pastes. Matériaux et Construction, 16(1), 19-25.

Park JJ, Kang ST, Koh KT, Kim SW. (2008). Influence of the ingredients on the compressive strength of UHPC as a fundamental study to optimize the mixing proportion. In: Fehling E, Schmidt M, Geisenhanslueke C, editors. Second International Symposium on Ultra High Performance Concrete. Kassel, Germany; 2008, p. 105–12.

Rangaraju P. R., Kizhakkumodom H., Li Z. and Schiff S.D. (2014). Development of High-Strength / High Performance Concrete / Grout Mixtures for Application in Shear Keys in Precast Bridges. Report No. FHWA-SC-13-04a. South Carolina Department of Transportation, Office of Materials and Research.

Rao, G.A., (2003). Investigations on the performance of silica fume-incorporated cement pastes and mortars. Cem. Concr. Res. 33(11), 1765–1770

Richard P. and Cheyrezy M. H. (1994). Reactive Powder Concretes With High Ductility and 200 - 800 MPa Compressive Strength. In: Metha PK editor. Concrete Technology. Past, Present, and Future. S. Francisco, USA American Concrete Institute, ACI SP 144-24; 1994. p. 507–518

Richard P., Cheryrezy M. (1995). Composition of reactive powder concretes. Cement and concrete research, vol. 25, No7, pp. 1501-1511.

Rimstidt J.D., Barnes H.L. (1980). The kinetics of silica-water reactions. Geochimica et Cosmochimica Acta. Volume 44, Issue 11, 1683–1699.

Rossi, P. et al. (2005). Bending and Compressive Behaviors of a New Cement Composite. Cement and Concrete Research. Vol. 35, No. 1, pp. 27–33.

Rothstein D, Thomas JJ, Christensen BJ, Jennings HM (2002). Solubility 51ehavior of Ca-, S-, Al-, and Si-bearing solid phases in Portland cement pore solutions as a function of hydration time. Cem Concr Res 32(10):1663–1671. Doi:10.1016/S0008-8846(02)00855-4

Russell H.G. and Graybeal B.A. (2013). Ultra-High Performance Concrete: A State-of-the-Art Report for the Bridge Community. Report No. FHWA-HRT-13-060. Federal Highway Administration.

SFA (2015). Silica fume presentation, version 1, Chapter 4. Working with Silica-fume concrete. Available at http://www.silicafume.org/media/sfa_ch4.ppt (Accessed 16 Aug 2015)

Siddique R. and Khan M. I. (2011). Supplementary Cementing Materials, Engineering Materials (Chapter 2. Silica Fume). Springer-Verlag Berlin Heidelberg.

Silva W.M. (2011). Microsilica-bonded magnesia-based refractory castables: Bonding mechanism and control of damage due to magnesia hydration. PhD thesis. TU Bergakademie Freiberg.

Simon, M. J. (2003). *Concrete mixture optimization using statistical methods: final report* (No. FHWA-RD-03-060,). US Department of Transportation, Federal Highway Administration, Research, Development and Technology, Turner-Fairbank Highway Research Center.

So H., Jang H., Khulgadai J., and So S. (2015). Mechanical Properties and Microstructure of Reactive Powder Concrete using Ternary Pozzolanic Materials at Elevated Temperature. Structural Engineering. pISSN 1226-7988.

Tam C. and Tam V. (2012). Microstructural behaviour of reactive powder concrete under different heating regimes. Magazine of Concrete Research. 64(3), 259–267.

Tam C.M., Tam V. W. Yand Ng K. M. (2010). Optimal conditions for producing reactive powder concrete. Magazine of Concrete Research. 62 (10), pp.701–716.

Tarun R. Naik, Shiw S. Singh, Mohammad M. Hossain. (1995). Properties of high performance concrete systems incorporating large amounts of high-lime fly ash. Construction and Building Materials, Volume 9, Issue 4, August 1995, Pages 195–204

Thomas, M.D.A. (2007). Optimizing the Use of Fly Ash in Concrete. PCA Report IS548, Portland Cement Association.

Toutanji, A. H., and Bayasi, Z. (1999). Effect of Curing Procedures on Properties of Silica Fume Concrete. Cement and Concrete Research. Vol 29(1999), pp. 497-501.

Tritthart, J., & Häußler, F. (2003). Pore solution analysis of cement pastes and nanostructural investigations of hydrated C3S. Cement and concrete research, 33(7), 1063-1070.

U.S. Geological Survey (2015). Cement Statistics and Information - Mineral Commodity Summaries. U.S. Geological Survey. Available at: http://minerals.usgs.gov/minerals/pubs/commodity/cement (Access: 07 May 2015).

Unluer C., Al-Tabbaa A. (2011) Green construction with carbonating reactive magnesia porous blocks: effect of cement and water contents. Future Concrete 2011: 2nd International Conference & the Environmental Construction Exhibition, Dubai, 12-14 December 2011)

Unluer, C., & Al-Tabbaa, A. (2013). Impact of hydrated magnesium carbonate additives on the carbonation of reactive MgO cements. Cement and Concrete Research, 54, 87-97.

Verbeck, G.J., and Helmuth R.A. (1968). Structures and physical properties of cement paste. Proc. 5th Int. Symp. On the Chemistry of Cement, Tokyo, Vol. 3, pp. 1-32.

Vernet C, De´moulian E, Gourdin P, Hawthorn F (1980a). Hydration kinetics of Portland cement. In: 7th International congress on the chemistry of cement, Paris, pp 219–224

Vernet C, De´moulian E, Gourdin P, Hawthorn F (1980b). Kinetics of slag cements hydration. In: 7th International congress on the chemistry of cement, Paris, pp 128–133

Vlaspoulos N., Cheeseman C.R. (2007). Use of Magnesium Oxide-cement binders for the production of blocks with lightweght aggregates. Sustainable Construction Materials and Technologies - Chun, Claisse, Naik&Ganjian (eds). Francis Group, London.

Vollpracht, A., Lothenbach, B., Snellings, R., & Haufe, J. (2016). The pore solution of blended cements: a review. *Materials and Structures*, *49*(8), 3341-3367.

WallingS. A.,KinoshitaH., BernalS. A.,CollieraN. C.,and ProvisJ. L. (2015). Structure and properties of binder gels formed in the system Mg(OH)2–SiO2–H2O for immobilisation of Magnox sludge. The Royal Society of Chemistry, Dalton Trans., 2015, 44, 8126–8137.

Way SJ., Shayan A. (1989). Early hydration of a Portland cement in water and sodium hydroxide solutions: composition of solutions and nature of solid phases. Cem Concr Res 19(5):759–769

WEI Jiangxiong, CHEN Yimin, LI Yongxin (2006). *The Reaction Mechanism between MgO and Microsilica at Room Temperature.* Journal of Wuhan University of Technology - Mater. Sci. Ed. 21(2), p88-91

Whiting, D., and Detwiler, R. (1988). Silica Fume Concrete for Bridge Decks. Report 410, National Cooperative Highway Research Program, Washington, DC, 1988, 107 pp.

Wille K., Naaman A.E., El-Tawil S., Parra-Montesinos G. (2012). Ultra-high performance concrete and fiber reinforced concrete: achieving strength and ductility without heat curing. Materials and Structures. 45, pp. 309-324.

Wille, K., Naaman, A.E., and El-Tawil, S. (2011). Optimizing Ultra-High Performance Fiber Reinforced Concrete. Concrete International, Vol. 33 (9), pp. 35–41.

Yang Y. (2000). Manufacturing Reactive Powder Concrete using common New Zealand Materials. Master Thesis. The University of Auckland.

Yazıcı H., Yardımcı M.Y., Aydın S., Karabulut A.S. (2009). Mechanical properties of reactive powder concrete containing mineral admixtures under different curing regimes. Construction and Building Materials. 23, 1223–1231.

Yu R., Spiesz P., Brouwers H. (2014). Static properties and impact resistance of a green Ultra-High Performance Hybrid Fibre Reinforced Concrete (UHPHFRC): Experiments and modeling. Construction and Building Materials. 68, pp. 158-171.

Yu R., Spiesz P., Brouwers H. (2014). Development of Ultra-high performance fibre reinforced concrete (UHPFRC): Towards an efficient utilisation of binders and fibres. Construction and Building Materials. 79, 273–282

Yu R., Spiesz P., Brouwers H. (2014). Mix design and properties assessment of Ultra-high Performance Fibre Reinforced Concrete (UHPFRC). Cement and concrete research, 56, pp. 29-39

Zdeb T. (2013). Ultra-high performance concrete - properties and technology. Bulletin of the polish academy of sciences technical sciences, Vol. 61 (1), 183-193.

Zhang T., Vandeperre L., Cheeseman C. (2011). Development of Magnesium Silicate Hydrate cement system for nuclear waste encapsulation. NUWCEM 2011: 1st International Symposium on Cement-based Materials for Nuclear Wastes, France – Avignon – 11 to 14 October, 2011. Vol 44, Issue03. Available at: https://inis.iaea.org/search/searchsinglerecord.aspx?recordsFor=SingleRecord&RN=44011470

Zhang T., Vandeperre L., Cheeseman C. (2014). Formation of magnesium silicate hydrate (M-S-H) cement pastes using sodium hexametaphosphate. Cement and Concrete Research 65 (2014) 8–14

Zhang, T., Cheeseman, C., & Vandeperre, L. J. (2012). Characterisation of corrosion of nuclear metal wastes encapsulated in magnesium silicate hydrate (M-S-H) cement. Ceramic Materials for Energy Applications II, 159-167.

CHAPTER 3
MATERIALS CHARACTERIZATION AND TESTING METHODS

Preamble

This chapter outlines the characteristics of materials and experimental methods used in the research project. The materials characterization includes chemical composition, morphology properties such as particle size distribution, particle shape and texture. The crystal or amorphous structures of materials are also investigated. It is known that material characteristics are directly related to the material reactivity, which will influence the reaction rate to form the binding phases of cement. The particle size, shape, texture and porosity also play important roles in fresh properties of concrete such as water demand, flowability, and viscosity. Achieving good workability with low mixing water content is desirable for cementitious materials to achieve high strength and durability.

The experimental results such as physical and chemical properties of the raw materials alongside the mechanical and durability properties are highly dependent on the testing methods. In this study, the experimental methods used to analyze the materials either complied with the current standards or where suitable standards were not available the tests were based on widely accepted non-standard techniques considered reliable in studies of cementitious materials.

3.1. MATERIAL SOURCES AND PROPERTIES

3.1.1. Binder constituents

Reactive MgO

M-S-H binder systems generally consist of reactive magnesium oxide and amorphous silica. Reactive MgO, obtained from magnesium carbonate, is calcined at temperatures of 700-1000 ^{o}C, which is very different from other two groups of MgO including hard-burned MgO (calcined at 1000-1400^{o}C) and dead-burned MgO (calcined at 1400-2000^{o}C). It is known that calcining temperatures have a large influence on the hydration of MgO (Fang, 2004; Aphane, 2009). The low calcination temperatures result in an amorphous microstructure and thus lead to the high reactivity of the light-burned MgO which is suitable for developing M-S-H cement. An increase of calcination temperature generally increases crystallinity and decreases the reactivity of MgO,

which might be detrimental to M-S-H binders as the large volume expansion often occurs at late ages.

The effect of different sources of MgO on the M-S-H binders has been reported in the literature (Jin et al., 2013). Therefore, only one source of light burnt magnesium oxide, calcined at temperatures of approximately 700°C was selected for this study. The highly reactive MgO was provided by Calix (Australia) with a particle size d_{50}=9μm.

Amorphous silica

Amorphous silica has been widely used as supplementary cementitious materials (SCMs) to improve mechanical and durability properties of the PC concrete. Replacement of PC with a source of SCMs generally results in the generation the additional binding phase C-S-H and an increases strength. The effects of SCMs depend on the type and amount of silica in the mix. Although silica fume and fly ash are among the most commonly used SCMs, other sources of silica such as natural pozzolan or agricultural waste (eg. rice husk ash) are increasingly used for similar purposes to develop sustainable building materials.

Numerous studies on the effect of SCMs in PC concrete have been found in the literature but few experiments have been carried out with M-S-H binders. For this reason, four sources of reactive silica were sought to compare their cementitious properties in M-S-H binders. Chemical compositions of the materials are presented in Table 3.1.

- Silica fume (SF) was supplied by SIKA NZ. The material (commercial name is SIKAFUME) is in condensed form including agglomerates of particle size d_{50}=100μm although the individual silica fume particles have particle size d_{50}=0.1 μm.
- Microsilica 600 (MS), a natural amorphous silica source, was quarried from a local site in New Zealand and marketed by Microsilica New Zealand Ltd (2017).
- Rice husk ash (RHA) is a source of highly reactive silica produced from raw rice husk, an agricultural by-product. The husk is converted into ash during a controlled firing process under the optimal temperature of 600-700°C (Chandra, 1996). The selected RHA, which was supplied by Guru Metachem (India), contains > 90 % amorphous silica.
- Fly ash (type F), supplied by a specialist merchant in New Zealand, was used to examine the effect of silica reactivity to cementing properties of M-S-H binders.

3.1.2. Aggregate

Aggregates were sourced locally. River sand (max particle size of 4.75 mm, finess modulus (FM) = 2.33) which is primarily siliceous in nature was prepared to meet the requirements of ASTM C33.

The sand used for mortar mixtures was sieved to a maximum particle size of 2.36 mm. Smooth and rounded stone used for concrete has maximum aggregate size of 16 mm.

Quartz sand (S) is used as aggregates for high strength mortar mixtures. Quartz filler (QF) is ground quartz sand using a ring mill to achieve desired particle size.

3.1.3. Portland cement

Control samples were prepared with a general purpose Portland cement provided by Holcim New Zealand.

3.1.4. Superplasticizer

As one of the most significant disadvantages of M-S-H binders using silica fume was the very poor workability due to the inclusion of high silica fume content, most previous studies of M-S-H binders used high w/c ratios of 0.50 or above even with the presence of superplasticizers (Wei et al., 2006l Jin and Al-Tabbaa, 2014; Walling et al., 2015). In this study, Viscocrete-5-555, a third-generation polymer-based superplasticizer supplied by Sika (New Zealand) was used and provided extremely high water reduction for M-S-H binder systems. Workable mixtures were achieved with w/c as low as 0.40.

3.1.5. Particle size distribution

Particle sizes of the binder constituents, PC and quartz filler were determined by LA-950 Laser diffraction analyzer. In addition, a scanning electron microscope (SEM) was used to determine individual silica fume particle sizes. A sieving method was used to obtain particle sizes for normal sand and coarse aggregates.

Particle size distributions of binder constituents (MgO and SCMs) are shown in Figure 3.1. Silica fume is an ultrafine material. Observation by SEM shows that conglomerates of condensed silica fume actually contain individual spherical particles having particle sizes of <0.1μm-5 μm. MS is natural pozzolan ground to high fineness to increase reactivity with particle sizes in the range of 0.4-75 μm. FA and RHA have larger particle sizes than MgO, SF and MS. Therefore, FA generally has lower activity than SF and MS. RHA had larger particle size than SF and MS, however, the reactivity of RHA is controlled by its microstructure which is very porous as shown in the SEM images. The activity of rice husk ash will be studied through experimental programmes.

Table 3.1. Chemical compositions of MgO and silica sources

Sample	**SiO_2**	**TiO_2**	**Al_2O_3**	**Fe_2O_3**	**MnO**	**MgO**	**CaO**	**Na_2O**	**K_2O**	**P_2O_5**	**LOI**	**SO_3**	**Total**
	(%)	**(%)**	**(%)**	**(%)**	**(%)**	**(%)**	**(%)**	**(%)**	**(%)**	**(%)**	**(%)**	**(%)**	**(%)**
M (MgO)	11.36	0.02	0.57	0.33	0.02	71.67	4.06	0.13	0.13	0.02	11.67	-	99.98
SF (Silica fume)	88.18	<0.01	0.62	1.39	0.14	3.28	0.93	0.85	2.67	0.22	1.66	-	99.92
MS (Microsilica)	85.14	0.95	6.31	0.41	0.01	<0.05	0.13	0.29	0.77	0.07	3.96	-	98.04
FA	49.87	1.04	21.88	7.78	0.06	2.54	8.91	0.50	1.20	0.20	3.31	1.50	98.79
RHA	92.62	0.05	0.61	0.31	0.02	0.19	0.41	0.33	0.90	-	3.46	-	98.90

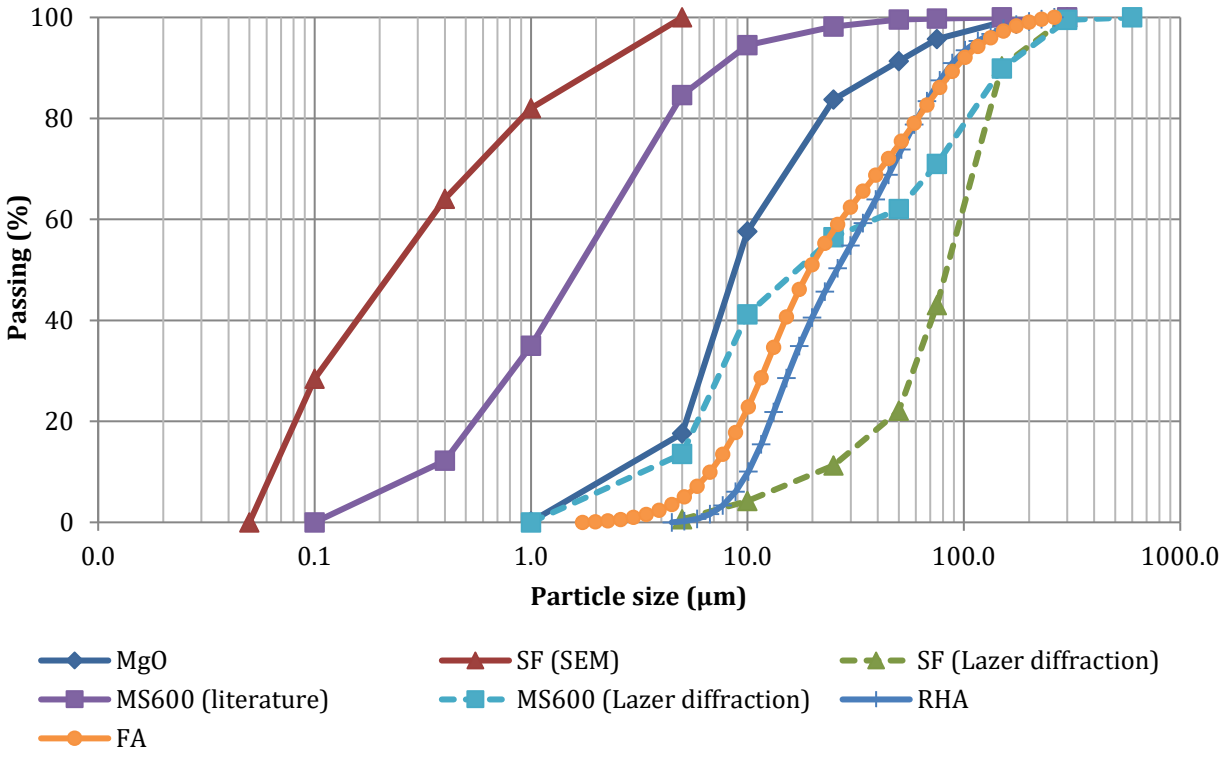

Figure 3.1. Particle size distributions of MgO and SCMs

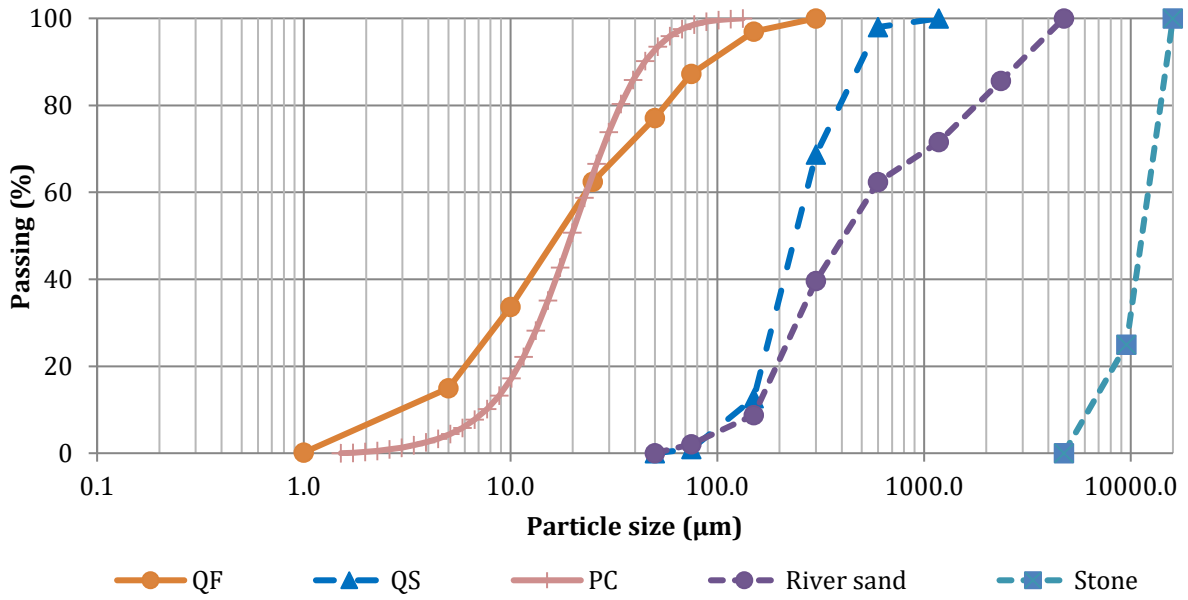

Figure 3.2. Particle size distributions of PC, filler and aggregates

Figure 3.2 shows the particle sizes of PC, crushed quartz fillers and aggregates. It can be seen that the particle size of the PC is somewhat larger than MgO, SF and MS. The M-S-H binder contains high amounts of MgO and SF/MS and the fineness of those main binder constituents greatly influences the amount of mixing water and the workability of the mixture. For this reason, the use

of crushed quartz fillers was used to reduce the water demand and improving workability caused by microfine particles of M-S-H binders. Quartz sand was ground to the high fineness with ring mill equipment. The particle size of crushed quartz fillers was close to PC.

3.1.6. **Morphology and texture**

SEM was used to examine morphology (particle size, shape and texture) of the raw materials which is expected to have a significant influence on the fresh properties (workability) and the packing density of the resulting cementitious materials. Figure 3.3 – 3.8 present the SEM images of the raw materials.

Morphology of MgO shows angular particle shape and rough surface. The different silica sources had very different characteristics of particle size, shape and texture. Silica fume with its ultrafine particle size may increase the amount of mixing water when used with significant quantities. MS includes very fine particles without roundness, so it is necessary to consider the adverse effect on workability. SEM images of RHA present large pores in the microstructure. The high specific surface area resulted from this very high porosity might increase reactivity but also potentially requires high water demand. As for fly ash, it can be seen that the coarse particle size and roundness are desirable for workability, however, the large particle size can reduce the reactivity.

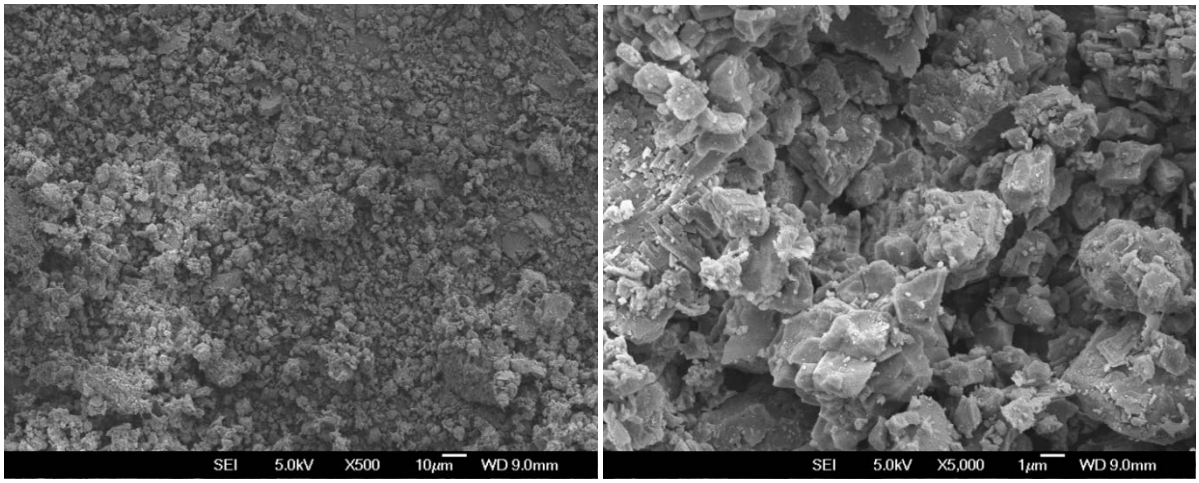

(a): x500 (b): x5000

Figure 3.3. SEM images of reactive MgO

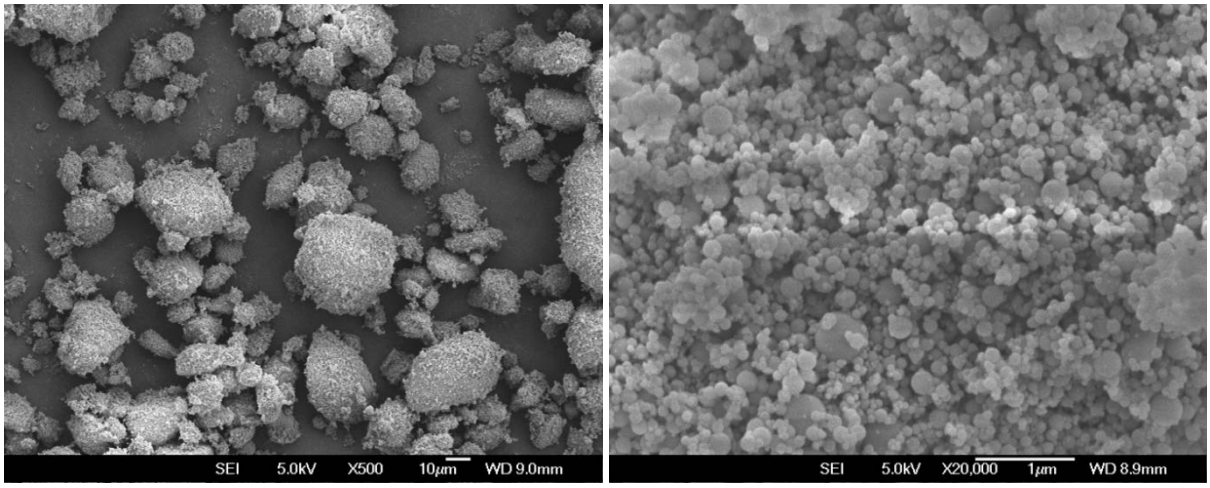

(a): x500 (b): x20000

Figure 3.4. SEM images of reactive SF

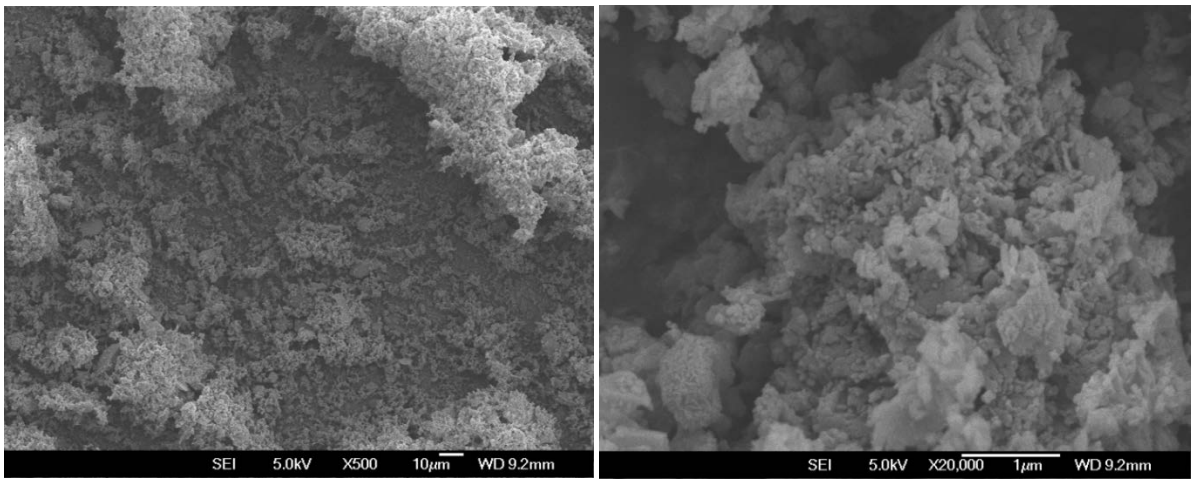

(a): x500 (b): x20000

Figure 3.5. SEM images of reactive MS

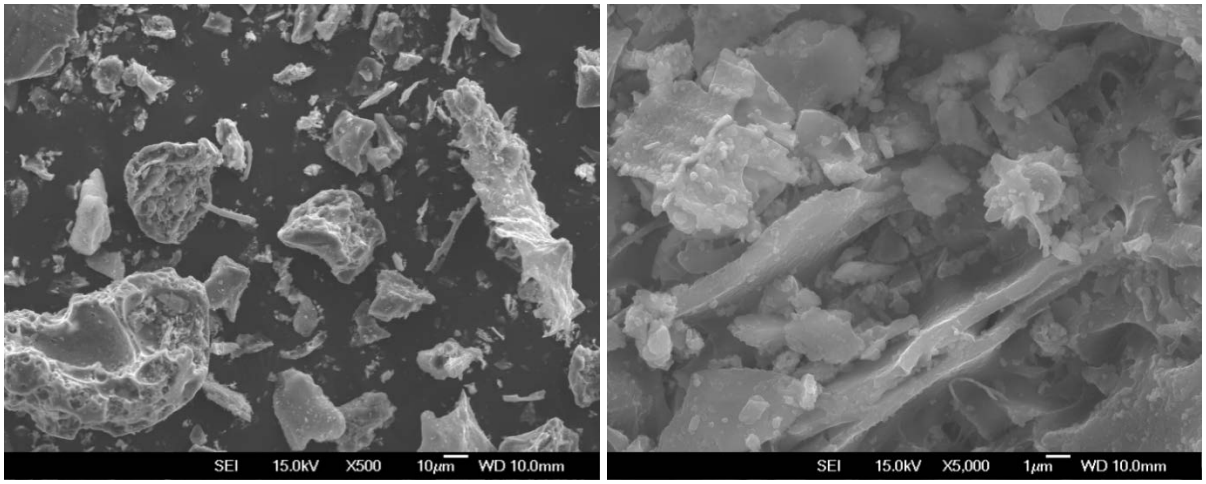

(a): x500 (b): x5000

Figure 3.6. SEM images of reactive RHA

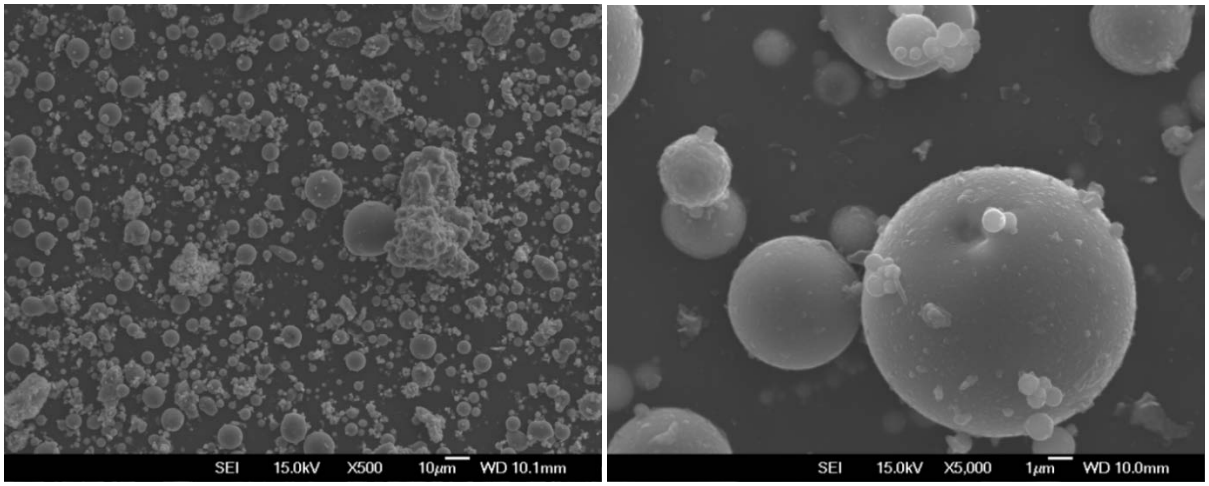

(a): x500 (b): x5000

Figure 3.7. SEM images of reactive FA

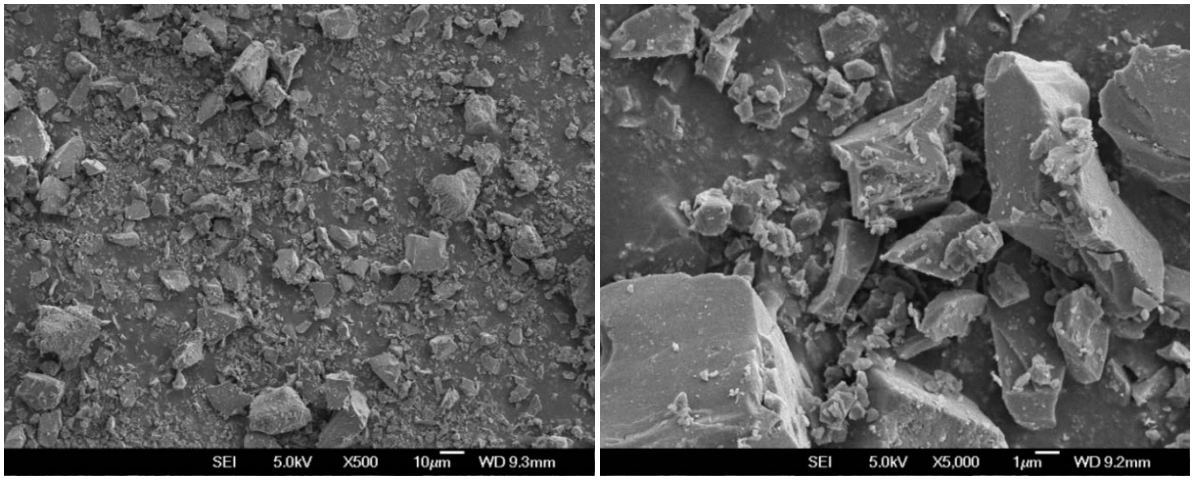

(a): x500 (b): x5000

Figure 3.8. SEM images of quartz filler (QF)

3.1.7. **XRD spectra**

The XRD analysis uses a Philips PW1729 X-ray diffractometer (Cu, 50 kV/40 mA) with a 3 to 70° 2θ scan range to characterize XRD spectra of the raw materials. XRD method is useful to determine the chemical composition of the material sources.

Figure 3.9 presents the XRD spectrum of reactive MgO used in this study. The reactive magnesia has three XRD peaks at 2θ ~37°, 43° and ~62°, however, it also contains a considerable amount of impurities including quartz and calcite.

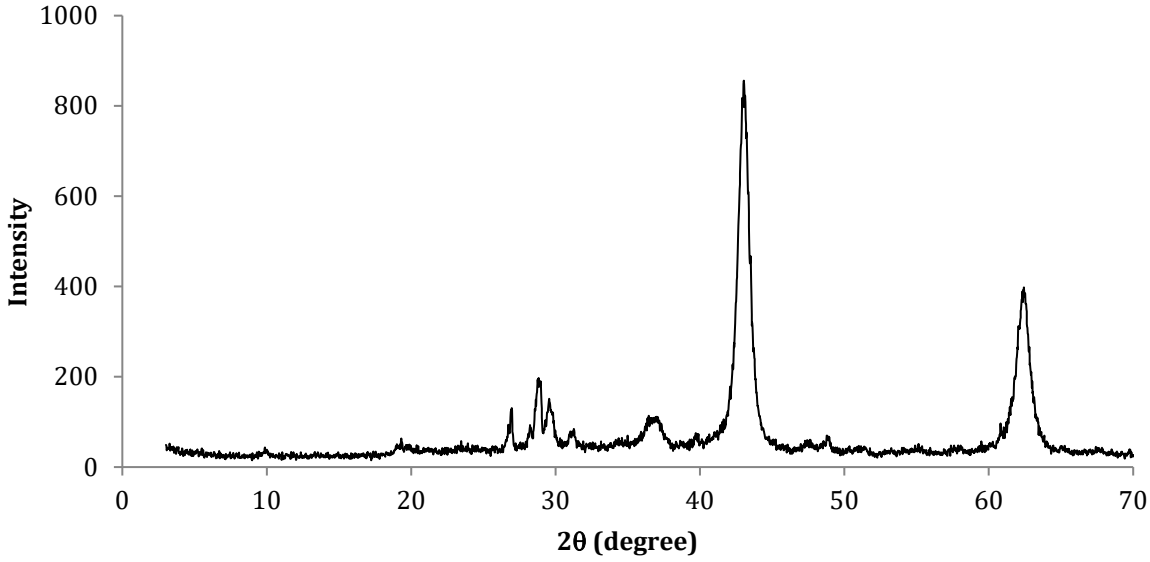

Figure 3.9. XRD spectra of the raw materials (MgO)

Figure 3.10 – 3.13 show XRD spectra of four silica sources including SF, MS, RHA and FA. It is known that amorphous silica is characterized by a broad peak at 2θ ~21° (Brew and Glasser, 2005; Ono and Wada, 2007) and all silica sources show this feature, which indicates the potential use of these materials to develop M-S-H binders. Nonetheless, the intensities of the peaks are very different for each silica source. The high quality amorphous structure of SF and RHA can be seen by the significant broad peaks of non-crystalline silica. MS is less pure than SF with respect to amorphous silica content, showing other peaks of impurities including crystalline silica with XRD peaks at 2θ ~ 21°, 27° and 30°. FA has expected to have a lower reactivity compared to other silica sources due to the low intensity of the peak of amorphous silica. The XRD of FA has shown the peaks of other impurity elements which account for a considerable proportion of the material, including: aluminum oxide, ferrous oxide, calcium oxide and quartz. The inclusion of a high content of impurities is expected to have a major influence on the reaction rate of MgO and FA and the quantity of resulting binding phases of the binders.

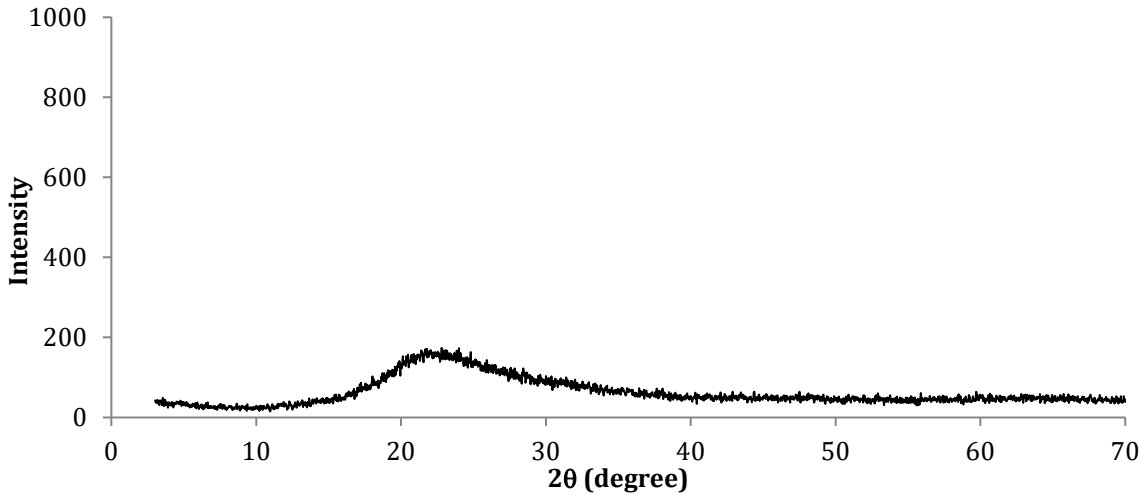

Figure 3.10. XRD spectra of the raw materials (SF)

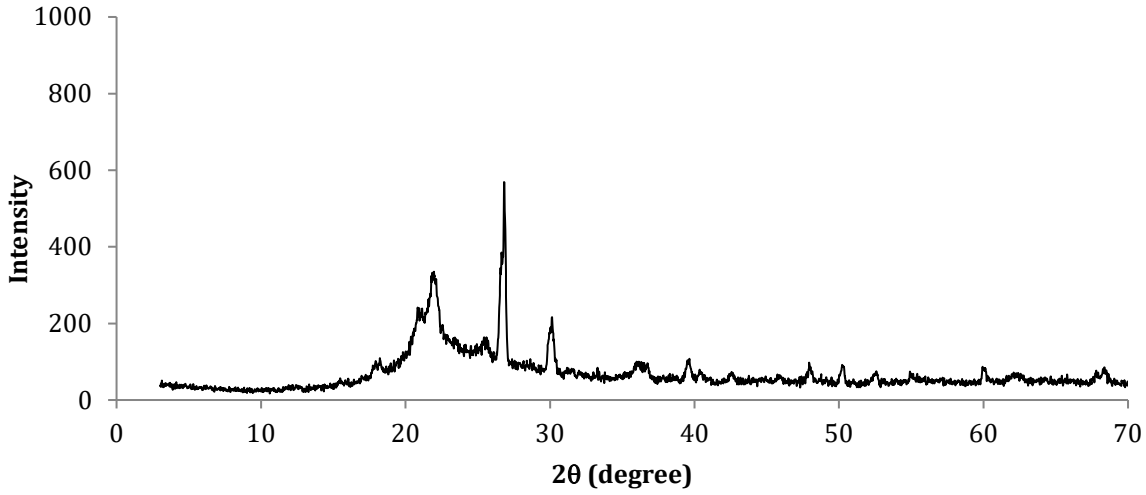

Figure 3.11. XRD spectra of the raw materials (MS)

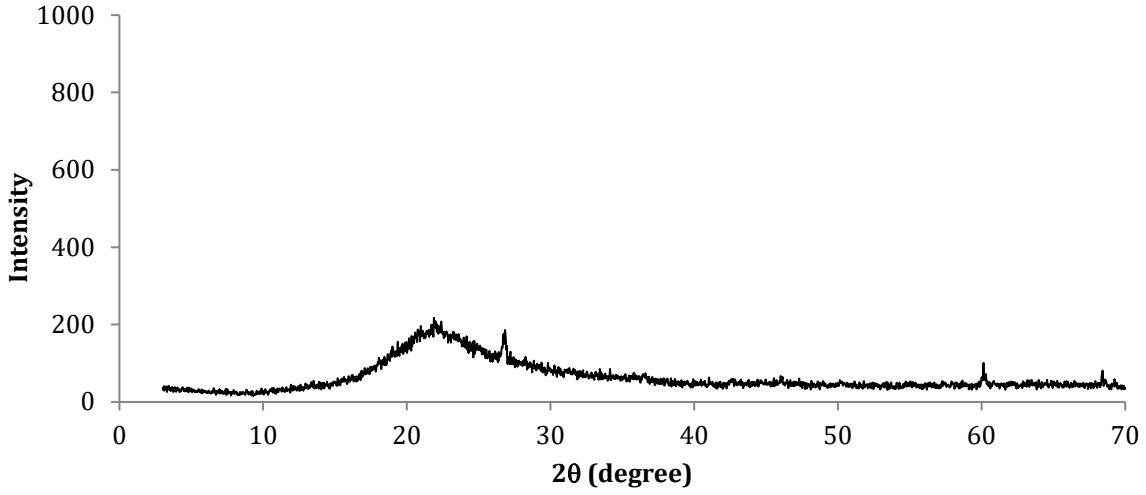

Figure 3.12. XRD spectra of the raw materials (RHA)

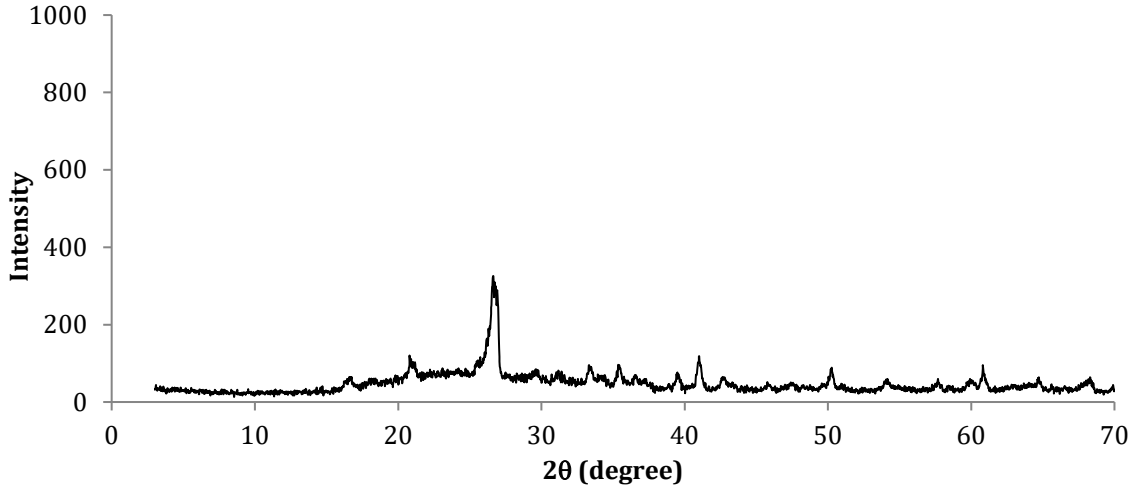

Figure 3.13. XRD spectra of the raw materials (FA)

3.2. TESTING METHODS

3.2.1. Flow test

The flow test measures the spread of a mixture by determining the mean diameter of a test sample compared to the original size of the mixture in the cone. The spread of the mix is an indication of the plasticity of the mixture which will affect the workability and rheology behavior of the mixture.

The flow test is performed following ASTM C1437 testing method. Fresh M-S-H paste/mortar is placed in the standard mold (50 mm in height, 70 mm internal top diameter, 100 mm internal base diameter) in two layers where each 25mm layer being tamped 20 times with the tamper. The mould is held firmly in place during this operation. The excess mortar is removed from the top of the mould with the trowel by a sawing motion to keep the top surface leveled. Wipe the table top and the area around the base of the mould clean. The mold is lifted up slowly away from the paste/mortar within 1 minute after completing the mixing operation and the table is immediately jolted 25 times in 15 s. Flow value of the M-S-H mixture is the increase in average base diameter of the mixture, expressed by percentage of the original base diameter. The measured value (in/mm) can be used as an alternative where necessary.

The main apparatus includes flow table, flow mold conforming to the requirements of ASTM C 230.

Figure 3.14. Apparatus for flow test of cement paste/mortar

3.2.2. Compressive strength test

Cement paste and mortars

The compressive strengths of cement paste and mortar are determined following the procedure specified in ASTM C109 designation using 2-in. (50mm) cube specimens, except that the mix proportions, water content and curing regimes are modified for different testing purposes.

The paste/mortar mixtures were mixed with an electrically driven Hobart mixer. Within 2 min and 30 s after completing mixing operation, the paste/mortar is placed in the molds. The mortar is filled in two layers of 25mm each and tamped for 32 times in 10 s in 4 rounds on the operating vibration table. After filling and tamping the molds were vibrated for 2 min to remove air bubbles. Immediately upon completion of molding, the specimens were stored in a moist chamber for 24 hours – 72 hours before demolding for different curing regimes until tested.

Three specimens from a batch of mortar are made for each test age. The cubes are tested with a compressive testing machine in which the load is applied to a face against the steel face of the mould. The loading capacity is 3000 kN and the loading rate is applied at 1-2 kN/s until failure within a time period of thirty to ninety seconds. The compressive strength is recorded to the nearest 1.0 N and the mean result reported to the nearest 0.1 N/mm^2 by the following formula:

$$fm = \frac{P}{A}$$

where:

fm = compressive strength in MPa

P = total maximum load in N

A = area of loaded surface in mm^2

Figure 3.15. Compressive test machine (Servo Plus Evolution Model)

Cylindrical concrete specimens

A Standard Test Method for Compressive Strength of Cylindrical Concrete Specimens is performed as per ASTM C39. The axial compressive load is applied to the cylindrical specimen until rupture occurs. The compressive strength is calculated by dividing the maximum load by the cross-section area:

$$S = \frac{P}{A}$$

S = compressive strength, MPa

P = total maximum load, N, and

A= cross-section area, mm^2

The testing machine has loading capacity of 3000 kN, loading rate is set at 2-3kN/s.

3.2.3. Split tensile test

Due to the complication of direct tensile strength test, the split tensile test was performed instead. The split tensile strength testing procedure was performed in accordance with the ASTM standard C496. Cylindrical concrete specimens are used for the test. The nominal diameter and length of the specimens are 100mm x 200mm. During the test, a diametral compressive force is applied along the length of the specimen until failure occurs. Two thin, plywood bearing strips are placed between the specimen and both the upper and lower bearing blocks of the testing machine to distribute the compressive load applied along the length of the cylinder.

Figure 3.16. Test setup for split tensile strength

The maximum load at failure of the sample is recorded to calculate the split tensile strength. The tensile stress which is acting in a direction perpendicular to the line of applied loading is given by the formula, following the equation:

$$T = \frac{2P}{\pi d d}$$

where:

T = splitting tensile strength, MPa

P = maximum applied load indicated by the testing machine, N

l = length, mm, and

d = diameter, mm.

3.2.4. Static Modulus of Elasticity

The static modulus of elasticity (MOE) of the M-S-H concrete specimens is determined using ASTM C469 test procedure with 100 mm x 200 mm (4 in. x 8 in.) cylindrical specimens.

Prior to performing the test, companion cylinder specimens were used to determine the compressive strength of the concrete according to the ASTM C39 test method. Subsequently, cylindrical specimens were instrumented to measure the static elastic modulus by the indicated stress and strain calculated from recorded load and deformation.

A compressometer was used for determining the modulus of elasticity using an unbonded sensing device that measures to the nearest 5 millionths the average deformation. The specimen, with the strain-measuring equipment attached, is then placed on the lower platen or bearing block of the testing machine. The applied loads and longitudinal strains at specified points was recorded without interruption of loading until the applied load was equal to 40 % of the ultimate load. The longitudinal strain is defined as the total longitudinal deformation divided by the effective gauge length.

Figure 3.17. Test setup for static modulus of elasticity

The modulus of elasticity is calculated to the nearest 200 MPa as follows:

$$E = (S_2 - S_1)/(\varepsilon_2 - 0.000050)$$

In which:

E = chord modulus of elasticity, MPa

S2 = stress corresponding to 40 % of ultimate load,

S1 = stress corresponding to a longitudinal strain, ε1, of 50 millionths, MPa, and

ε2 = longitudinal strain produced by stress S2.

3.2.5. **Oxygen Permeability**

The Oxygen Permeability Test was performed to the ease with which a gas (oxygen) can penetrate through the concrete. The Oxygen Permeability Index (OPI), determined from the test data, is related to the durability of the testing concrete.

The test used a falling head permeameter to apply an initial pressure to a concrete sample in which the pressure was allowed to decay as permeation proceeds. The faster reduction rate of pressure indicates the more gas (oxygen) permeability and possibly less durability of the concrete.

Each test procedure required preparation of 4 specimens at the age of 28 days in which each specimen consisted of a 100 mm diameter concrete disc with a thickness of 30± 2 mm. The sample was inserted in a compressible rubber collar, placed in the upper cell and then compressed so that

no gaps should be visible between the sides of the test specimen and the collar. The initial pressure was set as 100 kPa and the permeability test was terminated as the pressure reduced to 50 kPa or after 6 hours.

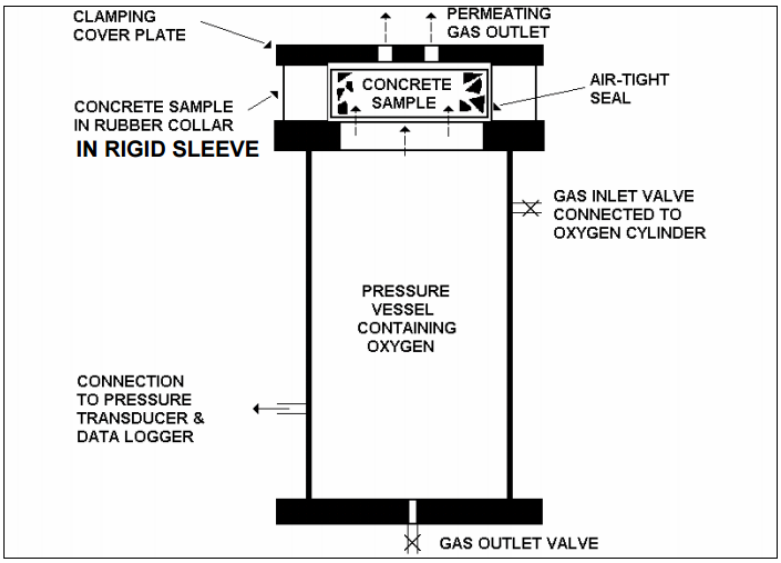

Figure 3.18. Permeability cell arrangement (Alexander, 1999)

The calculation of OPIs requires determining pressure decay curve which is plotted in the form of the logarithm of ratios of pressure over the time. The first step is to determine the D'arcy coefficient of permeability which is given by:

$$k = \frac{\varpi V g d}{R A \theta} \ln \frac{P_0}{P}$$

Where:

k = coefficient of permeability of test specimen (m/s)

ω = molecular mass of oxygen = 32 g/mol

V = volume of oxygen under pressure in permeameter (m3)

g = acceleration due to gravity (9.81 m/s2)

R = universal gas constant = (8.313 Nm/K mol)

d = average specimen thickness (m) to the nearest 0.02 mm

A is the cross sectional area of the specimen, in square meters

θ= absolute temperature (K)

The oxygen permeability index (OPI) is taken as the negative log of the average of the coefficients of permeability of the tested specimens, which is determined by the following equation:

OPI = - log10 [¼ (k1+k2+k3+k4)]

The calculated OPI can be used as an indicator of the durability of the concrete, based on the classification shown in Table 3.2.

Table 3.2. Suggested ranges for durability classification using index values (Alexander et al., 1999)

Durability Class	OPI (log scale)
Excellent	>10
Good	9.5 - 10
Poor	9.0 - 9.5
Very poor	< 9.0

Examples of OPI of PC concrete are shown in figure 3.19 to illustrate the effects of curing conditions on the durability of the PC concrete. The wet curing in conventional Portland cement concrete enhances the hydration process to facilitate the formation of binding phases and improves the microstructure of cement pastes, as opposed to the effect of dry curing regime. Accordingly, the wet-cured samples have a denser microstructure and low coefficient of permeability represented by higher OPI index of 10.15. On the other hand, a porous microstructure results in higher coefficient of permeability or lower OPI index of 9.50.

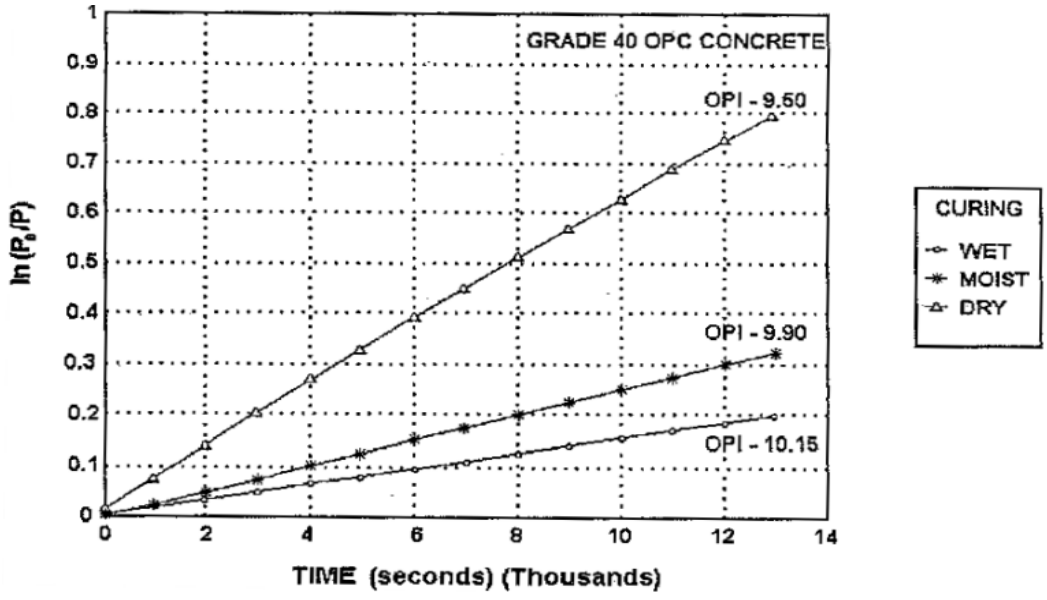

Figure 3.19. OPI of PC concrete at different curing conditions (Alexander et al., 1999).

3.2.6. **Resistivity Test**

The resistivity test provides a rapid indication of the likely penetration of chloride ions and reinforcing corrosion resistance of concrete. This test is faster to run compared to the Rapid Chloride Ion Permeation Test (RCPT) as specified in ASTM C1202 however it also presents high correlation with RCPT (Gudimettla and Crawford, 2015). A linear relationship between concrete electrical conductivity and corrosion rate has been found in previous studies (Bertolini 1997, Carino 1999, Alonso 1988, Andrade 1996, Gulikers 2005). The resistivity test is used to evaluate the electrical resistivity of M-S-H samples from the early age of 7 days to a long-term curing duration up to 365 days.

The resistivity test reused the same samples tested for oxygen permeability. After re-drying to a constant mass the samples were soaked in 3.5% NaCl solution in 22 h until saturated, the resistivity was measured from the applied voltage and corresponding current across the sample:

$$R = \left(V/I\right) \times \left(A/d\right)$$ (kOhm.cm)

V = applied voltage (mV)

I = current at 1 min (μA)

A = cross sectional area of the specimen (cm2)

d = average specimen thickness (cm)

Figure 3.20. Resistivity test arrangement (Tarig, 2016)

3.2.7. Porosity

Porosity presented by percent voids in hardened cementitious materials was determined as per ASTM C 642 with some modifications. The sizes of test specimens are 50x50x50mm (paste and mortar) and 100x100x100mm (concrete). The calculation of porosity requires the determination of oven-dry mass, saturated mass and apparent mass submerged in water. Instead of submerging specimens in boiling water as specified in ASTM C642, vacuum pressure was applied to remove the entrapped air in the oven-dried samples before saturating samples in water at approximately 21^{o}C. The porosity was calculated as the volume of permeable pore space voids:

$$P(\%) = (C - A) / (C - D) \times 100$$

where:

A = mass of oven-dried sample in air, g

C = mass of surface-dry sample in the air after vacuum pressure application and immersion, g

D = apparent mass of sample in water after vacuum pressure application and immersion, g

3.2.8. SEM analysis

The Scanning Electron Microscope (SEM) has been utilized extensively in material engineering for analysis of particle size, shape, texture (morphology), and material composition. An SEM is consist of an electric gun to produce electron beams, a system of lens, specimen stage, secondary electron detector and a display unit as described in figure 3.21.

The operation principle of SEM is the irradiation of specimens with a fine electron beam (electron probe) from an electric gun. The electron probe is adjusted and focused by a system of condenser and objective lens before reaching the specimen. As scanned with the electron probe, secondary electrons are emitted from the specimen surface. The secondary electrons are detected and analyzed by a secondary electron detector. The detector comprises of a collector and scintillator applied with a high voltage to attract secondary electron to general light and convert the light into electrons through a photo-multiplier tube (PMT) before amplifying these electrons to electric signals to produce SEM images (figure 3.22). The resolution of the SEM is dependent on the size of the electron beam convergence and the interaction between surface materials and electrons.

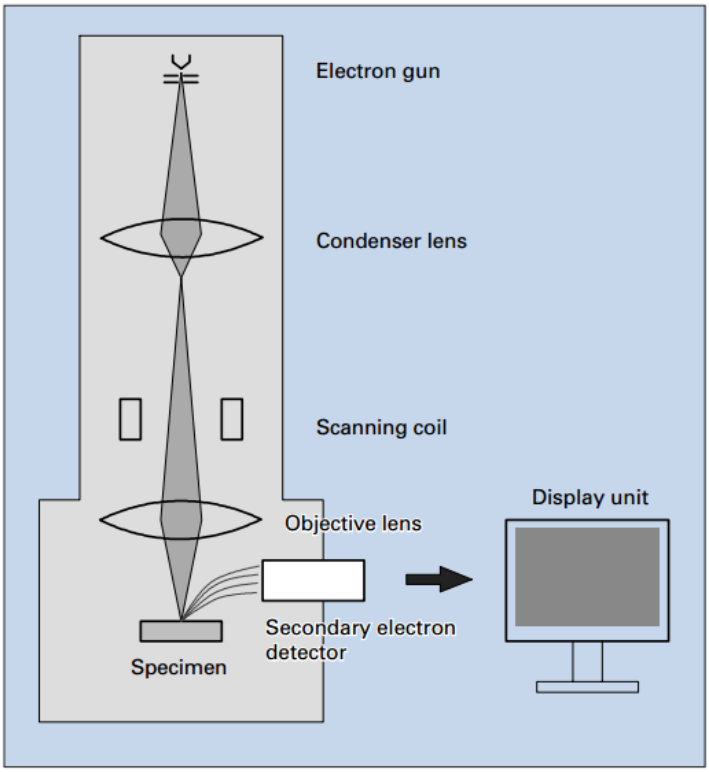

Figure 3.21. Construction of an SEM (JEOL, 2015)

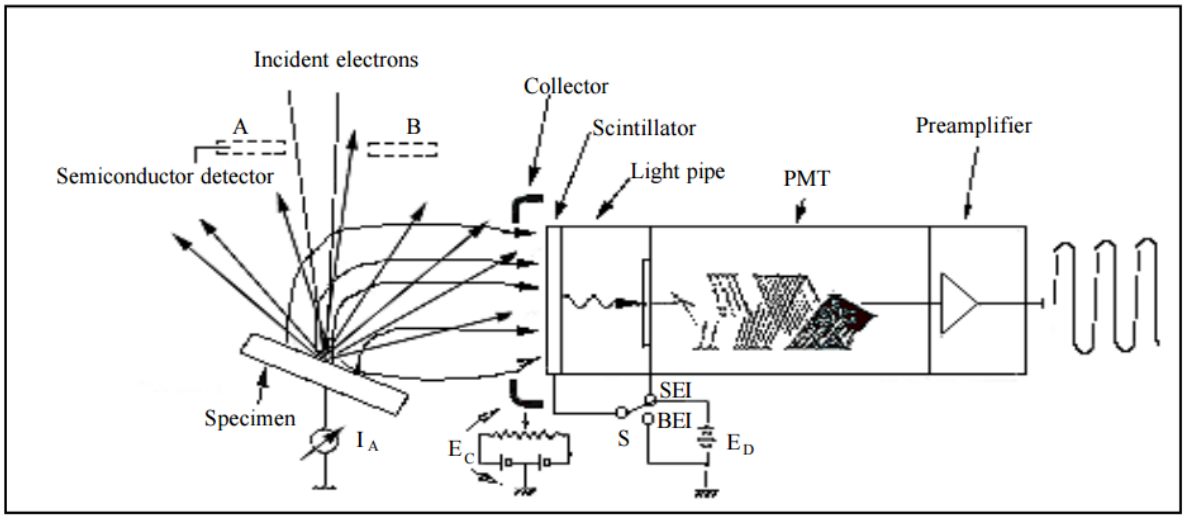

Figure 3.22. Secondary electron detector (JEOL, 2015)

A high resolution Scanning Electron Microscope equipment model JEOL JSM 7000F was used in the study to analyze topography of the materials (figure 3.23). The EDS function of the equipment allows detecting and quantifying compositions of the hydration products of the M-S-H cementitious materials.

Figure 3.23. SEM equipment (JEOL) at University of Canterbury

3.2.9. **XRD analysis**

XRD provides information on interatomic distances, bond angles and the main use of this method is to identify chemical composition in a specimen by a search/match procedure. When X-rays interact with a crystalline substance, the diffraction pattern of the substance is obtained and by comparing the powder diffraction to the standard data, the composition in a testing sample can be identified.

XRD equipment was used to identify the chemical composition of M-S-H pastes. The X-ray production uses Cu target metal, wavelength λ (Cu kα) = 1.54 Å and the angle increases from 10-70°C. The d-spacing is a function of 2θ from Bragg's law:

$$d = \lambda / 2\sin\theta$$

Peak positions related to d-spacings and lattice parameters characterize the phases in M-S-H hydration products. Also, each component in the sample is quantified by the relation to the areas under the peaks of each phase plotted in the XRD diffraction spectra. The development of hydration products was monitored by XRD using a Philips PW1729 X-ray diffractometer (Cu, 50 kV/40 mA) with a 3 to 70o 2θ scan range.

3.2.10. **Pore solution analysis**

The pore solution expression technique was first introduced by Longuet et al. (1973) using mechanical pressure to extract pore solution from cementitious materials (figure 3.26). The method has since been applied to study compositions of the pore solutions for specific ions to understand the hydration processes and durability of Portland cement pastes, mortars and blended cement.

A pore press apparatus (PPA) was produced as shown in figure 3.27. The equipment consists of a die body of two concentric thick-walled steel cylinders close fit together. The die body rests on a steel base in which both components were ground to be exactly on a level plane to allow even pressure transfer across the body of the equipment. The test sample was placed inside the inner cylinder and a polymer disk was placed on top of the sample followed by a steel piston to which compressive load was applied. The load was increased gradually to extract pore solution which was drained and collected via a groove ring in the base.

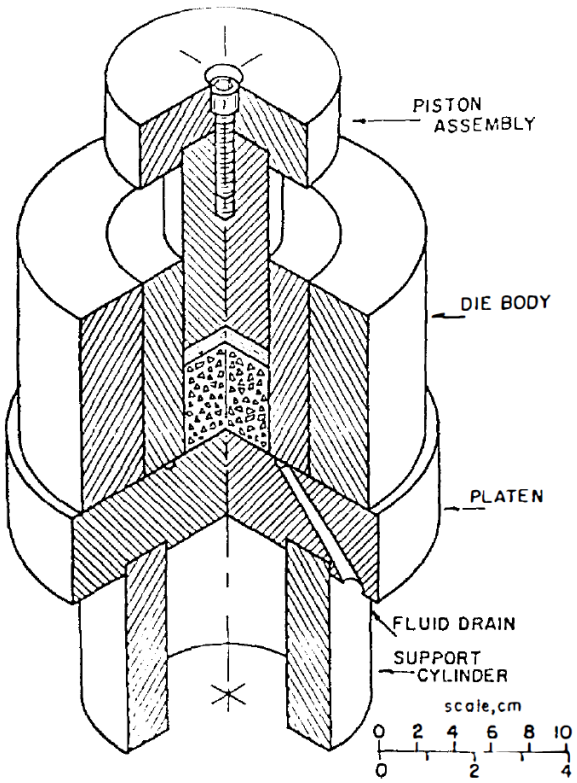

Figure 3.24. Schematic design of pore press expression apparatus (Barneyback and Diamond, 1981)

Figure 3.25. Pore press apparatus set up

Each sample was placed in the pore solution expression apparatus and loaded to 400 MPa at a rate of 0.25 MPa/s (taking about 25 min) and then held at this pressure for 30 seconds. The total volume of expressed pore solution was recorded and pH was measured within 1 h of collection using a digital pH meter (Figure 3.28). The collected pore solution was sealed in a container to prevent reaction with atmospheric carbon dioxide and stored under -18^{o}C temperature prior to analysis. ICP-MS method was used to analyze the ion concentrations of the solutions with a dilution factor between 500-2000 due to the detection limit of the analytical method.

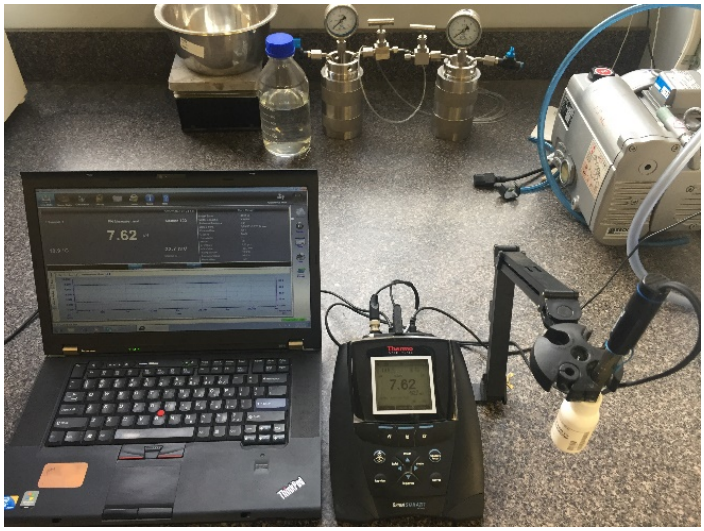

Figure 3.26. pH meter

3.3. CONCLUSIONS

Each MgO and amorphous silica source used for M-S-H binders had distinct physical and chemical properties. The material sources influence both fresh and hardened characteristics of the cement paste, mortar and concrete and will lead to very different material properties of the resulting binders such as reaction mechanism, strength and microstructure.

For M-S-H binders, MgO and silica are the main constituents accounting for 40-60% of the binder compositions and therefore the material sources will have significant impact on the formation of binding phases. Different characteristics of the raw materials including chemical composition, particle size, shape, texture and porosity play a key role in the variability of M-S-H binders. Results of experimental programmes are presented in the next chapters to discuss these effects of materials on the properties of M-S-H binder systems.

Experimental methods are of utmost importance to obtain accurate results of the physical and chemical properties of testing materials. A number of different experimental methods were used to provide comprehensive results on the material properties. The combination of various testing methods and equipment such as Lazer diffraction, SEM, XRD was able to provide accurate results on the chemical composition, microstructure and morphology images of ultrafine materials used in this study. Standard testing methods were used to determine mechanical properties of materials such as compressive strength, tensile strengths and elastic modulus. Some non-standard testing methods such as oxygen permeability test, pore solution extraction and ion concentrations analysis allow analyzing important durability properties such as pH development and identifying chemical reactions mechanism for studying and developing M-S-H binder systems.

3.4. REFERENCES

Alexander MG, Mackechnie JR and Ballim Y (1999) Guide to the use of durability indexes for achieving durability in concrete structures. Research monograph 2.

Alonso C, Andrade C, and Gonzalez J.A. (1988). Relation between resistivity and corrosion rate of reinforcements in carbonated mortar made with several cement types. Cement and Concrete Research, Vol. 18, no. 5, pp. 687–698.

Andrade C. and Alonso C. (1996). Corrosion rate monitoring in the laboratory and on-site. Construction and Building Materials, Vol.10,no.5,pp.315–328.

Aphane, M. E. (2009). The hydration of magnesium oxide with different reactivities by water and magnesium acetate (Masters dissertation). University of South Africa

ASTM (2001) C 39: Standard test method for compressive strength of cylindrical concrete specimens. ASTM International, West Conshohocken, PA, USA.

ASTM (2002) C 469: Standard test method for static modulus of elasticity and Poisson's ratio of concrete in compression. ASTM International, West Conshohocken, PA, USA.

ASTM (2004) C 496: Standard test method for splitting tensile strength of cylindrical concrete specimens. ASTM International, West Conshohocken, PA, USA.

ASTM (2006) C 642: Standard test method for density, absorption, and voids in hardened concrete. ASTM International, West Conshohocken, PA, USA.

ASTM C109 / C109M-02, Standard Test Method for Compressive Strength of Hydraulic Cement Mortars (Using 2-in. or [50-mm] Cube Specimens), ASTM International, West Conshohocken, PA, 2002, www.astm.org

ASTM C1437-15, Standard Test Method for Flow of Hydraulic Cement Mortar, ASTM International, West Conshohocken, PA, 2015, www.astm.org

ASTM C33 / C33M-18, Standard Specification for Concrete Aggregates, ASTM International, West Conshohocken, PA, 2018, www.astm.org

ASTM C642-06, Standard Test Method for Density, Absorption, and Voids in Hardened Concrete, ASTM International, West Conshohocken, PA, 2006, www.astm.org

Bertolini L. and Polder R. (1997). Concrete resistivity and reinforcement corrosion rate as a function of temperature and humidity of the environment TNO 97-NaN-R0574. Netherlands Organisation for Applied Scientific Research, Delft, The Netherlands.

Brew DRM and Glasser FP (1995) Synthesis and characterisation of magnesium silicate hydrate gels. Cement and concrete research **35(1):** 85-98.

Carino N. J. (1999). Nondestructive techniques to investigate corrosion status in concrete structures. Journal of Performance of Constructed Facilities, Vol.13,no.3,pp.96–106.

Chandra S (1996). Waste materials used in concrete manufacturing. Elsevier.

Fang, K.H. (2004). Hydration of MgO and its Influence on Autogenous Volume Expansion. Journal of Hydroelectric Engineering, 4, p45-49, (in Chinese).

Gudimettla, J.M., Crawford, G.L., "Field Experience in using Resistivity Tests for Concrete", in Transportation Research Board 94th Annual Meeting (No. 15-3357), 2015.

Gulikers J. (2005). Theoretical considerations on the supposed linear relationship between concrete resistivity and corrosion rate of steel reinforcement. Materials and Corrosion, Vol.56,no.6,pp.393–403.

Jin F, Gu K, Abdollahzadeh A and Al-Tabbaa A (2013). Effects of different reactive MgOs on the hydration of MgO-activated GGBS paste. Journal of Materials in Civil Engineering 27(7): B4014001

Jin F, Gu K, Abdollahzadeh A and Al-Tabbaa A (2013). Effects of different reactive MgOs on the hydration of MgO-activated GGBS paste. Journal of Materials in Civil Engineering 27(7): B4014001

Jin. F, Al-Tabbaa A. (2014). Strength and hydration products of reactive MgO–silica pastes. Cement & Concrete Composites 52 (2014) 27–33

Longuet P, Burglen L, Zelwer A. (1973). La phase liquide du ciment hydrate. Rev mate´r constr 676:35–41

Microsilica New Zealand (2017). General guidance to Microsilica. Microsilica New Zealand. http://www.goldenbay.co.nz, 2017 (accessed 01 Feb 2017)

Ono, H., & Wada, S. I. (2007). Properties of layer silicates formed from MgO-SiO2-H 2O mixtures at 25° C. Journal of the Faculty of Agriculture, Kyushu University, 52(1), 159-162.

Tariq, S. (2016). High volume utilization of waste glass powder as a cement replacement in the composition of self-compacting concrete. PhD thesis. University of Canterbury.

Walling S. A.,KinoshitaH., BernalS. A.,CollieraN. C.,and ProvisJ. L. (2015). Structure and properties of binder gels formed in the system Mg(OH)2–SiO2–H2O for immobilisation of Magnox sludge. The Royal Society of Chemistry, Dalton Trans., 2015, 44, 8126–8137.

Wei JX., Chen YM., Li YX. (2006). The Reaction Mechanism between MgO and Microsilica at Room Temperature. Journal of Wuhan University of Technology - Mater. Sci. Ed. 21(2), p88-91

CHAPTER 4
HYDRATION PRODUCTS AND MICROSTRUCTURE OF MAGNESIUM SILICATE HYDRATE BINDER SYSTEMS

Preamble

It's understood that the microstructure and reaction mechanisms of cement have a strong influence on the mechanical properties and durability of the resulting cementitious materials. The formation and strength of the hydration products, as well as the hydration rate, are decisive factors affecting strength development over the time. For M-S-H binders, previous studies also showed the influence of material sources on strength and durability. Chapter 3 outlined the material properties where significant differences were observed with different silica sources in terms of chemical composition, particles size distribution, and textures. It is expected that those properties may result in a variation of properties of M-S-H binders including microstructure, strength, workability, and durability. The study of microstructures of M-S-H cement pastes prepared with different materials is therefore of utmost importance to characterize the hydration process, which is directly related to the strength development and durability of the binders. This chapter proposed an experimental programme on the investigation of the microstructures of M-S-H cement pastes samples over 365 days curing period. The results provided a thorough understanding of the formation of hydration products. Effects of MgO/SiO2 ratio were discussed in search of the optimal binder composition for the formation of M-S-H binding phases. Other effects of the chemical composition and morphology of each silica were also discussed where the pros and cons of each silica sources were compared.

Abstract

The magnesium silicate hydrate (M-S-H) binding phases were formed readily in mixtures of reactive MgO and amorphous silica at low water content (w/c=0.40). XRD results showed that the hydration products after 1 day mainly include brucite while M-S-H phases are observed at 7 days and longer curing periods. At low MgO/SiO_2 ratio of 40/60 by mass (Mg/Si=1.0), MgO is completely hydrated and reacts with amorphous silica to form M-S-H gel over 365 days. The increase in MgO/SiO_2 ratio to 50/50 and 60/40 results in residual brucite in $MgO\text{-}SiO_2$ mixtures at all testing ages. The silica source and MgO/SiO_2 ratios were found to significantly affect the microstructure and hydration products of M-S-H systems. Supplementary cementitious materials such as silica fume, natural pozzolan and rice husk ask are highly reactive and react with hydrated MgO while the formation of M-S-H phases is not observed with fly ash due to its low reactivity compared to other sources of silica.

4.1. INTRODUCTION

Research on magnesium silicate hydrate binder systems as an alternative to Portland cement (PC) has significantly increased in the last decade since its cementitious properties have been reported (Wei et al., 2006). The production of M-S-H binder has potential benefits to the environment due to the low calcination temperature coupled with the incorporation of industrial by-products and suitable applications to heavy-metal-containing waste encapsulation (Zhang et al., 2009, 2011). Hence, the development of M-S-H binder systems for sustainable cementitious materials will become feasible if mechanical properties and microstructure of these binder systems are well studied and reported.

The constituents of M-S-H binder systems include reactive magnesium oxide and amorphous silica. The reactive magnesium oxide is traditionally produced from magnesite by decarbonation reactions at a low temperature of 650-750ºC (Tececo, 2017), hence it may require significantly less energy to produce than PC. A potential technology, which is claimed to have neutral or even negative CO_2 emissions, to produce MgO from abundant sources of about 10,000 billion tons of magnesium silicates in the earth's mantle is being developed by Novacem (Deolalkar, 2016). Magnesium carbonate will be converted from magnesium silicates under elevated temperatures (180 °C) and 150 bar pressure and then calcined at low temperatures of 700 °C to produce reactive MgO (Deolalkar, 2016). Silica fume has been used in M-S-H systems in most of the previous studies. However, other sources of amorphous silica such as natural pozzolans, rice husk ash, and fly ash can be potential alternatives.

The formation and microstructure of MgO-SiO_2-H_2O system have been investigated for decades since its appearance was discovered in the 1950s from the deterioration in a concrete sea wall by sulphate attack (Cole, 1953). A considerable divergence of M-S-H compositions exists in the literature. Factors including the reactivity and purity of light burnt MgO sources, Mg/Si mixing ratio and hydrothermal treatment conditions all play an important role in the composition of resultant M-S-H gel phases and crystallinity. In the natural deterioration of concrete in Mg-containing ground water, the decomposition of C-S-H gel resulted in the formation of M-S-H gel having Mg/Si molar ratio in a range of 1.0 – 2.0 (Bonen and Cohen, 1992; Bonen, 1992) or even as high as 4.0 (Cole, 1953). The M-S-H formed in sulphate attack of ordinary Portland cement was reported to have a cryptocrystalline form of serpentine ($C_3S_2H_2$) (Gollop and Taylor, 1992).

The microstructure and composition of synthesis M-S-H phases also have been studied extensively in the literature. The pozzolanic reaction between reactive magnesia and amorphous silica to form M-S-H gel should not be confused with reactions in MgO-based cement in which

hydrated MgO sequestrates CO_2 to produce magnesium carbonate to gain strength. At room temperatures, the low crystallinity M-S-H gel was formed readily even in short curing duration of 24h from sodium metasilicate and magnesium nitrate solutions at 25°C (Brew and Glasser, 2005) or from highly reactive MgO and reagent grade silica fume (Tonelli et al., 2006). The compositions of M-S-H phases formed at room temperatures have Mg/Si molar ratios in between 0.67 and 1.50 with structures resembling magnesium phyllosilicates such as talc or chrysotile (Lothenbach et al., 2015; Li et al., 2014; Roosz et al., 2015; Ono and Wada, 2007; Nied et al., 2016). In other cases, there has been a number of studies on the effect of hydrothermal conditions and pressure on synthesized magnesium silicate hydrates. Heated treatment facilitates the formation of M-S-H with improved crystallinity compared to reactions at room temperature (Kalousek and Mui, 1954; Yang, 1960; Mitsuda and Taguchi, 1977; Wei et al., 2011). For example, an M-S-H gel was formed from a mixture of $Mg(OH)_2$ and silicic acid (M/Si ratio = 1.0) after only 24h at 80°C (Temuujin,, 1998a). The MgO-SiO_2 mixtures prepared at elevated temperature (50°C) for 3 months obtained similar results as the same mixtures cured at 20°C for 1 year (Nied et al., 2016). The M-S-H phases formed by heated treatment have compositions close to talc ($(Mg_3(Si_4O_{10})(OH)_2$), or serpentine ($M_3S_2H_2$) with poorly crystalline layer structures (Mitsuda and Taguchi, 1977; Mitsuda, 1973; Speakman and Majumdar, 1974). At high temperature and pressure, the Mg/Si molar ratios occasionally increased to higher than 1.50 and close to 2.0 resembling the chemical composition of forsterite (Wei et al., 2011; Yamamoto and Akimoto, 1974).

Traditionally, hydration products of MgO-SiO_2 mixtures including brucite and M-S-H phases were considered to have little cementitious property as the formation of M-S-H mainly related to the concrete deterioration by sulphate attack in sea water. However, differing from a slow mechanism of sulphate attack or the reaction of hard burned MgO (impurities in the Portland cement) with silica, the hydration of reactive MgO in M-S-H systems is rapid so as not to cause significant expansion and cracking which might reduce strength. One of the first studies on cementing properties of M-S-H systems was published in 2006 in which M-S-H mortars obtained strengths of over 50MPa (Wei et al., 2006). However, due to the very high water demand of the raw materials, other studies reported fairly low strengths of M-S-H mixtures (Jin and Al-Tabbaa, 2014; Walling et al., 2015). Using sodium hexametaphosphate superplasticizer, a few studies have reported 28 days strength of over 60 MPa (Zhang et al., 2012a, 2012b, 2014; Marmol et al., 2016). The incorporation of crushed quartz into MgO-SiO_2 systems has increased strength to over 85 MPa (Tran and Scott, 2017).

Despite numerous studies on microstructure and strength of M-S-H, none of those has reported characterizations of the M-S-H systems prepared at low w/c and cured at ambient temperatures

and low humidity. Although the significant dependence of the properties of MgO-based binders on MgO sources has been well-studied (Jin and Al-Tabbaa, 2014; Jin et al., 2015), the effect of various amorphous silica sources has received relatively little attention. Therefore, the objectives of this chapter are to study the formation and microstructure of M-S-H systems at low w/c ratio of 0.40 and to compare four silica sources at different MgO/SiO_2 ratios. The experimental result is aimed at providing a greater understanding of M-S-H systems as potential construction materials for the widespread application of M-S-H systems in the future.

4.2. EXPERIMENTAL PROGRAMME

4.2.1. Materials

Binder constituents contain magnesium oxide and different sources of silica. Details of material properties are described in Chapter 3.

4.2.2. Sample preparation and testing methods

Binder compositions and mix proportions were designed using mass ratios. This approach has been widely used in the literature for ease of quantifying materials and useful in the production of a large number of samples. Given that chemical compositions of all materials are available, molar ratios can be obtained from the mass and molar mass of any compound where necessary to discuss the effect of molar ratios on the chemical reactions of the hydration process.

The paste samples of MgO and a source of silica were prepared using a planetary 20 L mixer. The MgO/SiO_2 ratios varied between 40/60 and 60/40 by mass. The lower limit of 40/60 was aimed at maximizing the formation of M-S-H gel with Mg/Si molar ratio close to 1.0 while the upper limit of 60/40 allowed examination of the formation of both brucite and M-S-H as hydration products. The fresh cement pastes were sealed in 50 ml containers and stored in an environmental chamber at 21oC until testing dates. Mix proportions are shown in Table 4.1.

The optimization of superplasticizer (SP) content (as presented in Chapter 6) found that a SP dosage of 3% of binder by mass was optimal for 40% MgO-60% SF mixture. This SP dosage were utilized for all of the pastes in Table 4.1 and no adjustment was required for workability.

SEM/EDS analysis was performed on hydrated paste samples at 7, 28, 90 and 365 days age using a JEOL 6400 Scanning Electron Microscope. The development of hydration products was monitored at 1, 7, 28, 90 and 365 days using a Philips PW1729 X-ray diffractometer (Cu, 50 kV/40 mA) with a 3 to 70^o 2θ scan range.

Table 4.1. Mix proportions of MgO-SiO_2 mixtures

Mixtures	Binder (MgO+SiO_2=1.0)					w/ (MgO+SiO_2)	SP (%, liquid)
	MgO	SF	MS	RHA	FA		
SF60	0.40	0.60				0.40	3%
SF50	0.50	0.50				0.40	3%
SF40	0.60	0.40				0.40	3%
MS60	0.40		0.60			0.40	3%
MS50	0.50		0.50			0.40	3%
MS40	0.60		0.40			0.40	3%
RHA60	0.40			0.60		0.40	3%
RHA50	0.50			0.50		0.40	3%
RHA40	0.60			0.40		0.40	3%
FA60	0.40				0.60	0.40	3%
FA50	0.50				0.50	0.40	3%
FA40	0.60				0.40	0.40	3%

4.3. XRD ANALYSIS

4.3.1. M-SF mixtures

Effect of ageing on the formation of M-S-H phases

Figure 4.1 presents XRD spectra of M-S-H paste mixtures with MgO/SiO_2 =40/60. The raw materials before mixing with water were denoted by age 0 while the hydration development was analyzed at 1, 7, 28, 90 and 365 days.

It was found that curing duration has a significant effect on the type of hydration products of M-SF mixtures. Much of the MgO was consumed in just the first day, illustrated by the reduction in intensity of MgO peaks, compared to the raw mixtures. As a result of the hydration of the MgO, a large amount of brucite was formed at this very early age, featured by brucite's peaks at $2\theta^o$ = 18^o, 38^o, 51^o, 59^o. This is consistent with what has been observed elsewhere (Vandeperre et al., 2008; Jin and Al-Tabbaa, 2013). The peaks of SF were almost unchanged indicates there were very little reactions of silica fume and brucite to form M-S-H after 1 day. The reaction of MgO with water was almost completed after 7 days. However, the observed amount of brucite at 7 days and 1 day was similar, as part of the freshly formed brucite proportion subsequently reacted with silica fume to form M-S-H gel, illustrated by the reduction in intensity of both the MgO peak and broad silica fume peak. According to previous studies (Gollop and Taylor, 1992; Temuujin et al., 1998a), three major broad peaks at 20–30^o, 32–39^o, and 58–62^o 2θ have been assigned to M-S-H gel. Due to the slow reaction between brucite and SF, these peaks were not obvious at a curing age of 7 days. At 28 days age, the decrease in brucite and SF peaks' intensity, and formation of new broad peaks

characteristic of M-S-H were evident, which indicate the formation of a poorly crystalline layered magnesium silicate hydrate phase resulting from the reaction between $Mg(OH)_2$ and silica fume. Although the freshly formed $Mg(OH)_2$ is highly reactive (Temuujin et al., 1998b) and even at a ratio of M/SF 40/60, which should have excess silica, a large amount of brucite was still present at 28 days age, which reveals that this pozzolanic reaction between brucite and silica fume occurred slowly at this early age up to 28 days. However, this pozzolanic reaction accelerated significantly with the long-term curing as the peaks associated with brucite completely disappeared at the age of 90 days and 365 days, which suggests that M-S-H is the only hydration product with samples containing 40%MgO-60%SF. It should be noted that the polymer-based superplasticizer used in this study has a critical role to permit the water reduction to w/c=0.40 while still providing sufficient water for hydration. In other studies (Zhang et al., 2014), a 40/60 MgO/SF mixture produced using sodium hexametaphosphate superplasticizer (w/c=0.40) still contained brucite and unreacted MgO even after 285 days curing.

Effect of MgO/SiO_2 ratio on the composition of M-S-H phases

Figure 4.2 and 4.3 present XRD spectra of M/SF mixtures with increasing MgO/SiO_2 ratio to 50/50 and 60/40, respectively. A change in MgO/SiO_2 ratio (M/Si molar ratio) significantly influences the hydration products. An increase in MgO content from 40% to 60% did not appear to affect the hydration rate of MgO as almost all MgO reacted with water to form brucite within 7 days. Consequently, the increase of MgO content increased the brucite content available at an early age to react with silica to form M-S-H phases.

While the appearance of M-S-H was observed at the same age across all the samples with various MgO/SiO_2 ratios, the peak intensities for the M-S-H phases decreased as the MgO/SiO_2 ratio increased from 40/60 to 60/40. After 90 days age, residual brucite almost did not appear in the mixture containing 50-60% SF (where Mg/Si ratio was close to 1.0-1.5), however, it was found in the 60/40 M/SF mixture (Mg/Si ratio close to 2.25). Accordingly, the Mg/Si ratio of resulting M-S-H after 90 days curing is close to 1.0 and no greater than 1.50, which indicates MgO/SiO_2 ratios in between 40/60 to 50/50 should be optimal for the formation of M-S-H gel. This result is consistent with previous studies (Nied et al., 2016) in which M-S-H phases synthesized at room temperature had Mg/Si molar ratios in between 0.70 and 1.50.

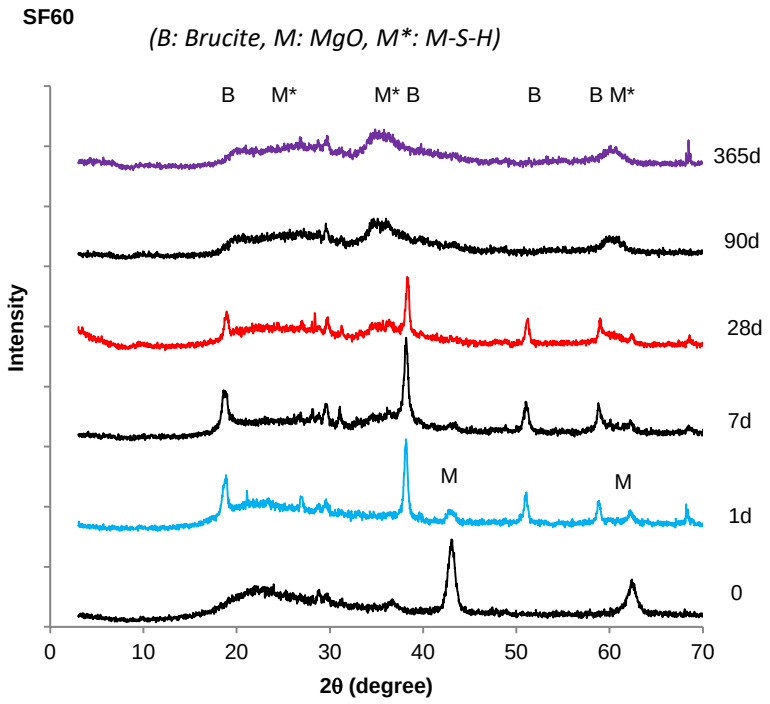

Figure 4.1. XRD spectra of M-SF paste samples (M/SF=40/60) over 365 days

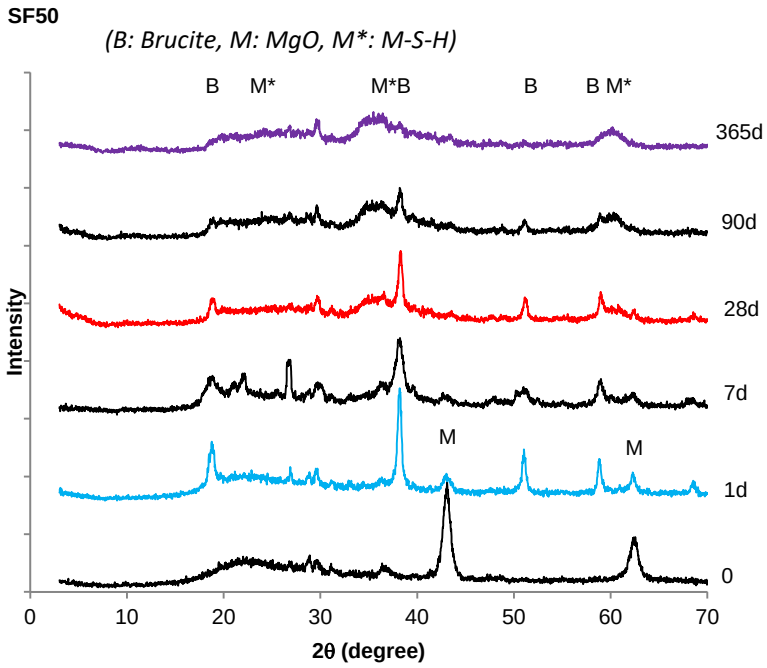

Figure 4.2. XRD spectra of M-SF paste samples (M/SF=50/50) over 365 days

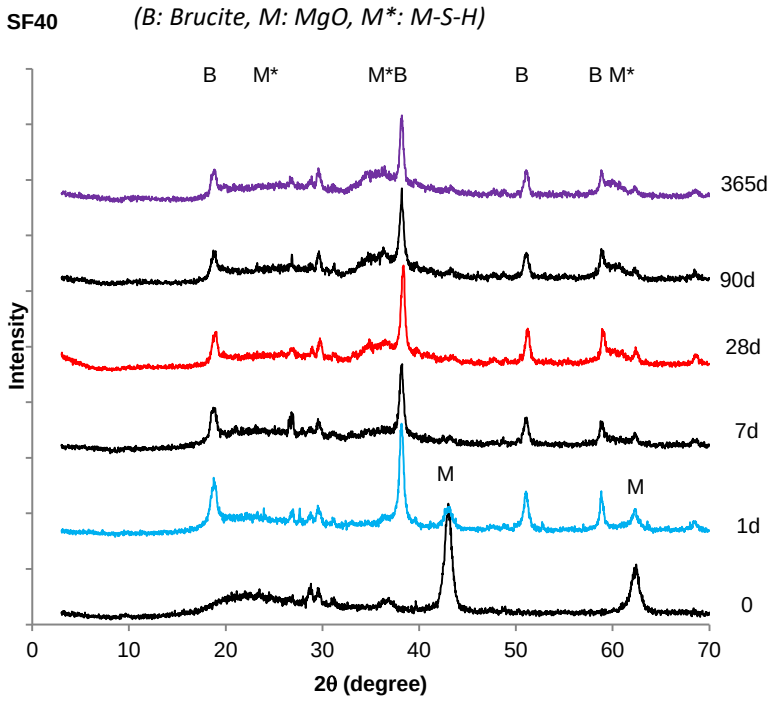

Figure 4.3. XRD spectra of M-SF paste samples (M/SF=60/40) over 365 days

4.3.2. Comparison of different amorphous silica sources

4.3.2.1. M-MS mixtures

Figure 4.4 presents XRD patterns of 40/60 M/MS mixture where a pozzolanic reaction similar to the M/SF mixtures also occurs between MgO and MS. The peak intensities show that MgO component in M-MS mixtures hydrated at a similar rate as seen in M-SF mixtures to form brucite at 1 day and the MgO hydration was almost complete after 7 days. The brucite peaks decreased over the curing period, indicating the formation of M-S-H gel at 7 days age. The M-MS pastes contained a higher amount of impurities (quartz) than M-SF mixtures and correspondingly showed various peaks at ~ 27°, 30° 2θ across the samples. The M-S-H gel observed at 28 and 90 days age increasingly formed over the curing period, as illustrated by the increase of the intensity of two broad peaks at 32–39°, 58–62° 2θ while other peaks at 20–30°2θ of M-S-H almost overlapped with the peak of impurity quartz in the mixtures. The XRD spectrum was almost unchanged between 90 to 365 days which indicates the reactions forming M-S-H phases almost finished after 90 days with the selected MgO/SiO_2 ratio.

Similar to the formation of M-S-H using SF, various MgO/SiO_2 ratios of M-MS mixtures led to changes in the amount of hydration products formed at different curing ages (Figure 4.5, Figure 4.6). The increase of MgO content also resulted in higher brucite content available to react with amorphous silica forming M-S-H gel. The XRD peaks of brucite formed in the MS60 and MS50 samples (Mg/Si =1.0-1.50) decreased and disappeared over 365 days, indicating the complete reactions between brucite and MS to form M-S-H gel with suggested Mg/Si molar ratio ranged from 1.0-1.50. It was found that the M-S-H gel were formed in a similar mechanism with the two sources of amorphous silica: SF and MS.

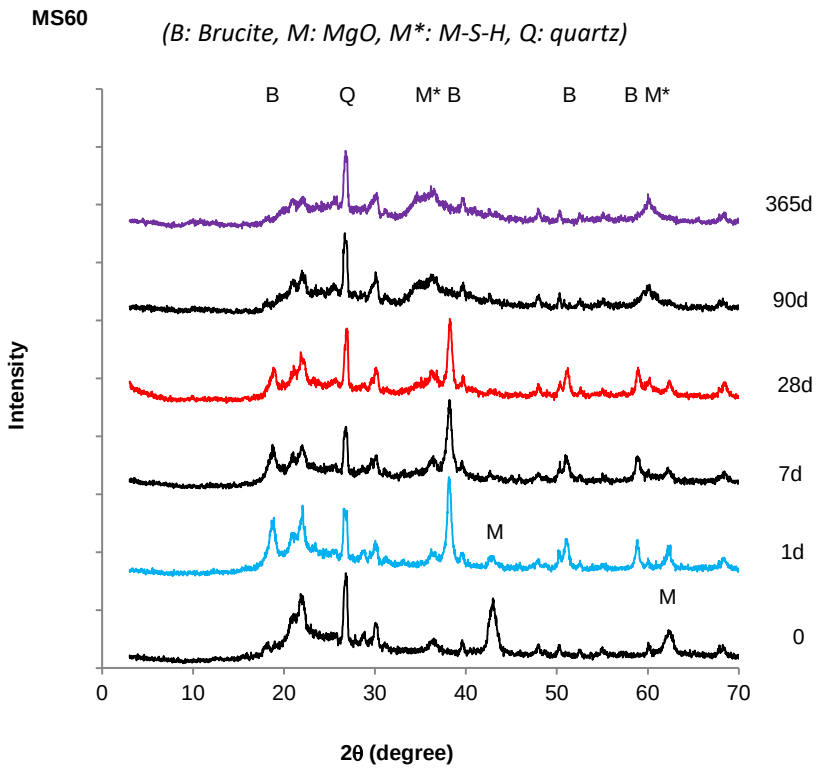

Figure 4.4. XRD spectra of M-MS paste samples (M/MS=40/60) over 365 days

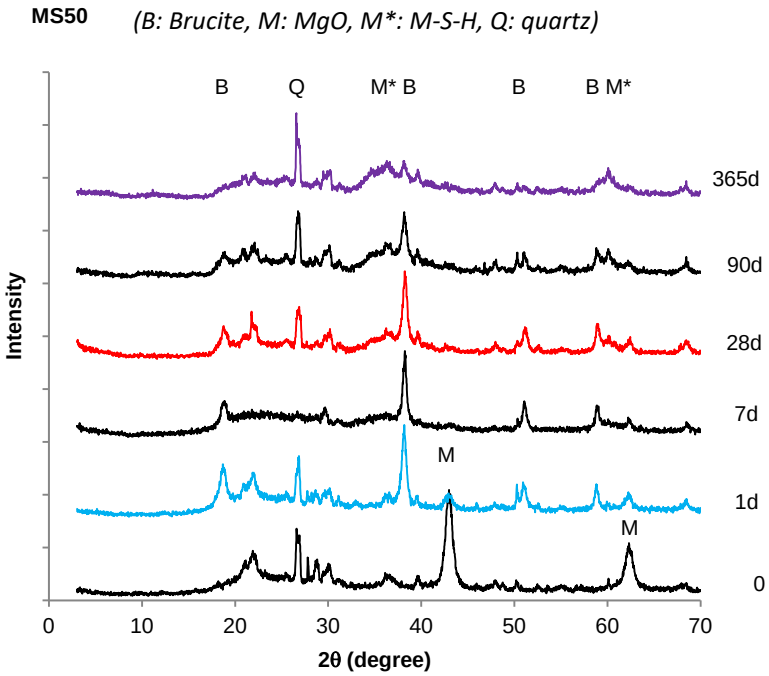

Figure 4.5. XRD spectra of M-MS paste samples (M/MS=50/50) over 365 days

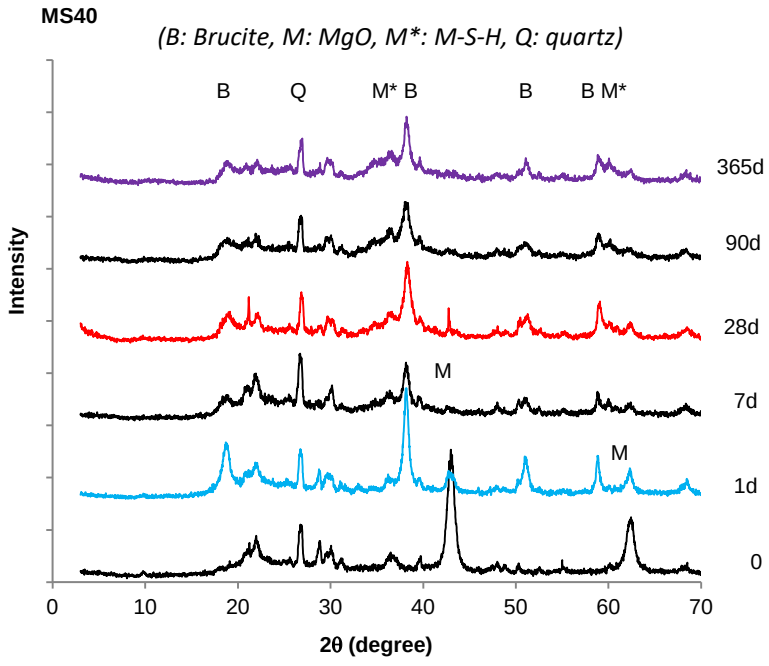

Figure 4.6. XRD spectra of M-MS paste samples (M/MS=60/40) over 365 days

4.3.2.2. M-RHA and M-FA mixtures

Figure 4.7 shows XRD patterns of M-RHA mixtures at 28, 90 and 365 days. M-RHA samples contain 60% of MgO and 40% of RHA in order to reduce the high porosity due to a very porous microstructure of RHA. At 28 days age, the peaks representing M-S-H phases was well observed. The predominance of XRD patterns of M-S-H phases indicates that most of hydrated MgO has reacted with RHA. The formation of M-S-H at this age and the unchanged XRD patterns after 28 days have shown the high reactivity of RHA results from the high amount of amorphous silica >90% in the chemical composition.

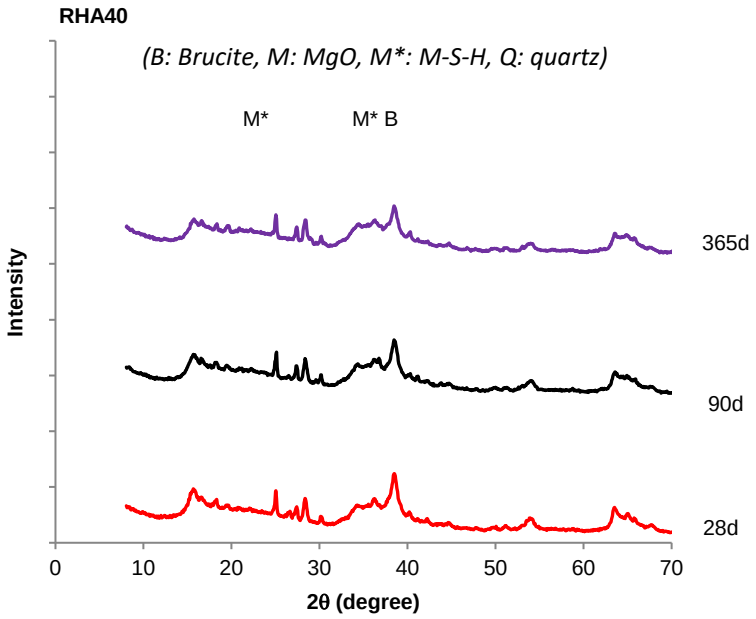

Figure 4.7. XRD spectra of M-RHA paste samples (M/RHA=60/40) over 365 days

Figure 4.8 presents XRD spectra of M-FA samples containing 60% MgO and 40% FA. The formation of M-S-H is very limited as the peaks representing M-S-H phases are not clearly shown in the XRD results. The XRD patterns of M-FA mixtures are pretty consistent over the curing period and there is no indication of the formation of M-S-H even after the long-term duration up to 365 days. The reason for the poor formation of M-S-H in M-FA mixtures could be attributed to the low reactivity of FA and the low amorphous silica content of FA in the mixtures. The chemical composition analysis of FA shows a low SiO_2 content (<50%) due to the availability of impurities such as aluminum, ferrous oxide and quartz in this source of silica. Therefore, it could be seen that

FA is not suitable to develop M-FA binary binder systems. The reactivity of MgO and silica is the most important factor for the chemical reactions forming binding phases.

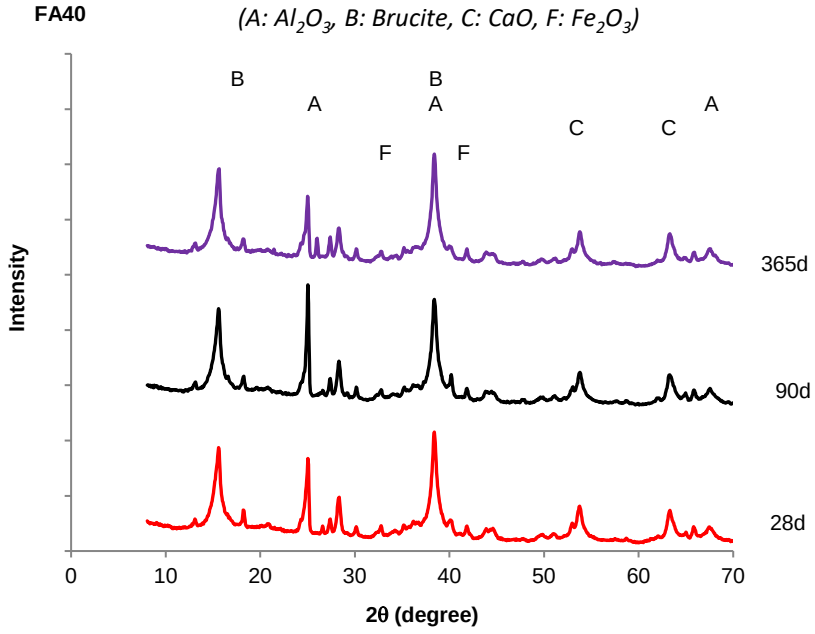

Figure 4.8. XRD spectra of M-FA paste samples (M/FA=60/40) over 365 days

Figure 4.9 compares 28-day XRD patterns of samples of the 60/40 MgO/SiO_2 ratio to illustrate the effect of silica sources to the hydration process of M-S-H systems. Each source of silica with its distinct features of chemical composition and morphology reacts differently with the same source of MgO in MgO-silica systems. It is known that the degree of hydration is strongly influenced by the reactivity of silica which is attributed to proportion of amorphous silica, particle size or specific surface area of the silica source. Various XRD patterns reflect the effect of the four testing silica sources on the formation of the hydration products. The formation of M-S-H phases illustrated by the corresponding peaks of the M-S-H compounds was well observed at 28 days age with mixtures using SF, MS, and RHA. These sources of silica with very high content of amorphous silica (>85%) and fineness due to the ultrafine particle size (SF, MS) and cellular microstructure (RHA) resulted in high degree of reaction with MgO in the mixtures. On the other hand, the formation of M-S-H phases in mixtures containing fly ash at 28 days age was negligible. It is obvious that the chemical composition of fly ash significantly differs from other sources of silica

with a low proportion of amorphous silica. The particle size analysis and SEM images (Chapter 3) show coarse spherical particles of FA with less porous microstructure. Such properties of a different source of silica significantly affect the reactivity of FA and may be the main reason for the poor formation of M-S-H phases in M-FA mixtures.

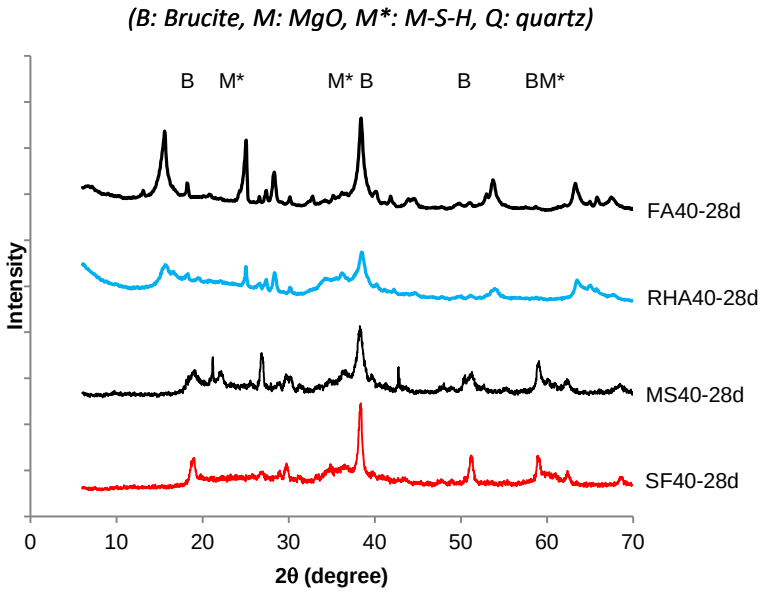

Figure 4.9. XRD spectra of MgO-silica mixtures with different silica sources at 28 days age

4.4. SEM ANALYSIS

4.4.1. M-SF mixtures

4.4.1.1. Effect of curing duration on microstructure of M-S-H phases

Since the hydration of reactive magnesia is fairly rapid (Du, 2005; Aphane, 2007; Jin, 2014), a control sample of 100% reactive MgO (w/c=0.40) cured for 28 days was considered to be fully hydrated brucite and used as a reference to examine the formation of M-S-H phases by SEM. The microstructure of 100% brucite was porous (Figure 4.10(a)) and included thin sheets as seen in the higher magnification image (Figure 4.10(b)).

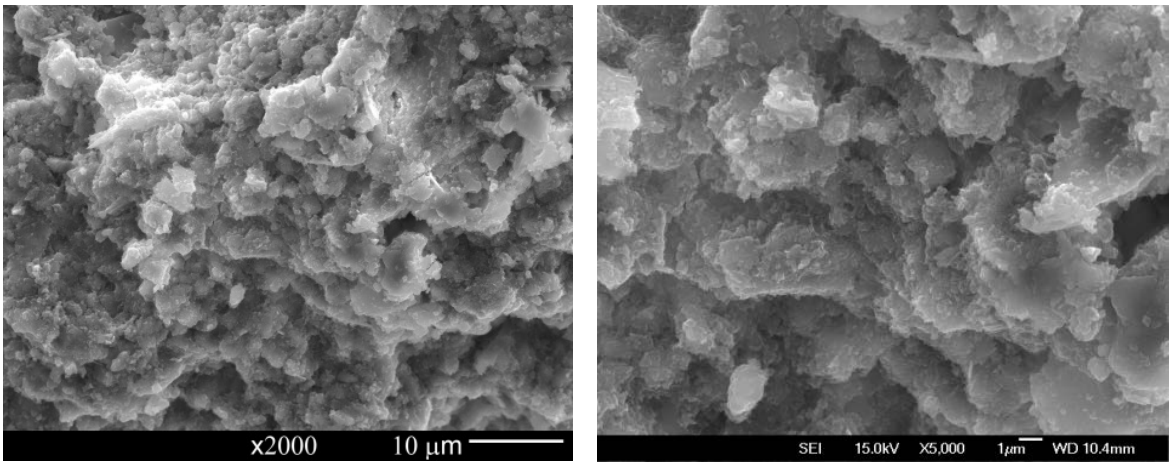

(a) *(b)*

Figure 4.10. SEM image of brucite at 28 days age (a): X2000 and (b) : X5000

Figure 4.11 shows the microstructure of MgO-SF mixtures with MgO/SiO_2 ratio of 40/60 over 365 days. The inclusion of silica fume particles resulted in much denser fracture surfaces compared with the 100% MgO sample (Figure 4.10). The formation of M-S-H gel at the early age of 7 days, which was not shown clearly by XRD results as previously discussed, can be observed in the microstructure of 40/60 M/SF samples (Figure 4.11(a)). There was unreacted brucite in 40/60 M/SF samples at 7 days age (Figure 4.11(a)), however, this content decreased over time as it reacted with silica fume. Figure 4.11(b) and 4.10(c) show the increase of M-S-H content and improved densities at 28 and 90 days. After 90 days, the mixture with MgO/SiO_2 ratio of 40/60 has a smooth fracture surface without any noticeable residual brucite. The SEM and XRD results are generally in agreement indicating the complete reaction of brucite with silica fume to form M-S-H by 90 days.

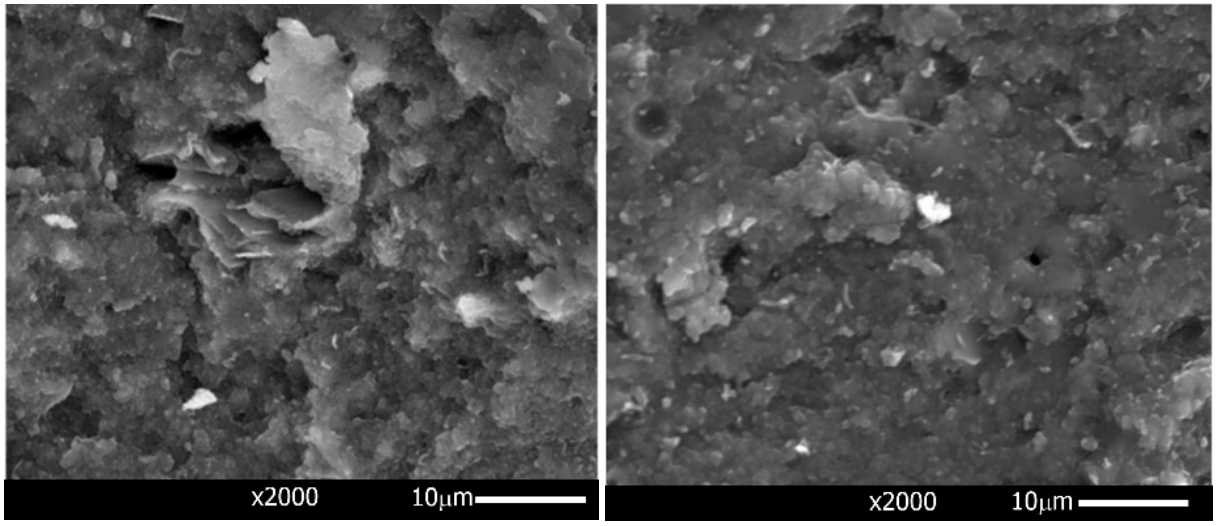

(a) SF60-7d *(b) SF60-28d*

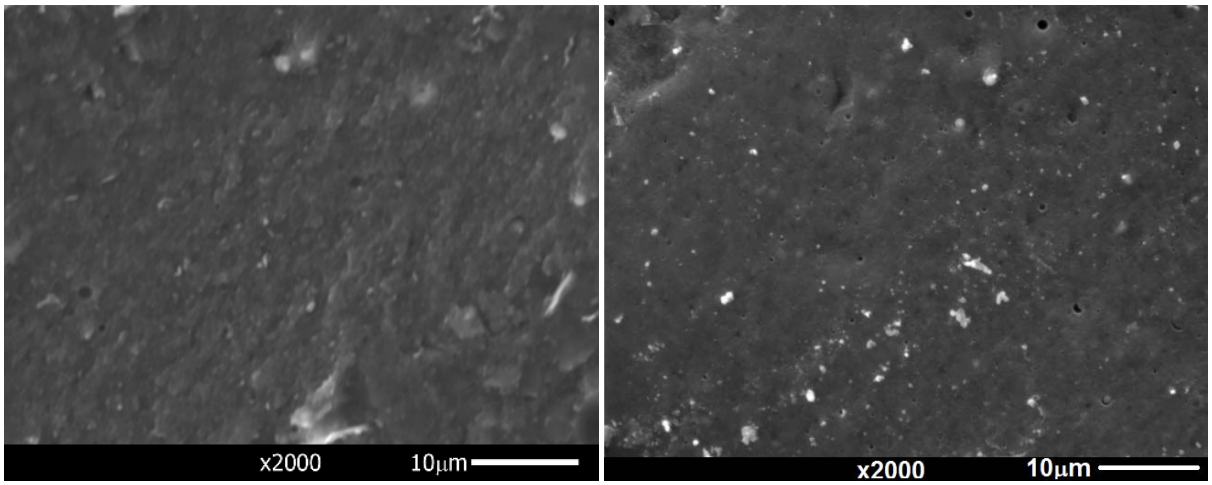

(c) SF60-90d *(d) SF60-365d*

Figure 4.11. SEM of M-SF paste samples (M/SF= 40/60) at 7 days (a), 28 days (b), 90 days (c) and 365 days (d)

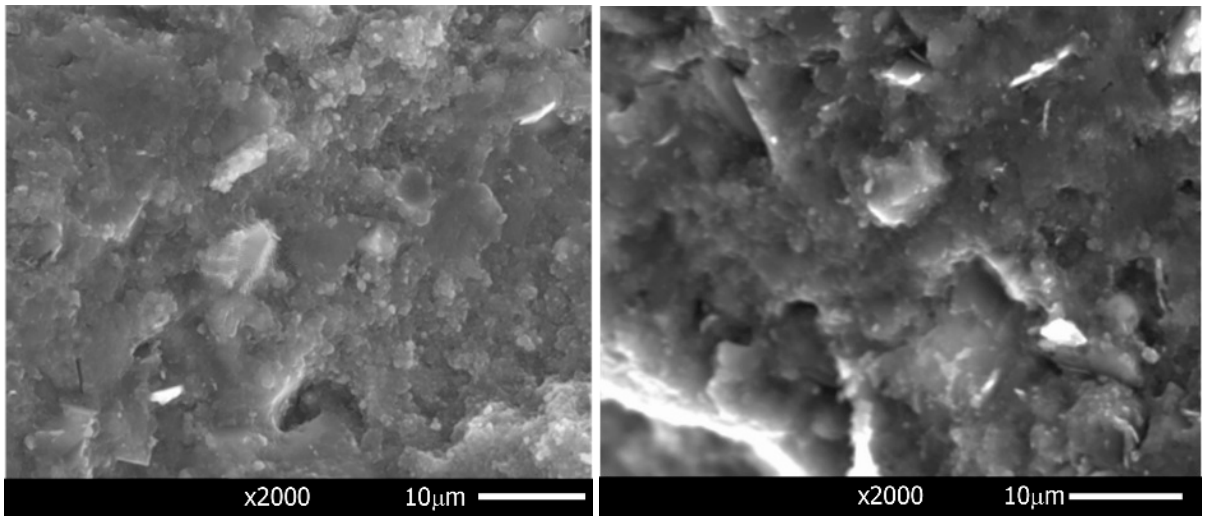

(a) SF50-7d *(b) SF50-28d*

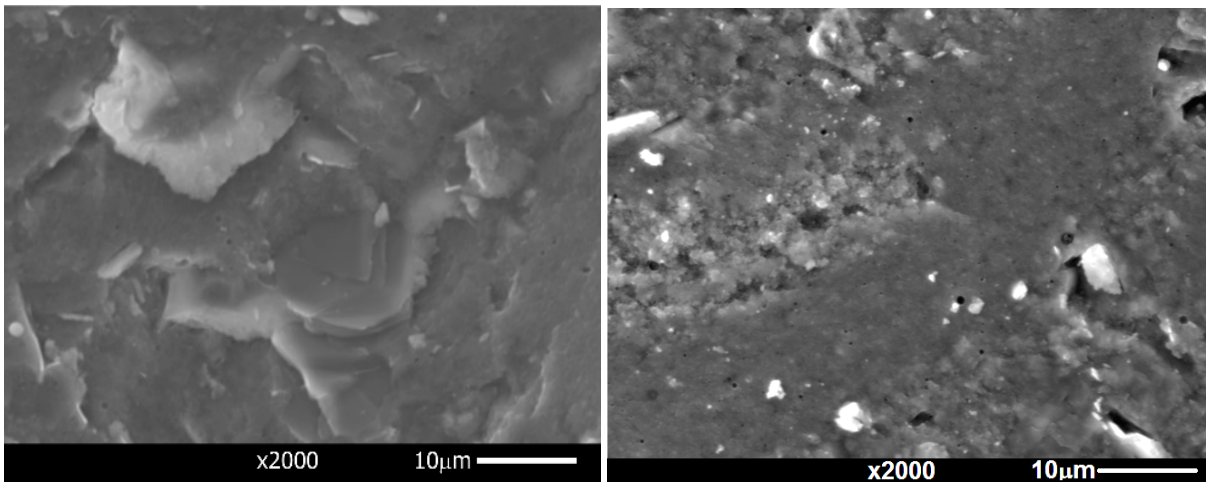

(c) SF50-90d *(d) SF50-365d*

Figure 4.12. SEM of M-SF paste samples (M/SF= 50/50) at 7 days (a), 28 days (b), 90 days (c) and 365 days (d)

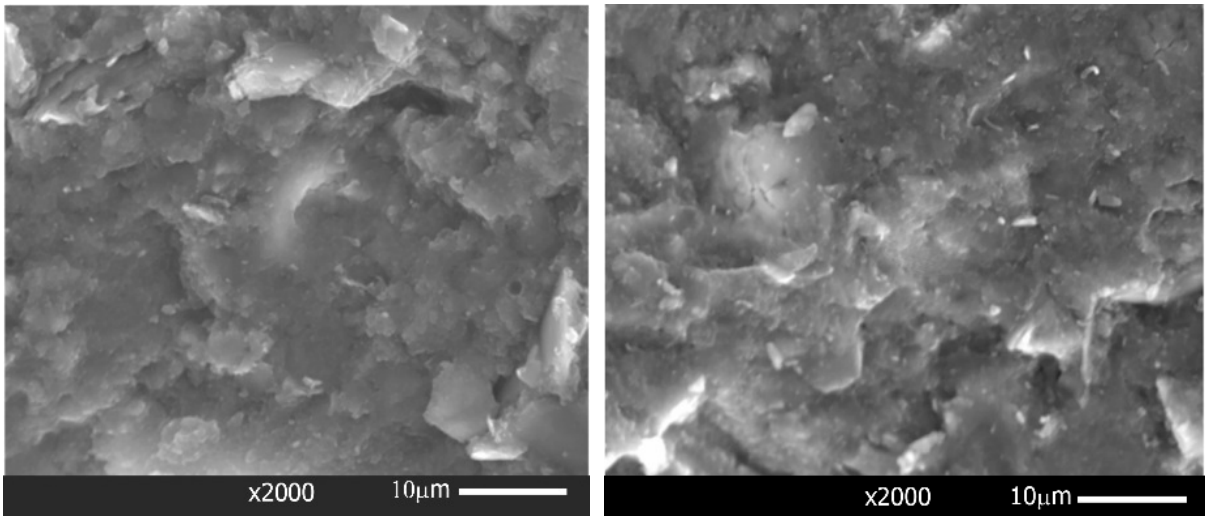

(a) SF40-7d *(b) SF40-28d*

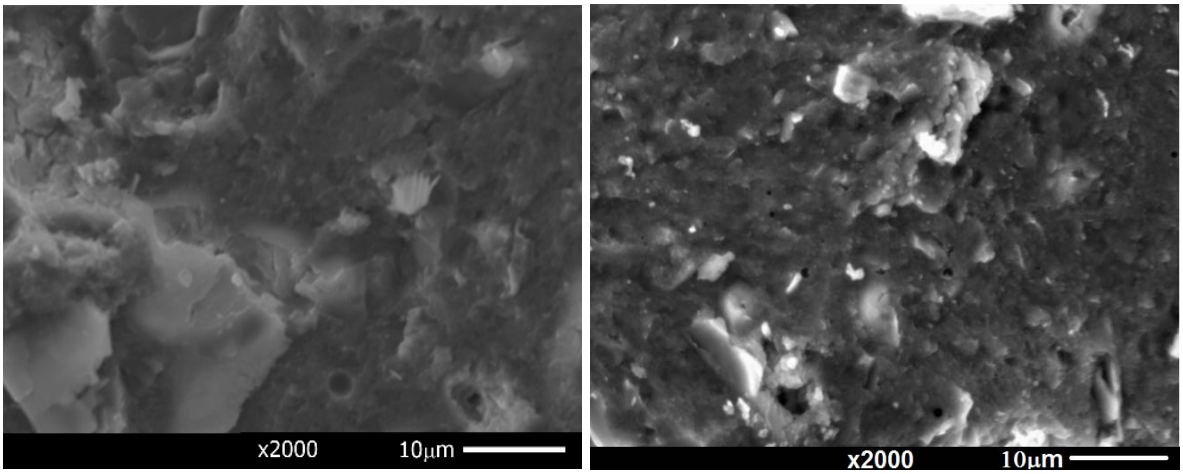

(c) SF40-90d *(d) SF40-365d*

Figure 4.13. SEM of M-SF paste samples (M/SF=60/40) at 7 days (a), 28 days (b), 90 days (c) and 365 days (d)

4.4.1.2. Effect of MgO/SiO_2 ratio on microstructure of M-S-H phases

While it was proved that all brucite can react with silica fume at low w/c=0.40 over 90 days with 40/60 M/SF mixture, residual brucite appeared in other mixtures even at 365 days as M/SF ratios increased to 50/50 (Figure 4.12(a)-4.11(d)) and 60/40 (Figure 4.13(a)-4.12(d)). It is obvious that

higher MgO content results in higher residual brucite which was observed at all curing ages. Accordingly, from the XRD and SEM results the most likely Mg/Si molar ratio of M-S-H formed in this investigation was below 1.50. The M/SF ratio for the optimal production of M-S-H and to limit the presence of residual brucite, therefore, should be close to 1.0.

4.4.2. Comparison of different amorphous silica sources

4.4.2.1. M-MS mixtures

SEM images of M-MS mixtures (Figure 4.14 - 4.15) show a similar formation of M-S-H phases as observed in M-SF mixtures (Figure 4.11 - 4.12). The MgO/SiO_2 ratio has a significant effect on the brucite content where there was some residual brucite in most of M-MS samples except those mixtures with the lowest MgO/SiO_2 ratio (M/MS=40/60). The microstructures of both M-MS and M-SF mixtures at 7 and 28 days were fairly porous with a similar appearance to the microstructure of 100% brucite sample (Figure 4.10). However, SEM images of M-MS samples show more porous structures compared to SF mixtures, likely a result of the MS particles having a more angular morphology and larger particle size than the SF. The formation of M-S-H increased with both SF and MS due to ageing effect over 365 days curing period. The texture of the microstructure is visibly improved with age; e.g. the porous texture at early ages was gradually replaced by more homogeneous and smooth surface due mainly to the increased formation of M-S-H gel.

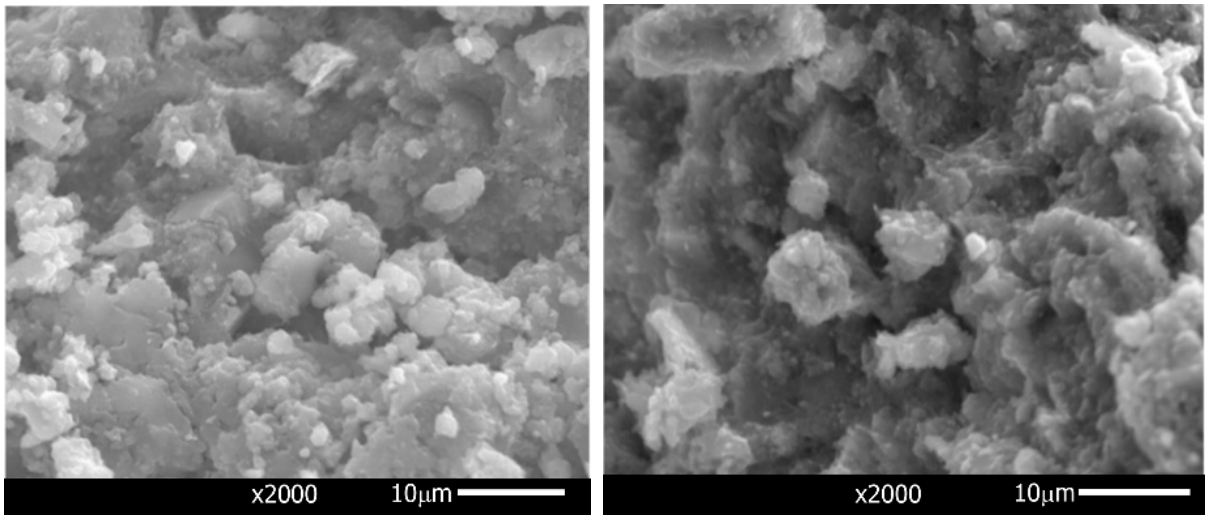

(a) MS60-7d *(b) MS60-28d*

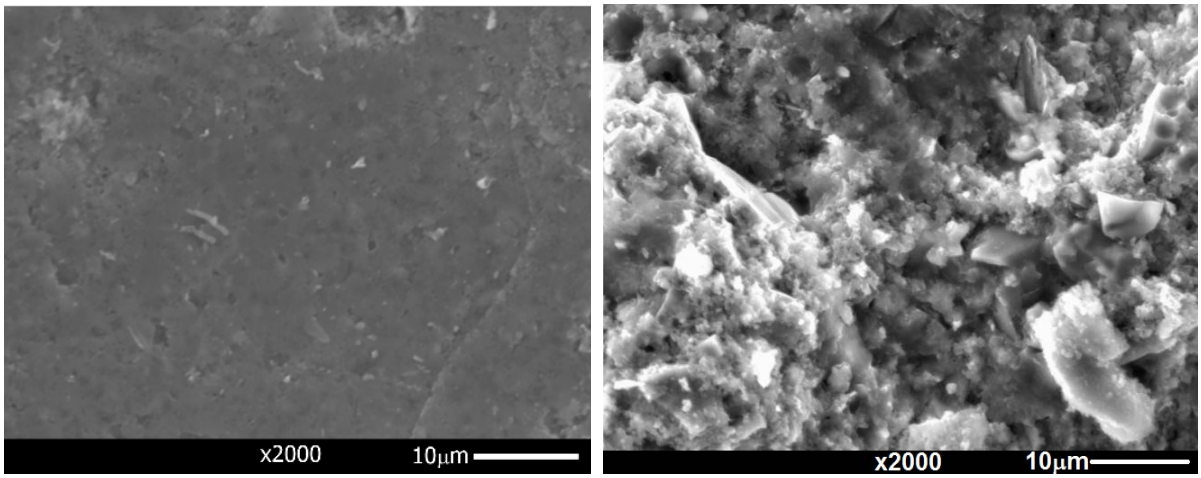

(c) MS60-90d *(d) MS60-365d*

Figure 4.14. SEM of M-MS paste samples (M/MS=40/60) at 7 days (a), 28 days (b), 90 days (c) and 365 days (d)

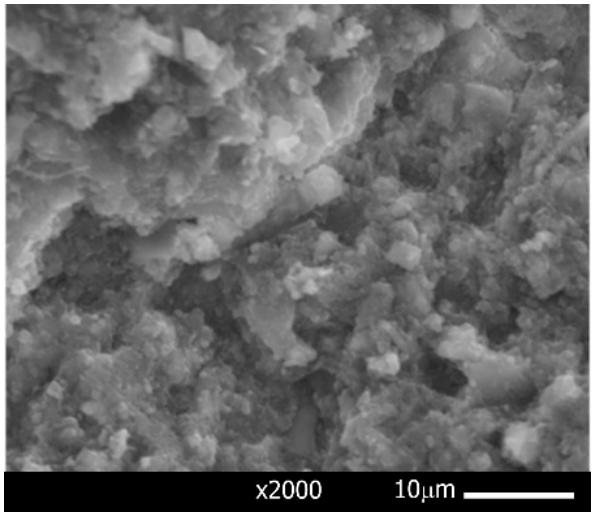

(d) MS50-7d

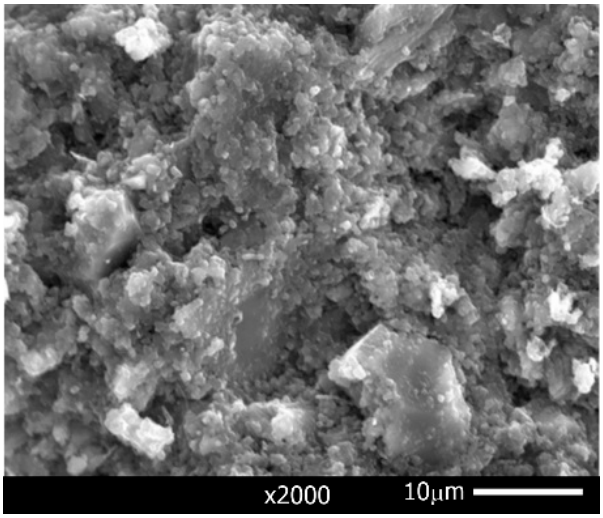

(e) MS50-28d

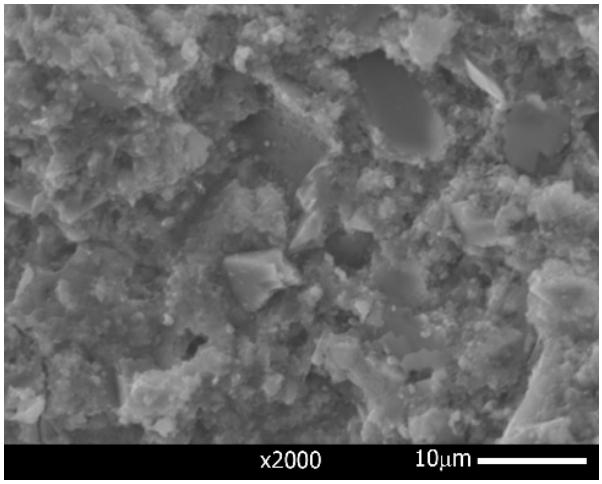

(f) MS50-90d

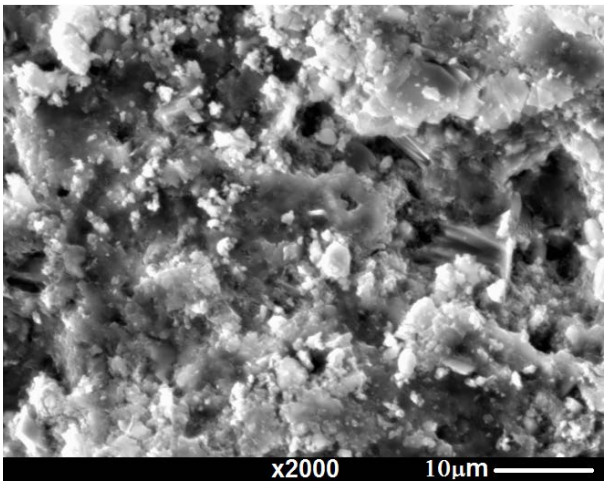

(f) MS50-365d

Figure 4.15. SEM of M-MS paste samples (M/MS=50/50) at 7 days (a), 28 days (b), 90 days (c) and 365 days (d)

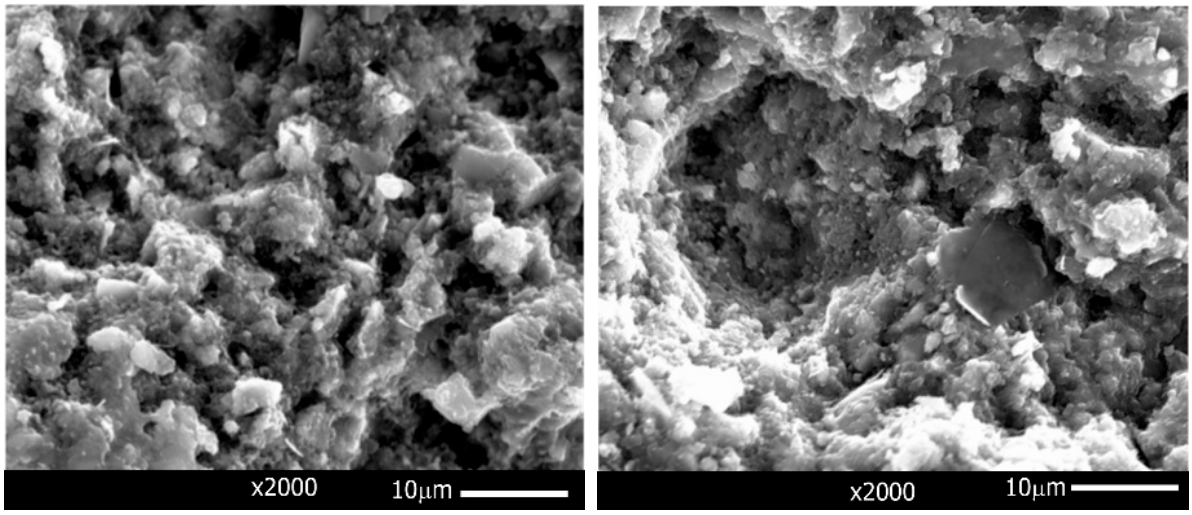

(g) MS40-7d *(h) MS40-28d*

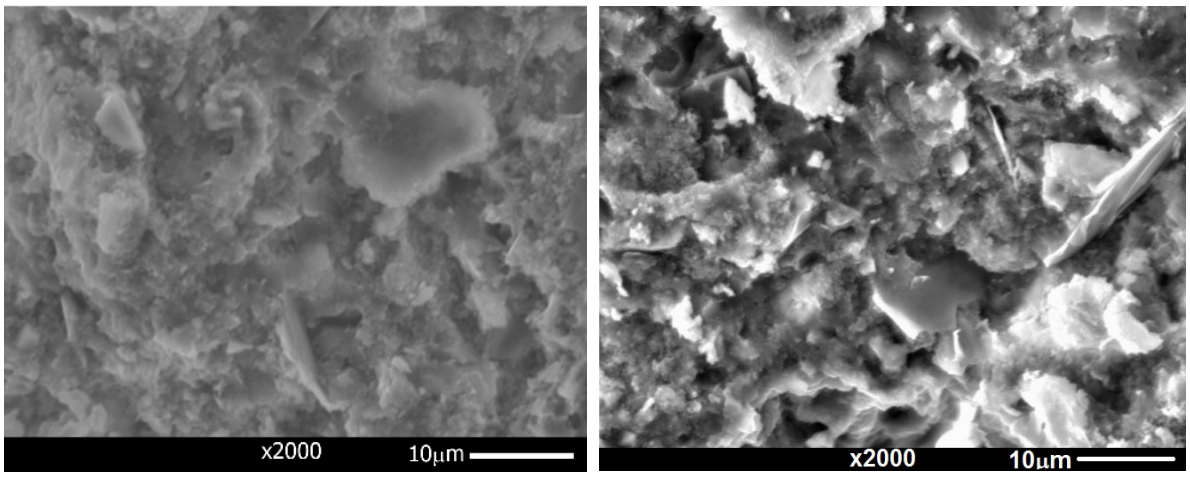

(c) MS40-90d *(d) MS40-365d*

Figure 4.16. SEM of M-MS paste samples (M/MS=60/40) at 7 days (a), 28 days (b), 90 days (c) and 365 days (d)

4.4.2.2. M-RHA and M-FA mixtures

Figure 4.17 presents SEM images of the microstructure of M-RHA mixtures over the curing duration up to 365 days. As experimental results from M-SF mixtures have shown that a high content of silica may result in porous microstructure, the selected M/RHA ratio was 60/40 to

reduce the porosity of M-RHA cement pastes. However, it is shown that the microstructures of M-RHA mixtures are not well-improved compared to 100% MgO sample as large pores still presented at all testing ages. The pastes are highly porous at 7 days age when there is only a small amount of M-S-H phases formed at this early age. The formation of M-S-H increases over the time and results in denser microstructures in the long-term (Figure 4.11d and Figure 10e). Although the formation of M-S-H was observed, the presence of large pores in M-RHA microstructures has shown that the porous structure and large particle size of RHA compared to SF might limit the strength development and durability of M-S-H binder systems using RHA.

Figure 4.18 shows the rough texture of M-FA mixtures with porous microstructures. There were very limited M-S-H phases formed in the mixtures due to the low reactivity of FA compared to other silica (SF, MS, RHA). A remarkable amount of spherical fly ash particles those are probably unreacted was observed throughout the curing duration up to 365 days age. The FA resulted in large pore sizes in microstructures of M-FA pastes. The composition of FA contains very low SiO_2 content (<50%) including impurities of crystalline silica. The low content of amorphous silica and coarse particle sizes result in the low reactivity of fly ash and the porous microstructure of the mixtures, although the spherical shape is known to enable good workability. The microstructure is therefore highly dependent on the silica sources which reactivity and particle size are of utmost importance to form M-S-H binding phases and dense cement pastes.

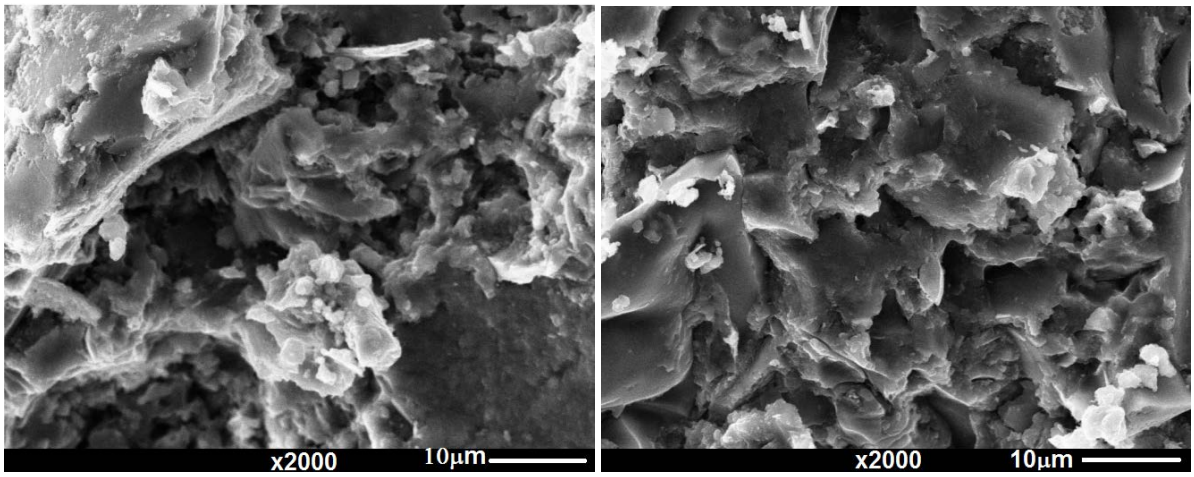

(a) RHA40-7d *(b) RHA40-28d*

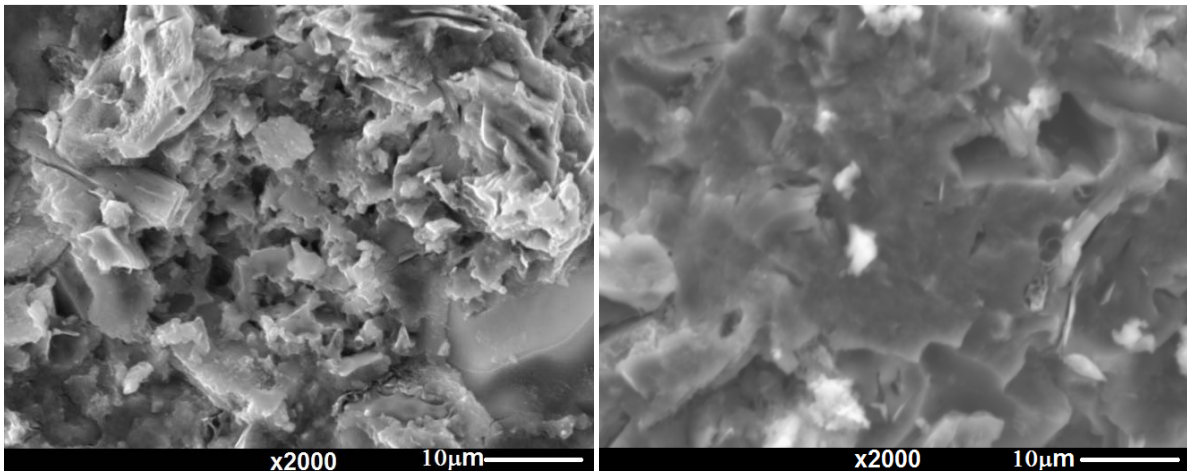

(c) RHA40-90d *(d) RHA40-365d*

Figure 4.17. SEM of M-RHA paste samples (M/RHA=60/40) at 7 days (a), 28 days (b), 90 days (c) and 365 days (d)

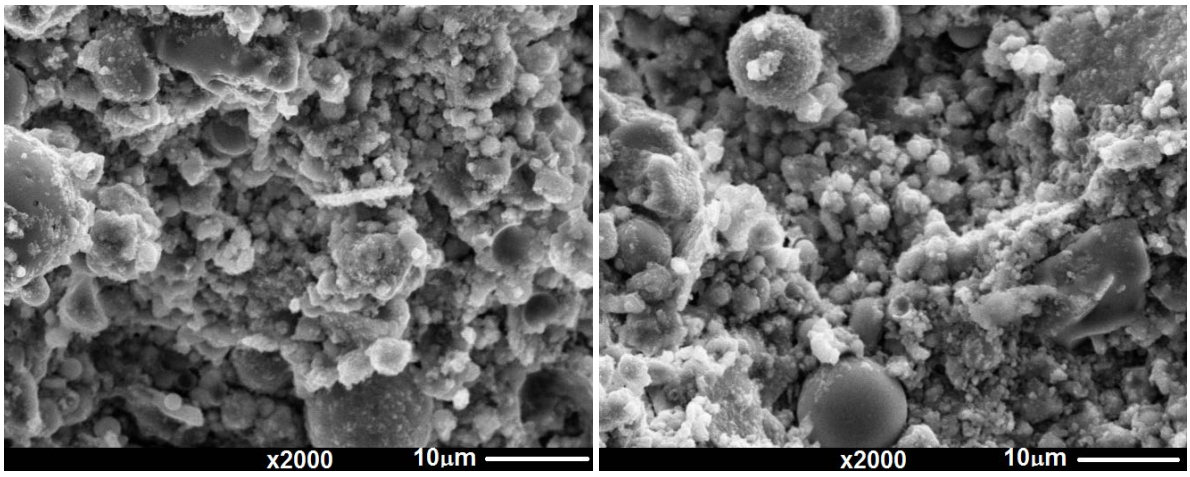

(a) FA40-7d *(b) FA40-28d*

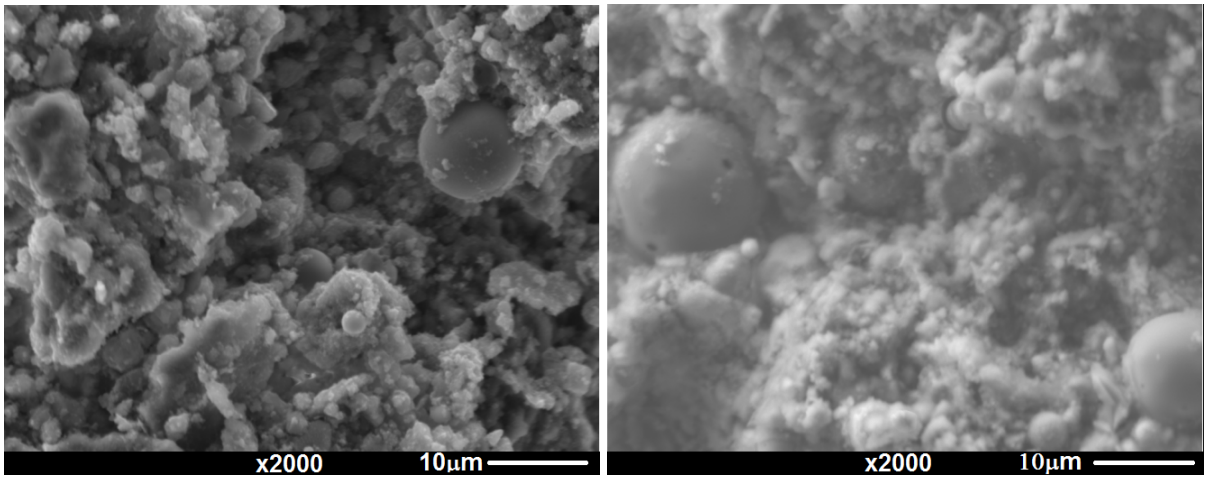

(c) FA40-90d *(d) FA40-365d*

Figure 4.18. SEM of M-FA paste samples (M/FA=60/40) at 7 days (a), 28 days (b), 90 days (c) and 365 days (d)

Figure 4.19 shows microstructures of PC samples to compare with M-S-H binder systems. The PC samples have homogeneous microstructures in which the micro-pores are well distributed on the fracture surfaces. In contrast, the microstructures of M-S-H binders appear to be porous. Although PC samples showed a porous microstructure at 7 days, denser pastes were observed over the time due to the formation of hydration products. As for M-S-H binders, the microstructure is dependent on the silica sources and porous textures are still observed even at the long-term curing after 365 days.

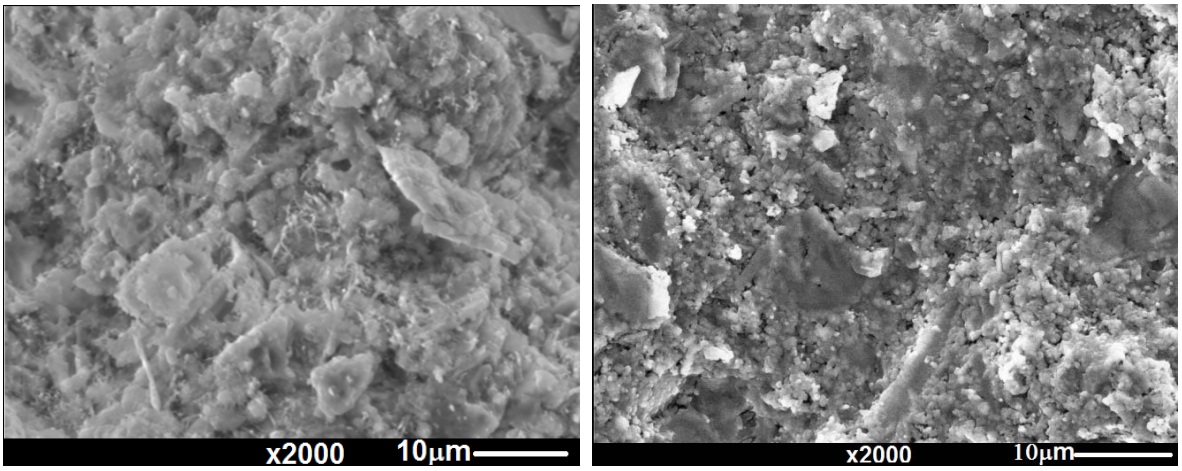

(a) PC-7d *(b) PC-28d*

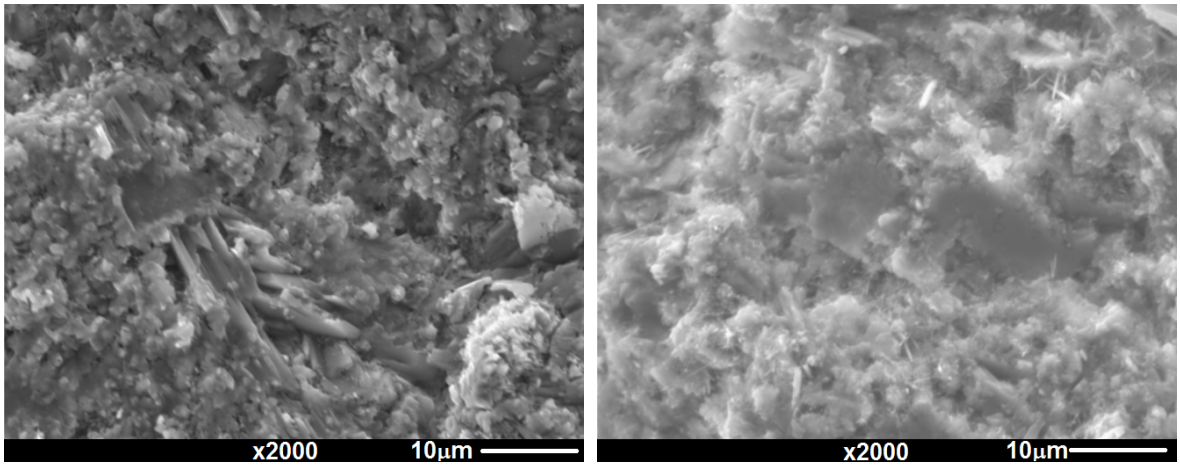

(c) PC-90d *(b) PC-365d*

Figure 4.19. SEM of PC paste samples at 7 days (a), 28 days (b), 90 days (c) and 365 days (d)

4.5. ENERGY DISPERSIVE X-RAY SPECTROSCOPY (EDS) ANALYSIS

While Scanning Electron Microscopy (SEM) allows for visual observation of specific locations, Energy Dispersive X-Ray Spectroscopy (EDS), sometimes referred to as EDAX or EDX, can be used to obtain quantitative elemental results of the same areas of interest.

In order to study elemental compositions of hydration products of M-S-H binders, SEM/EDS was conducted on the backscattered model of carbon coated samples. The picking points were selected at different locations of the fracture surfaces. The spectrum analysis reveals the concentrations of elements whereby the presence M-S-H gel, brucite or unreacted particles can be identified based

on the calculated Mg/Si molar ratios. Details of the EDS analysis of the mixtures of MgO and different silica sources are discussed below.

4.5.1. M-SF systems

To characterize the formation of M-S-H phases, quantitative study of Mg and Si elements at each curing age is performed using EDS analysis. Details of elemental spectra of M-SF mixtures are presented in Appendix C. The summary of Mg/Si molar ratios of SF60, SF50, SF40 samples at 7 days age are shown in Table 4.2.

A wide range of Mg/Si molar ratios of SF60 samples were observed. All the spectra have average molar ratios lower than 1.0. Some points have very low Mg/Si molar ratios of 0.1-0.3 which locate the areas of high Si concentrations. These ratios are lower than the minimum Mg/Si molar of 0.67 obtained in M-S-H gel (Brew and Glazer, 2005), and therefore possibly reveal the unreacted silica fume particles. At this early age, the reactions of brucite and silica fume appear to be incomplete and therefore, the unreacted silica fume with its ultra-high fineness and large surface area covers most of unreacted MgO or brucite particles.

The effect of changing MgO/SiO_2 ratio to the formation of M-S-H gel is well described by the Mg/Si molar ratios calculated from elemental spectra. An increase in M/SF ratio of the raw materials results in an increase in Mg/Si molar ratio of hydration products. Samples SF50 and SF40 contain higher brucite content than SF60 samples and possibly result in more Mg bound in M-S-H gel phases. Although the MgO/SiO_2 ratio or the precursors of SF40 samples is 2.25, the highest average Mg/Si molar ratio of the hydration products is only 0.78. M-S-H gel formed at early ages therefore has low Mg/Si molar ratios.

Table 4.2. EDS results of SF60 samples at 7 days age

System	Number of points / Spectrum	Mg wt%	Si wt%	Mg/Si (molar) of precursors	Mg/Si (molar) of hydration products
SF60	14	12.7	35.4	1.0	0.42
SF60	15	17.7	30.4	1.0	0.68
SF60	16	18.9	24.3	1.0	0.91
SF60	17	6.3	57.9	1.0	0.13
SF60-7d (average)	**4**			**1.0**	**0.53**
SF50	27	10.5	42.8	1.50	0.29
SF50	29	8.1	48.2	1.50	0.20
SF50	30	20.2	28.8	1.50	0.82
SF50	31	24.1	30.8	1.50	0.91
SF50	32	16.6	35.8	1.50	0.54
SF50	34	23.5	17.3	1.50	1.58
SF50-7d (average)	**6**			**1.50**	**0.72**
SF40	48	30.0	26.7	2.25	1.31
SF40	49	10.2	47.1	2.25	0.25
SF40	50	18.8	43.0	2.25	0.51
SF40	51	22.8	30.6	2.25	0.87
SF40	52	22.0	26.2	2.25	0.98
SF40-7d (average)	**5**			**2.25**	**0.78**

The Mg/Si molar ratios of samples at 28 days are shown in Table 4.3. At this age, there is an increase in Mg/Si molar ratios compared to 7 days age. Over the time, due to the dissolution of SF particles and the chemical reactions to form M-S-H, the concentrations of SF covering the surface of MgO particles reduce and result in the increase in Mg/Si molar ratios of the hydration products.

MgO/SiO_2 ratios of the raw materials have a strong influence on the chemical compositions of the hydration products. M-S-H gel phases are formed readily after 28 days curing with Mg/Si molar ratios in a range of 0.80 to 1.30, which is consistent with previous studies reported Mg/Si ratios of M-S-H phases in between 0.7 to 1.50 (Mitsuda and Taguchi, 1977). An increase in MgO content from 40% to 60% in the M-SF mixtures also leads to the higher Mg/Si molar ratios of the hydration products at 28 days age.

Table 4.3. EDS results of SF60 samples at 28 days age

System	Number of points / Spectrum	Mg wt%	Si wt%	Mg/Si (molar) of precursors	Mg/Si (molar) of hydration products
SF60	54	24.6	30.8	1.0	0.93
SF60	55	19.3	26.9	1.0	0.84
SF60	56	24.2	32.6	1.0	0.87
SF60	57	22.9	30.7	1.0	0.87
SF60	58	17.8	38.7	1.0	0.54
SF60-28d (average)	**5**			**1.0**	**0.81**
SF50	2	24.0	29.9	1.50	0.94
SF50	3	24.3	26.9	1.50	1.05
SF50	4	31.2	26.7	1.50	1.36
SF50	5	26.4	26.7	1.50	1.15
SF50	6	24.8	29.0	1.50	1.00
SF50-28d (average)	**5**			**1.50**	**1.10**
SF40	3	30.4	25.9	2.25	1.37
SF40	4	25.9	28.4	2.25	1.06
SF40	5	18.3	14.3	2.25	1.49
SF40	6	24.2	33.6	2.25	0.84
SF40	8	22.1	14.9	2.25	1.73
SF40-28d (average)	**5**			**2.25**	**1.30**

Table 4.4 and 4.5 present the EDS results over the long-term curing periods up to 90 days and 365 days. As also shown in Figure 4.20, Mg/Si molar ratios of the hydration products increase further to confirm the improvement of the crystallinity and the completion of the hydration process over the time. Mixture SF60 and SF50 have the Mg/Si molar ratios in a range of 0.80 to 1.21 over the long-term. For mixture SF40, the Mg/Si molar ratios after 365 days curing reached 1.59 and 2.09 at 90 and 365 days, respectively. The Mg/Si molar ratios exceeding 1.50 suggest the presence of residual brucite due to a high content of MgO in the binder composition.

The hydration process can be summarized as that at the early age up to 7 days, the main reaction is the hydration of MgO and brucite precipitates as the main hydration product. Reactions of silica fume and brucite take place slowly at this stage. The Mg/Si ratios of the M-S-H phases depend on the binder composition (MgO/SiO_2 ratio). MgO content higher than 50% results in unreacted

brucite while SF content should be limited below 60% of the binder for complete reactions with brucite. M-S-H phases at early ages have low Mg/Si molar ratios and long-term ageing increases these ratios.

Table 4.4. EDS results of SF60 samples at 90 days age

System	Number of points / Spectrum	Mg wt%	Si wt%	Mg/Si (molar) of precursors	Mg/Si (molar) of hydration products
SF60	7	19.6	25.6	1.0	0.89
SF60	8	21.3	28.7	1.0	0.87
SF60	9	20.9	25.4	1.0	0.96
SF60	10	22.5	29.6	1.0	0.89
SF60	11	22.7	26.7	1.0	0.99
SF60-90d (average)	**5**			**1.0**	**0.92**
SF50	13	25.4	21.2	1.50	1.40
SF50	14	24.1	26.2	1.50	1.07
SF50	15	20.5	27.8	1.50	0.86
SF50	16	24.0	25.0	1.50	1.12
SF50	17	26.2	25.9	1.50	1.18
SF50-90d (average)	**5**			**1.50**	**1.13**
SF40	41	28.6	18.0	2.25	1.85
SF40	42	29.3	14.0	2.25	2.44
SF40	43	26.0	22.9	2.25	1.32
SF40	44	26.4	20.6	2.25	1.50
SF40	45	25.9	22.9	2.25	1.32
SF40	46	21.9	23.5	2.25	1.09
SF40-90d (average)	**6**			**2.25**	**1.59**

Table 4.5. EDS results of SF60 samples at 365 days age

System	Number of points / Spectrum	Mg wt%	Si wt%	Mg/Si (molar) of precursors	Mg/Si (molar) of hydration products
SF60	66	18.9	27.0	1.0	0.82
SF60	67	19.2	27.4	1.0	0.82
SF60	68	18.7	27.6	1.0	0.79
SF60	69	18.7	27.5	1.0	0.79
SF60	70	18.6	27.5	1.0	0.79
SF60-365d (average)	**5**			**1.0**	**0.80**
SF50	8	24.7	25.0	1.50	1.15
SF50	9	25.2	26.4	1.50	1.11
SF50	10	27.8	23.4	1.50	1.39
SF50	11	27.1	24.3	1.50	1.30
SF50	12	25.4	26.7	1.50	1.11
SF50-365d (average)	**5**			**1.50**	**1.21**
SF40	19	31.1	17.0	2.25	2.13
SF40	20	26.8	22.2	2.25	1.41
SF40	21	35.2	15.4	2.25	2.67
SF40	22	33.9	15.9	2.25	2.49
SF40	23	30.0	20.1	2.25	1.74
SF40-365d (average)	**5**			**2.25**	**2.09**

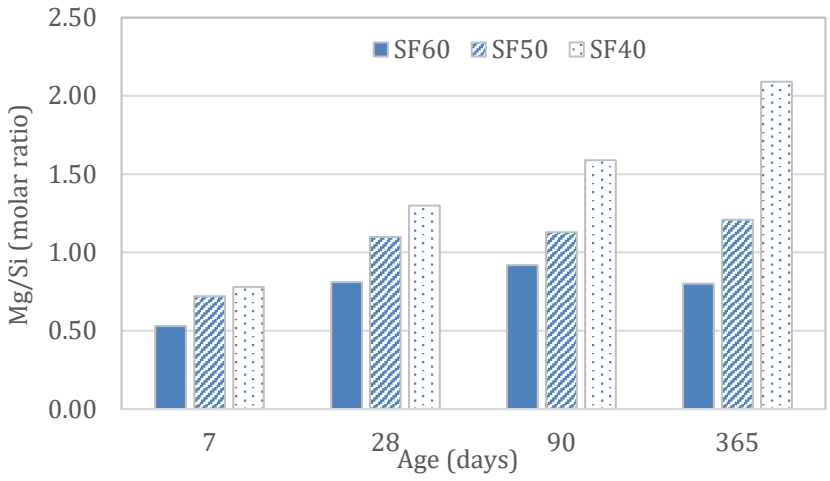

Figure 4.20. Average Mg/Si molar ratios of M-SF mixtures

4.5.2. M-MS systems

The summary of Mg/Si molar ratios of MS60, MS50, and MS40 samples at 7 days age are shown in Table 4.6. Details of EDS spectra of M-MS mixtures are available in Appendix C. The MS60 sample has a target Mg/Si ratio of 1.0, but the spectra at 7 days age only obtained lower Mg/Si ratios in a range of 0.36-1.09 with an average value of 0.68. Most of the spectra have Mg/Si ratios agreed well with M-S-H compositions in previous studies, indicating that M-S-H phases are also formed at an early age with M-MS mixtures. As MgO content in the binder compositions increases from 40% to 60%, the Mg/Si ratios of the hydration products in samples MS50 and MS40 also increase, indicating an additional amount of Mg is bound in the M-S-H phases. However, it can be seen that the Mg/Si ratios of the hydration products are always lower than the MgO/SiO_2 ratios of the raw materials. This proves that the reactions forming M-S-H phases at this early age occur slowly and the main reactions are the hydration of MgO.

Table 4.6. EDS results of M-MS mixtures at 7 days age

System	Number of points / Spectrum	Mg wt%	Si wt%	Mg/Si (molar) of precursors	Mg/Si (molar) of hydration products
MS60	17	12.1	23.5	1.0	0.60
MS60	18	10.5	33.7	1.0	0.36
MS60	19	14.8	27.3	1.0	0.63
MS60	20	22.6	38.9	1.0	0.68
MS60	21	22.3	23.9	1.0	1.09
MS60	22	17.2	27.8	1.0	0.72
MS60-7d (average)	**6**			**1.0**	**0.68**
MS50	69	11.2	35.7	1.50	0.37
MS50	70	19.3	20.2	1.50	1.11
MS50	71	8.7	30.8	1.50	0.33
MS50	72	25.6	23.0	1.50	1.30
MS50	73	21.1	36.1	1.50	0.68
MS50	74	16.7	29.8	1.50	0.65
MS50-7d (average)	**6**			**1.50**	**0.74**
MS40	34	23.4	16.6	2.25	1.64
MS40	35	24.2	20.4	2.25	1.38
MS40	36	17.2	24.4	2.25	0.82
MS40	37	21.6	31.5	2.25	0.80
MS40	38	27.9	15.7	2.25	2.07
MS40-7d (average)	**5**			**2.25**	**1.34**

Table 4.7 shows the Mg/Si molar ratios of samples at 28 days age in which increases of the Mg/Si molar ratios compared to 7 days age were observed. Over the time, due to the consumption of MS for the chemical reactions forming M-S-H, the concentrations of MS on the surface of MgO reduce and result in the increase of Mg/Si molar ratios of the hydration products.

The MgO/SiO_2 ratios of the binder compositions have a strong influence on the chemical compositions of the hydration products of M-MS mixtures. M-S-H phases are formed readily after 28 days curing with Mg/Si molar ratios in a range of 0.69 to 1.87, which is almost consistent with Mg/Si ratios of M-S-H suggested elsewhere in the literature (Wei et al., 2006). An increase in MgO content from 40% to 60% of the raw materials also leads to the higher Mg/Si molar ratios of the hydration products at 28 days age. However, some locations have Mg/Si molar ratios higher than 1.50 indicating the heterogeneity of the mixture containing excessive MgO (MS40 samples).

Table 4.7. EDS results of M-MS mixtures at 28 days age

System	Number of points / Spectrum	Mg wt%	Si wt%	Mg/Si (molar) of precursors	Mg/Si (molar) of hydration products
MS60	32	20.2	35.2	1.0	0.67
MS60	33	20.9	35.4	1.0	0.69
MS60	34	16.0	39.2	1.0	0.48
MS60	35	24.0	34.1	1.0	0.82
MS60	37	20.4	30.0	1.0	0.79
MS60-28d (average)	**5**			**1.0**	**0.69**
MS50	47	21.8	31.6	1.50	0.80
MS50	48	25.0	28.2	1.50	1.03
MS50	49	18.1	32.2	1.50	0.66
MS50	50	17.6	36.7	1.50	0.56
MS50	51	27.2	24.4	1.50	1.30
MS50-28d (average)				1.50	**0.87**
MS40	53	27.6	20.0	2.25	1.61
MS40	55	32.2	22.4	2.25	1.68
MS40	56	29.9	15.8	2.25	2.21
MS40	57	30.5	19.3	2.25	1.84
MS40	58	30.4	17.8	2.25	1.99
MS40-28d				2.25	**1.87 (average)**

Table 4.8 and 4.9 present the EDS results over the long-term curing up to 90 days and 365 days of M-MS mixtures. The comparison of average Mg/Si molar ratios of M-MS mixtures over the time is shown in Figure 4.21. Similar to M-SF samples, Mg/Si molar ratios of the hydration products increase further to confirm the improvement of the crystallinity and the completion of the hydration process. Mixture MS60 and MS50 have Mg/Si molar ratios in a range of 0.80 to 1.40 over the long-term, which is attributed to the formation of M-S-H gel. Mixture MS40 containing 60% MgO and 40% MS with a target Mg/Si molar ratio of 2.25 obtained very high Mg/Si molar ratios of 2.66 and 2.24 at 90 and 365 days, respectively. The Mg/Si molar ratios exceeding 1.50 reveal the non-uniformity of the MS40 mixture with the presence of residual brucite due to a high content of MgO in the binder composition.

Table 4.8. EDS results of M-MS mixtures at 90 days age

System	Number of points / Spectrum	Mg wt%	Si wt%	Mg/Si (molar) of precursors	Mg/Si (molar) of hydration products
MS60	52	27.5	31.4	1.0	1.02
MS60	53	18.7	38.4	1.0	0.57
MS60	54	25.1	26.2	1.0	1.12
MS60	55	7.2	31.8	1.0	0.26
MS60	56	20.5	31.0	1.0	0.77
MS60	57	23.0	29.4	1.0	0.91
MS60-90d (average)				**1.0**	**0.78**
MS50	64	21.5	33.1	1.50	0.76
MS50	65	26.5	27.5	1.50	1.12
MS50	66	30.1	24.4	1.50	1.44
MS50	67	27.5	21.9	1.50	1.46
MS50	68	23.7	36.6	1.50	0.76
MS50-90d (average)				1.50	**1.11**
MS40	69	34.5	16.4	2.25	2.45
MS40	70	29.0	22.4	2.25	1.51
MS40	71	26.7	29.2	2.25	1.07
MS40	72	28.2	15.0	2.25	2.19
MS40	73	35.9	6.9	2.25	6.07
MS40-90d (average)				2.25	**2.66**

Table 4.9. EDS results of M-MS mixtures at 365 days age

System	Number of points / Spectrum	Mg wt%	Si wt%	Mg/Si (molar) of precursors	Mg/Si (molar) of hydration products
MS60	34	24.8	26.0	1.0	1.11
MS60	35	22.1	23.5	1.0	1.10
MS60	36	8.6	40.2	1.0	0.25
MS60	37	23.4	30.5	1.0	0.90
MS60	38	24.8	26.5	1.0	1.09
MS60	39	20.0	27.6	1.0	0.85
MS60-365d (average)				**1.0**	**0.88**
MS50	45	27.1	19.5	1.50	1.62
MS50	46	25.6	22.6	1.50	1.32
MS50	47	24.6	21.3	1.50	1.35
MS50	48	25.7	18.8	1.50	1.59
MS50	49	21.4	24.5	1.50	1.02
MS50-365d (average)				1.50	**1.38**
MS40	50	29.8	18.5	2.25	1.88
MS40	51	30.3	15.8	2.25	2.24
MS40	53	33.7	17.4	2.25	2.26
MS40	54	35.4	13.6	2.25	3.04
MS40	55	25.6	16.7	2.25	1.79
MS40-365d (average)				2.25	**2.24**

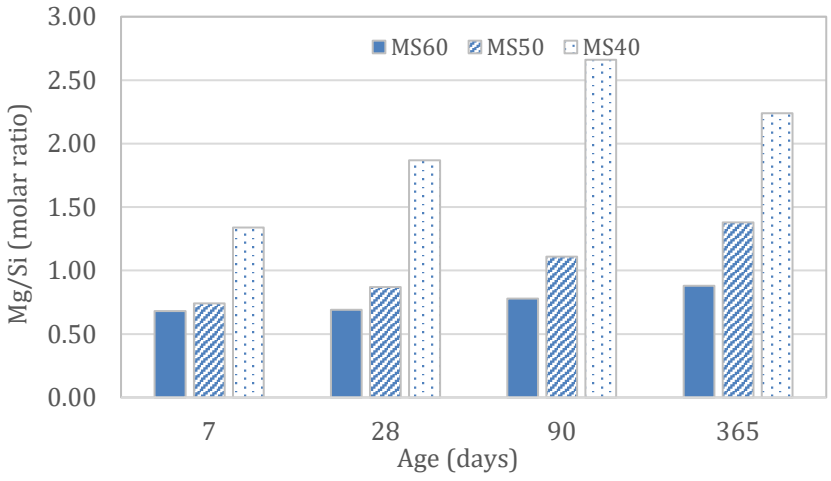

Figure 4.21. Average Mg/Si molar ratios of M-MS mixtures

The hydration process of M-MS mixtures is similar to that of M-SF mixtures however the Mg/Si molar ratios are slightly higher than those of M-SF mixtures. The difference of particle size, chemical composition and reactivity between the two silica sources can have a strong influence on the formation of M-S-H binding phases.

4.5.3. M-RHA and M-FA systems

Table 4.10 and Figure 4.22 presents EDS analysis of M-RHA mixture containing 60% and 40% RHA during 365 days curing period.

It is shown that the average Mg/Si ratio of RHA40 samples is in the range of 1.23 to 1.46, which is consistent with reported Mg/Si ratios of M-S-H phases. The formation of M-S-H binding phases in RHA40 samples was observed at the early age of 7 days which indicates the high reactivity of RHA. In comparison to M-SF and M-MS systems, Mg/Si ratios of M-S-H phases of RHA40 samples are quite stable over the 365 days as a result of the early completion of the reactions of RHA and brucite.

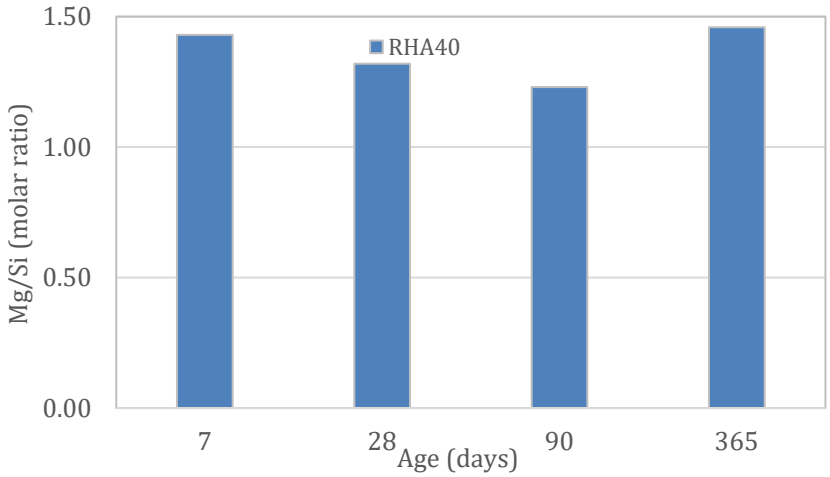

Figure 4.22. Average Mg/Si molar ratios of M-RHA mixtures

Table 4.10. EDS results of RHA40 samples at 7, 28, 90 and 365 days age

System	Number of points / Spectrum	Mg wt%	Si wt%	Mg/Si (molar) of precursors	Mg/Si (molar) of hydration products
RHA40	42	34.8	18.8	2.25	2.16
RHA40	43	21.7	29.7	2.25	0.85
RHA40	44	22.4	29.2	2.25	0.89
RHA40	45	37.3	17.1	2.25	2.54
RHA40	46	19.1	31.3	2.25	0.71
RHA40-7d (average)				**2.25**	**1.43**
RHA40	52	22.3	29.0	2.25	0.90
RHA40	53	30.8	22.2	2.25	1.62
RHA40	54	28.5	22.9	2.25	1.45
RHA40	55	24.8	27.2	2.25	1.06
RHA40	56	30.4	22.7	2.25	1.56
RHA40-28d (average)				2.25	**1.32**
RHA40	29	10.4	37.0	2.25	0.33
RHA40	30	27.5	34.1	2.25	0.94
RHA40	31	23.7	21.6	2.25	1.28
RHA40	32	27.2	30.4	2.25	1.04
RHA40	33	35.7	26.7	2.25	1.56
RHA40	36	39.4	20.8	2.25	2.21
RHA40-90d (average)				2.25	**1.23**
RHA40	16	31.0	19.3	2.25	1.87
RHA40	17	29.3	33.0	2.25	1.04
RHA40	18	30.4	24.4	2.25	1.45
RHA40	19	27.9	22.9	2.25	1.42
RHA40	20	31.0	23.9	2.25	1.51
RHA40-365d (average)				2.25	**1.46**

Table 4.11 and Figure 4.23 shows EDS results of M-FA mixtures containing 60% of MgO and 40% of FA. Due to the high MgO/FA ratio and the low SiO_2 content in FA (<50%), it is obvious that the Mg/Si ratios of the hydration products are very high compared to the use of other silica sources (SF. MS, RHA). The average Mg/Si ratio in FA40 samples is in between 5.0 - 6.50, which is out of the suggested range of Mg/Si molar ratios of M-S-H phases. It appears that M-S-H is not formed in these samples. In addition, the variation of Mg/Si ratios in each sample is very large. For example, the FA40 samples at 7 days had Mg/Si molar ratios varied from 0.06 to 12.89. Similarly, at the end of 365 days curing period, the Mg/Si ratios varied from 0.1 to 18.38. A low value of Mg/Si ratios represents the predominance of unreacted SiO_2 while a very high Mg/Si ratio can reflect the presence of MgO or $Mg(OH)_2$. The large variability of Mg/Si ratios has shown the heterogeneity of microstructure without reactions of FA and hydrated MgO. The EDS results are well agreed with the SEM and XRD analysis as mentioned above to identify the formation of M-S-H in the mixtures of MgO and different silica sources.

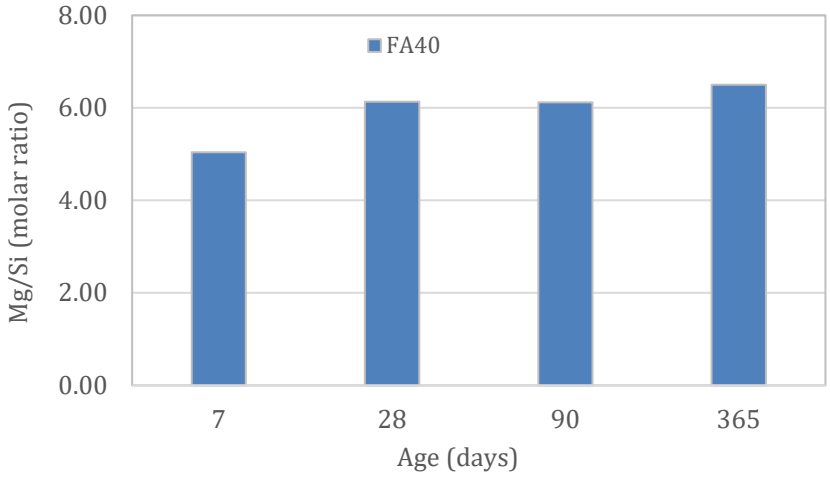

Figure 4.23. Average Mg/Si molar ratios of M-FA mixtures

Table 4.11. EDS results of FA40 samples at 7, 28, 90 and 365 days age

System	Number of points / Spectrum	Mg wt%	Si wt%	Mg/Si (molar) of precursors	Mg/Si (molar) of hydration products
FA40	75	49.7	4.5	2.25	12.89
FA40	76	2.0	30.8	2.25	0.08
FA40	77	44.9	5.0	2.25	10.48
FA40	78	2.4	43.2	2.25	0.06
FA40	79	27.9	19.2	2.25	1.70
FA40-7d (average)				**2.25**	**5.04**
FA40	95	39.2	7.2	2.25	6.35
FA40	96	41.9	6.8	2.25	7.19
FA40	97	46.9	5.0	2.25	10.94
FA40	98	36.2	7.3	2.25	5.79
FA40	99	5.7	17.7	2.25	0.38
FA40-28d (average)				2.25	**6.13**
FA40	80	32.0	5.9	2.25	6.33
FA40	81	45.1	4.6	2.25	11.44
FA40	82	37.4	6.0	2.25	7.27
FA40	83	34.7	7.4	2.25	5.47
FA40	84	2.0	30.9	2.25	0.08
FA40-90d (average)				2.25	**6.12**
FA40	70	9.1	2.3	2.25	4.62
FA40	71	3.0	27.1	2.25	0.13
FA40	72	1.7	19.6	2.25	0.10
FA40	73	23.2	11.2	2.25	2.42
FA40	74	37.8	2.4	2.25	18.38
FA40	75	39.0	3.4	2.25	13.38
FA40-365d (average)				2.25	**6.50**

Figure 4.24 compares Mg/Si molar ratios of M-S-H phases formed at 28 days ages of mixtures of MgO with four silica sources with a MgO/SiO_2 ratio of 60/40. The average Mg/Si molar ratios were calculated for each sample from EDS analysis which reflects the effect of each of the four testing silica sources on the hydration products. Various Mg/Si molar ratios were found which show a strong influence of the chemical composition of the silica sources. The average 28-day Mg/Si molar ratios of SF40 and RHA40 samples were 1.30 and 1.32 (respectively), which are consistent with other studies reporting common ratios of M-S-H phases in between 0.70-1.50 (Mitsuda and

Taguchi, 1977; Lothenbach et al., 2015). As for MS40 samples, the average molar ratios of M-S-H phases (1.87) was slightly higher than the reported range, which indicates the presence of unreacted $Mg(OH)_2$ as a hydration product alongside the formation of M-S-H. In contrast to the low Mg/Si molar ratios of SF40, RHA40, and MS40 samples, mixtures using FA exhibited an extremely high average Mg/Si molar ratio of the hydration products. This high Mg/Si ratio reveals the inhomogeneity of M-FA mixtures in which the formation of M-S-H phases is negligible and $Mg(OH)_2$ is the predominant hydration product. Therefore, each source of silica with its distinct features of chemical composition and morphology has a strong influence on the hydration products of MgO-silica systems, which may affect the mechanical and durability properties of the cementitious materials.

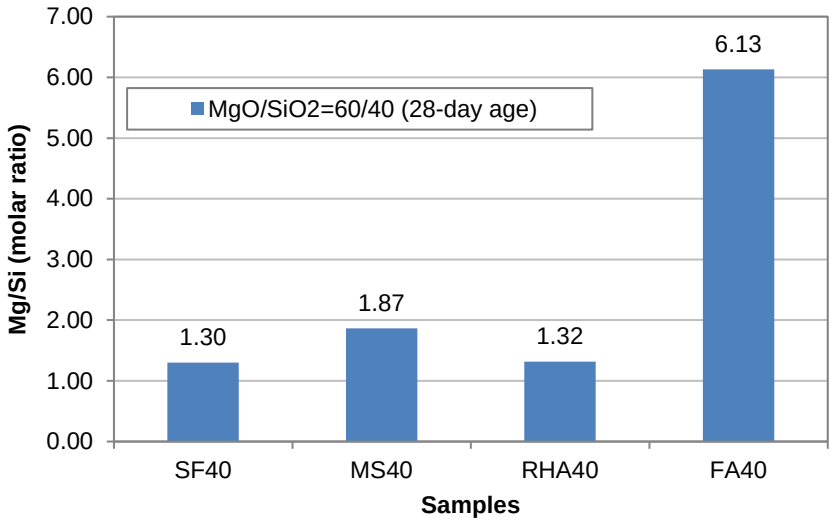

Figure 4.24. Mg/Si molar ratios of samples at 28 days age

4.6. CONCLUSIONS

This experimental work investigated the microstructure and hydration products of MgO-SiO_2 mixtures prepared at low water content (w/c=0.4) with different amorphous silica sources commonly used in concrete construction. The following conclusions can be drawn based on the findings of this study.

(1) M-S-H binding phases can be formed readily in mixtures of reactive MgO and different silica sources at w/c=0.40. The main hydration product after 1 day is brucite while M-S-H can be found as early as 7 days and at longer curing periods. Reactions of brucite and amorphous silica occur slowly before 28 days age and accelerate afterwards.

(2) The MgO/SiO_2 ratios significantly affect the microstructure and type of hydration products. The MgO/SiO_2 ratio of 1.0 (40/60 by mass) is ideal for the formation of M-S-H with a complete reaction of hydrated magnesium oxide and amorphous silica to form M-S-H gel over 365 days curing period. Higher MgO/SiO_2 ratios result in residual brucite in the mixture even after long-term curing.

(3) Silica sources with different material reactivity, purity and particle sizes also have a strong effect on the hydration products. The design of M-S-H binder systems is, therefore, complicated due to the influence of silica sources. EDS analysis shows the formation of M-S-H binding phases with different Mg/Si molar ratios results from different sources of silica. SF, MS, and RHA have high reactivity to activate hydrated MgO in M-S-H binder systems. However, the formation of M-S-H phases in M-FA systems is negligible due to the low reactivity of FA.

(4) Freshly formed M-S-H has low Mg/Si molar ratios due to the coverage of unreacted silica on the surface of brucite particles. Over the time, the brucite reacts further with silica and results in modified M-S-H phases of higher Mg/Si molar ratios.

(5) EDS analysis is well correlated with other experimental techniques such as XRD and SEM to characterize the hydration products of M-S-H binder systems.

4.7. REFERENCES

Aphane M.E. (2007). The hydration of magnesium oxide with different reactivities by water and magnesium acetate, Master Thesis, University of South Africa.

Bonen D. (1992). Composition and appearance of magnesium silicate hydrate and its relation to deterioration of cement-based materials, J. Am. Ceram. Soc. 75 2904–2906.

Bonen D., Cohen M.D. (1992). Magnesium sulfate attack on Portland cement paste—II. Chemical and mineralogical analyses, Cem. Concr. Res. 22 707–718.

Brew D.R.M., Glasser F.P. (2005). Synthesis and characterisation of magnesium silicate hydrate gels, Cem. Concr. Res. 35 85–98.

Cole W.F.A. (1953). Crystalline hydrated magnesium silicate formed in the breakdown of a concrete sea-wall, Nature 171 354–355.

Deolalkar S.P. (2016). Designing Green Cement Plants, BSP Books Pvt Ltd.

Du C. (2005). A review of magnesium oxide in concrete, Concrete international, 27 45-50.

Gollop R.S., Taylor H.F.W. (1992). Microstructural and microanalytical studies of sulfate attack. I. Ordinary Portland cement paste. Cement and Concrete Research, 22 1027-1038.

Jin F., Al-Tabbaa A. (2013). Thermogravimetric study on the hydration of reactive magnesia and silica mixture at room temperature, Thermochimica Acta, 566 162-168.

Jin F., Al-Tabbaa A. (2014). Characterisation of different commercial reactive magnesia, Advances in Cement Research, 26 101-113.

Jin F., Al-Tabbaa A. (2014). Strength and hydration products of reactive MgO–silica pastes, Cem. Concr. Compos. 52 27–33.

Jin F., Gu K., Abdollahzadeh A., Al-Tabbaa A. (2015). Effects of different reactive MgOs on the hydration of MgO-activated GGBS paste, Journal of Materials in Civil Engineering, 27.

Kalousek G.L., Mui D. (1954). Studies on Formation and Recrystallization of Intermediate Reaction Products in the System Magnesia-Silica-Water, Journal of the American Ceramic Society, 37 38-42.

Li Z., Zhang T., Hu J., Tang Y., Niu Y., Wei J., Yu Q. (2014). Characterization of reaction products and reaction process of MgO–SiO2–H2O system at room temperature, Constr. Build. Mater. 61 252–259

Lothenbach B., Nied D., L'Hopital E., Achiedo G., Dauzeres A. (2015). Magnesium and calcium silicate hydrates, Cem. Concr. Res. 77 60–68.

Mármol G., Savastano H., Tashima M.M., Provis J.L. (2016). Optimization of the MgO-SiO2 binding system for fiber-cement production with cellulosic reinforcing elements, Materials & Design, 105 251-261.

Mitsuda T. (1973). Paragenesis of 11 Å tobermorite and poorly crystalline hydrated magnesium silicate. Cement and Concrete Research, 3 71-80.

Mitsuda T., Taguchi H. (1977). Formation of magnesium silicate hydrate and its crystallization to talc, Cem. Concr. Res. 7 223–230.

Nied D., Enemark-Rasmussen K., L'Hopital E. , Skibsted J., & Lothenbach B. (2016). Properties of magnesium silicate hydrates (M-S-H), Cement and Concrete Research, 79, 323-332.

Ono H, Wada S. (2007). Properties of Layer Silicates Formed from MgO–SiO2–H2O Mixtures at 25 ˚C. J. Fac. Agr., Kyushu Univ., 52 (1) 159–162.

Roosz C., Grangeon S., Blanc P., Montouillout V., Lothenbach B., Henocq P., Giffaut E., Vieillard P., Gaboreau S. (2015). Crystal structure of magnesium silicate hydrates (M-S-H): The relation with 2:1 Mg–Si phyllosilicates, Cem. Concr. Res. 73 228–237.

Speakman K., Majumdar A.J. (1971). Synthetic 'deweylite', Mineral. Mag. 38 225-234.

Tececo (2017). Reactive magnesia. https://www.tececo.com/technical.reactive_magnesia.php, 2017 (accessed 01.02.17).

Temuujin J., Okada K., MacKenzie K.J. (1998a). Formation of layered magnesium silicate during the aging of magnesium hydroxide–silica mixtures, Journal of the American Ceramic Society 81 754-756.

Temuujin J., Okada K., MacKenzie K.J.D. (1998b). Role of water in the mechanochemical reactions of MgO–SiO2 systems, Journal of Solid State Chemistry, 138 169-177.

Tonelli M., Martini F., Calucci L., Fratini E., Geppi M., Ridi F., Borsacchi S., Baglioni P. (2016). Structural characterization of magnesium silicate hydrate: towards the design of eco-sustainable cements, Dalton Transactions 45, no. 8 3294-3304.

Tran H.M., Scott A. (2017). Strength and workability of magnesium silicate hydrate binder systems, Construction and Building Materials, 131 526-535.

Vandeperre L.J., Liska M., Al-Tabbaa A. (2008). Microstructures of reactive magnesia cement blends, Cement and Concrete Composites, 30 706-714.

Walling S.A., Kinoshita H., Bernal S.A., Colliera N.C., Provis J.L. (2015). Structure and properties of binder gels formed in the system Mg(OH)2–SiO2–H2O for immobilisation of Magnox sludge, The Royal Society of Chemistry, Dalton Trans. 44 8126–8137.

Wei J.X. , Chen Y.M., Li Y.X. (2006). The reaction mechanism between MgO and microsilica at room temperature, J. Wuhan Univ. Technol. – Mater. Sci. Ed. 21 88–91.

Wei J.X., Yu Q., Zhang W., Zhang H. (2011). Reaction products of MgO and microsilica cementitious materials at different temperatures, J. Wuhan Univ. Technol. Mater. Sci. Ed. 26 745–748.

Yamamoto K., Akimoto S.I. (1974). High pressure and high temperature investigations in the system MgO-SiO2-H2O, Journal of Solid State Chemistry, 9 187-195.

Yang J.C.S. (1960). The System Magnesia-Silica-Water Below 300° C.: I, Low-Temperature Phases from 100° to 300° C. and Their Properties, Journal of the American Ceramic Society, 43 542-549.

Zhang T, Cheeseman C., Vandeperre L.J. (2009). Development of novel low pH cement systems for encapsulation of wastes containing aluminium, Decommissioning, Immobilisation and Management of Nuclear Waste for Disposal.

Zhang T, Cheeseman C., Vandeperre L.J. (2011). Development of low pH cement systems forming magnesium silicate hydrate (M-S-H). Cement and concrete research, 41(4) 439-442.

Zhang T, Cheeseman C., Vandeperre L.J. (2012a). Characterisation of corrosion of nuclear metal wastes encapsulated in magnesium silicate hydrate (M–S–H) cement, Cer. Mater. Energy Appl. II (2012a) 159–167.

Zhang T, Cheeseman C., Vandeperre L.J. (2012b). Magnesium–silicate–hydrate cements for encapsulating problematic aluminium containing wastes, J. Sustain. Cement Based Mater. 1 34–45

Zhang T, Cheeseman C., Vandeperre L.J. (2014). Formation of magnesium silicate hydrate (M–S–H) cement pastes using sodium hexametaphosphate, Cem. Concr. Res. 65 8–14.

CHAPTER 5
PORE SOLUTION ANALYSIS OF MAGNESIUM SILICATE HYDRATE BINDER SYSTEMS

Preamble

In the earlier work on the microstructure analysis in chapter 4, the hydration process of M-S-H cement pastes was characterized using different techniques including XRD, SEM/EDS analysis. The mechanism of the formation of the M-S-H binding phases such as hydration products, hydration rate, and texture properties was discussed. The effects of different material sources and binder compositions on the hydration products and microstructures were also evaluated.

The XRD and SEM/EDS analysis are useful for the understanding of the strength development of a binder system (in chapter 7) in which hydration products can be identified and the quantitative analysis of the hydration products can be achieved. However, the nature of the chemical reactions forming the hydration products is not fully understood. The characterization of the chemical reaction requires a number of analytical techniques to investigate solubility, pH, and ion concentrations of elements of interest of the solutions extracted from cement paste samples.

For this reason, the pore solution analysis is presented in this chapter in which inductively coupled plasma mass spectrometry (ICP-MS) was utilized to analyze the development of ion concentrations of the pore solutions of M-S-H binders. Although the purpose of the analysis is not to quantify the hydration products directly, the determination of various metals and non-metals leads to an understanding of the nature of the pore solutions and provides insight into which hydrate phases are stable and can thus potentially precipitate or disolve. In addition, pHs of the pore solutions were measured to discuss the pH development as it significantly affects the solubility of the binder constituents as well as the potential durability (as discussed in chapter 8) of the resulting M-S-H cementitious materials.

Abstract

The pore solutions of magnesium silicate hydrate (M-S-H) binder systems are extracted to analyze chemical composition and pH. Mixtures contain reactive magnesium oxide and different sources of silica including silica fume (SF), natural microsilica (MS), rice husk ash (RHA) and fly ash (FA) with MgO/silica ratio varies in between 40-60 weight %.

M-S-H binders are naturally alkaline with pHs of the pore solutions strongly depend on the reactivity and alkalis content of the raw materials. The pHs of M-S-H binder systems decrease over time during 90 days testing period. SF, MS, or RHA mixed with MgO result in pHs at 2 days age in the range of 10.50 – 11.70 followed by the reduced pHs of well below 10.50 at 90 days. M-FA mixtures contain high content of sodium, potassium and calcium, which lead to high pHs in the pore solutions of above 11.00 at all testing ages.

The dominant ions available in the M-S-H binders include sodium, potassium, calcium, magnesium and silicon with the concentrations strongly influenced by the pH and solubility of the binder constituents. The formation of M-S-H phases in mixtures of low pHs under 10.50 after 90 days is confirmed with the increase of magnesium concentrations along with the decrease of silicon concentrations.

5.1. INTRODUCTION

The M-S-H binder systems are among potential sustainable cements due to the use of reactive magnesium oxide calcined at low temperatures (700-1000^{o}C) and industrial by products or waste materials such as silica fume, fly ash, rice husk or natural pozzolan.

A process which involves CO_2 sequestration by magnesium-rich minerals olivine and serpentine to produce magnesium hydroxide is being developed. Such technology if successful can produce carbon neutral magnesium-based binder materials in the future (Pacheco-Torgal, 2014). There are also other benefits of using M-S-H binders for the immobilization of nuclear wastes (Zhang et al., 2012; Walling et al., 2015).

An increasing number of publications have been found in the literature in the last decade concerning the characterization of the microstructure and mechanical properties of M-S-H binder systems. Since cementing properties of M-S-H binder were reported with strengths of over 50 MPa (Wei et al., 2006), other studies have achieved considerable higher strengths. Zhang et al. (2014) developed low pH M-S-H binder systems obtaining strengths of over 60 MPa. Marmol et al. (2016) produced 70 MPa fiber-cement with MgO-SiO_2 systems incorporating cellulosic reinforcing elements. By using quartz fillers, Tran and Scott (2017) proposed ternary mortar mixtures of MgO-SiO_2-quartz filler resulting in strengths exceeding 85 MPa. Chen et al. (2017) was able to produce pastes with a 28-day compressive strength in excess of 105 MPa at a w/c ratio of 0.2 by using a combination of CFB slag, reactive MgO and silica fume.

A number of studies including Mitsuda and Taguchi (1977) and Brew and Glasser (1995) have laid the foundations for the understanding of microstructure and reaction mechanism of reactive MgO and silica fume. Chemical reactions forming M-S-H phases at room temperature were also suggested (Li et al., 2014; Zhang et al., 2014). The MgO/SiO_2 ratio was found to have a large effect on the hydration products including brucite and M-S-H phases. The Mg/Si molar ratios of M-S-H phases range from 0.7-1.5 which are lower than Ca/Si ratios in Portland cement (Lothenbach et al., 2015; Nied et al., 2016).

There are however no studies on pore solutions extracted from M-S-H binder systems. It is known that the composition of the cement pore solution is essential as it reflects the hydration processes and determines which hydrate phases are stable and can thus potentially precipitate and vice versa (Vollpracht et al. (2016)). Different methods can be applied to obtain pore solutions of cementitious materials depending on the age and w/c ratio of the samples. Hardening pastes are generally required a high pressure device to extract the pore solutions. Such a high pressure device was first introduced by Longuet et al. (1973) to study the liquid phase of hydrate cement

and numerous studies (Barneyback and Diamond, 1981; Page et al., 1986; Kawamura et al., 1988; Andersson et al., 1989; Hussain and Al-Gahtani, 1991; Duchesne and Bérubé, 1994; Tritthart and Häußler, 2003; Buckley et al., 2007) have successfully applied similar techniques to obtain pore solutions of cement pastes with w/c = 0.60 and below.

Data such as ion concentrations and pH can be analyzed from collected pore solutions to understand the cement hydration processes. The pore solution analysis is very useful for understanding cement's deleterious reactions and durability (Hooton et al., 2010). Analytical techniques such as inductively coupled plasma optical emission spectroscopy (ICP-OES) or inductively coupled plasma mass spectrometry (ICP-MS) are available for elemental determinations.

Significance

Despite the availability of a number of studies on the formation of M-S-H binder systems, it is unlikely the binders system will find practical application in the near future due to a lack of the full understanding of the properties of the binder, in particular the pore solutions' chemical composition and durability, among other things. There is still the limitation of the very high water demand for workability compared to PC which results in fairly low strengths of the M-S-H binders (Jin and Al-Tabbaa, 2014; Walling et al., 2015). Also, the material source is reported to be one of the major causes for the strength variations of M-S-H binders (Jin et al., 2013). Tran et al. (2017) also reported the problems of slow strength development rate of M-S-H binders compared to PC.

The understanding of pH and ion concentrations of the pore solutions of the MgO-silica mixtures in this study will give important insights into the chemical processes and the interactions between solid and liquid phases of the M-S-H binder systems. In particular, underlying factors of the extreme variations of the resulting properties due to different material sources may be explained. Other findings are the relationship between the change of ion concentrations and reactions rate and causes of the slow strength development of the developing binder systems.

An understanding of the pore solution will aid in the determination of the potential durability of the new binder. The measured pHs of the pore solutions also explain potential vulnerability to the risk of corrosion if the cementitious materials are intended to have steel reinforcement. The measured concentrations of the main elements of the M-S-H binding phases may reveal the risk of leaching or loss of strength in the long term.

5.2. EXPERIMENTAL PROGRAMME

5.2.1. Materials

Reactive magnesium oxide (MgO) and four sources of reactive silica were supplied. Rice husk ash (RHA) and Fly ash (type F) was used to target low cost material sources for the M-S-H binders. Properties of materials are provided in Chapter 3.

5.2.2. Mix proportions and sample preparation

A series of samples for pore solution expression were prepared from freshly-mixed cement paste using deionized water. Mix proportions are shown in Table 5.1.

Table 5.1. Mix proportions of samples for pore solution expression

No.	Samples	Binder composition	w/b	SP (liquid % binder)	Test age and methods			
					2d	7d	28d	90d
1	SF60	0.4MgO+0.6SF	0.60	0.5	pH, ICP-MS	pH, ICP-MS	pH, ICP-MS	pH, ICP-MS
2	SF50	0.5MgO+0.5SF	0.60	0.5	pH, ICP-MS	pH, ICP-MS	pH, ICP-MS	pH, ICP-MS
3	SF40	0.6MgO+0.4SF	0.60	0.5	pH, ICP-MS	pH, ICP-MS	pH, ICP-MS	pH, ICP-MS
4	MS60	0.4MgO+0.6MS	0.60	1.0	pH, ICP-MS	pH, ICP-MS	pH, ICP-MS	pH, ICP-MS
5	MS50	0.5MgO+0.5MS	0.60	1.0	pH, ICP-MS	pH, ICP-MS	pH, ICP-MS	pH, ICP-MS
6	MS40	0.6MgO+0.4MS	0.60	1.0	pH, ICP-MS	pH, ICP-MS	pH, ICP-MS	pH, ICP-MS
7	RHA60	0.4MgO+0.6RHA	0.60	1.0	pH, ICP-MS	pH, ICP-MS	pH, ICP-MS	pH, ICP-MS
8	RHA50	0.5MgO+0.5RHA	0.60	1.0	pH, ICP-MS	pH, ICP-MS	pH, ICP-MS	pH, ICP-MS
9	RHA40	0.6MgO+0.4RHA	0.60	1.0	pH, ICP-MS	pH, ICP-MS	pH, ICP-MS	pH, ICP-MS
10	FA60	0.4MgO+0.6FA	0.60	-	pH, ICP-MS	pH, ICP-MS	pH, ICP-MS	pH, ICP-MS
11	FA50	0.5MgO+0.5FA	0.60	-	pH, ICP-MS	pH, ICP-MS	pH, ICP-MS	pH, ICP-MS
12	FA40	0.6MgO+0.4FA	0.60	-	pH, ICP-MS	pH, ICP-MS	pH, ICP-MS	pH, ICP-MS

The pastes were stored in 50 ml cylindrical laboratory tubes and sealed immediately following casting until prior to crushing to prevent both evaporation of the mix water and carbonation (Figure 5.1). Samples were cured at a room temperature of approximately 20 °C and tested at 2, 7, 28, and 90 days age.

Figure 5.1. Sample preparation

Details of the pore solution extraction method and the apparatus were described in Chapter 3. Samples (in 50 ml tubes) were taken out of the tubes and immediately placed into the apparatus followed by the compression procedure. The loading increased pressure up to 400 MPa at a rate of 0.25 MPa/s (taking about 25 minutes) and then held at this pressure for 30 seconds. Paste samples after extraction can be seen in Figure 5.2.

The volume of the pore solutions obtained by this method varied significantly with different silica sources and reduced significantly at longer curing durations. Typically, two 50 ml tube samples were used at each pressing and a volume of 4-40 ml of the pore solutions was collected at different testing ages of 2, 7, and 28 days. At 90 days age, the extraction were repeated twice with mixtures produced little pore solution. Table 5.2 shows volumes of pore solutions obtained with testing samples.

Table 5.2. Pore solution volumes (ml) of testing samples.

Sample / Age	SF60	SF50	SF40	MS60	MS50	MS40	R60	R50	R40	FA60	FA50	FA40
2 days	20	15	14	20	21	20	27	27	29	40	38	37
7 days	16	12	11	17	18	17	25	23	22	34	34	30
28 days	9	7	4	14	13	13	18	20	18	28	27	27
90 days	7*	3**	7**	11	10	12	19	18	14	23	24	22

** 2.5 samples were used; ** 5 samples were used*

The collected pore solution of each mixture was filtered and sealed in a container to prevent reactions with atmospheric carbon dioxide. The pH was measured within 1 h of collection using a pH benchtop meter (Thermo Scientific Orion Star A211). Samples for ICP-MS analysis were stored under -18^{o}C temperature until testing age. Due to the detection limit of the analytical method, samples were diluted prior to analysis. The dilution factor of M-SF, M-MS, and M-RHA mixtures was 500 (1 ml of the pore solution was diluted by 500ml of deionized water). The M-FA mixture was diluted with a dilution factor as high as 2000 due to the high content of alkalis in the pore solutions. Ion concentrations of the pore solutions were analyzed using the Agilent 7500cx ICP-MS instrument (Figure 5.3)

Figure 5.2. Paste samples after expression

Figure 5.3. Agilent 7500 Series ICP-MS analysis instrument (Agilent Technologies Inc., 2006)

5.3. RESULTS AND DISCUSSION

5.3.1. pH development of M-S-H binders

The reference pH of each material source is required to understand the interaction of the constituents in the M-S-H binders. To provide a control pH for each material source, a solution was prepared in which 5 g of each raw material was stirred in 100 ml of deionized water. Figure 5.4 shows the control pHs of each individual material measured at the same testing ages as the pore solutions (2, 7, 28, and 90 days).

The pH changes in the pore solutions of each mixture in comparison to its each binder constituents are discussed below.

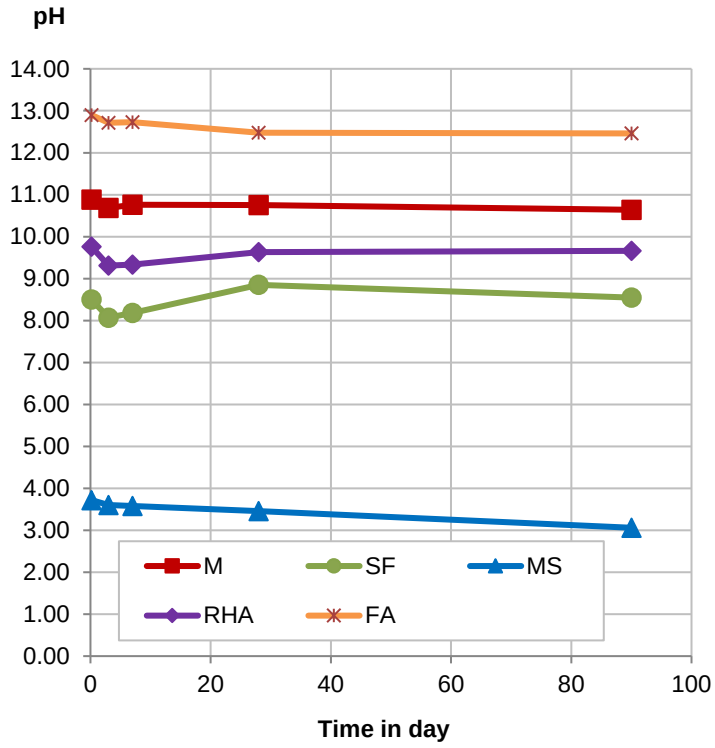

Figure 5.4. pH of raw material solutions (solid/water = 5/50 g/ml)

5.3.1.1. M-SF systems

Figure 5.5 shows pH-values of the pore solutions extracted from M-SF cement pastes. It is obvious that M-S-H binders are naturally alkaline though somewhat lower than PC. The pHs of the mixtures are dependent on the reactivity of MgO, silica, and in particular total content of alkali compounds such as N_2O, K_2O, CaO although available in the binders as impurities of the raw materials.

It is expected that reactive MgO can react quickly with water during the first few days to form brucite and the predominance of brucite in the mixture results in an alkaline pore solution. Theoretically, $Mg(OH)_2$ is reported to have a pH close to 10.50 (O'Neil, 2006).

The pHs of M-S-H pore solutions at 2 days age are well above 10.50 and close to 11.00. These high pH-values result from the presence of soluble alkalis in both MgO and SF. However, a sharp decrease of pHs to below 10.50 was observed with all M-SF mixtures at 7 days age and the pHs further decreased as curing age increased to 90 days. The pH changes in M-SF mixtures are opposed to pH patterns of the raw material solutions in which a stable pH close to 11.00 for the MgO solution was observed while SF solution showed slightly fluctuated pH-values as low as in between 8.00-9.00.

The effect of changing MgO/SF ratios on pHs of pore solutions is well observed particularly in the long-term. The pHs of mixtures at 90 days vary noticeably reflecting the reaction rate and stoichiometry. The low SF mixture (SF40) has a pH of just below 10.50 suggesting the presence of residual brucite as part of hydration products while the high SF mixture (SF60) shows a very low pH of only 9.20 at which most of brucite should react with SF and the M-S-H are formed as the main binding phases.

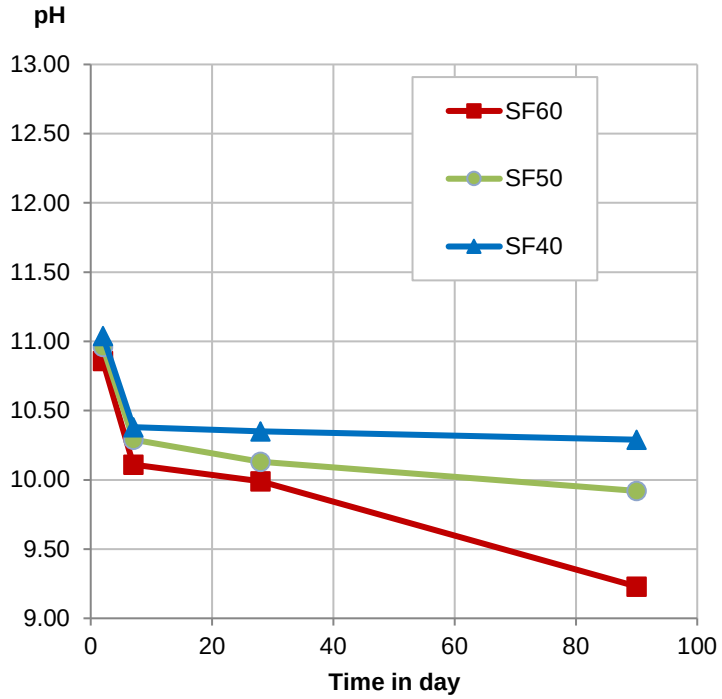

Figure 5.5. pH of pore solutions of M-SF binder systems

5.3.1.2. M-MS systems

Figure 5.6 presents the pHs of M-MS binder systems showing a decrease trend over the 90 days period which is similar to the pH patterns of M-SF samples.

The pHs of the pore solutions are determined by the chemical compositions of the raw materials. It is shown that the reference MS solution has the lowest pH-values of only between 3.0 and 4.0 over the 90 days compared to other silica sources. The reason is that although MS600 is rich in silica, the deposit also contains impurities including clay, ironsand, alunite, and elemental sulphur (Chrisholm, 1998). This low pH has affected the pHs of M-MS pore solutions resulting in a wide range of pH-values at early age up to 7 days as the MS content increases from 40 to 60%.

M-MS mixtures have a pH range of 10.20 to 11.00. The decrease rate of the pH-values is lower than the M-SF samples even no significant decrease is observed between 28 and 90 days. The pH decrease indicates some degree of reaction of MS and hydrated MgO forming M-S-H binding phases, however, a stable pH of about 10.20 at later stage also suggests that MS is less reactive than SF in M-S-H binder systems.

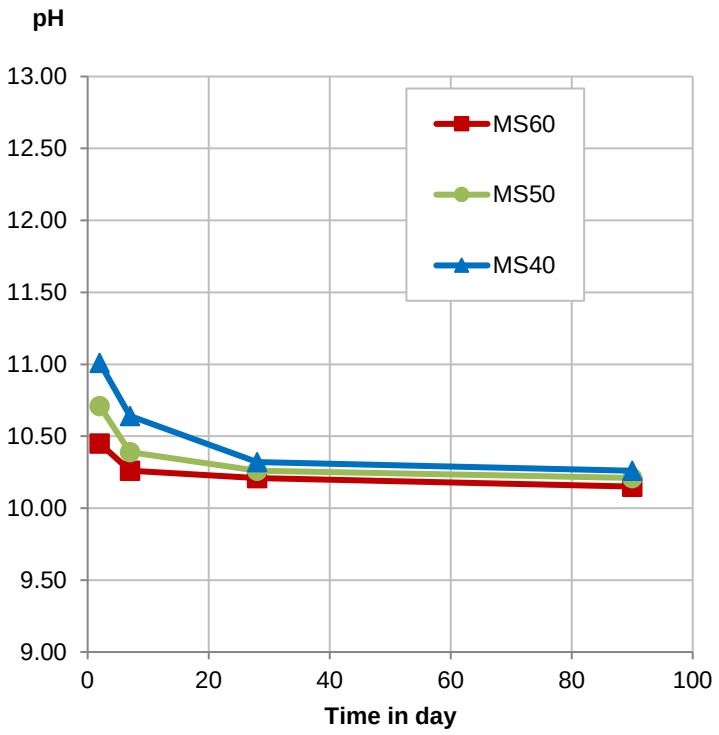

Figure 5.6. pH of pore solutions of M-MS binder systems

5.3.1.3. M-RHA systems

Figure 5.7 shows the pH evolution of M-RHA mixtures over 90 days hydration period. Again, a downward trend is observed with a sharp decrease of the pH-values during the first 7 days followed by a slow reduction from 7 to 90 days age.

The pore solutions have the high pHs at 2 days range from 11.40-11.70 resulted from the high pH of the RHA solution (pH = 9.30-9.80, Figure 5.4) compared to SF and MS. Nonetheless, the pHs of the pore solutions drop dramatically to around 10.50 after 7 days indicating some degree of reaction forming M-S-H phases. A further pH reduction at a slow rate to below 10.00 after 90 days confirms the increasing formation of M-S-H as a result of the reaction of hydrated MgO and RHA, which is almost similar to the pozzolanic reaction of calcium hydroxide and silica to form C-S-H in the blended PC.

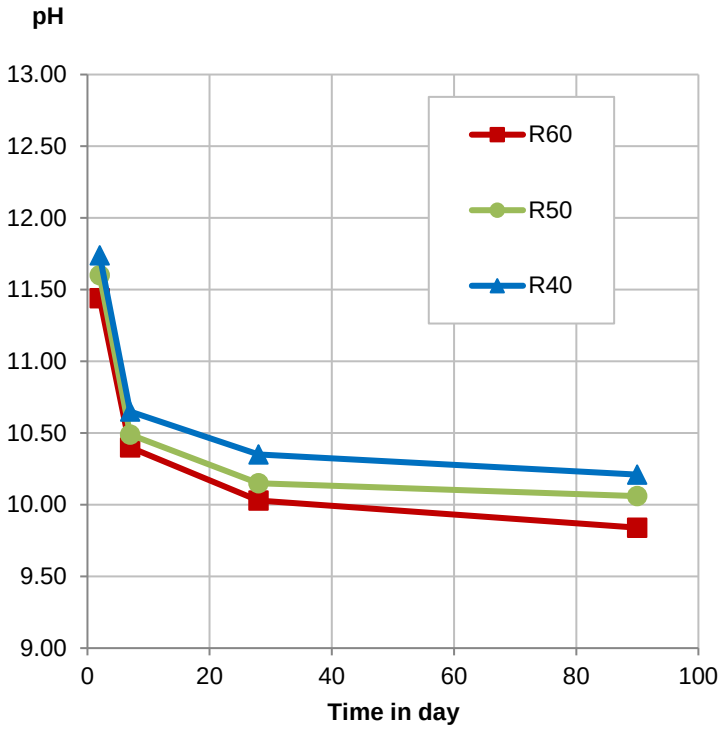

Figure 5.7. pH of pore solutions of M-RHA binder systems

5.3.1.4. M-FA systems

Figure 5.8 presents the pH development of the pore solutions of M-FA mixtures over the time. The decrease in pHs is observed however the pore solutions of M-FA mixtures have exceptionally high pHs during 90-day curing period compared to other mixtures. The total alkalis content (Na_2O, K_2O, CaO, MgO) in FA is far more higher than in other silica and possibly the main cause to raise pHs of the pore solutions. The pH of FA control solution fluctuated in between 12.50 to 12.90 during 90 days (Figure 5.4). As a result, the pore solutions of M-FA mixtures also showed high pH-values in between 11.30 and 12.80. The pHs of M-FA mixtures appear to decline linearly, which is in contrast to the sharp decrease during the first 7 days as seen with M-SF, M-MS, M-RHA mixtures.

The high pHs in M-FA mixtures could increase the dissolution of silica and accelerate the MgO-silica reactions. On the other hand, the high pH adversely affects the solubility of MgO which would reduce the reaction rate. The high pHs measured after a long period curing up to 90 days suggests a very limited degree of reaction between MgO and FA. The pH development therefore also reflects the lower reactivity of FA compared to other types of silica, which is consistent with the low amorphous silica content in the chemical composition of FA (in chapter 4) and the strength results of M-FA mixtures (in chapter 7).

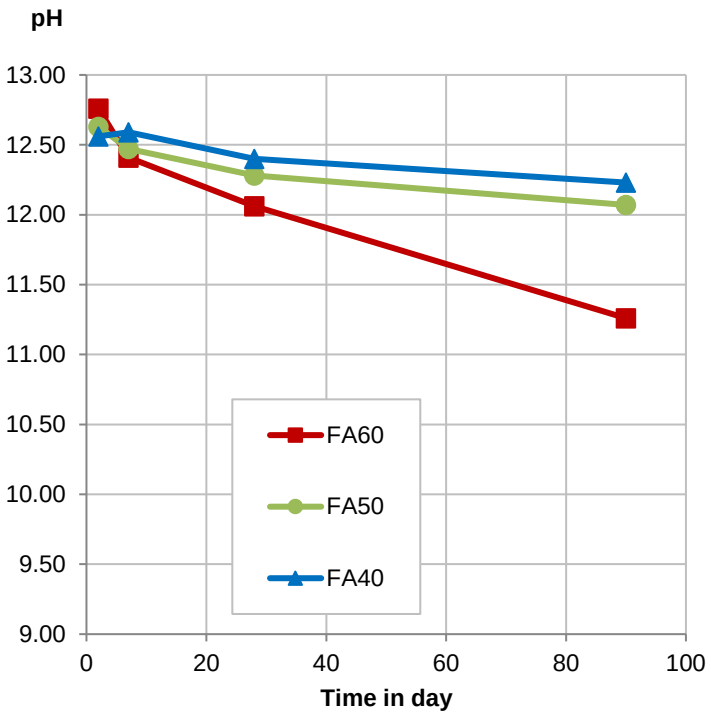

Figure 5.8. pH of pore solutions of M-FA binder systems

5.3.2. Chemical composition of M-S-H cement pore solutions

5.3.2.1. MgO-SF systems

a) Alkali concentrations (Na+, K+, Ca2+)

Alkalis are present in the raw materials of the binders. Both reactive magnesium oxide and silica have alkalis as impurities. In particular, fly ash contains a considerable amount of calcium oxide. It is known that alkalis (Na_2O, K_2O) dissolve rapidly within the first minutes when water is added and therefore have a strong influence on the pH and dissolution of other elements.

Three MgO/SF ratios were intentionally selected for SF60, SF50, SF40 mixtures to examine the influence of MgO/SF ratio on the ion concentrations. However it should be noted that only alkalis and magnesium ion concentrations of SF50 and SF40 mixtures were reported and discussed herein in Figure 5.9 – 5.12. The alkali concentrations of SF60 mixture at 28 days age are presented in Appendix D for reference only as they appears to be out of proportion to the other samples (SF 50 and SF40) and probably the result of a dilution error.

Alkali concentrations (Na+, K+, Ca2+) of SF50 and SF40 mixtures are shown in Figure 5.9, Figure 5.10, and Figure 5.11. The ion concentrations are dependent on the amount of the elements in the raw materials. As SF contains high amounts of Na and K (compared to other silica), high concentrations of Na and K were observed in the solutions, ranged widely from 300 to 1150 mg/L (Na) and 150 to 950 mg/L (K).

Although there is a considerable amount of CaO (4%) in the reactive MgO, the theoretical solubility of Ca is far less than Na and K, hence there is only a low concentration of Ca available in the solutions at all ages (Figure 5.11). Measured calcium concentrations are also far less than magnesium concentrations in the pore solutions of the binders.

b) Magnesium concentration

Figure 5.12 shows Mg concentrations of the pore solutions of MS50 and MS40 mixtures over 90 days period. During the early age, Mg concentrations are mainly controlled by the dissolution of MgO and affected by the reactivity of MgO and pH of the pore solutions. MgO is known to be practically insoluble in water. Due to a poor water solubility (86 mg/L at 30^{o} C (Patnaik, 2003)), the Mg^{2+} concentration at early age up to 7 days are very low and consistent with its theoretical solubility. The high MgO/SF ratio is expected to result in higher Mg concentration at this early age as the MgO content increases from 50% (in SF50 samples) to 60% (in SF40 samples). However, the low solubility of MgO has made this difference insignificant.

SF has a strong influence on the solubility of MgO, particularly after 7 days age. As SF is present, the dissolution of MgO is accelerated and the Mg concentration exceeds the water solubility limit. At 28 and 90 days age, an increase in Mg concentrations was observed along with the decrease of Si concentrations. The measured magnesium concentrations are even much higher than calcium concentrations in the pore solutions of the M-SF systems. This general trend of increasing magnesium concentrations indicates the reactions of hydrated MgO and SF to form M-S-H phases.

As hydrated MgO reacts with SF, the MgO/SF ratio also influences Mg concentrations. The high Mg^{2+} concentration was observed at 90 days age with SF50 mixture containing higher SF than SF40 mixture. The Mg ion concentrations were consistent with the theoretical stoichiometry of the reaction between MgO and SF to form M-S-H phases.

The reactivity of a silica source can be shown by the dissolution of MgO. A highly reactive silica source would accelerate the dissolution of MgO for the formation of M-S-H phases. The remarkable change in measured Mg concentrations has shown the high reactivity of silica fume used in M-SF systems.

c) Silicon concentration

Si concentration is correlated to the solubility of silica which is affected by the pH and the content of alkalis in the mixtures. It is known that the pore solutions have high pHs at early age due to the high solubility of alkalis and the high content of MgO (40-60%) in the binder. As a result, the Si concentrations (Figure 5.13) increased to the highest values at 2 days age. The Si concentrations decreased over the time along with the formation of M-S-H phases.

It is observed that MgO/SF ratios within the testing range have little effect on the solubility of SF in the mixtures, probably due to the high content of both MgO and SF. All M-SF mixtures exhibit similar patterns of a downward trend with marginal difference of the Si concentrations over the 90 days. The Si concentrations of M-SF mixtures reduce from the high value of 150 mg/L at 2 days age to the low value of about 100 mg/L at long-term of 90 days.

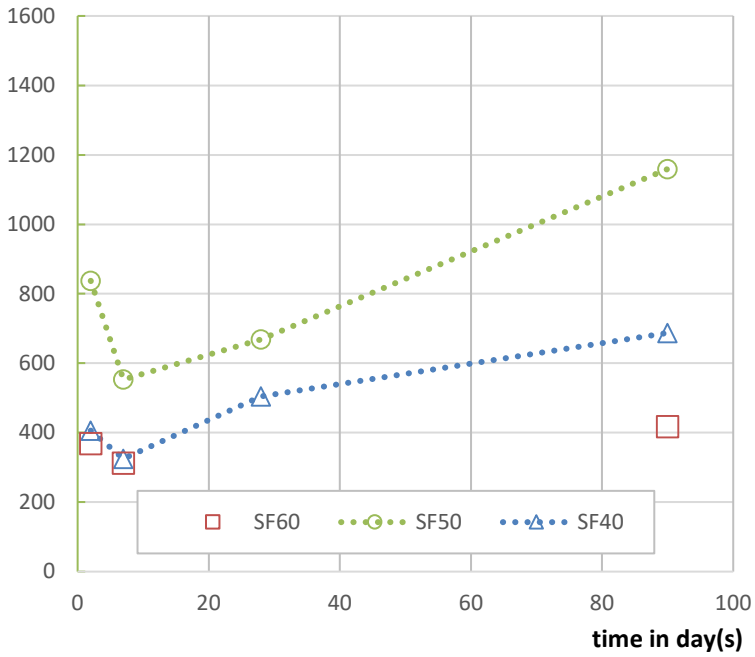

Figure 5.9. Na concentration (mg/L) in M-SF systems

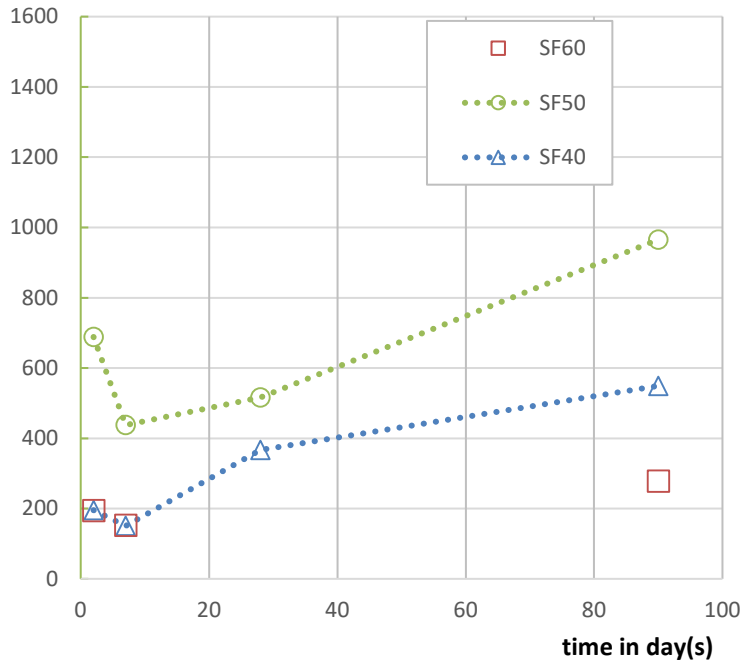

Figure 5.10. K concentration (mg/L) in M-SF systems

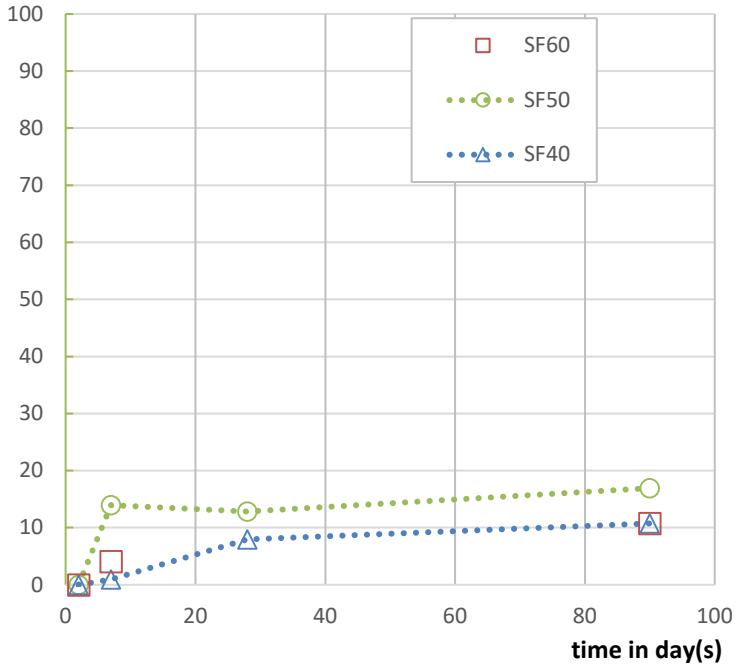

Figure 5.11. Ca concentration (mg/L) in M-SF systems

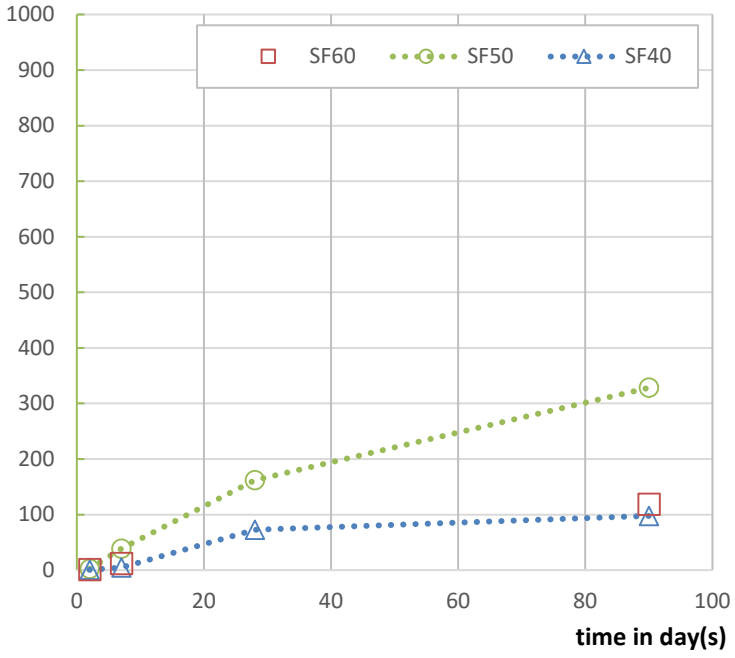

Figure 5.12. Mg concentration (mg/L) in M-SF systems

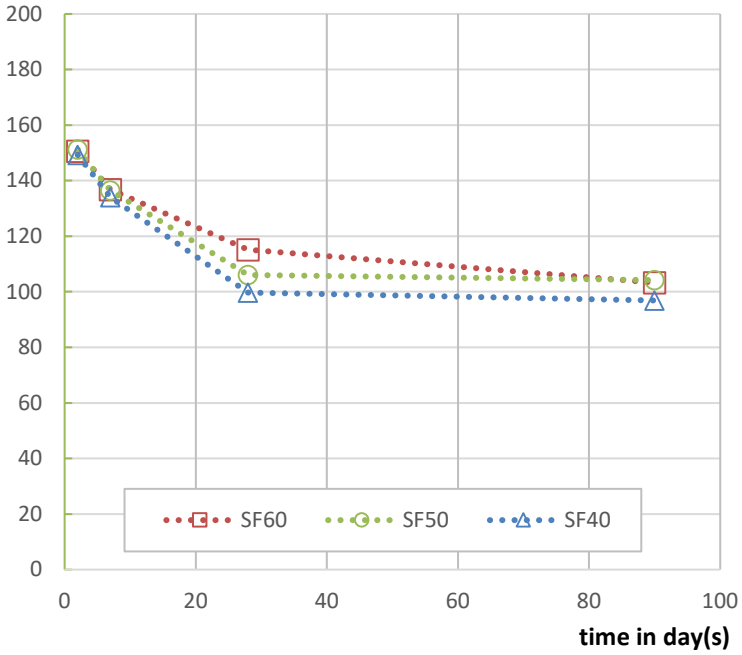

Figure 5.13. Silicon concentration (mg/L) in M-SF systems

5.3.2.2. MgO-MS systems

a) Alkali concentrations (Na^+, K^+, Ca^{2+})

The concentrations of alkalis in the pore solutions of M-MS paste samples are provided in Figure 5.14, Figure 5.15, and Figure 5.16. Due to the consumption of water during the hydration process and also a release of alkalis incorporated into binder constituents the alkali concentrations slightly increase over time, although a part of the alkalis is bound in the hydration products (brucite and M-S-H phases).

The concentrations of sodium, potassium and calcium depend on the total content of K_2O, N_2O and CaO of the binders. The total content of these oxides in MS is much lower than SF, which leads to far less alkali ion concentrations than M-SF mixtures. The sodium and potassium concentrations in M-MS mixtures reach up to 400 and 120 mg/L, compared to approximately 1600 and 1400 mg/L of M-SF samples, respectively. The low solubility also limits the calcium concentrations in the pore solutions. The highest calcium concentrations in M-MS mixtures over 90 days are below 30 mg/L while these concentrations in M-SF mixtures varies under 50 mg/L.

b) Magnesium concentration

Figure 5.17 shows Mg concentrations in the M-MS mixtures over 90 days period. During the early age, Mg concentrations are pretty low which are mainly controlled by the limited solubility of MgO in water. An increase of the Mg concentrations in the pore solution is observed for all binders over the time. The presence of MS has a strong influence on the dissolution of hydrated MgO after 7 days.

The Mg concentration ranges of M-MS mixtures are slightly lower than M-SF mixtures. The measured concentrations at 7 days are in between 20 and 100 mg/L, then rise to 50÷200 mg/L at 28 days and further increase to 150÷250 mg/L. The increasing Mg concentration would suggest the depletion of brucite to react with MS for the formation of M-S-H binding phases.

Mg concentrations are also influenced by MgO/MS ratios in M-MS mixtures. The variation of the concentration reflects the change of MS content. High amounts of MS can reduce pH faster to increase dissolution of MgO and reaction rate forming M-S-H phases. An increase in Mg concentration due to increasing MS content also indicates the high reactivity of MS as a supplementary cementitious materials.

c) Silicon concentration

Silicon concentrations of M-MS mixtures are shown in Figure 5.18. The results are almost in the same range as observed in M-SF mixtures in which the general trend is the decrease of Si concentrations over the 90 days period.

One possible reason for the reduced Si concentrations is the consumption of an amount of silica as a result of the formation of M-S-H. The pH also has strong impact on the solubility of silica. The decrease of the pHs of the pore solutions over the time generally reduces the dissolution of silica and leads to the reduction of Si concentrations.

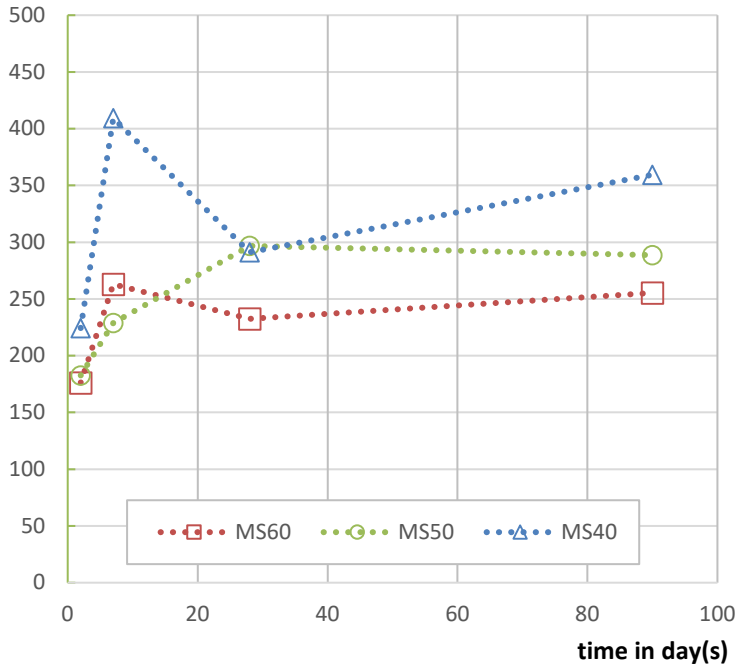

Figure 5.14. Na concentration (mg/L) in M-MS systems

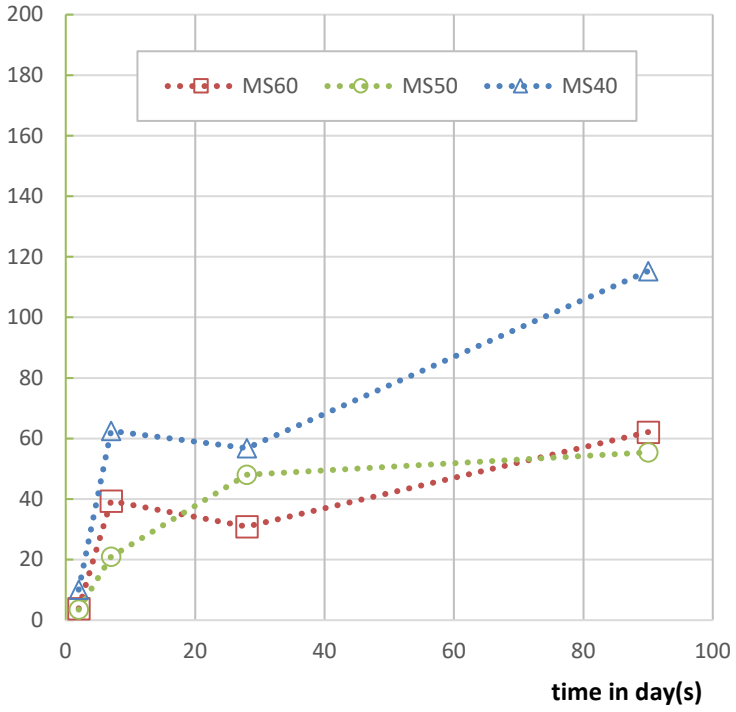

Figure 5.15. K concentration (mg/L) in M-MS systems

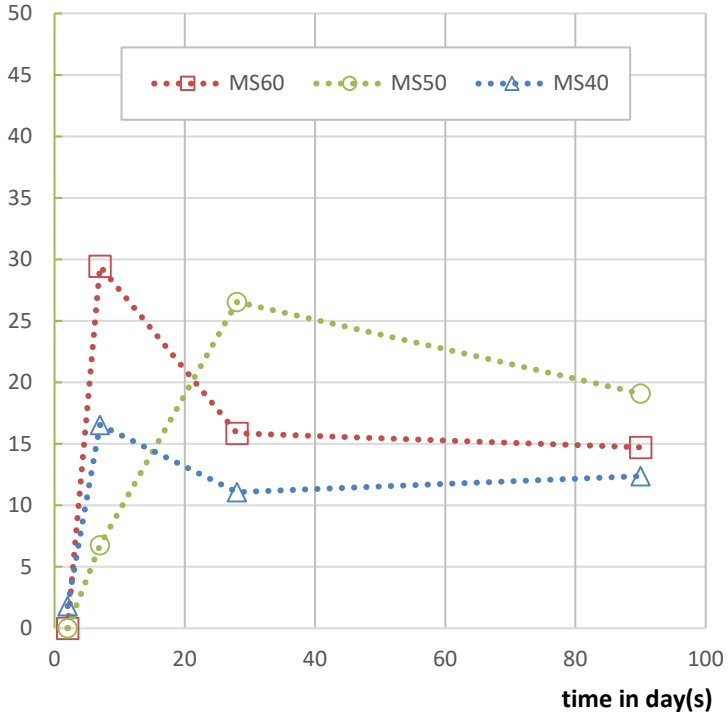

Figure 5.16. Ca concentration (mg/L) in M-MS systems

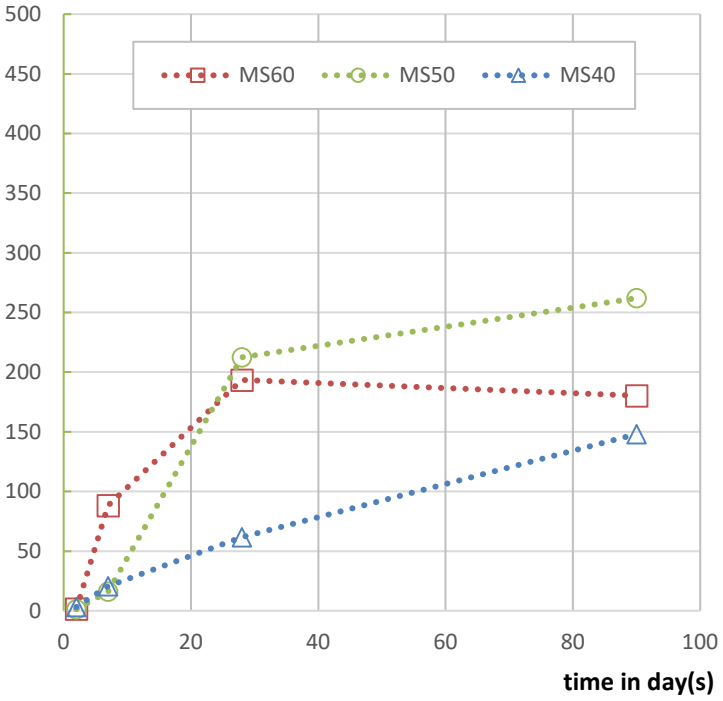

Figure 5.17. Mg concentration (mg/L) in M-MS systems

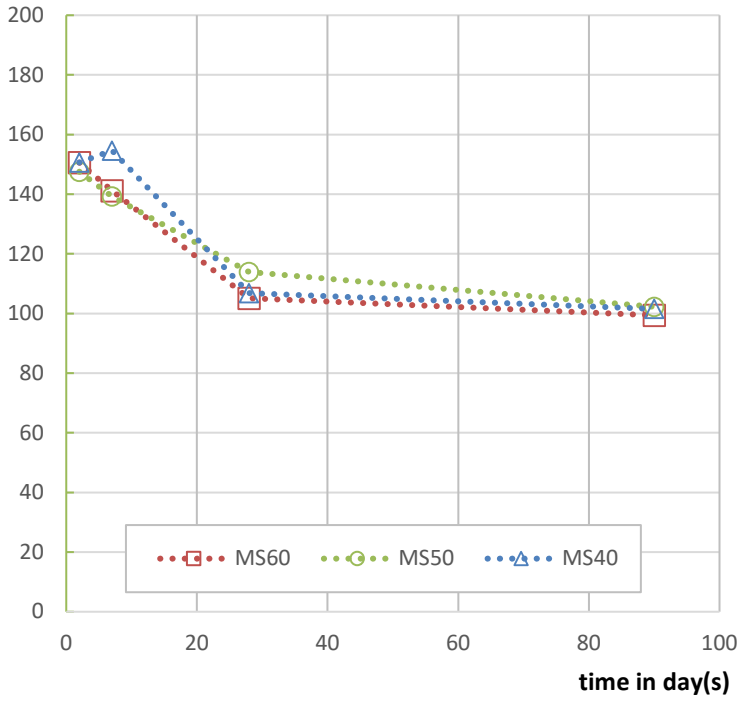

Figure 5.18. Si concentration (mg/L) in M-MS systems

5.3.2.3. MgO-RHA systems

a) Alkali concentrations (Na^+, K^+, Ca^{2+})

Figure 5.19 to Figure 5.21 present alkali concentrations of M-RHA pore solutions. Overall, the ion concentrations increase over 90 days curing period except a peak of Ca concentration at 7 days age.

A rapid increase of sodium and potassium concentrations is observed during the first 7 days. The increase rate then reduces over the time. The measured concentrations during 28 and 90 days are in range of 400-750 mg/L (sodium) and 350-600 mg/L (potassium). The calcium concentration is pretty low with the high of 30 mg/L at 90 days age. It is shown that the alkali concentrations of the pore solutions depend on the total content of each alkali compound in the binders.

b) Magnesium concentration

Magnesium concentrations in the pore solutions of M-RHA blends are shown in Figure 5.22. To compare with M-SF and M-MS pastes, no significant difference is observed except a slightly lower range of concentrations varies between 20 – 200 mg/L from 28 to 90 days.

The Mg^{2+} concentrations increase over the time due to the presence of RHA which leads to the decrease in pH of the pore solutions. The effect is obvious after 7 days as Mg concentrations increase considerably, particularly with mixtures contain high content of RHA (RHA50 and RHA60). A wide range of Mg concentrations changed at later stage proves the high reactivity of RHA and the formation of M-S-H phases. However the increase of Mg concentrations at later stage also suggests slow reactions of hydrated MgO and RHA in this M-S-H formation mechanism.

c) Silicon concentration

Silicon concentrations of M-RHA mixtures are shown in Figure 5.23. The Si concentrations of the pore solutions rise sharply during first 7 days followed by a quick decrease to 28 days. From 28 days to 90 days of the hydration process, only a slight decrease of the Si concentration is observed.

The slightly different trend of Si concentrations development compared to M-SF and M-MS mixtures reflects the pH development of the pore solutions. M-RHA pore solutions obtain higher pHs than those of M-SF and M-MS mixtures at early age, which lead to the sharp increase of Si concentrations at early age. The rapid decrease of the pHs from 7 to 28 days also causes a remarkable reduction of the Si concentrations in this period. The Si concentrations during the first 7 days of hydration are in the range from 140 – 200 mg/L, higher than those of M-SF and M-MS mixtures. However, the concentrations from 28 - 90 days slightly decrease, which are in the same range of 100-120 mg/L as for pore solutions of M-SF and M-MS samples.

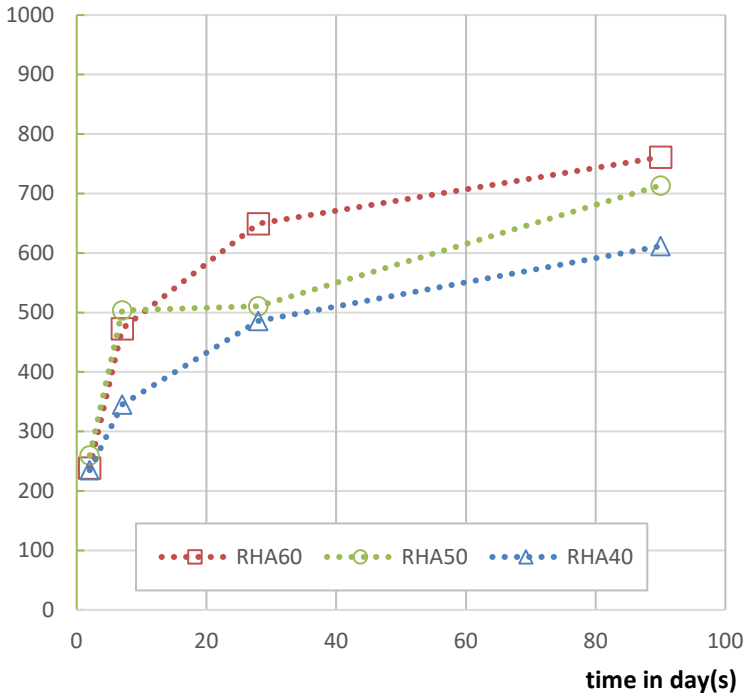

Figure 5.19. Na concentration (mg/L) in M-RHA systems

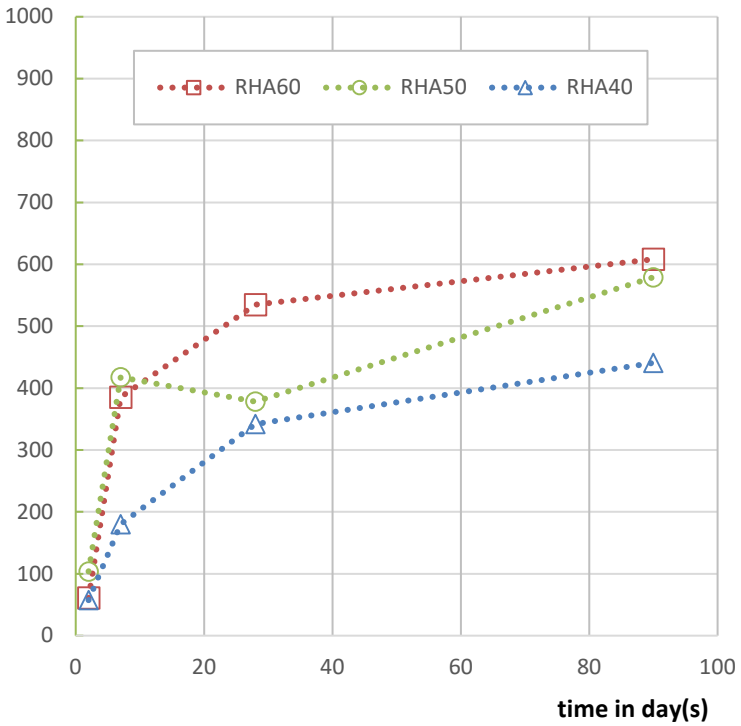

Figure 5.20. K concentration (mg/L) in M-RHA systems

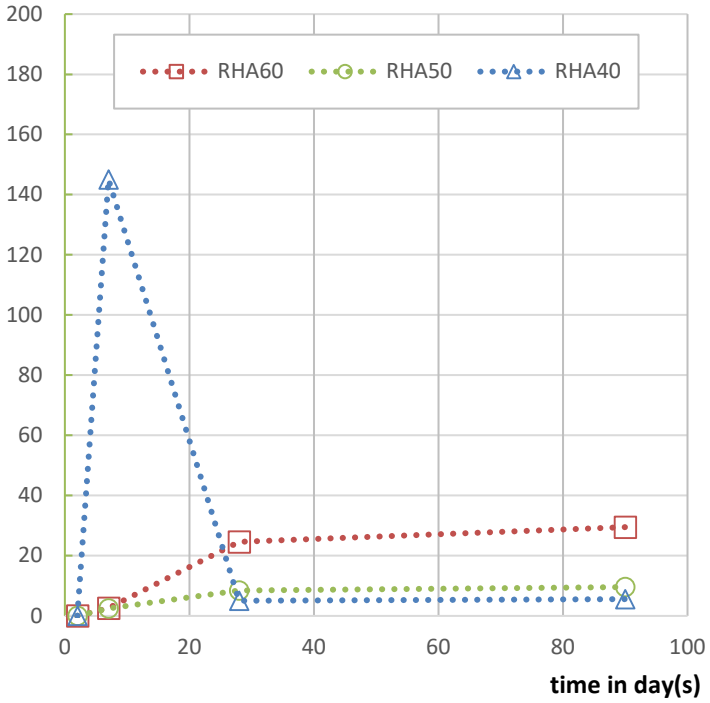

Figure 5.21. Ca concentration (mg/L) in M-RHA systems

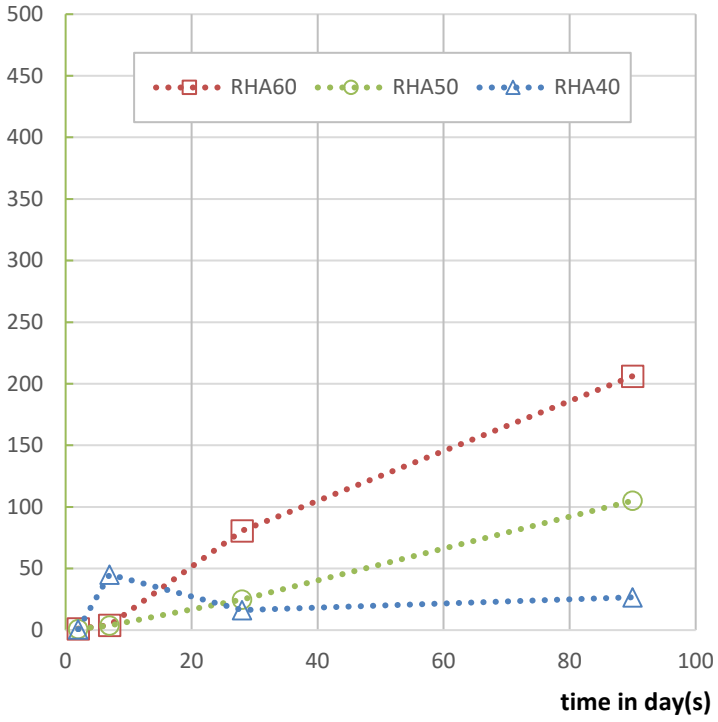

Figure 5.22. Mg concentration (mg/L) in M-RHA systems

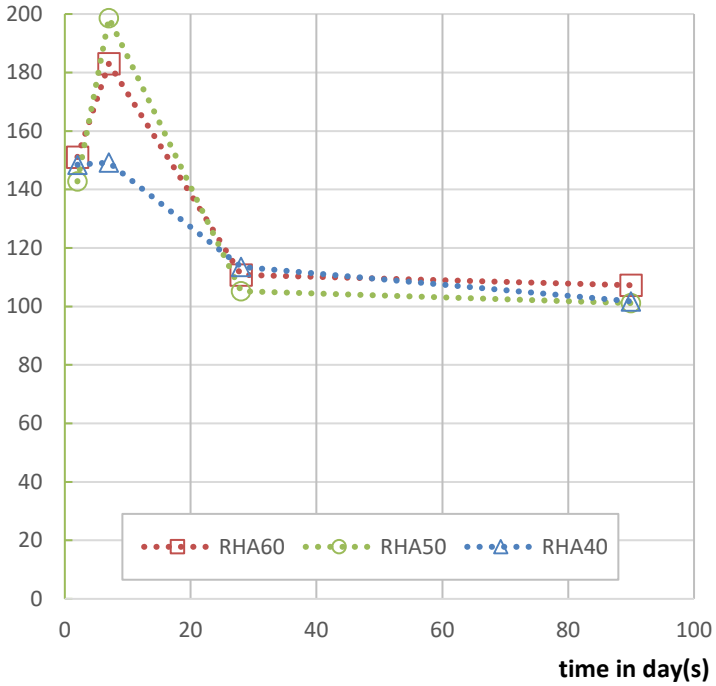

Figure 5.23. Si concentration (mg/L) in M-RHA systems

5.3.2.4. MgO-FA systems

a) Alkali concentrations (Na^+, K^+, Ca^{2+})

FA contains higher calcium content than other sources of silica. The sodium and potassium content of FA are also higher than those of MS and RHA. The chemical composition of FA therefore has strong influence on the alkali concentrations of the pore solutions of M-FA mixtures as shown in Figure 5.24 – Figure 5.26.

The high pHs at all ages result in different changing patterns of the alkali concentrations of M-FA mixtures compared to other mixtures containing SF, MS, and RHA. The concentrations of Na+, K+ in M-FA pore solutions increase rapidly in the early age up to 28 days of the hydration process, which is also seen with other silica. However, it is obvious that at later stage the concentrations almost remain stable. The range of sodium and potassium concentrations of the M-FA pore solutions are slightly less than M-SF pore solutions however higher than those of M-MS and M-RHA pore solutions, which agrees well with the total content of each sodium and potassium oxide in the binder compositions. In the meanwhile, there is a minor increase in Ca concentrations in the pore solutions of M-FA mixtures due to the high CaO content in the FA compared to other sources of silica.

b) Magnesium concentration

Figure 5.27 presents magnesium concentrations in the pore solutions of M-FA blends. The trend is very different compared to other silica sources. The Mg concentrations almost remain stable over the curing period, indicates very limited reactions of MgO with FA if occurred.

The different trend has shown the strong effect of material sources on the MgO-silica reactions. Mg concentrations are extremely low and less than Ca concentrations, while opposite results are observed for mixtures using different silica source (SF, MS or RHA). The low Mg concentration is possibly due to the rise of pH due to the very high content of alkalis (N_2O, K_2O, CaO). Mg concentrations at all ages are almost unchanged at as low as below 5 mg/L.

In contrast to effects of SF, MS or RHA on the MgO-silica systems, the increase of FA content in between 40-60% of the binder has little effect on the dissolution of MgO. The variation of Mg concentrations in pore solutions of M-FA samples is relatively small with increasing FA content. This may suggest a lower reactivity of FA compared to other sources of silica.

c) Silicon concentration

Figure 5.28 shows concentrations of silicon in the pore solutions of M-FA mixtures. Although the concentrations follow the general trend to decrease over the time, blending FA with MgO increases the Si concentrations in the pore solutions significantly compared to mixture of MgO with other silica sources.

The pHs of M-FA pore solutions never fall below 11.30 during 90 days hydration period. Such high pHs resulted from the high content of alkalis compound (Na_2O, K_2O, CaO) is the main cause of the increased solubility of silicon oxide in FA. The Si concentrations in the pore solutions of M-FA binders are out of the range of mixtures of MgO with other sources of silica. A high range of 400-600 mg/L is observed for Si concentrations in pore solutions of M-FA mixtures while the figures of binders using other silica sources vary in a much lower range of only 100- 200 mg/L.

The significant high Si concentrations in M-FA mixtures possibly suggest reactions forming silicon contained hydration products. Due to the availability of CaO and the limited dissolution of MgO represented by very low Mg concentrations, it is likely that the silica may react with calcium hydroxide to form C-S-H rather than the formation of M-S-H in the M-FA mixtures.

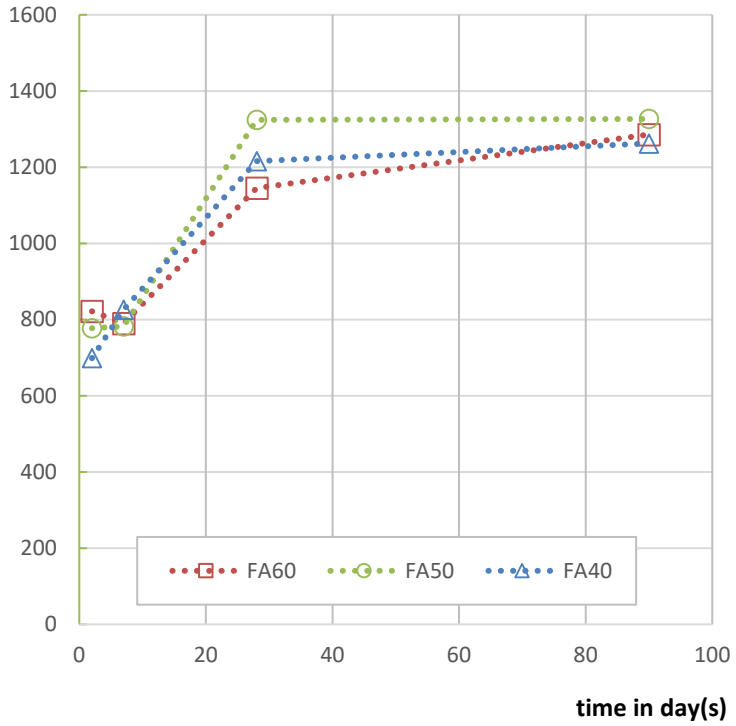

Figure 5.24. Na concentration (mg/L) in M-FA systems

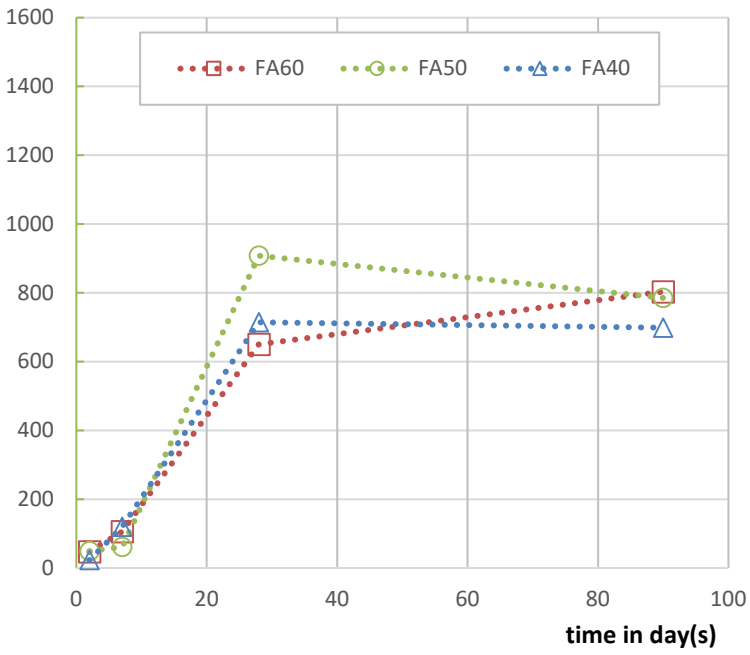

Figure 5.25. K concentration (mg/L) in M-FA systems

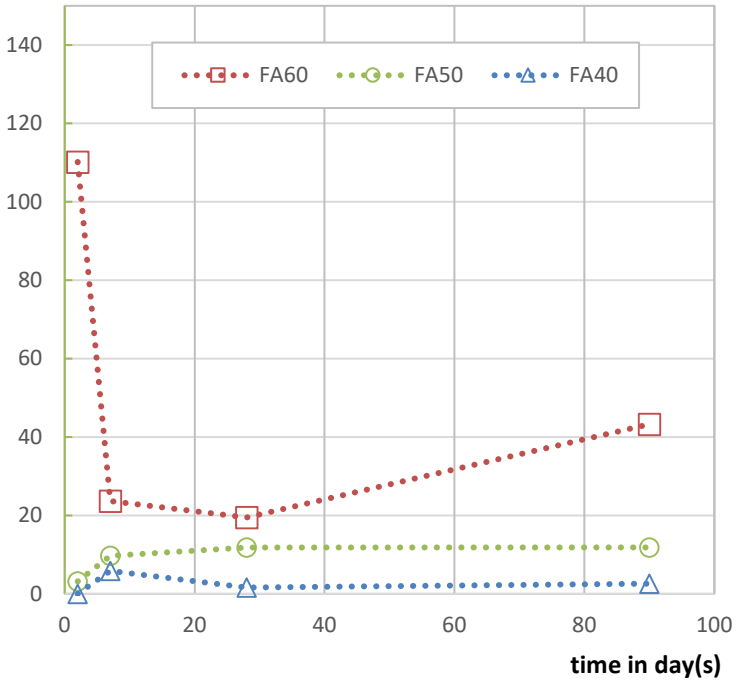

Figure 5.26. Ca concentration (mg/L) in M-FA systems

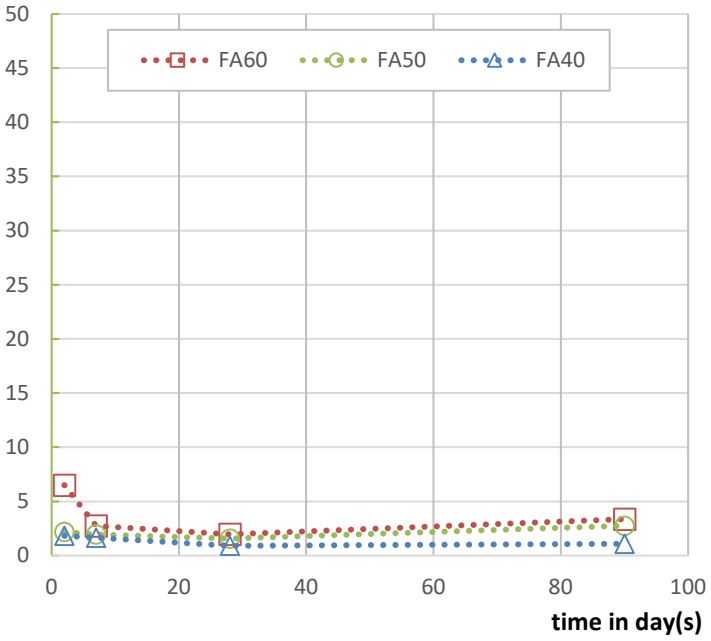

Figure 5.27. Mg concentration (mg/L) in M-FA systems

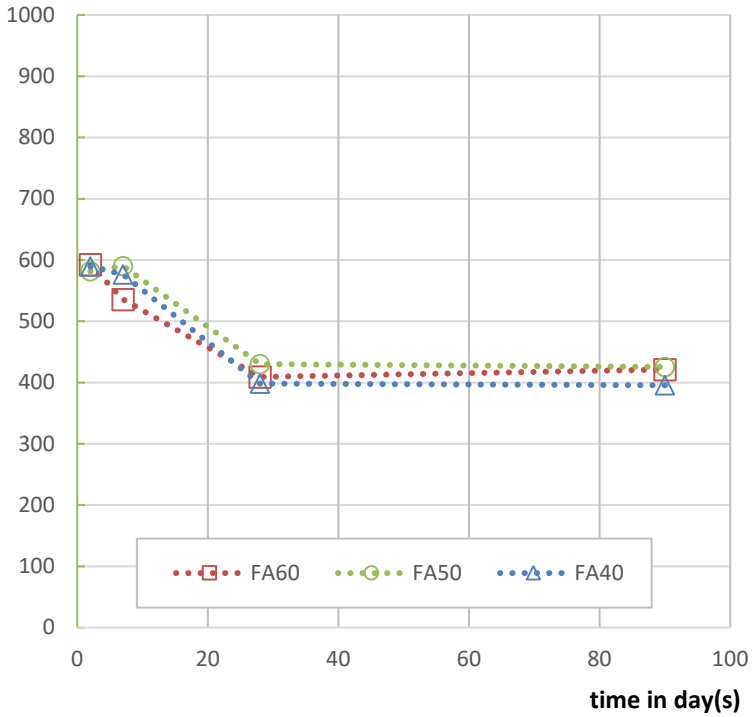

Figure 5.28. Si concentration (mg/L) in M-FA systems

5.3.3. Comparison of silica source effects on the pore solutions' pH and ion concentration

To illustrate the effect of silica sources on the hydration process of M-S-H systems, figure 5.29 shows the pH of pore solution with different silica sources at 90 days age. Each source of silica with its distinct features of chemical composition and morphology reacts differently in MgO-silica systems.

SF, with its high amorphous content and ultrafine particle size, appears to have the highest reactivity indicated by the lowest pH of SF50 samples at 90 days age. Similarly, MS50 and RHA50 samples had pH values below 10.50, suggesting the formation of M-S-H phases as a result of the high reactivity of MS and RHA. On the other hand, the pH of the M-FA samples were much higher than mixtures with other silica sources. The chemical composition of FA significantly differs from other sources of silica with a lower proportion of amorphous silica but high proportions of impurities. In addition, SEM images (Chapter 3) show coarse spherical particles of FA with a less porous microstructure. The difference of chemical composition and morphology significantly

affect the reactivity of FA and the pH of the pore solutions, which reflect the poor formation of M-S-H phases in M-FA mixtures.

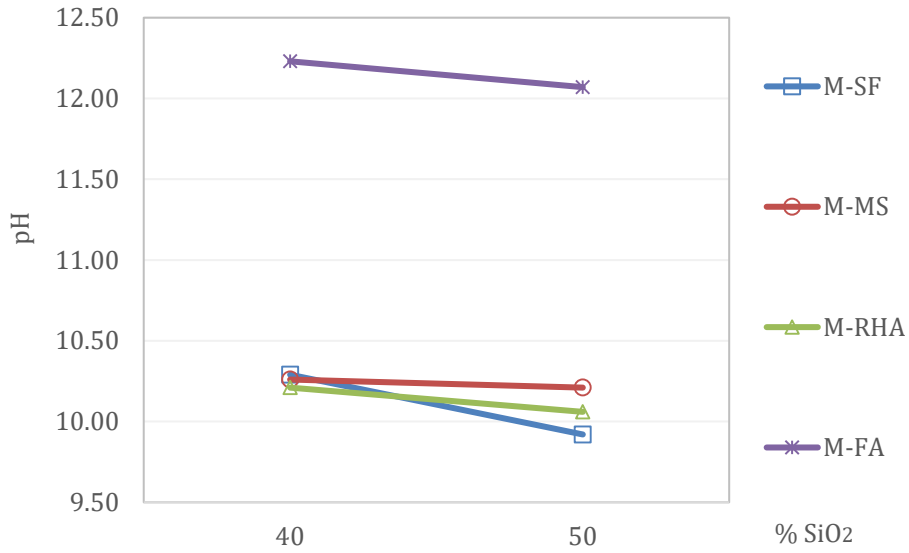

Figure 5.29. Pore solutions' pHs with different silica sources at 90 days age

Figure 5.30 compares Mg ion concentrations of the pore solutions with four silica sources at 90 days age. The highest concentration of Mg ions were found with SF50 samples which agrees well with the high reactivity of SF resulting in lowest pH, and greatest solubility of Mg^{2+}, as shown in Figure 5.29. Other highly reactive silica of MS and RHA also resulted in high Mg concentrations indicating the reactions to from M-S-H phases. In contrast, M-FA mixtures showed extremely low Mg concentrations in the pore solutions. This result reveals the poor dissolution of MgO, possibly results from the high pH of the FA mixtures. The low Mg concentrations also indicate the low reactivity of this type of FA, leading to the poor formation of M-S-H phases.

Si ion concentrations of the pore solutions with four silica sources at 90 days age are shown in Figure 5.31, which agrees with the measured pH values (Figure 5.29) and Mg concentrations (Figure 5.30). The high pH of M-FA mixtures increased the dissolution of silica, however lowered the dissolution of MgO. Meanwhile, mixtures with other silica (SF, MS, RHA) showed similar Si concentrations after 90 days age. The low Si concentrations in these mixtures with highly reactive silica sources (SF, MS, RHA) could be attributed to the consumption of a large amount of SiO_2 in the reactions with brucite to form M-S-H phases. The effects of material sources discussed herein also agree with the results of microstructure study (chapter 4) and compressive strength test (chapter 7).

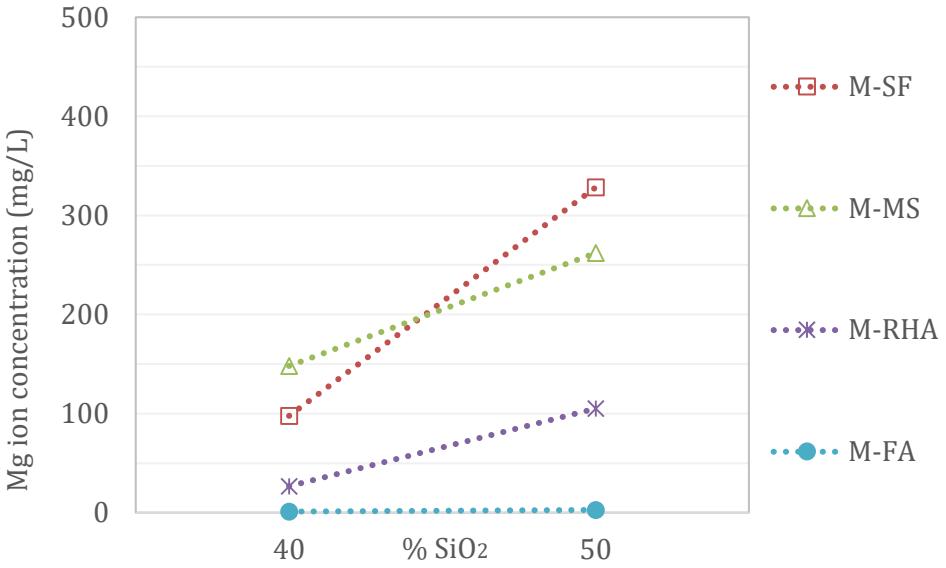

Figure 5.30. Pore solutions' Mg concentrations (mg/L) with different silica sources at 90 days age

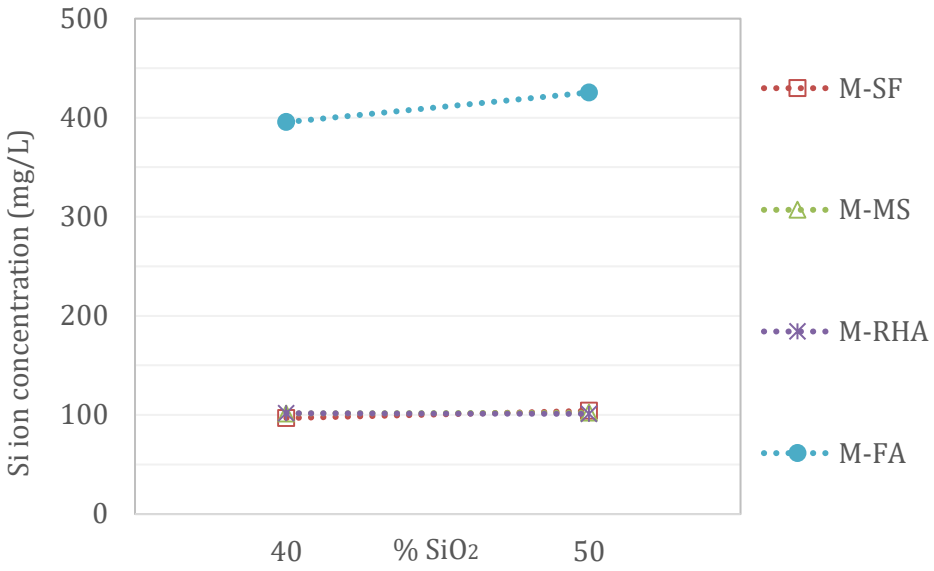

Figure 5.31. Pore solutions' Si concentrations (mg/L) with different silica sources at 90 days age

5.4. CONCLUSIONS

M-S-H binder systems using different silica sources and MgO/Silica ratios have been prepared to analyze chemical composition and pH of the pore solutions extracted from the paste samples. Based on experimental results of the selected materials, a further understanding of the hydration process of M-S-H binders has been provided.

Pore solutions of M-S-H binders are naturally alkaline. The pHs strongly depend on the reactivity and alkali content of the raw materials. For MgO-silica binders using highly reactive silica sources (SF, MS, RHA), pHs at 2 days age are generally high in the range of 10.50 – 11.70 due to the hydration of MgO and the effect of soluble alkalis. The pHs decrease to well below 10.50 from 7 days to 90 days as a result of the formation of M-S-H phases. An increase in silica content lowers the MgO and alkalis content hence lowering the pH of the resulting binders.

SF is most effective in reducing pH of the pore solutions of the M-S-H binders compared to other silica. FA contains high content of sodium, potassium and calcium, which results in high pHs of the pore solutions to above 11.00. The high pHs may severely reduce the dissolution of MgO and the formation of M-S-H phases.

ICP-MS analysis shows strong influences of binder chemical compositions on the ion concentrations of the pore solutions. Dominant ions available in the MgO-silica mixtures include sodium, potassium, calcium, magnesium and silicon. The measured ion concentrations reflect the solubility of the binder constituents. All M-S-H systems show very high sodium and potassium concentrations due to the effect of soluble alkalis in the binders while calcium concentrations are generally below 50 mg/L.

The formation of M-S-H phases can be associated with changes in the ion concentrations. The reaction mechanism involves the increasing of magnesium concentrations along with the decrease of silicon concentrations under the low pH environment.

Highly reactive silica sources containing low alkali content (SF, MS, RHA) accelerate MgO-silica reactions. Ion concentrations at 90 days in such systems are in between 100-300 mg/L (Mg) and 100 mg/L (Si). FA, generally less reactive and with a high pH, significantly limits the formation of M-S-H due to its adverse effect on the dissolution of MgO although remarkably increases silica concentrations. This large variation of ion concentrations of the pore solutions reflects a strong influence of material source on the properties of M-S-H binder systems.

The general trend of increasing Mg concentration and decreasing Si concentration during 7-90 days indicates this is the main period for the formation of M-S-H phases. This slow reaction mechanism and the increased Mg concentrations at later stage may be vulnerable to the

aggressive environments and require further studies on the durability of the M-S-H binder systems.

5.5. REFERENCES

Agilent Technologies, Inc. (2006) Specifications Agilent 7500 Series ICP-MS – Power, Flexibility, Sensitivity - The Ultimate in Metals Analysis. Agilent Technologies, Inc.

Andersson, K., Allard, B., Bengtsson, M. and Magnusson, B. (1989). Chemical composition of cement pore solutions. Cement and Concrete Research, 19(3), pp.327-332.

Barneyback, R.S. and Diamond, S. (1981). Expression and analysis of pore fluids from hardened cement pastes and mortars. Cement and Concrete Research, 11(2), pp.279-285.

Brew D.R.M., Glasser F.P. (2005). Synthesis and characterisation of magnesium silicate hydrate gels, Cement and Concrete Research 35, 85– 98.

Buckley, L. J., Carter, M. A., Wilson, M. A., & Scantlebury, J. D. (2007). Methods of obtaining pore solution from cement pastes and mortars for chloride analysis. Cement and Concrete Research, 37(11), 1544-1550.

Chandra, S (ed.) (1997). Waste materials used in concrete manufacturing. Noyes Publications, Westwood, New Jersey, USA.

Chen S, Wang L, Wu Z, Zhang T. (2017). Mechanical properties and reaction products of reactive magnesia and CFB slag/silica fume pastes. Advances in Cement Research, 11, https://doi.org/10.1680/jadcr.16.00171

Chrisholm, D.H. (1998). Performance characteristics of concrete incorporating a natural amorphous silica. Proceeding of The 3rd CANMET/ACI International Conference, Auckland, NZ, 1997.

Duchesne, J., & Bérubé, M. A. (1994). Evaluation of the validity of the pore solution expression method from hardened cement pastes and mortars. Cement and Concrete Research, 24(3), 456-462.

Hooton, R. D., Thomas, M. D. A., & Ramlochan, T. (2010). Use of pore solution analysis in design for concrete durability. Advances in Cement Research, 22(4), 203-210.

Hussain, S.E. and Al-Gahtani, A.S. (1991). Pore solution composition and reinforcement corrosion characteristics of microsilica blended cement concrete. Cement and Concrete Research, 21(6), pp.1035-1048.

Jin F. and Al-Tabbaa A. (2014). Strength and hydration products of reactive MgO–silica pastes. Cem. Concr. Compos. 52: 27–33.

Jin F, Gu K, Abdollahzadeh A and Al-Tabbaa A (2013). Effects of different reactive MgOs on the hydration of MgO-activated GGBS paste. Journal of Materials in Civil Engineering 27(7): B4014001

Kawamura, M., Kayyali, O. A., & Haque, M. N. (1988). Effects of a flyash on pore solution composition in calcium and sodium chloride-bearing mortars. Cement and Concrete Research, 18(5), 763-773.

Li Z, Zhang T, Hu J, Tang Y, Niu Y, Wei J and Yu Q (2014). Characterization of reaction products and reaction process of MgO–SiO2–H2O system at room temperature. Construction and Building Materials 61: 252-259.

Lothenbach B, Nied D, L'Hopital E, Achiedo G and Dauzeres A (2015). Magnesium and calcium silicate hydrates. Cem. Concr. Res. 77: 60–68.

Mármol G., Savastano H, Tashima MM. and Provis JL. (2016). Optimization of the MgO-SiO2 binding system for fiber-cement production with cellulosic reinforcing elements. Materials & Design 105: 251-261.

Nied D., Enemark-Rasmussen K., L'Hopital E., Skibsted J. and Lothenbach B. (2016). Properties of magnesium silicate hydrates (M-S-H). Cement and Concrete Research 79: 323-332.

O'Neil, M.J. (ed.) (2006). The Merck Index - An Encyclopedia of Chemicals, Drugs, and Biologicals. Whitehouse Station, NJ: Merck and Co., Inc., p. 983

P. Longuet, L. Burglen, A. Zelwer. (1973). La phase liquide du ciment hydrate, Revue Materiaux Construction Travaux 676, 35–41.

Pacheco-Torgal F., Cabeza L.F., Labrincha .J and De Magalhaes A.G. (2014). Eco-efficient construction and building materials: life cycle assessment (LCA), eco-labelling and case studies. Woodhead Publishing, p 226.

Page, C.L., Short, N.R., Holden, W.R. and Materials Research Group. (1986). The influence of different cements on chloride-induced corrosion of reinforcing steel. Cement and Concrete Research, 16(1), pp.79-86.

Patnaik P. (2003). Handbook of Inorganic Chemicals. New York, NY: McGraw-Hill p. 529

Mitsuda T., Taguchi H. (1977). Formation of Magnesium Silicate Hydrate and Its Crystallization to Talc, Cement and concrete research 7, 223-230.

Tran HM. and Scott A. (2017). Strength and workability of magnesium silicate hydrate binder systems. Construction and Building Materials 131: 526-535.

Tran H. M., Scott A., Dhakal R.P. (2017). Strength development of mortars using a magnesium silicate hydrate binder system under different curing conditions. Proceedings of the 2nd International RILEM Conference on Bio-based Building Materials, 21-23 June 2017, Clermont-Ferrand, France.

Tritthart, J., & Häußler, F. (2003). Pore solution analysis of cement pastes and nanostructural investigations of hydrated C3S. Cement and concrete research, 33(7), 1063-1070.

Vollpracht, A., Lothenbach, B., Snellings, R., & Haufe, J. (2016). The pore solution of blended cements: a review. Materials and Structures, 49(8), 3341-3367.

Walling S A., Kinoshita H., Bernal S A., Colliera N C. and Provis JL. (2015). Structure and properties of binder gels formed in the system Mg(OH)2–SiO2–H2O for immobilisation of Magnox sludge. The Royal Society of Chemistry, Dalton Trans. 44: 8126–8137.

Wei JX., Chen YM., Li YX. (2006). The Reaction Mechanism between MgO and Microsilica at Room Temperature. Journal of Wuhan University of Technology - Mater. Sci. Ed. 21(2): 88-91.

Zhang T., Vandeperre LJ. and Cheeseman CR. (2012). Magnesium-silicate-hydrate cements for encapsulating problematic aluminium containing wastes. Journal of Sustainable Cement-Based Materials 1 (1-2): 34-45.

Zhang T., Vandeperre LJ. and Cheeseman CR. (2014). Formation of magnesium silicate hydrate (M-S-H) cement pastes using sodium hexametaphosphate. Cement and Concrete Research 65: 8–14.

CHAPTER 6
OPTIMIZATION OF BINDER COMPOSITIONS FOR STRENGTH AND WORKABILITY OF MAGNESIUM SILICATE HYDRATE BINDER SYSTEMS

Tran, H. M., & Scott, A. (2017). Strength and workability of magnesium silicate hydrate binder systems. *Construction and Building Materials*, *131*, 526-535.

Preamble

In previous chapters, the microstructures and pore solution analysis were performed to characterize the reaction mechanism of M-S-H binders. Chapter 4 examined the hydration process and microstructures of the M-S-H pastes in which XRD and SEM/EDS analysis were presented. The reaction mechanism of the formation of the hydration products, hydration rate, and texture properties were discussed. In addition, the critical influence of the material sources and the binder compositions on the hydration products was evaluated. On the other hand, Chapter 5 provided the understanding of the pH development and ion concentrations of the pore solutions of the M-S-H cement pastes. The measured pHs and concentrations of alkalis, magnesium, and silicon showed the effect of pHs on the dissolution of reactive MgO and silica, which have a strong influence on the formation of the binding phases and the durability of the M-S-H binders.

Experimental results in chapter 4 and chapter 5 have confirmed the formation of M-S-H phases at room temperatures which is the basis for the development of M-S-H binder systems. Nonetheless, the application of any new binder is questionable if the desired strength and workability cannot be achieved and the limitation of M-S-H binders in strength and workability appears to exist in the literature.

This chapter discusses the optimization to achieve the desired strength and workability of mixtures of MgO and silica fume. Different binder compositions designed for pastes and mortars were compared to achieve normal to high strength and workable M-S-H cementitious materials. Ternary systems were proposed in combination with the use of polymer-based superplasticizer to overcome the existing limits of the strength and workability of M-S-H binder systems.

Abstract

This chapter discusses the optimization of magnesium silicate hydrate (M-S-H) binder systems to achieve desirable strength and workability properties of cement paste and mortar. The binary systems contain magnesia and silica fume in which each constituent accounts for 40-60% by mass of the binder. The ternary systems include 10 to 40% very fine crushed quartz which is used as a fine filler for the partial replacement for the cementitious materials. It was found that the pure M-S-H binder system has a much higher water demand compared to Portland cement due to the very high silica fume content. The use of polymer-based superplasticizer effectively reduced water to cementitious materials ratio (w/c) for M-S-H binder system. The optimal binary binder composition for strength and workability was found to contain 60% magnesium and 40% silica fume (Mg/Si molar ratio =2.25). The addition of very fine crushed quartz filler from 10-40%, as a partial replacement for the magnesia and silica fume, further improved the rheology of the mixture allowing for a workable mix with a w/c = 0.30. The highest compressive strength of mortar samples achieved with ternary M-S-H system is up to 87 MPa.

6.1. INTRODUCTION

The formation of the magnesium silicate hydrate (M-S-H) was first discovered in 1953 during an investigation on the deterioration mechanism of concrete in sea water (Cole, 1953). M-S-H formation since then had been generally considered a detrimental phenomenon associated with sulphate attack on concrete (Bonen and Cohen, 1992a, 1992b; Bonen, 1992; Gollop and Taylor, 1996) and attracted little research interest as cementitious materials. Based on microstructure analysis, potential chemical reactions forming M-S-H gel at room temperature were suggested as follows (Li et al., 2014; Zhang et al., 2014):

$$3Mg^{2+} + 6OH^- + 4SiO_2 \rightarrow Mg_3Si_4O_{10}(OH)_2 + 2H_2O \quad (1)$$

$$3Mg^{2+} + 6OH^- + 2SiO_2 \rightarrow Mg_3Si_2O_5(OH)_4 + H_2O \quad (2)$$

$$8MgO + 8SiO_2 + 16H_2O \rightarrow M_8Si_8O_{20}(OH)_8.12H_2O \quad (3)$$

The microstructure and chemical composition of M-S-H are related to the ratio of reactants and hydrothermal curing regimes. The M-S-H formed in sulphate attack of concrete was reported to have high Mg/Si molar ratio of between 1.0-4.0 (Cole, 1953; Bonen and Cohen, 1992a, 1992b). However, most of synthesized M-S-H gel in paste samples have lower Mg/Si ratio of between 0.67-1.5 (Mitsuda and Taguchi, 1977; Brew and Glasser, 2005; Wei et al., 2006; Zhang et al., 2014; Lothenbach et al, 2015; Roosz et al., 2015) which suggests that the optimal formation of M-S-H gel without residual brucite can be obtained when the MgO content accounts for 30-50% of the MgO-SiO_2 mixtures. Furthermore, higher Mg/Si ratio of M-S-H gel has been found at elevated temperature (Wei et al., 2011). The M-S-H microstructure consists of disordered intermediate phases and resembles the formation of talc (Mg/Si=0.75), serpentine or chrysotile (Mg/Si=1.5), or deweylite at Mg/Si ratios between 0.75-1.50 (Mitsuda and Taguchi, 1977).

Results from studies on the mechanical properties of M-S-H system in cementitious materials are quite varied and dependent on mix proportions and materials sources (Wei et al., 2006; Zhang et al., 2012a, 2012b, 2014; Jin and A. Al-Tabbaa, 2014; Walling et al., 2015). Wei et al (2006) prepared M-S-H binder mortars containing 60-90% reactive MgO (10-40% silica fume) whereby the mortar mix with M-S-H binder containing 70% MgO obtained the highest 28 day compressive strength result of 57.4 MPa. In such case, the MgO/SiO_2 ratio for optimal M-S-H gel formation did not result in the highest strength. In contrast, Jin and Al-Tabbaa (2014) have shown that compressive strength increases with increasing silica content in the range of 0 to 50% and this was despite an increase in w/c ratio at the higher silica replacement levels. The highest

compressive strength of 70 MPa at 28 days for a M-S-H binder mixture was reported by Zhang et al (2012b) in which the M-S-H binder system contained 20% MgO, 5% $MgCO_3$, 25% silica fume (SF) and 50% quart sand filler. Apart from these encouraging experimental results, other studies report poor compressive strengths for magnesium silicate hydrate binder system (Walling et al., 2015). In addition to the limited strength, one of the greatest challenges faced in the development of a M-S-H binder system compared to Portland cement (PC) is the very high water demand and poor workability of the binder, primarily due to fineness of SF and cell lattice structure of reactive magnesia (Eubank, 1951; Zhang et al., 2009).

The primary aim of this investigation is to develop an optimal composition based on the workability and compressive strength characteristics of M-S-H binder systems. In the first stage, the effects of superplasticizers type, dosage and MgO/SiO_2 ratios (in the range of 40:60 to 60:40) on water demand and strength were determined for a binary system of magnesia and SF. The MgO/SiO_2 range used in this study was chosen based on the variability of results found in the available literature and the high compressive strength in excess of 60 MPa achieved for the 40:60 MgO/SiO_2 mix (Zhang et al., 2014). The second stage involved replacing a portion of the Mg/SiO_2 binder with crushed quartz filler to produce a ternary system (MgO-SF-QF) with a low water demand for high compressive strength.

6.2. EXPERIMENTAL PROGRAMME

6.2.1. Materials

Binder compositions include reactive magnesium oxide and silica fume. Crushed quartz filler (QF) was ground in a ring mill from local quartz sand until obtaining desired particle size. Quartz sand (S) is a local fine aggregate. Two superplasticizers were used in this investigation; Viscocrete-5-555 (liquid), a third generation polymer-based superplasticizer was provided by Sika NZ and sodium hexametaphosphate (SHMP), an inorganic superplasticizer supplied by Ajax Chemicals (Australia) with chemical formula $Na(PO_3)_n.Na_2O$. Chemical compositions and particle sizes of the materials are presented in Chapter 3.

6.2.2. Optimization of superplasticizer dosage

The use of superplasticizers is crucial to reduce water demand and improve both the strength and workability of the mix. For these reasons, tests with superplasticizers were performed to optimize superplasticizer dosages for M-S-H binder. Viscocrete-5-555, a polymer-based superplasticizer was selected and compared to an inorganic superplasticizer (Sodium hexametaphosphate). The superplasticizer dosage optimization procedure is described as follows:

- Step 1: Prepare a set of containers with each container contained 50 g binder (40% MgO + 60% SF) dry mixed until homogeneous.
- Step 2: Place superplasticizer into each container. The superplasticizer dosage was increased from 0 to 5% by 1% unit increments.

  Step 3: Gradually add water in each container while slightly stirring until obtaining a flowable / self-levelling paste that has a specified flow of 150±5 mm as per ASTM C1437 without tamping. The amount of water poured into each container was recorded with an accuracy of ±1 ml. The superplasticizer efficiency was calculated based on the amount of added water including the water content contained in the superplasticizer. The mixture containing the lowest water content indicated optimal superplasticizer dosage.

6.2.3. Mix proportions

Three MgO/SiO_2 ratios (by mass) were selected and listed in Table 6.1. The low MgO/SiO_2 system (MgO/SiO_2 = 40/60) provided a high SF content binder to facilitate the formation of M-S-H gel (Brew and Glasser, 2005; Zhang et al., 2014). The high MgO/SiO_2 system (MgO/SiO_2 = 60/40) provided a greater portion of MgO particles, which are coarser than SF, with the intention of improving the packing density of the binder despite the possible reduction in the formation of M-S-H gel. In cases of higher MgO content, the hydration products might contain residual brucite ($Mg(OH)_2$) and in such conditions, both brucite and M-S-H gel would co-exist in the hardened concrete as cementing materials. The selection of the high MgO, low SF mix was also intended to reduce the detrimental workability effects associated with a high SF content.

Table 6.1. MgO/SiO_2 ratios (by mass) and Mg/Si molar ratios of M-S-H systems

MgO/SiO_2 by mass	**40:60**	**50:50**	**60:40**
Mg/Si molar ratio	1.00	1.50	2.25

Five series resulting in a total of 21 mixtures were prepared for compressive strength testing. The mix proportions, listed in Table 6.2 are described as follows:

Table 6.2. Mix proportions of M-S-H paste and mortar

No.	Mix Label	Binder composition (MgO+SF+QF=1.0)			Quartz sand	w/c	w/s	SP (liquid)	Flow (mm)	28-day compressive strength (MPa)	Standard deviation (s)
		MgO	SF	QF							
1	S1.60	0.40	0.60	-	-	0.40	-	3%	145	**29.9**	0.68
2	S1.50	0.50	0.50	-	-	0.40	-	3%	150	**39.3**	1.25
3	S1.40	0.60	0.40	-	-	0.40	-	3%	157	**42.8**	1.87
4	S2.60	0.40	0.60	-	0.50	0.45	-	3%	125	**25.9**	0.20
5	S2.50	0.50	0.50	-	0.50	0.45	-	3%	147	**29.4**	1.39
6	S2.40	0.60	0.40	-	0.50	0.45	-	3%	160	**36.3**	0.68
7	S3.0	0.40	0.60	0	0.50	0.45	0.45	3%	125	**25.9**	0.20
8	S3.10	0.36	0.54	0.10	0.50	0.41	0.37	3%	125	**33.3**	1.83
9	S3.20	0.32	0.48	0.20	0.50	0.45	0.34	3%	124	**33.4**	1.30
10	S3.30	0.28	0.42	0.30	0.50	0.40	0.27	3%	125	**39.2**	1.21
11	S3.40	0.24	0.36	0.40	0.50	0.42	0.25	3%	127	**43.0**	1.14
12	S4.0	0.50	0.50	0	0.50	0.38	0.38	3%	121	**42.1**	1.18
13	S4.10	0.45	0.45	0.10	0.50	0.34	0.31	3%	122	**54.1**	1.73
14	S4.20	0.40	0.40	0.20	0.50	0.35	0.28	3%	124	**68.9**	0.90
15	S4.30	0.35	0.35	0.30	0.50	0.36	0.25	3%	122	**64.6**	0.72
16	S4.40	0.30	0.30	0.40	0.50	0.38	0.23	3%	121	**56.9**	1.87
17	S5.0	0.60	0.40	0	0.50	0.36	0.36	3%	124	**43.7**	0.83
18	S5.10	0.54	0.36	0.10	0.50	0.30	0.27	3%	121	**85.0**	0.85
19	S5.20	0.48	0.32	0.20	0.50	0.31	0.25	3%	120	**83.1**	2.11
20	S5.30	0.42	0.28	0.30	0.50	0.33	0.23	3%	122	**84.3**	1.51
21	S5.40	0.36	0.24	0.40	0.50	0.35	0.21	3%	121	**87.3**	1.10

- w/c = mass of water / mass of (MgO +SF)
- w/s = mass of water / mass of (MgO+SF+QF)

- Series 1 included three M-S-H paste mixtures in with a water/cement (w/c) ratio of 0.40 and using a 3% polymer-based superplasticizer to achieve adequate workability. Mixes were labeled S1.40-S1.60 in accordance with silica fume content (%) by mass in the binder.

- Series 2 produced three M-S-H mortar mixtures in which quartz sand was used as fine aggregate to reduce shrinkage. A fixed amount of sand was selected (Sand to binder ratio, S/c = 0.5). The w/c required for workability increased to 0.45 with the use of 3% polymer-based superplasticizer. Mixes were labeled S2.40-S2.60 in accordance with silica fume content (%) by mass in the binder.

- Series 3 (mixes labeled S3.0-S3.40), series 4 (mixes labeled S4.0-S4.40) and series 5 (mixes labeled S5.0-S5.40) added crushed quartz filler (QF) to binary systems to form ternary systems of MgO-SF-QF (solids). The MgO/SiO_2 ratio in each series was 40/60 (Series 3), 50/50 (Series 4), and 40/60 (Series 5) while the crushed quartz filler increased from 0-40% to replace (MgO+SF) content in 10% increments. An amount of unground quartz sand content (S/(MgO+SF+QF) = 0.5) was included in the mortar to reduce shrinkage and improve packing density. To evaluate water reduction effect of crushed quartz filler, a fixed flow of 120-125 mm was selected for minimum workability whereby the water to solids ratio (w/s), which included the MgO, SF and QF, was modified corresponding to the variation of crushed quartz filler content.

6.2.4. Sample preparation and testing methods

The workability of the mixes was measured by flow test following ASTM C 1437. Compressive strength tests were performed according to ASTM C 109 using 50×50×50 mm cubes. Details of the testing methods are described in Chapter 3.

The microstructures were investigated using SEM and XRD methods. SEM analysis was performed on the three sets of hydrate paste samples after 28 days using a JEOL 6400 Scanning Electron Microscope. The development of hydration products of the paste samples was monitored at 1 day and 28 days by XRD using a Philips PW1729 X-ray diffractometer (Cu, 50kV/40mA) with a 3 to 70^{o} 2Θ scan range. The fresh paste samples were sealed in 50 ml containers immediately after mixing and stored at 20^{o}C until testing age.

6.3. OPTIMAL SUPERPLASTICIZER DOSAGES

The effects of superplasticizer type and dosage on the fluidity of a 40% MgO-60% SF binder are provided in Figure 6.1. The 1% dosage of inorganic superplasticizer SMHP was chosen for the optimal water reduction effect as reported in previous studies (Zhang et al., 2014; Walling et al., 2015). In the current investigation the use of 1% SHMP resulted in a 22% reduction in the water demand for the M-S-H binder system. The optimal superplasticizer dosage of Viscocrete 5-555 was found to be approximately 3-4% by binder (about 1-1.5% solids) for which the water demand was reduced up to 41%. Viscocrete-5-555 at a dosage of 3% was therefore shown to provide sufficient water reduction and used in the comparison for all the M-S-H mixes.

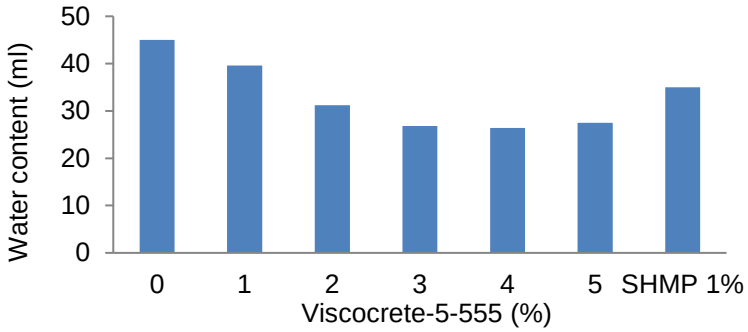

Figure 6.1. Water content for binder composed of MgO-SF (40%-60%)

The optimal superplasticizer content for 40% MgO-60% SF mixture was utilized for all other MgO-SF binder mixtures, although it is acknowledged that the superplasticizer content required for another mix (e.g. MgO-SF of 60%-40%) might be different. It was predicted that the decrease of silica fume content from 60% to 40% would lead to the improved workability due to the replacement of microfine silica fume particles with coarser MgO particles. Therefore, the SP dosage of 3% of the binder by mass might result in better workability for mixing and moulding samples with MgO/SF ratios other than 40/60. The test results (Figure 6.2) have proved this effect and no superplasticizer adjustment was required.

6.4. PROPERTIES OF M-S-H BINARY SYSTEM ($MgO\text{-}SiO_2$)

6.4.1. Influence of specific gravity on w/c of M-S-H binder

SF has a lower specific gravity (S.G) and bulk density than PC. Thus the high SF content in M-S-H binder composition results in a lighter M-S-H binder, compared to PC. The significant difference of specific gravities of M-S-H binder and PC leads to a variations in the w/c ratio of the two systems for a constant water content. Considering M-S-H and PC mixtures of a fixed binder volume *(V)*, calculation of the difference of w/c ratio is derived from:

$$V = \frac{M_{MSH}}{S.G_{MSH}} = \frac{M_{PC}}{S.G_{PC}} \qquad (4)$$

Where:

V =absolute volume of the binder

$M_{M\text{-}S\text{-}H}$ = mass of M-S-H binder in a binder volume of V

M_{PC} = mass of PC binder in a binder volume of V

$S.G_{M\text{-}S\text{-}H}$ = specific gravity of M-S-H binder

$S.G_{PC}$ = specific gravity of PC

If mixes with PC and M-S-H binder have the same mass of water (*w)*, (4) can be rewritten as:

$$\frac{w/M_{MSH}}{S.G_{MSH}} = \frac{w/M_{PC}}{S.G_{PC}} \qquad (5)$$

By rearranging equation (5), the difference in water to binder ratio by mass is:

$$\left(w/c\right)_{MSH} = \frac{S.G_{PC}}{S.G_{MSH}}\left(w/c\right)_{PC} \qquad (6)$$

where

$(w/c)_{MSH}$ = water to cementitious materials ratio of M-S-H binder mix

$(w/c)_{PC}$ = water to cement ratio of PC mix

Equation (6) shows that the deviation of w/c of M-S-H binder and PC is dependent on the ratio of specific gravities. The decrease of the specific gravity of M-S-H binder leads to an increase of $(w/c)_{M\text{-}S\text{-}H}$ compared to $(w/c)_{PC}$. Deviations of w/c for various M-S-H binder compositions corresponding to four $(w/c)_{PC}$ ratios ranging from 0.20-0.40 are presented in Table 6.3. The relative densities of MgO, SF and PC are taken as 3.15, 2.20 and 3.14, respectively.

When comparing different binder systems it is important therefore to consider the influence of the specific gravity on the volume of the paste produced. Using a fixed w/c ratio will result in a greater volume of paste and lower volume of sand in a M-S-H mortar system compared to a PC system. Conversely, to maintain the same volume of paste and w/c ratio in a M-S-H system both the mass of water and mass of binder would need to be reduced. Reducing the total water content for instance is likely to have a detrimental effect on the workability of the material.

Table 6.3. Deviation of w/cm of PC and M-S-H binder (at fixed water and paste volume)

Binder system	**Relative density**	**w/c**			
PC	3.14	0.20	0.30	0.40	0.50
MgO/SF=60/40	2.77	0.23	0.34	0.45	0.57
MgO/SF=50/50	2.68	0.23	0.35	0.47	0.59
MgO/SF=40/60	2.58	0.24	0.37	0.49	0.61

In this investigation all mix designs are based on a fixed ratio if the mass of water to binder and the volume paste is allowed to vary.

6.4.2. **Flow test**

The use of large volumes of SF results in a high water demand and stickiness, producing a less workable mix (FIB, 1988). The workability of M-S-H binder is of utmost importance if it is eventually to be used as a construction material and must be optimized to at low water content to ensure sufficient compaction for high strength.

Binder systems	**Before testing**	**After testing**	**Demoulded Cubes**
SF content 60%			
SF content 50%	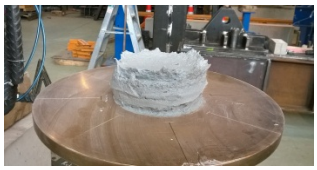		
SF content 40%			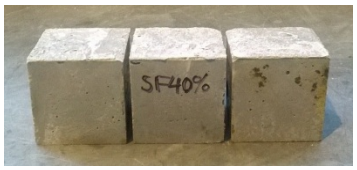

Figure 6.2. Fresh and hardened M-S-H pastes with different SF content (at w/cm=0.40 and 3% Viscocrete-5-555 superplasticizer)

Figure 6.2 shows the workability of paste mixes with various SF contents. Images (before and after flow tests) illustrate a significant improvement of workability as SF content decreases. An increase in stickiness was identified in higher SF mixes (images before testing). The high SF content mixture (60% SF) dried out very quickly, was difficult to finish and was vulnerable to plastic shrinkage, requiring moist cure right after casting to avoid cracking. The poor workability of the mix containing high SF content (60%) also affected compaction and resulted in compaction defects on the surfaces of the cubes after demoulding.

Figure 6.3 shows the flow of samples of series 1 and series 2, indicating a significant decrease in workability corresponding to an increase in SF content. Paste and mortar samples containing highest SF content (60%) had the lowest flows of only 140 mm (paste) and 125 mm (mortar). On the other hand, there is a significant improvement of workability as SF content reduced to 40%, illustrated by the increase of flow to 157 mm (paste) and 163 mm (mortar). Mixes containing low SF content (40%-50% binder) achieve better workability and therefore can be developed for low water content M-S-H binder.

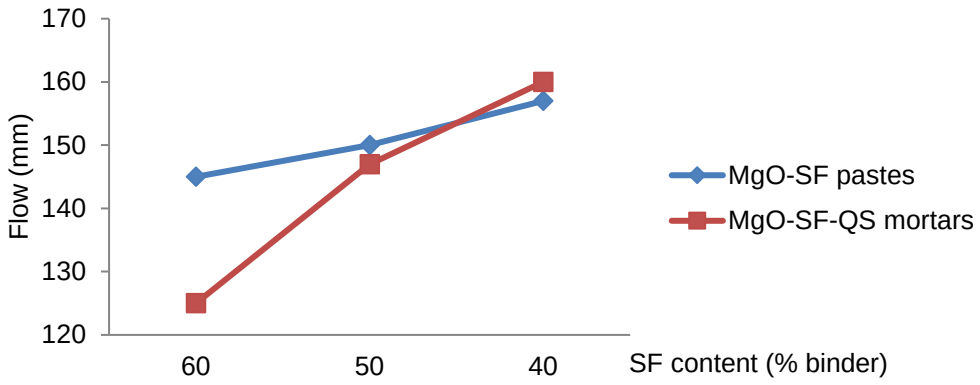

Figure 6.3. Effect of SF content on flow of M-S-H binder

6.4.3. **Microstructure analysis**

As the objective of this chapter is to study the workability and strength of M-S-H cement pastes and mortars in the early ages, the SEM and XRD results up to 28 days are presented. Preliminary studies have shown the high strength of mixtures using SF, rather than other silica sources. Accordingly, only M-SF mixtures are discussed herein in search for the optimal M-SF binder composition to provide the highest strength. A more comprehensive study of the microstructures of M-S-H binders with different silica sources and long-term curing up to 365 days was discussed in chapter 4.

SEM analysis was performed to investigate the effect of binder's morphology on the rheology of the paste and mortar. The SEM images provided information on the binder particle size, shape and surface texture, as shown in Figure 6.4.

The angular and rough surface of the MgO particles, as shown in Figure 6.4(a) and Figure 6.4(b) will result in generally poor workability. The relatively large particle size of d_{50} = 9 μm of the MgO offsets the negative effects of particle shape resulting in lower water demand compared to the SF

component of the binder. The high MgO content mixture (60% MgO-40%SF) therefore showed higher flow than other MgO-SF combinations.

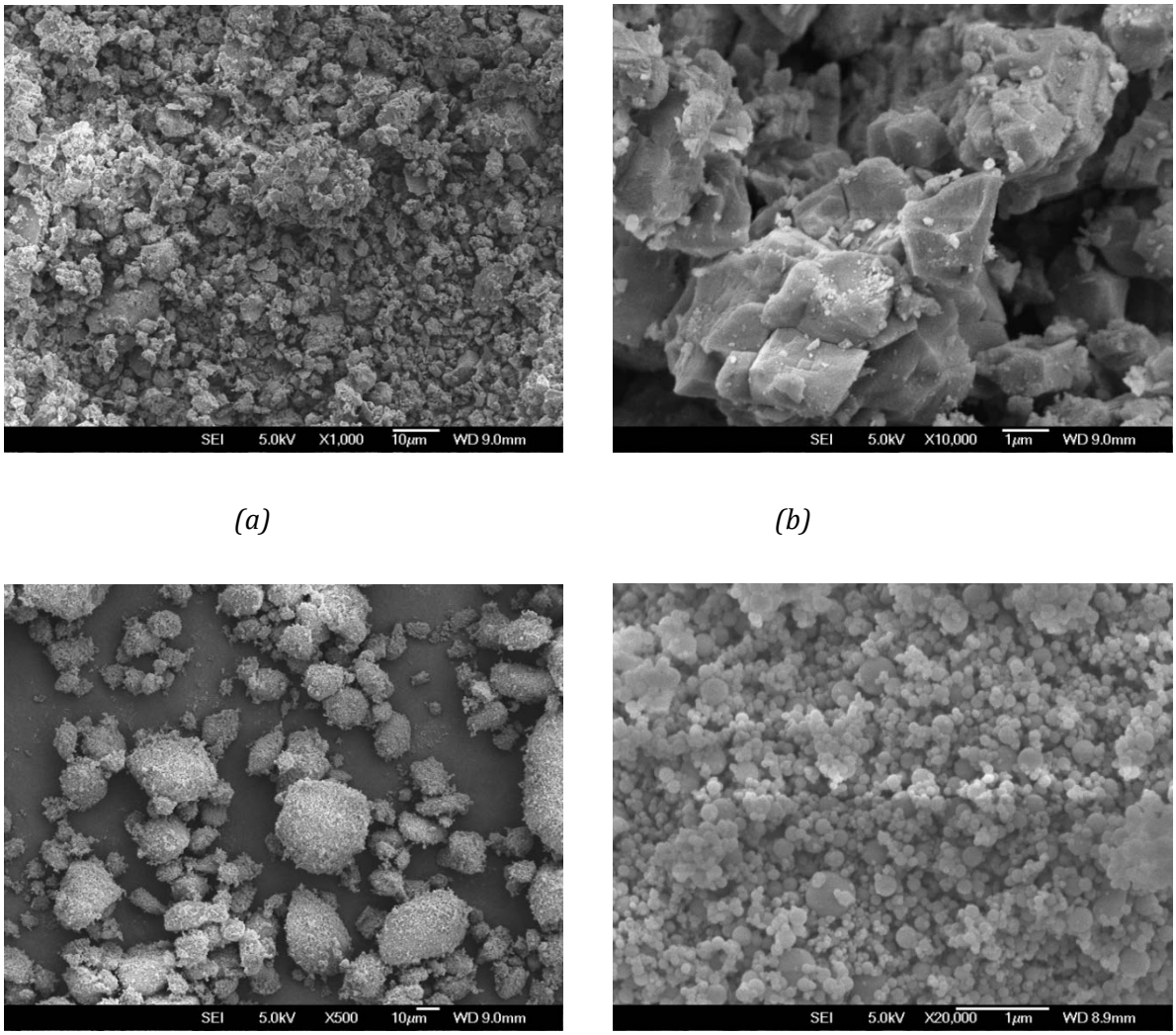

Figure 6.4. SEM images of magnesium oxide (a), (b) and condensed SF (c), (d).

The particle size distribution analyzed by laser diffraction shows that condensed SF contains agglomerates (d_{50} ≈ 88 μm). However, the mixing procedure breaks up these agglomerates resulting in original SF particles with d_{50} observed at about 0.10 μm. Despite the advantage of spherical shape (Figure 6.4(c), Figure 6.4(d)), the fineness of SF is the main cause of the very high water demand of M-S-H binder. The optimal binder composition for workability, mixing and vibration compaction is found to contain lowest SF content of 40% (Mg/Si molar ratio =2.25).

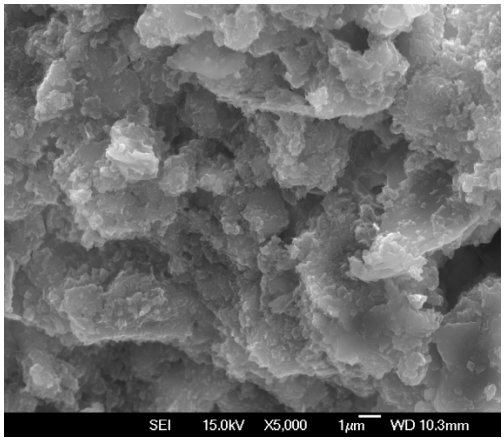

(a): *M100SF0 (100%MgO)*

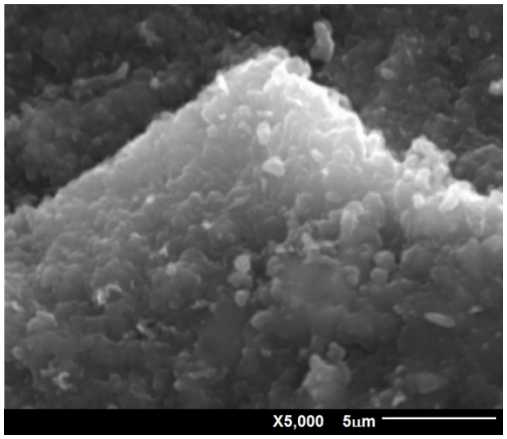

(b): *M40SF60 (40%MgO-60%SF)*

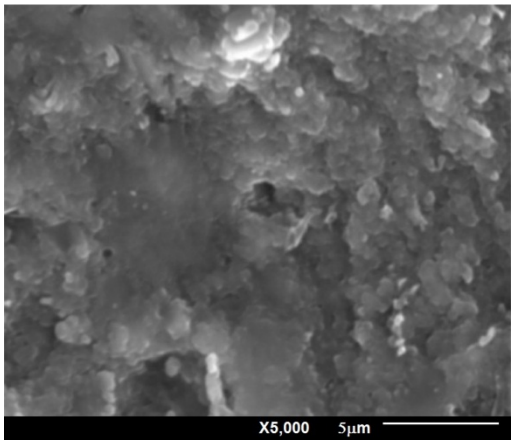

(c): *M50SF50 (50%MgO-50%SF)*

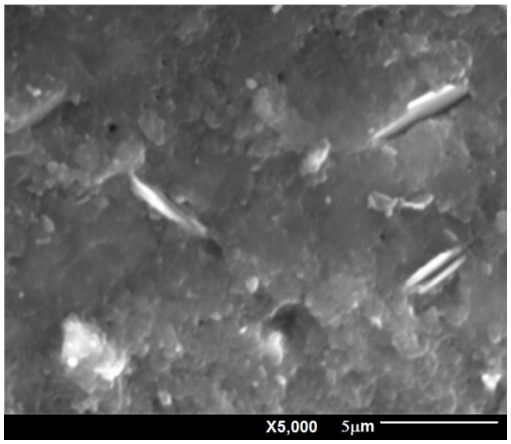

(d): *M60SF40 (60%MgO-40%SF)*

Figure 6.5. SEM images of brucite and M-S-H pastes at 28 days age (w/c=0.40)

The microstructure of brucite and M-S-H pastes at 28 days age is shown in Figure 6.5. Four mixtures were prepared in sealed tubes and cured at ambient conditions. Formation of brucite with thin platelets and layers structure were observed with mixture M100SF0 containing 100% MgO (Figure 6.5(a)). All other mixtures show the formation of M-S-H gel with presence of brucite and unreacted silica fume particles, indicating that the hydration was not completed at 28 days age. The slow reaction of MgO and SF possibly results in a low early strength but increased long-term strength for M-S-H binder compared to Portland cement as seen in previous studies (Zhang et al., 2012a, 2012b). With continued hydration the long-term strength of the mortar samples presented in this investigation is expected to increase considerably. There is an improvement of the homogeneity and density of the pastes as the SF content decreased. Sample Mg/SF=40/60 shows a relatively large pore structure compared to samples Mg/SF=50/50 and Mg/SF-60/40 with lower SF content.

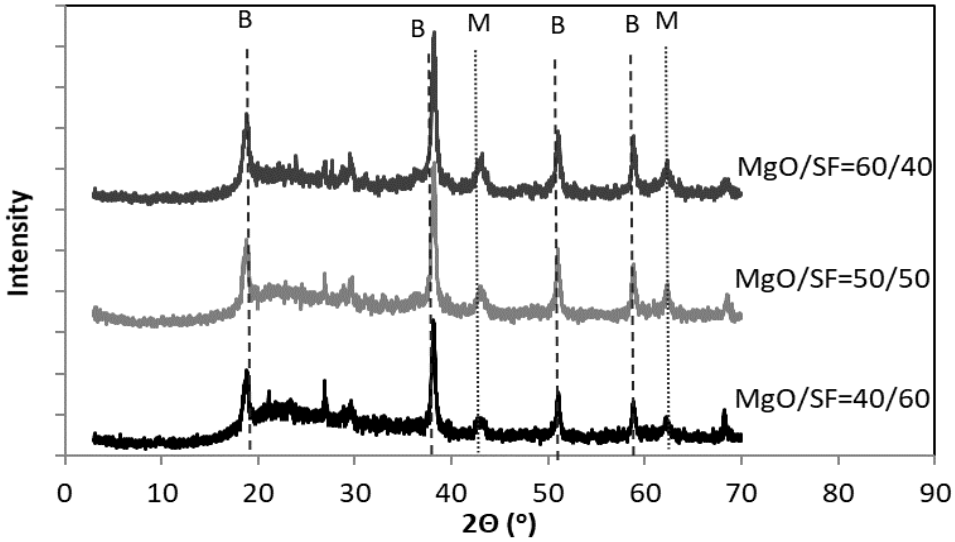

a) 1 day results

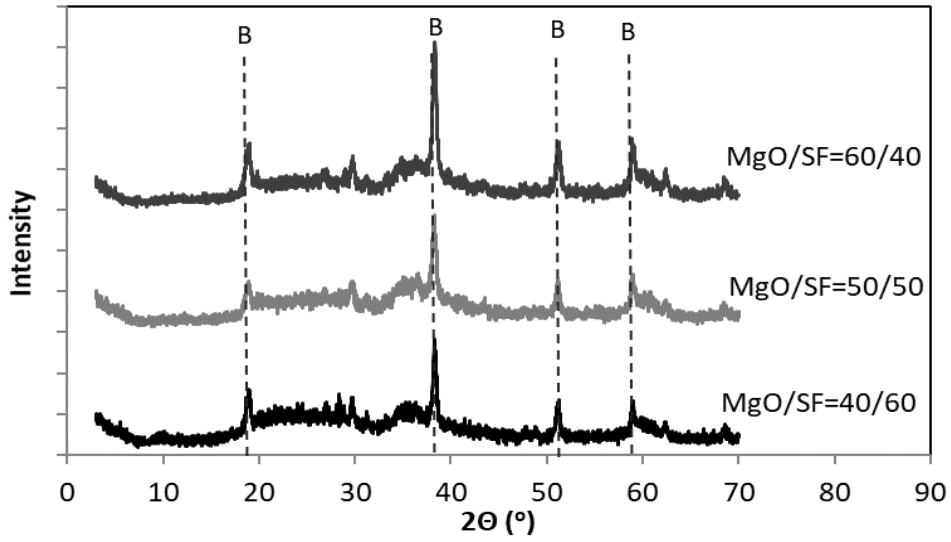

b) 28 day results

Figure 6.6. XRD results after 1 and 28 days hydration. (B – brucite, M – MgO, Q – Quartz SiO_2)

XRD results of all of the paste samples presented in Figure 6.6 show distinct brucite peaks, regardless of the MgO/SiO_2 ratio after 1 day of hydration. The intensity of the peaks however diminishes with a decrease in the MgO content. The broad peaks of the amorphous silica fume are evident in all the samples between approximately 20 and 30 ^{o} (2Θ). In addition to the brucite and MgO, the Mg/SF=40/60 paste sample also has a peak indicating crystalline SiO_2 which is not present in the samples with lower proportions of silica. After 28 days the majority of the brucite

has been consumed in the Mg/SF=40/60 sample while in the Mg/SF=50/50 and the Mg/SF-60/40 samples brucite is still clearly present. The broad peaks around 36° (2θ) are indicative of amorphous M-S-H gel (Zhang et al., 2014) and are visible in all three samples at 28 days.

6.4.4. **Compressive strength**

Due to the fineness, low density and high water demand, the SF content affects both physical and chemical properties of M-S-H binder. Therefore, even a minor change in MgO/SiO_2 ratio influences the strength of hardened mixtures as a result of the following properties:

- An increase in the SF content decrease binder specific gravity;
- Change of Mg/Si molar ratio affects the proportions of M-S-H gel and brucite in the hydration products;
- High SF content decreases workability and packing density of the mixture, as it was demonstrated that the dominance of fine particles generally reduce packing density compared to the case where coarse particles are dominant (Stovall et al., 1986; Larrard and Sedran, 1994; Larrard, 1999).

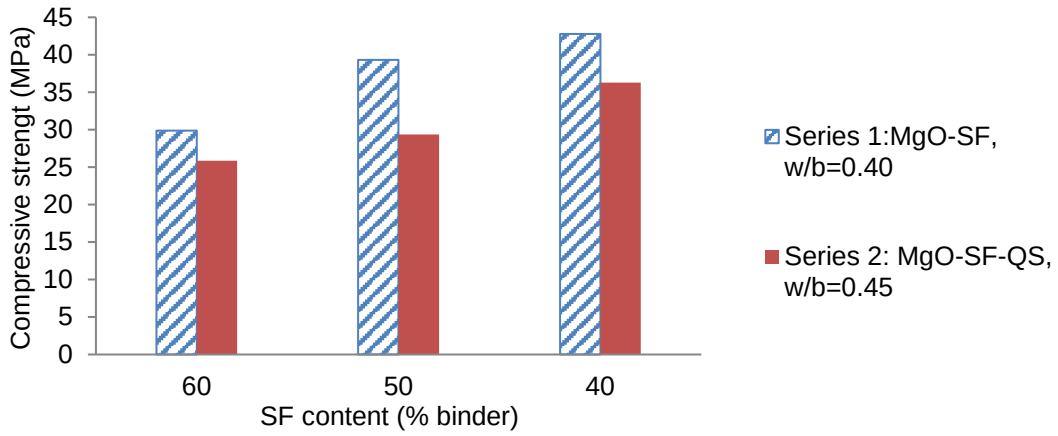

Figure 6.7. Compressive strength of M-S-H paste and mortar (at w/cm = 0.40 and 3% Viscocrete-5-555)

Figure 6.7 presents the compressive strength of Series 1 (paste) and Series 2 (mortar) samples using M-S-H binary binder system (MgO+SF). The MgO/SiO_2 ratio significantly affects 28-day compressive strength of all samples. In Series 1, mix S1.60 containing 40% MgO-60% SF obtained compressive strength of only 29.9 MPa. Surprisingly, as the SF content was reduced the compressive strength increases to the highest strength of 42.8 MPa for the mix S1.40 containing 60% MgO–40% SF. Zhang et al. (2014) have shown that in the excess of SF, the major hydration product of MgO-SF reaction is M-S-H gel which are associated with greater cementious properties.

Therefore the low strength of the high SF content mix might result from the very low packing density. Furthermore, both M-S-H gel and brucite ($Mg(OH)_2$) are present as hydration products and contribute to the strength of high MgO content mixes.

Series 2 includes M-S-H mortar mixtures with quartz sand to reduce shrinkage cracking. Due to the addition of quartz sand aggregate, the w/c was increased to 0.45 to achieve the desired workability. The increase of w/c to 0.45 lead to strength reductions of all mixes in Series 2 compared to Series 1. However, the two series exhibit a similar relation between the SF content and compressive strength. The 28-day compressive strength was only 25.9 MPa with mortar mix S2.60 containing the highest SF content (40% MgO-60% SF) while mortar mix S2.40 containing 60% MgO-40% SF achieved the highest compressive strength of 36.3 MPa.

6.5. PROPERTIES OF TERNARY SYSTEMS MgO-SF-QF

6.5.1. Effect of crushed quartz filler on water reduction

The idea of adding crushed quartz filler to M-S-H binder was derived from a study of Portland cement replacement with quartz filler to improve the rheology (Daukšys, 2010) due to the lower water absorption and smooth texture of finely ground quartz particles.

Figure 6.8 and Figure 6.9 show the reduction in water associated with adding crushed quartz filler to maintain a fixed flow of MgO-SF-QF ternary systems (Series 3, 4, 5). The replacement of cementitous materials by crushed quartz filler improves rheology considerably, expressed by the reduction of water content while maintaining a minimum flow of 120-125 mm for workability. The amount of reduced water is proportional to the increase of filler content from 10-40%. It is possible to achieve a low range w/s of 0.21-0.27 while maintaining workability by the use of crushed quartz filler. However, the reduction of w/s did not reduced w/c ratios in all samples. Mixes S5.10, S5.20 showed the lowest w/c of 0.30 were obtained by adding 10-20% of crushed quartz filler. Also, it's agreed that a minimum w/s ratio of 0.36 is required to react with the 40%MgO-60%SF sample to form M-S-H gel (Zhang et al., 2014), sufficient water was provided during the hydration process as water curing was applied in the experiments.

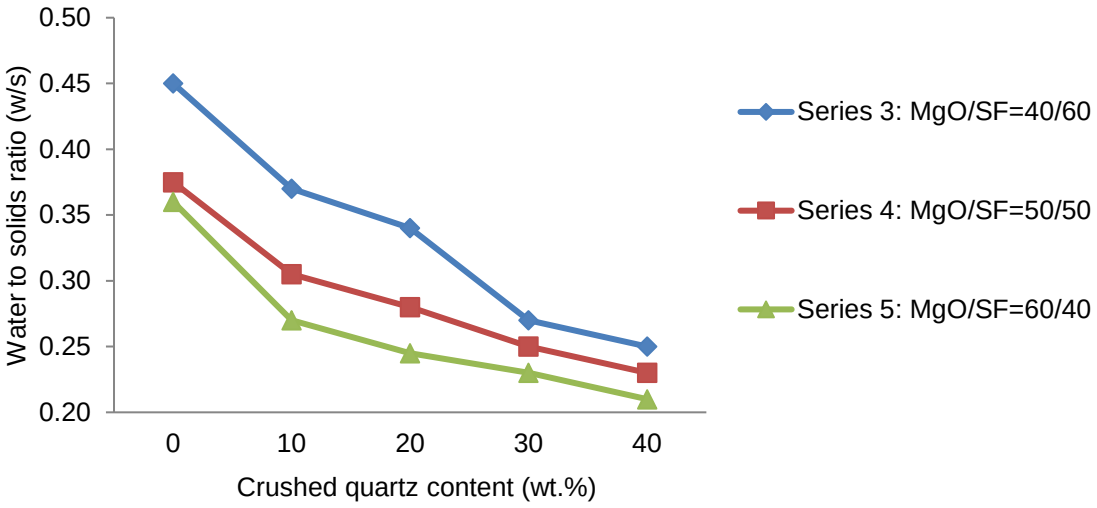

Figure 6.8. Change in w/s at 0-40% crushed quartz filler and fixed flow

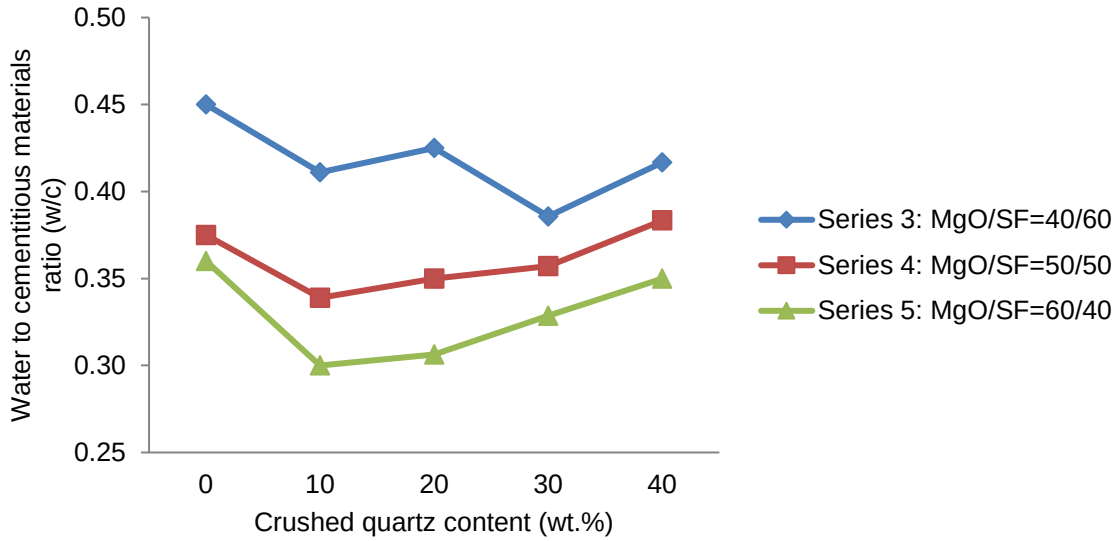

Figure 6.9. Change in w/cm at 0-40% crushed quartz filler and fixed flow

The shape and surface texture of the finely ground quartz filler is clearly show in Figure 6.10. The crushed quartz filler was ground in a ring mill to achieve a particle size of d_{50} = 21 µm. This particle size of crushed quartz is much larger than SF and also larger than magnesium particles. The particle size of the original SF is a function of its production process and not possible to change. An increase in magnesium particle size to improve workability would reduce its reactivity and consequently weaken the strength of the binder. Thus, a partial replacement of the MgO and SF with the coarser particle size of crushed quartz filler was able to effectively reduce the overall water content and improve packing density for the M-S-H binder system. The angular shape of the

ground quartz filler was offset by the smooth surface texture reducing the water demand and the stickiness of the mix caused by the high SF content.

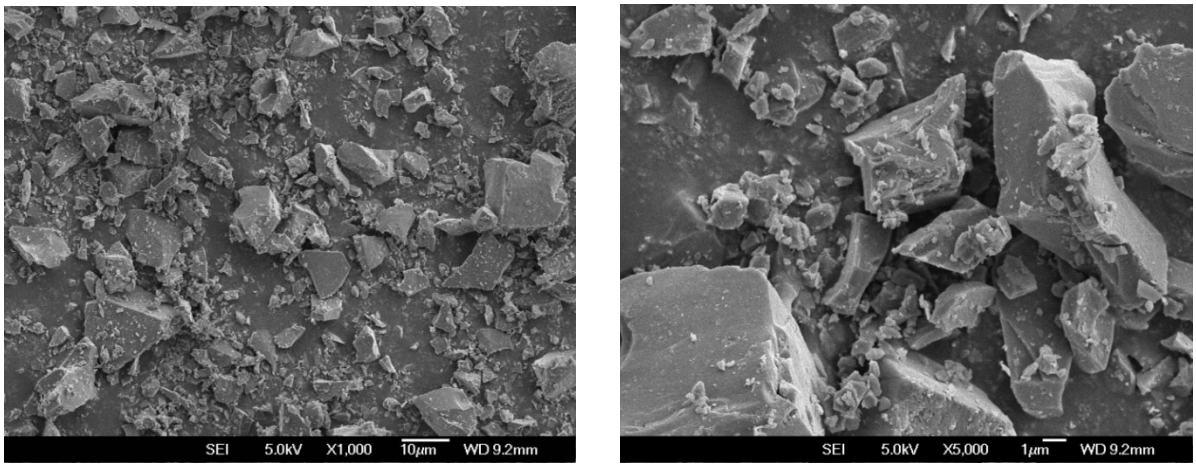

Figure 6.10. SEM images of finely crushed quartz

6.5.2. **Compressive strength**

The compressive strength of the mortar samples from series 3, 4 and 5 is compared against the percentage replaced by crushed quartz filler and w/s ratio in Figures 6.11 and Figure 6.12 respectively. The crushed quartz filler content was increased from 0-40% with an accompanying adjustment in the water content to maintain a fixed flow of 120-125 mm.

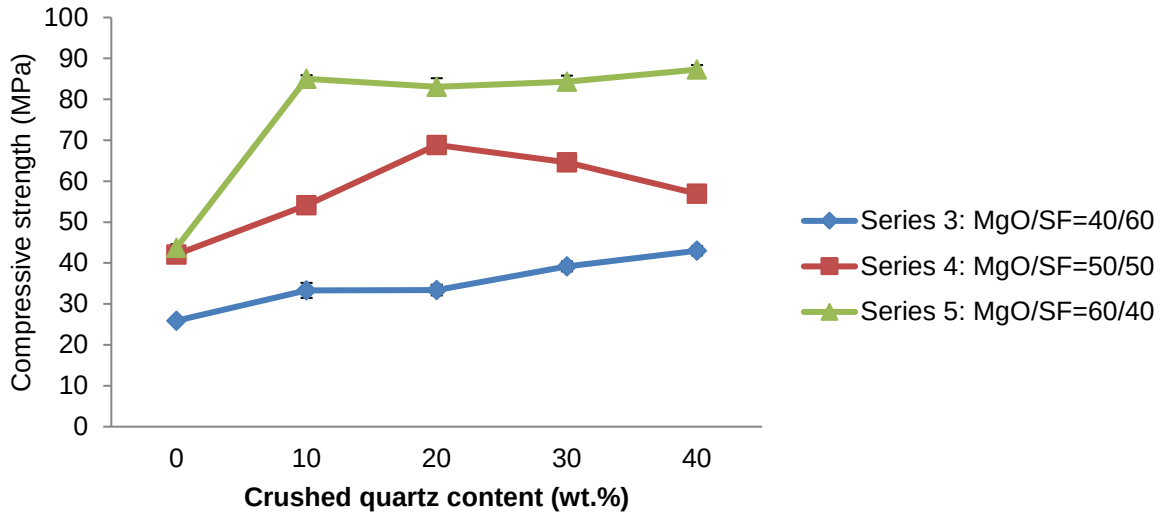

Figure 6.11. Effect of crushed quartz content on compressive strength of M-S-H ternary systems (at variation of w/cm for fixed flow)

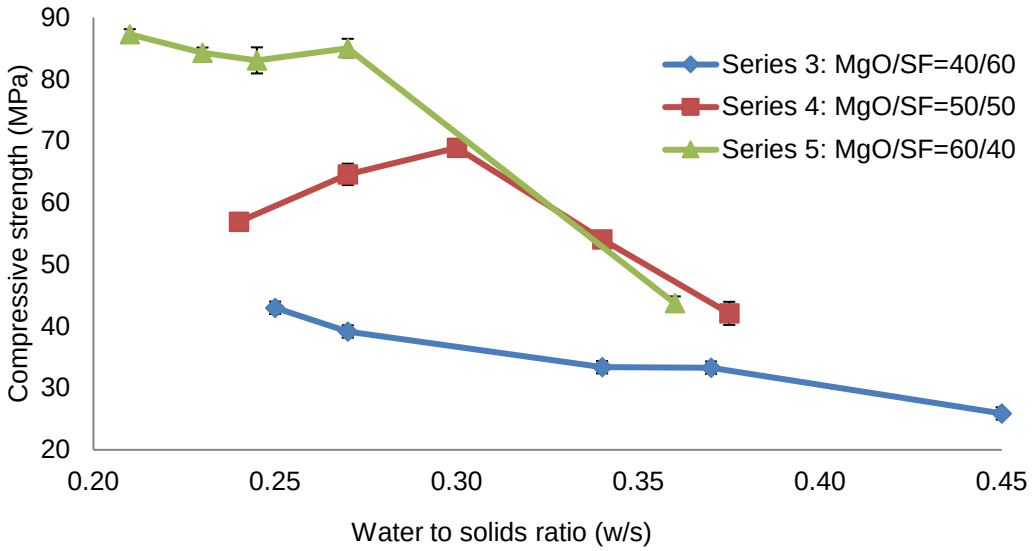

Figure 6.12. Effect of w/s to compressive strength of ternary M-S-H mortar

The crushed quartz filler content was found to considerably affect the strength of M-S-H samples in all testing series. For samples in Series 3 where MgO/SiO_2 was held at low ratio of 40/60 to optimize the formation of M-S-H gel, samples without fillers have the lowest compressive strength. The optimal M-S-H gel volume formed from high cementitious materials (MgO+SF) did not compensate for the loss of strength due to high porosity and poor packing density caused by high SF and water content, resulting in a 28-day compressive strength of only 25.9 MPa. The introduction of filler content, although at a minimum content of 10%, reduced the w/s from 0.45 (without filler) to 0.37, and increases compressive strength to 33.3 MPa. The change in w/c ratio was less dramatic but still noticeable with a decrease from 0.45 to 0.41. The compressive strength is proportional to the increase of filler content, due to coupling effect of water reduction, generally resulting in decreased w/c, and improved packing density. It should be noted that the highest compressive strength of 43 MPa was obtained with mix containing 40% crushed quartz filler where the w/c ratio was 0.42 compared to the 30% crushed quartz filler mix which had a w/c of 0.39 and a compressive strength of 39 MPa.

Series 4 samples exhibited higher strength than series 3 at the same replacement percentage of cementitious materials (MgO+SF). The strength increase is achieved from a further water reduction effect due to lower SF contents. The introduction of crushed quartz filler from 10-40% can reduce w/s from 0.375 to 0.23. This water reduction results in improved packing density and increases strength from 42.1 MPa (mix without filler) to 68.9 MPa (mix containing 20% filler).

Filler content of over 20% reduces strength as the overdosage of filler reduces gel volume, resulting in the segregation of cementitious materials (ACI, 2006).

The optimum binder composition for strength and workability was observed within Series 5 samples (MgO/SiO_2 = 60/40, Mg/Si molar ratio = 2.25). Samples without filler, although containing highest M-S-H gel volume, require the highest water content in the series (w/s=0.36) and obtain the lowest compressive strength of 43.7 MPa. The introduction of filler content, at only 10%, reduces water content dramatically to w/s=0.27 and impressively increases compressive strength to 85 MPa. Further increase of filler content to 40% results in higher reduction of water content to as low as w/s=0.21 with only a marginal increase of compressive strength to 87 MPa. It is obvious that ternary systems of MgO-SF-QF have higher compressive strength compared to binary system MgO-SF. Crushed quart filler is mainly "inert" at room temperature and primarily contributed to the increased strength through an improved packing density and workability in M-S-H ternary system (MgO-SF-QF). Benezet and Benhassaine (1999) however, note that fine quartz powder less than 5 μm displays pozzolanic properties when reacted with lime at 100°C. Some limited pozzolanic reaction between the very fine portion of the crushed quartz filler and Mg/SF binder may be possible.

The effective range of w/s to achieve the highest strength in each series can be clearly seen in Figure 6.12. As the total water content and w/s in the mix decrease, there is an increase in strength, with the exception of two mixes in series 4 (S4.30 and S4.40). These two mixes include very high filler content at 30-40% in which the decrease of water content might not compensate for the strength loss due to the reduction of cementitious materials (MgO + SF). To achieve a compressive strength over 80 MPa, the mortar mixtures required low SF content (MgO/SiO_2 = 60/40) in combination with low water content of w/s = 0.21-0.27 (equivalent to w/c = 0.30-0.35 from Table 6.2).

6.6. OPTIMAL BINDER COMPOSITION

It can be seen in Figure 6.13, that there is no common agreed binder composition for the optimal strength of M-S-H-based materials. Jin and Al-Tabbaa (2014) mixed MgO-SF pastes containing 0-50% SF at very high water content (w/cm=0.87) and obtained optimal strength with high SF content mix (50% MgO – 50% SF). Although the mix of high SF content has very poor packing density, it appears that the dominance of M-S-H gel controlled the strength.

On the other hand, in a study by Wei et al. (2006) mixing mortars with MgO-SF binder containing 10 - 40% SF (w/cm=0.50), the mix containing 30% SF resulted in higher compressive strength

than mix containing 40% SF. Considerable care however must be taken when comparing the results from different researchers as the source and preparation method of the magnesium oxide can have a significant effect on its reactivity and the strength development of the M-S-H system. Jin et al. (2013) have shown difference in reactivities of over an order of magnitude between various types of MgO. Some of the differences observed in the various properties of the concrete therefore may be due to the particular properties of the MgO rather than a result of differences in the MgO/SiO_2 ratios or even the w/c ratios.

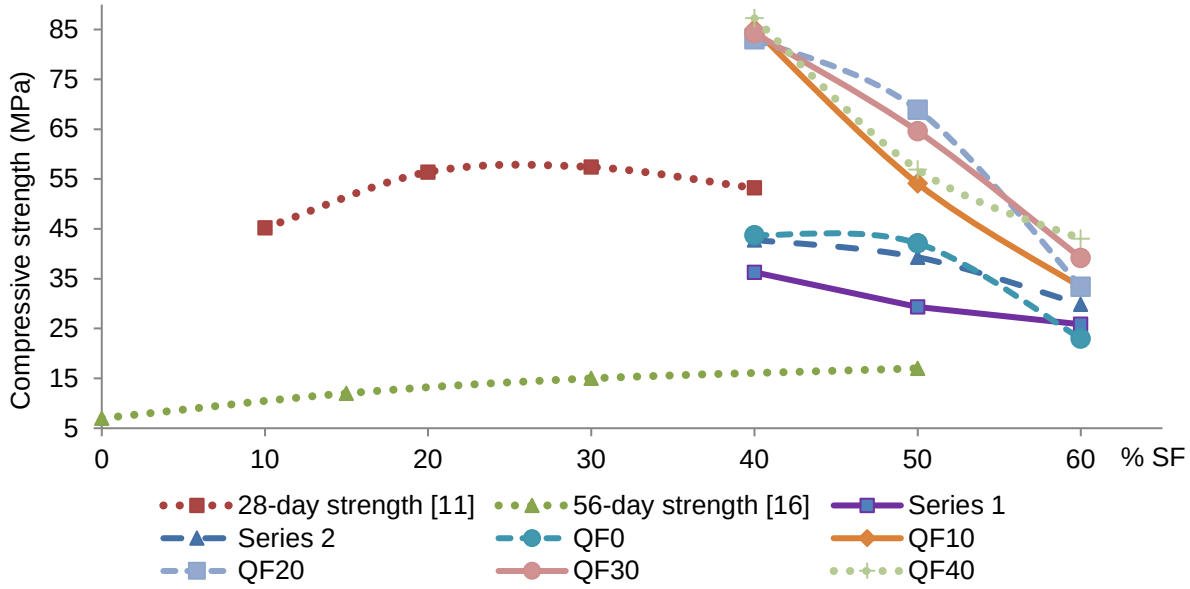

Figure 6.13. SF content and compressive strength of M-S-H paste (Series 1, 2) and mortar (QF0-QF40 denotes mortar samples containing 0-40% QF)

The experimental study in this paper also shows that high SF content mix did not always results in higher strength. High SF content binder might contain unreacted SF particles in low water content mixtures, resulting in poor particle packing and reduced strength.

From the testing of both binary and ternary systems it was observed that with mixture of 60/40 MgO/SF provided the greatest strength compared to the 40/60 MgO/SF ratio as required by stoichiometry for chemical reactions to form M-S-H gel. The optimal binder composition, therefore, is dependent not only on the MgO/SiO_2 ratio for maximum formation of M-S-H gel, but also the MgO/SiO_2 ratio for maximum packing density characterized by particle size and shape of each constituent in the binder. The addition of crushed quartz filler from 10-40% binder also

resulted in a considerable improvements to the workability which produced more consolidated less porous samples. Compressive strengths of QF20 and QF30 samples indicate the optimal replacement of crushed quartz filler was between 20-30%.

It should be noted that the optimization in this chapter was done for M-SF mixtures only and the optimal binder composition for the compressive strength is yet strongly dependent on the silica sources. A more detailed experimental programme using four silica sources is presented in chapter 7, mixtures of MgO and other amorphous silica such as MS or RHA obtained higher compressive strengths with MgO/SiO_2 of 50/50 and 40/60, which differs from M-SF systems. The mix designs used in chapter 7 were based on initial developments already discussed in this chapter.

6.7. CONCLUSIONS

In this wortk, M-S-H mixtures of MgO and SF have been prepared and tested to determine the optimal binder composition to obtain high compressive strength pastes and mortars using a M-S-H binder system. It should be noted that the results and conclusions are applicable to the specific materials used in this investigation and that other MgO or silica may give very different results. The following concluding remarks have been found from the optimization process:

(1) The M-S-H binder systems composed of MgO and SF require very high water demand compared to PC due to the low specific gravity and effects of particle size, shape and texture of the binder constituent materials.

(2) The use of suitable superplasticizer is critical to reduce water demand in which the optimal dosage of polymer-based superplasticizer (Viscocrete-5-555, liquid) is between 3-4% (1-1.5% solids).

(3) The formation of M-S-H-gel is not the only contributor to the strength of the binder. The MgO/SiO_2 ratio for optimal strength is also dependent on other factors including workability, packing density and water content. The MgO/SiO_2 ratio of 60/40 (Mg/Si molar = 2.25) is found to result in optimal compressive strength at w/c =0.45 and below.

(4) The use of crushed quartz filler is necessary to reduce water demand of the SF. The addition of crushed quartz filler from 10-40% results in highest strength mixtures of up to 87 MPa.

6.8. REFERENCES

ACI Committee 234 (2006). ACI 234R-06: Guide for the use of silica fume in concrete, ACI.

Benezet J.C., Benhassaine A. (1999). Grinding and pozzolanic reactivity of quartz powders, Powder Technology 105, 167-171.

Bonen D. (1992). Composition and Appearance of Magnesium Silicate Hydrate and Its Relation to Deterioration of Cement-Based Materials. Journal of the American Ceramic Society 75 (1992) 2904-2906.

Bonen D., Cohen M.D. (1992a). Magnesium sulfate attack on Portland cement paste-I. Microstructural analysis. Cement and concrete research 22, 169-180.

Bonen D., Cohen M.D. (1992b). Magnesium sulfate attack on Portland cement paste—II. Chemical and mineralogical analyses, Cement and concrete research 22, 707-718.

Brew D.R.M., Glasser F.P. (2005). Synthesis and characterisation of magnesium silicate hydrate gels, Cement and Concrete Research 35, 85– 98.

Cole W. F. A. (1953). Crystalline hydrated magnesium silicate formed in the breakdown of a concrete sea-wall, Nat 171, 354–355.

Daukšys M., Skripkiūnas G., Grinys A. (2010). Finely ground quartz sand and plasticizing admixtures influence on rheological properties of portland cement paste, Materials Science 16, 365-372.

De Larrard F. (1999). Concrete mixture proportioning: A scientific approach, CRC Press.

Eubank W. R. (1951). Calcination studies of magnesium oxides. Journal of the American Ceramic Society 34, 225-229.

FIB (1988). Condensed silica fume in concrete, Thomas Telford Ltd., London, 1988.

Gollop R., Taylor H. (1996). Microstructural and microanalytical studies of sulfate attack. IV. Reactions of a slag cement paste with sodium and magnesium sulfate solutions. Cem. Concr. Res. 26, 1013–1028.

Jin F., Abdollahzadeh A., Al-Tabbaa A. (2015). Effects of different reactive MgOs on the hydration of MgO-activated GGBS paste. J. Mater. Civ. Eng., 2015, 27(7): B4014001

Jin F., Al-Tabbaa A. (2014). Strength and hydration products of reactive MgO–silica pastes, Cement & Concrete Composites 52, 27–33.

Larrard F., Sedran T. (1994). Optimization of ultra-high-performance concrete by the use of a packing model, Cement and Concrete Research 24, 997-1009.

Li Z., Zhang T., Hu J., Tang Y., Niu Y., Wei J., Yu Q. (2014). Characterization of reaction products and reaction process of $MgO–SiO_2–H_2O$ system at room temperature. Construction and Building Materials 61, 252-259.

Lothenbach B., Nied D., L'Hopital E., Achiedo G., Dauzeres A. (2015). Magnesium and calcium silicate hydrates, Cement and concrete research 77, 60-68.

Malhotra V. M., Ramachandra V. S., Feldman R. F., Aitcin P. C. (1987). Condensed silica fume in concrete, No. 5657JD, 1987.

Mitsuda T., Taguchi H. (1977). Formation of Magnesium Silicate Hydrate and Its Crystallization to Talc, Cement and concrete research 7, 223-230.

Roosz C., Grangeon S., Blanc P., Montouillout V., Lothenbach B., Henocq P., Giffaut E., Vieillard P., Gaboreau S. (2015). Crystal structure of magnesium silicate hydrates (M-S-H): The relation with 2: 1 Mg–Si phyllosilicates, Cement and Concrete Research 73, 228-237.

Stovall T., De Larrard F., Buil M. (1986). Linear packing density model of grain mixtures, Powder Technology 48 (1986) 1-12.

Walling S. A., Kinoshita H., Bernal S. A., Colliera N. C., Provis J. L. (2015). Structure and properties of binder gels formed in the system $Mg(OH)_2–SiO_2–H_2O$ for immobilisation of Magnox sludge, The Royal Society of Chemistry, Dalton Trans. 44, 8126–8137.

Wei J. X., Yu Q., Zhang W., Zhang H. (2011). Reaction products of MgO and microsilica cementitious materials at different temperatures, Journal of Wuhan University of Technology-Mater. Sci. Ed. 26, 745-748.

Wei J.X., Chen Y.M., Li Y.X. (2006). The Reaction Mechanism between MgO and Microsilica at Room Temperature, Journal of Wuhan University of Technology - Mater. Sci. Ed. 21, 88-91.

Zhang T., Cheeseman C., Vandeperre L. J. (2009). Development of novel low pH cement systems for encapsulation of wastes containing aluminium, Decommissioning, Immobilisation and Management of Nuclear Waste for Disposal.

Zhang T., Cheeseman C., Vandeperre L. J. (2012a). Characterisation of corrosion of nuclear metal wastes encapsulated in magnesium silicate hydrate (M-S-H) cement, Ceramic Materials for Energy Applications II, 159-167.

Zhang T., Cheeseman C., Vandeperre L. J. (2012b). Magnesium-silicate-hydrate cements for encapsulating problematic aluminium containing wastes, Journal of Sustainable Cement-Based Materials 1, 34-45.

Zhang T., Vandeperre L., Cheeseman C. (2014). Formation of magnesium silicate hydrate (M-S-H) cement pastes using sodium hexametaphosphate. Cement and Concrete Research, 65, 8–14.

CHAPTER 7
EFFECTS OF CURING CONDITIONS AND SILICA SOURCES ON THE STRENGTH DEVELOPMENT OF MAGNESIUM SILICATE HYDRATE BINDER SYSTEMS

Tran H.M., Scott A., Dhakal R.P. (2017). Strength development of mortars using a magnesium silicate hydrate binder system under different curing conditions. *Proceedings of the 2nd International RILEM Conference on Bio-based Building Materials, 21-23 June 2017, Clermont-Ferrand, France,* 87-91.

Preamble

The previous chapters have discussed the reaction mechanisms and experimental results to confirm the formation of hydration products of M-S-H binder systems. In addition, a mix design for M-S-H cement pastes and mortars reached a 28-day strength of approximately 90 MPa which can be considered as Ultra-high performance concrete (UHPC) for use in specialist structural applications. To further improve and understand the mechanical properties of M-S-H binders, it is important to characterize the strength development of the binders under different curing conditions. The literature has shown a significant impact of curing conditions on the properties of resulting binder systems, for example, the effect of heated treatment on the early strengths of the PC concrete. Also, the testing of long-term strengths is required for further understanding of the durability of these new magnesium binders. Among the supplementary cementitious materials, silica fume is widely used to develop high-performance concrete (HPC) and UHPC and the content of silica fume is generally restricted to less 25% due to its high cost and engineering performance. The use of alternative silica sources without compromising engineering properties is essential to develop a cost-effective M-S-H binder. On this basis, this chapter continues to study the effects of curing conditions and different sources of silica on the strength development of the M-S-H cementitious materials over a medium-term duration up to 365 days.

Abstract

Mixtures of MgO, silica fume, natural pozzolan, rice husk ash and fly ash were prepared to study the effect of curing conditions and silica sources on the strength and microstructure of magnesium silicate hydrate (M-S-H) cementitious materials. A binder composition containing 60% magnesium oxide and 40% silica fume was selected for mortar samples with different curing regimes. It was found that curing conditions have a significant influence on the strength development of M-S-H binder mortar mixtures. Ambient conditions, oven curing for 1-3 days or water curing at elevated temperature for 1-3 days effectively increased early strengths for M-S-H binders, however, reduced long-term strengths over 90 days. The water curing longer than 90 days reduced 365-day strengths of M-SF mixtures. The M-S-H binder mixtures tend to have higher 28-day and 90-day strengths than PC control samples under ambient conditions but lower strengths than PC water cured samples at standard temperature (20°C). The silica sources had a strong influence on the strength and microstructure of the hardened M-S-H pastes due to the variation of reactivity, morphology and the material fineness. The highest compressive strengths of M-S-H mortar samples cured in different regimes reached 50 MPa, 53 MPa and 71 MPa at 7, 28 and 90 days age respectively, which is sufficient for a wide range of structural applications.

7.1. INTRODUCTION

The production of conventional Portland cement requires very high calcination temperatures of approximately 1450°C which is energy-intensive and can have a negative impact on the environment. As such, there has been a trend to develop low-energy binder systems capable of incorporating high volume of waste-related materials.

One of the constituents of magnesium-silicate-hydrate (M-S-H) binder systems is reactive magnesium oxide which can be calcined from magnesite at 700-1000°C (Thomas et al., 2014). Such decarbonation process at low temperature releases less CO_2 from burning fossil fuel than the production of Portland cement (Harison, 2007). Another potential technology to produce reactive magnesium oxide has been developing by Novacem which is claimed to be CO_2 neutral from processing magnesium silicates at low temperature and pressure (Gartner, 2011). The other constituent of M-S-H binders is amorphous silica which is available in various forms of industrial by-products or waste materials such as silica fume, rice husk ash, fly ash or alternatively from natural silica deposits.

Research on cementing properties of M-S-H binder systems reveals a number of distinct properties compared to Portland cement. The chemical reactions for the formation of M-S-H gel were proposed by a number of authors (Wei et al., 2006; Li et al., 2014; Zhang et al., 2014) whereby the M-S-H gel was formed in a similar mechanism to the pozzolanic reactions in Portland cement. The first stage is the hydration or magnesium oxide to form magnesium hydroxide:

$$MgO + H_2O = Mg(OH)_2 \quad (1)$$

The secondary reaction is then followed by the formation of magnesium silicate hydrates, for example (Zhang 2014):

$$8Mg(OH)_2 + 8SiO_2 + 8H_2O = M_8Si_8O_{20}(OH)_8.12H_2O \quad (2)$$

Studies of the microstructure revealed a poorly crystalline structure of M-S-H gel. The Mg/Si molar ratio of M-S-H gel was found to vary in a wide range in between 0.67 to 1.50 (Kalousek and Mui, 1954; Mitsuda and Taguchi, 1977; Brew and Glasser, 1995; Nied et al., 2016) while the Ca/Si ratio of the C-S-H gel of Portland cement is approximately 1.75 with a variable stoichiometry range of 1.2 to 2.1 (Taylor, 1997; Richardson, 1999).

There have been a number of studies on fresh and mechanical properties of M-S-H binder systems. In a M-S-H binder system containing a significant proportion of silica fume, the very high surface area results in a high water demand to achieve a reasonable level of workability which can adversely affect strength (Zhang et al., 2009; Walling et al., 2015). The MgO/SiO_2 ratio was reported to have remarkable effects on the optimal compressive strength of the binder systems.

Zhang et al. (2014) assumed that the low Mg/Si ratio systems (MgO/SiO_2=40/60 by mass) facilitated the formation of M-S-H gel which resulted in optimal compressive strength in excess of 60 MPa. On the other hand, Wei et al. (2006) suggested high MgO/SiO_2 ratios in which MgO content accounted for 60-70% of the binder composition resulted in better strengths. Tran and Scott (2017) proposed a ternary binder system containing magnesium oxide, silica fume and a small proportion of crushed quartz fillers to obtain compressive strength of over 85 MPa. The material source of both the MgO and the silica can have a major impact on the strengths of M-S-H binders. For example, the reactivity and CaO impurity content of MgO sources affect the solubility of silica and the formation of hydration products (Jin and Al-Tabbaa, 2014).

Significance

Despite the increasing research and interest in M-S-H binder systems, there is relatively little information on the effect of curing conditions and silica sources on the properties of the binders, particularly for the long-term curing duration. A part from a study on performance of $MgO–SiO_2$ binders under different curing conditions (Sonat et al., 2017), most previous studies on M-S-H binder systems controlled curing conditions at high humidity (RH≥95%) and temperature at or near 21^{o}C. Therefore, a number of silica sources and different hydrothermal curing conditions were investigated in this study to further understand the strength development and microstructures of M-S-H binder systems for potential use as a viable construction material.

7.2. EXPERIMENTAL PROGRAMME

7.2.1. Materials

M-S-H binders consist of magnesium oxide and amorphous silica. Control samples were prepared using a general purpose Portland cement. River sand, which is primarily siliceous in nature, was used to produce mortar samples. The sand was sieved to obtain a maximum particle size of 2.36mm and meets the requirement of ASTM C33.

As one of the major disadvantages associated with M-S-H binders with high proportions of silica fume is the poor workability, many previous studies of M-S-H binders used high w/c ratios of 0.50 or above even with the addition of superplasticizers (Wei et al., 2006l Jin and Al-Tabbaa, 2014; Walling et al., 2015). A third-generation polymer-based superplasticizer supplied by Sika (New Zealand) was used and provided extremely high water reduction for M-S-H binder systems, which produced workable mixtures with w/b as low as 0.40. The material properties are presented in Chapter 3.

7.2.2. Mix proportions

Three sample series were prepared to examine microstructure and individual effects of curing and silica sources on strength. A constant binder composition containing 60% MgO and 40% SF with sand/binder = 1.0 was selected as shown in Table 7.1 for M-S-H mortar samples in curing tests. The M-S-H samples required a superplasticizer (SP) content of 3% of binder by weight for workability.

Series 2 included MgO-silica mortar mixtures with different silica sources. MgO/silica ratio varied from 40/60 to 60/40. Due to the various water demand of silica, w/b = 0.40 and w/b=0.50 were used with varying superplasticizer dosages to achieve workable mixes. Mix proportions are shown in Table 7.2.

Series 3 contains MgO-silica paste samples for microstructure analysis using SEM in comparison to control samples using PC and 100% MgO mixture. Mix proportions of samples are shown in Table 7.3.

Table 7.1. M-SF mortar mixtures for different curing regimes

Mix labels	Binder			s/b ratio	w/b	SP, liquid (% of binder by weight)	Curing regime
	MgO	SF	PC				
SF40-A	0.6	0.4	-	1.0	0.40	3%	A
SF40-W7D	0.6	0.4	-	1.0	0.40	3%	W7D
SF40-W28D	0.6	0.4	-	1.0	0.40	3%	W28D
SF40-W90D	0.6	0.4	-	1.0	0.40	3%	W90D
SF40-W365D	0.6	0.4	-	1.0	0.40	3%	W365D
SF40-OV50-1D	0.6	0.4	-	1.0	0.40	3%	OV50-1D
SF40-OV50-3D	0.6	0.4	-	1.0	0.40	3%	OV50-3D
SF40-OV100-1D	0.6	0.4	-	1.0	0.40	3%	OV100-1D
SF40-OV100-3D	0.6	0.4	-	1.0	0.40	3%	OV100-3D
SF40-W60-1D	0.6	0.4	-	1.0	0.40	3%	HW60-1D
SF40-W60-3D	0.6	0.4	-	1.0	0.40	3%	HW60-3D
PC-A	-	-	1.0	1.0	0.40	-	A
PC-W365	-	-	1.0	1.0	0.40	-	W365D

Table 7.2. Mix proportions of mortar samples with different silica sources

Mix labels	Binder		s/b ratio	w/b	Super-plasticizer (% of binder by weight)	Curing regime
	MgO	SiO_2				
SF60	0.4	0.6	1.0	0.40	3%	W365D
SF50	0.5	0.5	1.0	0.40	3%	W365D
SF40	0.6	0.4	1.0	0.40	3%	W365D
MS60	0.4	0.6	1.0	0.40	3%	W365D
MS50	0.5	0.5	1.0	0.40	3%	W365D
MS40	0.6	0.4	1.0	0.40	3%	W365D
FA60	0.4	0.6	1.0	0.40	3%	W365D
FA50	0.5	0.5	1.0	0.40	3%	W365D
FA40	0.6	0.4	1.0	0.40	3%	W365D
MS60	0.4	0.6	1.0	0.50	2%	W365D
MS50	0.5	0.5	1.0	0.50	2%	W365D
MS40	0.6	0.4	1.0	0.50	2%	W365D
RHA60	0.4	0.6	1.0	0.50	5%	W365D
RHA50	0.5	0.5	1.0	0.50	4%	W365D
RHA40	0.6	0.4	1.0	0.50	3%	W365D

Table 7.3. Mix proportions of paste samples for microstructure analysis

Mix labels	Binder			w/c	Super-plasticizer (% of binder by weight)	Curing regime
	MgO	SiO_2	PC			
SF40	0.6	0.4	-	0.40	3%	A
MS40	0.6	0.4	-	0.40	3%	A
FA40	0.6	0.4	-	0.40	3%	A
RHA40	0.6	0.4	-	0.50	3%	A
PC	-	-	1.0	0.50	-	A
MgO	1.0	-	-	0.50	3%	A

7.2.3. Sample preparation and curing regimes

Mortar mixtures were produced using a Hobart mixer. Immediately after mixing, the mortars were placed in 50×50×50 mm cube molds and demolded after 24 h followed by curing in different conditions as follows:

- A (Ambient conditions): Samples were cured in an environmental chamber at a relative humidity RH=50% and a standard temperature of 20°C.
- W7D: Samples were cured in water at 20°C for 7 days followed by curing regime A until testing.
- W28D: Samples were cured in water at 20°C for 28 days followed by curing regime A until testing.
- W90D: Samples were cured in water at 20°C for 90 days curing period followed by curing regime A until testing.
- W365D: Samples were cured in water at 20°C for 365 days curing period.
- OV50-1D: Unsealed samples were cured in an oven at 50°C for 1 day followed by curing in water at 20°C until testing date.
- OV50-3D: Unsealed samples were cured in an oven at 50°C for 3 days followed by curing in water at 20°C until testing date.
- OV100-1D: Unsealed samples were cured in an oven at 100°C for 1 day followed by curing in water at 20°C until testing date.
- OV100-3D: Unsealed samples were cured in an oven at 100°C for 3 days followed by curing in water at 20°C until testing date.
- W60-1D: Samples were cured in hot water at 60°C for 1 day followed by curing in water at 20°C until testing date.
- W60-3D: Samples were cured in hot water at 60°C for 3 days followed by curing in water at 20°C until testing date.

7.2.4. Testing methods

Compressive strength tests were performed as per ASTM C 109-02. The tests were undertaken at 7, 28, 90, and 365 days age. The result of each test is the average compressive strength of three samples. SEM analysis was performed on the hydrated paste samples after 28 days using a JEOL 6400 Scanning Electron Microscope with the beam voltage 15kV, magnification ×2000.

7.3. RESULTS AND DISCUSSION

7.3.1. Effect of moist curing to M-S-H binder systems

The compressive strength of the mortar samples under different moist curing conditions is presented in Figure 7.1. At the early age of 7 days, it is surprising that the ambient conditions curing results in better strength than water curing method. The early age hydration products are known to contain a significant amount of brucite along with the freshly formed M-S-H phases (Wei et al. 2006). It is possible that under lower humidity of the ambient curing there is improved crystallinity of brucite and the possible formation magnesium carbonate due to exposure with the atmosphere compared to water curing at 7 days. Similar phenomenon was reported elsewhere (Grist et al., 2013) in a study of the strengths of dry-cured and water cured lime–pozzolan mortars in which the higher strength of dry-cured samples at 7 days age was attributed to the dewatering effect which results in a localised decrease in w/b ratio leading to a denser microstructure and the improvement of crystallisation of silica phases. At this early age, there also appears to be free water in the dry cured mixture which is sufficient for the hydration to form M-S-H gel from brucite and silica.

In addition, there might be potential effect of the moisture conditions on the compressive strength results. The compressive strength of each dry-cured mortar sample was tested without soaking it whereas the wet-cured samples were tested immediately after removing them from the water bath without allowing time to dry out. As the standard testing procedures do not explicitly state the difference of results due to different moisture conditions in which samples might be tested, this effect has not been investigated in detail in this project.

The strengths increase significantly up to 28 days for all the samples, especially those cured under ambient conditions (A) or short-term immersed in water for 7 days (W7D). Short-term curing in water followed by ambient curing can provide sufficient water for M-S-H gel formation while still maintaining the brucite. The W7D curing regime results in the highest compressive strength of over 50 MPa indicating that the formation of M-S-H gel is crucial to improve strength at this 28 days age. Water curing for a longer period (W28D) can provide additional water for the formation of M-S-H gel beyond 28 days, however, this affect the amount of brucite and possibly the formation of magnesium carbonate which results in lower strengths at 28 days age.

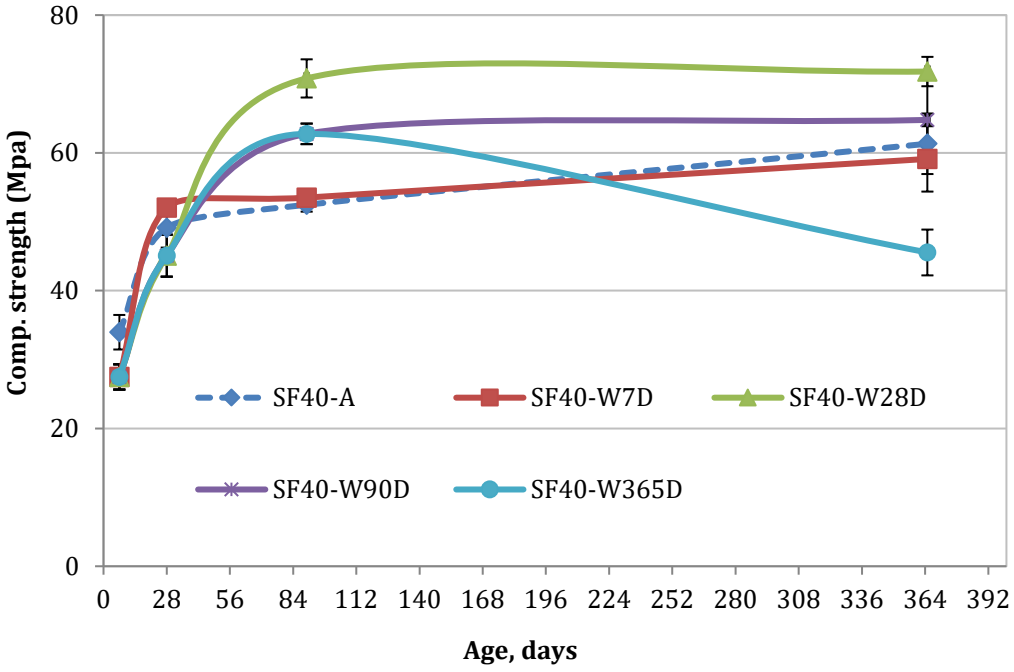

Figure 7.1. Compressive strengths versus (vs.) different moist curing conditions.

The optimal water curing duration for strengths of M-S-H binders was found to be dependent on the strength target at a particular age. The A and W7D curing conditions resulted in relatively little increase in strength up to 90 days while curing in water for 28 days (W28D) and longer up to 90 days (W90D) significantly improved the longer term strength development. It was found that the water curing duration has a large influence on the strength development of M-S-H binders in which the W28D results in the highest long-term strength over 70 MPa up to 365 days age, considerably higher than curing in A or W7D conditions. Hence, providing curing water longer than 7 days is crucial for hydration process. The pozzolanic reactions of brucite and silica to form M-S-H develops at a slow rate at the early age up to 7 days but improved considerably from 28 to 90 days when sufficient water is provided, which is associated with the strength increase at the later stages and indicates the significant contribution of the M-S-H gel rather than brucite in MgO-SiO_2 mixtures. However, it is very strange that the long-term strengths of samples continuously submerged in water up to 365 days decrease considerably after 90 days. It is possibly due to the high content of MgO in the binder composition and the adverse effect of water curing on the residual brucite resulting in a reduced strength. The long-term strength reduction of M-S-H binders has also reported elsewhere (Jin and Al-Tabbaa, 2014). Further studies are therefore necessary to characterize the influencing factors on the strength development of M-S-H binders in water for the long-term of a year or longer curing duration.

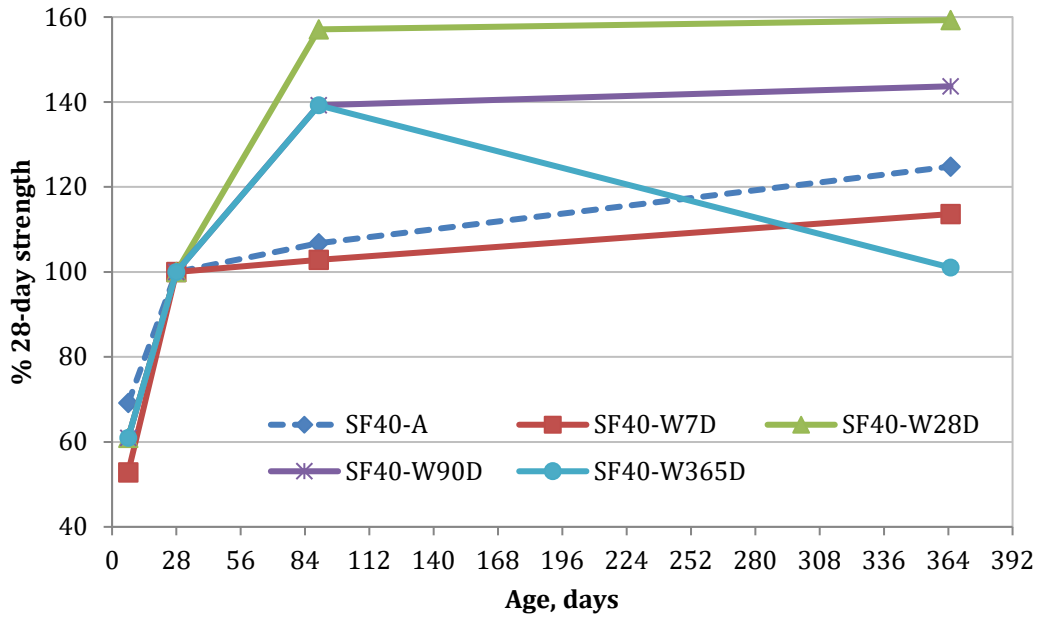

Figure 7.2. % 28-day strengths M-S-H and PC mortars under water and ambient curing

The strength development of samples presented by % 28 days strength is shown in Figure 7.2. Strengths of samples cured in ambient and W7D conditions increased slowly after 28 days compared to water curing due to the incomplete hydration process results from insufficient curing water. However, the long-term strengths up to 365 days of those samples increase considerably, possibly due to the continuous carbonation of brucite. In the meanwhile, the slow pozzolanic reactions between brucite and silica to form M-S-H binding phases result in significant strength increases with W28D and W90D curing regimes in between 28 and 90 days, presented by linear-like trends in this period and remains stable after 90 days.

However, it should be noted that the water curing regime W90D resulted in lower strength than W28D, and the long-term water curing regime W365D even reduced strengths of the samples further after 90 days. It is therefore indicated that that water curing up to 28 days provides sufficient water for the formation of M-S-H binding phases and further submerging samples in water has some detrimental effect on strengths of the samples.

7.3.2. **Effect of heat treated curing on M-S-H binder systems**

Figure 7.3 presents the compressive strengths of samples cured at different elevated temperatures. Both early and long-term strengths were influenced by oven heat treated curing. Early strengths at 7 days age of all samples cured in 50°C and 100°C were improved compared to

water curing regime (W365D). The highest 7-day strength achieved by elevated temperature curing (OV100-1D) was 40 MPa, an increase of 45% compared to water curing at standard temperature (20°C).

At 28 days age, the initial oven curing had little effect on compressive strengths compared to water curing. Heated treatment for 1 day (OV50-1D and OV100-1D curing regimes) resulted in a strength increase by 10% compared to W365D curing while longer heating duration up to 3 days did not improve strength significantly.

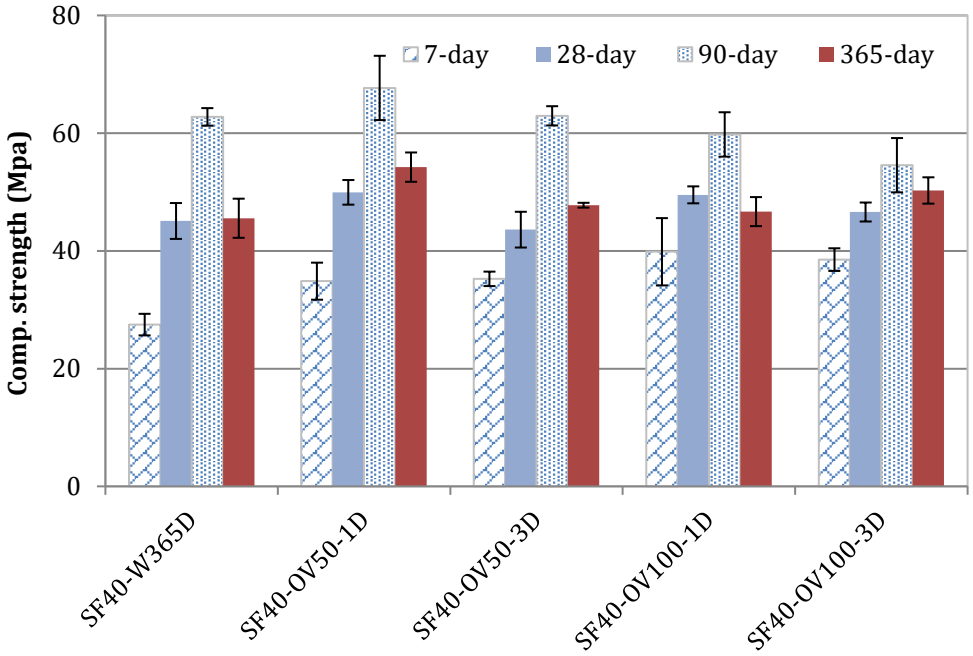

Figure 7.3. Compressive strengths vs. curing at different temperatures.

The 90-day strengths showed that only a mild increase of curing temperature for 1 day (OV50-1D) resulted in a higher strength (68 MPa) than water curing (63 MPa) while the extended heating duration to 3 days only had a marginal effect. At higher curing temperature (100°C), the 90-day strengths of M-S-H mortars were even negatively affected whereby samples exposed to OV100-1D curing obtained the lower strength (60MPa) than water curing (63MPa). The longer curing duration to 3 days (OV100-3D) further decreased the strength of the samples (55MPa) compared to OV100-1D cured samples. All samples exhibited a strength reduction from 90 to 365 days in which the 365-day strengths of oven curing samples were slightly higher than those of standard water curing at ambient temperatures.

The oven curing for 1 day at 50°C (OV50-1D) appears to be optimal for strength development as it is the only curing regime to increase strengths at all testing age (7, 28, 90 and 365 days) compared to standard water curing conditions.

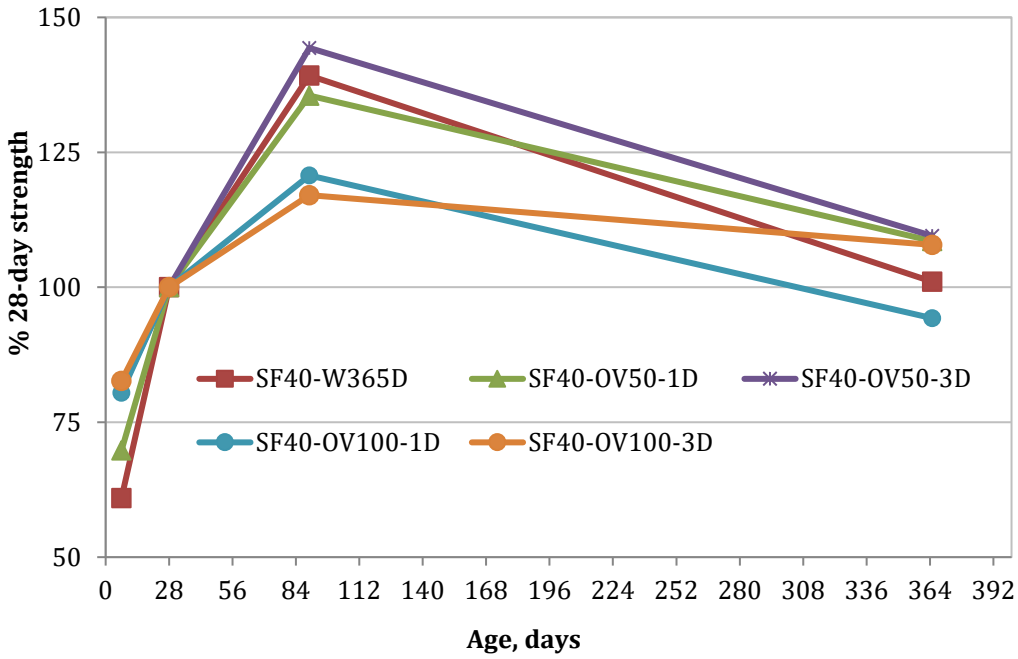

Figure 7.4. % 28-day strengths M-S-H and PC mortars under oven heated treatment

Strengths development measured by % 28-day strength is presented in Figure 7.4. It was found that heated treatment only increases strength development rate at the early age of 7 days however decreases these rates at 90-days age. Similar to its influence to PC, heated treatment might be an effective method to improve the strength development of the M-S-H binders. However, the temperature and heating duration should be carefully selected to avoid negative influences on the long-term strengths.

7.3.3. **Effect of hot water curing to M-S-H binder systems**

The coupled effect of moist curing and heat treatment was examined using hot water curing. Figure 7.5 presents the compressive strength of samples under hot water curing at 60^{o}C for 1 and 3 days in comparison to water curing at 20^{o}C. Hot water curing improves 7-day and 28-day strengths considerably, however reduced 90-day strengths and had little effect on the 365-day strengths. In addition, a longer curing period in hot water for 3 days resulted in higher strengths at 7 and 28 days age, but also decreased the 90-day and 365-day strengths by a greater extent compared to hot water treatment for 1 day. Samples cured in W60-3D achieved a 7-day strength of over 50 MPa, increased by 83% compared to water-cured samples obtained only 28 MPa although a trade-off was observed between early and long-term strengths.

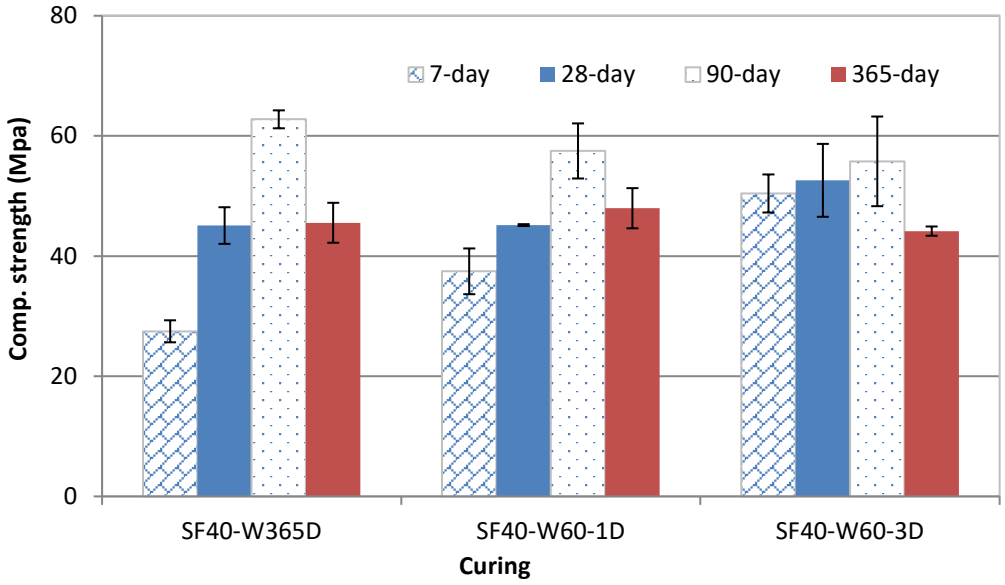

Figure 7.5. Compressive strengths vs. curing in hot water (60°C).

The % 28-day strengths of M-S-H mortars under hot water curing are displayed in Figure 7.6. The 7-day strength of samples cured with W60-3D regime reached 92% of the 28-day strength and further curing to 90 days only increase the strength to 108% while those rates of water curing samples at 7 and 90 days were 61% and 139%, respectively. As early strengths increase, samples cured in hot water develop strength at a higher rate compared to water curing at standard temperature. Although hot water curing regimes increase early strength, they reduce long-term strengths and therefore results in decreases in % 28-day strengths after 365 days curing period.

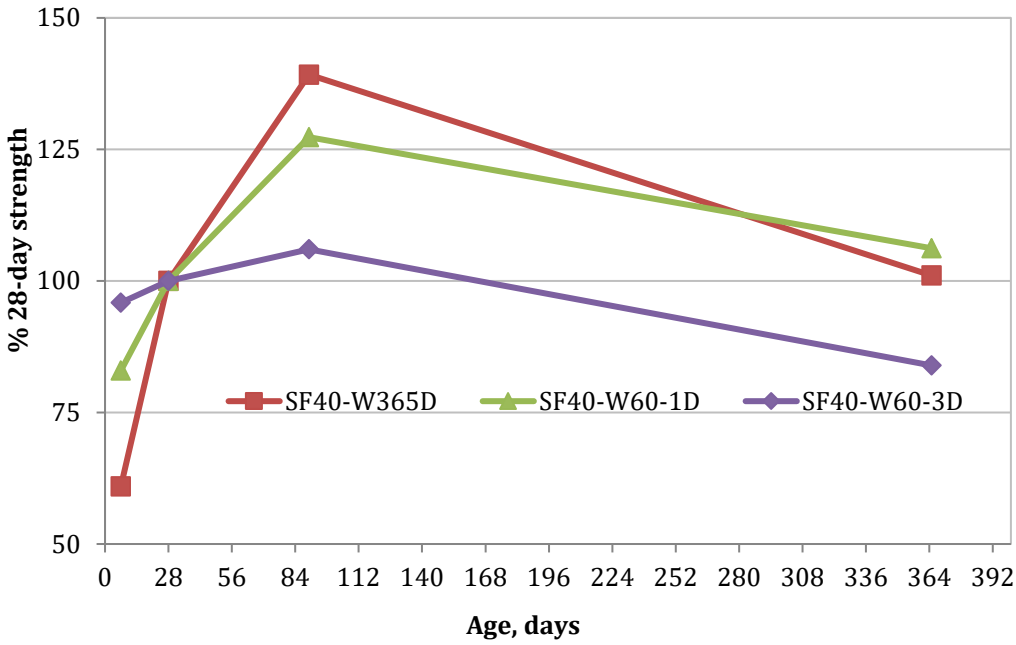

Figure 7.6. % 28-day strengths M-S-H mortars under hot water curing

7.3.4. Strength comparison of M-S-H and Portland cement mortar samples

Figure 7.7 and Figure 7.8 compare compressive strengths between M-S-H and Portland cement mortars. Two typical curing regimes of M-S-H binders were selected for this comparison including ambient conditions and water curing at standard temperatures. Surprisingly, M-S-H samples cured at ambient conditions achieved higher strength than PC samples at the ages of 28, 90, and 365 days, despite a lower strength at 7 days age. In contrast, the strengths of M-S-H samples cured in water were lower than those of control Portland cement samples (Figure 7.7).

For PC, the ambient curing conditions resulted in lower strengths than water curing at any ages between 7-365 days. The moist curing is crucial to provide sufficient water for the hydration of PC to gain strength. However, the water curing regime decreased strengths of M-S-H binder samples compared to ambient curing conditions and only increased the 90-day strengths. The 100%MgO samples had much lower strengths compared to 60/40 M/SF mixtures. It appears that due to containing high MgO content, the residual brucite formed is the weak phases of the hydration products and partially dissolve in curing water after 90 days resulting in the lower strengths at 365 days age. The M-S-H cementitious materials possibly are more durable for applications in low humidity rather than long-term submerged in water.

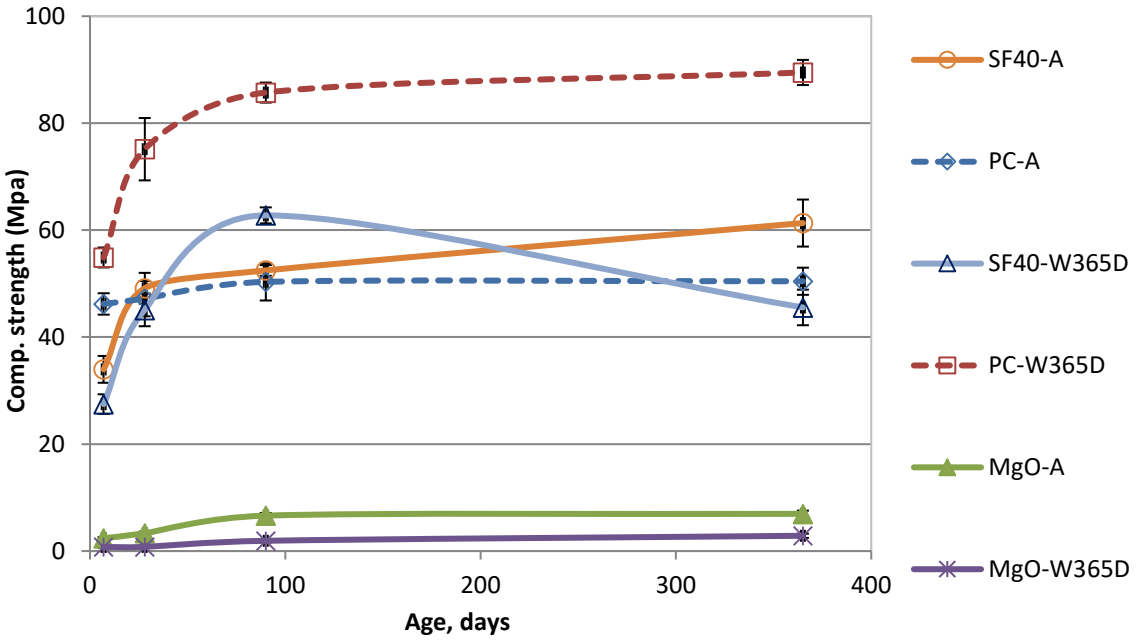

Figure 7.7. Compressive strength of M-S-H and PC samples (ambient conditions and water curing)

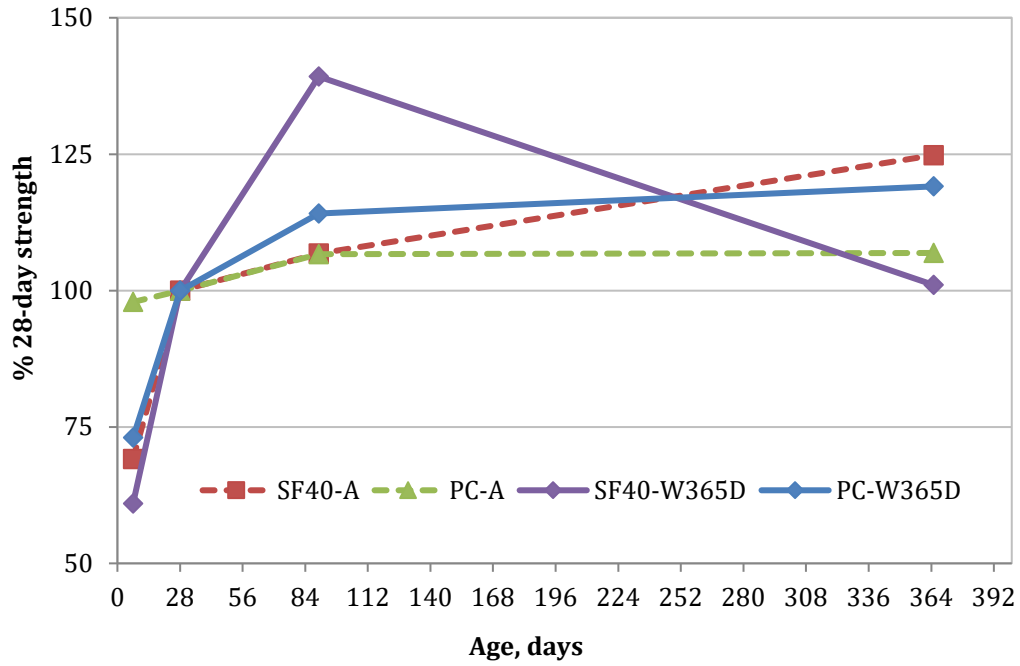

Figure 7.8. %28-day strengths of M-S-H and PC samples (ambient conditions and water curing)

In ambient conditions, the strength development of M-S-H binders was lower than PC samples in the early age up to 7 days however the rates were similar between 28 and 90 days and M-S-H samples particularly increased strengths after 90 days compared to PC control samples (Figure 7.8). The slow rates of strength development were more obvious with samples cured in water in which M-S-H samples developed strengths considerably between 28 and 90 days age which can be attributed to the slow pozzolanic reactions between hydrated magnesia and reactive silica in M-S-H binder systems. The unexpected strength reduction of water cured samples after 90 days has resulted in the 365-day strength similar to that at 28 days age.

7.3.5. Effect of silica sources (SF, MS, FA, RHA)

In chapter 6, the compressive strengths of MgO-SiO_2 mixtures with different MgO/SiO_2 ratio were tested to study the potential strength of M-S-H binders. At this stage, the tests were only carried out for samples of 28 days age and only SF was used. For a thorough understanding of the strength development of M-S-H binders, the experimental programme in this chapter includes both early age and long-term strengths of M-S-H samples up to 365 days. Also, comparisons of different silica sources were made possible as four silica sources were used to utilize the local and/or cost-effective materials.

Figure 7.9 presents the strengths of M-S-H mortar samples prepared with MgO and silica fume. The M/SF ratios and curing duration have a strong effect on the strength development of the samples. Surprisingly, the 40/60 M/SF had the lowest strength among the M/SF samples despite

having the highest proportion of M-S-H gel. SF60 samples have the lowest strengths at 7 days (21.25 MPa), 28 days (28.27 MPa), and 90 days (52.34 MPa). In contrast, SF40 samples obtain the highest strengths at these ages. The 90-day strength of SF40 samples was over 60 MPa, indicating a sufficient strength for a wide range of structural applications. However, all the samples present some degree of strength reduction in the long-term to under 50 MPa at 365 days age.

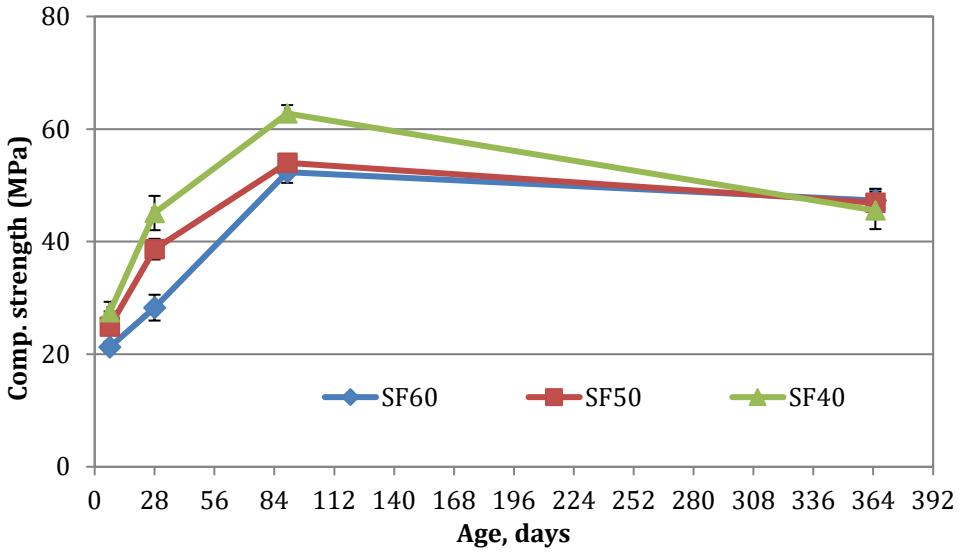

Figure 7.9. Compressive strength of M-SF mixtures (w/c=0.40)

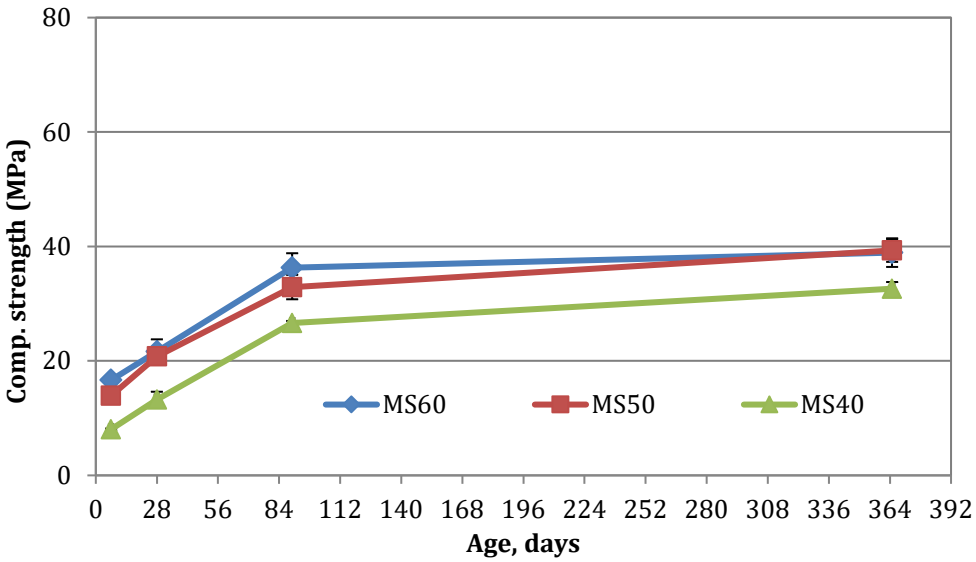

Figure 7.10. Compressive strength of M-MS mixtures (w/c=0.40)

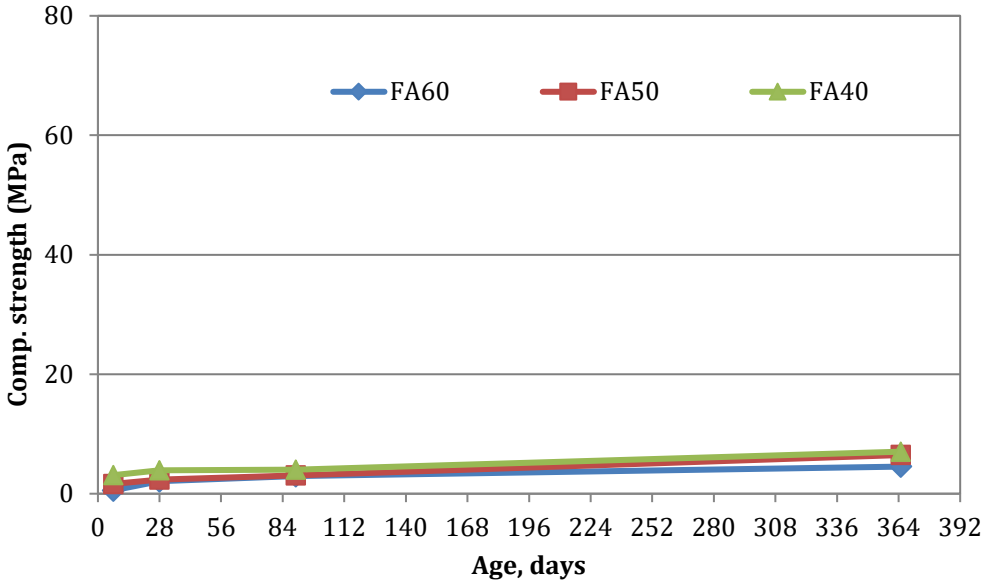

Figure 7.11. Compressive strength of M-FA mixtures (w/c=0.40)

The strength development of M-MS mixtures is presented in Figure 7.10. Mortar samples were prepared at w/b=0.40 for comparison with M-SF mixtures. It was found that the materials with different reactivity and morphology have strong effects on strengths of the resulting mortars. SF40 samples had the highest strengths of over 45 MPa at 28 days age and increased to over 62 MPa at 90 days age while M-MS mixtures resulted in far less compressive strengths. The M-MS mixtures containing 40%MgO-60%MS achieved the highest strength for that series and exhibited a linear strength increase from 17 MPa (7 days) to 22 MPa (28 days) and 36 MPa (90 days) followed by a slow increase to approximately 40 MPa at 365 days.

It was found that the replacement of silica fume by fly ash in M-S-H mortars did not produce strengths comparable to the silica fume, possibly due to the effect of material's reactivity, the presence of impurities and less homogenous structure of the resulting mortars. Similar results were observed in another study on the combination of MgO with pulverized fuel ash (Zhang et al., 2016). The pore solution analysis in chapter 5 has revealed that the M-FA mixtures have higher pHs compared to using other silica. Therefore, the presence of CaO significantly increased Si concentrations however limited the dissolution of MgO. Also, there is a possibility that FA may react with calcium hydroxide to form C-S-H along with the formation of M-S-H. However, the formation of C-S-H in M-FA mixtures was very limited, which is indicated by the very low compressive strength range varying only from 1 to 7 MPa during 365 days age. In addition, the formation of C-S-H was not shown obviously in SEM images and XRD results (presented in Chapter 4). The strength of M-S-H-based cementitious materials therefore greatly vary based on the sources of amorphous silica. The variation in material properties may lead to a wide range of

strength results reported in the literature (Wei et al., 2006; Walling et al., 2015; Tran and Scott, 2017).

Figure 7.12 and 7.13 show strengths of M-MS and M-RHA mixtures at a higher w/b=0.50. The w/b was increased for the workability of M-RHA mixtures due to the porous structure and high water demand of RHA. The mortar samples using RHA obtained higher strengths than M-MS samples at 7 and 28 days age however achieved similar strengths at longer curing durations up to 90 days and 365 days. Another study (Sonat and Unluer, 2019) also reported that amorphous RHA was able to replace silica fume in M-S-H cement but also bring in environmental and economic benefit.

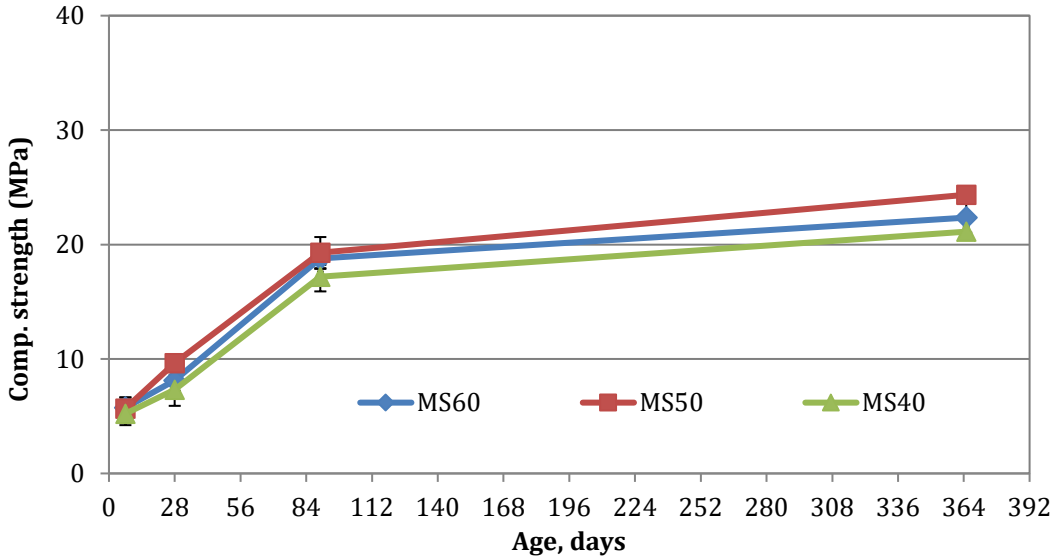

Figure 7.12. Compressive strength of M-MS mixtures (w/c=0.50)

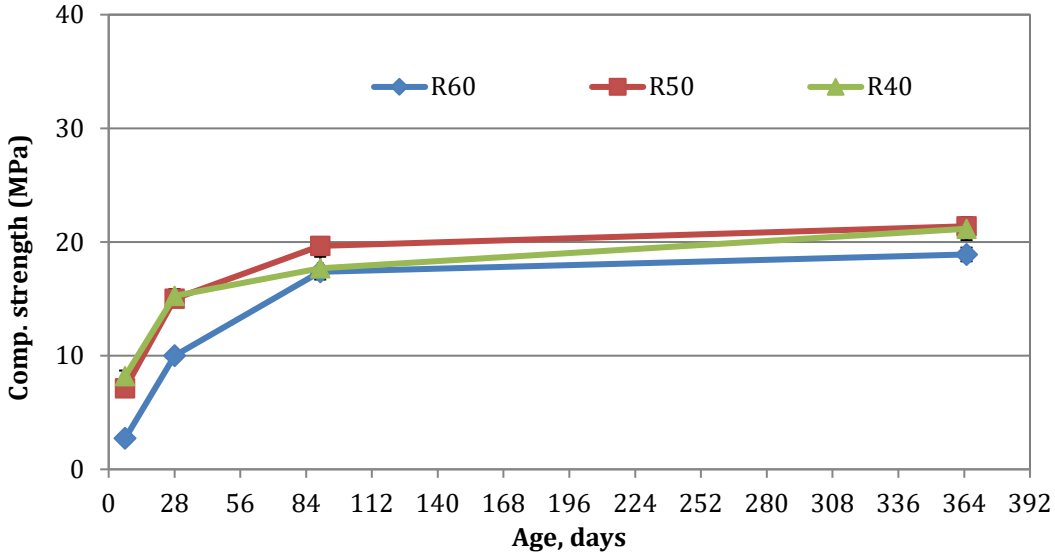

Figure 7.13. Compressive strength of M-RHA mixtures (w/c=0.50)

The strengths of M-S-H binders are shown to be strongly influenced by the w/b ratio. The increase of w/b ratio significantly reduces compressive strengths and vice versa. M-MS samples with w/b ratio of 0.40 achieved the highest strength of 39.3 MPa (Figure 7.10) however decreased considerably (by 38%) as only obtained the highest strength of 24.4 MPa as w/b increased to 0.50 (Figure 7.12). Similar effects of w/b ratio were discussed in chapter 6 where the decrease of w/b ratio resulted in the strength of approximately 90 MPa for the optimal M-SF mixture. M-S-H binders show the same trend as PC where the reduction of w/b ratio is crucial to improve compressive strengths of the cementitious materials.

The strength results have shown the effect of silica sources on the strengths of M-S-H mortars. SF, which has the highest reactivity resulted from a high content of amorphous silica and microfine particle size, is advantageous to react with MgO forming M-S-H gel to gain the highest strengths. On the other hand, FA has the least reactivity due to its low amorphous silica content and coarse particle size which consequently results in low strengths. It was found that the highly reactive silica reacts with hydrated MgO faster than less reactive silica and forms higher quantities of M-S-H gel to gain higher strengths. Such high dependence of strengths on silica sources indicates that the M-S-H gel is the main binding phase to contribute to strengths of the M-S-H binders other than hydrated MgO. The pure reactive MgO samples prepared as control samples showed the very low strength of brucite as a hydration product (Figure 7.7).

The optimal binder composition for compressive strength is also dependent on material sources. The MgO/SiO_2 ratio between 40/60 to 60/40 by mass has a strong effect on the strength development of M-S-H mortar samples. For M-SF mixtures, the low SF content of 40% is optimal for strength as discussed in details in Chapter 6. However, higher silica content up to 50 and 60% results in higher strengths for M-MS and M-RHA mixtures.

It is understood that the strength of the paste is attributed to the strength of the binding phases and the packing density of the mixture. The MS and RHA have coarse particle sizes than SF (as discussed in chapter 3) which may not lead to significant changes in the packing density as the MS/RHA content varies in between 40-60% of the mixtures. Hence, the compressive strengths of M-MS or M-RHA mixtures are mainly controlled by the hydration products.

The compressive strengths obtained with M-MS and M-RHA mixtures were also agreed with the microstructure and pore solutions analysis. In chapter 5, the pore solution analysis showed that the high content of silica reduced the pH of the pore solutions and increased the dissolution of MgO and silica which facilitate the formation of M-S-H phases. XRD results discussed in chapter 4 also confirmed the optimal MgO/SiO_2 ratio for the formation of M-S-H binding phases is 40/60

and therefore high silica content results in higher amounts of M-S-H phases in M-MS and M-RHA mixtures.

7.3.6. **SEM analysis**

Although a comprehensive study of the microstructures of M-S-H binders was provided in Chapter 4, the compressive strength test results have not been included. Therefore, this chapter presents SEM images of M-S-H binders at 28 days age to discuss the relationship between the microstructures and strengths of the mortar samples. The SEM analysis also addresses the microstructure of control samples using PC, which is not mentioned in previous chapters.

Figure 7.14 shows a PC sample having a homogeneous microstructure with micro-pores well distributed on the fracture surface. In contrast, the MgO sample without silica showed a highly porous structure of a rough surface with large pores between brucite particles (Figure 7.15). The heterogeneity of brucite's porous structure decreased while 40% of MgO was replaced with SF (M-SF mixtures in Figure 7.16). The microfine SF particles were well-dispersed and filled in the pores between MgO particles resulting in a denser microstructure with M-S-H formed on the surface of the brucite particles. The formation of M-S-H and the improvement of the microstructure are ascribed to the strength increase of the paste samples using silica fume.

The formation of M-S-H was also observed with mixtures using other silica sources such as MS and RHA (Figure 7.17 and Figure 7.18). However, microstructures of those M-MS and M-RHA mixtures were not significantly improved compared to 100% MgO sample as large pores still present in the pastes resulted in lower strengths than M-SF samples. One of the main factors is MS and RHA have coarser particle sizes which did not fill the pores between brucite particles to result in dense structures as seen with SF.

Figure 7.19 shows a rough surface of M-FA mixtures with a porous microstructure. There were very limited M-S-H phases formed in the mixture due to the low reactivity of FA compared to other silica (SF, MS, RHA). A remarkable amount of sphere fly ash particles representing unreacted fly ash was observed at 28 days age. The FA resulted in large pore sizes in microstructures of M-FA pastes compared to M-SF and PC control samples. The lowest strengths of M-FA samples as shown above can be attributed to the low reactivity of fly ash and the porous microstructure of the mixtures. Microstructure and mechanical properties of M-S-H cementitious materials therefore are highly dependent on the silica sources whose reactivity and particle size are of utmost importance to form M-S-H binding phases and dense paste structures.

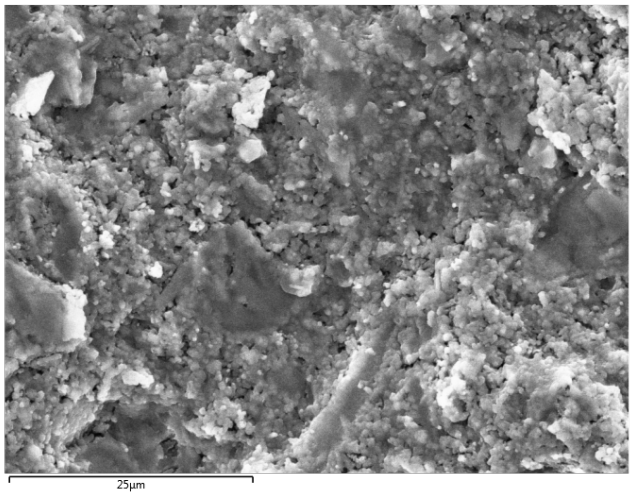

Figure 7.14. SEM image of PC paste sample (28 days age)

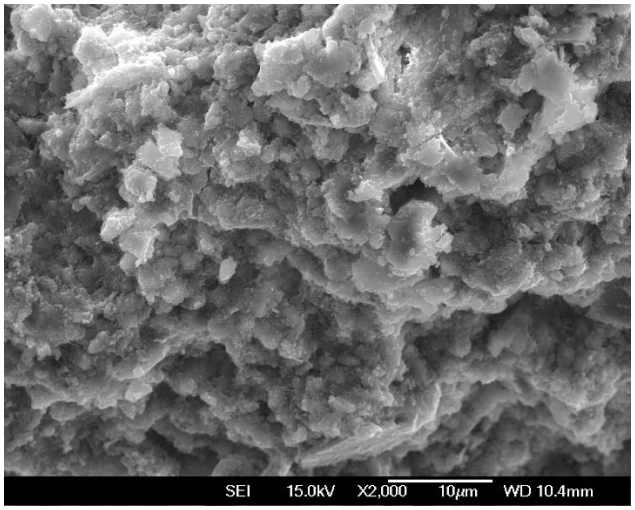

Figure 7.15. SEM image of 100% MgO paste sample (28 days age)

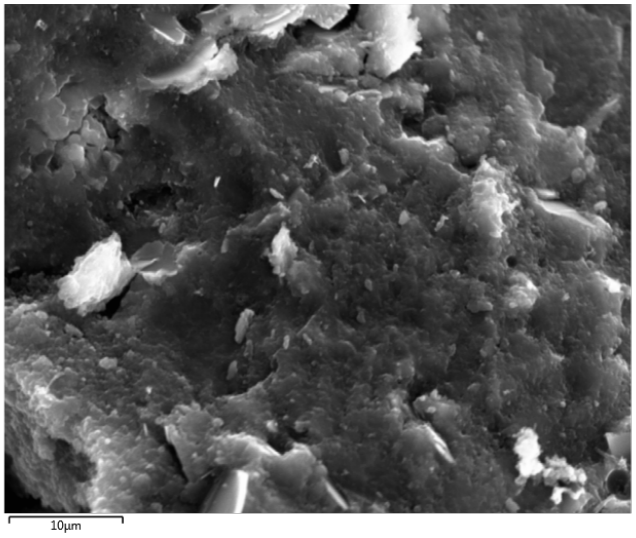

Figure 7.16. SEM image of M-SF paste sample (28 days age)

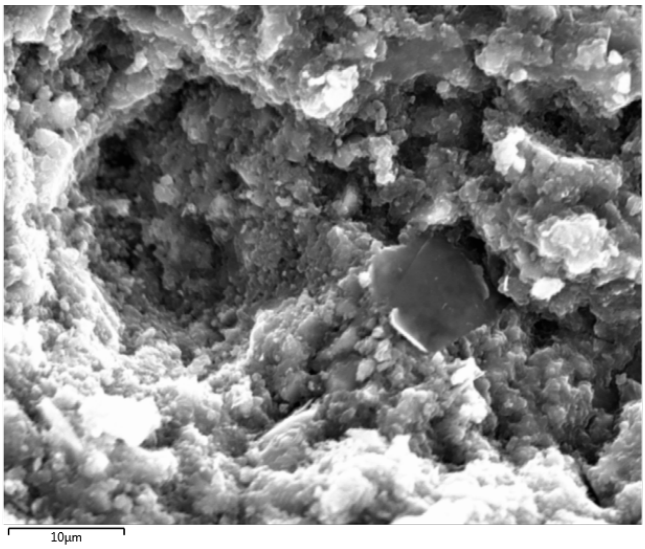

Figure 7.17. SEM image of M-MS paste sample (28 days age)

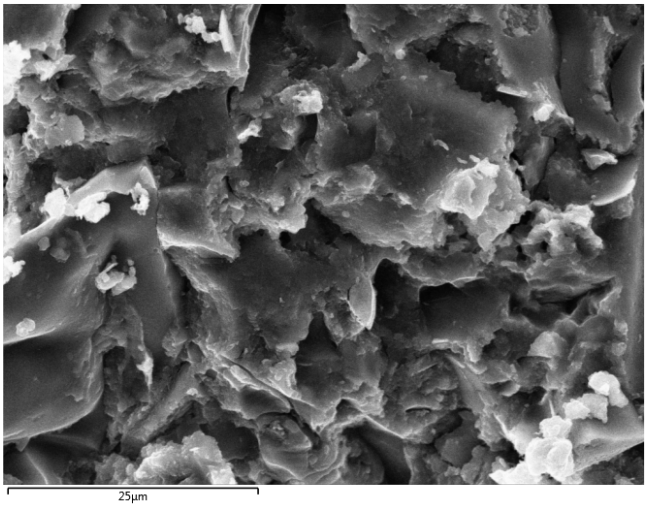

Figure 7.18. SEM image of M-RHA paste sample (28 days age)

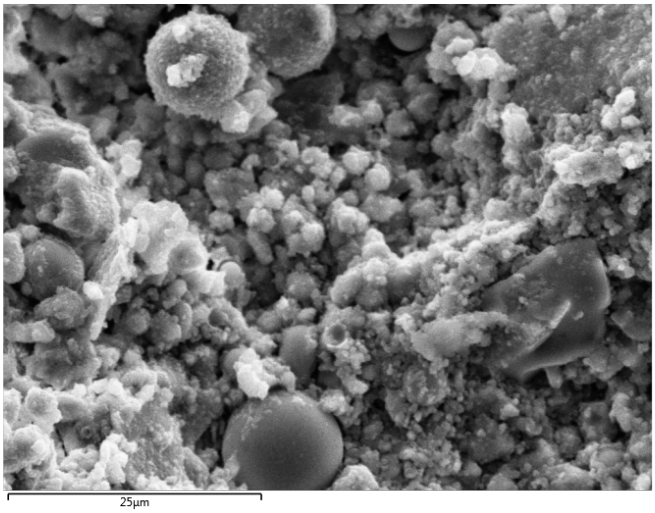

Figure 7.19. SEM image of M-FA paste sample (28 days age)

7.4. CONCLUSIONS

Based on the selected materials and experimental results in this study, the following conclusions can be derived:

Ambient conditions or short-term water curing up to 7 days increased the 28-day strength for M-S-H binders due to the presence of brucite and M-S-H, however, there was a reduction in long-term strength at 90 days due to insufficient water for the completion of the hydration processes. Water curing for longer durations from 28 to 90 days is crucial to facilitate the formation of M-S-H binding phases and increase 90-day strengths. The slow strength development resulted from slow pozzolanic reactions between MgO and silica to form M-S-H gel.

The effects of long-term water curing up to 365 days are not consistent for M-S-H binders using different silica. It is unusual that this curing regime reduced 365-day strength of M-SF mixtures, however, mixtures using MS and RHA still developed strengths over the period.

Heated treatment for M-S-H samples increased early strength but decreased long-term strength during 365 days curing. Higher temperature curing resulted in higher early strength but also reduced long-term strength to a greater extent.

Water curing at elevated temperature (60^{o}C) for 1 and 3 days improved 7-day and 28-day strengths significantly compared to ambient conditions and water curing at 20^{o}C, however, the effect was not obvious at the later stages of 90 and 365 days.

Strengths of M-S-H mortar samples cured in water were lower than those of PC control samples. Nonetheless, the M-S-H binder (60% MgO-40% SF) resulted in higher 28-day and 90-day strengths than PC for mortars with ambient curing conditions.

The silica sources significantly affect the strength and microstructure of M-S-H cementitious materials as a result of the variation of reactivity, morphology and fineness. The high reactivity and fineness of silica such as silica fume resulted in higher strengths and denser microstructure, which was opposed to the lower strengths and porous paste structures of other silica having coarse particle sizes and less reactivity such as FA. The M-S-H gel is the main binding phase to gain strengths other than hydrated MgO in MgO-silica mixtures.

Similar to PC, water content significantly affects the compressive strengths of M-S-H binders in which a reduction of w/b ratio is crucial to improving strengths. Workable mortar mixtůres of M-S-H binders with w/b of 0.40 was achieved using polymer-based superplasticizers. Water curing for 28 days is effective for M-S-H binders resulting in compressive strengths over 70 MPa.

7.5. REFERENCES

Brew DRM. and Glasser FP. (1995) Synthesis and characterisation of magnesium silicate hydrate gels. Cement and concrete research 35(1): 85-98.

Chandra S. (1996). Waste materials used in concrete manufacturing. Elsevier.

Gartner EM. (2011) Potential improvements in cement sustainability. In 31st Cement and Concrete Science Conference Novel Developments and Innovation in Cementitious Materials, 12–13 September, Imperial College London, United Kingdom.

Harrison J. (2007) Sustainability for the cement and concrete industry. Part 2, ZKG International, Knowledge 60 (2): 1-6.

Jin F. and Al-Tabbaa A. (2014) Strength and hydration products of reactive MgO–silica pastes. Cement & Concrete Composites 52: 27–33.

Grist E. R., Paine K. A., Heath A., Norman J., & Pinder H. (2013). Compressive strength development of binary and ternary lime–pozzolan mortars. Materials & Design (1980-2015), 52, 514-523.

Kalousek GL. and Mui D. (1954) Studies on Formation and Recrystallization of Intermediate Reaction Products in the System Magnesia-Silica-Water. Journal of the American Ceramic Society 37(2): 38-42.

Li Z., Zhang T., Hu J., Tang Y. et al. (2014) Characterization of reaction products and reaction process of MgO–SiO2–H2O system at room temperature. Construction and Building Materials 61: 252-259.

Mitsuda T. and Taguchi H. (1977) Formation of magnesium silicate hydrate and its crystallization to talc. Cement and Concrete Research 7: 223-230.

Nied D., Enemark-Rasmussen K., L'Hopital E., Skibsted J., Lothenbach B. (2016) Properties of magnesium silicate hydrates (M-S-H). Cement and Concrete Research 31(79): 323-332.

Richardson IG. (1999) The nature of C-S-H in hardened cements. Cement and Concrete Research 29: 1131-1147.

Sonat C., Dung N., Unluer C. (2017) Performance and microstructural development of MgO–SiO_2 binders under different curing conditions, Constr. Build. Mater. 154 (2017): 945-955.

Sonat C. and Unluer C. (2019). Development of magnesium-silicate-hydrate (M-S-H) cement with rice husk ash. Journal of Cleaner Production 211: p787-803.

Taylor HFW. (1997) Cement chemistry. Thomas Telford, London, UK.

Thomas JJ., Musso S., Prestini I. (2014) Kinetics and activation energy of magnesium oxide hydration. Journal of the American Ceramic Society 97(1): 275-282.

Tran HM., Scott A. (2017) Strength and workability of magnesium silicate hydrate binder systems. Construction and Building Materials 131: 526-535.

Walling SA., Kinoshita H., Bernal SA., Collier NC., Provis JL. (2015) Structure and properties of binder gels formed in the system $Mg(OH)_2$–SiO_2–H_2O for immobilisation of Magnox sludge. Dalton Transactions 44 (17): 8126-8137.

Wei JX., Chen YM., Li YX. (2006). The Reaction Mechanism between MgO and Microsilica at Room Temperature. Journal of Wuhan University of Technology - Mater. Sci. Ed. 21: 88-91.

Zhang T., Cheeseman C., Vandeperre L. (2009) Development of novel low pH cement systems for encapsulation of wastes containing aluminium. Decommissioning, Immobilisation and Management of Nuclear Waste for Disposal 2009; York, UK.

Zhang T., Vandeperre L., Cheeseman C. (2014) Formation of magnesium silicate hydrate (M-S-H) cement pastes using sodium hexametaphosphate. Cement and Concrete Research 65: 8–14.

Zhang T., Du Y.N., Sun Y.J., He Z.M., Wu Z.L. (2016). Development of magnesium-silicate-hydrate cement by pulverized fuel ash. Key Eng. Mater., Trans Tech Publ 709: 61-65.

CHAPTER 8
MECHANICAL AND DURABILITY PROPERTIES OF CONCRETE WITH MAGNESIUM SILICATE HYDRATE BINDER SYSTEMS

Tran, H.M., Scott, A., Dhakal, R.P. (2017). Mechanical and durability properties of a concrete using magnesium silicate hydrate binder system. *Proceedings of the Concrete 2017, the 28th Biennial National Conference of the Concrete Institute of Australia, held in conjunction with the 3rd International Congress on Durability of Concrete (ICDC), Adelaide, Australia, 22 October to 25 October 2017.*

Tran H, Scott A and Dhakal R (2019). Mechanical and durability properties of magnesium silicate hydrate binder concrete. *Magazine of Concrete Research*, https://doi.org/10.1680/jmacr.18.00217

Preamble

Based on the findings of previous chapters, M-S-H binder is able to develop the required strength and obtain adequate workability for a wide range of applications including building and civil structures. Chapter 4-5 have confirmed the formation of binding phases based on the examination of microstructures and pore solution analysis using XRD, SEM/EDS, and ICP-MS methods. Chapter 6-7 have shown the ability of M-S-H binder to produce normal to high strength cement pastes and mortars. Such promising properties have suggested the potential for M-S-H binders to produce normal to high strength and durable concrete which can complement or even replace PC as a construction material. However, most of the previous studies on M-S-H binder systems were performed with cement pastes and mortars and such studies on the mechanical and durability properties of M-S-H concrete appear not to be available in the literature. In addition, there are still concerns about other engineering properties such as tensile strength and modulus of elasticity of the M-S-H binder.

To provide a better understanding of the mechanical and durability properties of M-S-H binder concrete, this chapter presents the testing of concrete using M-S-H binders with and without crushed fillers based on the earlier work in chapter 6. The experimental work was among the first studies on the mechanical properties and durability of concrete using M-S-H binder systems. Mechanical properties including compressive strength, tensile strength, and modulus of elasticity were tested and durability indexes such as oxygen permeability, porosity and resistivity were discussed.

Abstract

Mechanical and durability properties of concrete made with magnesium silicate hydrate (M-S-H) binder systems were tested in comparison with Portland cement. The M-S-H binary binder system included 60% MgO and 40% SiO_2 while the ternary system replaced 10% of the M-S-H binder with 10% crushed quartz filler. It was found that the 28 day compressive strength of M-S-H concrete samples, produced at a water/cement ratio of 0.4, was approximately 40 MPa with little further increase after this age. The M-S-H concrete had lower tensile strengths and modulus of elasticity than PC control samples. The stress strain relationship of the M-S-H concrete showed an unusual non-linear relationship at a loading range up to 40% of the compressive strength. The porosity and permeability of concrete using M-S-H binders were higher than PC. The addition of crushed quartz filler was shown to improve microstructure, mechanical and durability properties of M-S-H binder concrete for potential structural applications.

8.1. INTRODUCTION

Research on alternative binder systems for Portland cement (PC) has increased considerably due to the urgent need to reduce the negative impacts of CO_2 emissions on the environment. The synthesis M-S-H binder systems are known to be less energy intensive than PC production process, due to the use of reactive magnesium oxide calcined at low temperatures (700-1000^{o}C) and the high proportion of silica, including industrial by products or waste materials such as silica fume, fly ash, rice husk or natural pozzolan. Other alternatives to develop a carbon neutral or negative magnesium-based binder materials are under investigation. One process involves CO_2 sequestration by magnesium-rich minerals olivine and serpentine to form magnesium carbonates which are then decarbonated to produce reactive magnesium hydroxide (Pacheco-Torgal, 2014). There are also potential benefits of using M-S-H binders for the immobilization of nuclear wastes (Zhang et al., 2012; Walling et al., 2015).

The mechanical properties of M-S-H pastes and mortars have been reported in the literature with a wide range of strength values. Wei et al. (2006) were among the first authors reporting cementitious property of M-S-H mortars of over 50 MPa. Zhang et al. (2014) developed M-S-H binder systems for immobilization of nuclear wastes obtaining strengths of over 60 MPa. Marmol et al. (2016) studied M-S-H and Portland cement pastes in which M-S-H samples achieved superior strength compared to PC samples at a similar water to cement ratio. Tran and Scott (2017) optimized ternary mortar mixtures of MgO-SiO_2-quartz filler resulting in strengths exceeding 85 MPa. On the other hand, Jin and Al-Tabbaa (2014) and Walling et al. (2015) reported fairly low strengths of M-S-H binder systems due to the very high water content for workability. Material source was reported to be one of the major causes for these strength variations of M-S-H binders (Jin et al., 2013). By using a combination of CFB slag, reactive MgO and silica fume Chen et al. 2017 where able to produce pastes with a 28 day compressive strength in excess of 105 MPa at a w/c ratio of 0.2.

The reaction mechanism of MgO-SiO_2 mixtures have been studied in the literature in which MgO/SiO_2 ratio has a large effect on the hydration products. Zhang et al. (2011, 2014) reported that brucite ($Mg(OH)_2$), a reaction product of reactive magnesium oxide and water, will react with silica fume (SF) to form M-S-H gel in mixtures containing 40% MgO and 60% SF. Wei et al. (2006) showed that at higher MgO/SiO_2 ratios, residual brucite and M-S-H phases co-existed in the resulting pastes. The Mg/Si molar ratio was found to be lower than Ca/Si in Portland cement (Lothenbach et al., 2015) and varied in a range of 0.7-1.5 (Nied et al., 2016).

Research significance

Previous studies have focused on the compressive strength and microstructure of cement paste and mortar samples, but few experiments have been carried out to examine the mechanical properties and potential durability of M-S-H binder based concrete. This work represents a preliminary investigation on the possibility of producing a strong and durable M-S-H concrete which is comparable with conventional PC concrete. The experimental study will practically contribute to the understanding of the magnesium silicate hydrate binder system by using commonly available industrial materials to examine fundamental structural properties including: compressive strength, split tensile strength and modulus of elasticity, in addition to the durability properties of porosity and oxygen permeability. As the materials are already produced on a large scale they have the potential for commercial application provided sufficient physical and durability properties can be achieved. The results from this investigation will provide direction for future studies to improve the quality of M-S-H concrete and its use as a viable sustainable construction material.

8.2. EXPERIMENTAL PROGRAMME

8.2.1. Materials

Reactive magnesium oxide, calcined at temperatures of below 700^{o}C, was supplied by Calix Ltd. (Australia). Silica fume, a highly reactive silica source, was provided by Sika NZ in condensed form. Quartz filler (QF) was ground from local quartz sand in a ring mill for 2 minutes to obtain the desired particle size. Aggregates including river sand (max particle size of 4.75 mm) and stone (max aggregate size of 16 mm) were sourced from locally. Control Portland cement samples were produced using a general purpose cement provided by Holcim New Zealand.

Particle size distributions are shown in Figure 8.1. The chemical compositions of the binders are presented in Chapter 3.

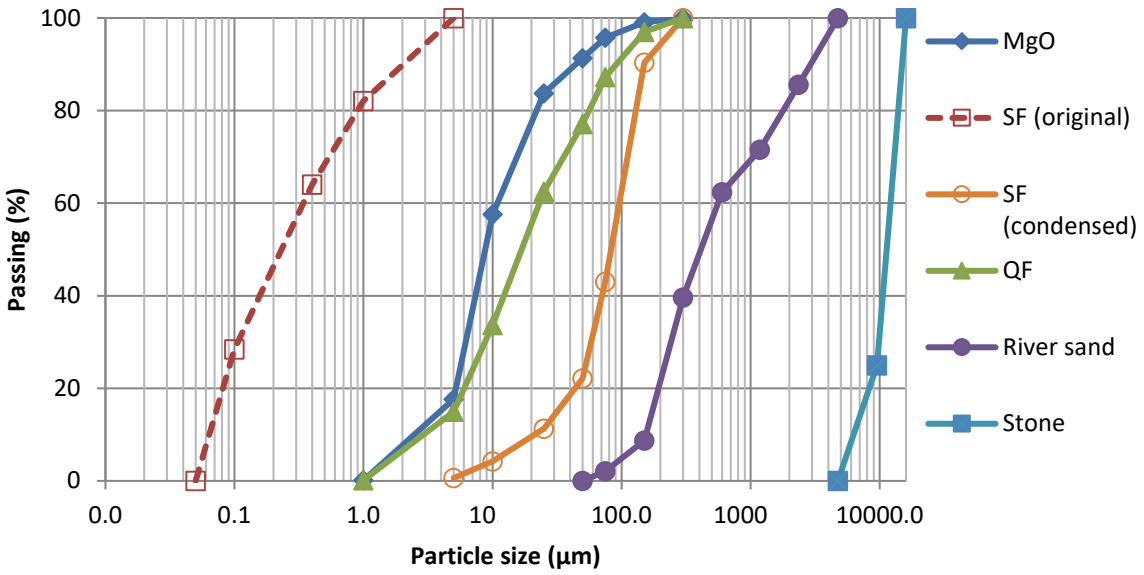

Figure 8.1. Particle size distribution of materials

8.2.2. **Mix proportions**

Concrete samples were prepared for mechanical and durability tests while paste samples were prepared for microstructure analysis. Sample labels and mix proportions are presented in Table 8.1. The MgO/SiO_2 ratio of 60/40 (by mass) was selected based on the optimal strength performance of the pastes compared to other binder compositions (Tran and Scott, 2017). Based on earlier work in chapter 6, quartz filler was introduced at 10% M-S-H binder replacement to test the effects of inert fillers on the mechanical and durability properties of the resulting cementitious materials. As the quartz filler is intentionally included in the w/c, it is expected that the quartz filler can improve the workability and microstructure of the M-S-H binder concrete. The sand and stone contents for M-S-H and control PC concrete were specified based on typical PC concrete mixes.

Due to the high volumes of silica fume, a superplasticizer (Sika ViscoCrete-5-555 (NZ)) was used to ensure adequate workability. The superplasticizer dosage and w/c ratio were selected based on pervious work by Tran and Scott (2017) (Chapter 6) which describes the fresh properties of various MgO-silica mixes. The target flow for M-S-H paste mixtures was approximately 160 mm ± 10 mm, using a cone with dimensions: 50 mm in height, 70 mm internal top diameter, 100 mm internal base diameter. While no quantitative data is available, the different concrete mixes were observed to achieve adequate workability with the selected superplasticizer dosage and w/c ratio.

Table 8.1. Relative mix proportions of pastes and concrete mixes (by mass)

Mix label	PC	MgO	Silica fume	Quartz filler	Sand	Stone	w/c ratio	SP (% of binder, liquid)
SF40 (paste)	-	0.60	0.40	-	-	-	0.40	3%
Q10 (paste)	-	0.54	0.36	0.10	-	-	0.40	3%
PC (paste)	1.0	-	-	-	-	-	0.40	-
SF40	-	0.60	0.40	-	1.25	2.0	0.40	3%
Q10	-	0.54	0.36	0.10	1.25	2.0	0.40	3%
PC	1.0	-	-	-	1.25	2.0	0.40	-

8.3. EXPERIMENTAL METHODS

8.3.1. Fresh and mechanical properties testing

As flow tests were carried out showing adequate workability of M-S-H cement paste and mortar, no slump test result was reported in this chapter. However, it is understood that some slump tests have been conducted with some trial mixes and the observation of mixing, moulding and compacting processes has shown the adequate workability of the produced M-S-H binder concrete. Also, it is suggested that future studies of M-S-H binder concrete should report and discuss slump test results to compare the workability of concrete produced with M-S-H and other binders.

Concrete cylinders sized 100 mm diameter × 200 mm height were cast for compressive strength, split tensile strength, modulus of elasticity testing and durability property testing. Samples were demolded after 24 h before curing in water at 20°C until tested at 7, 28 and 90 days. Three cylindrical samples were tested to calculate the average value for each reported result.

Compressive strengths were determined as per standard ASTM C39. Split tensile strength tests were performed instead of direct tensile tests following ASTM C496. The static modulus of elasticity (MOE) of the M-S-H and PC concrete specimens was tested in accordance with ASTM C469.

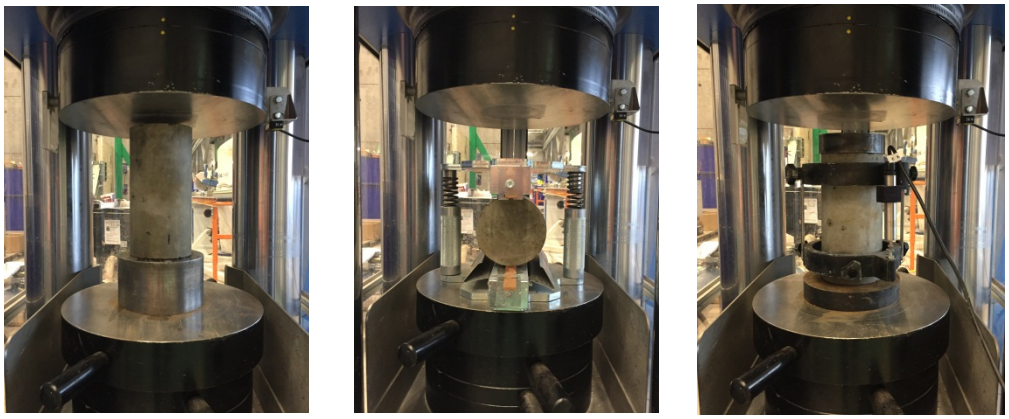

(a) (b) (c)

Figure 8.2. Mechanical testing setup

(a): Compressive strength, (b): Split tensile strength, (c): Modulus of elasticity

8.3.2. **Durability properties testing**

8.3.2.1. Porosity

The porosity presented as the percent of voids in hardened cementitious materials was determined based on ASTM C642 but using a vacuum saturation technique. Four testing cylinders were cut from 100 × 200 mm concrete cylindrical samples to produce specimens with a thickness of 30 ± 3 mm. The samples were oven dried at 50°C until the change in mass was less than 0.5% over 24 hours. The samples were placed under vacuum for 3 hours before water was introduced and a vacuum applied for an addition hour after which the chamber was open to the atmosphere and samples allowed to soak for a further 18 hours. The porosity was calculated from the formula of volume of permeable pore space voids:

$$P(\%) = (C - A)/(C - D) \times 100$$

where:

A = oven-dried mass in air, g

C = surface-dried mass in air after vacuumed and immersed in water, g

D = apparent mass in water after vacuumed and immersed in water, g

8.3.2.2. Oxygen Permeability Index

The Oxygen Permeability Test was performed to determine gas permeability coefficient of the concrete, which are related to the concrete durability. The applied testing procedure was introduced by Alexander et al. (1999). A falling head permeameter was used to apply pressure to a concrete sample whereby the pressure was allowed to decay as permeation proceeds. A rapid reduction in the pressure indicates a high permeability to gas (oxygen) and possibly a reduction in the durability of the concrete (Alexander et al., 1999).

Four cylinders of 30 ± 3 mm thick were cut from 100 × 200 mm concrete cylinders. The samples were preconditioned by oven drying at 50°C for at least 7 days until the change in mass was less than 0.5% over 24 hours, due to the sensitivity of gas transport to the moisture content of concrete. Each sample was inserted into a rubber collar, and compressed in the test rig to provide a seal around the samples. An initial pressure was set at 100 kPa and the test was terminated as the pressure reduced to 50 kPa or after 6 hours.

The calculation of the OPI required determining pressure decay curve which was plotted in the form of the logarithm of the ratio of pressure heads over the time, based on the D'arcy coefficient of permeability:

$$k = \frac{\varpi V g d}{R A \theta} \ln \frac{P_0}{P}$$

where:

k = coefficient of permeability of test specimen (m/s)

ω = molecular mass of oxygen = 32 g/mol

V = volume of oxygen under pressure in permeameter (m^3)

g = acceleration due to gravity (9.81 m/s^2)

R = universal gas constant = (8.313 Nm/K mol)

d = average specimen thickness (m) to the nearest 0.02 mm

A is the cross sectional area of the specimen (m^2)

θ= absolute temperature (K)

The OPI was taken as the negative log of the average of the 4 samples' coefficients of permeability (k_1, k_2, k_3, k_4), which was determined by the equation:

$$OPI = -\log 10\left[\tfrac{1}{4}(k_1 + k_2 + k_3 + k_4)\right]$$

Figure 8.3. Permeability cell arrangement

8.3.2.3. Resistivity Test

Resistivity test provides a rapid indication of the penetration of chloride ions and the likely resistance of concrete to the corrosion. This test is faster to run compared to the Rapid Chloride Ion Permeation Test (RCPT) as specified in ASTM C1202 however it also presents high correlation with RCPT

(Gudimettla and Crawford, 2015). Resistivity test is used to evaluate the electrical resistivity of M-S-H samples from the early age of 7 days to a long-term curing duration up to 90 days.

The resistivity test reused the samples as described in OPI tests. After re-drying to a constant mass the samples were vacuum saturated with 3.5% NaCl, the resistivity was measured from the applied voltage and corresponding current across the sample.

8.3.3. XRD and microstructure analysis

The XRD and microstructure analysis was conducted on the paste samples using a scanning electron microscope to investigate the relations of the mechanical and durability properties. Cement pastes were mixed by a Hobart mixer and poured into 50 ml laboratory tubes. Paste tubes were sealed and inserted into a rotating apparatus for 24 h immediately after molding to improve the homogeneity, and then stored in ambient conditions until examined at 28 and 90 days. The paste samples were cut into 10 mm thick slides and carbon coated for SEM analysis using JEOL JSM 7000F scanning electron microscope. The development of hydration products was examined over 90 days period by XRD using a Philips PW1729 X-ray diffractometer (Cu, 50kV/40mA) with a 3 to 70^{o} 2θ scan range.

8.4. RESULTS AND DISCUSSION

8.4.1. Compressive strength

Compressive strengths of M-S-H and PC concrete samples are shown in Figure 8.4. The PC concrete samples generally obtained higher compressive strengths than M-S-H concrete samples. At 7 days, the SF40 and Q10 mixes using M-S-H binders obtained strengths of over 20 MPa while the PC concrete reached over 50 MPa. At the 28 days age, SF40 and Q10 mixes increased strength by 75% and ~ 80% to 40 MPa and 44 MPa whereas PC concrete increased strength to 62 MPa. The M-S-H concrete shows a slower early strength development rate compared to PC possibly due to the slow pozzolanic reactions of brucite and silica fume.

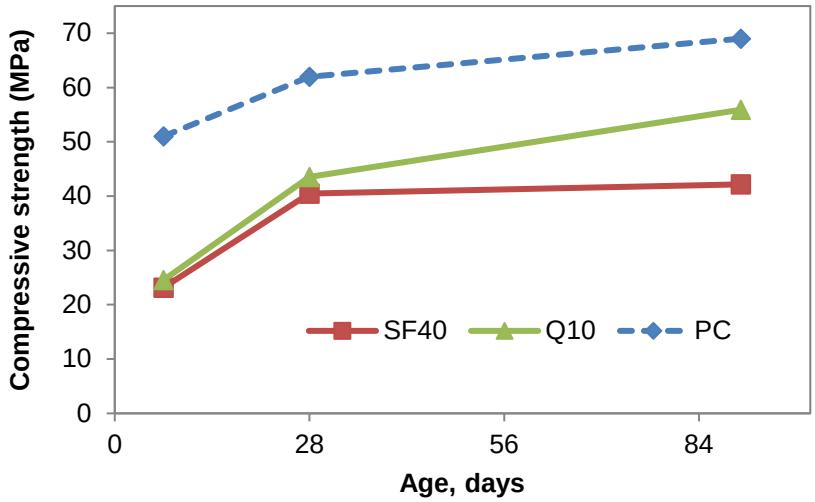

Figure 8.4. Compressive strength of M-S-H and PC concrete

For long-term curing up to 90 days, it was found that the strength of SF40 sample remained stable at over 40 MPa while PC samples still increased strengths to approximately 70 MPa. The 90-day strength of the Q10 samples continued to increase to 56 MPa, which was much higher than that of SF40 samples and close to the compressive strength of PC control samples. The addition of quartz filler considerably increased compressive strengths of the M-S-H binders, particularly in the long-term. The fact that the strength of non-filler M-S-H samples did not increase after 28 days might result from two scenarios (i) the hydration process to form binding phases of M-S-H and brucite completed after this age or (ii) the hydration products are formed continuously however the M-S-H concrete has a weak interfacial transition zones (ITZ) limiting the strength development of the concrete. The latter has been found more likely as the strength of the Q10 samples was found to increase after 28 days and the XRD results (Figure 8.5) also show the continued formation of M-S-H between 28 and 90 days.

The addition of 10% quartz filler, although almost inert at ambient curing temperature, appears to accelerate further the hydration, improve the microstructure and particle packing of the paste hence increases strengths of the resulting cementitious materials. The homogeneity of the paste containing the quartz filler was also observed compared to the samples without filler. The filler particles with its fineness and high surface area possibly act as nucleation sites, thus improving the hydration and distribution of hydration products and results in higher compressive strength.

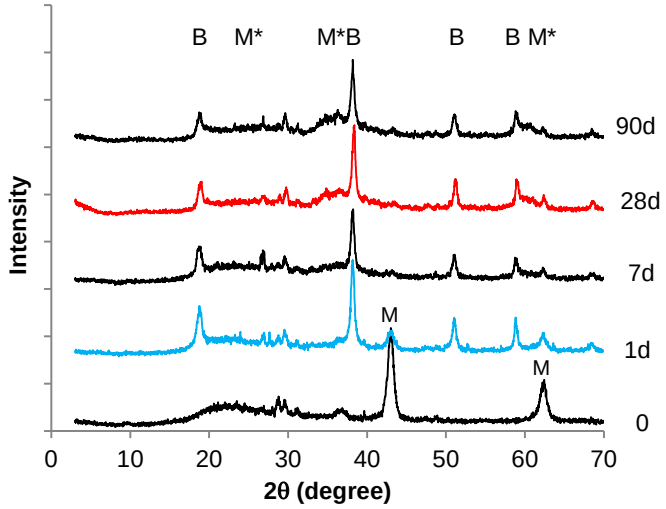

Figure 8.5. XRD spectra of SF40 paste samples over 90 days (B: Brucite, M: MgO, M: M-S-H, Q: quartz)*

8.4.2. **Split tensile strength**

Figure 8.6 presents split tensile strengths of M-S-H and the control PC concrete. The SF40 samples had relatively low split tensile strengths which only increased marginally from 7 to 28 days and remained stable under 2.0 MPa at all curing periods. The split tensile strengths of the Q10 samples benefited from the addition of quartz filler and reached 2.8 MPa at 7 days and rose to approximately 3.5 MPa at 90 days. The quartz filler likely improved the homogeneity and packing density of the microstructure of the Q10 samples which results in higher split tensile strengths than those of non-filler SF40 samples. However, it was obvious that the PC samples achieved considerably higher tensile strengths than the M-S-H concrete in which the 28 and 90 days strengths were almost double the strengths of the Q10 samples.

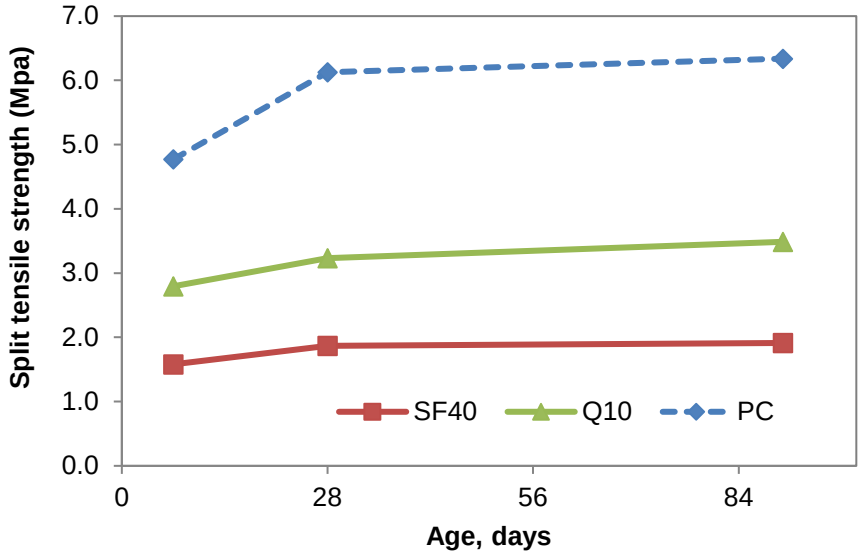

Figure 8.6. Split tensile strength of M-S-H and PC concrete

8.4.3. **Modulus of elasticity**

Figure 8.7 shows the stress-strain relations to determine the modulus of elasticity (MOE) of M-S-H and PC concrete. At loads up to 40% of the compressive strength, the SF40 mixes show unusual highly non-linear strain hardening behaviour compared to either the quartz filler M-S-H or the PC concrete. The behaviour of the SF40 mixes is similar to that observed when timber is loaded in compression perpendicular to the grain (Basta et al. 2012) or in the case of tendons and ligaments under tension where there is un-crimping of the collagen fibrils (Calc et al. 2013). The structure of the paste produced in the SF mixes may be more open and porous compared to the other mixes resulting in a lower initial stress-strain response until the M-S-H sheets have compacted. It should be noted that the reported porosities in this investigation are a bulk measure of the volume of permeable voids and do not account for gel pores which could be substantially higher in the SF mixes compared to the other mixes. Further investigation is needed to confirm the cause of the non-linear stress strain response.

The PC mixes show the expected linear stress-strain responses at loads less than 40% of the ultimate compressive strength. The addition of quartz filler at 10% MgO-SF mixture replacement had a significant effect on the stress-strain behavior of the concrete. The Q10 samples showed a linear stress-strain behaviour similar to that of PC rather than the non-linear stress-strain behavior observed with the SF40 samples.

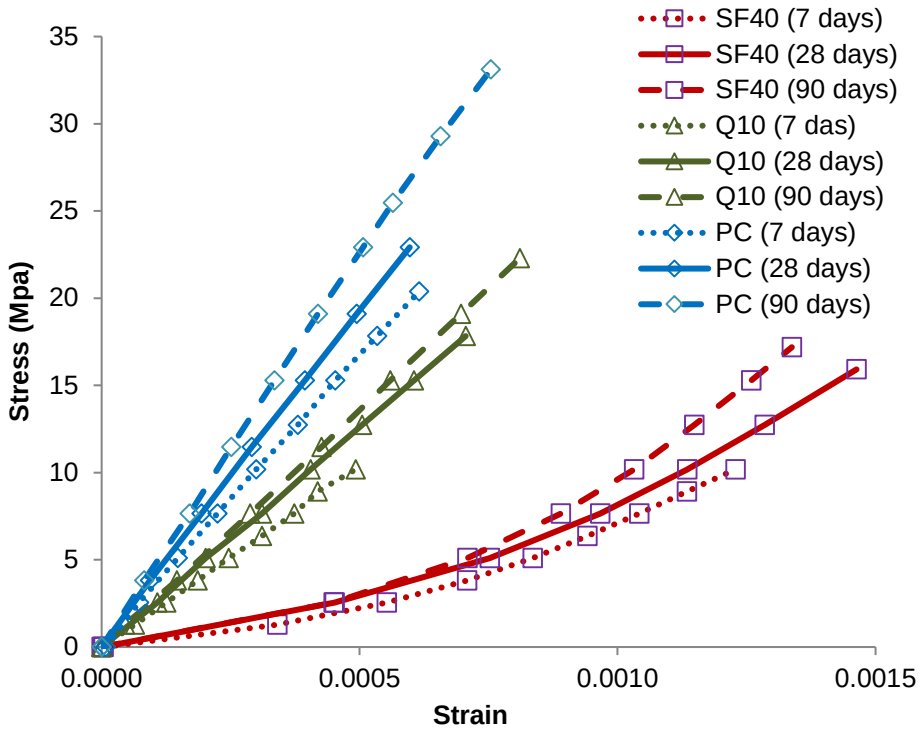

Figure 8.7. MOEs of PC and M-S-H concrete

Table 8.2 presents modulus of elasticity (MOE) of M-S-H and PC concrete. Secant modulus was used to measure MOE of SF40 samples for non-linear stress-strain behaviors in comparison to other samples showing linear stress-strain behaviors (PC and Q10). The SF40 mix had the lowest MOE at all testing ages with the secant modulus values of 8.2, 10.9, and 12.8 GPa respective at 7, 28 and 90 days. The PC concrete exhibited the highest MOE, achieving 33.5, 38.7, 44.7 GPa at the ages of 7, 28 and 90 days (respectively). Although the Q10 samples had a lower MOE than the PC samples, they were found to have much higher MOE (115-150%) compared to SF40 samples, and reaching 20.7 GPa, 25.2 GPa and 27.3 GPa at 7, 28 and 90 days.

The low MOE and rather unusual non-linear stress-strain behavior of M-S-H binder concrete might limit its structural application. However, the addition of quartz filler seems to provide a viable solution to improve MOE and modify stress-strain behaviors for a wider range of structural applications with M-S-H concrete.

Table 8.2. Modulus of elasticity of M-S-H and PC concrete

(Secant) MOEs	7 days (GPa)	28 days (GPa)	90 days (GPa)
PC	33.5	38.7	44.7
SF40	8.2	10.9	12.8
Q10	20.7	25.2	27.3

8.4.4. Durability-related properties

8.4.4.1. Porosity

Figure 8.8 shows the porosities of M-S-H and PC concrete. It was obvious that PC samples had the lowest porosity values < 10% at all curing ages. The substitution of PC by M-S-H binder increased the voids ratio of the concrete mixture whereby SF40 samples had the highest porosities of over 12% at all testing ages. The incorporation of quartz filler reduced porosities of the Q10 samples to around 11%. It was found that the porosities of PC concrete over 90 days curing period decreased while those using M-S-H binders slightly increased over the same period.

The volume change of hydration products in the formation of calcium silicates is among the key factors for the decrease of porosity in PC concrete over the long-term. For M-S-H binders, the hydration of reactive MgO at early ages absorbs free water to form brucite which might cause considerable volume increase (Harison, 2015) and reduces the capillary pores. However, the inclusion of a high content of fine SF particles appears to result in higher porosities of SF40 and Q10 samples at 7 days compared to PC. In the later stages, it was suggested that the chemical reactions of brucite and SF to form M-S-H binding phases did not incorporate additional free water to fill capillary pores (Zhang et al., 2014; Li et al., 2014; Nied et al., 2016) and this might be a reason for the high porosities of M-S-H concrete samples over the long-term.

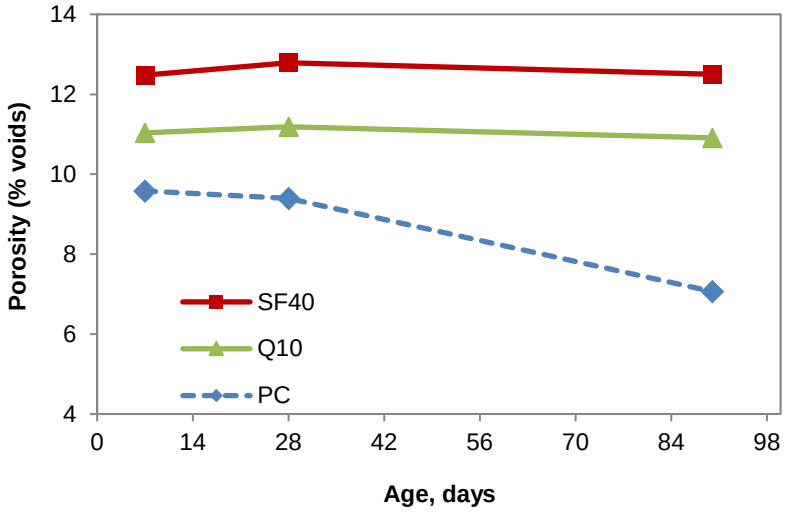

Figure 8.8. Porosity of PC and M-S-H concrete

Porosity has strong relationships with mechanical properties of concrete such that a one percent increase in porosity causes a reduction in concrete strength in the range of 5 - 6% (Massazza, 1996). It is clear that for the PC concrete there is an increase in strength associated with a decrease in porosity. For M-S-H samples, there was relatively little increase in strength over the 90 days associated with a reduction in porosities. The strength developed that did occur during the 90 days was mainly attributed to the reactions between brucite and silica to form the main binding phase M-S-H. The higher porosity partially explains the lower strength and modulus of elasticity of M-S-H compared to PC concrete. The adverse effects of the high porosity were reduced somewhat by the replacement of MgO-SF mixture by quartz filler. The quartz filler increases packing density by improving particle size distribution of the binder.

8.4.4.2. Oxygen Permeability Index (OPI)

The durability transport properties of concrete can be assessed by measuring the resistance of the concrete to the movement of gasses such as oxygen. The empirical studies show a reasonable relation between the carbonation resistance of concrete for instance and the early age (28 days) OPI values, such that the OPI can be used as a durability indicator in a carbonation-type service life models in which high OPI suggests low carbonation depth (EN, 2009). The OPI is related to permeability coefficient by the equation:

$$OPI = -\log 10(k)$$

Concrete typically has an OPI ranging from approximately 8.5–10.5 (equivalent K from approximately 3.2×10^{-9} to 3.2×10^{-11} m/s) (Beushausen and Luco, 2015). Mackechnie and Scott (2012) suggest OPI values above 10.0 indicate low permeability and those less than 8.0 high permeability in concrete. Specification, used by the South African National Roads Agency Limited (SANRAL) provide a lower OPI limit of 9.0 ($k=10x10^{-10}$) for concrete used in potentially aggressive environments for highway bridges (Beushausen and Luco, 2015).

Figure 8.9 presents oxygen permeability coefficients of M-S-H and PC concrete over the 90-day curing period. It was found that both M-S-H and PC concrete samples could be considered to have excellent durability at 7 days with a low coefficient of oxygen permeability. As the hydration process proceeded however, the permeability coefficients at 28 and 90 days for the SF40 and 10% quartz filler mixes increased considerably indicating a more open pore structure for the concrete. The trend of increasing permeability with time for the M-S-H binder systems is very different from what was observed for the traditional PC concrete which showed a decrease in permeability coefficient attributed to a densification of the pore structure. The permeability increase of M-S-H concrete over the 90 days curing period suggests an increasing level of pore connectivity or microcracking associated with the formation of M-S-H binding phases. It is possible that the consumption of brucite and silica to form M-S-H overtime reduced the total volume of hydration products despite the on-going hydration. Further investigation is necessary to determine the true cause of the increase in permeability and the long-term implications on the durability of the M-S-H binder system.

The incorporation of 10% quartz filler however was able to limit the increase in permeability $k = 10 \times 10^{-10}$ (m/s) for the Q10 samples compared to SF40 samples without quartz filler. The M-S-H concrete is therefore predicted to be more permeable and potentially less durable than PC concrete due to the more open pore structure.

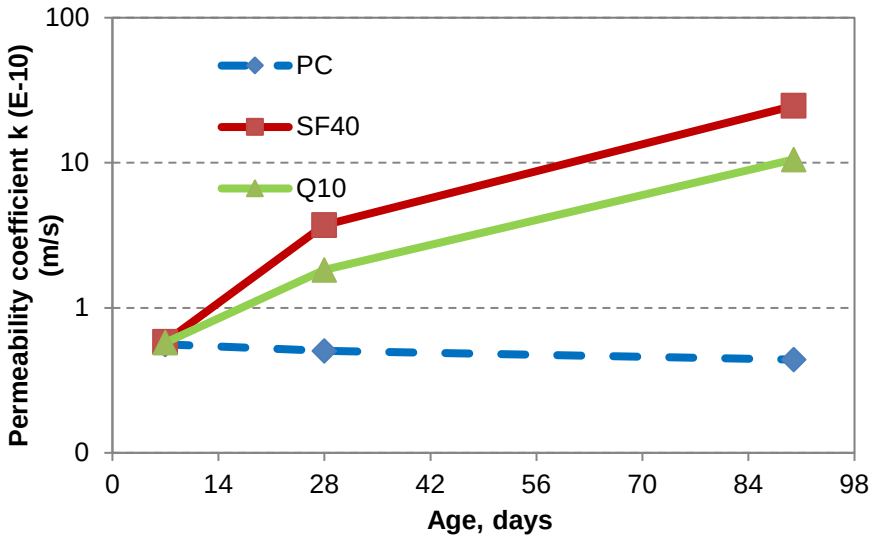

Figure 8.9. Permeability coefficient of M-S-H and PC concrete

8.4.4.3. Resistivity Test

Resistivity test was performed to evaluate the electrical resistivity of M-S-H samples compared to PC. The test provides a rapid indication of the penetration resistance of concrete to the movement of ions (chloride ions in particular). It is important to note that resistivity is a function of both the pore solution composition and the pore structure of the concrete. The pH, and by extension, conductivity of the pore solution of PC paste is typically several times greater than that of the M-S-H paste. The use of 3.5% NaCl to saturate the concrete was intended to counter the differences in the pore solution and to allow for a more accurate comparison of transport properties between the various types of binders. The values presented in Table 8.3 shows the relation of Rapid Chloride Penetration (RCP) and Resistivity tests reported in previous studies based on saturation with tap water rather than NaCl and are directly comparable to the results from this investigation. They are only meant to provide a general indication on chloride penetration resistance of the concrete.

Table 8.3. Chloride Ion Penetration and resistivity classification

(Adapted from AASHTO (2011) and Gudimettla and Crawford (2016))

Chloride Ion Penetration	**RCP Test Charges Passed (Coulombs)**	**Bulk Resistivity Test (KOhm.cm)**
High	> 4,000	<6.3
Moderate	2000-4000	6.3-11
Low	1000-2000	11-19.5
Very Low	100-1000	19.5-134
Negligible	<100	>134

Resistivity results of concrete samples from the early age of 7 days to a long-term curing duration up to 90 days are presented in Figure 8.10.

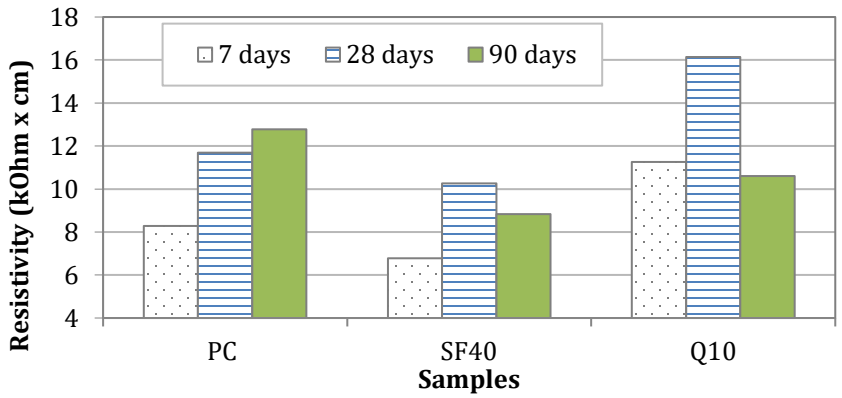

Figure 8.10. Permeability coefficient of M-S-H and PC concrete

For PC concrete, resistivity increases over the time due to the formation of C-S-H phases which result in dense cement pastes and reduce the connectivity of the pores in the microstructure. The resistivity indexes of PC samples at 28 and 90 days are over 11.0 and classified as low risk of Chloride ion penetration (Table 8.3). The resistivity of M-S-H samples increases up to 28 days however decreases considerably at 90 days age to reflect the unusual trend of increasing permeability over the long-term. It can be seen that the M-S-H binder replacement by 10% of quartz fillers results in a remarkable

improvement of the resistivity for M-S-H concrete and even obtains higher resistivity indexes than PC samples at 7 and 28 days age.

Although M-S-H concrete has higher porosity and permeability than PC concrete, it is shown that some resistivity indexes of M-S-H concrete are higher than those of PC, which is not correlated with porosity and OPI testing results and is likely a function of the lower pH in the pore solution of the M-S-H binder.

8.4.5. **Microstructure**

Microstructures of M-S-H and PC paste samples analyzed by SEM imaging are shown in Figure 8.11, 8.12, 8.13. Figure 8.11 presents fracture surfaces of PC pastes with homogenous microstructures showing a decrease in very small pores from 28 days (Figure 8.11(a)) to 90 days (Figure 8.11(b)). Figure 8.12(a) shows SF40 paste samples without quartz filler in which large pores were observed. Unreacted brucite laminae were visible at 28 days age while the M-S-H gel were formed connecting and covering the reacted brucite particles. The presence of micro-cracks during the hydration up to 90 days in Figure 8.12(b) might result from the high shrinkage of M-S-H binder, which could be one of the causes for the increase of permeability compared to PC as previously discussed. Connected pores were also observed in the M-S-H pastes (Figure 8.12(b) and Figure 8.13(b)), possibly results from the conversion of brucite and SF to M-S-H gel as identified by the XRD results provided in Figure 8.5. Since brucite is the predominant early hydration product in M-S-H concrete, the effect of connected pores from brucite dissolution might be significant and adversely affect the permeability. It was also shown in the Q10 paste samples that quart filler improved the dispersion of MgO and SF particles, resulting in denser pastes with virtually no micro-crack was found (Figure 8.13). The presence of connected pores was somewhat lower with the Q10 samples compared to SF40 samples without quartz filler. Further investigation is suggested to counter the effect of those connected pores to M-S-H binders.

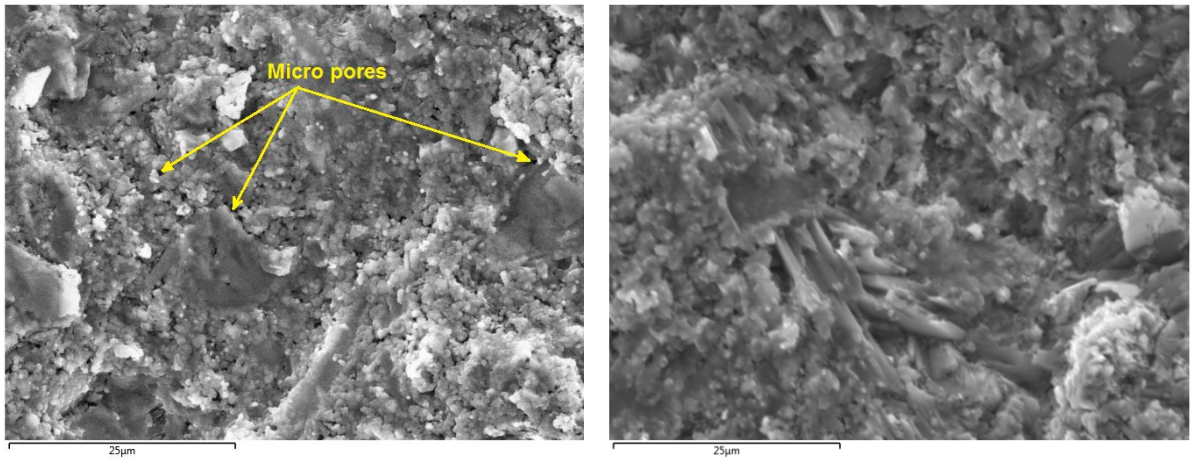

(a) PC - 28 days *(b) PC - 90 days*

Figure 8.11. SEM images of PC paste samples at 28 and 90 days

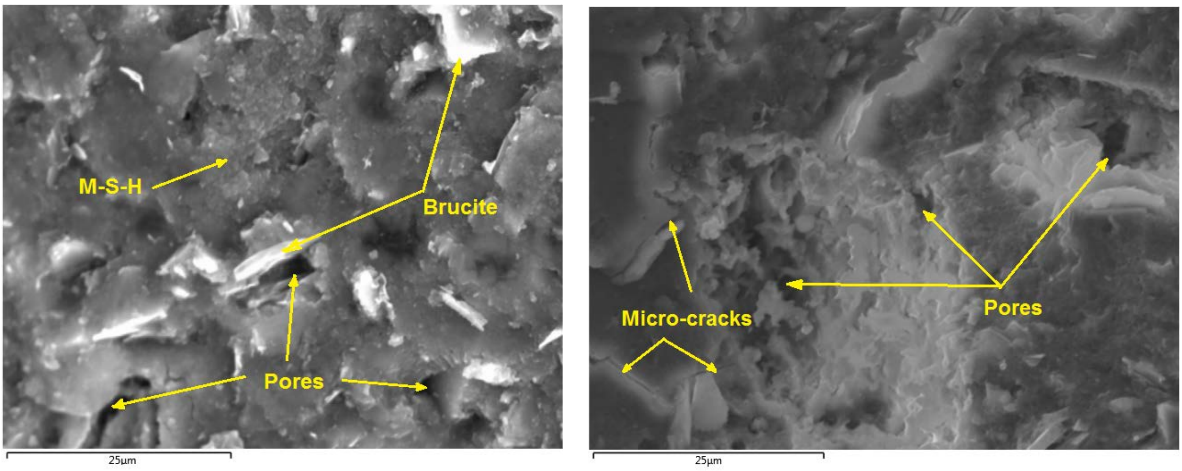

(a) SF40 - 28 days *(b) SF40 – 90 days*

Figure 8.12. SEM images of M-S-H paste samples at 28 and 90 days

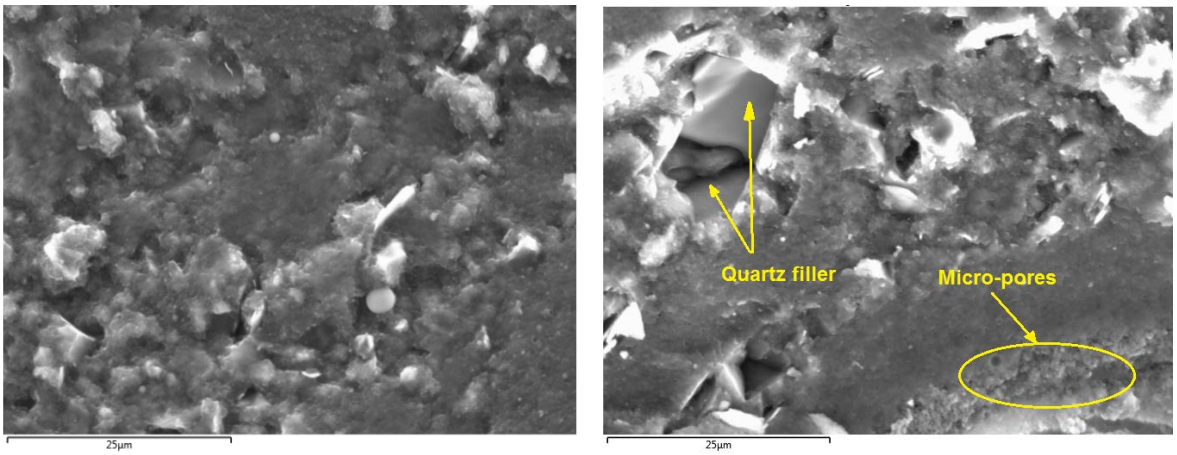

(a) Q10 – 28 days (b) Q10 – 90 days

Figure 8.13. SEM images of 10% quartz filler M-S-H paste samples at 28 and 90 days

8.5. CONCLUSIONS

Mechanical and durability properties of concrete using mixtures of reactive magnesium oxide and silica fume as the binder were investigated. The following conclusions can be drawn based on the experimental results of the selected materials:

The M-S-H binder system composed of 60% MgO and 40% SiO_2 enables the production of concrete with compressive strengths over 40 MPa at 28 days which may be suitable for a wide range of structural applications. The mechanical properties and durability of M-S-H concrete (compressive strength, tensile strength, modulus of elasticity) are somewhat lower than those of control PC concrete at the same mix proportions and water to binder ratio.

The selected binder composition of 60/40 MgO/SF results in an unusual non-linear stress-strain relationships in the loading range up to 40% of compressive strength.

The concrete using 60/40 MgO/SF binder system had a higher permeability and porosity than the control PC concrete, which indicates a higher potential risk for long-term deterioration. The formation of M-S-H phases appeared to result in an increased pore connectivity over the 90 days curing period.

The incorporation of 10% quartz filler into the 60/40 MgO/SF system can significantly increase the compressive strength, tensile strength and modulus of elasticity. M-S-H concrete containing 10% quartz filer showed a linear stress-strain behavior unlike the MgO/SF only concrete.

The use 10% quartz filler appeared to improve the M-S-H binder's homogeneity, dispersion and packing density to reduce porosity and permeability compared to the non-filler binder system.

8.6. REFERENCES

AASHTO (2011) AASHTO TP-95. Surface Resistivity Indication of Concrete's Ability to Resist Chloride Ion Penetration, 2011, Washington, D.C.

ACI Committee 318 (2015) Building Code Requirements for Structural Concrete (ACI 318-14): An ACI Standard: Commentary on Building Code Requirements for Structural Concrete (ACI 318R-14), an ACI Report. American Concrete Institute, Farmington Hills, MI, USA.

Alexander MG, Mackechnie JR and Ballim Y (1999) Guide to the use of durability indexes for achieving durability in concrete structures. Research monograph 2.

ASTM (2001) C 39: Standard test method for compressive strength of cylindrical concrete specimens. ASTM International, West Conshohocken, PA, USA.

ASTM (2004) C 496: Standard test method for splitting tensile strength of cylindrical concrete specimens. ASTM International, West Conshohocken, PA, USA.

ASTM (2002) C 469: Standard test method for static modulus of elasticity and Poisson's ratio of concrete in compression. ASTM International, West Conshohocken, PA, USA.

ASTM (2006) C 642: Standard test method for density, absorption, and voids in hardened concrete. ASTM International, West Conshohocken, PA, USA.

Basta C, Gupta R, Leichti R, Sinha A (2012) Applications of perpendicular-to-grain compression behavior in real wood construction assemblies. Wood and Fiber Science **44(2):** 155-167.

Beushausen H and Luco LF (eds.) (2015) Performance-based Specifications and Control of Concrete Durability: State-of-the-art Report. RILEM TC 230-PSC, Vol. 18, Springer.

Calc R, Naranda J, Kuhta M, Vorgrin M (2013) The physiology of sports injuries and repair processes, in: Hamlin M, Draper N, Kathiravel Y, (Eds.). Current Issues in Sports and Exercise Medicine: 43-86.

Chen S, Wang L, Wu Z, Zhang T (2017) Mechanical properties and reaction products of reactive magnesia and CFB slag/silica fume pastes. Advances in Cement Research, 11, https://doi.org/10.1680/jadcr.16.00171

EN (2009) EN 13670:2009: Execution of concrete structures, BSI.

Gudimettla J and Crawford G (2016) Resistivity Tests for Concrete--Recent Field Experience. ACI Materials Journal, 113(4): 505-512.

Harrison A.J.W (2005) Carbonating and Hydraulic Mortars - the difference is not only in the binder, aggregates are also important. Proceeding of the 10th Canadian Masonry Symposium, Banff, Alberta, June 8 – 12, 2005.

Jin F, Gu K, Abdollahzadeh A and Al-Tabbaa A (2013) Effects of different reactive MgOs on the hydration of MgO-activated GGBS paste. Journal of Materials in Civil Engineering **27(7)**: B4014001

Jin F and Al-Tabbaa A (2014) Strength and hydration products of reactive MgO–silica pastes. Cem. Concr. Compos. **52**: 27–33.

Li Z, Zhang T, Hu J, Tang Y, Niu Y, Wei J and Yu Q (2014) Characterization of reaction products and reaction process of $MgO–SiO_2–H_2O$ system at room temperature. Construction and Building Materials **61**: 252-259.

Lothenbach B, Nied D, L'Hopital E, Achiedo G and Dauzeres A (2015) Magnesium and calcium silicate hydrates. Cem. Concr. Res. **77**: 60–68.

Mackechnie JR and Scott CAN (2012) Durability properties of inorganic polymer concrete using fly ash and slag. In Concrete Repair, Rehabilitation and Retrofitting III: 3rd International Conference on Concrete Repair, Rehabilitation and Retrofitting, ICCRRR-3, 3-5 September 2012, Cape Town, South Africa, CRC Press, p 64.

Mármol G, Savastano H, Tashima MM and Provis JL (2016) Optimization of the $MgO-SiO_2$ binding system for fiber-cement production with cellulosic reinforcing elements. Materials & Design **105**: 251-261.

Massazza F (1996) Action of Environmental Conditions. Rilem Report 11: Interfacial Transition Zone in Concrete (Maso JC (ed.)). E&FN SPON, London, England, U.K., First Edition, pp. 132-149.

Nied D, Enemark-Rasmussen K, L'Hopital E, Skibsted J and Lothenbach B (2016) Properties of magnesium silicate hydrates (M-S-H). Cement and Concrete Research **79**: 323-332.

Pacheco-Torgal F, Cabeza LF, Labrincha J and De Magalhaes AG (2014) Eco-efficient construction and building materials: life cycle assessment (LCA), eco-labelling and case studies. Woodhead Publishing, p 226.

Tran HM and Scott A (2017) Strength and workability of magnesium silicate hydrate binder systems. Construction and Building Materials **131**: 526-535.

Walling S A, Kinoshita H, Bernal S A, Colliera N C and Provis JL (2015) Structure and properties of binder gels formed in the system Mg(OH)2–SiO_2–H_2O for immobilisation of Magnox sludge. The Royal Society of Chemistry, Dalton Trans. **44**: 8126–8137.

Wei JX, Chen YM, Li YX (2006) The Reaction Mechanism between MgO and Microsilica at Room Temperature. Journal of Wuhan University of Technology - Mater. Sci. Ed. **21(2)**: 88-91.

Zhang T, Cheeseman CR and Vandeperre LJ (2011). Development of low pH cement systems forming magnesium silicate hydrate (MSH). Cement and concrete research 41(4): 439-442.

Zhang T, Vandeperre LJ and Cheeseman CR (2012) Magnesium-silicate-hydrate cements for encapsulating problematic aluminium containing wastes. Journal of Sustainable Cement-Based Materials **1 (1-2)**: 34-45.

Zhang T, Vandeperre LJ and Cheeseman CR (2014) Formation of magnesium silicate hydrate (M-S-H) cement pastes using sodium hexametaphosphate. Cement and Concrete Research **65**: 8–14.

CHAPTER 9
EXPERIMENTAL STUDY ON MODULUS OF ELASTICITY OF M-S-H BINDER SYSTEMS

Preamble

The experimental programmes presented in previous chapters have studied a number of fundamental engineering properties of M-S-H cement pastes and mortars. The microstructures and hydration process analysis in chapter 4 has confirmed the ease of the formation of M-S-H binding phases at room temperatures, which laid the foundation for the development of M-S-H binder systems. The pore solution analysis of M-S-H paste samples in chapter 5 also showed the effects of pHs and chemical compositions of the raw materials on the hydration process which was consistent with XRD and SEM/EDS results.

The compressive strength, which is widely considered as one of the most important mechanical properties of cementitious materials, were well studied in chapter 6 and chapter 7. While chapter 6 focused on finding the strength capacity of M-S-H binders and the optimal binder composition for strength and workability, chapter 7 expanded the compressive strength tests to a wide range of silica sources. In particular, the effects of different curing conditions such as different moisture conditions and curing temperatures were investigated.

The developed M-S-H binder systems have obtained normal-to-high compressive strengths for a wide range of structural applications. Chapter 6, 7, 8 have shown that the optimal binder composition was able to achieve compressive strengths up to approximately 90 MPa and over 40 MPa with mortars and concrete mixes, respectively. However, other mechanical properties such as elastic modulus or tensile strength are also important in order to meet structural design requirements. In the literature, the stress-strain behaviours of M-S-H cementitious materials were not fully understood due to a lack of studies in this field. This chapter, therefore, further presents the characteristics of elastic moduli of M-S-H cement pastes with the aim to bridge this gap in the literature and evaluate stress-strain behaviors for the purpose of structural design considerations of M-S-H cementitious materials.

Abstract

Experimental study on modulus of elasticity and Poisson's ratio of magnesium silicate hydrate (M-S-H) cement pastes was performed in comparison with Portland cement. Mixtures of MgO with various silica sources were prepared with silica contents ranging between 40-60%. It was found that the 28-day compressive strengths of M-S-H cement pastes are lower than PC. The M-S-H binders also result in a lower modulus of elasticity than PC control samples. The stress-strain behavior of the M-S-H cement pastes shows a high degree of nonlinearity after elastic range. The silica sources was found to significantly affect the Poisson's ratio for the M-S-H binder which ranged from 0.10 to 0.21. The material source is one of the major factors of the high variability of the properties of M-S-H cement pastes compared to PC.

9.1. INTRODUCTION

Recent research on M-S-H binder systems has generally focuses on the potential benefits of the binder as an alternative to Portland cement (PC) to reduce the negative impacts of CO_2 emissions on the environment. The synthesis M-S-H binder systems use reactive magnesium oxide calcined at low temperatures (700-1000^{o}C) and are able to incorporate a high proportion of silica, including industrial by-products or waste materials such as silica fume, fly ash, rice husk or natural pozzolans. Other magnesium-based binders under development have claimed to be carbon neutral or even carbon negative involving CO_2 sequestration by magnesium-rich minerals olivine and serpentine to form magnesium carbonates which are then decarbonated to produce reactive magnesium hydroxide (Pacheco-Torgal, 2014). There are also potential benefits of using M-S-H binders for the immobilization of nuclear wastes (Zhang et al., 2012; Walling et al., 2015).

A number of studies have focused on the improvement of workability and optimization of strengths of M-S-H binders (Wei et al., 2006; Zhang et al., 2014; Marmol et al, 2016; Tran and Scott, 2017). The microstructure was also investigated to characterize the formation of the M-S-H binding phases (Li et al., 2014; Lothenbach., 2015., Nied et al., 2016). In addition, the material source was also considered to have a major influence on the consistency and possibly be one of the biggest challenges to develop M-S-H binders (Jin et al., 2013).

Despite the availability of the previous studies, the modulus of elasticity of the M-S-H binders has not been addressed adequately. For PC concrete, the modulus of elasticity was well studied and the relationship of the modulus of elasticity and compressive strength of PC cementitious materials was specified extensively in structural design guidance including NZS 3101 (2006). For M-S-H binders, chapter 8 has shown that M-S-H concrete might achieve compressive strength of over 40 MPa, or even beyond. However, the concrete samples also exhibited the unusual non-linear stress-strain behaviors at stress even below 40% of the ultimate strength. It is understood that the stress-strain responses are of utmost importance for structural design considerations. Accordingly, further experimental studies on stress-strain behaviors of M-S-H binders in various conditions were required. As chapter 8 discussed the elastic modulus of the M-S-H concrete, this chapter particularly studies modulus of elasticity of M-S-H cement pastes to understand the stress-strain responses of the pastes compared to concrete samples in chapter 8. The testing of stress - lateral strain responses was also conducted to evaluate the Poisson's ratio of cement pastes using M-S-H binders. In addition, comparison of different silica sources and control cement paste samples using PC were discussed.

9.2. EXPERIMENTAL PROGRAMME

9.2.1. Materials

Magnesium oxide (MgO), silica fume (SF), microsilica (MS) and rice husk ash (RHA) were used for modulus tests. Details of material properties are described in Chapter 3.

9.2.2. Mix proportions

Pastes samples with different silica sources were prepared for modulus of elasticity tests in comparison to control samples using Portland cement. Sample labels and mix proportions are presented in Table 9.1. Effects of binder compositions on resulting cement pastes are examined by varying MgO/SiO_2 ratios from 40/60 to 60/40 (by mass).

Due to the high water demand of M-S-H binders, a superplasticizer (Sika ViscoCrete-5-555 (NZ)) was used to obtain adequate workability. The superplasticizer dosage and w/c ratio were selected based on a previous work (Tran and Scott, 2017) (Chapter 6) which describes the fresh properties of various MgO-silica mixtures.

Table 9.1. Mix proportions (be mass) and 28 day results for M-S-H paste samples

Mix	MgO	Silica	w/c	SP	Curing	Comp. strength (MPa)	MOE (MPa)	Secant MOE (MPa)	Secant MOE /MOE ratio	Poisson's ratio
SF60	0.4	0.6	0.45	0.03	Sealed	8.6	1.5	1.0	0.66	**0.21**
SF50	0.5	0.5	0.45	0.03	Sealed	12.2	3.6	2.4	0.67	**0.18**
SF40	0.6	0.4	0.45	0.03	Sealed	13.9	5.3	4.3	0.82	**0.21**
MS60	0.4	0.6	0.45	0.03	Sealed	6.0	2.2	0.6	0.28	**0.16**
MS50	0.5	0.5	0.45	0.03	Sealed	9.8	5.1	1.8	0.34	**0.20**
MS40	0.6	0.4	0.45	0.03	Sealed	13.6	6.7	4.9	0.73	**0.18**
R60	0.4	0.6	0.45	0.04	Sealed	8.4	2.4	0.9	0.38	**0.15**
R50	0.5	0.5	0.45	0.03	Sealed	14.1	7.4	5.6	0.75	**0.17**
R40	0.6	0.4	0.45	0.03	Sealed	18.4	8.4	5.8	0.69	**0.10**
PC	-	-	0.45	-	Sealed	34.3	16.8	14.6	0.87	**0.17**

9.2.3. **Testing methods**

Paste cylinders sized 50 mm diameter × 100 mm height were cast for modulus of elasticity testing. The samples were demolded after 48 h before curing at room temperature in sealed containers until tested at 28 days age. Two strain gauges were attached to the surface of each sample to measure the longitudinal and transverse strains of each sample (Figure 9.1). Three cylindrical samples were tested to calculate the average value for each reported result. The static modulus of elasticity of the paste samples was determined in accordance with ASTM C469.

Figure 9.1. Cylindrical paste samples prepared for MOE test

9.3. RESULTS AND DISCUSSION

9.3.1. Compressive strength

Figure 9.2 shows the compressive strengths of M-S-H pastes compared to a control sample using PC. Mixtures of MgO and each silica sources are discussed as follows:

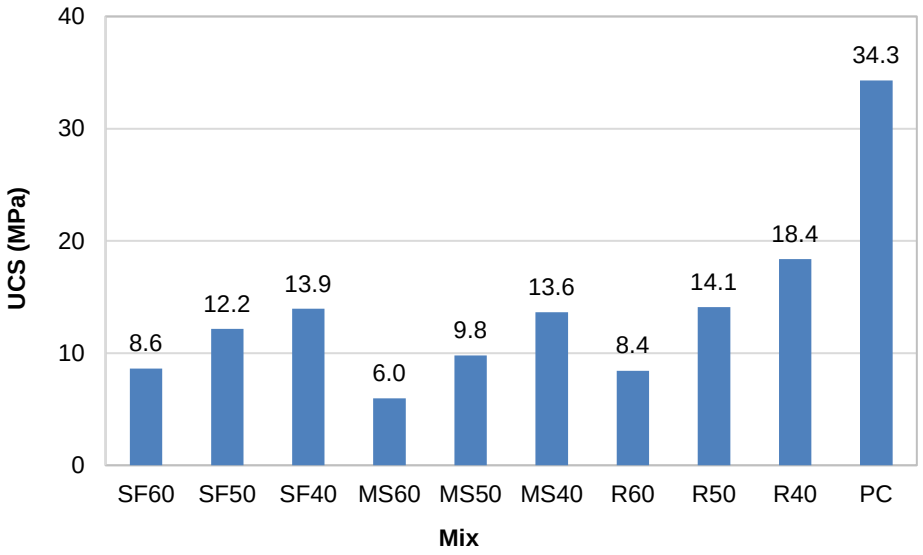

Figure 9.2. Compressive strength of cement pastes samples at 28 days age

M-SF mixtures

M-SF paste samples obtained relatively low compressive strengths at 28 days age. The strengths varied from 8.6 MPa for mixtures containing 60% silica fume to almost double strength of 13.9 MPa for mixtures containing 40% silica fume.

Particle size and bulk density of SF have a large influence on the strengths of the binders. The SF particles are microfine with a mean particle size of approximate 0.1 μm and low bulk density. Such properties can result in a very high microfine content and consequently increase the porosity of mixtures as SF content increases from 40-60%. Although the stoichiometry of M-S-H formation reactions may favor an optimal 40/60 MgO/SF ratio, the high SF content also results in high porosity and adversely affects the strength. Similar results of MgO/SF ratio for optimal strength and workability have also been reported in Chapter 6.

It was observed that w/c ratio also significantly influenced the strengths of the pastes. In this experiment, in order to produce the mixtures with a constant w/c and compare different silica sources, the w/c = 0.45 was required mainly for the workability of M-RHA and M-MS pastes even though 3-4% superplasticizer was used. However, this high w/c appears to result in high capillary

porosity for the M-SF paste samples. In chapter 6, a series of M-SF paste samples achieved good workability with lower w/c of only 0.40 due to the use of superplasticizer and such lower w/c resulted in higher strengths compared to M-SF mixtures of w/c=0.45 presented here. Testing results in chapter 6 also showed that with M-SF mortar mixtures and w/c=0.45, the inclusion of quartz sand (quartz/binder ratio = 0.5/1.0) also reduced the water content of the mixtures, increased packing density and therefore increased strengths of the mortars compared to the pastes. The inclusion of RHA as another silica source occurred as a later addition in this study of the M-S-H system and as a result was not included in the work at w/c=0.4 presented in chapter 6.

M-MS mixtures

Mixtures of M-MS show the same trend as observed with M-SF samples in which the increase in MS content reduces the compressive strength. The range of the strengths is lower than M-SF mixtures varying from only 6.0 MPa (M-MS40 samples) to 13.6 MPa (the highest among M-MS samples). The MS was ground to a very high fineness to increase reactivity. However the adverse effects of grinding to the high fineness and angular morphology occurred in which the use of a high proportion of MS increased the porosity of the cement pastes.

M-RHA mixtures

M-RHA pastes have higher strengths than using SF and MS in which the 28-day compressive strength was able to reach 18.4 MPa. The high strengths show the high reactivity of RHA and its potential use as silica fume replacement to reduce the cost of blended cement.

The mean particle size of RHA is 40 μm, which is far higher than SF and MS and even higher than MgO. The particle size of RHA would not affect the density to the same extent as SF or MS, however, the very porous microstructure of RHA, its low bulk density and angular morphology may increase the porosity of the resulting binders and require a high water demand for workability. A minimum w/b of 0.45 is required for workable M-RHA mixtures.

PC sample

The PC paste samples show a higher compressive strength than all M-S-H mixtures at 28 days age. One of the reasons is the slow strength development of M-S-H binders which can develop significant strength from 28 to 90 days age as discussed in Chapter 7.

Overall, it can be seen that M-S-H paste samples showed lower strengths than PC. The factors that influence strength development are not only the optimal MgO/Silica ratio for chemical reactions

forming M-S-H as the main binding phases but also the silica properties such as particle size, morphology, and microstructure.

9.3.2. Stress-strain behaviours at low range of compressive strengths

The stress-strain behaviour of PC cementitious materials is generally considered to be elastic at the low range of stress up to 40% of the compressive strength. For M-S-H binders, the study of concrete mixes in chapter 8 showed the unusual stress-strain relationship in which the non-linear stress-strain responses occurred and can be described as concave curves. Such stress-strain nonlinearity is not desirable in structural design and therefore the study of stress-strain relationships of M-S-H cementitious materials at the low range of stress and in other conditions is of importance for the application of the new binders in building/civil structures.

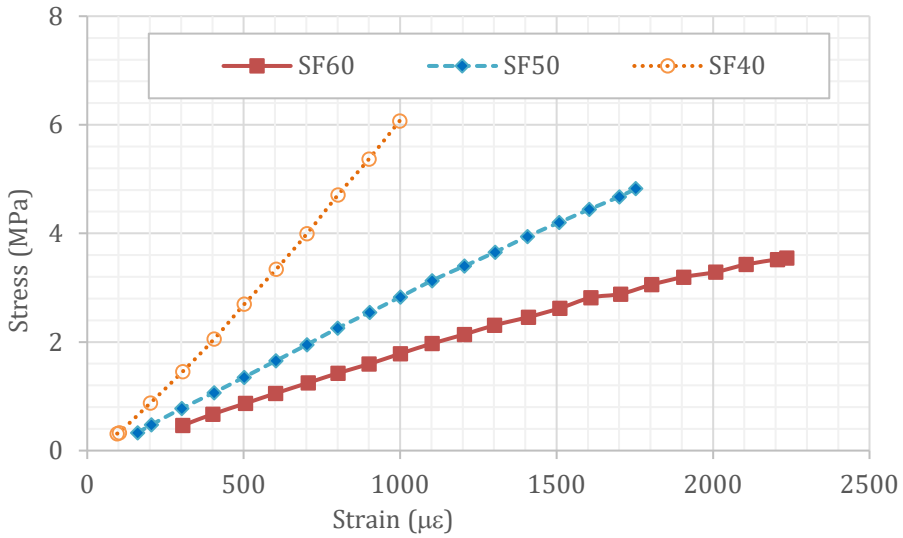

Figure 9.3. Stress-strain behaviours of M-SF paste samples at 28 days age

Figure 9.3 shows typical stress-strain behaviours of M-SF cement pastes under stress up to 40% compressive strengths. Samples were prepared with three different MgO/SF ratios (40/60, 50/50, 40/60) to evaluate the effect of MgO/SF ratio on the modulus of elasticity.

It was found that different MgO/SF ratios resulted in different stress-strain behaviours of the resulting paste samples. It was observed that for the paste of high MgO/SiO_2 ratio (MgO/SF = 60/40) the typical stress-strain relationship was slightly non-linear in a concave curve. On the other hand, the high SF content paste sample (MgO/SF = 40/60) showed another form of non-linearity as a convex curve while a linear-like stress-strain behaviour was shown with 50/50 MgO/SF mixtures.

The strength, microstructure, and porosity are possibly among the most influencing factors of the stress-strain behaviours. It was obvious that MgO/SF ratio significantly affected the strength and microstructure of the resulting binders in which hydration products (brucite and M-S-H phases) were formed with different proportions, as discussed in chapter 6. The change of MgO/SF also resulted in mixtures of various packing density/porosities. Accordingly, the variation of strength, microstructure and porosity may lead to different behaviours of the stress-strain relationship of the cement pastes with different MgO/SF ratios. For example, the excess amount of silica resulted in poor packing density and lower compressive strengths for SF60 mixes compared to SF40 mixes. The lower compressive strength is possibly the reason why SF60 mixes resulted in higher strain than SF40 mixes under same level of stress.

9.3.3. **Comparison of cement paste and concrete samples using M-SF binders**

In chapter 8, the concrete samples were produced for testing mechanical and durability properties. A binder composition of 60% MgO-40% SF was selected for the concrete and the mix without quartz filler showed a non-linear stress-strain relationship as shown in Figure 9.4.

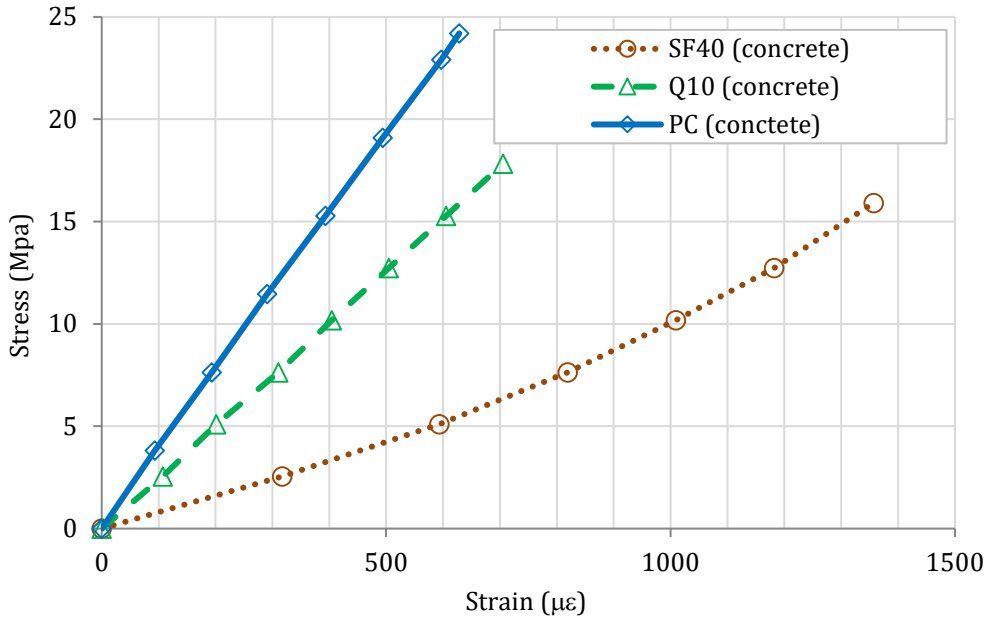

Figure 9.4. Stress-strain behaviours of M-SF concrete samples at 28 days age (Adapted from Figure 8.7 – chapter 8)

The stress-strain relationships of the paste samples (Figure 9.3) were compared to those of concrete samples (Figure 9.4) to give further understanding of stress-strain responses of the M-

S-H cementitious materials in various conditions. It should be noted that there were some difference in the paste and concrete samples as follows:

- The w/c ratio of the concrete was only 0.40 due to the good workability achieved with the use of superplasticizer and the inclusion of round coarse aggregate. On the other hand, the w/c of the paste was increased to 0.45.
- The mix proportions of the concrete include the fine and coarse aggregates which differed from the paste without aggregates.
- The concrete was water-cured while the paste was sealed and cured in room temperatures. Such conditions resulted in different moisture conditions of the concrete and paste samples at the time of testing.

In comparison to SF40 concrete mix, it was observed that the SF40 paste samples resulted in similar non-linear stress-strain behaviours and those curves were slightly concave. The non-linearity of the stress-strain relationship of the concrete samples was therefore influenced by the cement paste. It can be seen that both cement paste and concrete samples showed some degree of non-linear stress-strain behaviour at the low range of stress, which is not desirable in structural design, and the solution to modify those non-linear responses is required.

However, it was found that the stress-strain relationship of the paste can be modified using different MgO/SF ratios (Figure 9.3). Therefore, it appears that suitable selections of the binder compositions may result in desirable stress-strain behaviour of the M-S-H cementitious materials. Another viable solution to adjust the stress-strain behaviour of the concrete is the use of quartz filler was also discussed in chapter 8.

9.3.4. Effect of silica sources

The stress-strain relationships of M-MS paste samples are shown in Figure 9.5. The typical stress-strain behaviours of M-MS mixtures are almost similar to M-SF mixtures in which the MgO/SiO_2 ratio has a significant impact. At low MgO/MS ratio of 40/60, the stress-strain response was slightly non-linear as a convex curve. As the MgO/MS increased to 50/50, the linear stress-strain response was observed which was similar to the 50/50 MgO/SF paste sample. The high MgO/MS ratio of 60/40 resulted in a non-linear stress-strain response however the nonlinearity was slightly different from 60/40 MgO/SF paste sample. As for M-RHA paste samples (Figure 9.6), typical stress-strain responses with all MgO/RHA ratios were non-linear as convex curves.

The similarity and difference of the stress-strain responses of M-S-H cement pastes using different silica sources were subject to the MgO/SiO_2 ratios. The change of binder compositions was known

in microstructure study (Chapter 4 and 5) to result in various proportions of hydration products including brucite and M-S-H phases, which may play a key role in the stress-strain behaviours. In mixtures containing high silica content (MgO/SiO_2 = 40/60) where the majority of the hydration products were M-S-H phases, the stress-strain behaviours were consistent in which the slightly convex curves were observed. In contrast, the high MgO/SiO_2 ratio of 60/40 which often results in the high brucite proportion of the hydration products, have shown the unstable stress-strain responses. In addition, the variation of microstructure and porosity results from changing binder compositions are other potential influencing factors on stress-strain behaviours. Although the non-linear stress-strain behaviour is undesirable for structural design, it was found that the M-S-H binders might result in both linear and non-linear stress-strain responses, and the modification of binder composition was able to alter the stress-strain behaviours to obtain linear responses.

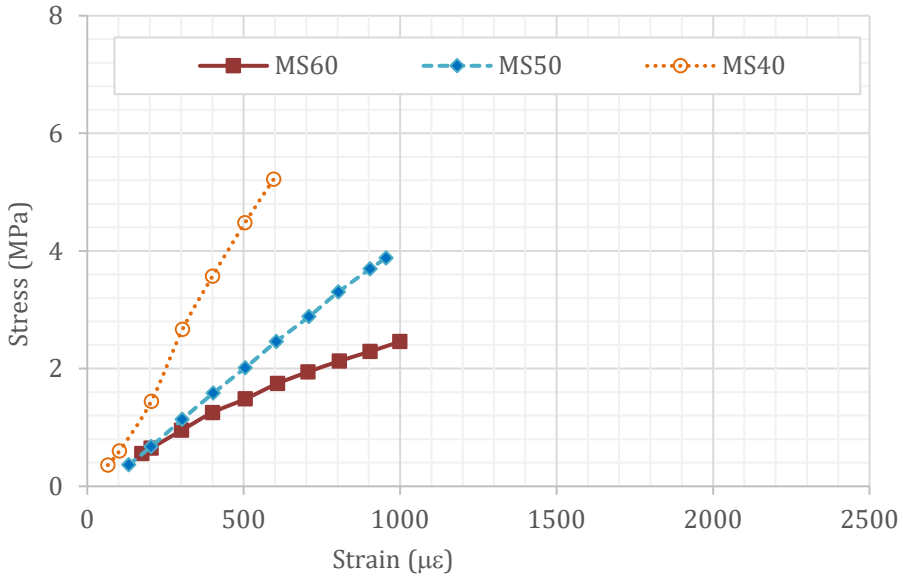

Figure 9.5. Stress-strain behaviours of M-MS paste samples at 28 days age

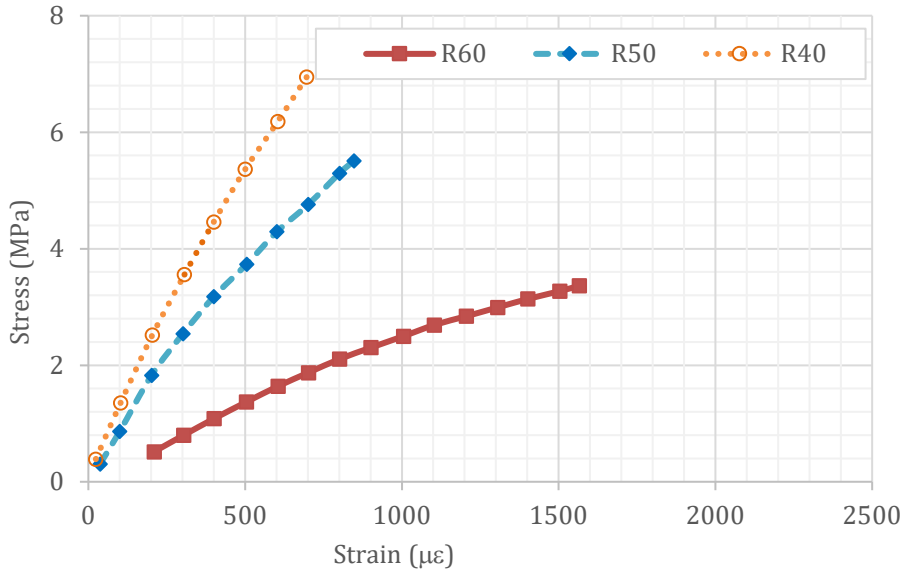

Figure 9.6. Stress-strain behaviours of M-RHA paste samples at 28 days age

9.3.5. **Modulus of elasticity (MOE)**

The modulus of elasticity of cementitious materials, which is defined as the ratio between normal stress to strain of the linear proportion of the stress-strain relationship, is a critical design parameter to measure instantaneous elastic deformation of the structures. The MOEs of the samples are calculated according to ASTM C469 adopting the assumption of a linear range up to 40% of the ultimate compressive strength for the stress-strain relationship.

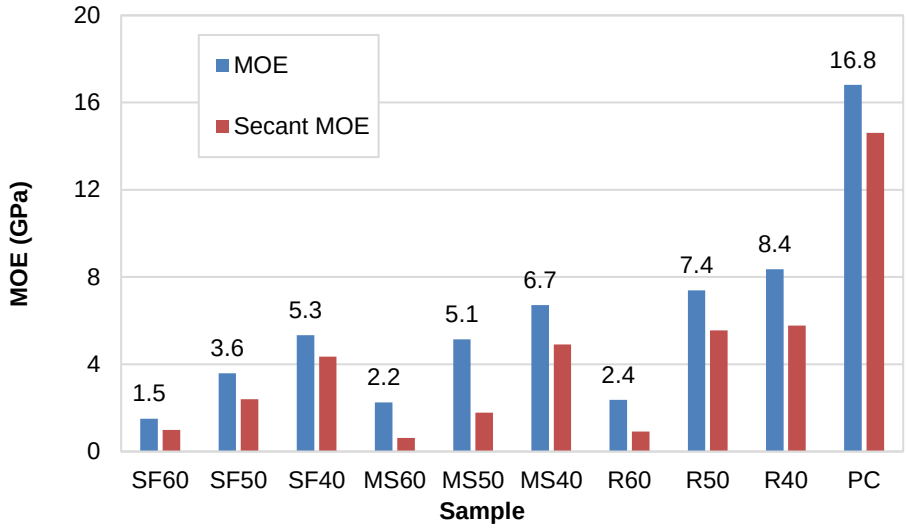

Figure 9.7. MOEs of M-S-H and PC pastes (w/c = 0.45)

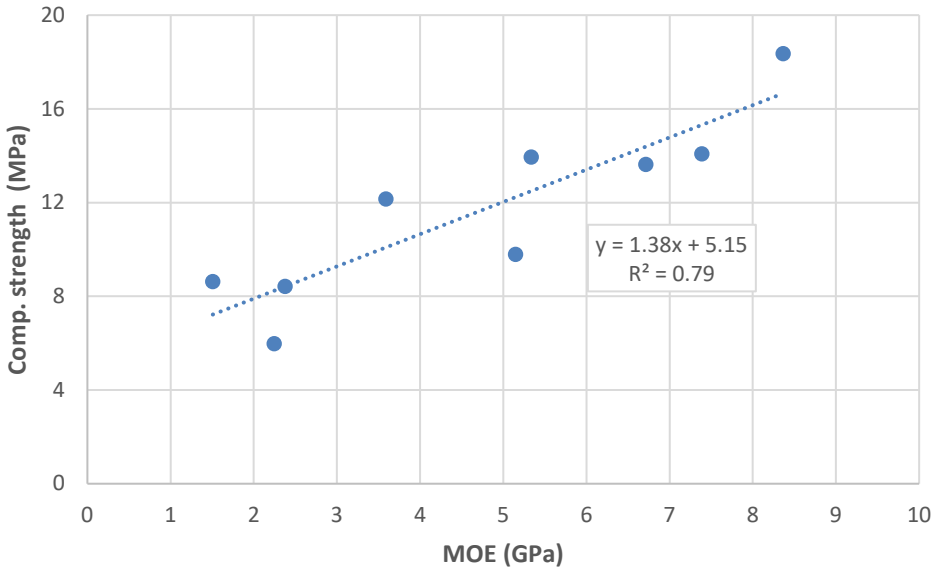

Figure 9.8. Relationship of MOE and Compressive strength of M-S-H cement pastes (w/c = 0.45)

Figure 9.7 presents the MOEs of M-S-H binders compared to PC sample. M-SF samples have the lowest MOEs only in the range from 1.5 to 5.3 GPa. M-RHA samples have the highest MOEs in all M-S-H cement pastes varying from 2.4 GPa (R60 mixture) to 8.4 GPa (R40 mixture). It is obvious that PC sample has higher MOE than M-S-H samples. MOE testing results show a common upward trend as silica content decreases from 60% to 40%. As discussed before, the MgO/Silica ratio has been attributed to having an influence on the compressive strength and therefore has affected the MOEs of resulting binders. Such a relationship between compressive strengths and MOEs is shown in Figure 9.8. The correlation of linear regression analysis indicates the proportional increase of MOEs results from the increase of compressive strengths. However only a limited number of samples were tested, further studies are necessary to characterize the relationship between strength and elastic modulus of M-S-H binder systems.

9.3.6. **Non-linear stress-strain behaviour**

As the load increases out of elastic range, the stress-strain relationship becomes unproportional and is known as plastic behaviour. Such nonlinearity can be assessed by the degree of curvature of the stress-strain graph in which generally MOEs decrease as the strain increases at higher rates than the applied stress. In this study, a point "immediately" before failure (without bonding failure of the strain gauge and sample) is used to determine the non-linear behaviour of the pastes. The secant modulus between the point of 50 millionths strain and the failure point is determined.

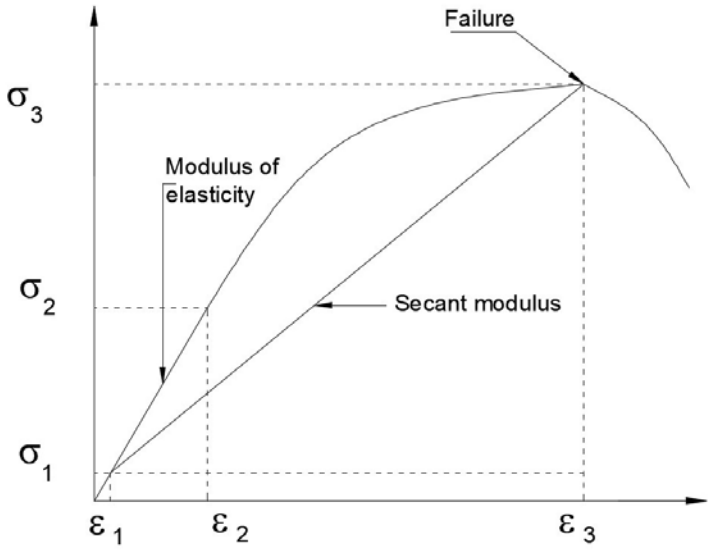

Figure 9.9. Representation of the stress-strain relation for M-S-H cement pastes

The ratios of secant MOE and MOE (MOE_{secant}/MOE) reflect the stress-strain behaviour in the plastic state as the stress exceeds 40% of the ultimate compressive strength. A linear stress-strain behaviour should have a MOE_{secant}/MOE ratio equal to 1.0. For other cases, the lower the MOE_{secant}/MOE ratios, the more the secant MOEs decrease which indicates the increase in the deformation of the samples (Figure 9.9).

The secant modulus of each M-S-H and PC sample at plastic state compared to its MOE is also presented in Figure 9.7 above. The measured secant moduli are lower than MOEs for all samples as the strain generally increases before failure. The decrease of MOEs represented by MOE_{secant}/MOE ratios is illustrated in Figure 9.10. A ratio close to 1.0 indicates a high proportion of linear stress-strain behavior, for example, PC sample has an average MOE_{secant}/MOE ratio equal to 0.87. On the other hand, all M-S-H samples show lower MOE_{secant}/MOE ratios in the range from 0.28 to 0.82 which suggests a large decrease of secant moduli and also a large increase of strains of M-S-H pastes, particularly the M-MS samples. The low MOE_{secant}/MOE ratios may also indicate a lower portion of linear stress-strain behavior compared to PC. The full stress-strain behaviour graphs of all mixtures from zero load until debonding failure between samples and strain gauges are shown in Figures 9.11 – Figure 9.20.

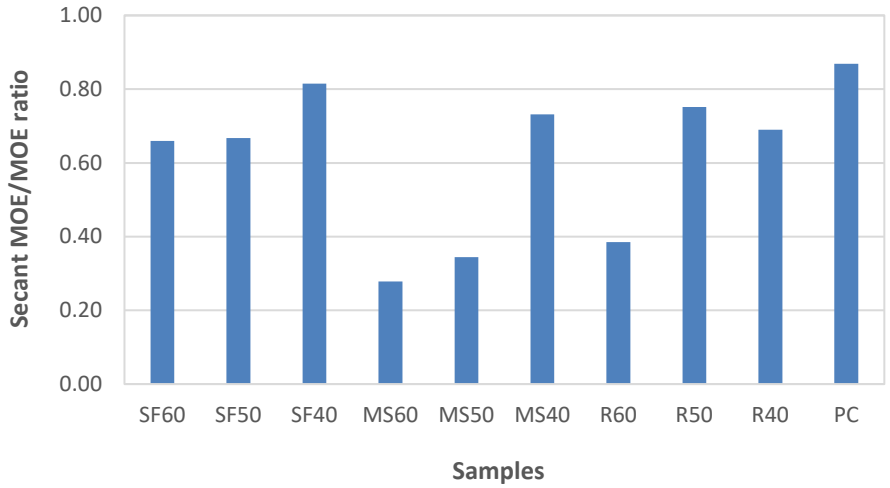

Figure 9.10. Representation of the stress-strain relationship for M-S-H cement pastes

Silica content also influences the stress-strain relationship of M-S-H binders. Although a MgO/silica ratio of 40/60 wt% may be optimal for the formation of M-S-H phases as described in the previous chapters, such high silica content also generally results in low MOEs and a high degree of nonlinearity of stress-strain behavior. The low MOEs in combination with a low portion of stress-strain behavior may be result in challenges for the design of structures using M-S-H binders.

The experimental results are obtained from the pastes samples cured at room temperature under sealed conditions. However, it is known that other factors such as aggregate type, proportion, and curing conditions also have a strong impact on the stress-strain behavior of the resulting cementitious materials. For example, the M-S-H concrete introduced in Chapter 8 has shown unusual non-linear stress-strain behavior instead of linearity at a low range of stress. Further research on MOEs of M-S-H binders is recommended in future studies for the structural design of the new binder systems.

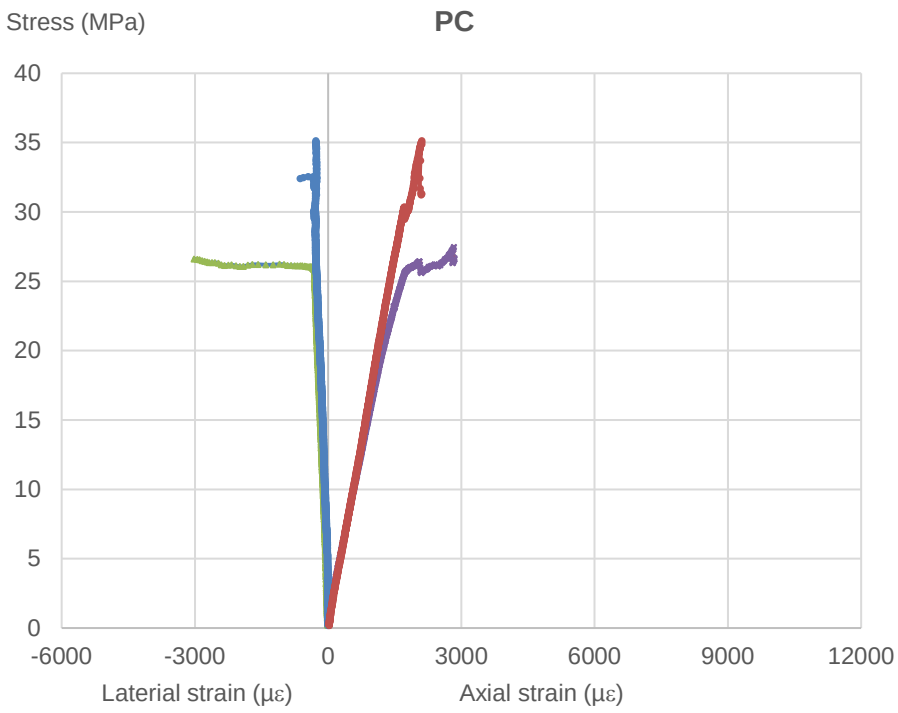

Figure 9.11. Stress-strain behaviour of PC paste sample

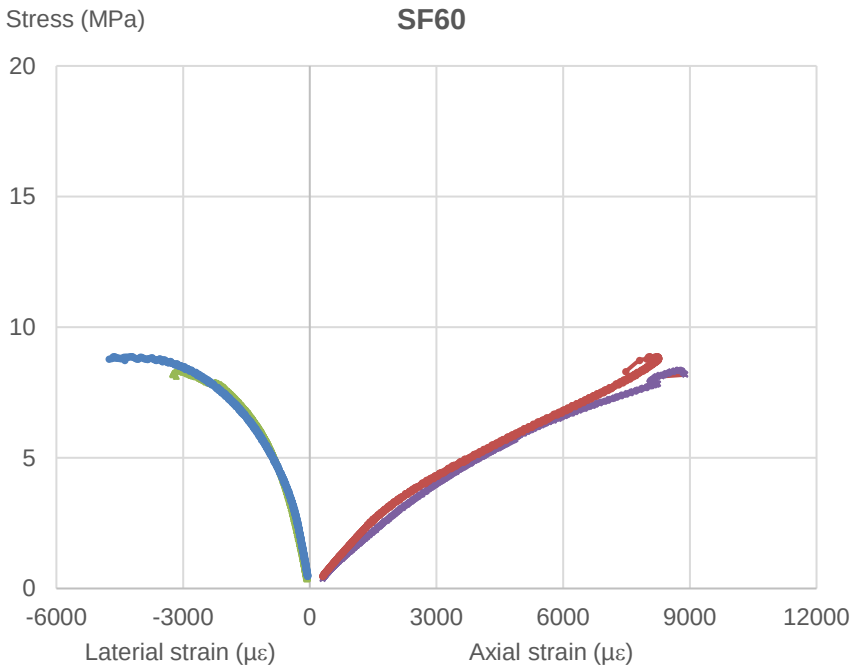

Figure 9.12. Stress-strain behaviour of SF60 paste sample

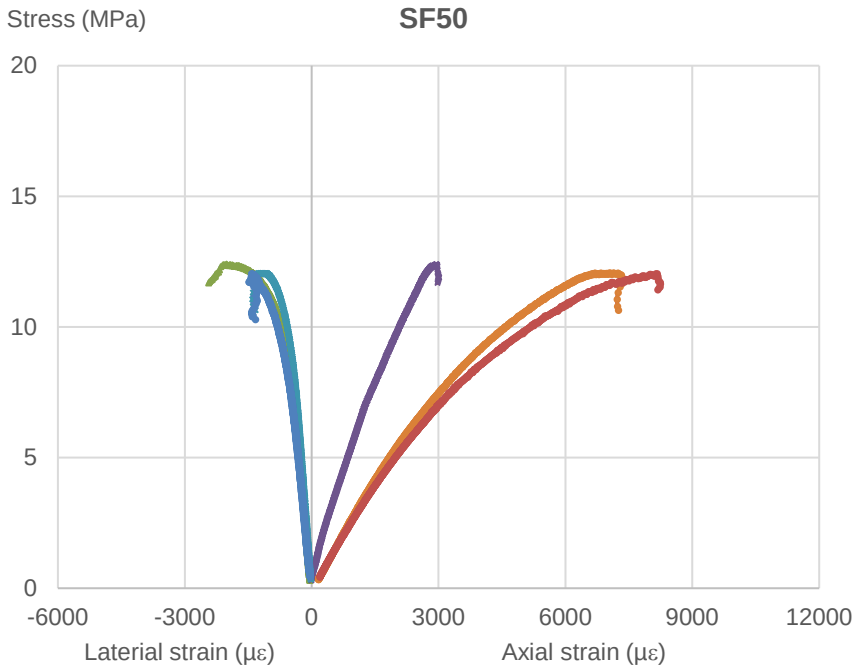

Figure 9.13. Stress-strain behaviour of SF50 paste sample

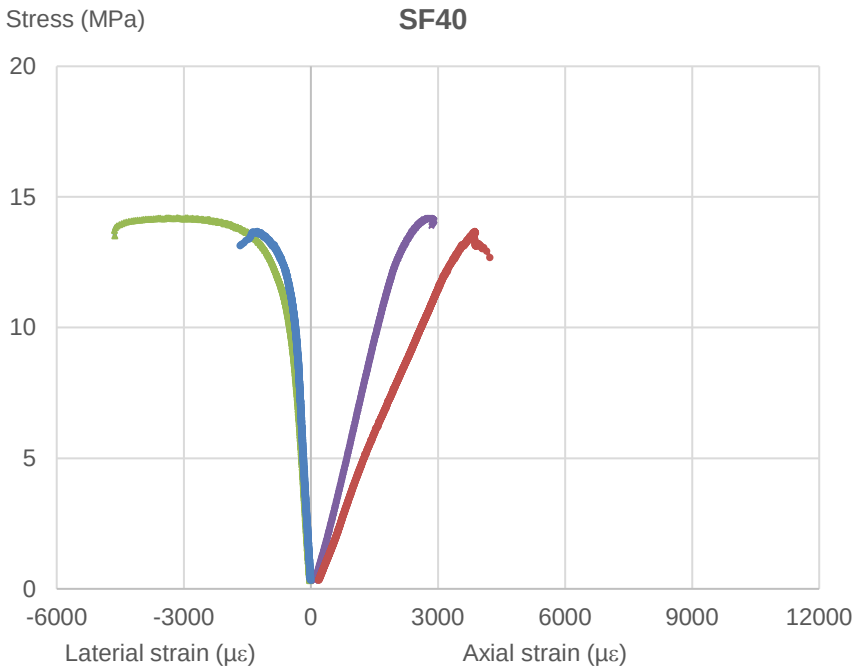

Figure 9.14. Stress-strain behaviour of SF40 paste sample

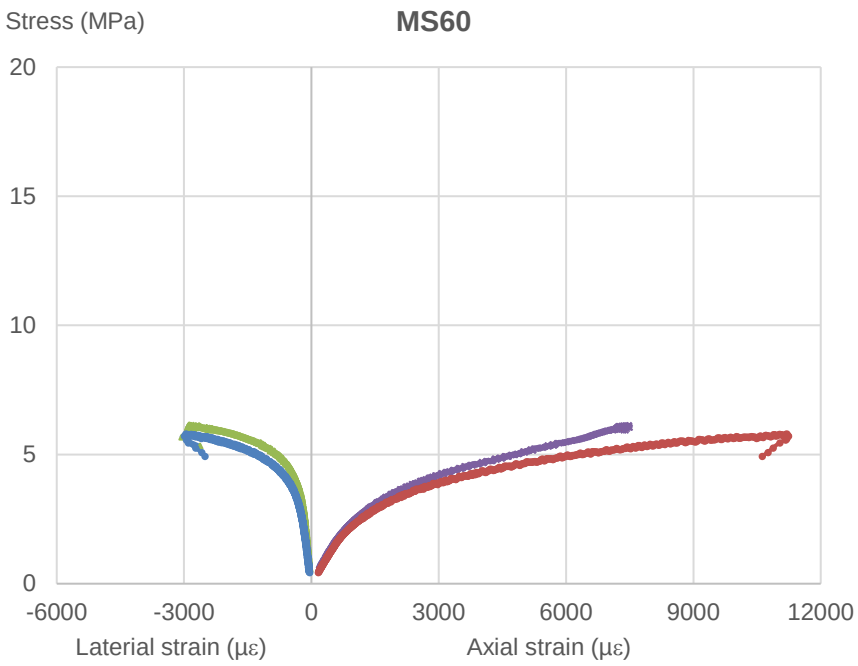

Figure 9.15. Stress-strain behaviour of MS60 paste sample

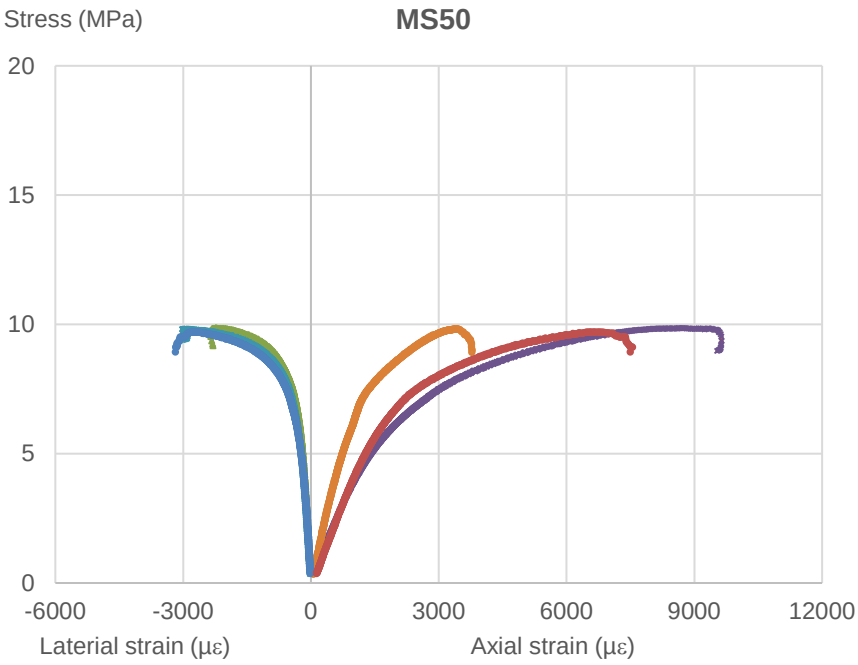

Figure 9.16. Stress-strain behaviour of MS50 paste sample

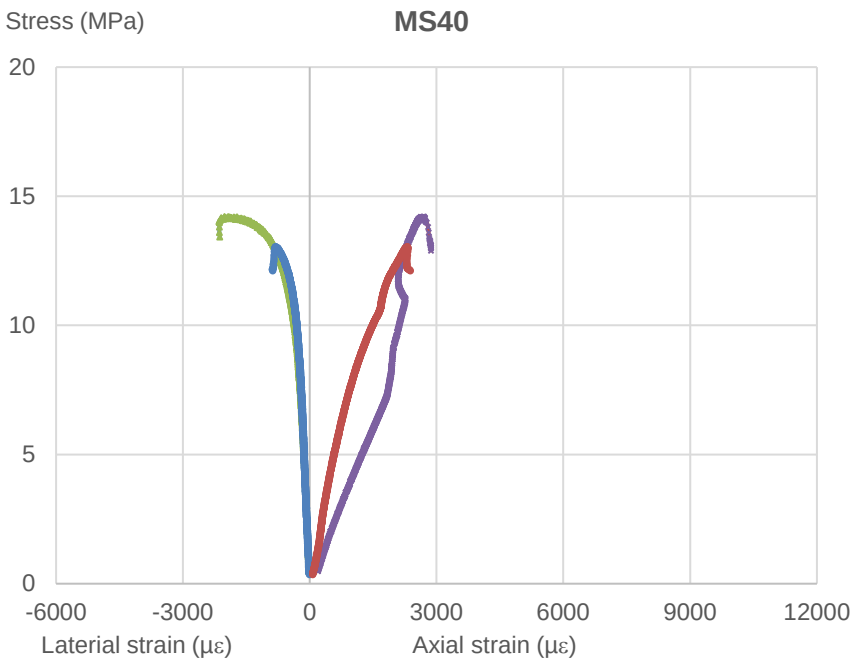

Figure 9.17. Stress-strain behaviour of MS40 paste sample

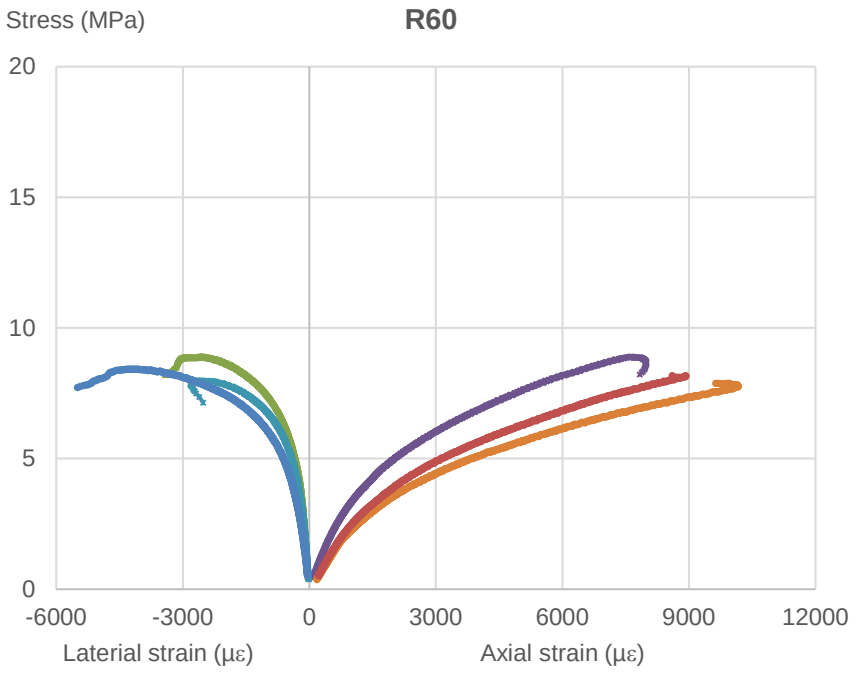

Figure 9.18. Stress-strain behaviour of R60 paste sample

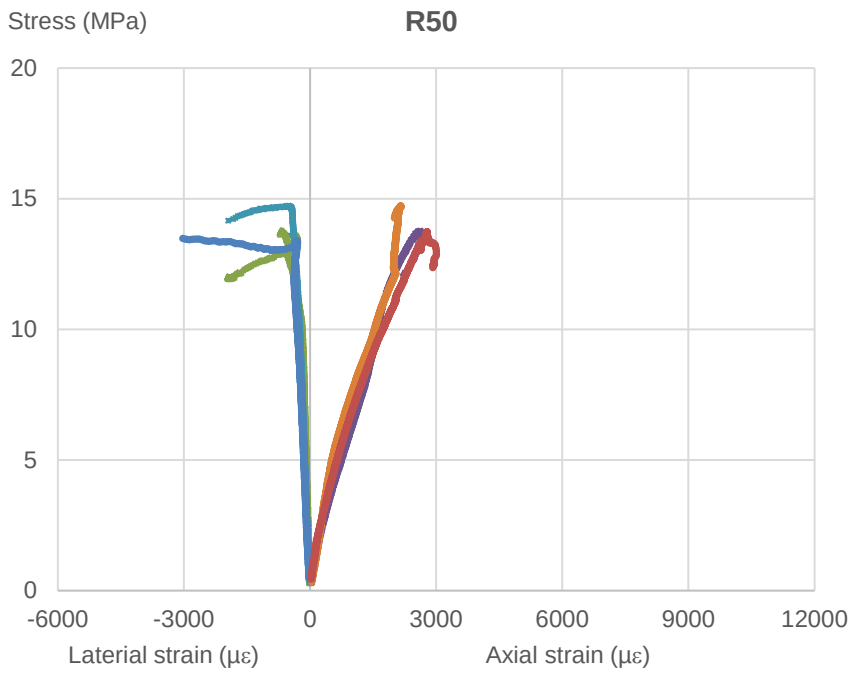

Figure 9.19. Stress-strain behaviour of R50 paste sample

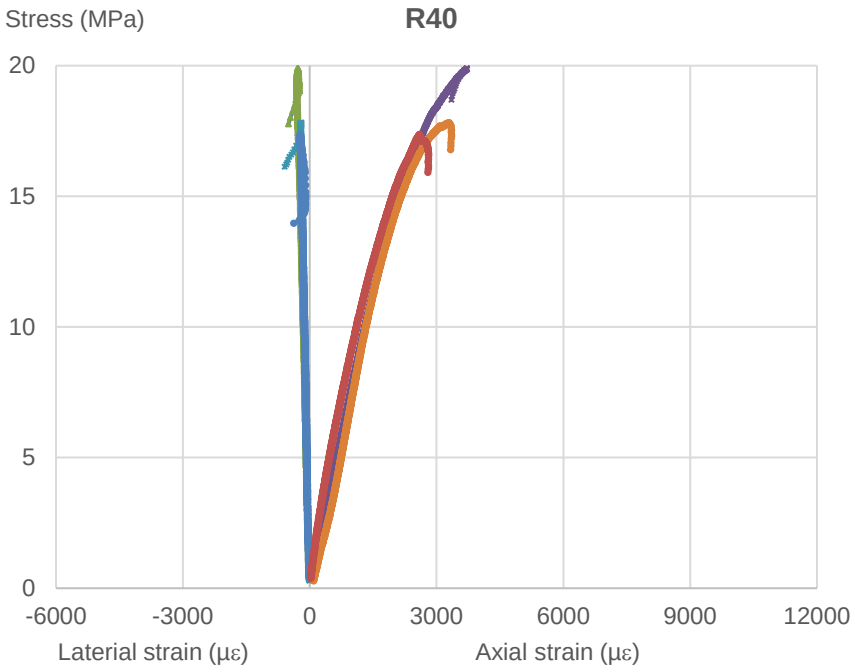

Figure 9.20. Stress-strain behaviour of R40 paste sample

9.3.7. Poisson's ratios

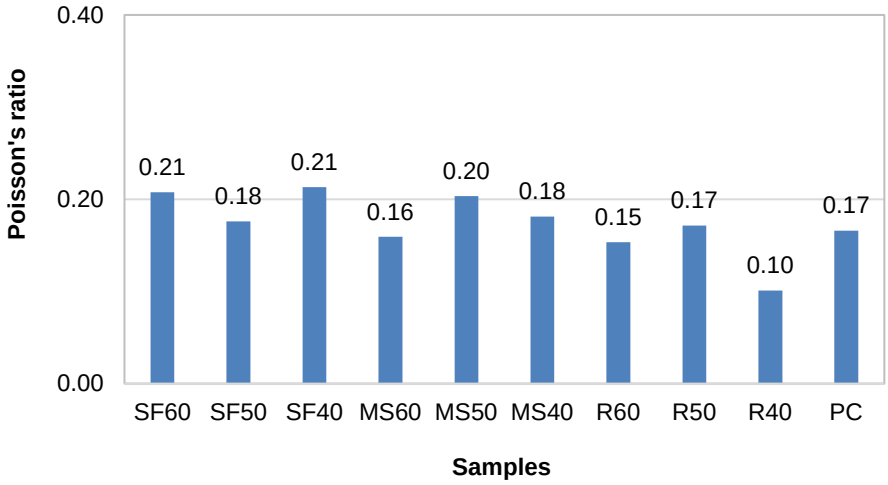

Figure 9.21. Poisson's ratios of M-S-H and PC paste samples

Figure 9.21 presents Poisson's ratios of M-S-H pastes compared to PC samples. Various binder compositions result in different Poisson's ratios as for M-S-H samples. M-SF samples have Poisson's ratios slightly higher than M-MS samples with the highest value of 0.21. The M-RHA samples have lowest Poisson's ratios compared to all other samples in which R40 mixture only obtains a Poisson's ratio of 0.10. In average, M-S-H binders have Poisson's ratio of 0.17, which is similar to the control PC sample.

9.4. CONCLUSIONS

The stress-strain relationship of M-S-H cement pastes strongly depends on the source of silica and binder compositions. Compressive strengths of M-S-H cement pastes using SF, MS, and RHA are generally lower than PC. For paste samples of a fixed w/b of 0.45, the lower silica content in a range of 40-60% of the binder leads to higher compressive strength.

At the low range of stress up to 40% of the compressive strength, MgO/SF ratios have a significant influence on the stress-strain behaviour of the paste and the concrete which may result in different stress-strain behaviours including both linear and non-linear responses. The selection of suitable binder composition may result in a more desirable stress-strain behaviour, similar in shape to PC.

Modulus of elasticity is highly influenced by the compressive strength. The higher compressive strength results in the higher modulus of elasticity for M-S-H binders and PC.

MOEs of M-S-H pastes samples are lower than PC, possibly due to the slow strength development of M-S-H binders. Also, the increase in nonlinearity after elastic range shows the high deformation of M-S-H cement pastes. Further studies are recommended to improve the MOEs of M-S-H cementitious materials for structural applications.

Although having a lower MOEs and a high degree of non-linearity, M-S-H cement pastes have Poisson's ratios comparable to PC.

9.5. REFERENCES

ASTM (2002) C 469: Standard test method for static modulus of elasticity and Poisson's ratio of concrete in compression. ASTM International, West Conshohocken, PA, USA.

Jin F, Gu K, Abdollahzadeh A and Al-Tabbaa A (2013) Effects of different reactive MgOs on the hydration of MgO-activated GGBS paste. Journal of Materials in Civil Engineering **27(7)**: B4014001

Li Z, Zhang T, Hu J, Tang Y, Niu Y, Wei J and Yu Q (2014) Characterization of reaction products and reaction process of $MgO–SiO_2–H_2O$ system at room temperature. Construction and Building Materials **61**: 252-259.

Lothenbach B, Nied D, L'Hopital E, Achiedo G and Dauzeres A (2015) Magnesium and calcium silicate hydrates. Cem. Concr. Res. **77**: 60–68.

Mármol G, Savastano H, Tashima MM and Provis JL (2016) Optimization of the $MgO\text{-}SiO_2$ binding system for fiber-cement production with cellulosic reinforcing elements. Materials & Design **105**: 251-261.

Nied D, Enemark-Rasmussen K, L'Hopital E, Skibsted J and Lothenbach B (2016) Properties of magnesium silicate hydrates (M-S-H). Cement and Concrete Research **79**: 323-332.

Pacheco-Torgal F, Cabeza LF, Labrincha J and De Magalhaes AG (2014) Eco-efficient construction and building materials: life cycle assessment (LCA), eco-labelling and case studies. Woodhead Publishing, p 226.

Tran HM and Scott A (2017) Strength and workability of magnesium silicate hydrate binder systems. Construction and Building Materials **131**: 526-535.

Walling S A, Kinoshita H, Bernal S A, Colliera N C and Provis JL (2015) Structure and properties of binder gels formed in the system Mg(OH)2–SiO_2–H_2O for immobilisation of Magnox sludge. The Royal Society of Chemistry, Dalton Trans. **44**: 8126–8137.

Wei JX, Chen YM, Li YX (2006) The Reaction Mechanism between MgO and Microsilica at Room Temperature. Journal of Wuhan University of Technology - Mater. Sci. Ed. **21(2)**: 88-91.

Zhang T, Vandeperre LJ and Cheeseman CR (2012) Magnesium-silicate-hydrate cements for encapsulating problematic aluminium containing wastes. Journal of Sustainable Cement-Based Materials **1 (1-2)**: 34-45.

Zhang T, Vandeperre LJ and Cheeseman CR (2014) Formation of magnesium silicate hydrate (M-S-H) cement pastes using sodium hexametaphosphate. Cement and Concrete Research **65**: 8–14.

CHAPTER 10
CONCLUSIONS AND RECCOMMENDATIONS ON FUTURE STUDIES

This research on M-S-H binder systems has been carried out with the purpose of developing new cementitious materials focussed on sustainable development requirements in the context of reducing the negative impact of cement production to the environment. This work includes extensive experimental programmes that have yielded valuable results for a variety of related topics which are of fundamental importance for the application of M-S-H binders. The research findings have been analyzed and closed a number of current research gaps, and also give directions for future studies of the M-S-H binders, which have only been developed as a cementitious material since the last decade (2006). Below is a summary of the main contributions of the thesis arranged in the order of the presented chapters. The final section provides a recommendation for future research directions for further understanding and improvement of M-S-H cement materials.

Characteristics of M-S-H binder constituents

The MgO and silica sources used in this study were commercially available in large scale to the construction industry, so they can be used in practice if the required engineering properties are met. The selected magnesium oxide had MgO content of above 70%. The silica sources of silica fume, natural pozzolan and rice husk ash all had SiO_2 content of over 80%. The fly ash had the lowest silica content of approximately 50%. Each MgO and amorphous silica source used for M-S-H binders had distinct features of chemical composition, particle size, shape, texture and porosity. The material sources influenced both fresh and hardened cement paste, mortar and concrete and led to very different material properties of the resulting binders such as reaction mechanism, strength and microstructure. The details of the various properties and the effect of silica source on those properties are dicussed in the following sections.

10.1. Hydration products and microstructures of M-S-H binder systems (Objectives 1 -i, ii)

XRD spectra was used to explain the hydration process and the hydration products of M-S-H cement over a long-term curing period up to 365 days. The hydration process showed a combination of two reaction mechanisms. The first stage involved the hydration of reactive MgO, followed by the formation of M-S-H as a reaction between brucite (hydrated MgO) and amorphous

silica in MgO-silica. The hydration of MgO is completed within about 7 days for the selected MgO source. The reactions to form M-S-H are not clearly shown by XRD peaks of M-S-H at the age of 7 days, but it is confirmed by the intensity reduction of XRD peaks of MgO and $Mg(OH)_2$. The formation of M-S-H is clearly visible in the period of 28-90 days. The reaction mechanism shows the existence of brucite as a primary hydration product in the binders, at least up to 28 days age. The second stage is the formation of M-S-H binding phases in which M-S-H will gradually replace the brucite which is associated with an increase in strength. The slow hydration process of forming M-S-H strongly affects the strength development of M-S-H at early ages.

The MgO/SiO_2 ratios significantly affect the hydration products. The MgO/SiO_2 molar ratio of 1.0 (40/60 by mass) appears ideal for the formation of M-S-H with a complete reaction of hydrated magnesium oxide and amorphous silica to form M-S-H gel over 90 days curing period. MgO/SiO_2 molar ratios higher than 1.50 (50/50 by mass) result in residual brucite in the mixture even after long-term curing. Silica sources with different material reactivity, purity and particle sizes also have a strong effect on the hydration products. SF, MS, and RHA have high reactivity to activate hydrated MgO in M-S-H binder systems. However, the formation of M-S-H phases in M-FA systems is negligible due to the low reactivity and high pH of FA. The design of M-S-H binder systems is, therefore, complicated due to the influence of silica sources.

By using SEM, the microstructure of M-S-H cement pastes have been investigated and compared to PC. The very porous structure of M-S-H pastes have been found, basically due to the high porosity of reactive MgO and silica, especially silica fume with ultrafine particle size and RHA with porous microstructure due to being calcined at low temperatures. The SEM images over the time also reflect the microstructure change to increase the homogeneity of the cement pastes due to the formation of M-S-H phases. The SEM images show the effect of MgO/SiO_2 ratio and material sources on the hydration process. Residual brucite is clearly observed when the MgO content increases in the binder composition. In addition, fly ash is regarded as a less reactive source of silica as found almost unreacted after a long-term curing duration.

The SEM/EDS analysis is able to give additional information on the formation of hydration products over the time by quantifying the elements on the surface of the samples. M-S-H binding phases are readily formed with highly reactive silica (SF, MS, RHA). The amount of M-S-H in cement pastes gradually increases and is proportional to the consumption of brucite and silica. For M-FA mixtures, the Mg/Si ratio is very high, showing the poor distribution of SiO_2 in the mixture, and therefore the formation of M-S-H is negligible. The EDS analysis well agrees with XRD results in reflecting the reaction mechanisms of the formation of M-S-H. The Mg/Si molar ratios

of M-S-H binding phases are found to be in between 1.0 to 1.50, which are consistent with reported results in the literature.

10.2. Pore solution analysis of M-S-H binder systesms (Objectives 1 -iii, iv)

The pore solution analysis represents a significant contribution of this study as no other similar work has been found in the literature. Knowledge of the chemical composition of the cement pore solution is essential as it reflects the hydration process and and the durability of hydrate phases over the time. In addition, the understanding of pH and ion concentrations in the pore solution is useful for the evaluation of the corrosion risk if steel reinforcement is used in the structures. A high pressure device was built at University of Canterbury to extract the pore solutions. Such device was successfully applied to the paste samples prepared with w/c of 0.60 to obtain sufficient pore solutions for the analysis. Mixtures contain reactive magnesium oxide and each source of silica including silica fume (SF), natural microsilica (MS), rice husk ash (RHA) and fly ash (FA) with MgO/silica ratios varying in between 40-60 weight %.

M-S-H binders are naturally alkaline in which the pH of the pore solutions strongly depends on the reactivity and alkalis content of the raw materials. The typical trend of the pH development of M-S-H binder systems was a fairly rapid initial decrease over the first few days followed by a more gradual decrease over time during 90 days testing period. SF, MS, or RHA mixed with MgO results in pH at 2 days age in the range of 10.50 – 11.70 followed by a pH reduction to below 10.50 at 90 days. M-FA mixtures had a higher pH in the pore solutions of above 11.00 at all testing ages due to the high content of impurities including sodium, potassium and calcium compounds. The ICP-MS analysis showed the dominant ions available in the M-S-H binders were sodium, potassium, calcium, magnesium and silicon with the concentrations strongly influenced by the pH and solubility of the binder constituents. The pH and ion concentrations also indicate the formation of M-S-H phases in mixtures of MgO with different silica sources. The reaction mechanism reveals the increase in magnesium concentrations along with the decrease in silicon concentrations under the low pH environment. The highly reactive silica sources such as SF, MS, RHA are vital for the formation of M-S-H phases while fly ash appears not to react with reactive MgO in M-S-H binder systems.

10.3. Optimization of strength and workability of MgO-silica fume mixtures (Objectives 2 – v to vii)

Based on previous studies, low strength and poor workability are among the most common challenges of M-S-H cement compared to PC. However, the experimental work in this study has shown significant improvements to the workability of M-S-H cementitious materials. One of the

main reasons of the high w/c ratio is related to the very low bulk specific gravity of amorphous silica which results in an increase in the w/c ratios. The porous structure of materials such as rice husk ash and the ultra-fine particle sizes of silica fume and MS require high water demand. Moreover, the angular shape of ground materials is detrimental for the workability. To improve the workability, experimental results have confirmed the effective water reduction of polymer-based superplasticizers. It is now feasible to achieve workable mixes using M-S-H binders with w/c lower than 0.40.

Compressive strength is probably the most important property of construction materials, especially for structural applications. This research project has studied binary systems of MgO-silica as a basis for strength capacity of M-S-H binders and it is possible to produce cement pastes and mortars using MgO-silica mixtures to obtain 28-day strength of up to 43.7 MPa, which can be sufficient for a wide range of structures. In addition, a significant improvement to the compressive strength was observed when quartz fillers were added into produce a ternary systems. Quartz fillers play a very important role in improving the microstructure, packing density, and the dispersion of MgO and silica in ternary binder systems (MgO-silica-quartz fillers). Quartz fillers were highly effective at improving the strength and workability of M-S-H cement. The highest compressive strength results from the optimization of M-S-H binder composition was approximately 90 MPa. This high strength confirms the high strength capacity of M-S-H cement which can be widely used for construction materials.

10.4. Strength development of M-S-H binders with different silica sources and under different curing conditions (Objectives 2 – viii, ix)

Although a compressive strength of approximately 90 MPa was achieved, M-S-H binders contain very high content of amorphous silica and therefore may be sensitive to different curing regimes. For this reason, an experimental programme was conducted to characterize the effects of curing conditions and different sources of materials on the strength development of the M-S-H cementitious materials over a long-term curing duration up to 365 days.

In general, water curing is crucial for the hydration process of PC. Surprisingly, M-S-H samples cured at ambient conditions achieved higher strength than PC samples at the ages of 28, 90, and 365 days, despite a lower strength at 7 days age. On the other hand, strengths of M-S-H samples cured in water were significantly lower than those of Portland cement samples. It is found that the water curing duration had a large influence on the strength development of M-S-H binders in which the water curing with up to 28 days age resulting in the highest long-term strength of over 70 MPa at 365 days age. The water curing longer than 90 days reduced long term 365-day strengths of M-SF mixtures. Heated treatment also had a significant influence on the strength

development of M-S-H binder mortar mixtures. Heated treatment for 1-3 days effectively increases early strengths for M-S-H binders, however, reduced long-term strengths over 90 days. Although heated treatment might be an effective method to improve the early strengths of M-S-H binders, the temperature and heating duration should be carefully selected to avoid negative influences on the long-term strengths.

The source of silica had a strong influence on the strength and microstructure of the hardened M-S-H pastes due to the variation of reactivity, morphology and the material fineness. To compare four silica sources, it can be seen that the reactivity plays a key role in the compressive strengths. SF had a high reactivity with ultra-fine particles size resultling in the highest strengths while FA results in very low strengths as a result of the low reactivity. As previously noted, water curing adversely affected the long-term strength development of M-SF mixtures. However, when using MS and RHA the strength continued to develop over the investigation period.

The experimental programme also compared strengths of hydration products of MgO-silica mixtures including M-S-H binding phases and brucite. It is shown that the brucite formed as the weak biding phases with very low strengths while the M-S-H gel obtain much higher strengths and can be regarded as the main binding phases to develop strengths in M-S-H binder systems. The tests over the long-term up to 365 days also revealed the slow strength development of M-S-H binders which probably resulted from the slow chemical reactions between brucite and silica to form M-S-H binding phases. While PC samples develop most of their strength before 28 days age, the M-S-H binders obtain a significant portion of their strength between 28 and 90 days curing period.

10.5. Mechanical and durability-related properties of concrete using M-S-H binders. (Objectives 2 – x, xi, Objective 3 - xii)

Production and testing of concrete samples using M-S-H binders is essential for the purpose of PC replacement in a large scale. Therefore, an experimental programme was performed to study the important mechanical and durability properties of concrete samples. Concrete using M-S-H binders can achieve normal strength of over 40 MPa for a wide range of structural applications. However, the tensile strength of M-S-H concrete is relatively low at approximately 3.5 MPa. It may be possible to improve this low tensile strength by using steel or fiber reinforcement, but this was not specifically investigated in this study. There are some options to reduce corrosion risk due to the low pH if steel reinforcement is incorporated in M-S-H binder systems. However, the suitability of using stainless steel, corrosion inhibitors or cathode protection methods should be carefully investigated in future studies. The elastic modulus is another important characteristic related to the deformation of concrete structures. In this study, stress-strain behaviors of M-S-H

cement pastes and concrete samples have been tested. The results show that M-S-H cementitious materials have lower elastic moduli than control samples using PC.

Some basic durability-related properties of M-S-H concrete such as oxygen permeability and porosity have been investigated in which M-S-H concrete shows higher porosity and oxygen permeability compared to PC concrete. Also, it is unusual that the oxygen permeability of M-S-H concrete increased over the time of the hydration process during the formation of the M-S-H binding phases. This unexpected phenomenon of M-S-H concrete is very different from that of PC when the formation of hydration products can fill the capillary pores to result in a denser cement paste with a lower permeability.

To improve the mechanical and durability properties of M-S-H concrete, quartz fillers have been introduced in ternary systems of MgO-silica-quartz fillers. With 10% of M-S-H binder replacement, quartz fillers significantly improve microstructures and hydration process as well as reduce the porosity of the pastes. Accordingly, quartz fillers increased compressive strength, tensile strength and elastic modulus of the concrete samples. The successful production of normal strength concrete of over 40 MPa has shown the potential of using the developing M-S-H binders in the large scale for the benefits to the environment.

10.6. Reccommendations and future research directions

This thesis has thoroughly studied the engineering properties of M-S-H binder systems and shown the potential to use this new material in construction industry. Although important progress has been made, it can be seen that there are still a number of challenges in the developing M-S-H binders and future studies are recommended to achieve desirable properties of this binder in practice. Key issues in future reseach directions may include:

The search for new material sources of reactive MgO and reactive silica is necessary to utilize different sources of material to achieve greater environmental benefits. New technologies are crucial to produce high quality and cost-competitive material sources for PC replacement in the near future.

Although adequate workability has been achieved with M-S-H binders, the new binder still requires an increased amount of mixing water and superplasticizer to maintain its workability. Therefore, it is necessary to study additional solutions to further improve the workability of M-S-H cement, especially for structural applications in large scale.

The quartz fillers result in improved microstructure and mechanical properties of M-S-H binders. Thus, effects of different fillers and the optimization of fillers should be studied to develop multi-

component systems containing reactive MgO and silica. It is recommended that microstructural analysis on the actual mortar and concrete samples incorporated fillers should be further studied to be able to establish an accurate correlation between the mechanical tests and microstructure.

The experimental programmes of M-S-H cementitious materials in this thesis were conducted for a curing duration up to 365 days age. There are some cases where the long-term strengths of water-cured M-S-H samples decreased after 90 days age. It is also unfavorable that the M-S-H concrete showed increasing permeability over the time. Future studies of properties of M-S-H binders in the long-term up to 365 days and longer are therefore necessary for a full understanding and finding of solutions for those limitations of M-S-H binder systems.

A tremendous experimental programme has been carried out in this research. Yet, the analysis of hydration kinetics, the quantification of hydration products, and the analysis of the chemical structure of hydration products is strongly recommended to provide useful information to complement the existing findings. Other research interest in all aspects of M-S-H binders is enrouraged to improve the quality of the raw materials, the microstructures, the mechanical properties and durability of M-S-H binders. The contribution of this thesis and future studies will play a key role for the use of M-S-H cement in practice as a sustainable construction material.

Appendix A (Chapter 2)

A.1. Ultra-high performance concrete (UHPC) approach

Mix proportioning methods of Reactive Powder Concrete (RPC) and Ultra-high performance concrete (UHPC) have been studied extensively in the literature. One of the first reported mix designs is the development of RPC by Richard and Cheyrezy (1994) in which the produced concrete achieved compressive strength of 170-230 MPa with heat-treatment up to 90^{o}C.

In general, the key principles of RPC concrete in comparison to other PC concrete are:

- Enhancement of the homogeneity by total elimination of coarse aggregate. Aggregates include only fine sand with a maximum particle size of 400-600μm.
- Enhancement of compacted density by elaborate selection of granular gradation.
- Reducing water to binder ratio to a minimum demand in use of high content of high-range water reducer.
- Enhancement of microstructure by temperature curing and adding reactive silica (crushed quartz, silica fume and other pozzolanic materials).
- Enhancement of ductility by integration of fibers in the concrete matrix.

Numerous studies have been conducted towards the development of RPC/UHPC family of concrete. Summary of mix proportions of RPC/UHPC in the previous studies is presented in Table A1. It is commonly accepted that there are no widely agreed specific and scientific proportioning techniques that result in reliable and expected mechanical properties as seen in the conventional concrete mix design. However, it can be seen that majority of the mixtures resulted in high strength require high cementitious materials content (700-1000 kg cement) in addition to low water to binder ratio. The pozzolanic reaction is utilized by the addition of siliceous materials (silica fume at 25-33 wt.% and quartz powder at 0-39 wt.% of cement). The recommended aggregate content varies substantially in which aggregate/cement ratio is as low at 0.49 in CEMTEC concrete (Rossil et al., 2005) or as high as 1.75 in Ductal concrete (Graybeal, 2006). The suggested optimal aggregate/binder ratios are inconsistent and varies in a wide range in between 1.0 and 1.5 (Richard and Cheyrezy, 1995; Park et al., 2008; Wille et al., 2012; Rangaraju et al., 2014).

In New Zealand context, there are few publications on reactive powder concrete as no expertise on this type of material had been developed until 2000 (Yang, 2000). The early study on the manufacturing of RPC using common New Zealand materials was conducted by Yang (2000) with compressive strength achieved at 100-117 MPa. One of the most recent studies was conducted by Lee and Chrisholm (2005) confirmed the success of production of RPC with both local and

commercial materials in New Zealand with compressive strength of up to 211 MPa, except the unsuccessful replacement of silica fume by a local pozzolan (Microsilica 600) which obtained compressive strength of only 43-84 MPa.

The key principles of UHPC approach have considerably improved mechanical properties and durability of UHPC compared to normal PC. The high strength and durability of UHPC, in conjunction with the similarity of the two binder systems (consisting of high microfine siliceous materials content), indicates potential applications of UHPC mix proportioning, mixing and curing method to improve properties of M-S-H binder systems.

Table A.1. Typical UHPC compositions and compressive strength

References	Unit	PC	Silica fume	Aggregate		Crushed quartz / Fillers	Fiber	Max w/b (PC + SF)	Super-plasticizer kg/%/litre	Water kg/m3	Comp. strength Different curing regimes
				Type	Mass/ Ratio						
Aydin and Baradan (2013)	Mass (kg/m3)	720	180	Quartz, dmax=3mm	1278.5	-	117.8	0.17	50	123	176.1-214.6
Aydin et al. (2010)	Mass (kg/m3)	940	282	Quartz, dmax=4mm	1000	200	234	0.13	43 (litre)	125	170-200
Aydin et al. (2010)	Mass (kg/m3)	940	282	Lime-stone, dmax=4mm	960	-	234	0.13	43 (litre)	125	180-200
Blais and Couture (1999)	Mass (kg/m3)	710	230	silica sand	1010	210	190	0.21	19 (litre)	200	200
Bonneau et al. (1997)	Mass (kg/m3)	695-705	225-230	Quartz, dmean=300 µm	990-1010	210 dmean=15µm	0-140	0.20-0.21	2%	-	150-217
Charron et al. (2007)	Mass (kg/m3)	1051	273	d_{max}=0.5 mm	733	-	468	0.12	35	165	168
Cheyrezy (1999)	Mass (kg/m3)	710	230	Fine sand, d_{max} =1mm	1020	215	160	0.15	10	140	200
Collepardi et al. (1997)	Mass (kg/m3)	665-847	166-212	Quartz + Coarse, d=0-8mm	1146-1383	-	188-189	0.18-0.23	12.8-12.9 (solid)	192-195	130-150
Collepardi et al. (1997)	Mass (kg/m3)	933-937	234-235	Quartz + Coarse, d=0-8mm	0-1031	-	187	0.18	12.7 (solid)	200-215	160-180
Collepardi et al. (1997)	Mass (kg/m3)	754-934	189-234	Quartz + Coarse, d=0-8mm	1029-1252	-	187-188	0.18-0.22	12.7-12.8 (solid)	202-215	140-160
Corinaldesi and Moriconi (2012)	Mass (kg/m3)	960	240	Fine, d≤100 µm	960	-	192	0.16-0.26	24 (dry mass)	196-306	110-156
Dugat et al. (1996)	Mass (kg/m3)	950	237	Silica sand, d50=250µm	997	-	146 L=13mm	0.15	16 (solid)	180	194-203
Graybeal and Hartmann (2003)	(%)	1.0	0.33	Fine sand, d=0-0.6mm	1.43	0.30	0.22	0.15	4.3%, Glenium 3000NS	-	124-193

Graybeal (2006)	Mass (kg/m3)	712.0	231	-	1020	211	156	0.12	30.7, Glenium 3000NS	109	126
Habel et al. (2006)	Mass (kg/m3)	1050	275	Quartz, d≤500 μm	730	-	470	0.14	35	190	160
HDR (2002)	(%)	37.0	9	Quartz	41	-	6% mass	0.18	2.00%	-	160
Kamal et al.(2013)	(%)	874.0	97.00	Silica sand, FM=2.72	1012.00	-	-	0.30	0.50%	291	127
Larrard and Sedran (1994)	Mass (kg/m3)	1080.6	334.2	Quartz, dmax=0.4mm	813.2		-	0.14		198.2	164.9-237.9
Larrard and Sedran (1994)	Mass (kg/m3)	868	269.3	Quartz, dmax=0.4mm	1088.3		-	0.17		191.3	224
Larrard and Sedran (1994)	Mass (kg/m3)	1682.8	420.7		0		-	0.13		274.5	244.9
Lee and Chisholm (2005)	(%)	1	0.25	Silica/ River sand, d=0.15-2.36mm	1.1	0	0.175	0.11-0.21	0.74-0.84 % (solids)	-	128-197
	(%)	1	0.23	Silica/ River sand, d=0.15-2.36mm	1.1	0.39 d50≈20μm	0.175	0.17-0.26	1.61-2.49 % (solids)	-	162-204
Máca (2013)	Mass (kg/m3)	800	200	Fine sand, d=0.1-0.8mm	1136	200	0-160	0.18	40 (liquid)	176	132.4-151.7
Máca (2012)	(%)	1	0.25	Fine sand, d=0.1-0.8mm	1.22	0.25 Glass powder	0-3% volume	0.22	2-5 % Viscocrete (liquid)	-	140-180
Monosi et al. (2000)	Mass (kg/m3)	928.7	232	Lime-stone, d=0.1-8mm	1021.6	-	185.7	0.21	12.6 (solid)	241.4	175-185
Monosi et al. (2000)	Mass (kg/m3)	930	232.5	Quartz sand, d=0.1-0.4mm	1023	-	186	0.20	12.6 (solid)	232.5	175-200
Rangaraju et al. (2014)	(%)	1.0	0.1-0.4	Normal sand, d=0.075-2.36mm	0.95-1.25	-	-	0.225	1.5 %, Melfux 6681F (solids)	-	80-100
Richard and Cheyrezy (1995)	(%)	1	0.25	Quartz, d≤0.6mm	1.1	0	0-0.175	0.15	0.6-1.6% (solids)	-	170
Richard and Cheyrezy (1995)	(%)	1	0.23	Quartz, d≤0.6mm	1.1	0.39 d50=10μm	0-0.175	0.15	0.6-1.6% (solids)	-	230
Richard and Cheyrezy (1994)	Mass (kg/m3)	955	229	Find sand, d=0.15-0.4mm	1051	10	191	0.13	13	153	100.6-230

Rossi et al. (2005): CEMTEC	Mass (kg/m3)	1050.1	268.1	Quartz, d=0-1.0mm	1002.3	-	858	0.16	44 (liquid)	180.3	220
Russell and Graybeal (2013)	Mass (kg/m3)	712.0	231	Find sand	1020	211	156	0.12	30.7	109	140-200
Shaheen and Shrive (2006)	(%)	1.0	0.23	Quartz, d=0.15-0.40mm	1.1	0.39 5-25µm	0.125 Carbon 3mm	0.14-0.15	0.019	-	243-288
So et al. (2015)	Mass (kg/m3)	868	217	Quartz, d=0.15-0.5mm	756	174 (0-45µm)	240	0.19	52 (liquid)	-	145-157
Tam and Tam(2012)	Mass (kg/m3)	761	247	Quartz, d=0.15-0.6mm	1090	226 (10-45µm)	-	0.20	19 (2-5% cement)	202	70.44-210.30
Tam et al. (2010)	Mass (kg/m3)	761	247	Quartz, d=0.15-0.60 mm	1090	226 (10-45µm)	-	0.20	2.5% Visco-Crete 1250NT	202	134.1-145.4
Wille and Boisvert-Cotulio (2015)	(%)	1.0	0.25	Fine+Coarse, d≤12.5mm	1.0-2.0	0.25	-	0.2-0.3	0.03	-	155-200
Wille (2011a)	(%)	1.0	0.25	Mixed Sand, d≤0.80mm	1.01-1.38	0.25 Glass Powder	-	0.18-0.22	0.5-1.14 % (solids)	-	194-246
Wille (2011b)	(%)	1.0	0.25	-	0.92	-	0.22-0.31	0.18-0.20	1.08 % (solids)	-	140-200
Yang (2000)	Mass (kg/m3)	705-740	230-241	Fine sand, d≤0.6mm	1010-954	210-220 (Silica Sand/ greywacke)	-	0.21-0.27	11.6-32.9 (litre) Viscocrere-5	195-255	100.6-161.9
Yazici et al. (2009)	Mass (kg/m3)	830	291	Quartz, d≤3.0mm	977	-	234	0.16	55 (liquid)	151	202-255
Yu et al. (2014b)	Mass (kg/m3)	594.2	24.8 (nano 0.1µm)	Normal sand, d≤2mm	1282.3	265.3 (limestone, d50=10µm)	0-2% volume	0.20	44.2 (liquid)	176.9	99-141.5
Yu et al. (2014a)	Mass (kg/m3)	612.4 - 874.9	43.7	Normal sand, d≤2mm	1273.4	0-262.5 limestone/ quartz, d50=10µm)	0.5-2.5% volume	0.23-0.30	45.9 (liquid)	202.1	142-156
Zdeb (2013)	(%)	1.0	0.20	Quartz	0.81	0.34	-	0.24	0.03	-	194-212

A.2. Particle packing models

Concrete is a mixture of at least three components of water, binder and aggregate. For a given set of materials, variations of those components and other additives directly influence the properties of both fresh and hardened concrete. Numerous studies in the literature have shown the improvement of the fluidity and strength of concrete with a high packing density. The following outlines the key principles of the packing density theory which can be used to optimize the binder composition to increase particle packing for desired mechanical properties and workability of the developing M-S-H binder systems.

A.2.1. Packing density

Packing density of a constituent in a mix is measured by the ratio of solid volume of the particle to the bulk volume occupied by the particles, following the equation:

$$\alpha = \frac{V_p}{V_b} = \frac{\rho_{bulk}}{\rho_\rho}$$

Voids content, is then calculated by the equation:

$$\varepsilon = 1 - \alpha$$

The dry packing density of particles, when measured by mass of particles filled in a container and subjected to a certain compaction condition, can be determined following the formula:

$$\alpha = \frac{m_p}{\rho_\rho V_{container}}$$

Fennis (2012) note that the packing density of concrete aggregates may vary from 0.55 to 0.80. However, the packing density of a mix combined by a series of constituents subjected to a number of variables include packing density and volume fraction of each constituents, particle shape and texture, compaction conditions. There are a number of packing density models applicable to M-S-H binder system which are discussed below.

A.2.2. Continuous particle packing models

Packing density of grades affect produced concrete properties in which maximum strength will be achieved in accordance with a minimal void of the mixture. Numerous studies (Fuller and Thomson, 1907; Adreasen, 1930; Funk and Dinger, 1980) assumed that a continuous grade of all grades between minimum and maximum size existing in the mix with a specific distribution resulted in densest packing. It means that each discrete grade will be mixed with another grade with adjacent size to fill in the void of the larger grade. The broad particle size distribution to infinite small particle size will therefore result in densest particle packing.

In 1907, Fuller and Thomson proposed an empirical relationship of continuous granulation, which is called “Fuller ideal curve”, presented the cumulative finer volume fraction as an exponent function of maximum size diameter, in which a minimal void to be achieve when exponent n equals to 0.5.

$$CPFT = \left(\frac{d}{d_{\max}} \right)^n$$

CPFT - cumulative finer volume fraction

d – particle diameter being considered

d_{max} – maximum particle diameter in the mixture

n – exponent adjusts the curve for fineness or coarseness

As the “Fuller ideal curve” is a simple formula without consideration of particle shape, in 1930 Andreasen recognized that there is always possibility to include finer particles in residual void of a certain curve, in particular the case of aggregates with sharp shape. The exponent was modifier to account for the fineness or coarseness of the grades with. The smaller exponent, the more fineness effect but the exponent will be in the range of 0.21-0.37.

A fundamental problem with those equations above is the assumption of infinitesimal small particles to fill the voids of an infinite distribution, which is not the case. As a lack of small size restriction resulted in inaccuracy, Funker and Dinger (1980) pointed out that both maximum and minimum particle size have influence on the optimal density. The formula was modified with the inclusion of minimum particle d_{min} and an exponent of 0.37 for a better expression of continuous curve, as follows:

$$P(d) = \frac{d^q - d_{\min}^q}{d_{\max}^q - d_{\min}^q}$$

Ideal packing curves according to Fuller, Andreasen and Funk and Dinger are shown in Figure A1. The simple method of ideal curves could be useful for preliminary design as it reflects the ideal proportion of each particle size in the mixture in a way to achieve a high packing density where continuous grade is available.

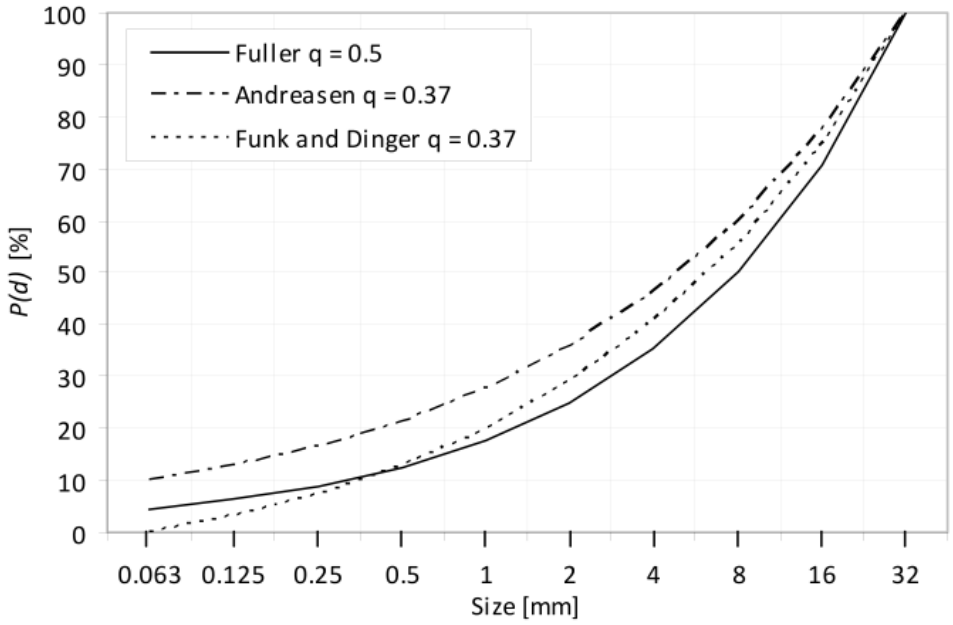

Figure A.1. Ideal packing curves according to Fuller, Andreasen and Funk and Dinger for a maximum particle diameter of 32 mm and a minimum particle diameter of 63 μm (Fennis, 2011).

The advantage of the ideal curves methods are their relative simplicity, being based on a few variables of particle sizes, proportions and fixed exponent. However, without consideration to shape, compression effect, there is always deviation from the real packing density. Also, there is no relation between the ideal curve functions and the real packing density. Since those limitations exist, the ideal curve method needs to be used in conjunction with other optimal techniques of mix proportioning.

A.2.3. Discrete packing models

In contrast to "ideal curves" method, the discrete models including Furnas Model, Linear Particle Packing Model (LPPM), Compressible Packing Model (CPM) consider the packing density of mixture of different sizes. While Furnas model is simple and can only apply for a binary mix, the LPPM and CPM model are more complicated however can apply for multi-component mixture with computer aid programme. The basics of these models are summarized below.

(1) Furnas model for binary mixture

The first discrete packing model was reported to be proposed by Furnas (1929). The Furnas model considers the maximum density of a binary system of fine and coarse grain sizes with $d_1 >> d_2$. Denoting the mutual volume fractions of fine and coarse grains are r_1, $r_2 (r_1+r_2=1)$, the volume fractions of fine and coarse grains in a unit bulk volume are φ_1, φ_2 and the packing densities of individual grains are α_1, α_2, there are two cases of domination of coarse grains ($r_1 >> r_2$) and fine grains ($r_1 << r_2$) in which the packing density of the mixture is determined respectively:

Case 1 ($r_1>>r_2$): In this case, the large particles fill in a unit bulk volume with packing density α_1 as if there is no small particle. The small particles are then filled in the voids between the large particles. The total packing density is calculated by the volume of large particles, plus the volume of small particles in a unit volume.

$$\Phi = \varphi_1 + \varphi_2 = \alpha_1 + \varphi_2 = \frac{\alpha_1}{1 - r_2} = \frac{\alpha_1}{r_1} \quad (1)$$

Case 2 ($r_1<<r_2$): In this case large particles are added in a volume unit of a matrix of small particles. Large particles are separated and there is no void between them. The small particles fill in the rest of unit volume ($1-\varphi_1$) with their maximum packing density α_2.

$$\Phi = \varphi_1 + \varphi_2 = \varphi_1 + (1 - \varphi_1)\alpha_2 = \frac{1}{r_1 + r_2/\alpha_2} \quad (2)$$

There is only one optimum total packing density in which all the voids between large particles are filled by small particles. In this case, the packing densities calculated by formula (1) and (2) equal. In other cases, the minimum value of formula (1) and (2) is the packing density of the mixture.

The Furnas model can be used only for binary system with particle size of $d_1>>d_2$.

(2) Linear packing density model

As Furnas model was limited to binary system, other authors studied and extended the model for polydisperse system. Stovall et al (1986), Larrard and Sedran (1994) proposed linear packing model to determine the maximum packing density of a mix with n classes of grains. The assumptions are the multi-component system comprises n grains size $d_1>>d_2>>d_3>>...>>d_n$; the mutual volume fractions of each pure components are $y_1, y_2, \dots, y_n$ in which $\sum y_i = 1 (i = 1 \text{ to } n)$; each component has packing density denoted by $\alpha_1, \alpha_2, \dots, \alpha_n$ determined as they are packed individually. Also, in linear packing density, the effect of particle size to packing density is considered, by integration of the loosening and wall effect functions. For a t size class of grains ($d_1 = D \geq t \geq d = d_n$), the maximum packing density of the mixture is calculated by:

$$c = \min\left(c(t)\right)$$

$$c(t) = \frac{\alpha(t)}{1 - \int_d^t y(x) f(x/t) dx - [1 - \alpha(t)] \int_t^D y(x) g(t/x) dx}$$

The loosening effect f(z) is caused by particle sizes smaller than t-size class when filled in the void between t-size particles while the wall effect is caused by particle sizes larger than t-size and

reduce packing density of t-size particles. These functions are determined by the following equations:

$$f(z = x/t) = 0.7(1-z) + 0.3(1-z)^{12}$$
$$g(z = t/x) = (1-z)^{1.3}$$

The advance of linear packing density is the ability to apply the model to any mixture of unlimited size and number of monosize classes. This LPPM has shown good correlations in practice to predict optimal proportions of superplasticizer cementitious materials (Larrard and Sedran, 1994).

(3) Compressible packing density model for grain mixtures

The packing density, to its nature, deal with the geometry of the granular materials to determine the maximum and actual packing density of a mix. The three factors affect the density of a mix of grains are listed as the size, the shape of the grains and the packing method.

The compressible packing model (CPM) is the third generation model developed by LCPC and proposed by Larrard (1999). The CPM is the only model accounting for all three main parameters controlling the packing density of a mix. The CPM is able to determine the actual packing density of a polydisperse mix of any size and shape, however, is also considered the most complicated model. Given a mix of n mono classes with particle size d_i (i=1 to n), the procedure to determine actual packing density then requires a number of steps as follows:

Total virtual packing density of the mixture

The difference in the LPPM and CPM model is that instead of using the experimental packing density α(t), the CPM used the virtual packing density of each individual monosize grain β_i to calculate the total virtual packing density. The CPM model has same method of formulating equations as shown in Furnas and LPPM models. The general model derived from simple binary and ternary mix before a generalized equation can be deducted.

In consideration of binary mix of two mono-sized classes, having β_1, β_2 as individual virtual packing density and Φ_1, Φ_2 as partial volume in a unit volume of the mix. The virtual packing density of the mix may be calculated as:

$$\gamma = \Phi_1 + \Phi_2$$

$$y_1 = \frac{\Phi_1}{\Phi_1 + \Phi_2};\ y_2 = \frac{\Phi_2}{\Phi_1 + \Phi_2}$$

In the case of dominance of class 1, the virtual packing density is calculated by:

$$\gamma = \gamma_1 = \beta_1 + \Phi_2 = \frac{\beta_1}{1 - y_2}$$

In the case of dominance of class 2, the virtual packing density is calculated by:

$$\gamma = \gamma_2 = \Phi_1 + \beta_2(1 - \Phi_1) = \frac{\beta_2}{1 - (1 - \beta_2)y_1}$$

Figure A2 illustrated the packing density of monosized grains and mixture. The AB segment depicted the dominance of coarse grain with void filled efficiently by fine and an optimal packing density was obtained at a specific fine content. As the fine content is dominant and exceeded the optimal Figure (segment BC), the packing density decreased proportional with the increase of fine content. Without consideration of dominant class, virtual packing density of any combination of the two classes is then written as:

$$\gamma = \min \gamma_i (1 \le i \le n)$$

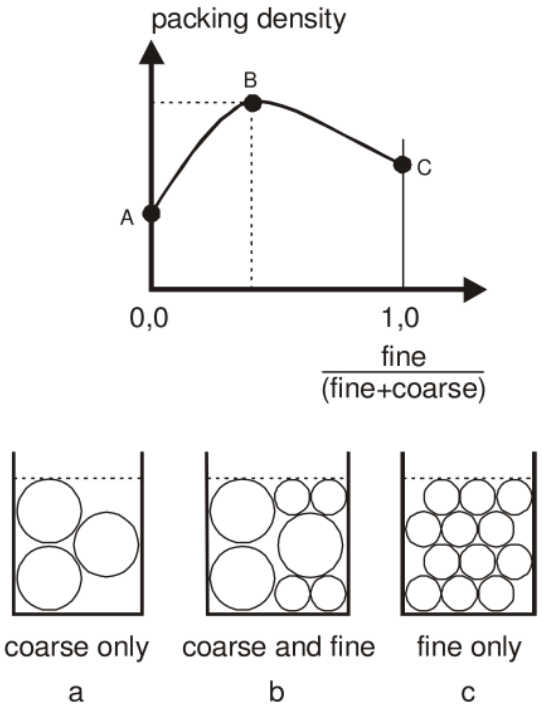

Figure A.2. General case of the packing density of granular mixtures with only coarse (a), only fine (c), and the combined fine and coarse aggregate grains (b) (Marković, 2006).

A general formula to calculate virtual packing density of a mix of n classes (n>2), hence can be written as:

$$\gamma = \gamma_i = \frac{\beta_i}{1 - (1 - \beta_i)\sum_{j=1}^{i-1} y_j - \sum_{j=i+1}^{n} y_j}$$

Where $$\gamma = \min \gamma_i \left(1 \le i \le n\right)$$

In account for the interaction of loosening (opening) and wall-effect, the final formula of γ_i is deducted:

$$\gamma = \min \gamma_i \left(1 \le i \le n\right) = \min\left(\frac{\beta_i}{1 - \sum_{j=1}^{i-1} \left[1 - \beta_i + b_{ij}\beta_i\left(1 - 1/\beta_j\right)\right] y_j - \sum_{j=i+1}^{n} \left[1 - a_{ij}\beta_i / \beta_j\right] y_j} \right)$$

In which the loosening effect and wall effect are introduced by the introduction of a_{ij} and b_{ij} factors, determined by the equations:

$$a_{ij} = \sqrt{1 - \left(1 - d_j/d_i\right)^{1.02}} \text{ and } b_{ij} = 1 - \left(1 - d_i/d_j\right)^{1.50}$$

The virtual (non-random) packing density of each monosize class, β_i, is determined from the relation with experimental packing density of the respective class, α_i. In fact, a mix with a virtual packing density can obtain different actual packing density, depending on the compaction process. The effect of compaction energy, which was not mentioned in the previous model, is proposed by the introduction of compaction factor K. The larger the K factor, the higher actual packing density, expressed by the relation:

$$K = \frac{1}{\beta_i/\alpha_i - 1} \Leftrightarrow \beta_i = \alpha_i\left(1 + 1/K\right)$$

As seen from the equation (1), the K value is required to determine the virtual packing density of each individual component, based on the experimental (actual) packing density. Larrard (1999) suggested K factor for different compacting methods: 4.1 (pouring), 4.5 (dry rodding), 4.75 (vibration), 6.7 (wet compacting), 9 (vibration plus 10 kPa pressure applied).

Actual packing density of polydisperse system

The total virtual packing density only represents a potential maximum packing density in which particles are arranged one by one and this does not occur in practice. However, the highest actual packing density can be determined from maximum virtual packing density in Compressible packing model.

Similar to individual components, actual packing density of the multi-component system depends on the compaction method of the whole multi-component system. Effect of different compaction method, applied to the mix, expressed by the following equation:

$$K = \sum_{i=1}^{n} K_i = \sum_{i=1}^{n} \left(\frac{\Phi_i / \Phi_i^*}{1 - \Phi_i / \Phi_i^*} \right) = \sum_{i=1}^{n} \frac{y_i / \beta_i}{1/\Phi - 1/\gamma_i} \quad (1)$$

As seen from the equation, the actual density Φ can be determined from the pre-determined parameters including solid fractional volumes, virtual packing densities of the pure classes and the mix, and the compaction index K. It is shown that the K factor is proportional with Φ and the higher K will result in better packing density. For a polydisperse system, it is complicated to solve the equation and normally the computer programme is needed.

A.3. Curing of PC concrete containing silica fume

The curing regime is one of particular importance after mixing to ensure adequate mechanical and durable properties of the concrete materials. In the case of high micro-fines and low w/b mixture, the curing effect is even more importance to provide sufficient water for the hydration process. Curing influence both early-age and long term mechanical properties and microstructure of the produced concrete.

Effect of water curing to mechanical properties

In plastic shrinkage cracking as water evaporates from the concrete surface faster than being supplied by bleeding, tensile stresses will develop and ultimately exceed the resistance of still-plastic concrete, results in cracking. It is widely accepted that silica fume concrete has less bleeding and this cause silica fume concrete to be more vulnerable to plastic shrinkage cracking (SFA, 2015).

Continuous protection during placing, finishing and curing is crucial for silica fume concrete. The risk of plastic shrinkage cracking increases with the increase of silica fume content and the reduction in water to binder ratio. Whiting and Detwiler (1988) studied silica fume concrete for bridge decks and suggested that the silica fume content did not affect the cracking if the mixtures were given 7 days of continuous moist curing. It was recommended a minimum 7 days moist curing for silica fume concrete to avoid plastic shrinkage cracking and get the most benefit from silica fume (Holland, 1987; Whiting and Detwiler, 1988).

Appropriate moist curing on compressive strength of hardened silica fume concrete is also critical in which a lack of moisture normally causes detrimental effect. Tountanji and Bayasi (1999) studied silica fume concrete with silica fume content ranged from 10-30% in three curing regimes including air cure, moist cure and steam cure at 80^{o}C. At the test age of 35 days, concrete cured in air with low humidity had a considerably lower compressive strength, compared to samples cured in moist of 100% humidity. Steam cure at 80^{o}C resulted in the highest compressive strength of samples in the experiment. Apart from influence on compressive strength, the author confirmed that curing in high humidity also resulted in a low permeability concrete with greater durability. The similar conclusions were found in a study on influence of dry and wet curing conditions on compressive strength of silica fume concrete (Atis et al., 2005). The comparisons showed that concrete cured at dry condition (65% humidity) achieved 28-day compressive strength of 13% lower than that of curing in 100% humidity ($f'c_{dry} = 0.87f'c_{wet}$). Other important remarks were that the negative effect of dry cure increased with the increase of silica fume replacement ratio and the increase of water to binder ratio.

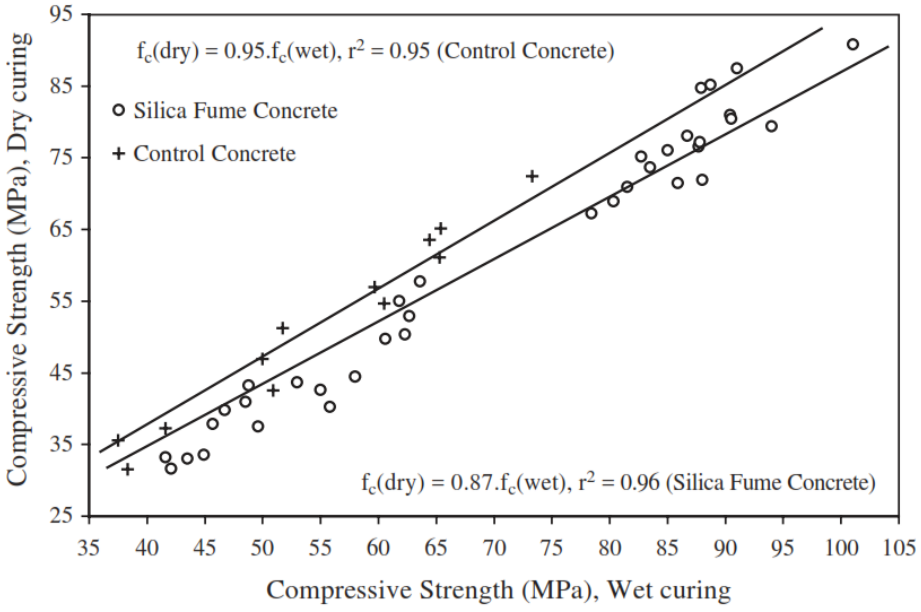

Figure A.3. Relation between dry-cured and wet-cured compressive strength (Atis et al., 2005)

Effect of heated-treatment to microstructure

The heated-treatment of PC concrete has been well-investigated in the literature, but little information on the curing M-S-H concrete has been found. It is useful to outline effect of different temperature cured regimes to UHPC using PC based on different curing temperature as follows:

At ambient temperature (20^{o}C), it is reported that the pozzolanic reaction of silica fume was weak and slow. At higher curing temperature of 50^{o}C-65^{o}C, the pozzolanic reaction rate increased without modifying the microstructure.

Curing temperature at 90^{o}C or higher enabled the modification of microstructures of hydrates as longer amorphous C-S-H chain were formed and pozzolacnic reaction was substantially accelerated (Richard and Cheyrezy, 1995; Cheyreze et al., 1995). The reason was explained that elevated temperature caused increase in SiO_2 solubility, regardless of its amorphous or crystalline forms, resulting in additional quantities of binding gel phase (Zdeb, 2013). In a study by Benezet and Benhassaine (1999) of grinding and pozzolanic reactivity of quartz powder, it was found that the chemical reaction of quartz powder and calcium hydroxide took place at about 100^{o}C. The reaction rate was confirmed to depend chiefly on the sizes and particle distribution. There is a criticle particle size at which smaller particles contributed to the major pozzolanic effect. Benezet and Benhassaine (1999) suggested a critical median d_{50} of 5µm whereas higher mean particle size of 10µm – 25µm was used by Richard and Cheyrezy (1995) and Menzel (1934). Tam and Tam (2012) also confirmed the pozzolanic reaction of both silica fume and crushed quartz at 100^{o}C

curing. The pozzolanic reaction of silica fillers was described in the following equation (Benezet and Benhassaine, 1999):

$$SiO_2 + CaO + H_2O \rightarrow (CaO)_{1.1}(SiO_2) \times H_20$$

Large effects of heated treatment occurred at 200-400°C, demonstrated by crystallization of amorphous cement hydration products ($C_3S_2H_3$) into tobernorite ($C_5S_6H_5$) and xonotlite (C_6S_6H), along with presence of pozzolan and crushed quartz powder to lower C/Si molar ratio in C-S-H gel phases (Cheyrezy et al., 1995).

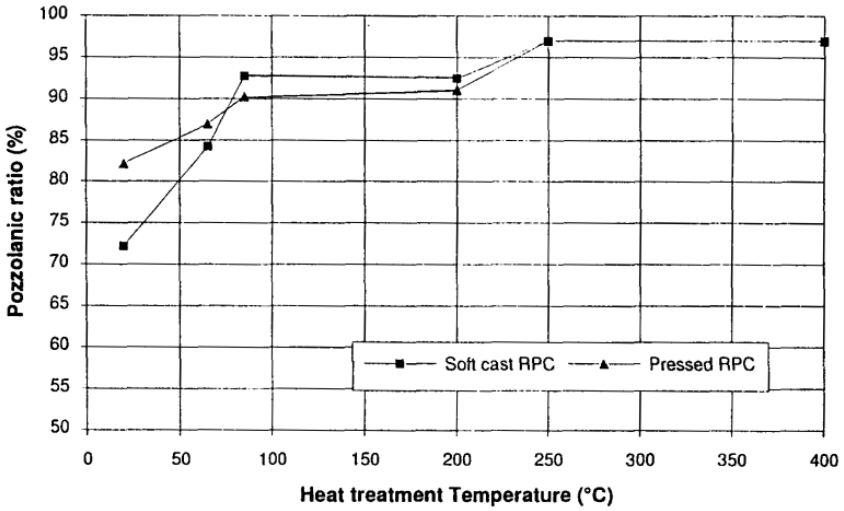

Figure A.4. Pozzolanic ratio versus heat treatment temperature of RPC (Cheyrezy et al., 1995)

The relationship of pozzolanic reaction and temperature was described in figure A4 (Cheyrezy et al, 1995) in which two effective curing temperatures was found at 90°C and 250°C for maximum pozzolanic reaction and microstructure modification. Tam and Tam (2012) described that the hydration product were amorphous below 100°C, the crystallinity started with tobermorite formed at 150°C and became coarse and denser at 200°C, followed by the formation of xonotlite at 250°C. The quality of crystal formation was improved better with longer heating duration while curing temperature increased. However, it should be noted that the micro cracks and voids might be appeared in heated treatment samples without fibers.

Effect of heated-treatment to compressive strength development

Silica fume concrete is more sensitive to curing temperature than ordinary Portland cement concrete, illustrated by greater strength acceleration on condensed silica fume concrete than on control sample without silica fume (Yang, 2000). Strength development would be dependent upon silica fume/cement ratio and temperature range.

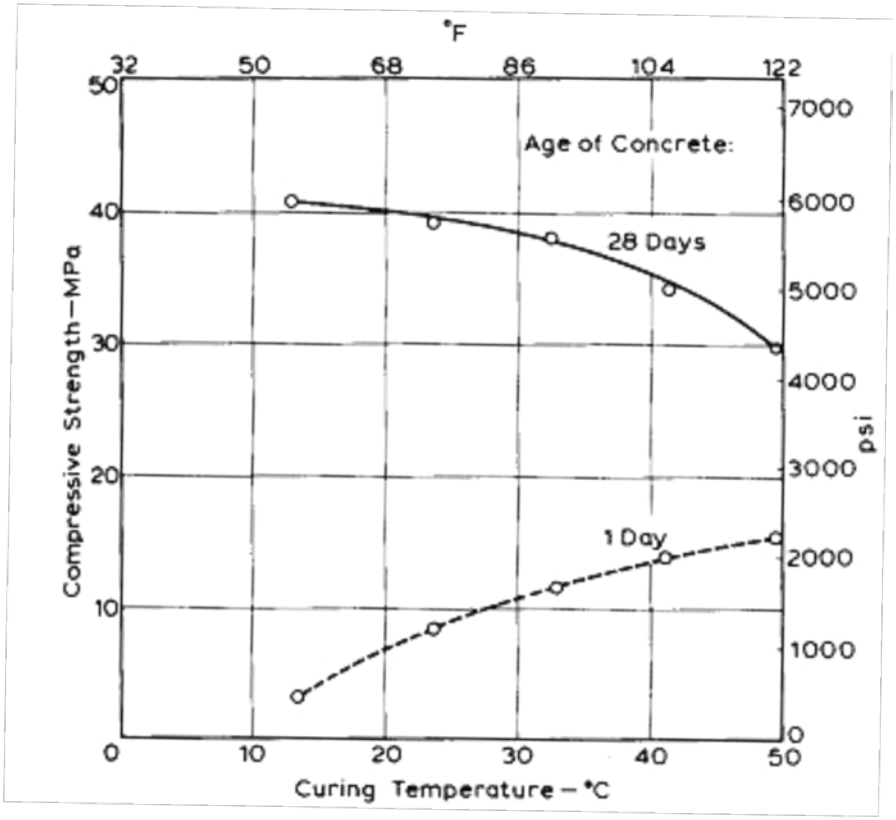

Figure A.5. Effect of curing temperature on concrete strength development (Verbeck and Helmuth, 1968)

Curing at temperatures below 20°C and high silica fume content appeared to retard strength development of condensed silica fume concrete more for control concrete (FIB, 1988). The increase of curing temperature to 35-65°C accelerated pozzolanic reaction of silica fume concrete, consequently increased early strength. An example was that condensed silica fume concrete cured at 50 °C had 1-day strength comparable to a control sample of equivalent proportions cured at standard conditions (FIB, 1988). Verbeck and Helmuth (1968) also showed the effect of different temperatures (10-50°C) on strengths at 1 day and 28 days age (Figure A5). Sabir (1995) reported that the average ratio of 7 and 28 day compressive strengths was up to 97% with 50°C water curing, instead of only 76% with 20°C water curing, whereas the 91 day strengths were not influenced by the two curing temperatures.

On the other hand, Ozyildirim (1998) studied compressive strength of 7% silica fume concrete with moist curing at 4 different temperatures (5, 10, 23 and 38°C). The results shown in figure A6 revealed that curing below 23°C reduced both early and long-term compressive strength, while curing at 38°C had a positive effect on early age strength up to 28 days followed by negative effect

on long-term strength at 1 year age. The reason for long-term strength reduction was well studied in PC concrete by a number of authors and it was widely accepted that high curing temperature (up to 60°C) normally resulted in rapid hydration but retarded subsequent hydration, consequently formed coarse and interconnected pores structure of high porosity (Verbeck and Helmuth, 1968; Goto and Roy, 1981; Kjelsen et al., 1990a,1990b; Acquaye, 2006).

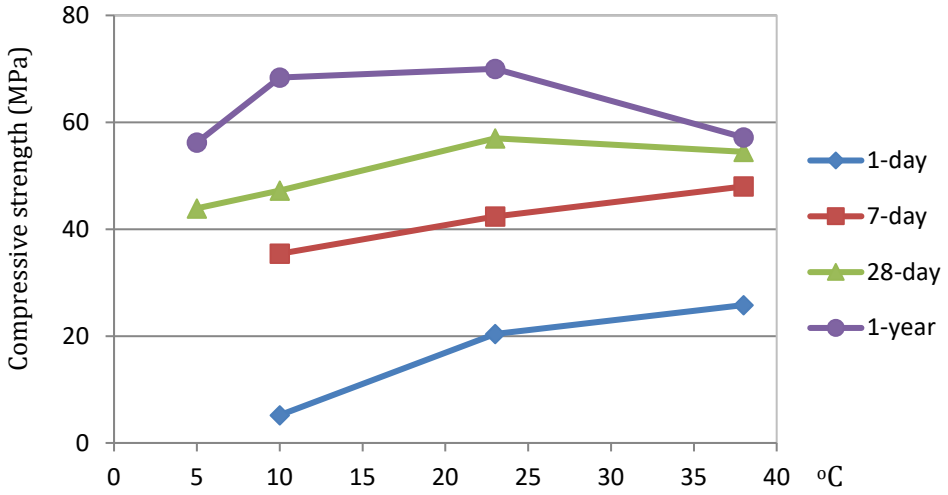

Figure A.6. Effect of temperature curing at 5, 10, 23, and 38°C to PC concrete of 7% silica fume cement replacement (adapted from Ozyildirim (1998)).

Temperature curing of 90°C and higher has been applied particularly to reactive powder and ultra-high performance concrete to improve early and long-term strength (figure A7). Pozzolanic reaction of silica fume is activated by temperature and a gain of 30 % strength is obtained by curing at 90°C during two days (Richard and Cheyrezy, 1994). Yazici et al. (2009) also tested reactive powder concrete containing silica fume of 25% binder under different curing regimes. Compressive strength test at 4 days age of samples demolded at 1 day followed by steam curing at 100°C in 3 days showed an increase of 26%, compared to samples cured in water and tested at 28 days age.

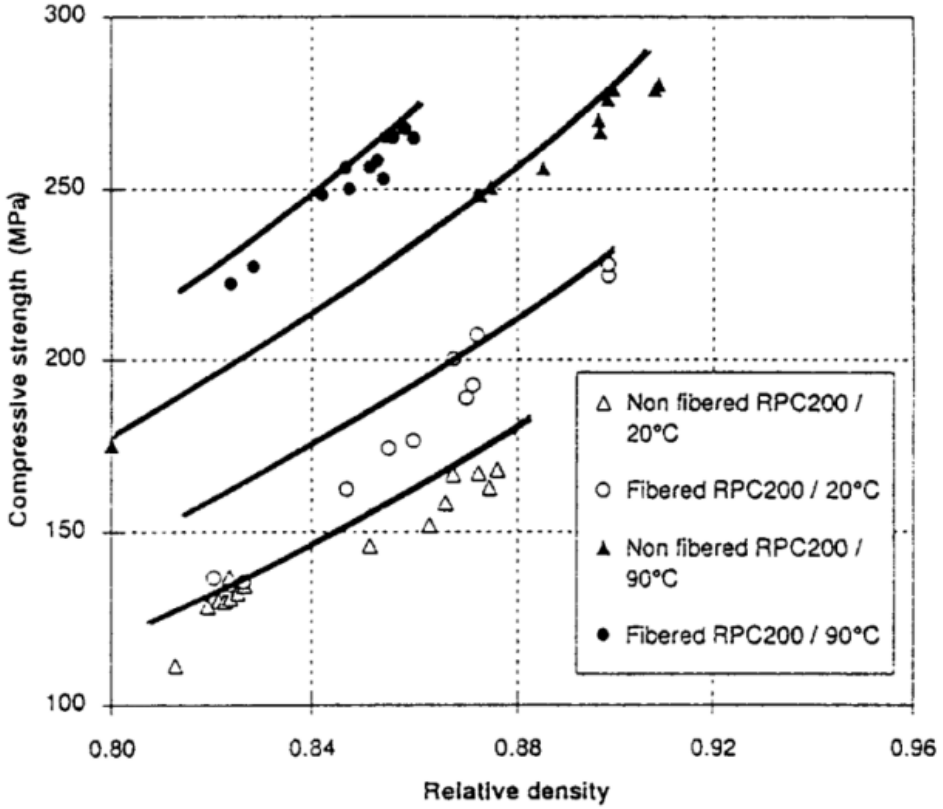

Figure A.7. Optimum strength values obtained for different relative densities and temperature (Richard and Cheyrezy, 1995)

The highest curing temperature was currently applied at 250-400°C. The resulting hydrates were very strong and the microstructure was modified with the formation of higher density crystalline, therefore resulted in rapid strength development. RPC cured at 250-400°C coupled with pre-setting pressurization achieved compressive strength up to 680 MPa (Richard and Cheyrezy, 1995).

Canbaz (2014) studied effect of high temperature on reactive powder concrete in which the concrete was exposed to temperatures ranged from 20 to 900°C for 3 hours after demoulding. The results shown in figure A8 indicated an effective range for the temperature curing and improvement of mechanical properties of concrete. For samples without fiber, the compressive strength increased as temperature increased up to 100°C, and decreased as temperature continued increasing. On the other hand, adding fiber will improve compressive strength and fire resistance of concrete, illustrated by a strength increase when exposed to temperature up to 400°C. Addition of fiber also enhanced ductility as in heated-treatment, the fracture energies of the materials sharply reduced while compressive strength increased (Richard and Cheyrezy, 1995).

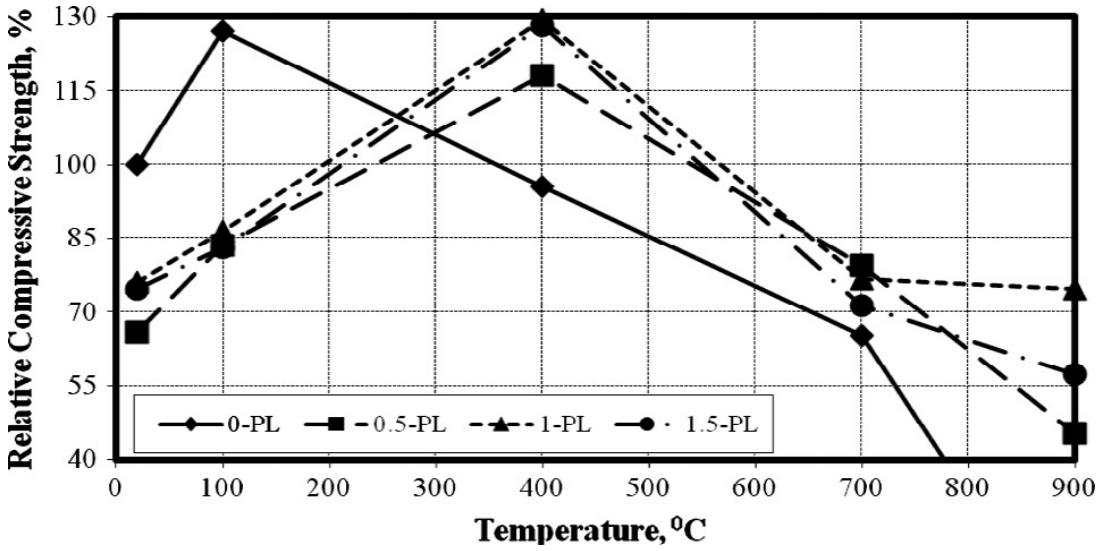

Figure A.8. Relative compressive strength of RPC at high temperatures (Canbaz, 2014).

Optimal heating duration

There is always an optimal heating duration at a given curing temperature. Larrard and Sedran (1994) tested ultra-high performance concrete cured in 90°C at normal pressure and humidity for 2 and 4 days. It was shown that the temperature curing for longer than 2 days resulted in the same compressive strength. On the other hand, Tam and Tam (2012) investigated reactive powder concrete cured at 8, 16, 24, 36, 48 hours and found that the optimal heating duration increased as the curing temperature increased. At 100°C, the difference of compressive strength cured at 8h and 24h was only 5.1%, suggested a curing duration of 8 h might be sufficient. However, at 250°C, the difference of compressive strength cured at 8h and 24 h was 18.5% and increased by 5% from 24h to 48h curing, revealed that a heating duration of 24 h was optimal, even longer heating duration may improve compressive strength. For the achievement of maximum compressive strength, the common heating duration of 24-48 hours was found in most of previous studies.

To sum up, moisture and temperature are of utmost importance factors affecting mechanical of silica fume concrete. As silica fume concrete is more sensitive to temperature and moisture than conventional concrete, it appears that particular consideration is required for M-S-H concrete to achieve desirable properties. Temperatures below 20°C and dry curing delay strength development while higher curing temperature should be based on desired compressive strength at specified age. Heated-treatment without modifying microstructure (<90°C) may increase early strength but reduce long-term strength. Higher temperature cure (90°C and above) may be more suitable for reactive powder concrete whereas microstructure can be enhanced in presence of ground quartz. Continuous moist curing is always needed to avoid plastic and dry shrinkage cracking. However, it should be noted that M-S-H binders have different compositions and

reaction mechanisms compared to PC. Therefore studies should be carried out to investigate whether different curing regimes have effects on the mechanical and durability properties of M-S-H binder systems.

Appendix B (Chapter 3)

Table B.1. Particle size distributions (MgO, SF, MS, QF, QS, River sand, Stone)

t (µm)	Passing (%)								
	MgO	**SF (Lazer diffraction method)**	**SF (SEM)**	**MS600 (literature)**	**MS600 (Lazer diffraction)**	**QF (d50 =16 µm)**	**Quartz sand**	**River sand**	**Stone**
0.05			0.00						
0.10			28.45	0.00					
0.40			64.05	12.20					
1.00	0.14		82.04	35.00	0.00	0.16			
5.00	17.63	0.61	100.00	84.60	13.54	14.93			
10	57.60	4.25		94.50	41.18	33.65			
25	83.71	11.26		98.18	56.44	62.48			
50	91.36	22.11		99.60	62.05	77.12	0.00	0.00	
75	95.74	43.00		99.80	70.98	87.28	0.97	2.10	
150	99.09	90.35		100.00	89.87	96.99	12.68	8.75	
300	100.00	100.00		100.00	99.52	100.00	68.69	39.62	
600					100.00		98.00	62.37	
1180							100.00	71.57	
2360								85.60	
4750								100.00	0.00
9530									25.00
16000									100.00

Table B.2. Particle size distributions (RHA, FA, PC)

t (μm)	Passing (%)				
	RHA (d50=40μm)		**FA (d50=37μm)**		**PC (d50=24μm)**
4.47	0.00	1.73	0.00	1.51	0.00
5.12	0.21	1.98	0.11	1.73	0.12
5.87	0.68	2.27	0.28	1.98	0.30
6.72	1.63	2.60	0.56	2.27	0.54
7.70	3.33	2.98	0.97	2.60	0.87
8.82	6.06	3.41	1.56	2.98	1.29
10.10	10.05	3.91	2.39	3.41	1.83
11.57	15.48	4.47	3.52	3.91	2.50
13.25	21.88	5.12	5.07	4.47	3.36
15.17	28.56	5.87	7.16	5.12	4.45
17.38	34.89	6.72	9.92	5.87	5.87
19.90	40.59	7.70	13.46	6.72	7.72
22.80	45.68	8.82	17.79	7.70	10.14
26.11	50.34	10.10	22.87	8.82	13.27
29.91	54.80	11.57	28.62	10.10	17.25
34.26	59.27	13.25	34.69	11.57	22.21
39.23	63.92	15.17	40.66	13.25	28.19
44.94	68.83	17.38	46.16	15.17	35.10
51.47	73.86	19.90	51.04	17.38	42.71
58.95	78.81	22.80	55.29	19.90	50.72
67.52	83.43	26.11	59.02	22.80	58.78
77.34	87.54	29.91	62.41	26.11	66.59
88.58	90.93	34.26	65.60	29.91	73.86
101.46	93.50	39.23	68.77	34.26	80.34
116.21	95.34	44.94	72.06	39.23	85.83
133.10	96.71	51.47	75.50	44.94	90.20
152.45	97.76	58.95	79.06	51.47	93.52
174.62	98.56	67.52	82.64	58.95	95.91
200.00	99.18	77.34	86.12	67.52	97.54
229.08	99.65	88.58	89.34	77.34	98.61
262.38	100.00	101.46	92.09	88.58	99.27
		116.21	94.25	101.46	99.65
		133.10	95.96	116.21	99.87
		152.45	97.30	133.10	100.00
		174.62	98.33		
		200.00	99.09		
		229.08	99.63		
		262.38	100.00		

Appendix C (Chapter 4)

EDS locations and spectra of M-S-H binder systems

C.1. M-SF mixtures - 7 days age: SF60 sample

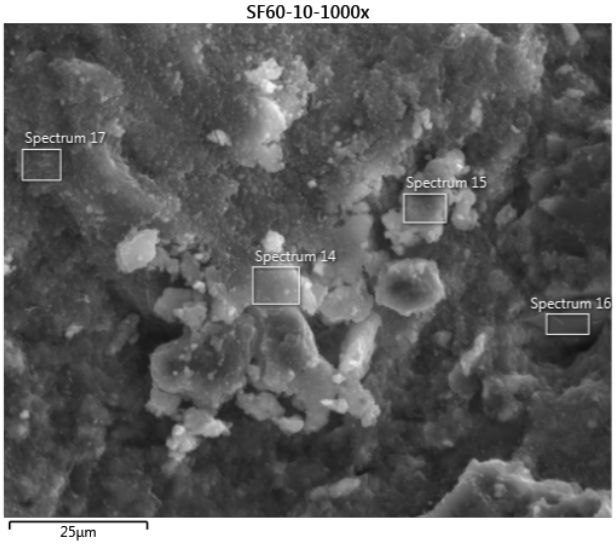

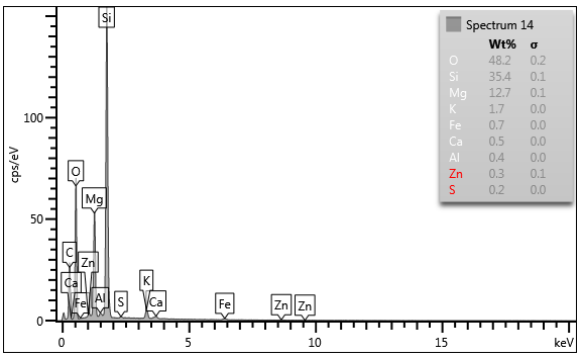

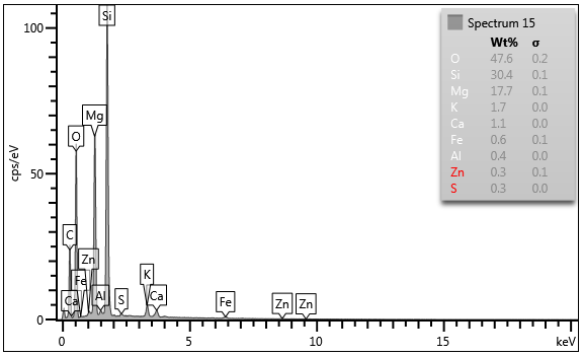

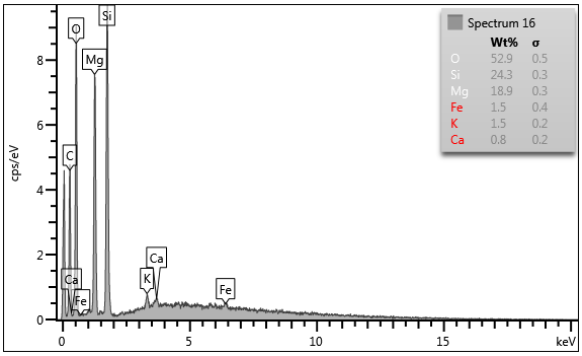

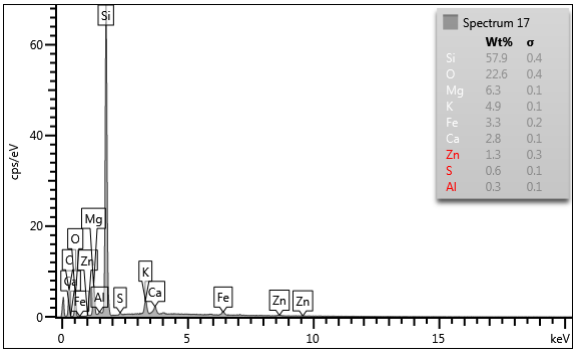

SF50 samples

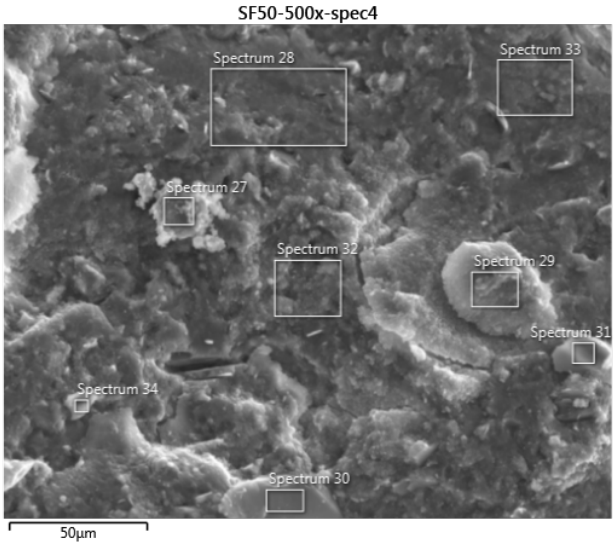

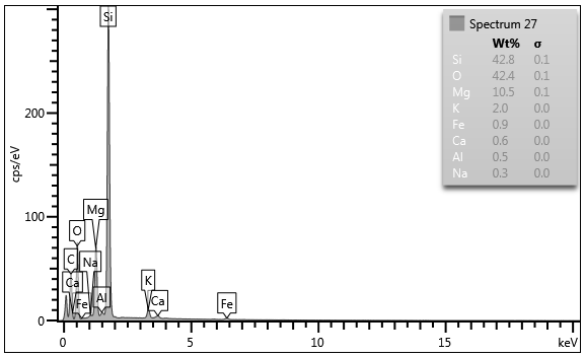

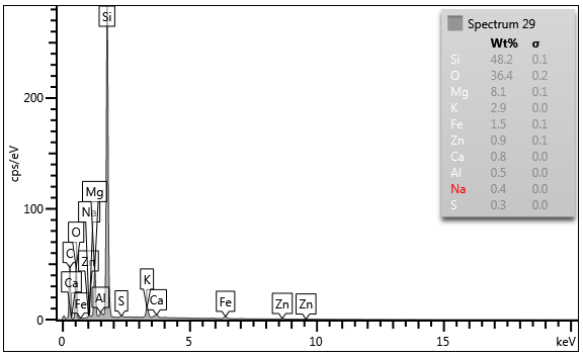

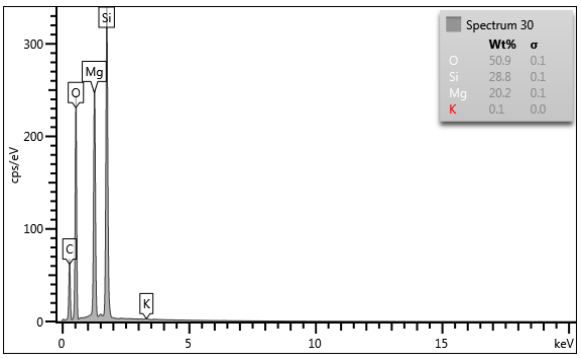

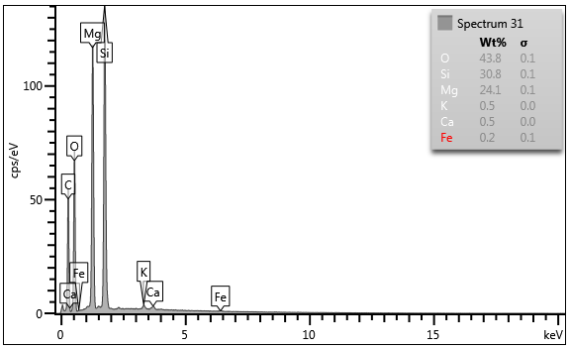

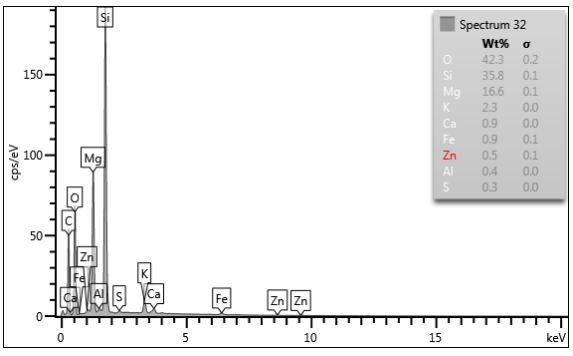

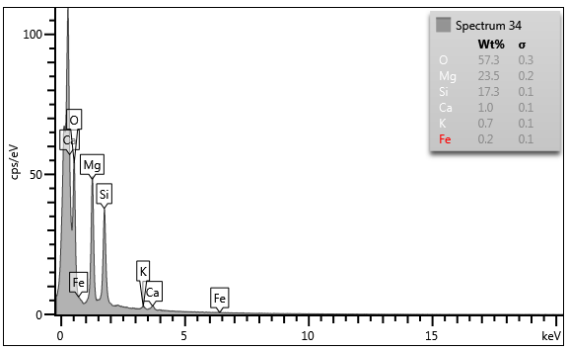

SF40 samples

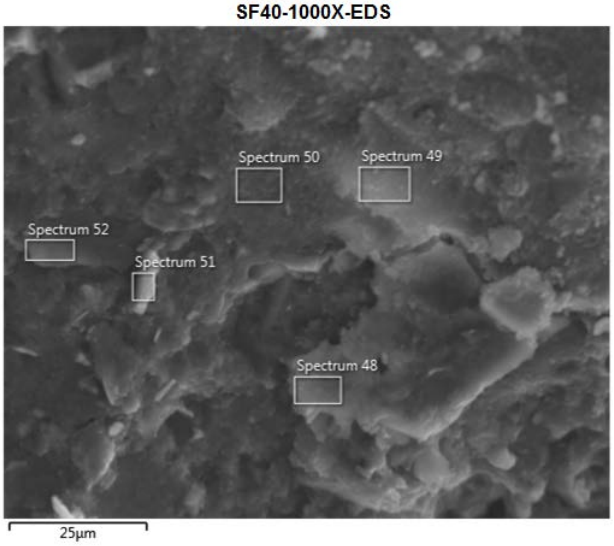

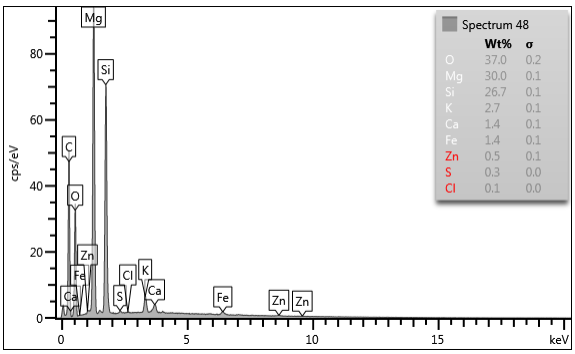

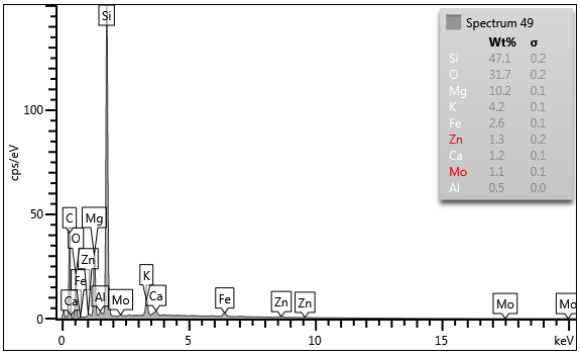

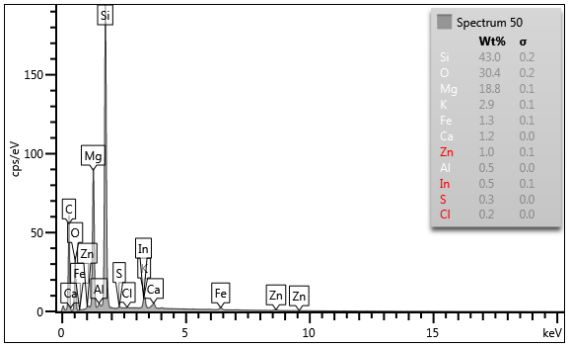

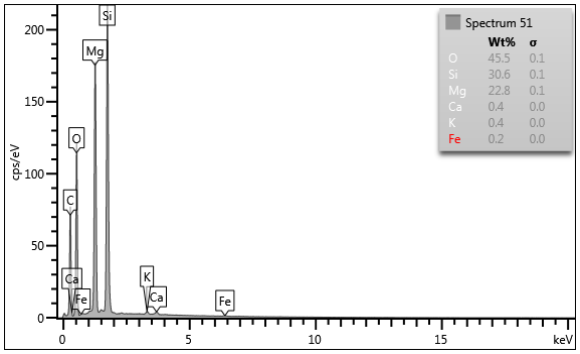

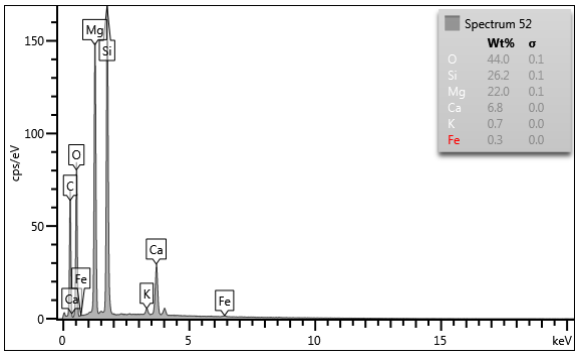

C.2 M-SF mixtures - 28 days age: SF60 samples

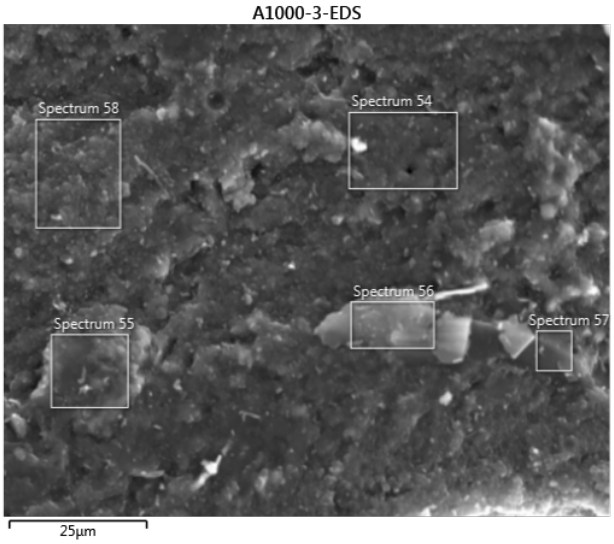

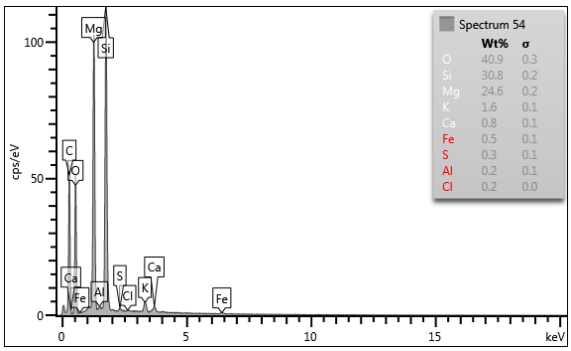

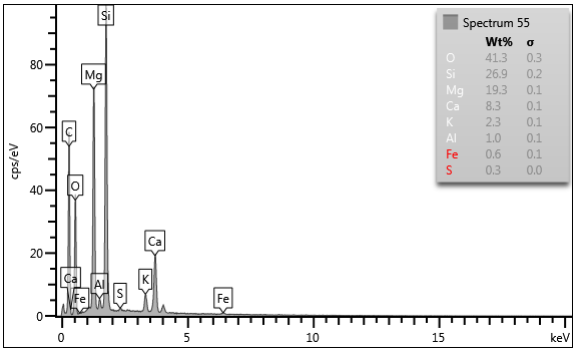

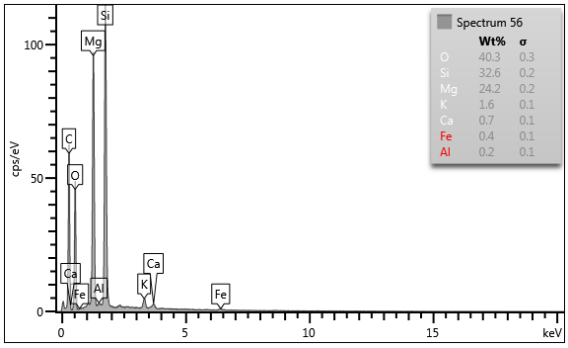

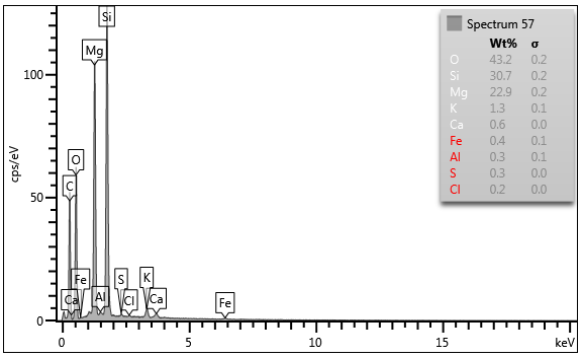

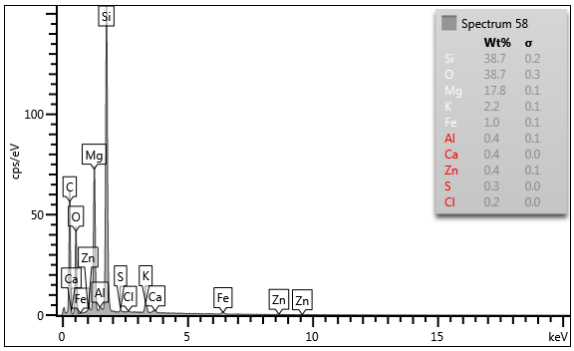

SF50 samples

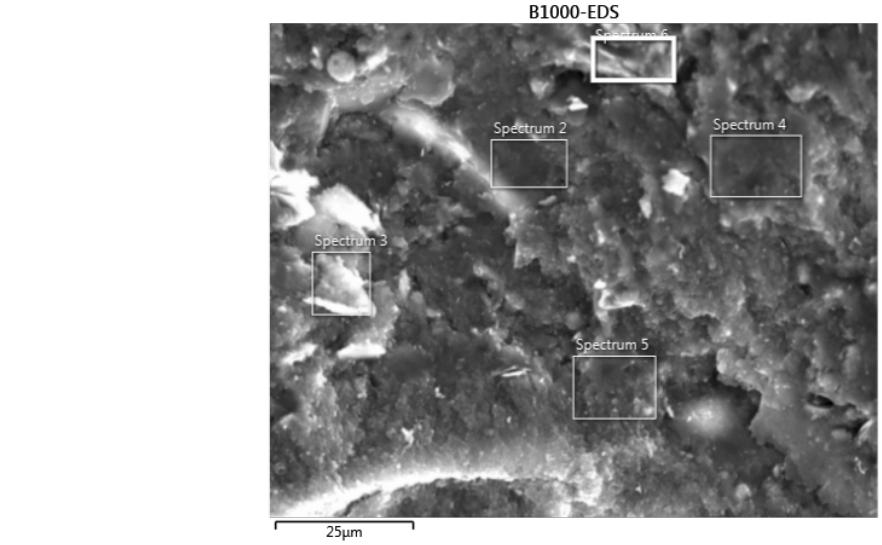

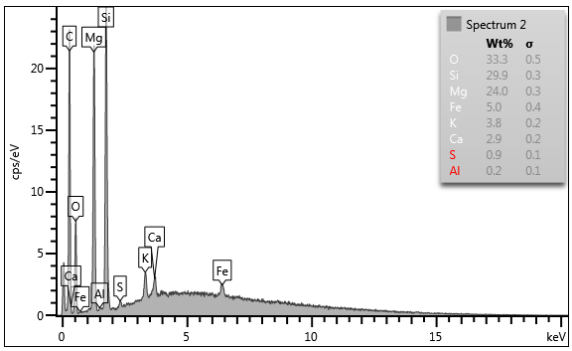

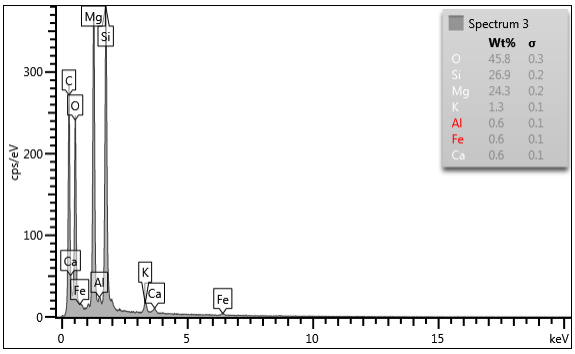

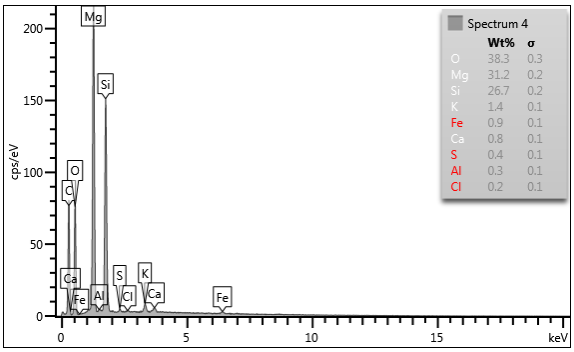

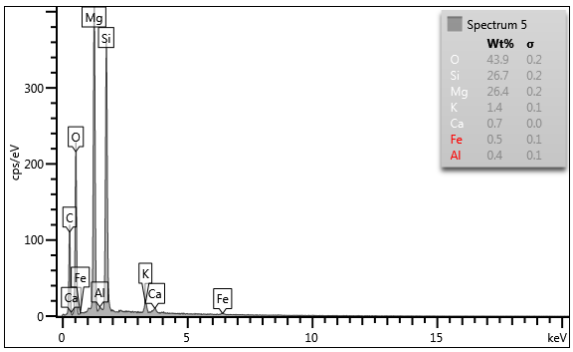

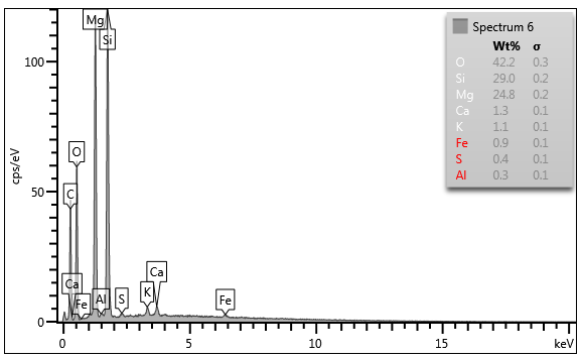

SF40 samples

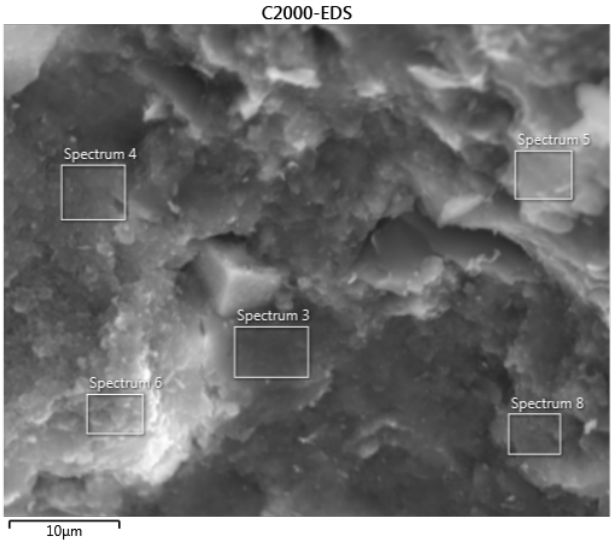

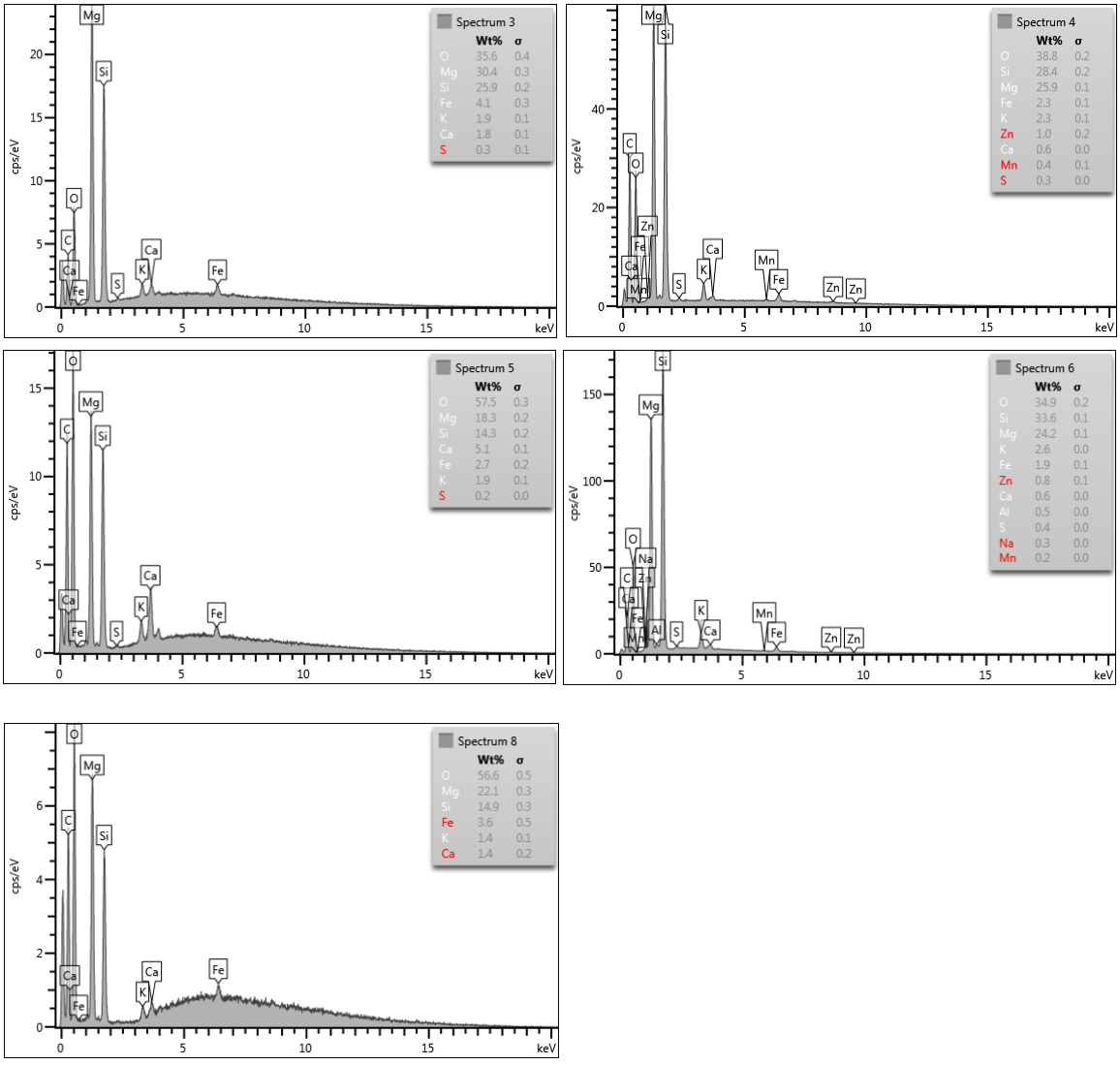

C.3. M-SF mixtures - 90 days age: SF60 samples

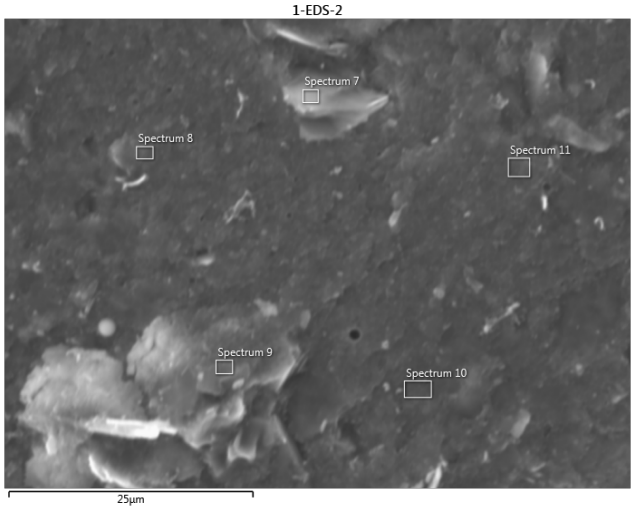

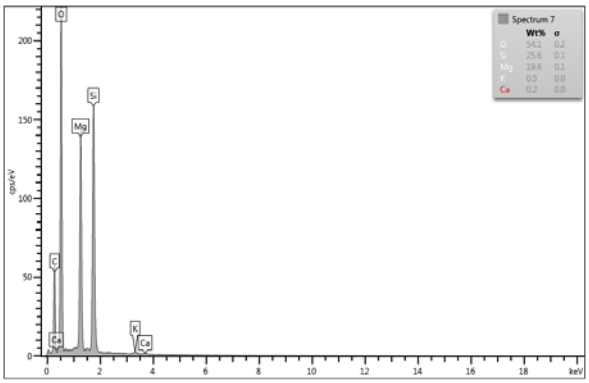

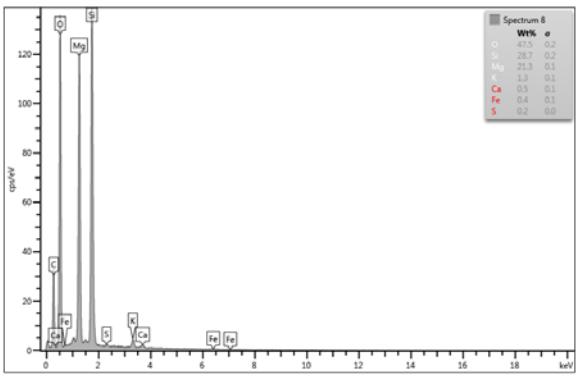

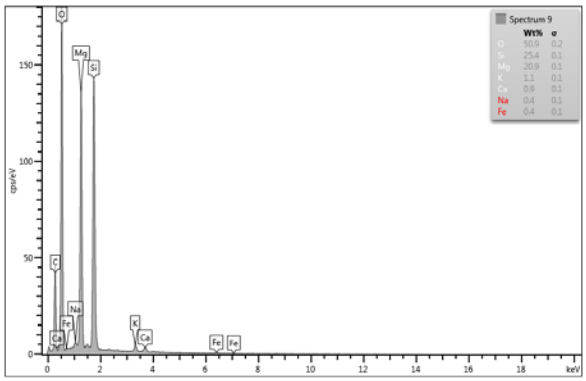

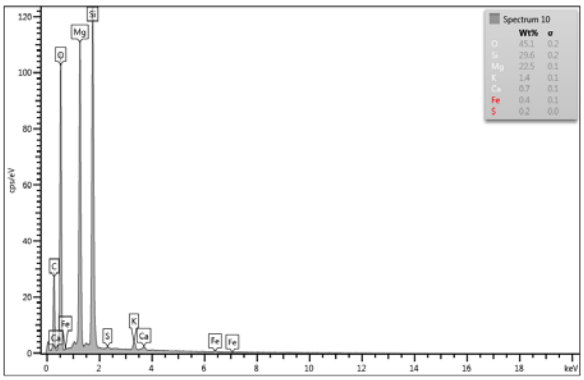

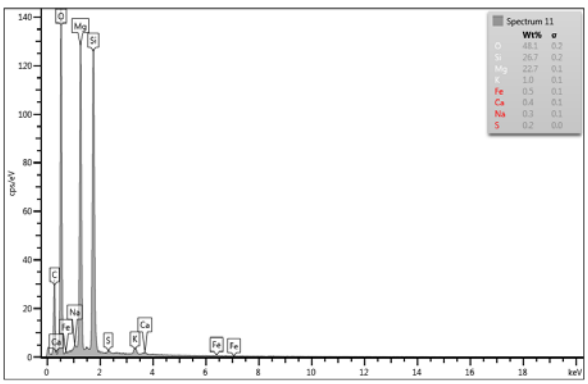

SF50 samples

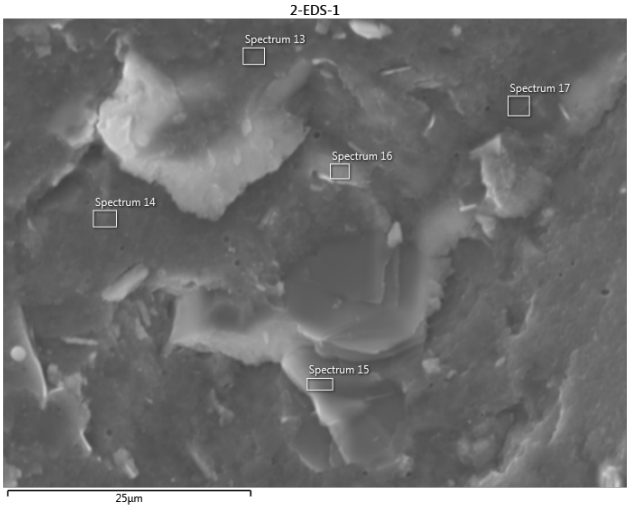

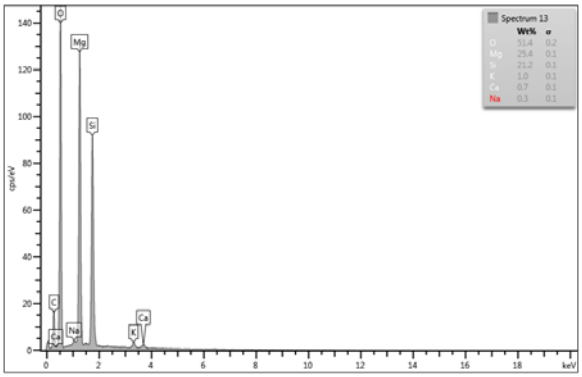

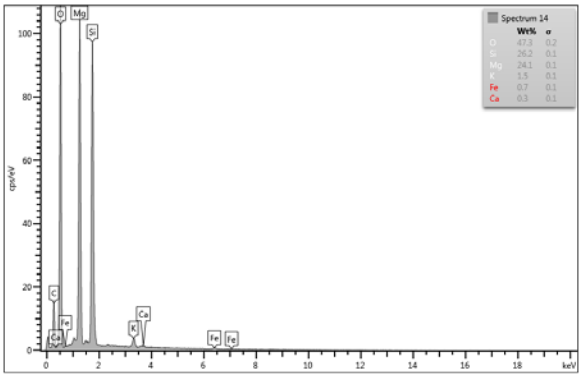

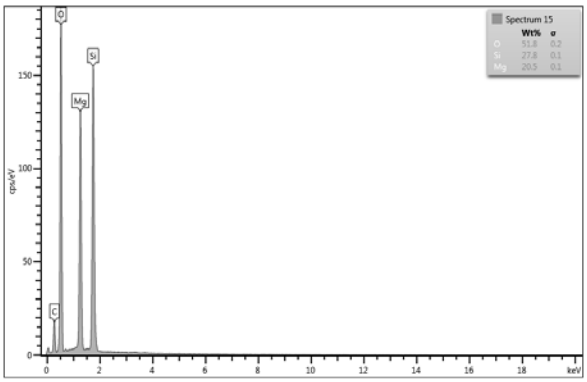

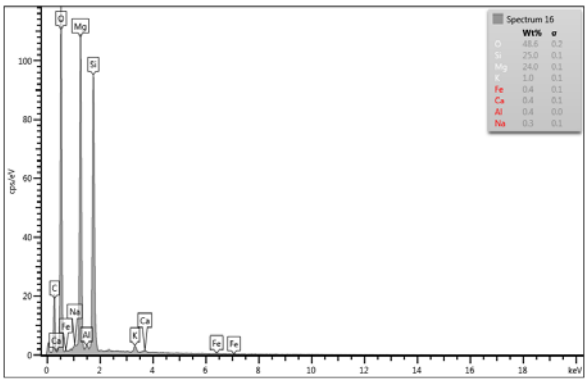

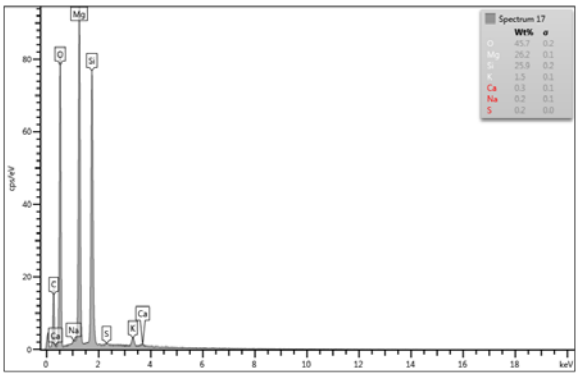

SF40 samples

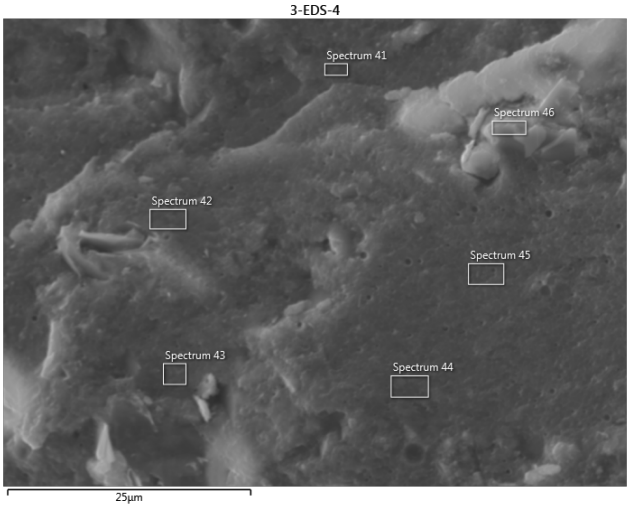

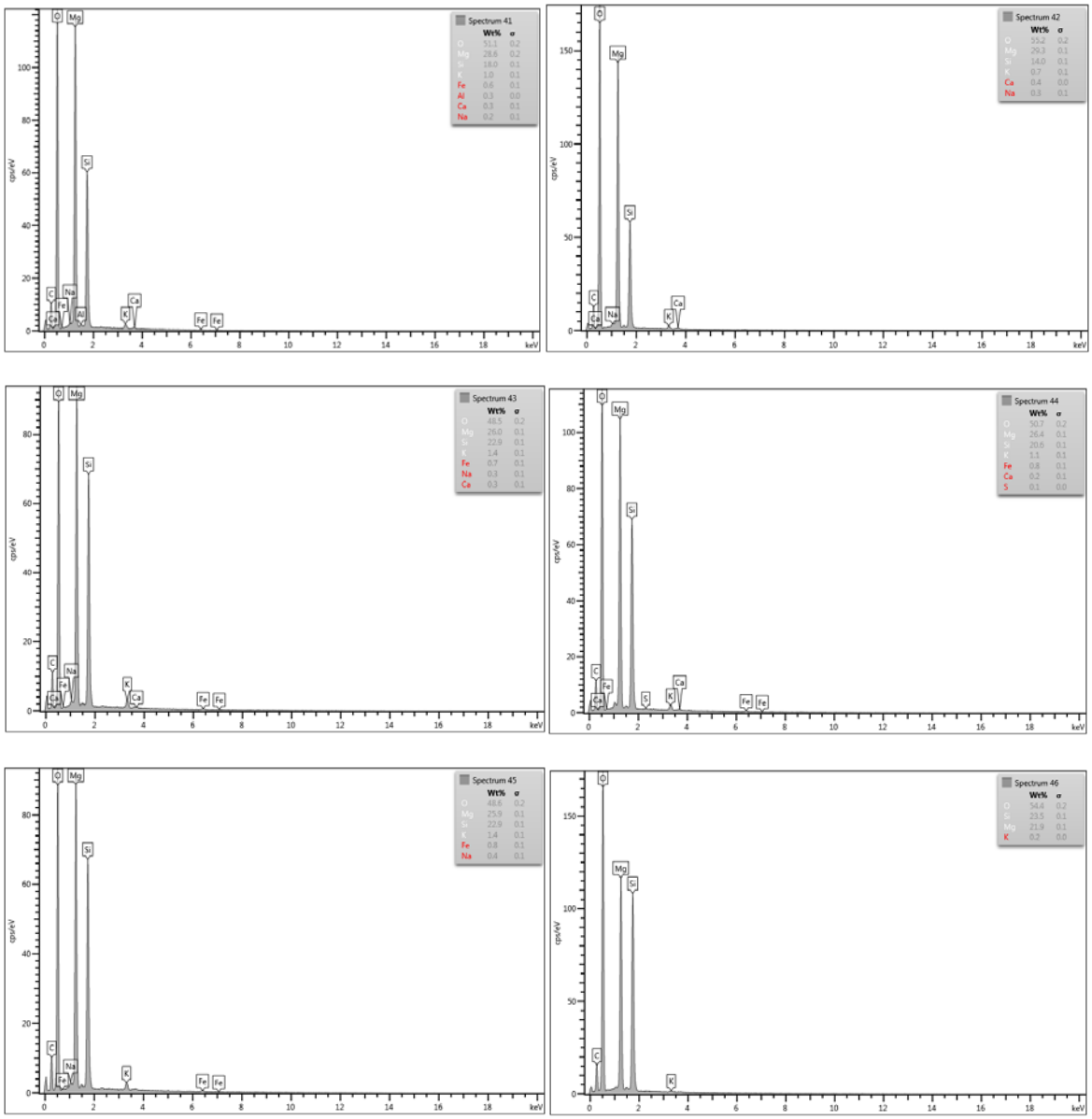

C.4. M-SF mixture 365 days: SF60 samples

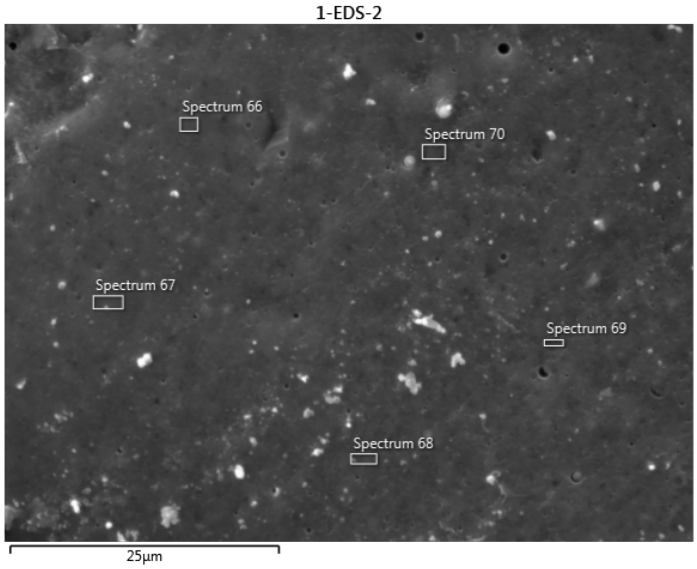

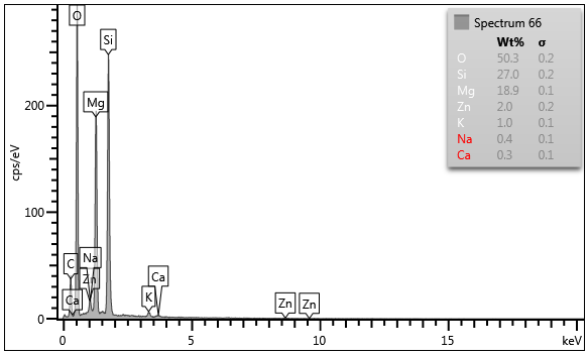

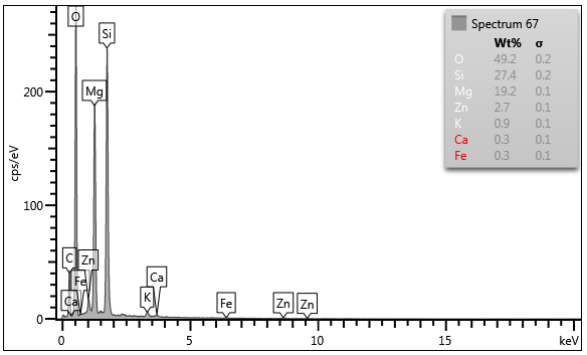

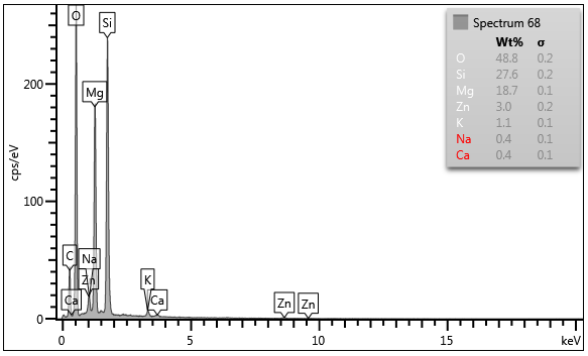

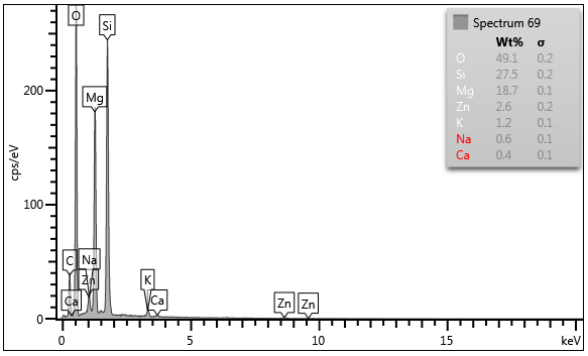

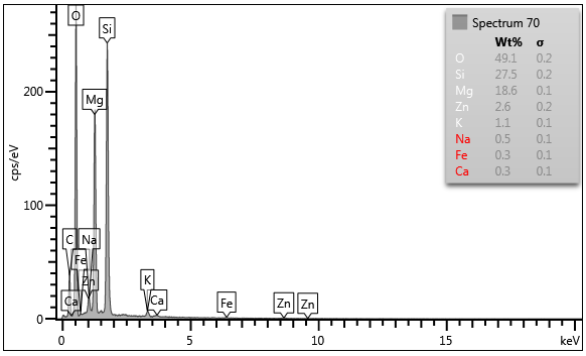

SF50 samples

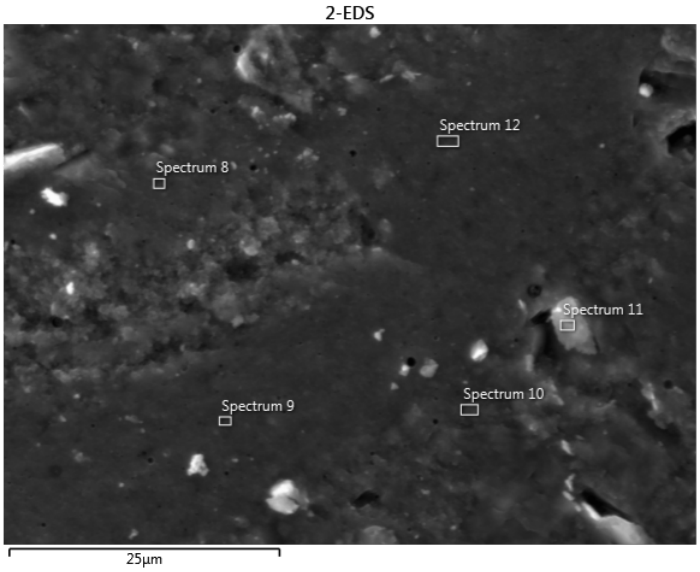

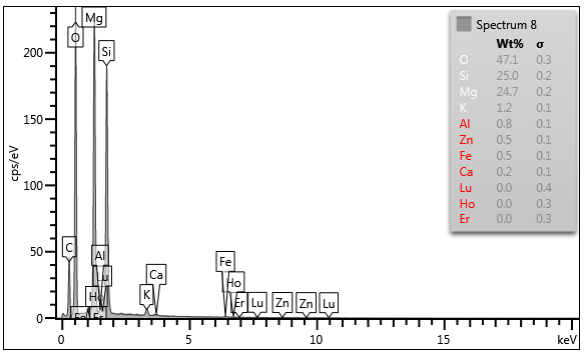

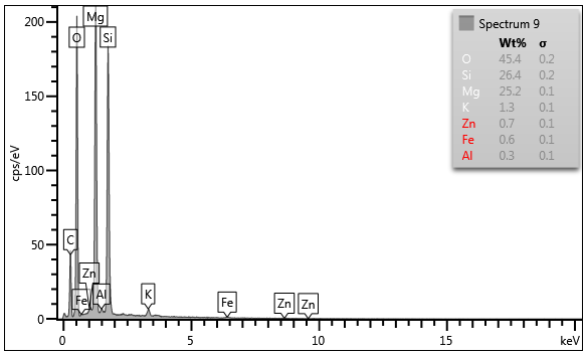

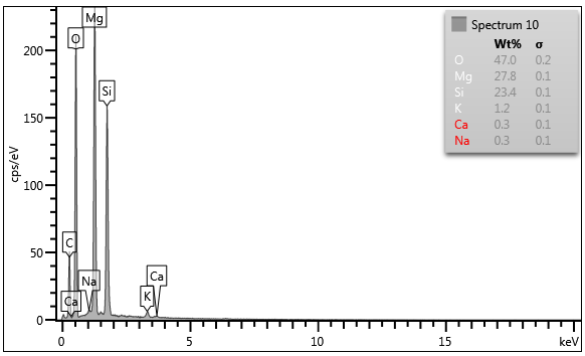

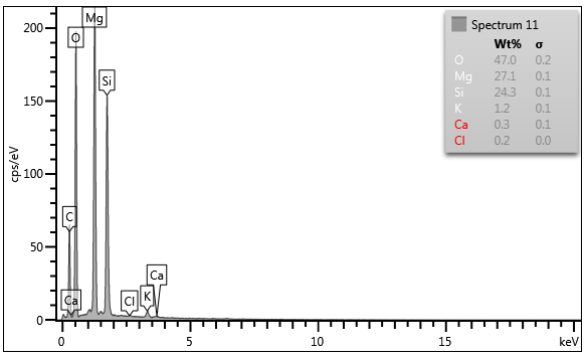

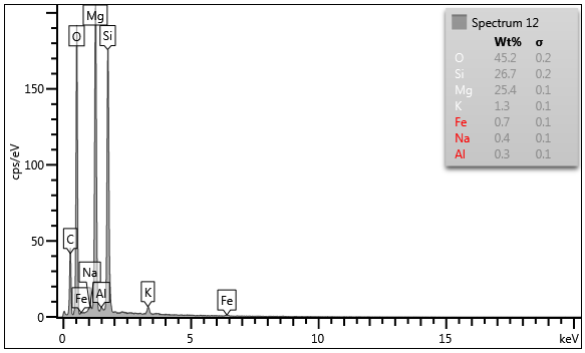

SF40 samples

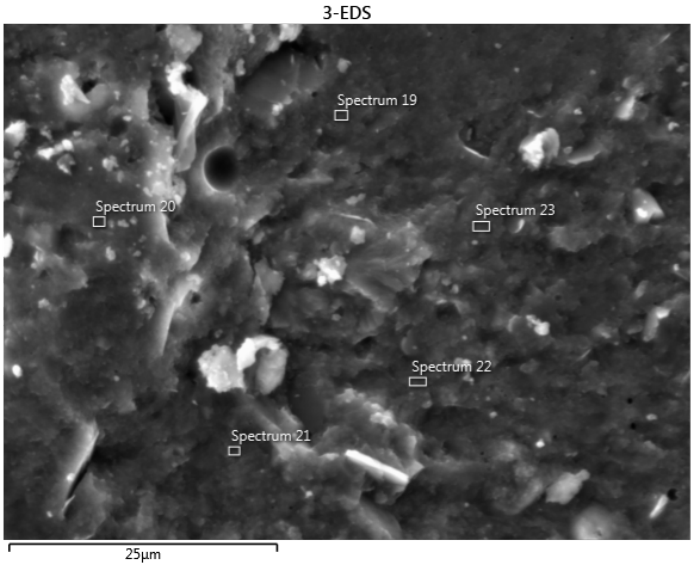

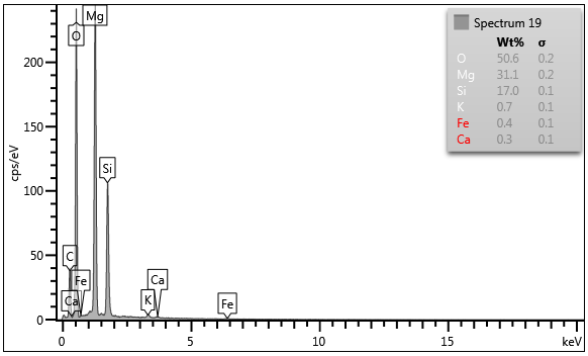

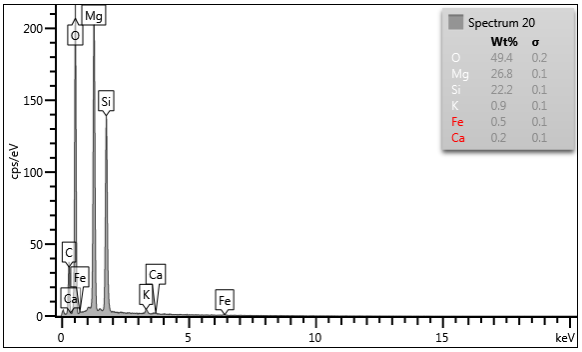

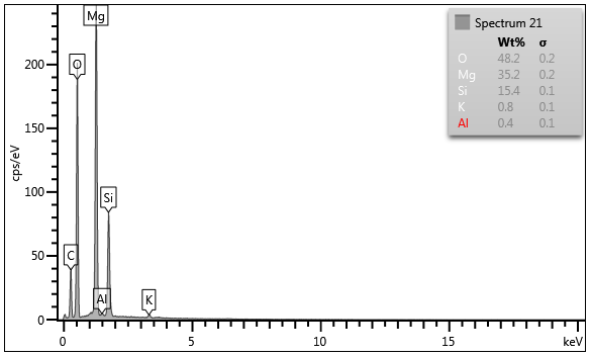

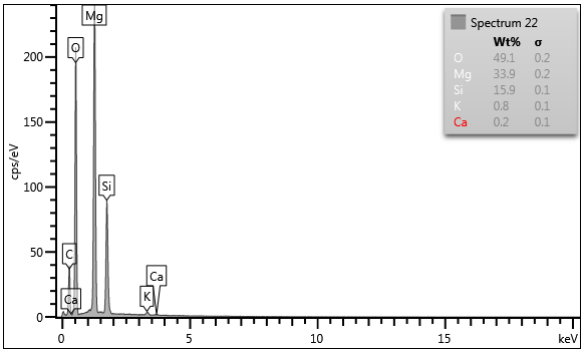

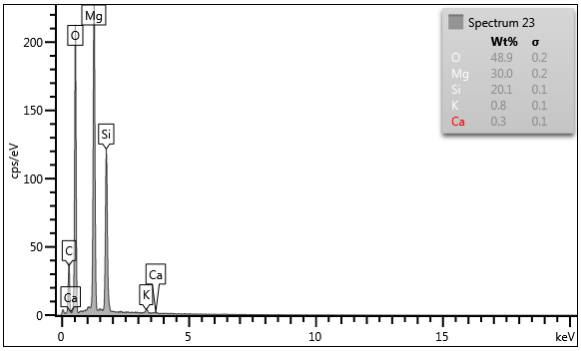

C.5. M-MS mixtures - 7-days age: MS60 samples

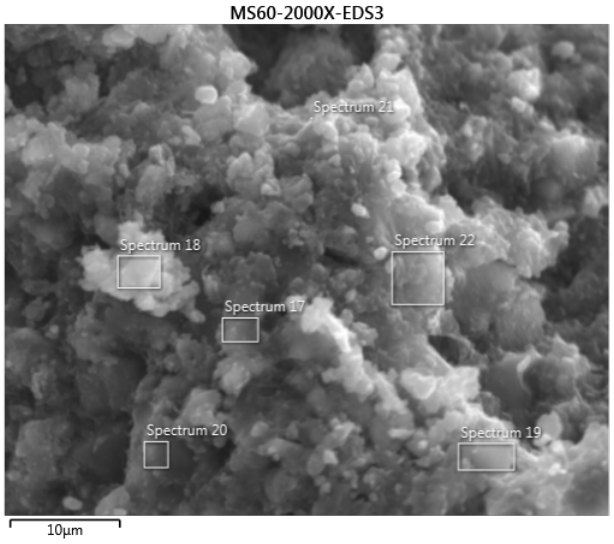

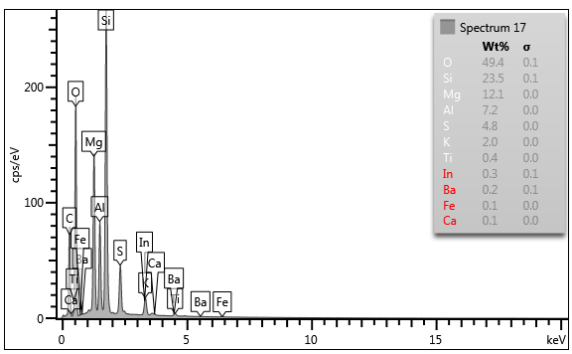

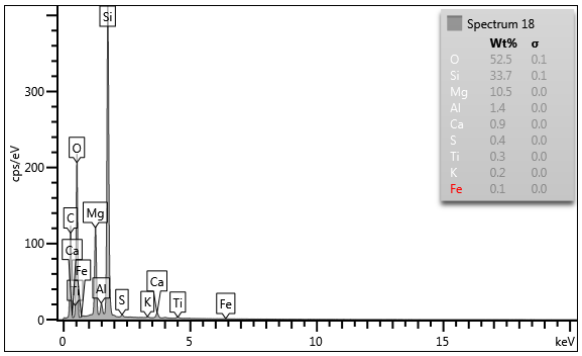

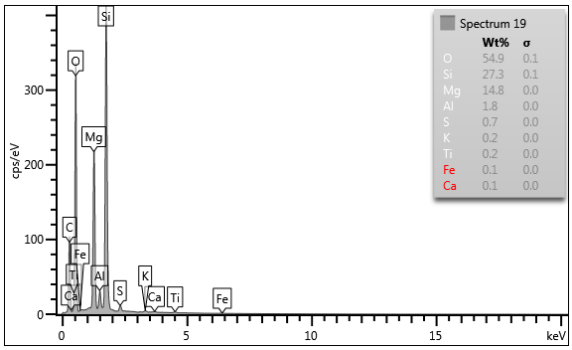

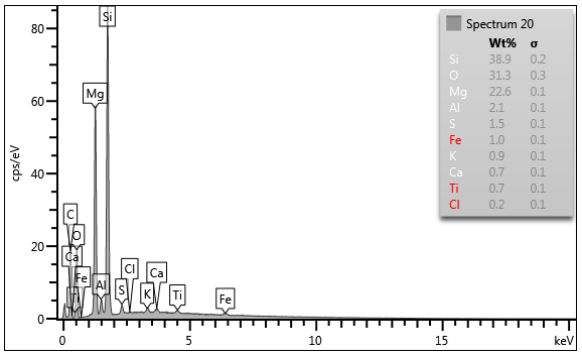

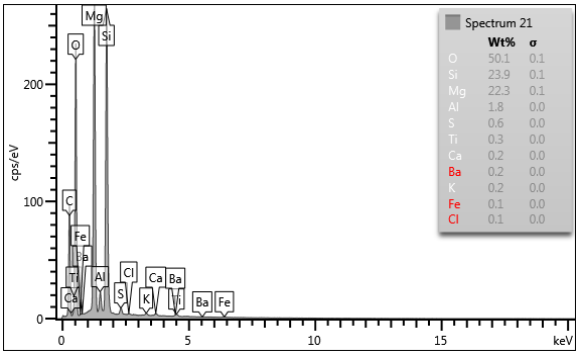

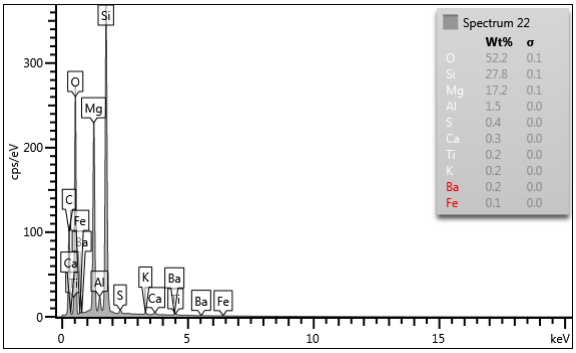

MS50 samples

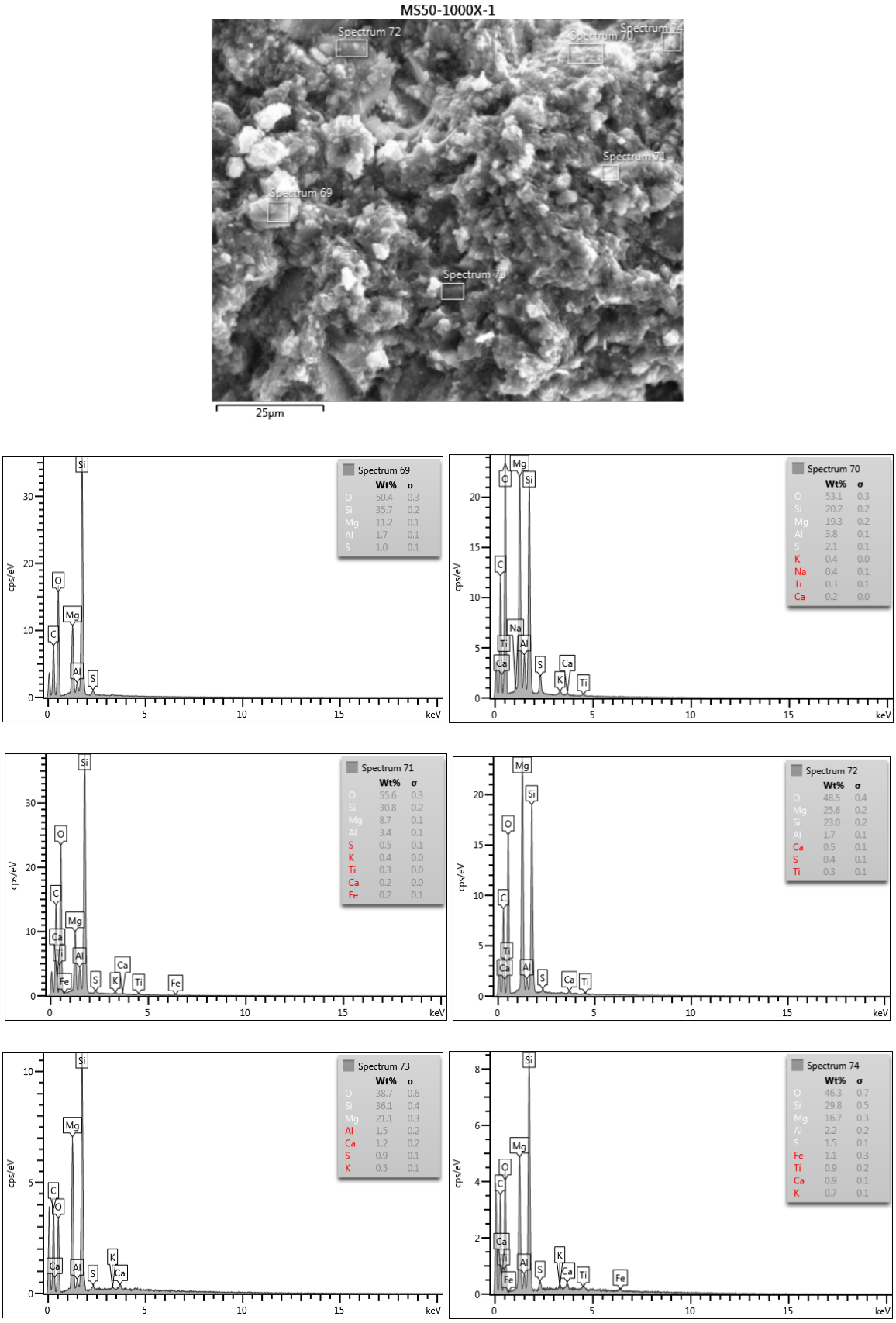

MS40 samples

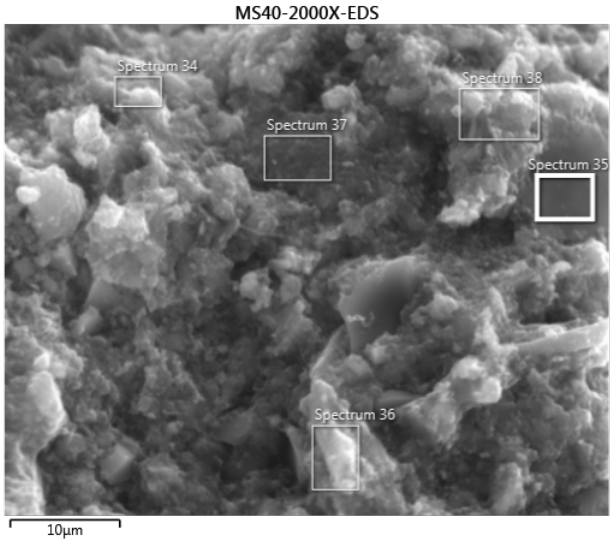

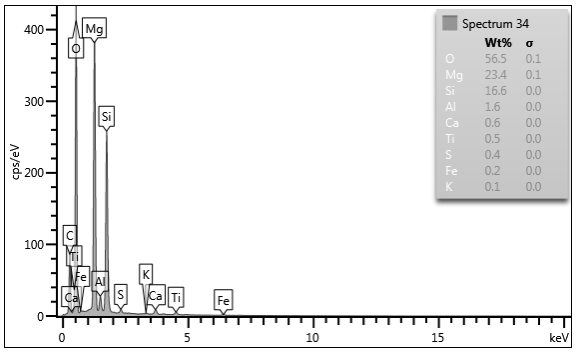

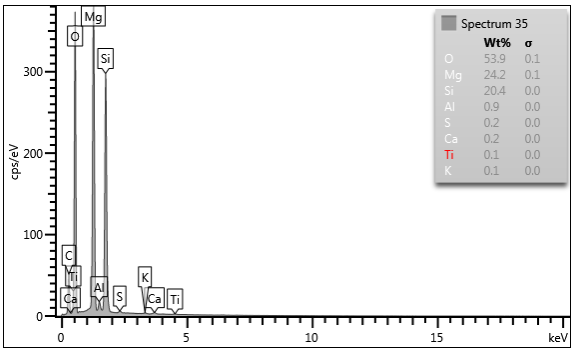

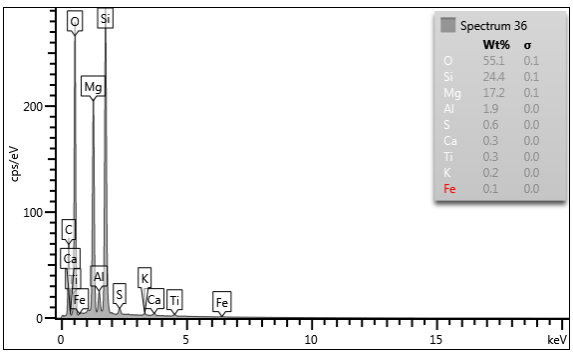

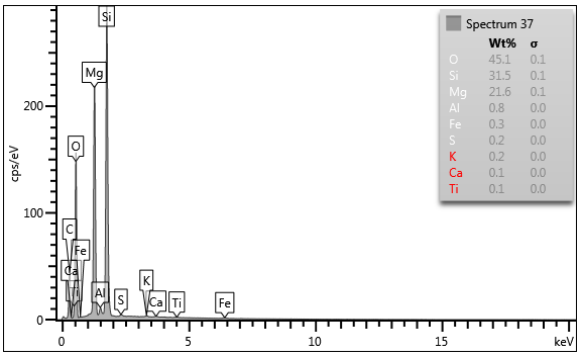

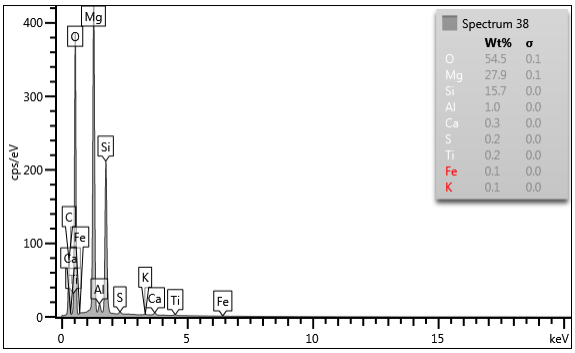

C.6. M-MS mixtures – 28 days age: MS60 samples

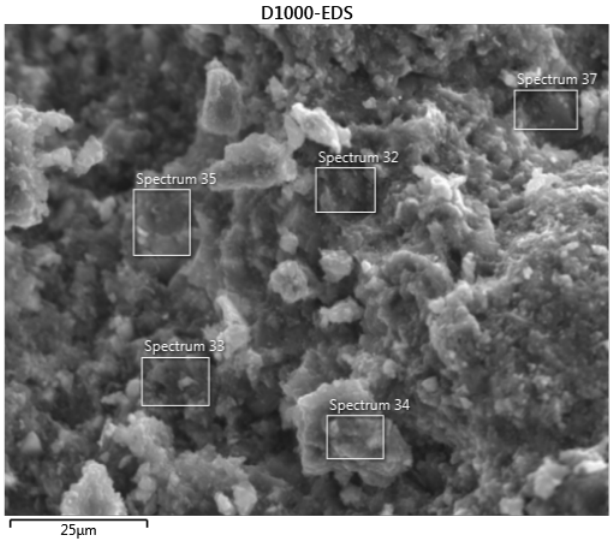

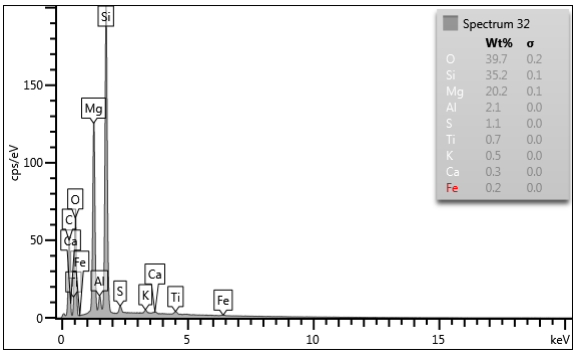

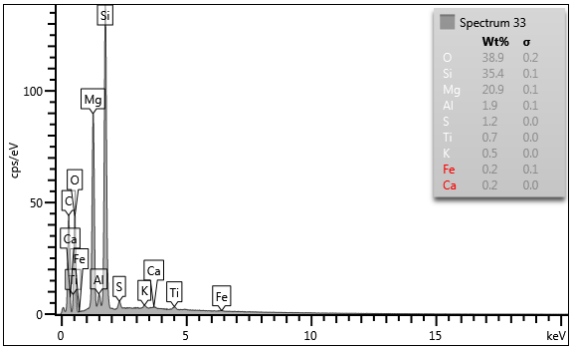

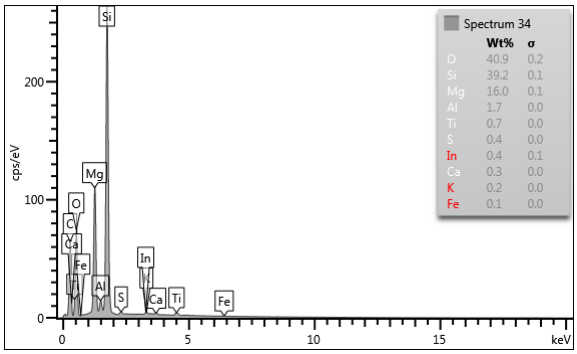

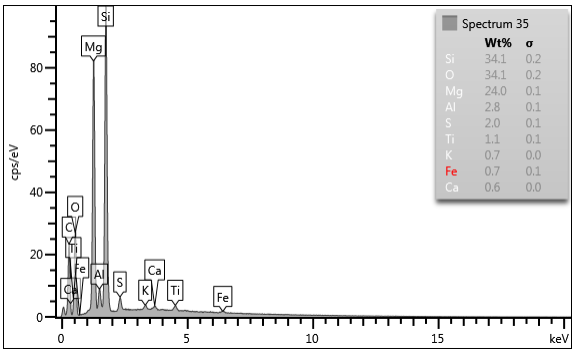

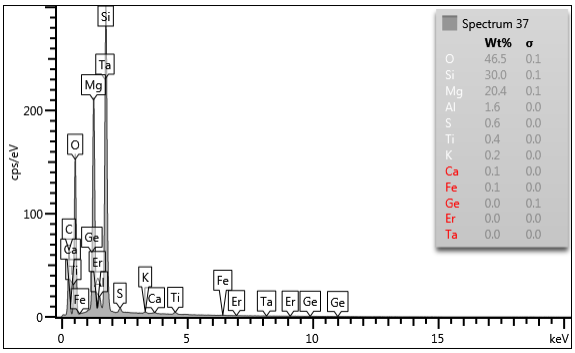

MS50 samples

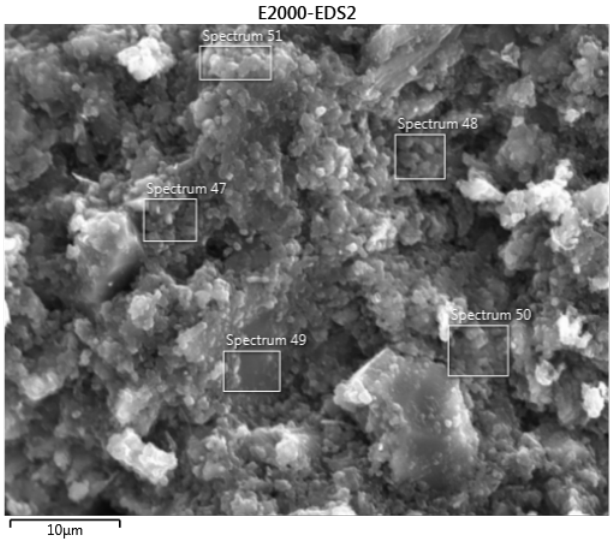

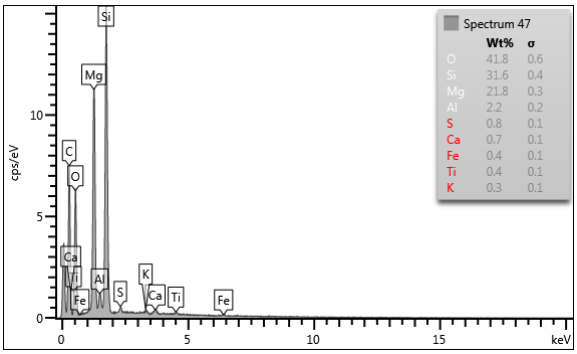

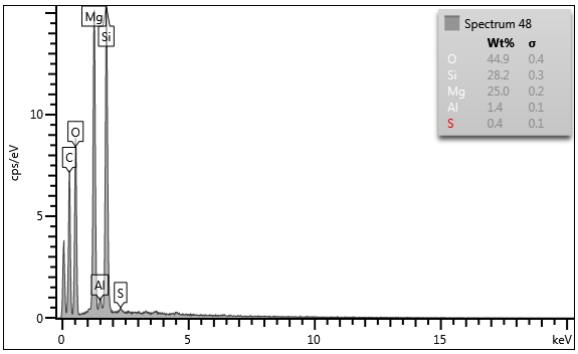

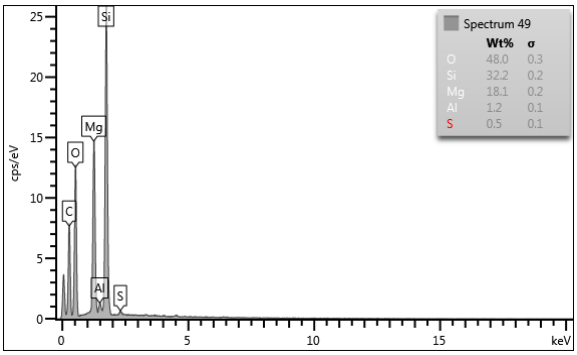

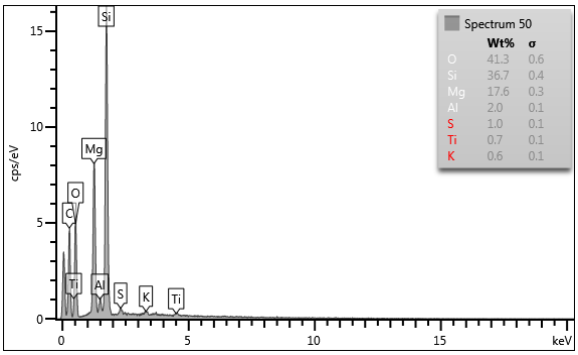

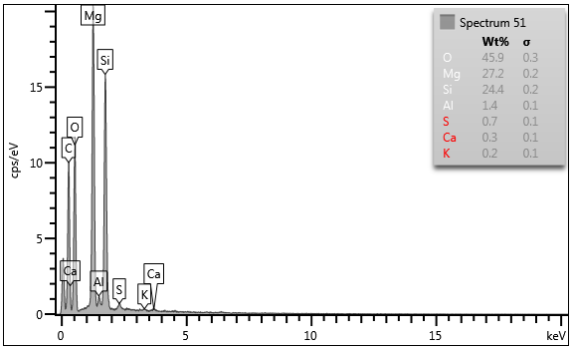

MS40 samples

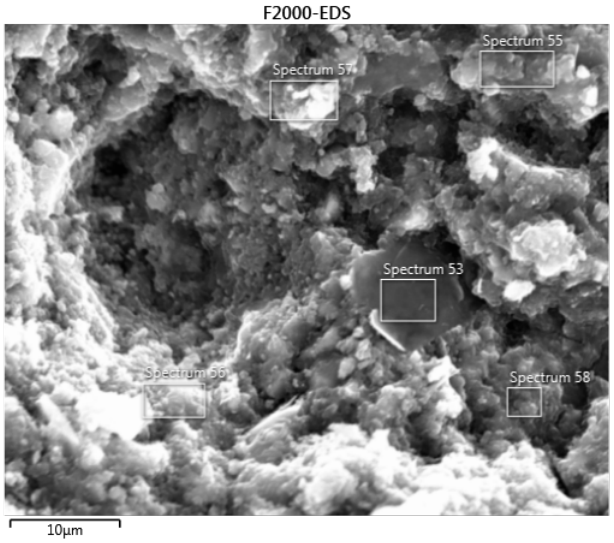

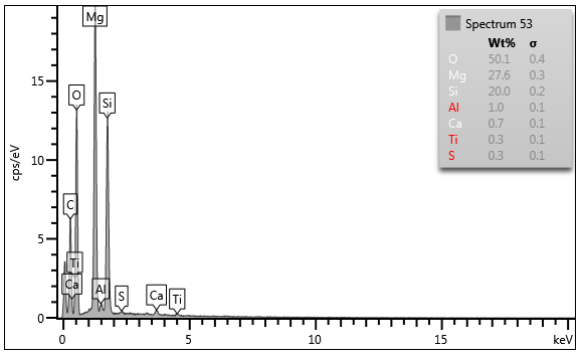

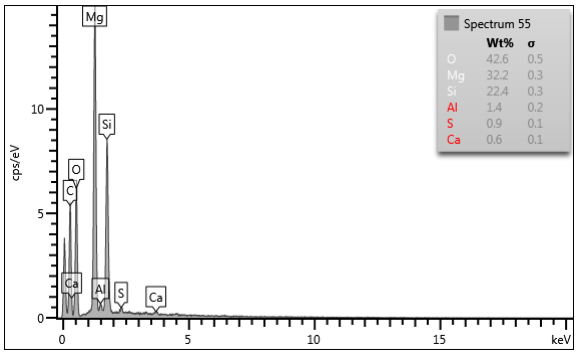

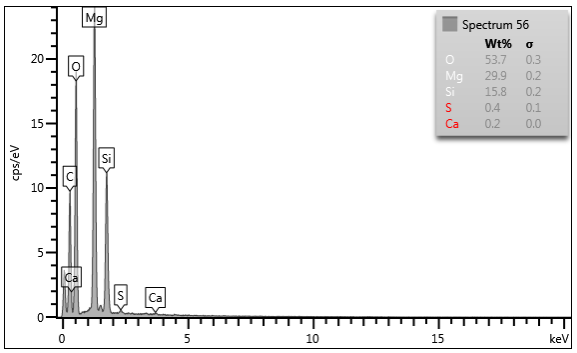

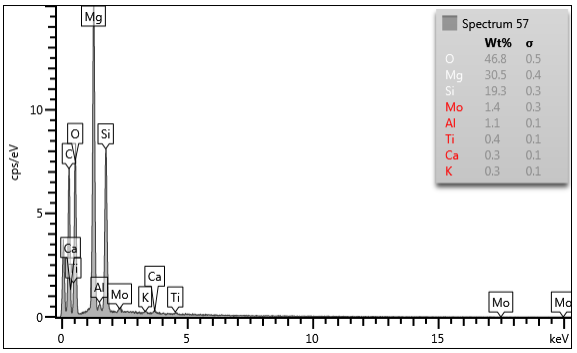

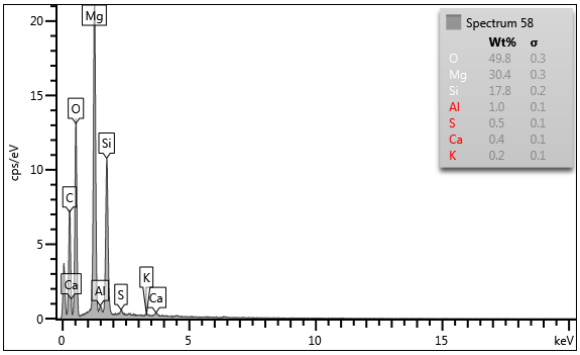

C.7. M-MS mixtures – 90 days age: MS60 samples

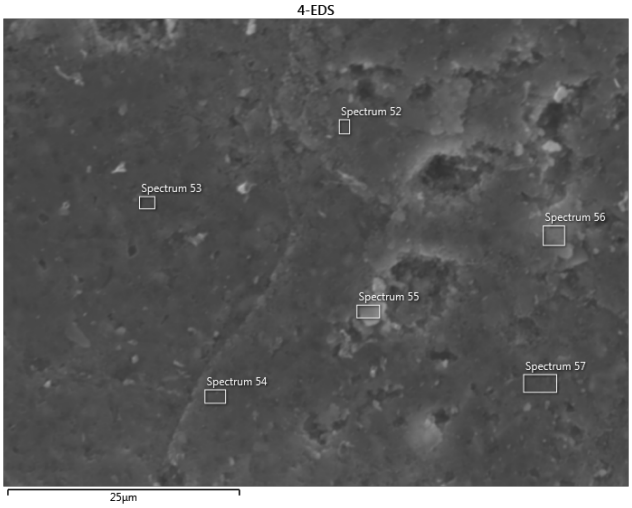

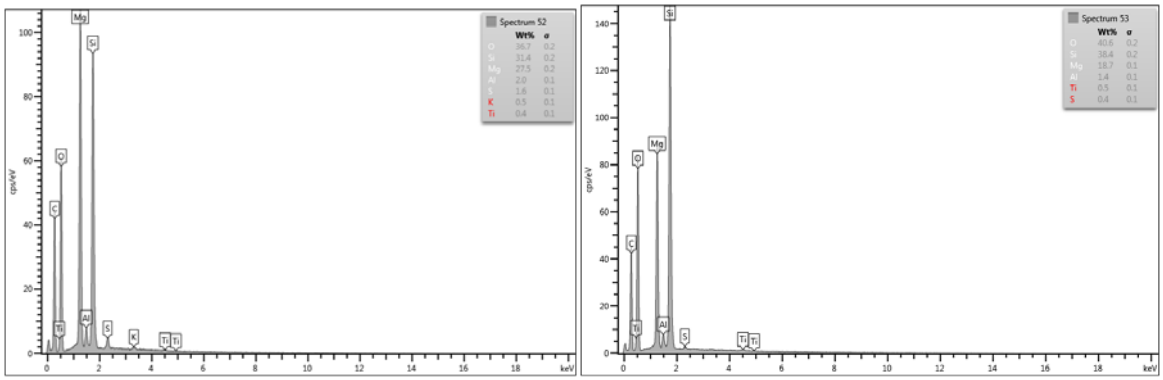

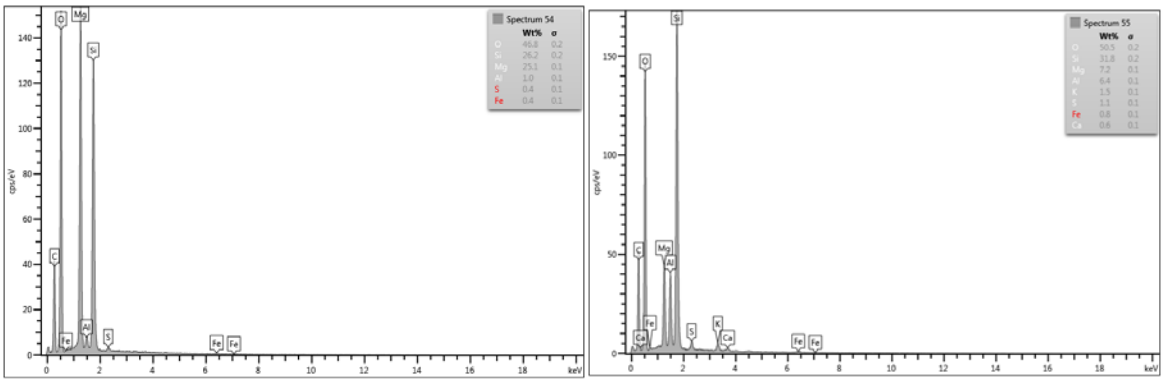

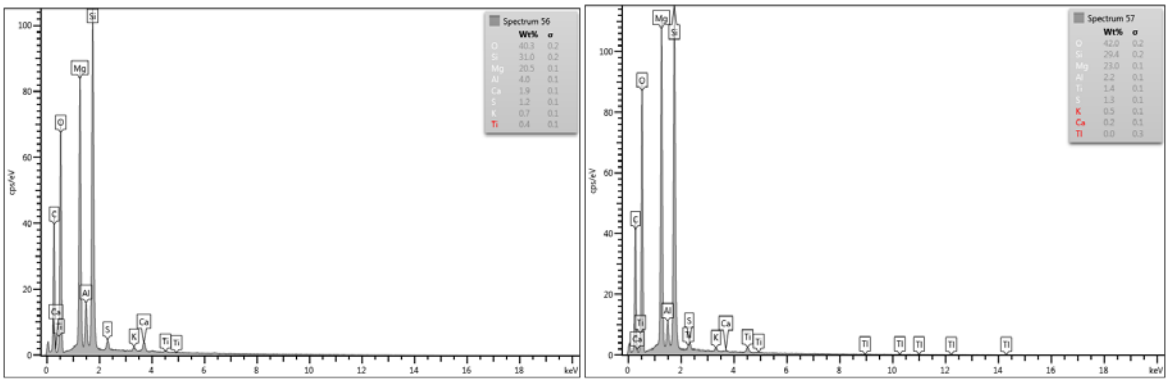

MS50 samples

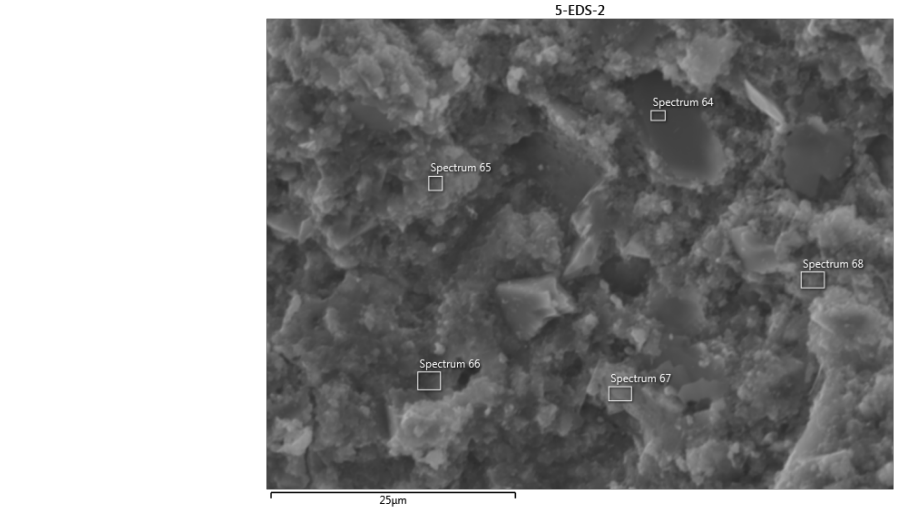

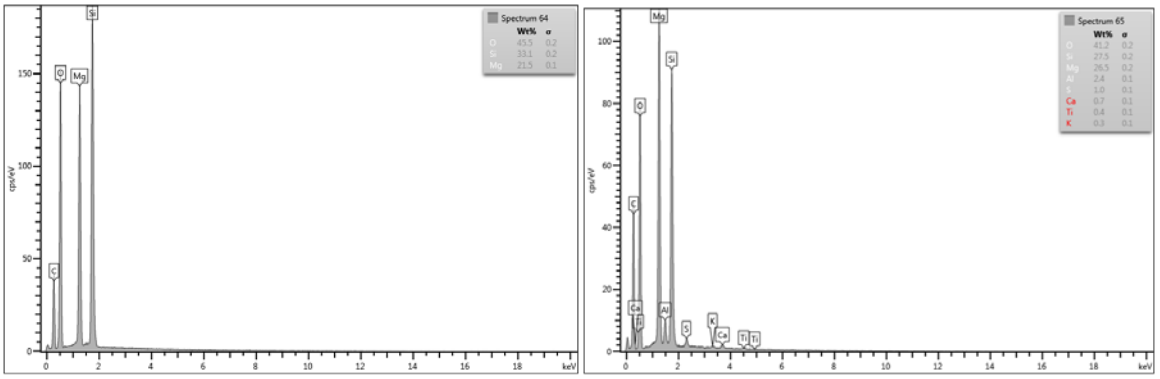

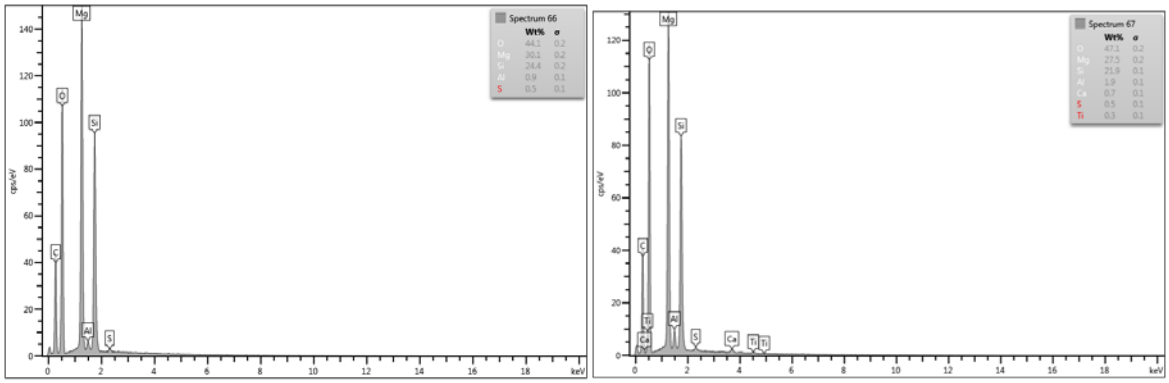

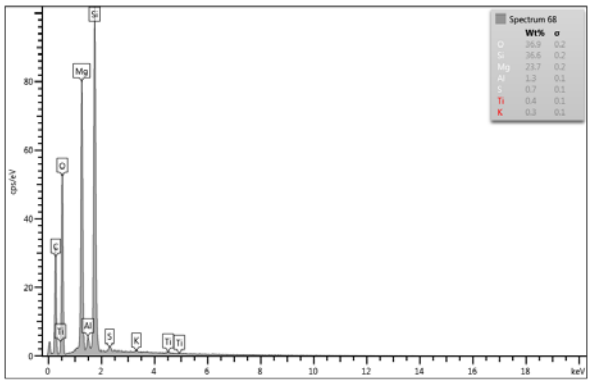

MS40 samples

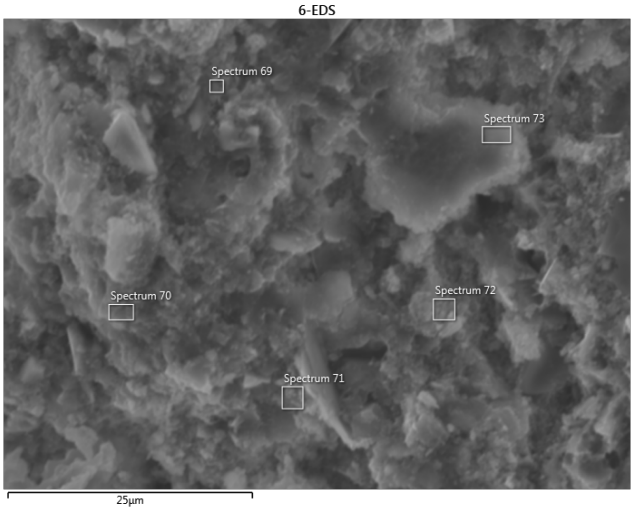

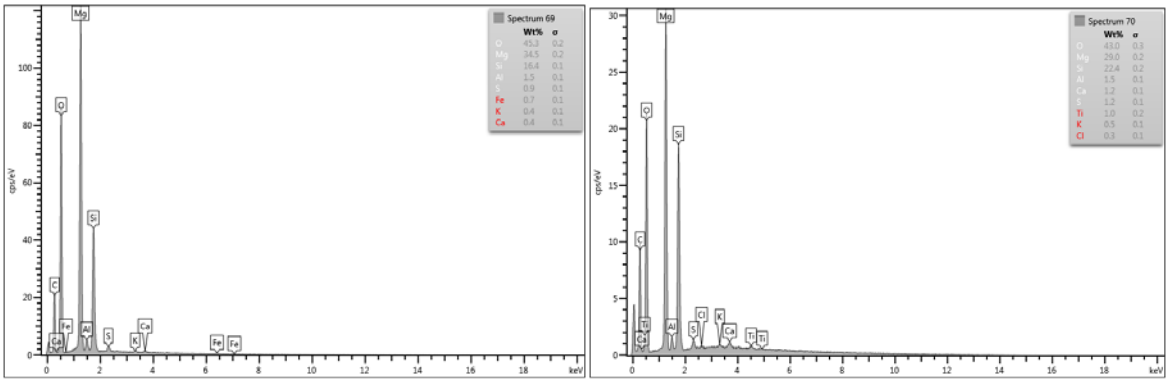

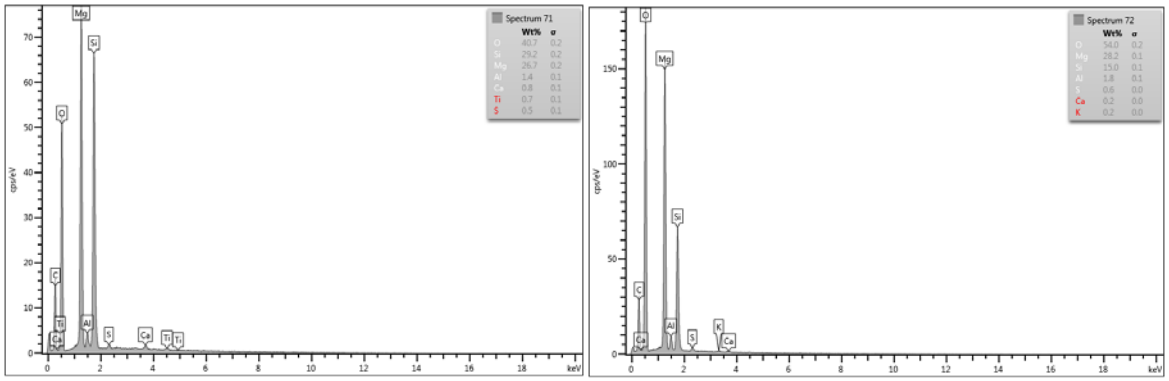

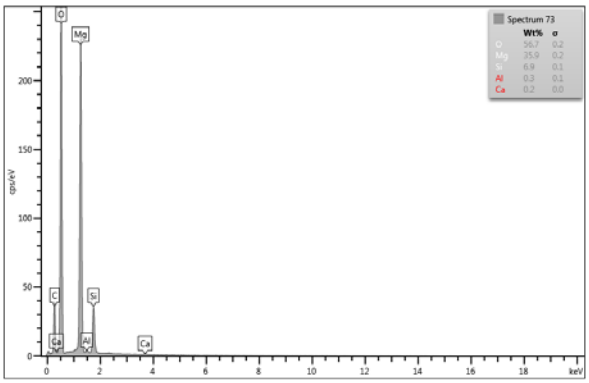

C.8. M-MS mixtures - 365 days age: MS60 samples

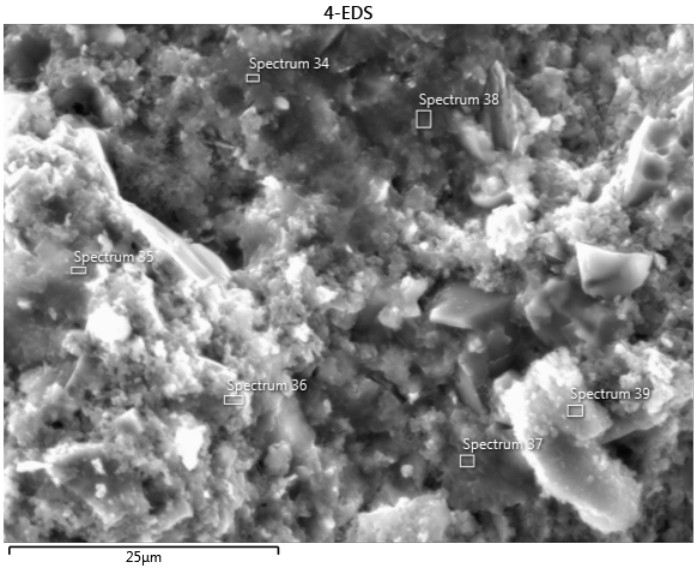

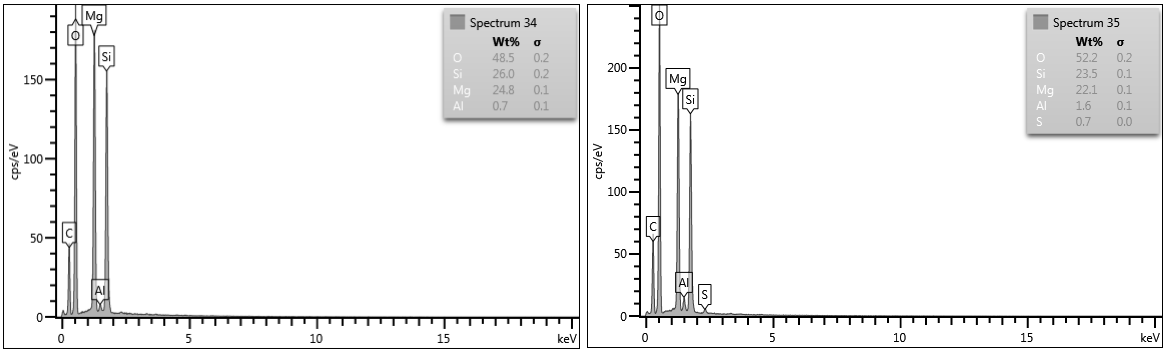

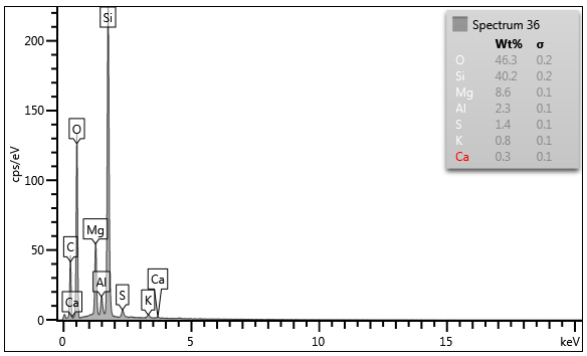

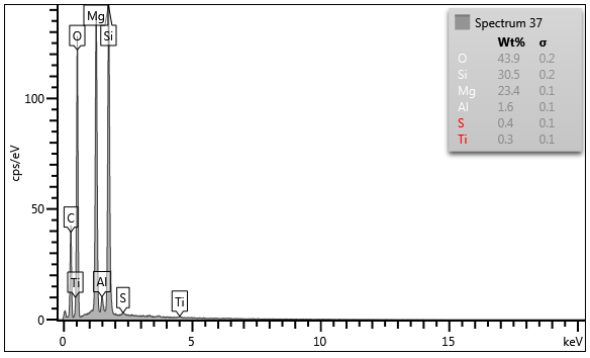

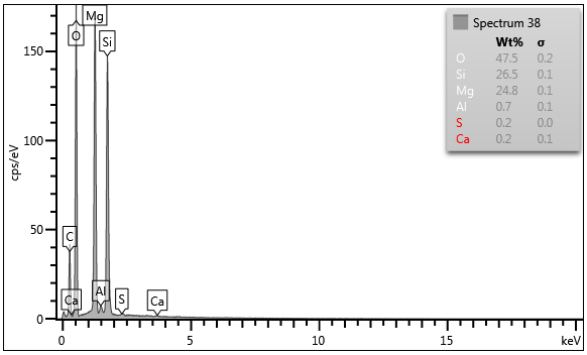

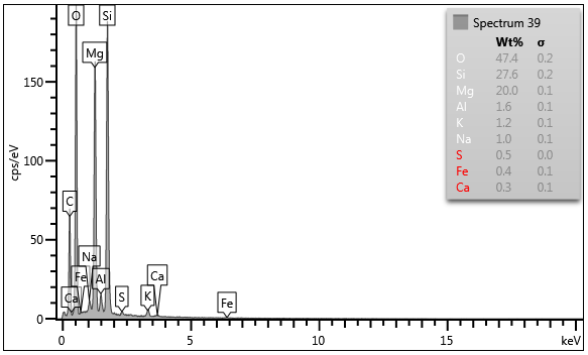

MS50 samples

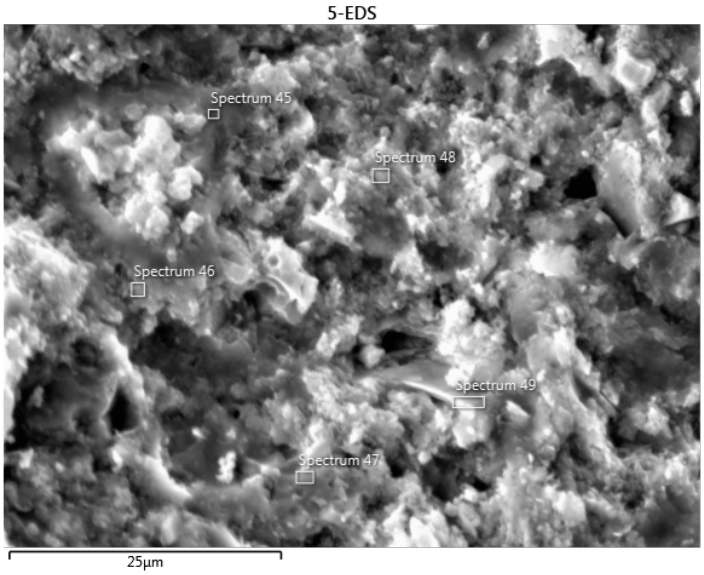

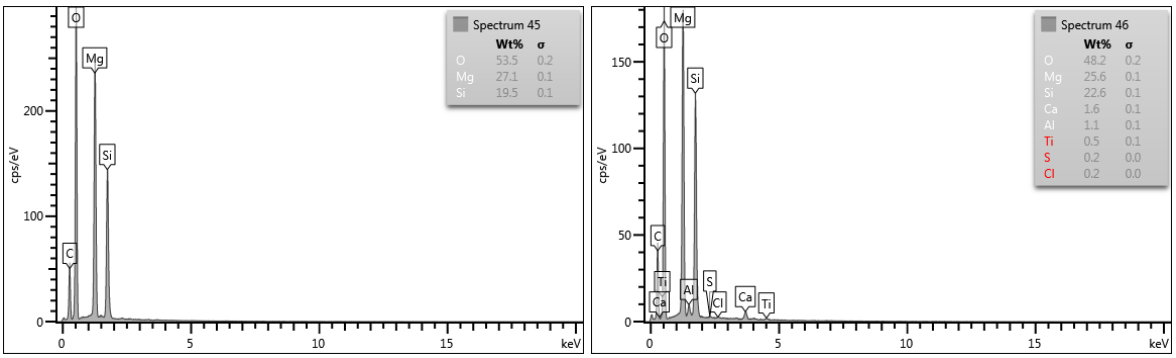

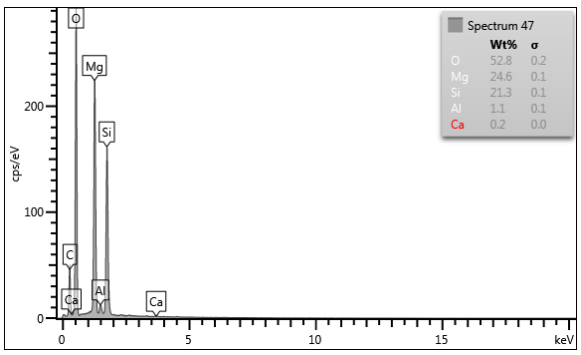

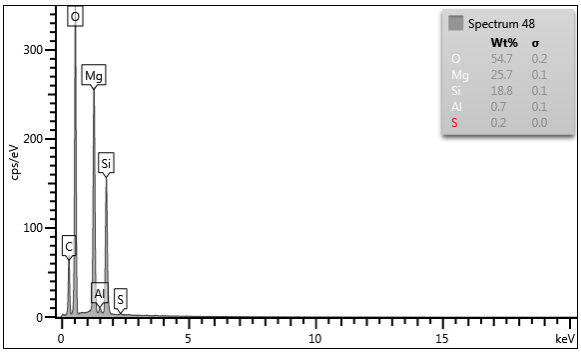

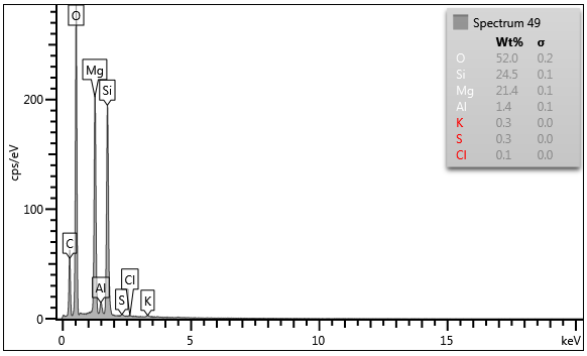

MS40 samples

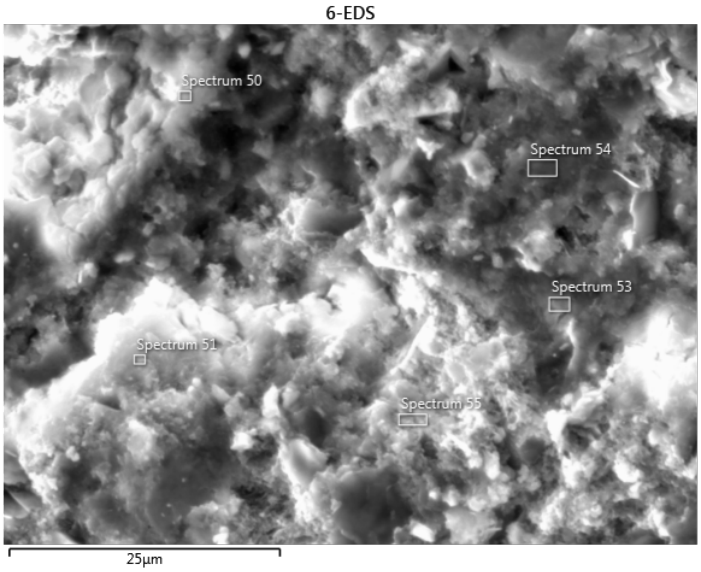

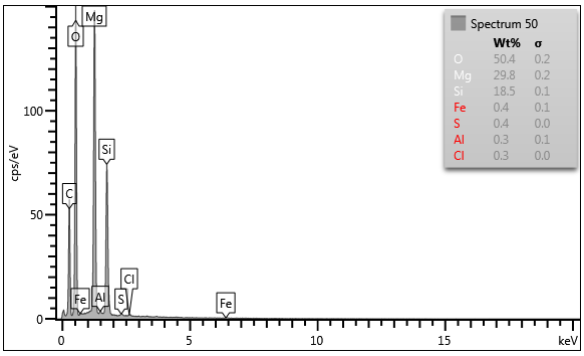

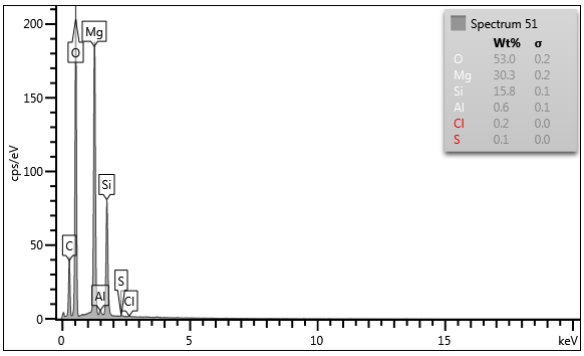

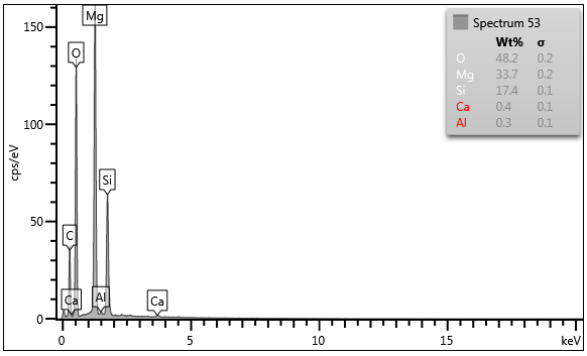

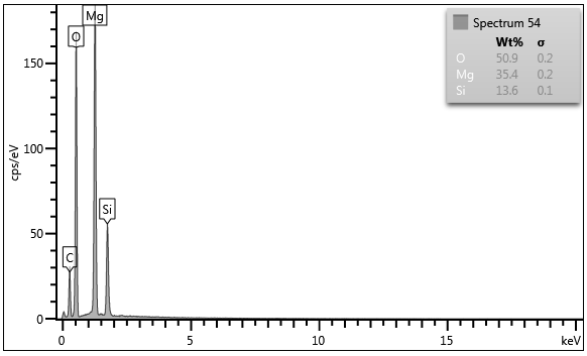

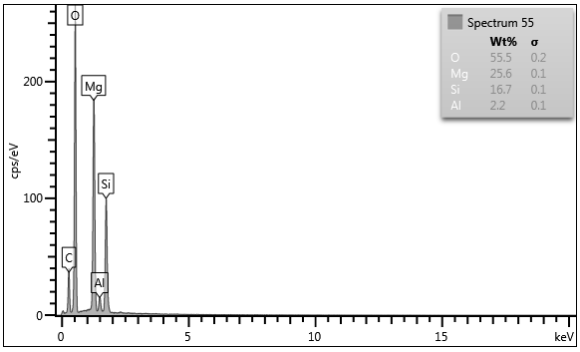

C.9. M-RHA mixtures - 7 days age: RHA40 samples

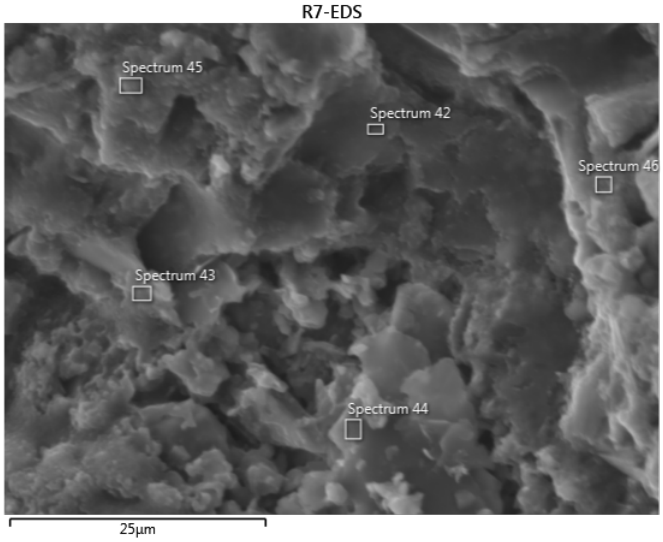

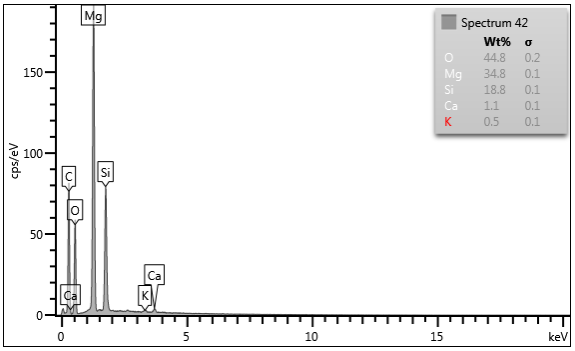

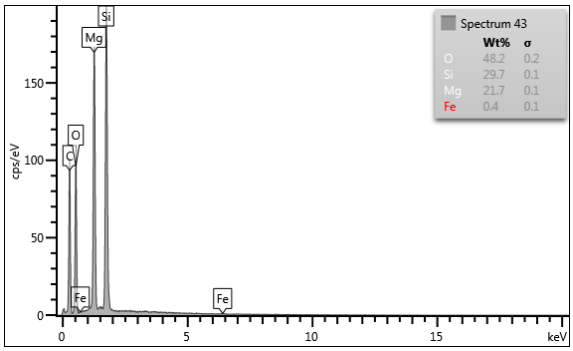

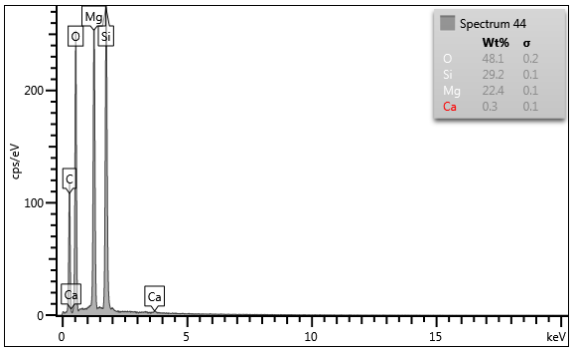

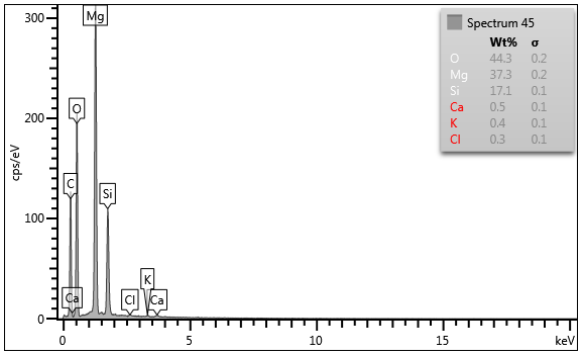

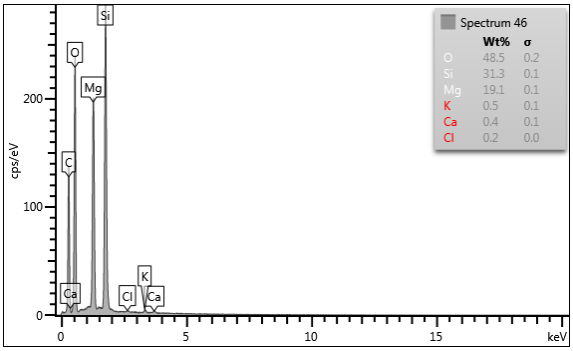

C.10. M-RHA mixtures - 28 days age: RHA40 samples

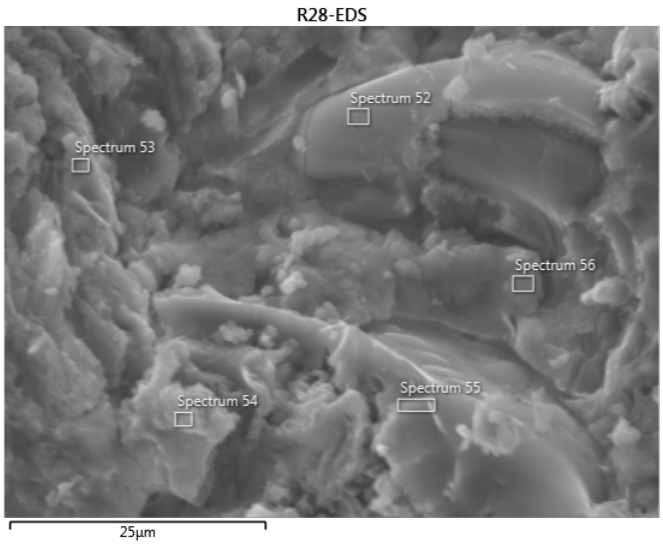

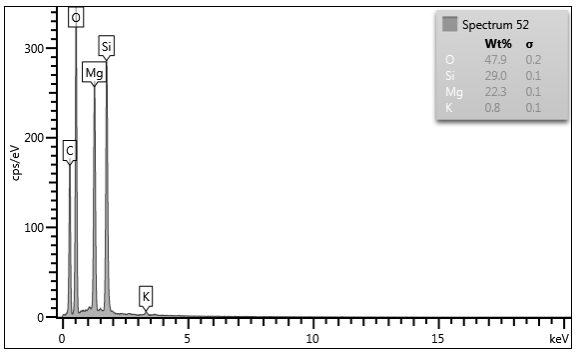

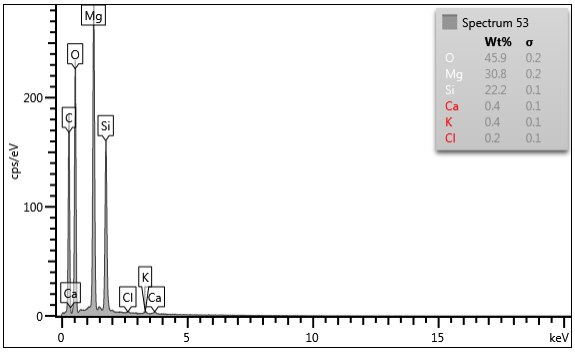

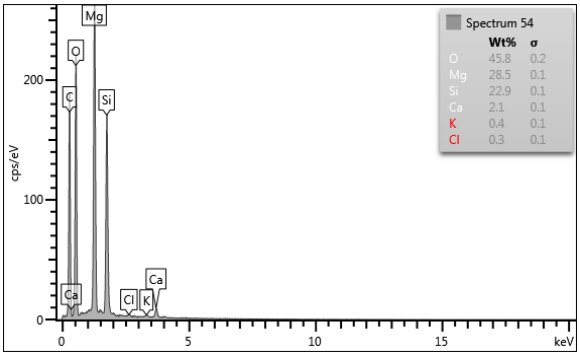

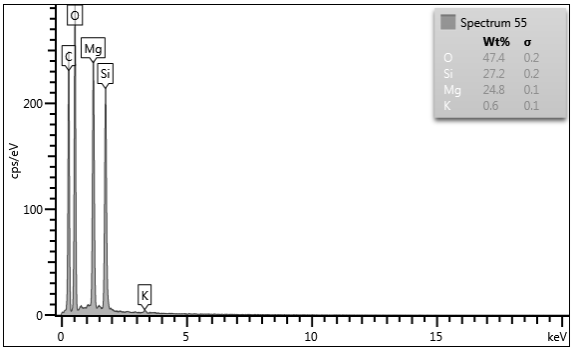

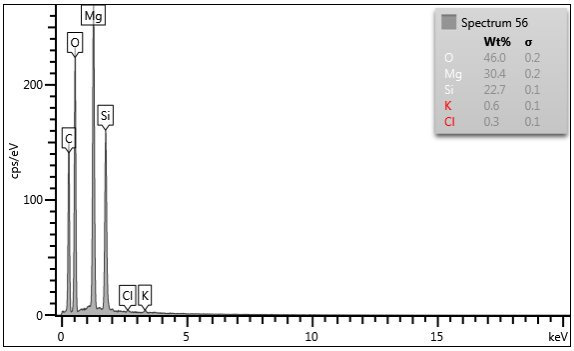

C.11. M-RHA mixtures - 90 days age: RHA40 samples

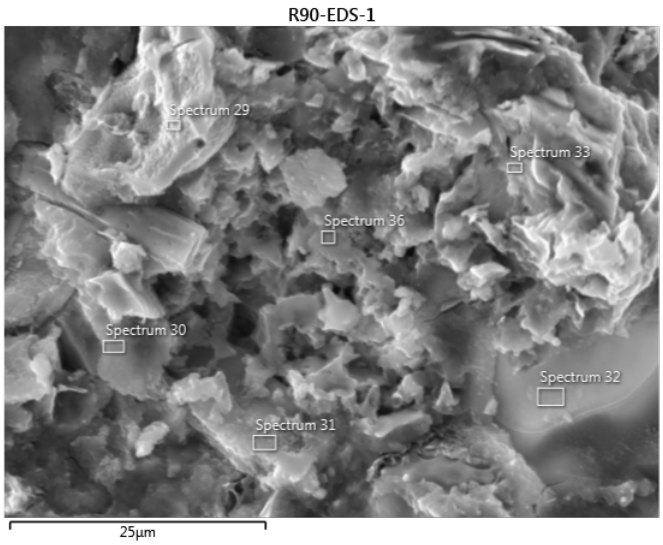

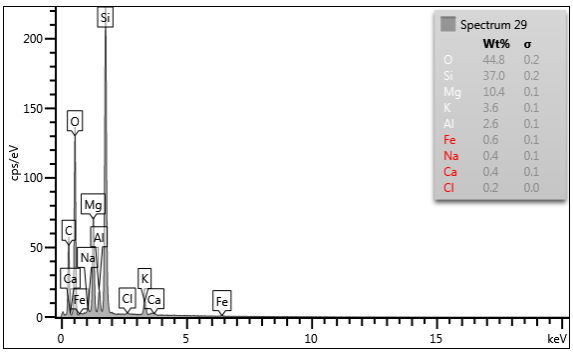

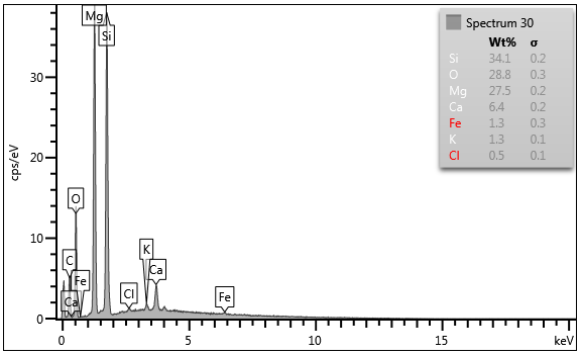

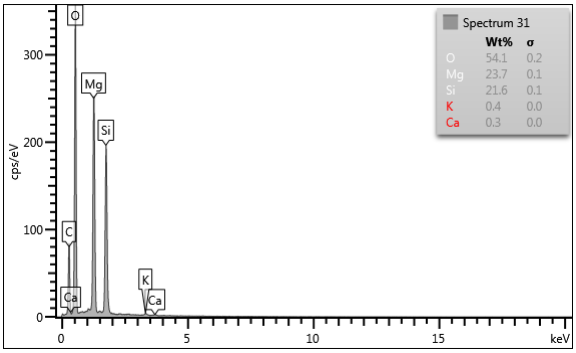

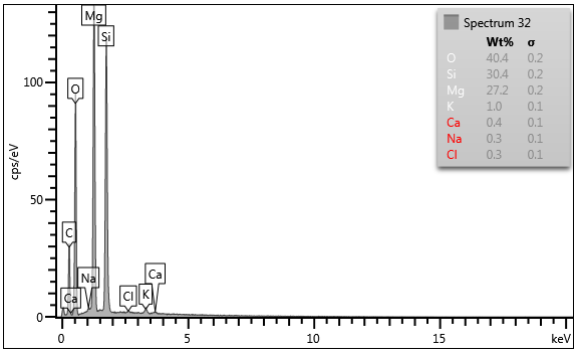

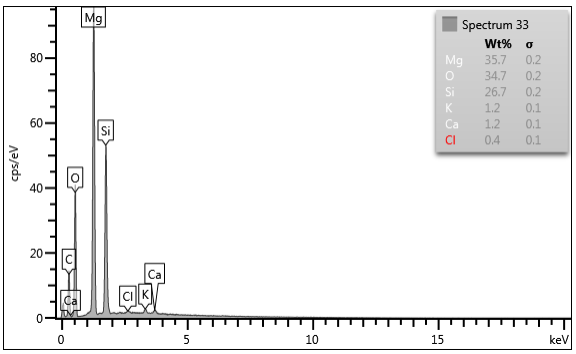

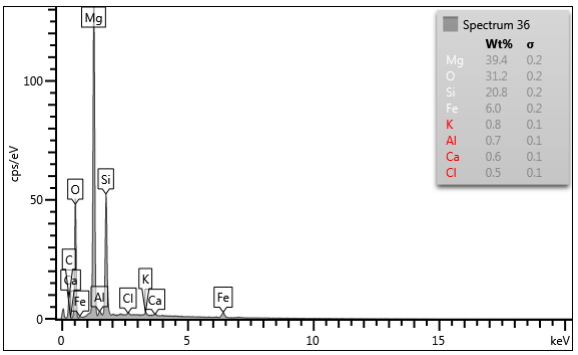

C.12. M-RHA mixtures - 365 days age: RHA 40 samples

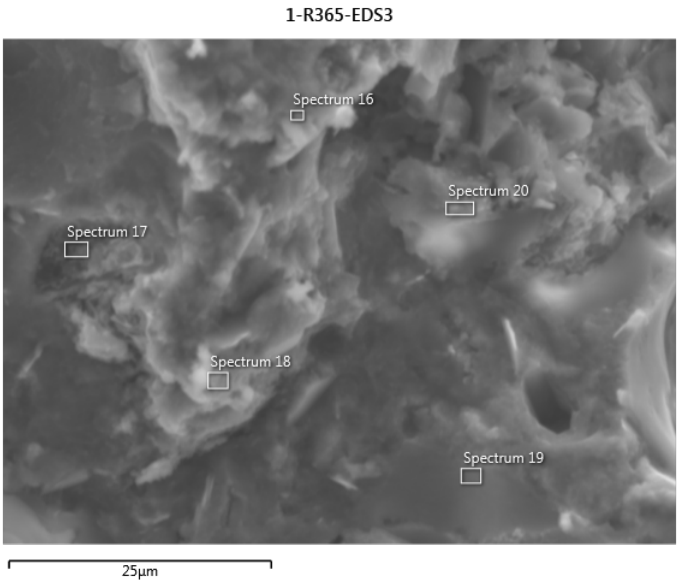

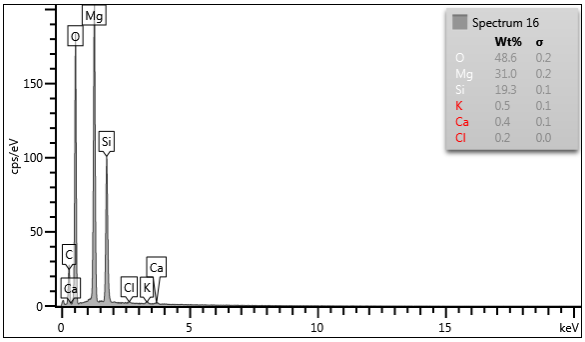

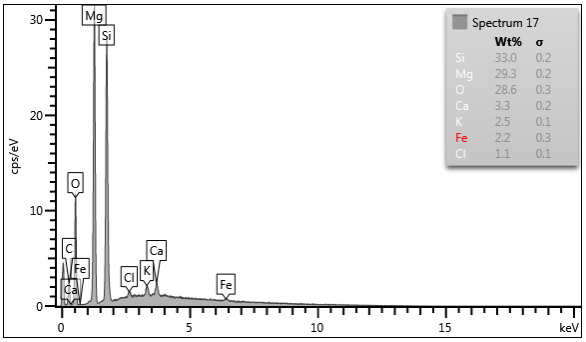

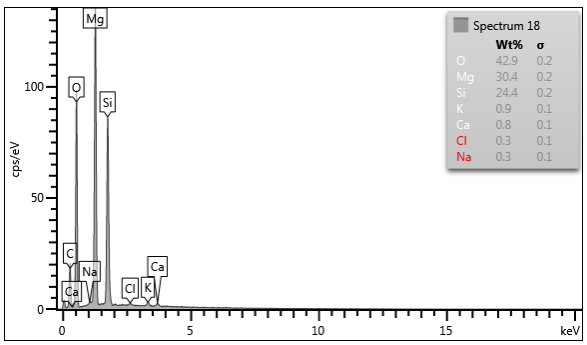

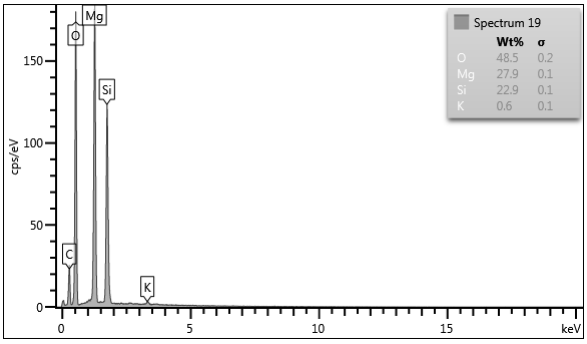

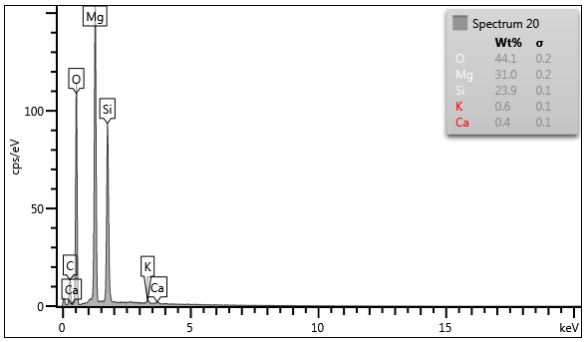

C.13. M-FA mixtures - 7 days age: FA40 samples

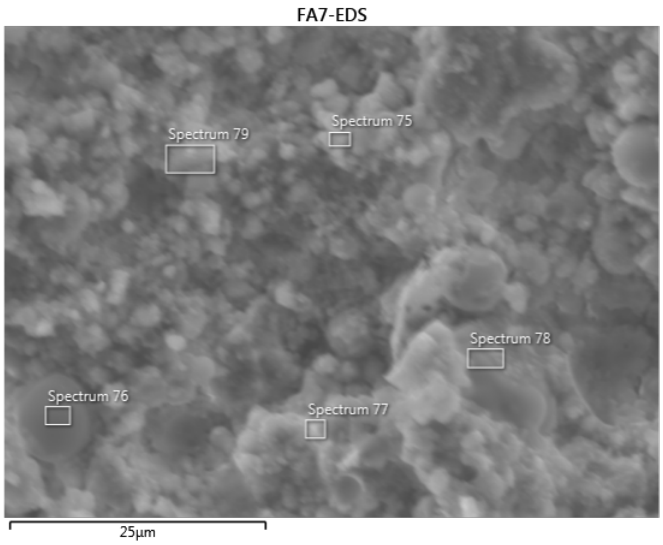

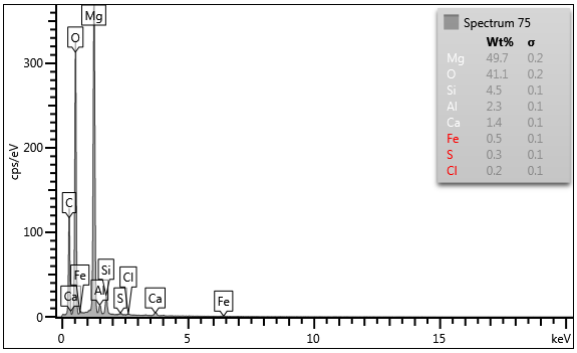

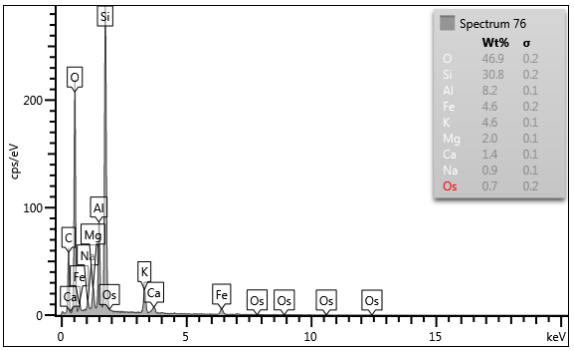

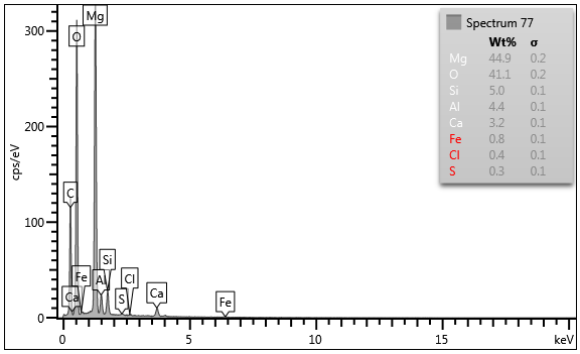

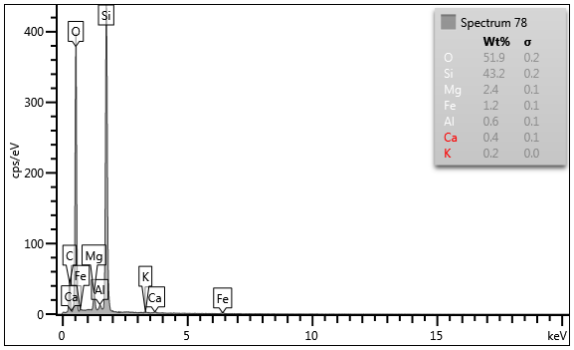

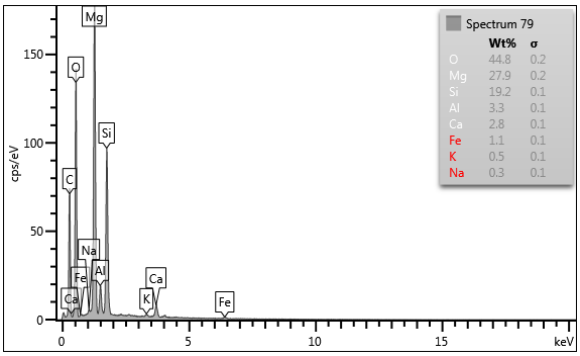

C.14. M-FA mixtures - 28 days age: FA40 samples

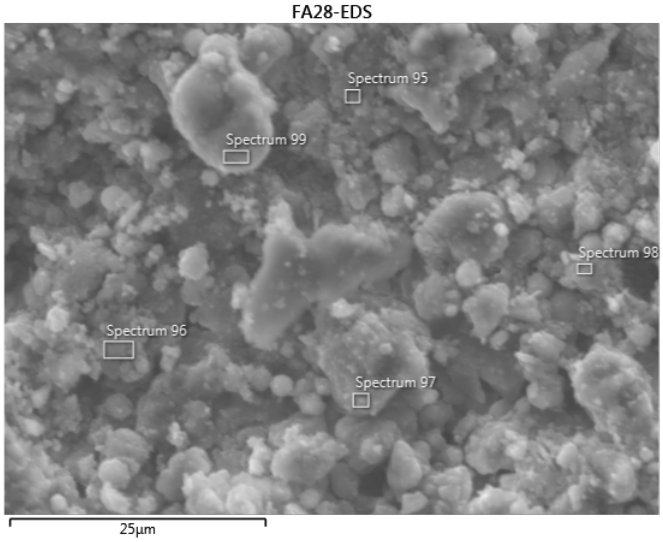

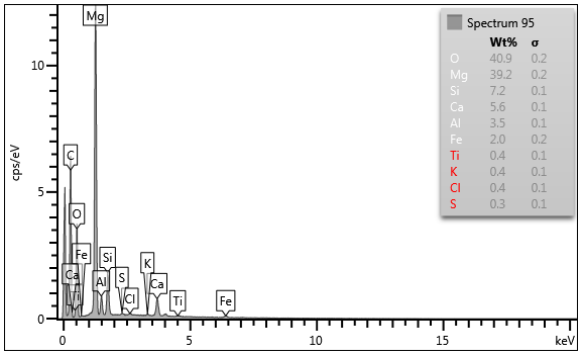

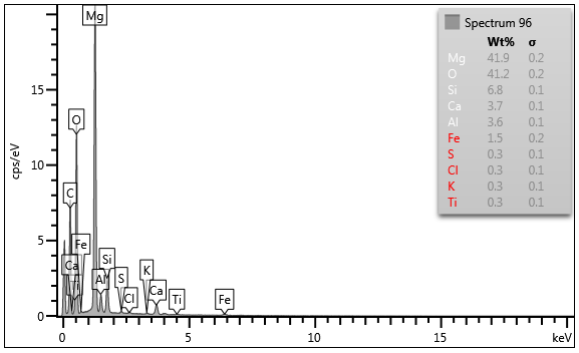

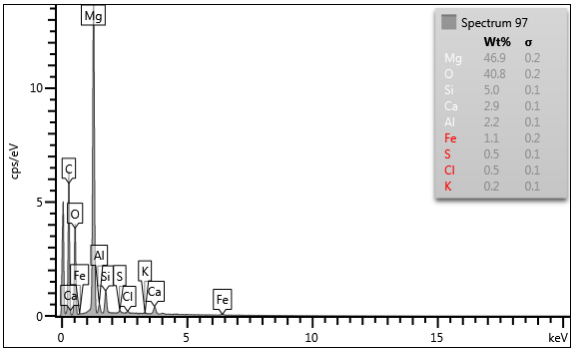

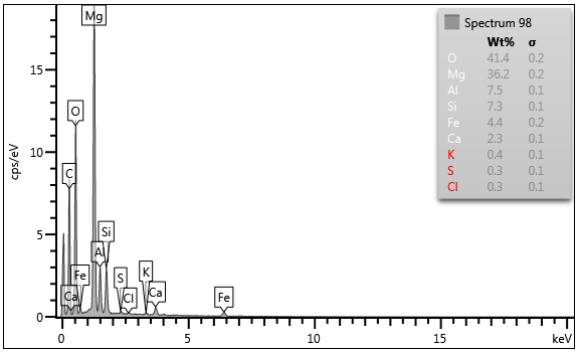

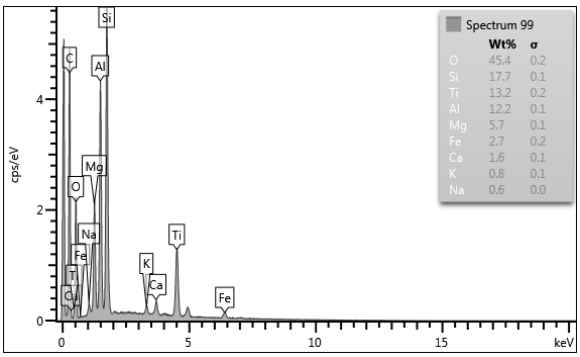

C.15. M-FA mixtures - 90 days age: FA40 samples

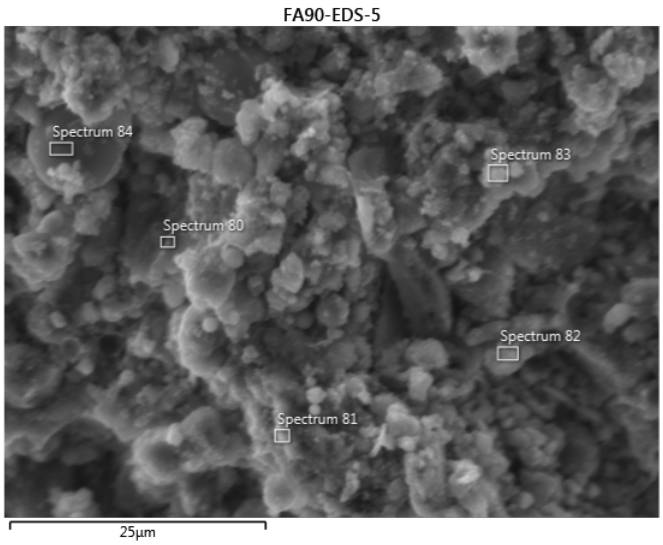

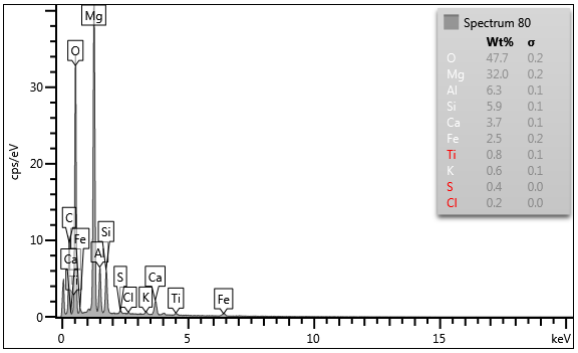

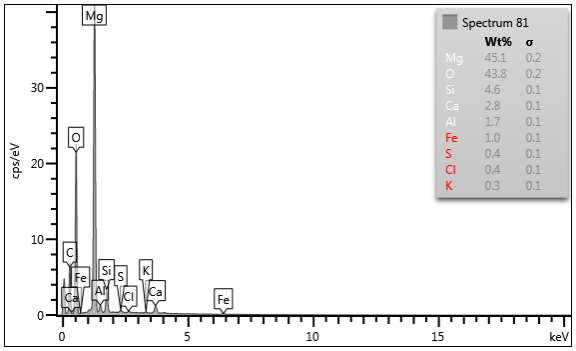

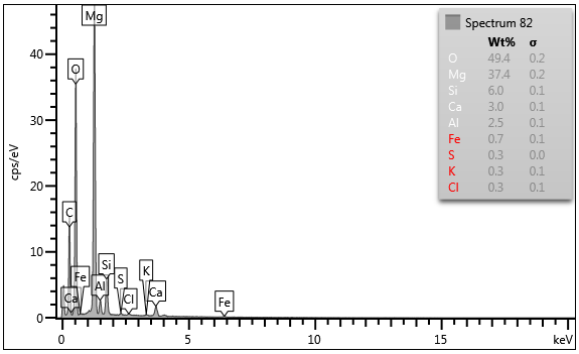

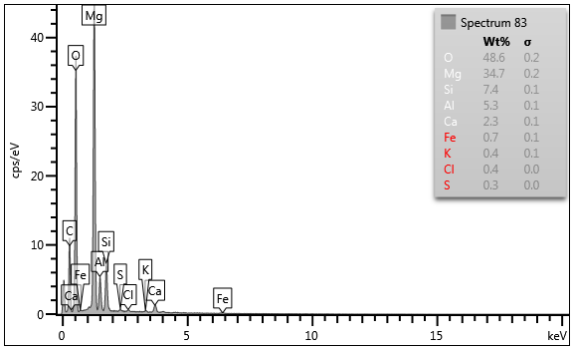

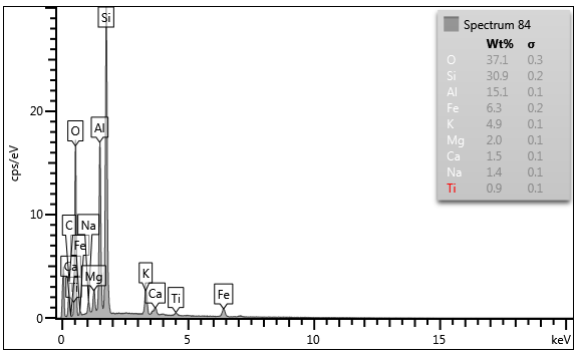

C.16. M-FA mixtures - 365 days age: FA40 samples

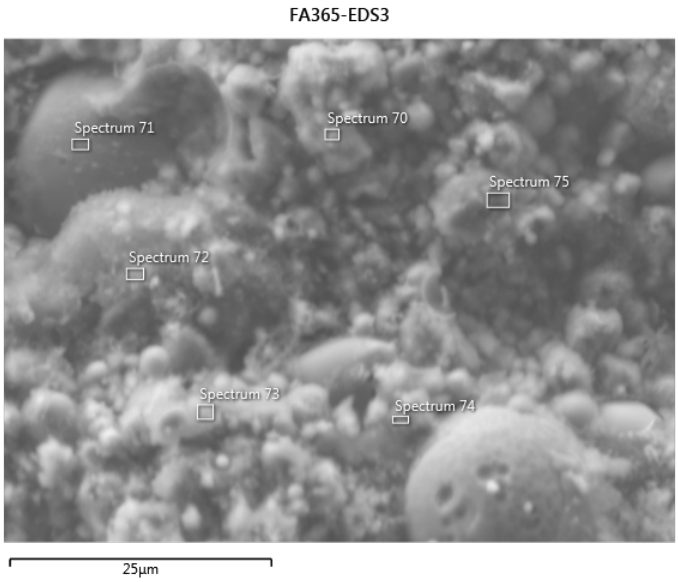

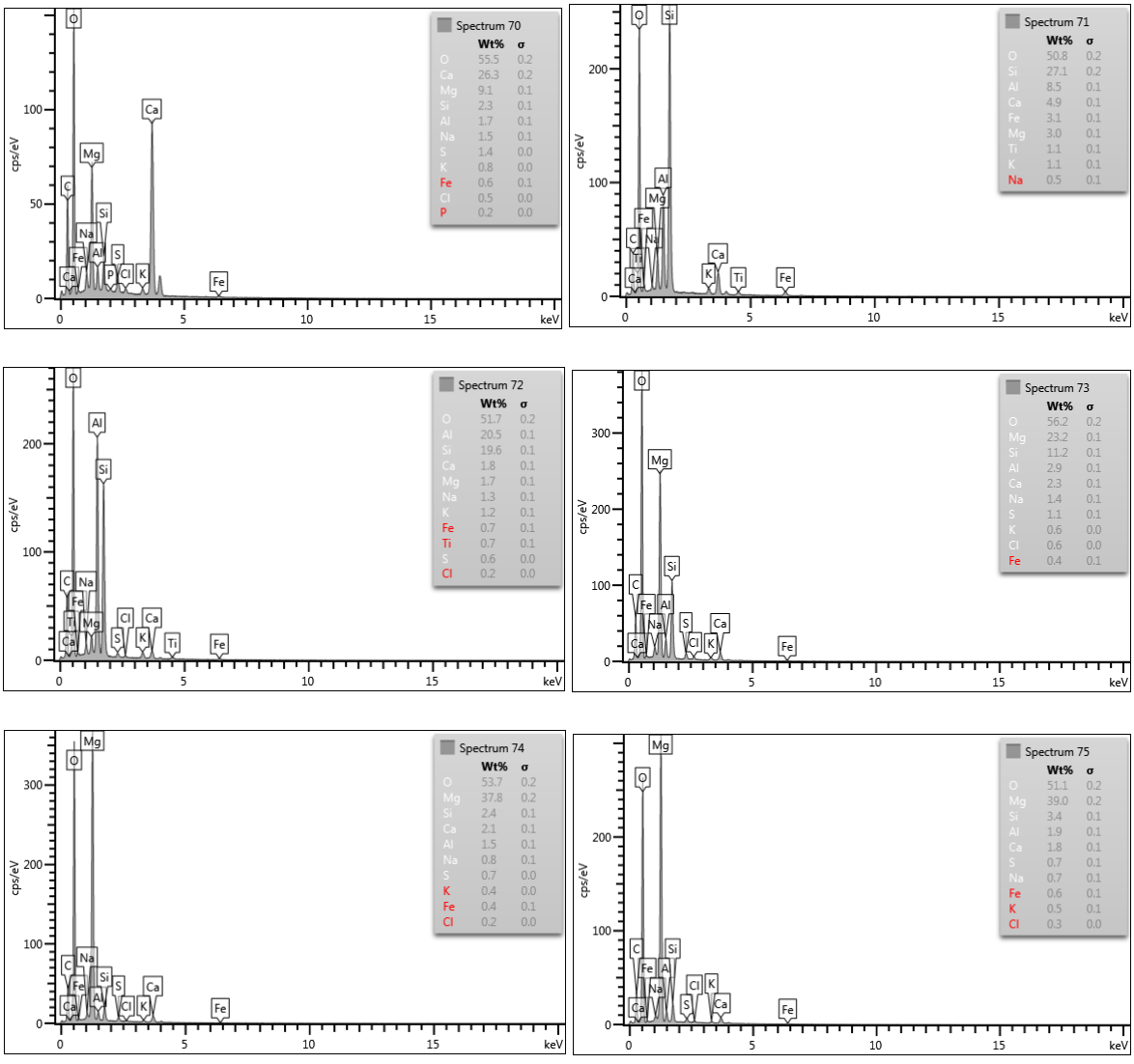

Appendix D (Chapter 5)

Alkali ion concentrations of M-SF mixtures

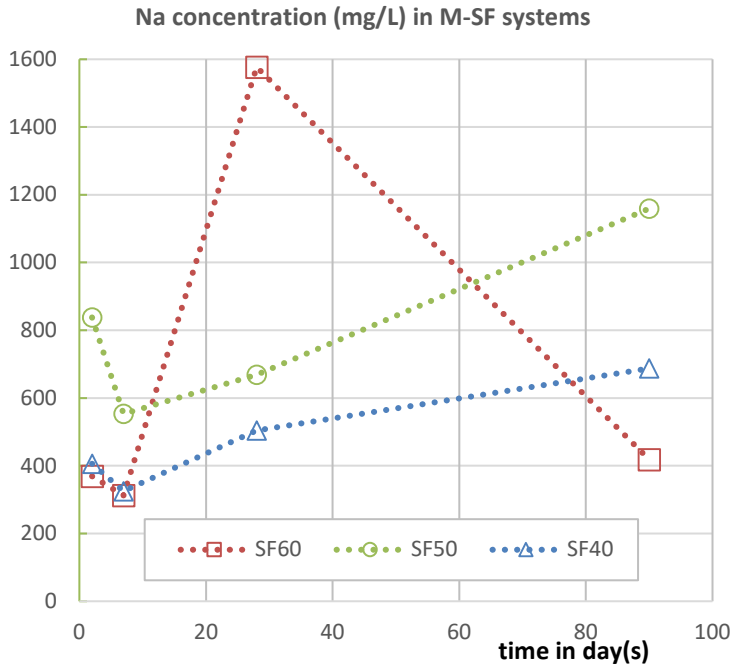

Figure D.1. Na concentration (mg/L) in M-SF systems

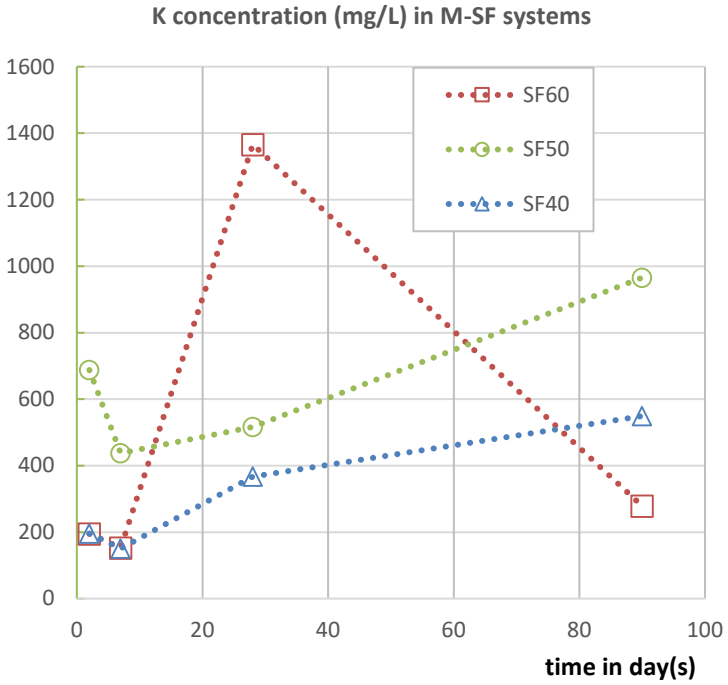

Figure D.2. K concentration (mg/L) in M-SF systems

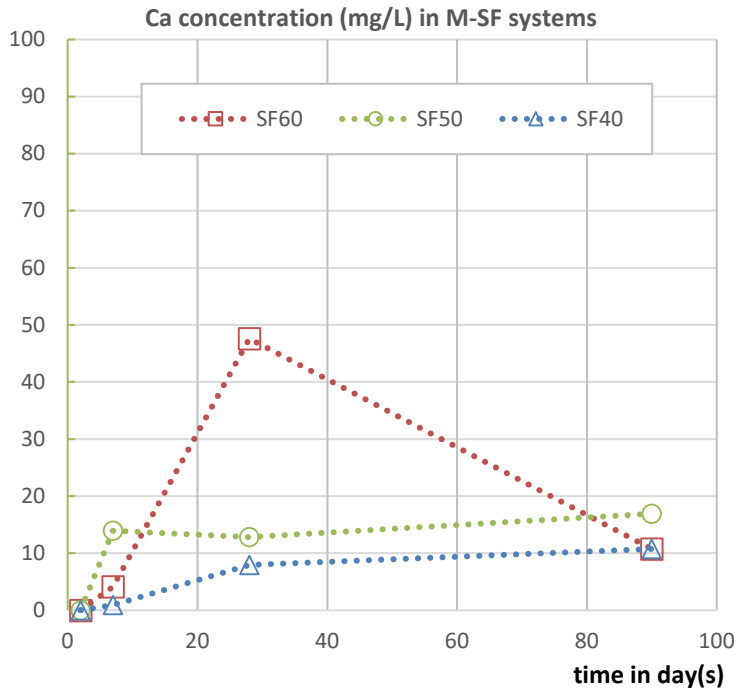

Figure D.3. Ca concentration (mg/L) in M-SF systems

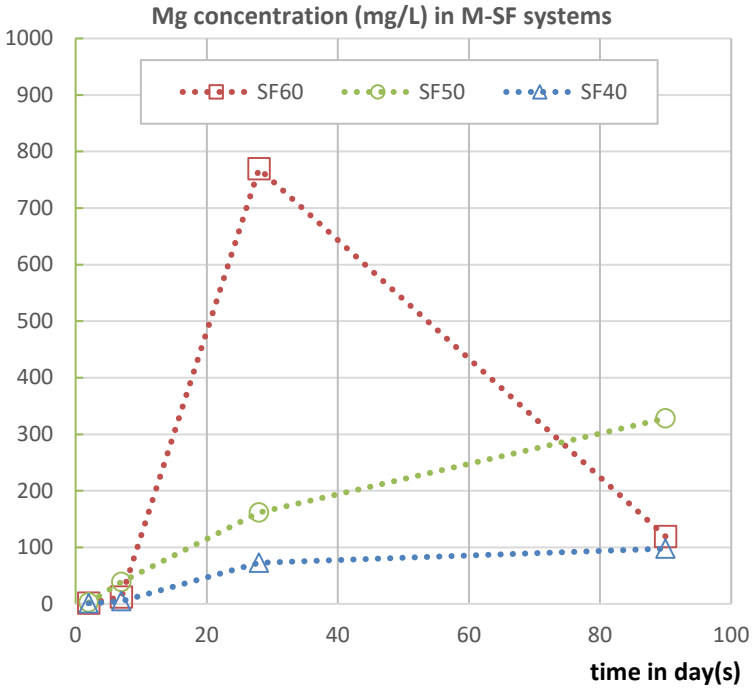

Figure D.4. Mg concentration (mg/L) in M-SF systems

Appendix E (Chapter 7)

Table E.1. Compressive strengths of M-S-H and PC samples with different curing conditions

Mix series	Mix Proportions (Label)	Binder		Sand		w/ (MgO+ SF)	SP (liquid %/g)	Slump/ Flow (mm)	Compressive strength MPa)				% 28-day compressive strength			
		MgO	Silica fume	PS (mm)	S/B Ratio				7	28	90	365	7	28	90	365
Curing effects to strength development (s/B=1.0, 7-28-90-365 days)																
Moisture	SF40-A	0.6	0.4	0-2.36	1.0	0.4	3%	~140-150	34.0	49.1	52.5	61.3	69	100	107	125
Moisture	SF40-W7D	0.6	0.4	0-2.36	1.0	0.4	3%	~140-150	27.5	52.0	53.5	59.1	53	100	103	114
Moisture	SF40-W28D	0.6	0.4	0-2.36	1.0	0.4	3%	~140-150	27.5	45.1	70.8	71.8	61	100	157	159
Moisture	SF40-W90D	0.6	0.4	0-2.36	1.0	0.4	3%	~140-150	27.5	45.1	62.8	64.8	61	100	139	144
Moisture	SF40-W365D	0.6	0.4	0-2.36	1.0	0.4	3%	~140-150	27.5	45.1	62.8	45.5	61	100	139	101
Oven-dried curing	SF40-OV50-1D	0.6	0.4	0-2.36	1.0	0.4	3%	~140-150	34.9	50.0	67.7	54.2	70	100	136	109
Oven-dried curing	SF40-OV50-3D	0.6	0.4	0-2.36	1.0	0.4	3%	~140-150	35.3	43.6	62.9	47.8	81	100	144	110
Oven-dried curing	SF40-OV100-1D	0.6	0.4	0-2.36	1.0	0.4	3%	~140-150	39.9	49.5	59.8	46.7	80	100	121	94
Oven-dried curing	SF40-OV100-3D	0.6	0.4	0-2.36	1.0	0.4	3%	~140-150	38.5	46.6	54.6	50.3	83	100	117	108
Hot water curing	SF40-W60-1D	0.6	0.4	0-2.36	1.0	0.4	3%	~140-150	37.5	45.2	57.5	48.0	83	100	127	106
Hot water curing	SF40-W60-3D	0.6	0.4	0-2.36	1.0	0.4	3%	~140-150	50.4	52.6	55.8	44.2	96	100	106	84
PC control mix																
PC	PC-A			0-2.36	1.0	0.4	-	~140-150	46.2	47.2	50.3	50.4	98	100	107	107
PC	PC-W365D			0-2.36	1.0	0.4	-	~140-150	54.9	75.1	85.7	89.5	73	100	114	119

Table E.2. Effect of silica sources to strength development of M-S-H binder systems

Mix series	Mix Proportions (Label)	Binder		Sand		w/ ($MgO+SiO_2$)	SP (liquid %/g)	Compressive strength (MPa)			
		MgO	Silica fume	PS (mm)	S/B Ratio			7-day	28-day	90-day	365-day
Effect of silica sources to strength development of MSH binder systems											
M-SF mixtures	SF60	0.4	0.6	0-2.36	1	0.4	3%	21.3	28.3	52.3	47.3
M-SF mixtures	SF50	0.5	0.5	0-2.36	1	0.4	3%	24.9	38.7	54.0	46.9
M-SF mixtures	SF40	0.6	0.4	0-2.36	1	0.4	3%	27.5	45.1	62.8	45.5
M-MS mixtures	MS60	0.4	0.6 MS	0-2.36	1	0.4	3%	16.6	21.6	36.3	38.9
M-MS mixtures	MS50	0.5	0.5 MS	0-2.36	1	0.4	3%	13.9	20.8	32.9	39.3
M-MS mixtures	MS40	0.6	0.4 MS	0-2.36	1	0.4	3%	8.0	13.3	26.6	32.6
M-FA mixtures	FA60	0.4	0.6FA	0-2.36	1	0.4	1%	0.6	2.1	3.0	4.5
M-FA mixtures	FA50	0.5	0.5FA	0-2.36	1	0.4	1%	1.6	2.4	3.1	6.5
M-FA mixtures	FA40	0.6	0.4FA	0-2.36	1	0.4	3%	3.1	3.9	4.0	7.0
M-MS mixtures	MS60	0.4	0.6 MS	0-2.36	1	0.5	2%	5.7	8.1	18.8	22.4
M-MS mixtures	MS50	0.5	0.5 MS	0-2.36	1	0.5	2%	5.7	9.6	19.3	24.4
M-MS mixtures	MS40	0.6	0.4 MS	0-2.36	1	0.5	2%	5.2	7.3	17.2	21.1
M-RHA mixtures	R60	0.4	0.6R	0-2.36	1	0.5	5%	2.7	10.0	17.4	18.9
M-RHA mixtures	R50	0.5	0.5R	0-2.36	1	0.5	4%	7.1	15.0	19.7	21.4
M-RHA mixtures	R40	0.6	0.4R	0-2.36	1	0.5	3%	8.2	15.3	17.7	21.2
100% MgO	MgO-W365D	100		0-2.36	1	0.6	3%	0.8	0.8	1.9	2.9
100% MgO	MgO-A	100		0-2.36	1	0.6	3%	2.4	3.3	6.6	7.0

Appendix F (Chapter 8)

Table F.1. Compressive strengths of concrete samples

Mix labels	7-day comp. strength (MPa)	28-day comp. strength (MPa)	90-day comp. strength (MPa)
SF40	23.2	40.5	42.2
Q10	24.5	43.5	55.9
PC	51.0	62.0	69.0

Table F.2. Split tensile strengths of concrete samples

Mix labels	7-day split tensile strength (MPa)	28-day split tensile strength (MPa)	90-day split tensile strength (MPa)
SF40	1.6	1.9	1.9
Q10	2.8	3.2	3.5
PC	4.8	6.1	6.3

Table F.3. Stress-strain testing results of PC concrete samples (7 days age)

Load (kN)	PC-Sample 1		PC-Sample 2		PC-Sample 3		Load (MPa)	Strain (average)
	Reading 1	Reading 2	Reading 1	Reading 2	Reading 1	Reading 2		
0	0.002	0.006	0.002	0.003	0.000	0.000	0.0	0.0000
20	0.019	0.019	0.023	0.023	0.016	0.016	2.5	0.0001
40	0.039	0.039	0.045	0.044	0.034	0.034	5.1	0.0001
60	0.058	0.060	0.066	0.066	0.055	0.053	7.6	0.0002
80	0.079	0.079	0.089	0.087	0.073	0.071	10.2	0.0003
100	0.100	0.106	0.110	0.108	0.092	0.091	12.7	0.0004
120	0.121	0.120	0.131	0.128	0.112	0.110	15.3	0.0005
140	0.142	0.141	0.155	0.150	0.134	0.130	17.8	0.0005
160	0.163	0.162	0.178	0.174	0.155	0.150	20.4	0.0006

Table F.4. Stress-strain testing results of SF40 concrete samples (7 days age)

Load (kN)	SF40-Sample 1		SF40-Sample 2		SF40-Sample 3		Load (MPa)	Strain (average)
	Reading 1	Reading 2	Reading 1	Reading 2	Reading 1	Reading 2		
0	0.002	0.002	0.002	0.000	0.000	0.000	0.0	0.000004
10	0.113	0.105	0.078	0.095	0.070	0.082	1.3	0.000340
20	0.175	0.168	0.133	0.154	0.121	0.131	2.5	0.000553
30	0.215	0.209	0.179	0.194	0.163	0.170	3.8	0.000708
40	0.247	0.243	0.220	0.225	0.199	0.199	5.1	0.000835
50	0.273	0.270	0.255	0.251	0.230	0.223	6.4	0.000941
60	0.298	0.294	0.285	0.278	0.259	0.249	7.6	0.001042
70	0.322	0.319	0.312	0.301	0.286	0.270	8.9	0.001134
80	0.347	0.345	0.340	0.325	0.314	0.292	10.2	0.001229

Table F.5. Stress-strain testing results of Q10 concrete samples (7 days age)

Load (kN)	Q10-03.04.17		Q10-05.04.17		Q10-16.04.17		Load (MPa)	Strain (average)
	Reading 1	Reading 2	Reading 1	Reading 2	Reading 1	Reading 2		
0	0	0	0	0	0	0	0.0	0.0000
10	0.011	0.014	0.019	0.027	0.017	0.017	1.3	0.0001
20	0.024	0.028	0.040	0.039	0.034	0.034	2.5	0.0001
30	0.038	0.042	0.058	0.060	0.050	0.050	3.8	0.0002
40	0.051	0.058	0.074	0.078	0.066	0.066	5.1	0.0002
50	0.066	0.074	0.092	0.097	0.084	0.084	6.4	0.0003
60	0.080	0.089	0.110	0.116	0.101	0.101	7.6	0.0004
70	0.090	0.100	0.123	0.130	0.113	0.113	8.9	0.0004
80	0.107	0.118	0.143	0.151	0.133	0.133	10.2	0.0005

Table F.6. Stress-strain testing results of PC concrete samples (28 days age)

Load (kN)	PC-Sample 1		PC-Sample 2		PC-Sample 3		Load (MPa)	Strain (average)
	Reading 1	Reading 2	Reading 1	Reading 2	Reading 1	Reading 2		
0	0.000	0.000	0.000	0.000	0.000	0.000	0.0	0.0000
30	0.023	0.024	0.029	0.026	0.024	0.023	3.8	0.0001
60	0.049	0.050	0.058	0.055	0.049	0.048	7.6	0.0002
90	0.074	0.076	0.084	0.082	0.074	0.074	11.5	0.0003
120	0.102	0.102	0.110	0.112	0.102	0.100	15.3	0.0004
150	0.129	0.128	0.138	0.137	0.129	0.128	19.1	0.0005
180	0.154	0.154	0.167	0.167	0.157	0.154	22.9	0.0006
190	0.165	0.163	0.173	0.175	0.165	0.162	24.2	0.0006

Table F.7. Stress-strain testing results of SF40 concrete samples (28 days age)

Load (kN)	SF-Sample 1		SF-Sample 2		SF-Sample 3		Load (MPa)	Strain (average)
	Reading 1	Reading 2	Reading 1	Reading 2	Reading 1	Reading 2		
0	0.002	0.000	0.000	0.000	0.000	0.000	0.0	0.0000
20	0.128	0.144	0.107	0.125	0.100	0.116	2.5	0.0005
40	0.213	0.228	0.191	0.205	0.176	0.188	5.1	0.0008
60	0.277	0.283	0.252	0.260	0.231	0.239	7.6	0.0010
80	0.323	0.328	0.299	0.304	0.277	0.280	10.2	0.0011
100	0.369	0.365	0.343	0.341	0.319	0.314	12.7	0.0013
125	0.420	0.411	0.395	0.386	0.367	0.356	15.9	0.0015

Table F.8. Stress-strain testing results of Q10 concrete samples (28 days age)

Load (kN)	Q10-03.04.17		Q10-05.04.17		Q10-16.04.17		Load (MPa)	Strain (average)
	Reading 1	Reading 2	Reading 1	Reading 2	Reading 1	Reading 2		
0	0	-	0	0	0	0	0.0	0.0000
20	0.024	-	0.034	-	0.028	-	2.5	0.0001
40	0.047	-	0.066	-	0.048	-	5.1	0.0002
60	0.073	-	0.099	-	0.076	-	7.6	0.0003
80	0.097	-	0.128	-	0.098	-	10.2	0.0004
100	0.121	-	0.157	-	0.125	-	12.7	0.0005
120	0.146	-	0.184	-	0.153	-	15.3	0.0006
140	0.171	-	0.211	-	0.181	-	17.8	0.0007

Table F.9. Stress-strain testing results of PC concrete samples (90 days age)

Load (kN)	PC-Sample 1		PC-Sample 2		PC-Sample 3		Load (MPa)	Strain (average)
	Reading 1	Reading 2	Reading 1	Reading 2	Reading 1	Reading 2		
0	0	0	0	0	0	0	0.0	0.0000
30	0.023	0.024	0.024	0.023	0.021	0.016	3.8	0.0001
60	0.049	0.050	0.050	0.047	0.040	0.036	7.6	0.0002
90	0.070	0.074	0.073	0.073	0.058	0.053	11.5	0.0003
120	0.094	0.099	0.097	0.099	0.074	0.071	15.3	0.0003
150	0.120	0.125	0.123	0.123	0.089	0.089	19.1	0.0004
180	0.146	0.151	0.147	0.150	0.105	0.110	22.9	0.0005
200	0.162	0.167	0.165	0.168	0.116	0.123	25.5	0.0006
230	0.189	0.192	0.193	0.194	0.136	0.144	29.3	0.0007
260	0.216	0.217	0.223	0.222	0.157	0.169	33.1	0.0008

Table F.10. Stress-strain testing results of SF40 concrete samples (90 days age)

Load (kN)	SF-Sample 1		SF-Sample 2		SF-Sample 3		Load (MPa)	Strain (average)
	Reading 1	Reading 2	Reading 1	Reading 2	Reading 1	Reading 2		
0	0	0	0	0	0	0	0.0	0.000000
20	0.084	0.095	0.136	0.155	0.121	0.126	2.5	0.000449
40	0.155	0.168	0.202	0.228	0.189	0.189	5.1	0.000709
60	0.197	0.213	0.251	0.280	0.241	0.238	7.6	0.000890
80	0.223	0.241	0.294	0.320	0.285	0.284	10.2	0.001032
100	0.243	0.260	0.336	0.357	0.327	0.310	12.7	0.001148
120	0.254	0.272	0.375	0.395	0.367	0.346	15.3	0.001259
135	0.267	0.282	0.403	0.419	0.395	0.368	17.2	0.001338

Table F.11. Stress-strain testing results of Q10 concrete samples (90 days age)

Load (kN)	Q10-03.04.17		Q10-14.04.17		Q10-15.04.17		Load (MPa)	Strain (average)
	Reading 1	Reading 2	Reading 1	Reading 2	Reading 1	Reading 2		
0	0	0	0	0	0	0	0.0	0.00000000
10	0.011	0.011	0.011	0.011	0.013	0.015	1.3	0.00004511
30	0.037	0.036	0.036	0.037	0.042	0.044	3.8	0.00014536
60	0.074	0.072	0.074	0.076	0.081	0.082	7.6	0.00028759
90	0.112	0.108	0.113	0.113	0.116	0.118	11.5	0.00042607
120	0.149	0.142	0.150	0.150	0.150	0.152	15.3	0.00055952
150	0.187	0.177	0.188	0.188	0.185	0.186	19.1	0.00069627
175	0.218	0.207	0.220	0.220	0.215	0.214	22.3	0.00081023

Table F.12. Porosity (% voids) of concrete samples

Mix labels	7-day (% voids)	28-day (% voids)	90-day (% voids)
PC	9.6	9.4	7.1
SF40	12.5	12.8	12.5
Q10	11.0	11.2	10.9

Table F.13. Coefficient of permeability (10^{-10} m/s) of concrete samples

Mix labels	7-day coefficient of permeability	28-day coefficient of permeability	90-day coefficient of permeability
PC	0.56	0.50	0.44
SF40	0.58	3.71	24.71
Q10	0.58	1.82	10.55

Table F.14. Resistivity indexes of concrete samples

Mix labels	7-day	28-day	90-day
PC	8.3	11.7	12.8
SF40	6.8	10.3	8.8
Q10	11.3	16.1	10.6